

# Glueballs, Hybrids, Multiquarks. Experimental facts versus QCD inspired concepts.

Eberhard Klempt<sup>a</sup> and Alexander Zaitsev<sup>b</sup>

<sup>a</sup> Helmholtz-Institut für Strahlen- und Kernphysik der Rheinischen Friedrich-Wilhelms Universität,  
Nußallee 14-16, D-53115 Bonn, Germany

<sup>b</sup> Institute for High-Energy Physics, Moscow Region, RU-142284 Protvino, Russia

## Abstract

Glueballs, hybrids and multiquark states are predicted as bound states in models guided by quantum chromodynamics, by QCD sum rules or QCD on a lattice. Estimates for the (scalar) glueball ground state are in the mass range from 1000 to 1800 MeV, followed by a tensor and a pseudoscalar glueball at higher mass. Experiments have reported evidence for an abundance of meson resonances with  $0^{-+}$ ,  $0^{++}$  and  $2^{++}$  quantum numbers. In particular the sector of scalar mesons is full of surprises starting from the elusive  $\sigma$  and  $\kappa$  mesons. The  $a_0(980)$  and  $f_0(980)$ , discussed extensively in the literature, are reviewed with emphasis on their Janus-like appearance as  $K\bar{K}$  molecules, tetraquark states or  $q\bar{q}$  mesons. Most exciting is the possibility that the three mesons  $f_0(1370)$ ,  $f_0(1500)$ , and  $f_0(1710)$  might reflect the appearance of a scalar glueball in the world of quarkonia. However, the existence of  $f_0(1370)$  is not beyond doubt and there is evidence that both  $f_0(1500)$  and  $f_0(1710)$  are flavour octet states, possibly in a tetraquark composition. We suggest a scheme in which the scalar glueball is dissolved into the wide background into which all scalar flavour singlet mesons collapse.

There is an abundance of meson resonances with the quantum numbers of the  $\eta$ . Three states are reported below  $1.5 \text{ GeV}/c^2$  whereas quark models expect only one, perhaps two. One of these states,  $\iota(1440)$ , was the prime glueball candidate for a long time. We show that  $\iota(1440)$  is the first radial excitation of the  $\eta$  meson.

Hybrids may have exotic quantum numbers which are not accessible by  $q\bar{q}$  mesons. There are several claims for  $J^{PC} = 1^{-+}$  exotics, some of them with properties as predicted from the flux tube model interpreting the quark-antiquark binding by a gluon string. The evidence for these states depends partly on the assumption that meson-meson interactions are dominated by s-channel resonances. Hybrids with non-exotic quantum numbers should appear as additional states. Light-quark mesons exhibit a spectrum of (squared) masses which are proportional to the sum of orbital angular momentum and radial quantum numbers. Two states do not fall under this classification. They are discussed as hybrid candidates.

The concept of multiquark states has received revived interest due to new resonances in the spectrum of states with open and hidden charm. The new states are surprisingly narrow and their masses and their decay modes often do not agree with simple quark-model expectations.

Lattice gauge theories have made strong claims that glueballs and hybrids should appear in the meson spectrum. However, the existence of a scalar glueball, at least with a reasonable width, is highly questionable. It is possible that hybrids will turn up in complex multibody final states even though so far, no convincing case has been made for them by experimental data. Lattice gauge theories fail to identify the nonet of scalar mesons. Thus, at the present status of approximations, lattice gauge theories seem not to provide a trustworthy guide into unknown territory in meson spectroscopy.

PACS: 12.38.-t; 12.39.-x; 13.25.-k; 13.75.Lb; 14.40.-a

## Contents

1	Introduction	9
1.1	Highlights and perspectives	9
1.1.1	Scope of the review	9
1.1.2	Recent outstanding achievements	9
1.1.3	New insights	10
1.1.4	Critique of QCD folklore	13
1.1.5	Successes and limitations of lattice QCD	14
1.1.6	Future options	15
1.1.7	Hints for expert readers	17
1.1.8	Outline	18
1.1.9	A guide to the literature	19
1.2	Phenomenology of $q\bar{q}$ mesons	20
1.2.1	The A,B,C, .. of meson spectroscopy: the naming scheme	20
1.2.2	Meson nonets	23
1.2.3	Mixing	24
1.2.4	The Zweig rule	26
1.2.5	Regge trajectories	27
1.2.6	Flavour independence of forces	28
1.2.7	The light meson spectrum and quark model assignments	30
2	From QCD to strong interactions	34
2.1	Quantum Chromo Dynamics	34
2.1.1	The QCD Lagrangian	34
2.1.2	Chiral symmetry	35
2.1.3	Instantons	36
2.2	Chiral Perturbation Theory $\chi$ PT	36
2.3	Lattice QCD	37
2.3.1	Confinement	38
2.3.2	Glueballs	38

2.3.3	Ground-state $q\bar{q}$ mesons . . . . .	40
2.3.4	Hybrids . . . . .	41
2.4	QCD sum rules . . . . .	42
2.5	Flux-tube model . . . . .	43
2.6	Quark models . . . . .	44
2.6.1	Gluon-exchange interactions . . . . .	44
2.6.2	Exchange of Goldstone particles . . . . .	45
2.6.3	Instanton-induced interactions . . . . .	45
2.6.4	Heavy Quark Symmetry . . . . .	47
2.7	Meson decays . . . . .	48
2.8	Effective chiral symmetry restoration . . . . .	48
2.9	Solvable models . . . . .	49
2.10	Have we gained insight from $q\bar{q}$ mesons? . . . . .	49
3	Major experiments . . . . .	51
3.1	Diffractive and charge exchange experiments . . . . .	51
3.1.1	The CERN-Munich experiment . . . . .	51
3.1.2	The WA3 experiment . . . . .	51
3.1.3	The LASS experiment . . . . .	52
3.1.4	The VES experiment . . . . .	52
3.1.5	Experiment E852 at BNL . . . . .	53
3.2	Central production experiments . . . . .	54
3.2.1	The WA76 and WA91 experiments . . . . .	54
3.2.2	The GAMS experiment . . . . .	55
3.2.3	WA102 experiment . . . . .	55
3.3	Antiproton-proton annihilation . . . . .	55
3.3.1	The Asterix experiment . . . . .	55
3.3.2	The Crystal Barrel experiment . . . . .	55
3.3.3	The Obelix experiment . . . . .	56
3.3.4	Experiment E760/E835 at FNAL . . . . .	57

3.4	Electron-positron annihilation experiments at $\Phi$ and $c\bar{c}$ factories .....	58
3.4.1	VEPP .....	58
3.4.2	KLOE at Daphne .....	59
3.4.3	Argus, Mark3 and DM2 .....	60
3.4.4	BES .....	60
3.5	Heavy-quark spectroscopy .....	60
3.5.1	Experiments at FNAL .....	60
3.5.2	CLEO .....	61
3.5.3	Meson spectroscopy at the $\bar{b}b$ factories BaBar and BELLE .....	62
3.6	Meson spectroscopy at LEP .....	64
3.6.1	The Aleph experiment .....	64
3.6.2	The Delphi experiment .....	65
3.6.3	The L3 experiment .....	65
3.6.4	The Opal experiment .....	65
4	Experimental methods .....	67
4.1	Meson resonances in production experiments .....	67
4.1.1	Charge exchange and strangeness exchange scattering .....	67
4.1.2	Two-photon fusion .....	69
4.1.3	Central production .....	71
4.1.4	The Deck effect .....	76
4.1.5	Antiproton-proton annihilation .....	77
4.1.6	Flavour tagging .....	78
4.2	Meson resonances in formation experiments .....	81
4.2.1	$e^+e^-$ annihilation .....	81
4.2.2	Width of the $J/\psi$ .....	82
4.2.3	Initial state radiation .....	83
4.2.4	Decay of $\tau$ mesons .....	84
4.2.5	The $\chi$ states in $\bar{p}p$ annihilation .....	84
4.3	Glueball rich processes .....	84

5	Heavy-quark spectroscopy .....	87
5.1	The $J/\psi$ states below the $D\bar{D}$ threshold .....	88
5.1.1	The $h_c(1P)$ .....	88
5.1.2	The $\eta_c(2S)$ .....	89
5.1.3	The 12% rule and the $\rho\pi$ puzzle .....	90
5.1.4	Two-pion transitions .....	91
5.2	The $J/\psi$ states above the $D\bar{D}$ threshold .....	92
5.2.1	$X(3872)$ .....	93
5.2.2	The $X, Y, Z$ resonances at $3940 \text{ MeV}/c^2$ .....	98
5.2.3	A new $\bar{c}c$ vector state $Y(4260)$ .....	99
5.2.4	Conclusions .....	101
5.2.5	A charged charmonium state ? .....	102
5.3	Heavy-light quark systems .....	102
5.3.1	$D$ and $D_s$ mesons and their low-mass excitations .....	102
5.3.2	Further mesons with open charm .....	106
5.3.3	Mesons with open beauty .....	108
6	Radial and orbital excitations of light mesons .....	110
6.1	Patterns at high $l, n$ .....	110
6.2	Systematic of $q\bar{q}$ mesons in $(n, M^2)$ and $(J, M^2)$ planes .....	112
6.3	Threshold dynamics .....	114
6.4	Hybrids candidates .....	114
6.4.1	$J^{PC} = 1^{--}$ .....	115
6.4.2	$J^{PC} = 1^{++}$ .....	116
6.4.3	$J^{PC} = 2^{++}$ and search for the tensor glueball .....	116
6.4.4	$J^{PC} = 2^{-+}$ .....	118
7	Mesons with exotic quantum numbers .....	120
7.1	Model predictions for exotic mesons .....	120
7.1.1	Hybrid mesons .....	120
7.1.2	Multiquark states .....	121

7.1.3	Molecular states . . . . .	122
7.2	Experimental results for $J^{PC} = 1^{-+}$ . . . . .	122
7.2.1	The wave $J^{PC} = 1^{-+}$ in the $\eta\pi$ channel. . . . .	122
7.2.2	The wave $J^{PC} = 1^{-+}$ in the $\eta'\pi$ channel. . . . .	126
7.2.3	Partial wave analyses of the diffractively produced $\pi^+\pi^-\pi^-$ system . . . . .	128
7.2.4	The wave $J^{PC} = 1^{-+}$ in the $\omega\pi\pi$ channel. . . . .	131
7.2.5	The wave $J^{PC} = 1^{-+}$ in the $f_1\pi$ channel. . . . .	132
7.2.6	Conclusion on $J^{PC} = 1^{-+}$ exotics . . . . .	132
7.3	Further $J^{PC}$ exotic waves . . . . .	134
7.3.1	$J^{PC} = 0^{+-}, 2^{+-}$ . . . . .	134
7.3.2	Isospin exotics . . . . .	134
8	Pseudoscalar mesons . . . . .	138
8.1	The $\pi$ radial excitations . . . . .	138
8.1.1	The $\pi(1300)$ . . . . .	138
8.1.2	The $\pi(1800)$ . . . . .	139
8.2	The $K$ radial excitations . . . . .	142
8.2.1	The $K(1460)$ . . . . .	142
8.2.2	The $K(1830)$ . . . . .	142
8.3	Isoscalar resonances . . . . .	142
8.3.1	The $\eta(1295)$ . . . . .	142
8.3.2	The $\eta(1440)$ . . . . .	143
8.3.3	The split $\eta(1440)$ . . . . .	144
8.3.4	Isoscalar resonances revisited. . . . .	146
8.4	Higher-mass $\eta$ excitations . . . . .	149
8.4.1	Selection rules . . . . .	149
8.4.2	$\eta$ excitations from radiative $J/\psi$ decays . . . . .	150
8.4.3	Baryon-antibaryon threshold enhancements . . . . .	152
8.5	The nonet of pseudoscalar radial excitations . . . . .	154
8.5.1	Other interpretations . . . . .	156

9	Scalar mesons: $\sigma, \kappa, \delta, S^*$	157
9.1	$\pi\pi$ scattering	159
9.2	$K\pi$ scattering	163
9.3	Isovector $\pi\eta$ interactions	164
9.3.1	The reaction $\pi^- p \rightarrow \eta\pi^0 n$	164
9.3.2	The $a_0(980)$ and $f_0(980)$ from $p\bar{p}$ annihilation	164
9.4	Scalar mesons in radiative $\phi$ decays	166
9.5	Scalar mesons in 2-photon fusion	168
9.6	Production of $f_0(980)$ as a function of $t$	170
9.7	Scalar mesons in fragmentation	171
9.8	Scalar mesons from chiral symmetry	172
9.9	A low-mass nonet of scalar mesons	173
10	Scalar mesons above 1 GeV	176
10.1	Charge exchange	176
10.2	Scalar resonances from central production	178
10.3	Scalar resonances from $p\bar{p}$ annihilation	184
10.4	The $f_0(1370)$ and $f_0(1500)$ resonances	187
10.4.1	The $f_0(1370)/f_0(1500)$ partial decay widths	187
10.4.2	Is $f_0(1370)$ a resonance?	187
10.5	Scalar mesons in $D, D_s$ and $B$ decays	189
10.6	Scalar mesons in hadronic $J/\psi$ decays	193
10.7	Scalar mesons in radiative $J/\psi$ decays	196
10.8	Scalar mesons in radiative $\Upsilon$ decays	199
10.9	Scalar mesons in $\chi_{cJ}$ decays	200
10.10	Scalar mesons in two-photon fusion	200
11	Scalar mesons and their interpretation	201
11.1	Global views of scalar mesons and the scalar glueball	201
11.2	Glueball- $q\bar{q}$ mixing scenarios	202
11.3	The Anisovich-Sarantsev picture	204

11.4	The red dragon of Minkowski and Ochs .....	208
11.5	Scalar mesons with instanton-induced interactions .....	208
11.6	Our own interpretation.....	210
11.6.1	Light scalar nonets .....	210
11.6.2	Dynamical generation of resonances and flavour exotics .....	213
11.6.3	Scalar states from the $\sigma$ to $\chi_{b0}(1P)$ .....	215
12	Outlook ... and a look back .....	217
	References.....	220

# 1 Introduction

## 1.1 Highlights and perspectives

### 1.1.1 Scope of the review

One of the most challenging topics in contemporary particle physics is the dynamics of non-Abelian gauge theories. Quantum Chromo Dynamics (QCD) is the most explored example of a class of theories in which the bosonic field quanta carry the charge of the fermionic agents. QCD predicts very new effects like confinement, quark and gluon condensates, glueballs and hybrids, perhaps instantons. Some of them have been observed, others not. We start to understand how the enigmatic  $\sigma(485)$  meson is created but we do not know if gluons add new degrees of freedom to spectroscopy. We know that the structure of the QCD vacuum plays a decisive rôle, but we are unable to link the vacuum structure to the confinement property of QCD.

Spectroscopy is a unique way to access QCD, and substantial progress has been made in recent years. This review covers topical features in meson spectroscopy, from light quark mesons to heavy quarkonia, from glueballs and hybrids to multiquark states. We are convinced that a global view of the whole field provides better insight than even a detailed discussion of separate issues would provide. At present, such a global view cannot be derived from first principles. A general frame needs to be defined within which detailed observations can be discussed. For this reason, we begin this report with a summary of highlights. This will allow us to discuss in the subsequent sections important results and their rôle for the full picture. Meson spectroscopy is an active field of research which implies that the frontier is open and that the interpretation of new results is often controversial. This review tries to give a fair account of the different views and still to emphasize our own position. We do not claim evidence for new physics when observations find consistent explanations with a minimal set of assumptions: ‘plurality ought never be posed without necessity’ (Occam’s razor). As authors we take the privilege to present, here in the summary, our own view in a series of clear statements with little reasoning or justifications. We are convinced that we have identified questions and that we give answers that should guide further theoretical and experimental work. Readers interested in other interpretations and in the scientific *if’s* and *why’s* would have to read the full text. Our conclusions and suggestions for future directions will be presented in this section as well.

### 1.1.2 Recent outstanding achievements

There have been outstanding achievements in recent years:

- (1) The long-sought  $h_c(1P)$  state has been found precisely at the mass given by the centre-of-gravity of the  $\chi_{cJ}(1P)$  states. The  $\eta_c$  first radial excitation  $\eta_c(2S)$  is now established. With these two discoveries, all charmonium states expected by quark models to fall below the  $D\bar{D}$  threshold are found, and no additional state. This is an important confirmation of the quark model; the precise mass values provide stringent constraints to model builders on the structure of the confining interactions.
- (2) Several unexpectedly narrow states,  $X(3872)$ ,  $X(3940)$ ,  $Y(3940)$ ,  $Z(3930)$ ,  $Y(4230)$ , were discovered over the last years. Their interpretation as  $c\bar{c}$  states, as molecules, or as hybrids is hotly debated. In the channel  $e^+e^- \rightarrow J/\psi$  plus recoil mesons, peaks due to  $\eta_c(1S)$ ,  $\eta_c(2S)$ , and  $X(3940)$  are observed (and a convolution of  $\chi_{cJ}(1P)$  states). We suggest to

identify  $X(3940)$  with  $\eta_c(3S)$ . The  $Z(3930)$  resonance is observed in  $\gamma\gamma \rightarrow D\bar{D}$  with a helicity distribution consistent with a  $\chi_{c2}(2P)$  interpretation. The  $Y(3940)$ , observed in its  $J/\psi\omega$  decay mode, is tentatively interpreted by us as the  $\chi_{c0}(2P)$   $q\bar{q}$  state with a strong tetraquark component, in analogy with the  $\phi\omega$  decay mode of  $f_0(1760)$ . The  $\chi_{c1}(2P)$  quark model state is identified with  $X(3872)$ . The state is attracted by the  $DD^*$  threshold to which it couples strongly. We present reasons why we interpret  $Y(4260)$  as  $\psi(4S)$  quark-model state and identify  $\psi(4415)$  with  $\psi(5S)$ .

- (3) New mesons with open charm, those which are found and those which are not found, and their decays provide new insight into the rôle of tetraquark configurations. The properties of these mesons are often dominated by their strong affinity to  $q\bar{q}\bar{q}\bar{q}$ . In spite of this, also these mesons are compatible with a  $q\bar{q}$  assignment: there are no ‘flavour-exotics’. The  $q\bar{q}$  component is essential to form a resonant state.
- (4) In the light-quark sector, a very large number of high-mass states was suggested and awaits future confirmation. They follow a simple mass pattern compatible with a string picture of mesonic excitations. Contributions from exotic partial waves, with quantum numbers beyond the quark model, have been identified. Their resonant nature is controversially discussed. Particular interest has been focussed on scalar mesons, their properties and abundance. A generally accepted consistent picture has not yet emerged.
- (5)  $J/\psi$  decays – studied at the Beijing storage ring BES – have yielded unexpected results, in particular on scalar mesons. Their production and decay pattern when recoiling against an  $\omega$  or  $\phi$  meson is a key witness of their anomalous structure.
- (6) Last not least, the  $\sigma$  at  $\sim 500 \text{ MeV}/c^2$ , called  $\sigma(485)$  in this report, and  $\kappa$  mesons at  $\sim 700 \text{ MeV}/c^2$  called  $\kappa(700)$  seem to be firmly established, not only because of new data but also due to substantial advances in the theoretical description of low-energy  $\pi\pi$  (and  $K\pi$ ) interactions. Both particles are now understood as consequence of chiral symmetry and unitarity, constraints which can both be met only when these two particles are introduced.

### 1.1.3 New insights

*Glueballs, hybrids, tetraquarks* and their rôle in *meson spectroscopy* are the central themes of this review.

- (1) A unified picture of *meson spectroscopy* emerges from new (and old) experimental findings connecting the family of  $\Upsilon$  states with light-quark spectroscopy, a view emphasized often by Nathan Isgur. The first orbital excitation energy, the mass difference between the first tensor and the first vector meson (with quantum numbers  $J^{PC} = 2^{++}$  and  $1^{--}$ , respectively), is about  $500 \text{ MeV}/c^2$ , independent of the quark flavour. The hyperfine splitting between the two  $S$ -wave ground states (with quantum numbers  $J^{PC} = 1^{--}$  and  $0^{-+}$ , respectively) scales with  $1/M$  as expected for a magnetic hyperfine interaction originating from one-gluon exchange. Only the – predicted –  $\Upsilon$ - $\eta_b$  mass difference breaks this simple rule. The pion plays a very special rôle in meson spectroscopy due to its dual nature as  $q\bar{q}$  meson and as Goldstone boson of QCD with massless quarks. It is extremely surprising that the  $1/M$  dependence is obeyed by all states from the  $J/\psi$ - $\eta_c$  mass difference down to the  $\rho$ - $\pi$  splitting. These two characteristic mass gaps can be identified even in the baryon excitation spectrum (see Fig. 6 in section 1.2.6).
- (2) We do not discuss individual high orbital and radial excitations. Rather, we point out regularities in their mass spectrum. For sufficiently high excitations in orbital angular momentum  $l$  and for small radial quantum numbers  $n$ , the squared masses of light mesons are proportional

to  $l + n$  (see Fig. 54 in section 6). The  $l + n$  dependence of meson masses can be derived in a string model but not in constituent quark models which are close to a  $l + 2n$  behaviour. Note that  $n = 0$  is allowed. The ground states have  $N = 1$ , we define  $n = N - 1$ .

- (3) The  $l + n$  dependence of meson masses leads naturally to a mass-degeneracy of even- and odd-parity resonances for all but ‘stretched’ states (with  $j = l + s$ ). Chiral symmetry restoration, suggested to be responsible for the mass-degeneracy, does not give an explanation why stretched states have no parity partners. In the string model, this aspect follows automatically.
- (4) *Hybrids* may have exotic or non-exotic spin-parity quantum numbers. In the sector of non-exotic states, there are two outstanding observations which do not fit into any quark-model assignment and which have the properties predicted for hybrids. These are the resonances  $\pi_2(1880)$  and  $\eta_2(1870)$ . Comparatively narrow hybrids are predicted in this partial wave. On the other hand, the  $1^{++}$  sector would be an ideal case to find hybrids as well; but no candidate has been seen. One important difference between these two partial waves is that the  $2^{-+}$  wave has important  $S$ -wave couplings to  $2^{++} + 0^{-+}$  mesons while there are no strong  $S$ -wave decays of the  $1^{++}$  wave. Further careful studies of dynamical effects induced by thresholds are therefore certainly needed before the claims for  $\pi_2(1880)$  and  $\eta_2(1870)$  can be accepted as resonant states of exotic nature.
- (5) Exotic mesons have quantum numbers which are not accessible to  $q\bar{q}$  configurations. Spin-parity exotic states can have contributions from  $q\bar{q}g$ ,  $qq\bar{q}q$ , and meson-meson configurations; flavour exotics are restricted to  $qq\bar{q}q$  and meson-meson dynamics. Since there is no established evidence for flavour exotics, the most likely interpretation of spin-parity exotic states would be that they are hybrids.

Exotic partial waves are an established phenomenon. However, there is still a controversy if exotic waves show a resonant behaviour. The ‘best case’, the  $\pi_1(1400)$ , has decay modes which rule out a hybrid interpretation. As  $\pi\eta$  system in a  $qq\bar{q}q$  decuplet-antidecuplet configuration, it should be accompanied by flavour exotic partners like  $K^+\pi^+$ . The latter configuration does not show any phase motion. The interpretation of the  $\pi\eta$  exotic wave in terms of non-resonant meson-meson interactions seems thus more likely than hybrid interpretations even though practical fits based on such assumptions yield a worse  $\chi^2$ . The  $\pi_1(1600)$  is a much more viable hybrid candidate. But as long as the experimental evidence for  $\pi_1(1400)$  and  $\pi_1(1600)$  is of similar quality, doubts remain why to reject  $\pi_1(1400)$  on general grounds and why to accept  $\pi_1(1600)$ .

- (6) There is a long controversy concerning the rôle of  $gg$ ,  $q\bar{q}$ ,  $q\bar{q}g$ ,  $qq\bar{q}q$ , and meson-meson configurations in meson spectroscopy. ( $gg$  and  $q\bar{q}g$  are short-hand notations for glueballs and hybrids.) A meson wave function of a ‘normal’ meson like  $f_2(1270)$  may contain contributions from all these configurations, at an – unknown – momentum-dependent fraction. The main emphasis is therefore laid on states beyond the quark model expectations.

So far, there are no forcing arguments for the existence of any *multiquark states* which could not be accommodated as a  $q\bar{q}$  object. For example, there are good arguments to interpret the narrow  $D_{s0}^{*+}(2317)$  state as  $DK$  bound state. Since  $D$  and  $K$  both have isospin  $1/2$ , an isospin singlet and a triplet of states (with charges  $0, 1, 2$ ) should be expected. Yet, only the singlet was found. The latter state is compatible with a  $c\bar{s}$  assignment. Thus we conjecture that there must be a  $c\bar{s}$  ‘seed’. Generalising this concept, the  $q\bar{q}$  seed is essential for all states which are seemingly of tetraquark or molecular nature. The  $q\bar{q}$  seed may dress into a tetraquark configuration if this is energetically favoured (e.g. due to diquark-diquark correlations). These correlations act by merging the quark-antiquark pairs into two colour-neutral mesons. Thus, a molecular component develops. The fractional contributions of these three configurations depend on the vicinity of thresholds for hadronic decays, and can be functions

of the spatial separations or of the momentum transfer with which the system is probed. At large momentum transfer, in fragmentation, the  $q\bar{q}$  nature is explored and seemingly molecular states are produced with the same rate as ordinary mesons. Soft processes (like the decay chain  $\phi \rightarrow \gamma f_0(980); f_0(980) \rightarrow K\bar{K}$  with minimal momentum transfers) reveal the molecular character of a state.

- (7) The  $q\bar{q}$ , tetraquark, and molecular components lead to a rich phenomenology, in particular for scalar mesons. Some mesons like  $a_0(980)$ ,  $\sigma(485)$ ,  $f_0(980)$ , and  $\kappa(700)$  reveal clearly a molecular character: their pole positions are very close to their respective thresholds and the poles can be generated from hadronic loops of the decay products. These arguments exclude tightly bound tetraquark configurations. The need for hadronic loops does not imply that the forces between the constituents are of molecular type. Two pseudoscalar mesons in the  $0^+$  channel, e.g. in the 1 GeV region, may interact attractively because at short distances their constitutive quarks can form diquarks with energetically favoured correlations.

The mass difference of the ground-state scalar meson to the threshold defined by the mass of the two related pseudoscalar mesons (i.e.  $M_{\chi_{b0}(1P)} - M_{B\bar{B}}$ ,  $\dots$ ,  $M_{f_0(980)} - M_{K\bar{K}}$ ,  $M_{\sigma(485)} - M_{\pi\pi}$ ) is a smooth function of the mass of the decay products (see Fig. 117a in section 11.6.3). The  $\chi_{b0}(1P)$  has a mass 700 MeV/c<sup>2</sup> below the threshold for  $B\bar{B}$  decays. It connects via  $\chi_{c0}(1P)$ , via  $D_{s0}^*(2317)$ , via a postulated  $D_0^*(1980)$ , via  $f_0(980)$  and  $\kappa(700)$  to the  $\sigma(485)$ . The  $\sigma(485)$  mass is 200 MeV/c<sup>2</sup> above the  $\pi\pi$  threshold. Current views mostly assume the  $\sigma(485)$  to be a  $\pi\pi$  effect, unrelated to  $q\bar{q}$  spectroscopy. The continuous transition from  $\chi_{b0}(1P)$  to the  $\sigma(485)$  does of course not imply similar wave functions for these two mesons. Instead, their nature is very different as evidenced by the  $1/N_c$  behaviour of their unitarized chiral amplitude (see Fig. 92 in section 9.8). The by far predominant part of the  $\chi_{b0}(1P)$  wave function is of  $b\bar{b}$  nature. When the quark mass is slowly reduced from the  $b$ -quark mass to light-quark masses, the  $\chi_{b0}(1P)$  state changes continuously into the  $\sigma(485)$ , a predominantly  $\pi\pi$  molecular object. But it has a  $q\bar{q}$  seed. If a low-mass light-quark  $q\bar{q}$  pair is created with vacuum quantum numbers, the  $\sigma(485)$  is created with unit probability. It has a complicated wave function but it is still the  ${}^3P_0$  scalar ground state; there is no additional light-quark scalar meson with  $q\bar{q}$  structure. It is the  $\sigma(485)$  which occupies the slot reserved for the  ${}^3P_0$  ground state. QCD provides very different mesonic wave functions when a quark and an antiquark is created out of the vacuum: the wave function for a clean  $q\bar{q}$  meson in case of  $b$  quarks, a highly correlated and complex system having the appearance of a  $\pi\pi$  interaction phenomenon when light quarks are involved.

- (8) Likewise,  $\chi_{b0}(2P)$ ,  $\chi_{c0}(2P)$ , the disputed Selex state  $D_s^{*+}(2630)$ ,  $D_0^*(2350)$ ,  $f_0(1500)$ ,  $K_0^*(1430)$ , and  $f_0(1300)$  may form a group of first radial excitations. The postulated  $D_0^*(1980)$  is below the  $D\pi$  threshold and can decay either via its high-mass tail (if the coupling is strong enough) or by weak interactions only. Its existence would resolve the apparent puzzle with the  $D_{s0}^*(2317)$  mass which should not be below the  $D_0^*(2350)$  mass if these two mesons just differ by the exchange of an  $s$  quark into a  $d$  or  $u$  quark. The  $f_0(1300)$  is the wide scalar background which was called  $\epsilon(1300)$  for a long time.
- (9) In our view, the scalar flavour-singlet mesons are very wide and merge into one continuous scalar background. Their widths arise from their strong coupling to the QCD vacuum by emission of two Goldstone bosons, i.e. of two pions. The  $\sigma(485)$  is part of this background. The wide poles at  $\sim 500$ ,  $\sim 1300$ , and  $\sim 1540$  MeV/c<sup>2</sup> reported in the literature are very far from the real axis. These states are supposed to be flavour-singlet mesons having  $\frac{1}{\sqrt{3}}|\bar{u}u + \bar{d}d + \bar{s}s\rangle$  and  $\frac{1}{\sqrt{3}}|\bar{u}u\bar{d}\bar{d} + \bar{d}\bar{d}\bar{s}\bar{s} + \bar{u}\bar{u}\bar{s}\bar{s}\rangle$  components. One exception is the  $\sigma(485)$  meson. Due to its low mass, flavour SU(3) is broken and the  $\bar{s}s$  part of its wave function is small. The wide background interferes with the flavour-octet scalar mesons,  $f_0(980)$ ,  $f_0(1500)$ ,  $f_0(1760)$ , and

$f_0(2100)$ , which have normal hadronic widths. At present, the flavour content of these mesons cannot be deduced experimentally like, e.g., the flavour decomposition of  $\eta$  and  $\eta'$  or of  $\omega$  and  $\phi$ . Dynamical arguments and indirect evidence need to be invoked. Any data shedding light on the flavour wave functions of scalar mesons is therefore extremely welcome.

- (10) We propose that the three observed meson states called  $f_0(1710)$ ,  $f_0(1790)$ , and  $f_0(1810)$  originate from one single meson,  $f_0(1760)$ , which has a (mainly) flavour-octet wave function with a large tetraquark component. The peculiar  $f_0(1760)$  production and decay pattern observed in  $J/\psi$  decays into  $\omega f_0(1760)$ ,  $\phi f_0(1760)$ , and  $\gamma f_0(1760)$  is interpreted as dressing of the initially formed  $q\bar{q}$  system into  $qq\bar{q}\bar{q}$  and its interference with a broad flavour-singlet background amplitude. The glueball candidate  $f_0(1500)$  is interpreted as being mainly a flavour octet meson. All scalar mesons have sizable  $q\bar{q}$  and  $qq\bar{q}\bar{q}$  components. Their  $q\bar{q}$  nature is revealed in their production. Their decays and mass pattern require substantial  $qq\bar{q}\bar{q}$  components. There is no 'narrow'  $f_0(1370)$ .
- (11) In our view, the  $f_0(980)$  resonance is a flavour-octet meson, at least in its  $q\bar{q}$  component. The vicinity of the  $K\bar{K}$  threshold breaks SU(3) symmetry and transforms  $f_0(980)$  into state with a  $\frac{1}{\sqrt{2}}(u\bar{u} + d\bar{d})s\bar{s}$  flavour structure of largely molecular decomposition.
- (12) There is no evidence for a narrow scalar *glueball* below  $1.8 \text{ GeV}/c^2$  in mass, or for a scalar decuplet consisting of a  $q\bar{q}$  nonet and a glueball with mixing of two isoscalar  ${}^3P_0$  states. The wide flavour singlet background may contain a glueball fraction. The glueball content can be searched for in the same way as a glueball fraction was sought for in the wave function of the  $\eta'$ . The existence of glueballs is an unproven hypothesis.
- (13) Glueballs could exist as broad objects with  $1 \text{ GeV}$  widths, or even broader. For scalar, pseudoscalar and tensor quantum numbers, broad and likely flavour-blind intensities have been identified. It is, of course, very difficult to establish a phase motion of such broad states. Even if the existence of such a wide state is accepted, this does not imply a particular interpretation: in  $J/\psi$  decays a very wide object with quantum numbers of the  $\rho$  has been reported which could be a molecular background, generated by  $t$ -channel exchange forces, a hybrid, but certainly not a glueball.
- (14) The  $\eta(1295)$  is unlikely to be the radial excitation of the  $\eta$  meson; more likely it is faked by feedthrough from the mass-degenerate  $f_1(1285)$  and the Deck effect in  $\eta$ - $\sigma$   $S$ -wave interactions. The  $\eta(1440)$  is not split into  $\eta(1405)$  and  $\eta(1475)$ ; rather, the node in the  $\eta(1440)$  wave function - expected for a radial excitation - leads to an apparent splitting of  $\eta(1440)$ . The  $\eta(1440)$ , the newly suggested  $X(1835)$  (if it proves to have pseudoscalar quantum numbers), the  $\pi(1375)$  and  $K(1450)$  form a consistent nonet of pseudoscalar radial excitations. A second nonet of pseudoscalar radial excitations is proposed but all four states require experimental confirmation. The excitation energies for the first and second radial excitation of pseudoscalar mesons decrease monotonously with increasing meson mass, when going from  $\pi$  to  $K$ ,  $\eta$ ,  $\eta'$ , and to  $\eta_c$  (see Fig. 78 in section 8.5).

#### 1.1.4 Critique of QCD folklore

In our view, efforts in this field have too often been driven by the quest for discoveries instead of the search for a deeper understanding. In this report, we review critically some QCD folklore. We conclude the following:

- (1) Central production in a  $450 \text{ GeV}/c$  proton beam is not dominated by Pomeron-Pomeron interactions; Regge exchange is still important. The so-called 'glueball filter' finds a straightforward interpretation; it does not project out extraordinary states.

- (2) In radiative  $J/\psi$  decays, the dominance of initial-state radiation is often assumed but experimentally not proven.
- (3) Proton-antiproton annihilation has no large affinity to glue-rich states. The process prefers (partial) rearrangement of quarks.

There is no experimental evidence that one of these three processes is a source of glueballs.

### 1.1.5 Successes and limitations of lattice QCD

Lattice QCD is growing into a predictive theory of strong interactions. Its many achievements include: accurate calculations of meson and baryon ground state masses, reliable calculations of weak matrix elements and of hadron decays, enlightening studies of chiral symmetry breaking, instanton induced interactions, and the confinement problem. The numerical successes of Lattice QCD are most striking when they can be connected to extrapolations using chiral perturbation theory. There are, however, questions for which no chiral expansion exists; the usefulness of Lattice QCD for this kind of applications needs to be tested with scrutiny. We emphasize that glueballs are predicted in Yang-Mills theories, hybrids in quenched QCD. It is an open issue if these concepts find their correspondence in Nature.

Many of the experimental findings and their interpretation suggested here are at variance with firm predictions of Lattice QCD, other important phenomena were not predicted. A large number of Lattice QCD results were preceded by results obtained within ‘QCD inspired models’. In this general overview, we restrict ourselves however to a discussion of Lattice QCD and list a few conclusions which are based on our personal interpretation of the spectrum of scalar mesons:

- (1) A full spectrum of glueballs is predicted but not even its ground state exists as identifiable object.
- (2) Hybrids are predicted to exist. Present data give only little evidence for hybrid degrees of freedom in meson spectroscopy but do not exclude their existence.
- (3) Lattice calculations did not find that scalar mesons are organised along their flavour structure, into singlet and octet states.
- (4) Lattice calculations did not predict the large rôle of tetraquark configurations for scalar mesons.
- (5) Lattice calculations missed the continuous transition from  $\chi_{b0}(1P)$  to the  $\sigma(485)$  when quark masses are changed from the  $b$  mass to  $u$  and  $d$  quark masses.
- (6) Lattice calculations seem to fail to reproduce mass gaps due to excitations with vacuum quantum numbers. This is an observation outside of meson spectroscopy, but Lattice QCD prefers a mass of the Roper  $N(1440)P_{11}$  above and not below  $N(1535)S_{11}$ . In this case, a chiral extrapolation to realistic quark masses exists but has not cured the problem.

Some of the most important questions in meson spectroscopy got answers from Lattice QCD (with the presently required approximations) which turned out to be misleading. Other important questions are out of reach of present-day Lattice QCD. It is certainly premature to question if QCD as fundamental theory is valid also in the low energy domain. Intense computing and new ideas are needed to study flavour-singlet mesons in tetraquark configuration in Lattice QCD and to unquench glueballs ready to decay into  $135\text{ MeV}/c^2$  pions. It is an irony of science that answers from Lattice QCD which we believe to be in conflict with experimental findings led to an enormous stimulation of the field and to a much improved understanding of strong interactions.

### 1.1.6 Future options

We conclude this section by defining open issues, by listing some specific propositions and by giving some general recommendations. The aim of experiments is not just to define basic resonance parameters like masses, widths and decay branching fractions but rather to learn more about the structure of mesons. Hence it is important to use a variety of different methods. Production of mesons in hard reactions depends on the mesonic wave function at the origin of the centre-of-mass system. Diffractive production of light-quark resonances off nuclei is sensitive to the spatial extent of the wave function, colour transparency of charmonium states gives access to its  $q^2$  evolution. The amplitude of radiative decays is proportional to the inverse of the quark mass  $m_q^{-1}$ . But, how does a constituent quark mass change if one considers high orbital excitations?

- (1) Physics is an open science with competing ideas, also in data analysis. After publication, data should be made public. In baryon physics, data are accessible via internet. In meson spectroscopy, data are private property of collaborations also beyond publication. This can be changed; look at web page  
<http://hadrondb.hiskp.uni-bonn.de>  
 where you find Dalitz plots and full data samples for multibody final states, both real data and Monte Carlo data. An open-access policy should be enforced not only for journals but also for data.
- (2) Quantum numbers and decay properties of the recently discovered states with open and hidden charm need to be studied. The  $B$  factories and the CLEO experiment have opened a window to a new spectroscopy but the existence of many of the states is based on poor statistics. A substantial increase of statistics (and running time) is required. Since BaBar – and SLAC as particle laboratory – will be closed, the hope for advances in the immediate future rests on BELLE. In the time of continuous evaluations, the citation index is an important aspect of science. Half of the BELLE papers with more than 100 citations report discoveries in spectroscopy. Surprisingly, also CDF and  $D\bar{O}$  are shown to be capable to make significant contributions to this field, and additional results can be hoped for from LHCb.
- (3) An intense antiproton source is part of the FAIR project at GSI, Darmstadt. The spectroscopy of open and hidden charm states is a central issue of PANDA, a universal detector proposed to be installed at the antiproton facility. Mass and widths of states below the  $c\bar{c}$  threshold and their decay rates will be measured with high precision. Above the  $c\bar{c}$  threshold, there are candidates for all  $N = 1$  and  $N = 2$  states which can be interpreted in the quark model as  $S$ - and  $P$ -states; the  $D$  states (except the  ${}^3D_1$  states which can be observed in  $e^+e^-$  annihilation) are unknown. The completion of the quark model and the search for states beyond the quark model are central themes at FAIR. In this report we argue that there is no forcing evidence for states beyond the quark model. The high-mass charmonium region is likely the best place to search for mesons with exotic quantum numbers, exotic in spin-parity like  $J^{PC} = 1^{-+}$ , or exotic in their flavour structure like charged companions of the  $X, Y, Z$  states at 3940 MeV (with flavour content  $cud\bar{c}, \dots$ ).
- (4) Scalar mesons still remain a most fascinating research object. In this report, a new view is developed which is in conflict with generally accepted interpretations. Interpretational differences manifest themselves in the flavour wave functions of scalar isoscalar mesons. The best approach to substantiate or to reject the view are likely coupled channel analyses of  $J/\psi$  decays into vector plus scalar mesons. Urgently needed are high-statistics and high-quality data on processes like  $J/\psi \rightarrow \gamma, \omega, \phi$  recoiling against  $\pi^0\pi^0, \eta\eta, \eta\eta'$  and  $\eta'\eta'$ . Radiative decays like  $f_0 \rightarrow \gamma\omega$  and  $f_0 \rightarrow \gamma\phi$  will constrain the flavour structure. The possibility of a sizeable glueball fraction in the  $\eta'$  was studied in the so-called Rosner plot (see Fig. 3 in section

1.2.3). A similar plot is required for  $f_0(980)$ ,  $f_0(1500)$ ,  $f_0(1760)$ , and for the region between the narrow resonances. Such experiments will become feasible at BESIII.

A coupled-channel partial wave analysis on  $J/\psi$  data on  $\gamma, \omega, \phi$  recoiling against  $\pi\pi$ ,  $K\bar{K}$ ,  $4\pi$ , and  $\omega\omega$  should be performed on existing data. An amplitude for the broad isoscalar scalar background should be included in the fit. If possible, a mass independent phase shift analysis should be made, not an isobar fit only.

The two scalar mesons  $f_0(1500)$  and  $f_0(1760)$  are interpreted here as flavour octet states. At present, experimental data permit the interpretation of  $f_0(2100)$  as a glueball (even though we believe it to be an octet meson). The most direct way to decide this alternative is to measure the ratio of its decay modes into  $\eta'\eta'$  and  $\eta\eta'$ . BESIII should have good chances to search for both channels in radiative  $J/\psi$  decays.

- (5) The systematic of scalar mesons suggests the existence of a (nearly) stable scalar charm state, called  $D_0^*(1980)$  here, with a mass below its only hadronic decay mode  $D\pi$ . The experimental  $D\pi$  mass distribution exhibits a – statistically not significant – threshold spike and wider scalar background contribution (see Fig. 49b in section 5); the partial wave analysis of  $D\pi\pi$  data assigns a fraction of the data to two subthreshold virtual  $D^*$  intermediate states. The possibility that this is a  $D_0^*$  object was not tested. One of these observations might be a trace of the postulated state.
- (6) There is the possibility that a narrow  $D_0^*$  exists at about  $2450\text{ MeV}/c^2$ , just below the  $D_s K$  threshold, the analogue of  $a_0(980)$  with open charm. It would be an isodoublet. Both these states can be searched for at PANDA. If our scheme to organize scalar mesons is right, it will not be found.
- (7) The  $X(3872)$  is observed in its  $\gamma J/\psi$  decay. The  $X(3872) \rightarrow \gamma\psi(2S)$  decay mode should be searched for. The  $\chi_{bJ=1,2}(2P)$  states have decay branching ratios to  $\Upsilon(2S)$  which exceed those to the  $\Upsilon(1S)$  ground state by a factor 2; for the  $\chi_{b0}(2P)$  state, this enhancement factor is 5. The relative yield of  $X(3872) \rightarrow \gamma\psi(2S)$  should shed light on the  $X(3872)$  structure.
- (8) The  $D^*$ ,  $D_s^*$  and  $B$  decays display the flavour structure of isoscalar scalar mesons; the statistics is, however, at the lower limit for far-reaching conclusions. A Super  $b$  factory planned at Frascati will provide  $10^{10}$   $B$  and  $B_s$  mesons; in recent years, the discovery potential of  $B$  decays for meson spectroscopy was demonstrated in an impressive way. An immediate remedy would be to combine the data from BaBar and BELLE, and for  $D^*$ ,  $D_s^*$  decays those of Focus, E687 and E791 in addition. Such a combined effort would also help to see if the threshold spike in the  $D\pi$  mass distribution in  $B \rightarrow D\pi\pi$  decays is fake or real, and if its quantum numbers are  $0^{++}$  or  $1^{--}$ .
- (9) In our view, data analysis was often guided by prejudices. Of course, it is boring (and unnecessary) to test charge conjugation invariance in every new reaction. However, it is a legitimate question to ask to what extend isovector mesons are suppressed in radiative  $J/\psi$  decays. For this kind of process, the Particle Data Group lists one entry only,  $J/\psi \rightarrow \gamma\pi^0$ , which is small but in a very unfavourable kinematical region. Radiative yields for  $f_2(1270)$  are known, for  $a_2(1320)$  they are not. Likewise, radiative yields for  $J/\psi \rightarrow \gamma f_4(2050)$  or  $\gamma f_1(1285)$  and  $\gamma f_1(1420)$  are large, but no upper limits exist for their isovector counterparts. Not only  $J/\psi \rightarrow \gamma\pi^0\pi^0$ ,  $J/\psi \rightarrow \gamma\eta\eta$ ,  $J/\psi \rightarrow \gamma\rho\rho$ , and  $J/\psi \rightarrow \gamma\omega\omega$  should be studied but  $J/\psi \rightarrow \gamma\pi^0\eta$  and  $J/\psi \rightarrow \gamma\rho\omega$  as well. It is unclear whether these modes have just not been published, if they escaped detection so far because nobody looked, or if the modes are suppressed.

In central production, isoscalar final states were studied intensively, but isovector states were not. The collaborations focussed on detection of glueballs in Pomeron-Pomeron fusion, hence final states like  $\rho\rho$  and  $\omega\omega$  were believed to be interesting,  $\rho\omega$  not. A large fraction of the data had a forward  $\Delta^{++}$  (instead of a fast proton). These data were not analysed. The

$\Delta^{++}$  requires Regge exchanges to be produced; the  $\Delta^{++}$  - proton ratio depends on fraction of Regge exchange in the data. The Compass experiment at CERN is going to clarify many of the open issues.

- (10) There are several experiments which will study exotic partial waves. New information can be expected from Pomeron-Regge (Compass) and from Pomeron-photon fusion. First evidence for the latter process has been reported by the STAR collaboration at BNL. The search for exotic mesons is also a central topic of the Hall D project at JLab.
- (11) The high-mass spectrum of light-quark mesons gives information on the confinement region. Pioneering new results have been presented on antiproton-proton annihilation in flight. This process appears to give the best access to the full meson spectrum. By their nature,  $p\bar{p}$  formation experiments do not allow the study of exotic waves; this is however possible in subsystems. At FAIR, glueballs are hoped to show up at high energy as narrow states above a continuum background; light meson spectroscopy is not one of the research goals. Hegels ‘craft of reason’ (List der Vernunft) will entail the quest for a detailed knowledge of the ‘background’ of  $q\bar{q}$  mesons. Thus an improved understanding of confinement physics will emerge from the FAIR research. Experimentally, an extracted low-energy antiproton beam with momenta between 400 MeV/c and 2.5 to 3 GeV/c is required. The extended energy range (compared to LEAR) gives access to states at even higher masses. This will provide information on whether the linear Regge trajectories start to bend, stop, or continue their linear rise as a function of the squared mass. For part of the data, a polarised target should be used. A source of polarised antiprotons as foreseen by the PAX collaboration at FAIR would of course lead to very significant constraints in the partial wave analysis. The upper part of the spectrum will be covered by the planned facilities; here, the PANDA detector is an ideal instrument. For momenta antiproton below 2 GeV/c, the options are not yet clear. In case, a second facility would be required, the asymmetric BaBar detector would be an ideal detector.

Antiproton-proton annihilation formation experiments give access only to non-strange mesons; mesons with hidden strangeness are formed only to the extent to which they mix with  $n\bar{n}$ . In production experiments, planned to be performed with PANDA, the full meson spectrum including exotic partial waves can be covered. We lack knowledge of mesons carrying strangeness. With the intense antiproton beams available at FAIR, a strangeness exchange reaction  $p\bar{p} \rightarrow \Lambda\bar{\Lambda}$  will produce a source of  $\bar{\Lambda}$ . Exploiting secondary reactions should help to understand the spectrum of Kaon excitations.

- (12) Baryons – which are not discussed here – have the potential to provide additional insights into strong interactions which cannot be gained studying mesons alone.

### 1.1.7 *Hints for expert readers*

Experts in meson spectroscopy may not have time to read through this lengthy paper but might be interested to see new developments and interpretations.

Readers interested in the history of meson spectroscopy may consult subsection 1.2.1. The subsection 1.2.5 contains a brief discussion of the basics of string models not commonly known to experimental physicists. Section 5 on heavy quark spectroscopy is rather compact, and our personal view of the newly discovered narrow states is presented along with the experimental data.

For high-mass states, a remarkable mass pattern evolves which we believe to provide very significant constraints on the dynamics of quarks at large excitation energies. In subsection 6.1, we scrutinise the conjecture of restored chiral symmetry under these conditions.

The search for hybrids, for mesons with exotic quantum numbers, is reviewed in section 7.

The  $\eta(1440)$  is a long-discussed particle and deeply connected with the search for glueballs among  $q\bar{q}$  mesons. Our view is given in subsections 8.3.4 and 8.5.

An update on the existence of the  $\sigma(485)$  and  $\kappa(700)$  can be found in section 9. There is a full section on different interpretations of scalar mesons (11). Our interpretation containing new ideas on the dynamical rôle of tetraquark configurations for scalar mesons is given in section 11.1. Comments on dynamically generated resonances and on multiquark states are presented in subsection 11.6.2. A global view of scalar mesons from heavy to light quarks is given at the end of this review, in section 11.6.3.

### 1.1.8 Outline

After the introductory section, the review begins with a survey of expectations based on lattice gauge calculations and QCD-inspired models (section 2). These expectations provide a ‘coordinate system’ for experiments and their interpretations. In section 3 major experiments in this field are introduced to allow the reader to appreciate better the significance of results. The spectrum of meson resonances seen in a particular experiment depends critically on the method applied. Fusion of  $2\gamma$  e.g. couples to quark charges, while radiative  $J/\psi$  decays are a good place to search for glueballs. The main experimental methods are described in section 4. In this part, some experimental results are discussed which are of general interest for  $q\bar{q}$  spectroscopy but unrelated to the main issues of this report.

The spectroscopy of heavy quarks – reviewed in section 5 – reveals a very simple pattern and serves as textbook example providing evidence for Coulomb-like interactions and a linear confinement potential between a heavy quark and an antiquark at large separations. In spite of this apparent simplicity, surprising discoveries were made recently. Some  $D_s^*$  resonances are surprisingly narrow and have masses which fall much below the expected values. The  $X(3872)$  resonance has large decay branching ratios into both, a  $J/\psi$  recoiling against a  $\rho$  or against an  $\omega$  meson. These two decays are observed with similar strengths, hence isospin symmetry is broken violently. Higher mass states,  $X(3940)$ ,  $Y(3940)$ ,  $Z(3930)$ , and  $X(4260)$ , are observed which could need an interpretation beyond the standard  $q\bar{q}$  scenario.

The discussion of light-quark spectroscopy and of searches for glueballs and hybrids begins in section 6 with a global survey of the meson spectrum. A statistical approach to the numerous results exhibits striking regularities pointing at a simple structure of the confining interactions. The regularities are very helpful in assigning spectroscopic quantum numbers to the observed states and to identify mesons which fall outside of the usual nonet classification of meson resonances. These additional mesons may be glueballs, hybrids or multiquark states.

In hybrids, the gluonic fields transmitting the forces between quark and antiquark are themselves excited. The gluon field may acquire an effective ‘constituent’ mass and thus hybrids are no longer two-particle bound states; they may have quantum numbers outside of the  $q\bar{q}$  scheme. Mesons with exotic quantum numbers have been reported but the evidence for their existence as resonant states is not beyond doubt; their interpretation as hybrids (instead of  $qq\bar{q}\bar{q}$  tetraquark states) is not yet based on solid experimental facts. Evidence for exotic mesons is reviewed in section 7.

Light-quark spectroscopy receives its continued fascination from the QCD-based prediction that

the self-interaction between gluons as mediators of strong interactions should lead to new forms of hadronic matter. Glueballs were predicted as mesonic bound states having no valence quarks. The  $\eta(1440)$  was for a long time a prime glueball candidate; its rôle is discussed in section 8 in the context of other pseudoscalar mesons.

Most exciting is the possibility that the three mesons  $f_0(1370)$ ,  $f_0(1500)$ , and  $f_0(1710)$  might reflect the intrusion of a scalar glueball into the world of quarkonia. However, the existence of  $f_0(1370)$  is not beyond doubt, and there is no unanimous agreement if and how gluonic degrees of freedom manifest themselves in spectroscopy. The interpretation of the scalar meson spectrum is a most controversial topic which is discussed in sections 9 - 11.

A short outlook is given in section 12. A summary of the report and our conclusions were already presented above.

### 1.1.9 *A guide to the literature*

There is an enormous number of papers related to meson spectroscopy covering a wide range of topics and results. It is of course impossible to discuss them all in depth or even just to mention them. The selection of results presented in this review may reflect personal biases and even important contributions may have escaped our attention. Apologies go to all authors whose results are missing or not properly represented here.

A prime source of information is of course contained in the Review of Particle Properties which contains most published results on meson spectroscopy. The last one which is used for this review appeared in 2006 [1]. The main review is published in even years; in odd years, additions can be found in the web edition. The Review was first issued by Gell-Mann and Rosenfeld in 1957 [2]. This was the birth of series which is indispensable for any particle physicists. This year (2007), the 50<sup>th</sup> anniversary is celebrated.

The development of meson spectroscopy can be followed closely by reading the Proceedings of specialised Conferences and Workshops. The series of International Conferences on Meson Spectroscopy was begun in 1969 and continued for 14 years [3–9]; after 1985 it was held regularly as biennial conference on Hadron Spectroscopy [10–20]. The last conference of this series took place in Rio de Janeiro in 2005; Hadron07 will be hosted by Frascati. In some years, additional workshops were organised which were often devoted to specific topics or were born out of regional needs: an incomplete list comprises [21–26]. Confinement and other theoretical aspects were felt to require a deeper discussion in an own conference series on Quark Confinement and the Hadron Spectrum [27–33].

More pedagogical introductions can be found in the Proceedings of dedicated Schools. We quote here a few lectures which may still be useful, from the CERN summer school [34], the PSI summer school at Zuoz [35], The Advanced School on Quantum Chromodynamics at Benasque in Spain [36], the Schools at Erice, Sicily [37], the Scottish Universities Summer School [38], and the Hampton University Graduate School at Jefferson Lab [39, 40].

Meson spectroscopy is part of the much wider field of strong interaction physics. Related are workshops and conference series' devoted to chiral dynamics [41], lattice QCD [42], hadron structure [43] or to meson and nuclear physics [44]. Often, interesting results in meson spectroscopy are discussed. We give here references only to the most recent workshop.

Finally, we refer to some recent reviews on meson spectroscopy. Godfrey and Napolitano [45] provide a good introduction to the field; recent reviews concentrate on gluonic degrees of freedom [46–50]. Due to the non-Abelian structure of QCD, the dynamics of quarks and gluons cannot be calculated analytically from QCD but effective theories provide quantitative predictions in restricted areas. At low energies, strong interactions can be expanded in terms of (low) pion momenta and the pion mass; reviews on Chiral Perturbation Theories can be found in [51–55]. If one of the quarks is very heavy, it remains stationary in the hadron rest frame and the spin remains frozen. This gives rise to Heavy Quark Effective Theories [56, 57]. QCD inspired models still play a decisive rôle for understanding the phenomenology. Three papers by Barnes and colleagues present detailed information on meson masses and decays [58–60]. The remarkable progress in QCD simulations on a lattice is reviewed extensively in [61, 62]. An detailed documentation of the physics of heavy quarkonia can be found in [63].

## 1.2 Phenomenology of $q\bar{q}$ mesons

### 1.2.1 The $A, B, C, \dots$ of meson spectroscopy: the naming scheme

Particles have names which go back into the early history of particle physics. Today, a rational scheme is used where letter and subscripts have a precise meaning. When the first mesons were discovered, no scheme existed, and names were often invented to memorise the discoverer, his wife or his children.

The naming of mesons started with a lepton. The mesotron had a mass between proton and electron mass and proved quickly not be the predicted mediator of nuclear forces. The name changed to  $\mu$ -meson and to muon to avoid any confusion with hadronic mesons. The quantum of nuclear interaction proved to be the  $\pi$ -meson, discovered [64] by Cecil Frank Powell who received the Nobel prize in 1950 for this discovery. It became convention to use Greek symbols for new particles. The  $\eta$  followed, discovered by Ahud Pevsner [65], the  $\omega$  [66], the  $\phi$  discovered by P.L. Connolly [67] (the name  $\phi$  was suggested by Sakurai). The  $\sigma$  (with mass  $\sim 500 \text{ MeV}/c^2$ ) was introduced to describe nuclear interactions by meson exchange current and later understood as scalar  $2\pi$  correlation effect. It is separated in mass from the  $\epsilon$  (with mass  $\sim 1300 \text{ MeV}/c^2$ ) by a deep valley, for some time called S\*. The strange analogue of the  $\sigma$  is the  $\kappa$ . The  $\theta$  and  $\tau$  particles proved to be same particle which was then named Kaon  $K$ . Then the habit changed to denote new meson resonances by roman letters.

**A:** The  $a_2(1320)$  meson e.g. was formerly called **A** meson. Later it was observed to be split into a pseudovectorial state  $A_1$  and a tensor  $A_2$ . The couple Gerson and Sulamith Goldhaber discovered jointly the resonance complex at the Bevatron in Berkeley [68], and decided to call it **A** because of their son **Amos**. Sulamith died a year after the discovery, in 1965, at an age of 42 after having made remarkable contributions to particle physics.

**B:** None of us authors knows if A. Bondar played a leading rôle in the discovery of the  $b_1(1235)$ , formerly called **B** meson [69]. It used to have the nickname **Buddha** particle, a buddhist member of the collaboration suggested this name. In  $\bar{p}p$  annihilation into  $\omega\pi\pi$ , it resides like a **Buddha** on the  $\omega\pi$  background.

**C:** The **C** meson, now called  $K_1(1270)$ , was discovered by Lucien Montanet and others [70]. Its

name reminds of its discovery at CERN.

**D:** The ***D*** meson, or  $f_1(1285)$ , was discovered independently at BNL [71] and at CERN [72]<sup>1</sup>. The first author Donald H. Miller had a son Douglas Allen. The letter *D* is now used to denote mesons with open charm.

**E:** The history of the ***E*** or  $\eta(1440)$  meson is particularly interesting. It was first reported in 1965 at the Sienna conference on High Energy Physics. It was found in  $p\bar{p}$  annihilation at rest and was the first meson discovered in Europe. People at CERN were obviously very cautious not to present a wrong result, only two years later the ***E*** meson was reported in a journal publication [73]. A detailed study was presented which included several final states and a full partial wave analysis yielding pseudoscalar quantum numbers. The name ***E*** meson may stand for Europe but remembers also Lucien Montanet's daughter Elisabeth. In the same year, a second meson was discovered which is now called  $f_1(1420)$ . It has nearly the same mass as the ***E*** meson and was called ***E***, too, since the quantum numbers in [73] were believed to be possibly wrong (see, however, [74]). Now we know that the state produced in  $p\bar{p}$  annihilation has pseudoscalar quantum numbers. But this confusion led the MarkIII collaboration to call a state at  $1440 \text{ MeV}/c^2$ , discovered in radiative  $J/\psi$  decay [75], *iota*(1440) or  $\iota(1440)$  to underline the claim [76] that the first glueball was discovered ( $\iota = 1$  in Greek). Indeed, the meson proved to have pseudoscalar quantum numbers [77]. The history of this meson is not yet closed and the discussion will be resumed in this report.

**F:** The  $f_2(1270)$  was introduced by Walter Selove as ***f*** meson to memorise his wife **Fay Ajzenberg** [78]. Fay herself is a well-known nuclear physicist awarded with 3 doctorates honoris causa. She wrote the book ‘A Matter of Choices: Memoirs of a Female Physicist (Lives of Women in Science)’. For some time,  $D_s$  mesons were called F mesons.

**G,H:** The former ***G***-meson was discovered by **Goldberg** and others [79] (now  $\rho_3(1690)$ ), the ***H*** (claimed at  $975 \text{ MeV}/c^2$ ) [80] has become the  $h_1(1170)$ . The letter *G* was later used to claim the discovery of a glueball. The  $g_s(1470)$  [81] may have been an early sighting of the glueball candidate  $f_0(1500)$ . Certainly the  $G(1590)$  [82] is closely related to it. A tensor glueball was suggested to be mixed into 3 tensor resonances  $g_T(2010)$ ,  $g'_T(2300)$  and  $g''_T(2340)$  [83].

**J:** The  **$J/\psi$**  must not be missed. This narrow resonance revolutionised physics, it was discovered independently in 1974 at Brookhaven National Laboratory (BNL) in Long Island, New York, in the process proton + Be  $\rightarrow e^+e^-$  + anything [84]. The group leader was Samuel Chao Chung Ting, the Chinese symbol for Ting reads ***J***. At Stanford University, the new resonance was observed in the SPEAR storage ring in  $e^+e^-$  annihilation to  $\mu^+\mu^-$ ,  $e^+e^-$  and into hadrons [85]. It was seen in a series  $\psi$ ,  $\psi'$ ,  $\psi''$ . Its name is derived from the  $\psi$ -shaped pattern in  $\psi'$  decays into  $\pi^+\pi^-$  pair and the  $J/\psi$  (decaying into  $e^+e^-$ ), see Fig. 1. The name  $J/\psi$  honours both discoveries.

**K,L, ... Z:** The Kaon ***K*** was already mentioned; the  $K_2(1770)$  was discovered as ***L*(1770)** [86]. The ***M*(1405)** was a precursor of the  $\pi_1(1400)$  [87]. The ***N*** and ***P*** are reserved for neutron/nucleon and proton, the ***O*** is void. There were two ***Q*** mesons (now  $K_1(1270)$  and  $K_1(1400)$ ), **R**, **S**, **T** were used to name enhancements in the missing mass in the reaction  $\pi^-p \rightarrow pX$  [88]. With the

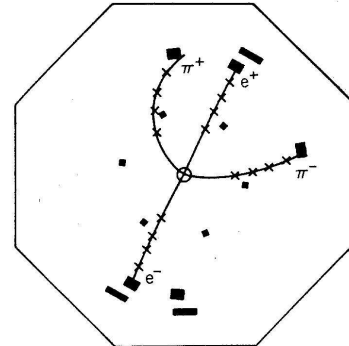


Fig. 1. Decay of a  $\psi'$  into  $\pi^+\pi^-J/\psi$  with  $J/\psi$  decaying into a high-energy  $e^+e^-$  pair in the MARKIII experiment.

<sup>1</sup> [71] was submitted in May 1965 and published in June, two weeks after [72] was submitted.

$W$  as charged weak interaction boson, with  $X$  as the unknown, with  $\Upsilon$  as bottomonium family and with  $Z$  as neutral weak interaction boson, the alphabet was exhausted.

With the increasing number of inhabitants in the particle zoo, rules had to be invented like Carl v. Linné (Linnaeus, 1707 - 1778) did in biology. The system was introduced by the Particle Data Group in 1986. New particle symbols were chosen which are simple, convey the quantum numbers, and are close, whenever possible, to the traditional names listed above. Table 1 translates meson names into quantum numbers. Mesons are characterised by their quantum numbers, their total angular momentum  $J$ , their parity  $P$  and their charge conjugation parity  $C$ :

$$P = (-1)^{L+1} \quad C = (-1)^{L+S} \quad (1.1)$$

where  $L$  denotes the intrinsic orbital angular momentum in the  $q\bar{q}$  meson and  $S$  the total spin of the  $q\bar{q}$  pair. The notation  $J^{PC}$  is used not only for the neutral mesons for which  $C$  parity is a good quantum number but also for the other components of a SU(3) nonet. For instance, since  $C\pi^0 = \pi^0$ , we define  $C\pi^\pm = \pi^\mp$ , and  $CK^0 = \bar{K}^0$ , and with  $C\rho^0 = -\rho^0$ , we adopt  $C\rho^\pm = -\rho^\mp$  and  $CK^{*\pm} = -\bar{K}^{*\mp}$ . In addition, a sign for each flavour needs to be defined. The convention is used that the sign of a flavour is the sign of its charge,  $c$  quarks have positive charm,  $s$  quarks have negative strangeness.

The *up* and the *down* quark form an isospin doublet. We define antiquarks by  $\bar{u} = Cu$  and  $\bar{d} = Cd$ . We obtain:

$$\begin{aligned} |I=1, I_3=1\rangle &= -|\bar{d}u\rangle, \\ |I=1, I_3=0\rangle &= \frac{1}{\sqrt{2}}(|\bar{u}u\rangle - |\bar{d}d\rangle), \\ |I=1, I_3=-1\rangle &= |\bar{u}d\rangle, \\ |I=0, I_3=0\rangle &= \frac{1}{\sqrt{2}}(|\bar{u}u\rangle + |\bar{d}d\rangle) = |\bar{n}n\rangle, \\ |I=0, I_3=0\rangle &= |\bar{s}s\rangle. \end{aligned} \quad (1.2)$$

The  $|\bar{n}n\rangle$  and  $|\bar{s}s\rangle$  states have the same quantum numbers and mix to form two physical states. With  $n$  we denote the two lightest quarks,  $u$  and  $d$ , the symbol  $q$  stands for any quark, including heavy quarks.

The  $G$ -parity is approximately conserved in strong interactions. It is defined as charge conjugation followed by a rotation in isospin space about the  $y$ -axis,

$$G = Ce^{i\pi I_y} = (-1)^I C = (-1)^{L+S+I}. \quad (1.3)$$

For a system of  $n_\pi$  pions,  $G = (-1)^{n_\pi}$ . The  $G$ -parity plays a similar rôle as  $C$ -parity in QED where the relation  $C = (-1)^n$  holds for  $e^+e^- \rightarrow n\gamma$ .

The  $\omega_3$  is a isoscalar meson with a flavour wave function  $\frac{1}{\sqrt{2}}(d\bar{d} + u\bar{u}) = \bar{n}n$  even though it may have a small  $s\bar{s}$  component, its total angular momentum is  $J = 3$ , its intrinsic orbital angular momentum is even (with  $L = 2$  dominant), and it is member of the spin triplet  $\omega_1, \omega_2, \omega_3$ . Only the  $\omega_3(1670)$  is experimentally known. The mass is added to identify a meson. The index for  $J$  and the mass are omitted when no confusion can occur like for the  $\pi, \eta$ , or  $\phi$ . The name  $J/\psi$  is kept.

Table 1  
Symbols of mesons with no open strangeness, charm or beauty

$q\bar{q}$ content	$^{2S+1}L_J =$	$^1(L \text{ even})_J$	$^1(L \text{ odd})_J$	$^3(L \text{ even})_J$	$^3(L \text{ odd})_J$
	$J^{PC}$	$0^{-+}, 2^{-+} \dots$	$1^{+-}, 3^{+-} \dots$	$1^{--}, 2^{--}, 3^{--} \dots$	$0^{++}, 1^{++}, 2^{++} \dots$
$u\bar{d}, d\bar{d} - u\bar{u}, d\bar{u}$		$\pi$	$b$	$\rho$	$a$
$d\bar{d} + u\bar{u}, s\bar{s}$		$\eta, \eta'$	$h, h'$	$\omega, \phi$	$f, f'$
$c\bar{c}$		$\eta_c$	$h_c$	$\psi$	$\chi_c$
$b\bar{b}$		$\eta_b$	$h_b$	$\Upsilon$	$\chi_b$

Mesons with open strangeness, charm or beauty are no charge-conjugation eigenstates and the four columns of Table 1 collapse into two. The normal series ( $^1(L \text{ odd})_J, ^3(L \text{ odd})_J$ ) with  $J^P = 0^+, 1^-, \dots$  is tagged by a star, the 'anomalous' series ( $^1(L \text{ even})_J, ^3(L \text{ even})_J$ ) with  $J^P = 0^-, 1^+, \dots$  is untagged. Mesons belonging to the normal series are, e.g.,  $K_3^*$  and  $D_{s0}^{*+}(2317)$ . The latter describes a  $c\bar{s}$  state with  $J = 0$  and positive parity. Anomalous mesons have no star, like the  $D_{s1}^+(2460)$  with  $J = 1$  and  $P = +1$ . Bottom mesons  $B^\pm$  have a mass of more than  $5 \text{ GeV}/c^2$ ; their decays cover the full charmonium spectrum and may even contribute to glueball spectroscopy. The wave functions of the  $K_1(1270)$  and  $K_1(1400)$  have  $L$  even and can have intrinsic quark spin 1 or 0 (and would then belong to the  $a_1(1260)$  or the  $b_1(1235)$  nonet, respectively). In practice, they are mixtures of the two quark model configurations.

Quantum numbers like  $J^{PC} = 0^{+-}, 1^{-+}, 2^{+-} \dots$  are not accessible in fermion-antifermion systems. In analogy to the  $\pi$  (with  $J^{PC} = 0^{-+}$ ) and  $\pi_2(1670)$  (with  $J^{PC} = 2^{-+}$ ), these states are called  $\pi_1$ . Its isoscalar companion would be  $\eta_1$ . If a  $J^{PC} = 1^{-+}$  exotic resonance in the charmonium spectrum would be discovered, its name would be  $\eta_{c1}$ . Exotic states  $b_0, h_0, b_2, h_2$  with  $0^{+-}$  and  $2^{+-}$ , respectively, may exist as well. So far, only evidence for states with exotic quantum numbers  $(I^G)J^{PC} = (1^-)1^{-+}$  has been reported.

### 1.2.2 Meson nonets

SU(3) symmetry considerations have shown to be extremely useful in classifying mesons and baryons [89] as composed of quarks and antiquark or of 3 quarks, respectively. Light mesons with  $u, d$  and  $s$  quarks have a flavour wave function which is conveniently decomposed into a flavour basis. For pseudoscalar mesons, this is given by  $\pi^+ = -d\bar{u}$ ,  $\pi^- = \bar{u}d$ ,  $K^0 = \bar{s}d$ ,  $K^+ = \bar{s}u$ ,  $\bar{K}^0 = \bar{d}s$ ,  $K^- = \bar{u}s$ . The quark model representation of the neutral pseudoscalar mesons is  $\pi^0 = \frac{1}{\sqrt{2}}(\bar{u}u - \bar{d}d)$ ,

$$\eta_8 = \sqrt{\frac{1}{6}}(\bar{u}u + \bar{d}d - 2\bar{s}s) , \quad \text{and} \quad \eta_1 = \sqrt{\frac{1}{3}}(\bar{u}u + \bar{d}d + \bar{s}s) . \quad (1.4)$$

We thus have families of nine mesons with the same radial and angular-momentum structure of the wave function. For pseudoscalar mesons, a nonet is shown in Fig. 2.

Other nonets are formed by the ground state vector mesons with  $J^{PC} = 1^{--}$ ,  $\{\rho, \phi, \omega, K^*\}$ , by tensor mesons with  $J^{PC} = 2^{++}$ ,  $\{a_2(1320), f'_2(1525), f_2(1270), K_2^*(1430)\}$ , and many others.

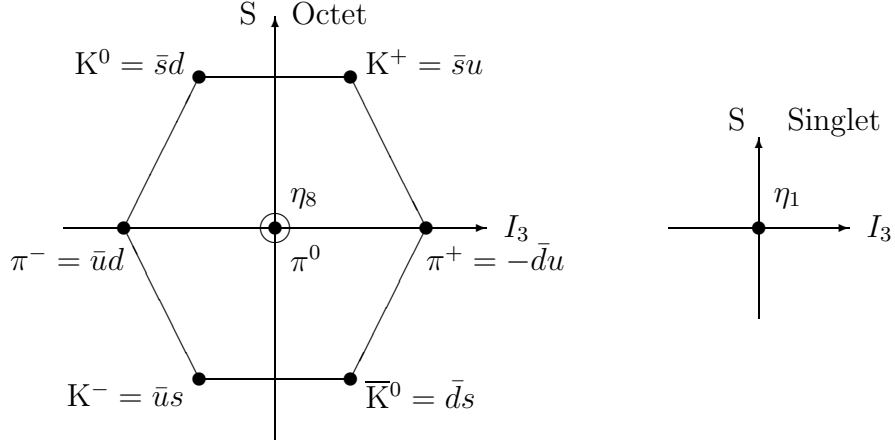


Fig. 2. The nonet of pseudoscalar mesons.

### 1.2.3 Mixing

Mesons having identical external quantum numbers can mix even if they have different internal flavour structures or different angular momentum configurations. The isoscalar pseudoscalar mesons are not realised as SU(3) eigenstates; the physical mass eigenstates, using the abbreviation  $\bar{n}n = \frac{1}{\sqrt{2}}(\bar{u}u + \bar{d}d)$ , can be written as

$$\begin{aligned} |\eta\rangle &= \cos\Theta_P |\bar{n}n\rangle - \sin\Theta_P |\bar{s}s\rangle = \cos\theta_P |\eta_8\rangle - \sin\theta_P |\eta_1\rangle \\ |\eta'\rangle &= \sin\Theta_P |\bar{n}n\rangle + \cos\Theta_P |\bar{s}s\rangle = \sin\theta_P |\eta_8\rangle + \cos\theta_P |\eta_1\rangle. \end{aligned} \quad (1.5)$$

Nothing forbids the wave functions to have a  $c\bar{c}$  component. The huge mass difference between  $\eta$  and  $\eta_c$  makes, however, the mixing angle very small. The pseudoscalar mixing angle is defined using eigenstates of SU(3) symmetry as basis vectors. The two mixing angles are related by  $\Theta_P = \theta_P - \Theta_{id} + \pi/2$ . The angle  $\Theta_{id} = \arctan(1/\sqrt{2})$  is defined below.

This mixing scheme is highly simplified: it is assumed that the spatial wave functions of all ground-state pseudoscalar mesons are identical. Clearly, it is not to be expected that these assumptions hold to a good precision, that the wave function of the pion is the same as that of the  $\bar{n}n$  component of the  $\eta$  and the  $\eta'$ . Further, the  $\eta$  and  $\eta'$  could also mix with other states, in particular with a pseudoscalar glueball. This has led to speculations that the  $\eta'$  (and to a lesser extend also the  $\eta$ ) may contain a large fraction of glue. There is an abundant literature on this subject, and we refer the reader to [90].

In a simplified form, one can extend the mixing scheme 1.5 to include an inert (gluonic) component which does not couple to charges. The  $\eta$  and  $\eta'$  wave functions are then written as

$$\begin{aligned} |\eta\rangle &= X_\eta |\eta_q\rangle + Y_\eta |\eta_s\rangle + Z_\eta |G\rangle, \\ |\eta'\rangle &= X_{\eta'} |\eta_q\rangle + Y_{\eta'} |\eta_s\rangle + Z_{\eta'} |G\rangle, \end{aligned} \quad (1.6)$$

with  $X_{\eta(\eta')}^2 + Y_{\eta(\eta')}^2 + Z_{\eta(\eta')}^2 = 1$  and thus  $X_{\eta(\eta')}^2 + Y_{\eta(\eta')}^2 \leq 1$ . A gluonic admixture implies that  $Z_{\eta(\eta')}^2 = 1 - X_{\eta(\eta')}^2 - Y_{\eta(\eta')}^2$  must take on a positive value. The mixing scheme assumes isospin

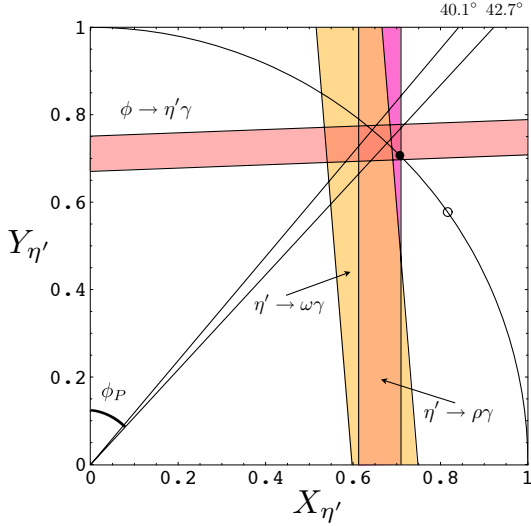


Fig. 3. Constraints on the flavour wave function of  $\eta'$  mesons from radiative decays. A point in the plane defines the non-strange ( $X_{\eta'}$ ) and strange ( $Y_{\eta'}$ ) component in the  $\eta'$ . The relation  $X_{\eta(\eta')}^2 + Y_{\eta(\eta')}^2 \leq 1$  must hold. The two small circles define a pure singlet wave function (open circle) or a mixing angle of  $-11.1^\circ$  in the basis of eqs. (1.4). The vertical and inclined bands show the constraints for  $X_{\eta'}$  and  $Y_{\eta'}$  from  $\eta' \rightarrow (\rho, \omega)\gamma$  and  $\phi \rightarrow \eta'\gamma$  transitions. Symmetry, *i.e.* excludes mixing with  $\pi^0$ , and neglects other possible admixtures from  $c\bar{c}$  states and/or radial excitations. In absence of gluonium,  $Z_{\eta(\eta')} \equiv 0$ , the mixing parametrisation (1.6) is reduced to the scheme (1.5).

The first analysis of this type was carried out by Rosner [91] and diagram 3 is often called Rosner plot. New data on the ratio  $R_\phi = BR(\phi \rightarrow \eta'\gamma)/BR(\phi \rightarrow \eta\gamma)$  led the KLOE collaboration to estimate the gluonium fractional content of  $\eta'$  meson as  $Z^2 = 0.14 \pm 0.04$ .

A re-evaluation of this data and data on radiative decays of vector to pseudoscalar and to pseudoscalar to vector mesons by Escrivano and Nadal was presented in [92]. The radiative widths for  $\eta' \rightarrow \rho\gamma$  and  $\eta' \rightarrow \omega\gamma$  decays are proportional to the  $n\bar{n}$  content of the  $\eta'$  wave function, and a measurement of the rate constrains  $X'_{\eta'}$ . The  $\omega$  meson has a small  $s\bar{s}$  component and the area allowed by experiment is tilted (see Fig. 3). The  $\phi \rightarrow \eta\gamma$  and  $\phi \rightarrow \eta'\gamma$  yields determine the  $s\bar{s}$  components.

The latter analysis is consistent with a negligible gluonic content in  $\eta'$  (and in  $\eta$ ) mesons,  $Z_{\eta'}^2 = 0.04 \pm 0.10$ ;  $Z_\eta^2 = 0.00 \pm 0.07$ . For a vanishing gluonic component, the  $\eta$  and  $\eta'$  mixing angle is found to be  $\Theta_P = (41.5 \pm 1.2)^\circ$  in the quark-basis scheme and  $\theta_P = -(13.2 \pm 1.2)^\circ$  in the singlet-octet scheme. A variety of reactions has been used in the past to determine the pseudoscalar mixing angles. Recently, the transition form factors  $F_{\eta\gamma}(Q^2)$  and  $F_{\eta'\gamma}(Q^2)$  have been used to derive  $\Theta_P = 38.0^\circ \pm 1.0^\circ \pm 2.0^\circ$  [93] where references to earlier work can be found.

The sign in (1.5) is a convention used only for pseudoscalar mesons; for all other meson nonets, the convention is chosen as for the vector meson nonet:

$$\begin{aligned} |\omega\rangle &= \cos \Theta_V |\omega_1\rangle + \sin \Theta_V |\omega_8\rangle \\ |\phi\rangle &= -\sin \Theta_V |\omega_1\rangle + \cos \Theta_V |\omega_8\rangle \end{aligned} \quad (1.7)$$

For  $\Theta_V = \Theta_{\text{id}} = \arctan(1/\sqrt{2})$ , the wave functions reduce to  $|\omega\rangle = |\bar{n}n\rangle$ ,  $|\phi\rangle = |\bar{s}s\rangle$ . This angle is called *ideal mixing angle*  $\Theta_{\text{id}}$ .

A second mixing example was already discussed: there are two nonets with  $J^{PC} = 1^{++}$  and  $1^{+-}$ , respectively, the  $\{a_1(1260), f_1(1285), f_1(1510), K_{1A}\}$  and  $\{b_1(1235), h_1(1170), h_1(1380), K_{1B}\}$ .  $K_{1A}, K_{1B}$  are defined as spin triplet and spin singlet states. The internal quark spin is not a measurable quantity, the two states  $|1^1P_1\rangle$  and  $|1^3P_1\rangle$  mix forming  $K_1(1280)$  and  $K_1(1400)$ .

$$|K_1(1280)\rangle = +\cos(\theta)|1^1P_1\rangle + \sin(\theta)|1^3P_1\rangle \quad (1.8)$$

and

$$|K_1(1400)\rangle = -\sin(\theta)|1^1P_1\rangle + \cos(\theta)|1^3P_1\rangle. \quad (1.9)$$

The charge conjugation operator  $\mathcal{C}$  gives opposite phases when applied to  $|1^1P_1\rangle$  and  $|1^3P_1\rangle$  basis states. We impose  $K_1(1280)$  and  $\bar{K}_1(1280)$  to have the same decomposition into  $|1^1P_1\rangle$  and  $|1^3P_1\rangle$ , then  $\theta$  must be  $\pi/4$ . This is compatible with data on  $K_1$  decays. Likewise, there is evidence for two states  $K_2(1770)$  and  $K_2(1820)$  which are driven by the quark model states  $|1^1D_2\rangle$  and  $|1^3D_2\rangle$ . Similar mixing phenomena can be expected for the  $D$  and  $B$  families.

#### 1.2.4 The Zweig rule

The Zweig or OZI rule, after Okubo, Zweig and Iizuka [94–96], has played an important rôle in the development of the quark model. The  $\phi(1020)$  is e.g. an isoscalar vector meson like the  $\omega$ . But it is much narrower, in spite of the more favourable phase-space. It decays preferential into  $K\bar{K}$  pairs, and rarely into three pions. The suppression of the  $\phi \rightarrow 3\pi$  decay was explained by its almost pure  $s\bar{s}$  flavour function and the assumption that the decay proceeds mostly with the strange quark and antiquark flowing from the initial state to one of the final-state mesons, as seen in Fig. 4, left, while disconnected diagrams (centre) are suppressed. The decay  $\phi \rightarrow \pi\pi\pi$  is attributed to the small  $n\bar{n}$  component which is mixed into the dominantly  $s\bar{s}$  wave function. The  $n\bar{n}$  component decays into pions by a perfectly allowed process (right). Vector mesons have

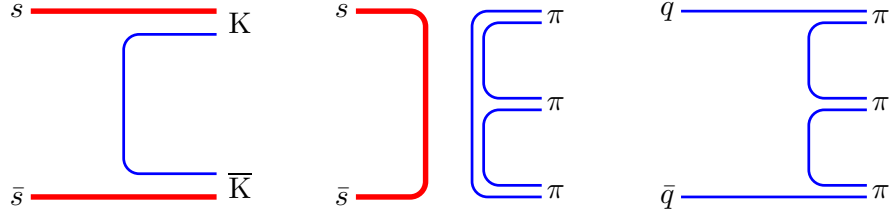


Fig. 4. Connected (left) and disconnected (centre) contribution to  $\phi(1020)$  decay. The latter contribution to  $\phi(1020) \rightarrow \pi\pi\pi$  can be described as an allowed decay from a small impurity in the wave function (right).

a mixing angle of  $\Theta_V = 39^\circ$  which deviates from the ideal mixing angle  $\Theta_{id}$  by  $\delta_V = 3.7^\circ$ . The physical  $\phi(1020)$  is then written

$$\begin{aligned} |\phi\rangle &= \cos\delta_V |s\bar{s}\rangle + \sin\delta_V |n\bar{n}\rangle, & |\omega\rangle &= -\sin\delta_V |s\bar{s}\rangle + \cos\delta_V |n\bar{n}\rangle \\ |f'_2(1525)\rangle &= \cos\delta_T |s\bar{s}\rangle + \sin\delta_T |n\bar{n}\rangle, & |f_2(1270)\rangle &= -\sin\delta_T |s\bar{s}\rangle + \cos\delta_T |n\bar{n}\rangle \end{aligned} \quad (1.10)$$

The mixing angle of tensor mesons is about  $\delta_T = -6^\circ$ .

The OZI rule was decisive when the narrow  $J/\psi$  was discovered with its high mass and narrow width of about  $90\text{ KeV}/c^2$ . Its narrow width entailed – together with the OZI rule – that a new quark flavour was discovered, and that  $J/\psi$  is a  $c\bar{c}$  state.

### 1.2.5 Regge trajectories

Light mesons have been observed with large angular momenta, up to  $J = 6$ . Fig. 5 shows the meson mass square as a function of the total angular momentum  $J$ . Spin of  $q\bar{q}$  resonances are

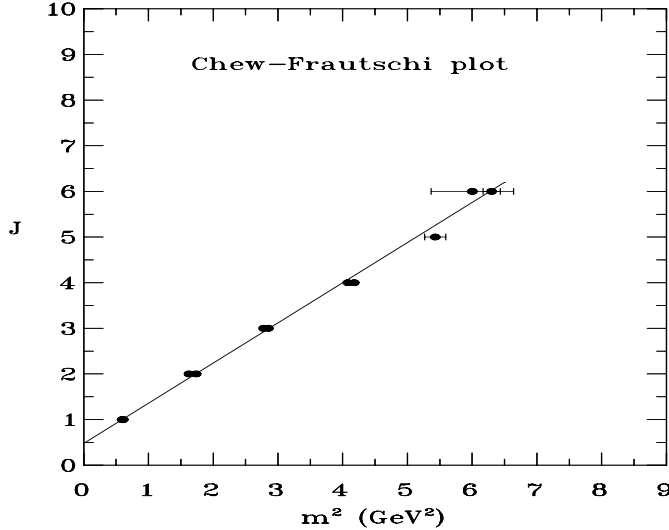


Fig. 5. Spin of meson resonances versus  $M^2$  [97]. The squared masses of  $\rho, \omega, f_2(1270), a_2(1320), \omega_3, \rho_3, a_4(2040), f_4(2050), \rho_5(2350)$ , and  $a_6(2450), f_6(2510)$  are plotted against their total angular momentum. For all mesons shown,  $j = l + s$ . In Regge theory, non-integer spins  $\alpha$  are allowed in exchange processes. Particles have integer spins.

linearly related to their squared masses over the full range of  $M^2$  and  $J$ . The width of resonances increases with their available phase space for decay; the widths are approximately given by a constant ratio  $\Gamma/M \simeq 0.1$ .

Regge theory relates the particle spectrum to the forces between the particles and the high-energy behaviour of the scattering amplitude. If scattering data on the Regge trajectory are included (for momentum transfer  $q^2 = t \leq 0$ ), Regge trajectories require a nonlinear term. An important question is related to these observations: do trajectories continue to arbitrarily high values of  $J$  or is there a trajectory termination point beyond which no resonances occur?<sup>2</sup> Abundant literature can be found on this topic. We refer to a few recent papers [100–102].

An attractive interpretation of linear Regge trajectories was proposed by Nambu [103]. He assumed that the gluon flux between the two quarks is concentrated in a rotating flux tube or a rotating string with a homogeneous mass density. The velocity at the ends may be the velocity of light. Then the total mass of the string is given by

$$Mc^2 = 2 \int_0^{r_0} \frac{\sigma dr}{\sqrt{1 - v^2/c^2}} = \pi \sigma r_0$$

and the angular momentum by

$$l = \frac{2}{\hbar c^2} \int_0^{r_0} \frac{\sigma r v dr}{\sqrt{1 - v^2/c^2}} = \frac{\pi \sigma r_0^2}{2 \hbar c} + \text{constant} = \frac{M^2}{2 \pi \sigma \hbar c} + \text{constant}$$

<sup>2</sup> Amazingly, our galaxy falls onto the same Regge trajectory as mesons and baryons as Muradian discovered [98,99].

where  $\sigma$  is the string tension. We set the constant to  $-\frac{1}{2}$  (thus replacing  $l$  by  $l + \frac{1}{2}$ ). From the slope in Fig. 5 we find  $\sigma = 0.182 \text{ (GeV)}^2/\hbar c = 0.92 \text{ GeV/fm}$ , and diameters of

$$r_0(\rho) = 0.26 \text{ fm} \quad r_0(a_6) = 0.86 \text{ fm}$$

Mass and radius  $r_0$ , and mass and width, are proportional. Hence the total width of resonances is proportional to  $r_0$ : the probability of string breaking per unit length is a constant. The  $a_6^+(2450)$  is a meson with a mass of  $2450 \text{ MeV}/c^2$  in which a  $u$  quark and a  $\bar{d}$  quark are bound by the confining forces; both quark spins are parallel, the orbital angular momentum between  $u$  and  $\bar{d}$  is  $l = 5\hbar$ . Quark and antiquark are separated by  $1.7 \text{ fm}$ .

This is a mechanical picture of a quantum system which was expanded by Baker and Steinke [104] and by Baker [105] to a field theoretical approach. The origin of the string connecting quark and antiquark is an effect, similar to the Meissner effect in superconductivity, which confines the colour electric fields to a narrow tube. For quark-antiquark separations larger than the tube size, a linear potential develops that confines the quarks in hadrons. Flux tube fluctuations to this quark-antiquark potential can be determined by path integral methods. Regge trajectories of light mesons can then be calculated by attaching massless scalar quarks to the ends of a rotating string. A path integral is then calculated around the classical rotating straight string solution. After quantisation of the quark motion at the end of the string, energy levels of a rotating string at large excitations are obtained:

$$M_n^2(l) = 2\pi\sigma \left( l + n + \frac{1}{2} \right). \quad (1.11)$$

Eq. (1.11) contains an important message: for large  $l, n$  and  $l \gg n^2$ , degeneracy of orbital and radial excitations is expected. Quark spins are not included in the picture. Spin-spin interactions vanish with the inverse meson mass forces, see right panel of Fig. 6 and consider  $M_1^2 - M_2^2 = (M_1 - M_2) \cdot (M_1 + M_2) = \text{constant}$ . Spin-orbit interactions are known to be small even though this was an unexpected observation.

This semiclassical picture can be reproduced within a ‘5-dimensional theory holographically dual to strongly coupled QCD (AdS/QCD)’. In [106], the linearity of the mass square spectrum is used as a constraint for the infrared behaviour of the theory. Two variants have been proposed how to model confinement: by a ‘hard wall’ [107] or by a ‘soft wall’ [106] which cut off effectively AdS space in the infrared region. The two variants lead to different relations between mass and orbital and radial quantum numbers. The hard wall solutions gives  $M_n(l) \sim l + 2n$ , the soft wall  $M_n^2(l) \sim l + n$ .

The duality between the anti-de-Sitter space and conformal field theories seems to us as one of the most promising directions to clarify the relation between hadron properties, including the excitation spectrum, and their structure functions [108]. A very short introduction can be found in section 2.9.

### 1.2.6 Flavour independence of forces

Meson masses vary over a wide range; e.g.  $\omega(782)$  and  $\Upsilon(9460)$  are both ground state vector mesons. The different masses are due to different quark masses, the interactions are the same: gluons do not experience any difference when coupling to a *blue* up, down or bottom quark.

Quarks having different flavour couple to gluons with their colour, irrespective of their flavour. Surprisingly, the flavour independence of quark-antiquark interactions can be seen in meson mass spectra (Fig. 6). The spectra show a similarity of mass splittings from very light to very heavy mesons implying that even the wave functions must be similar.

The left panel of Fig. 6 shows the mass gap for  $L = 1$  excitations with quark spins aligned for mesons and some baryons. An arbitrary (model) error of  $30 \text{ MeV}/c^2$  is assigned to the masses. The mass difference between the lowest-mass tensor meson and the lowest-mass vector meson are given for different flavours. The figure starts with the difference of the mean  $f_2(1270)$ ,  $a_2(1320)$  mass and the mean  $\omega$ ,  $\rho$  mass, and ends with the difference in mass of  $\chi_{b2}(1P)$  and  $\Upsilon(1S)$ . For baryons, the mass difference is given for the mean value of the orbital angular momentum  $L=1$  excitations,  $\Delta_{1/2^-}(1620)$  and  $\Delta_{3/2^-}(1700)$ , and the ground state  $\Delta_{3/2^+}(1232)$ , and for the corresponding  $\Sigma$  states  $\Sigma_{3/2^+}(1385)$ ,  $\Sigma_{1/2^-}(1750)$ , and  $\Sigma_{5/2^-}(1775)$ . For the comparison of baryon excitations, it is important to select states in which either spin or isospin wave functions are symmetrical with respect to exchange of two quarks. The first orbital angular momentum excitation of the nucleon,  $N_{1/2^-}(1520)$ , would be inappropriate to use for this comparison. It has a larger excitation energy with respect to the nucleon ground state; both, nucleon mass and  $N_{1/2^-}(1520)$  mass are reduced by spin-spin interactions (likely induced by instantons) which are absent for members of a decuplet.

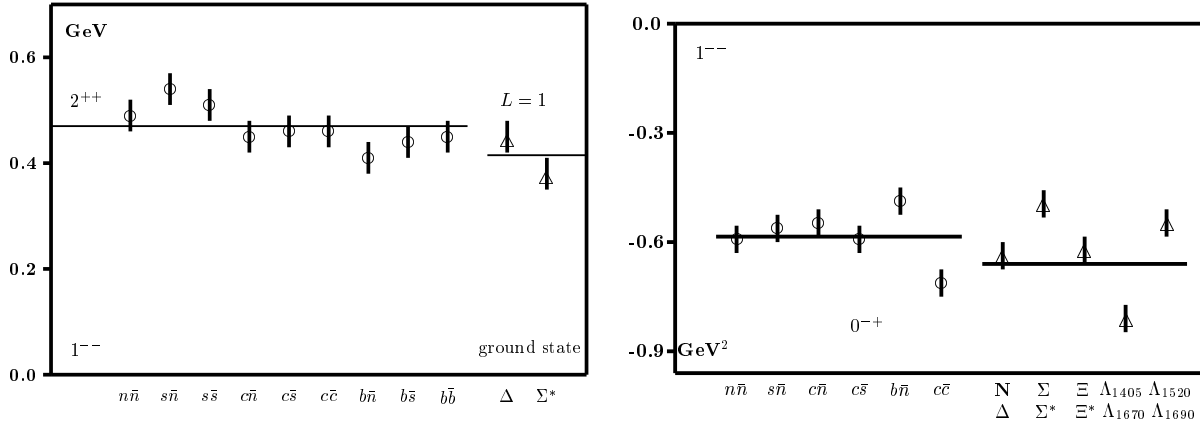


Fig. 6. Flavour independence of the strong forces: Left panel: Mass differences for  $L = 1$  excitations of mesons and baryons (for systems with aligned spin). Right panel: Mass square differences between pseudoscalar and vector mesons, for ground states ( $L = 0$ ) octet- and decuplet-baryons, and for  $L = 1$  excited singlet- and octet-baryons.

On the right panel of Fig. 6, the 'magnetic' mass splitting between states with aligned and not aligned spins is plotted. In this case, the differences in mass square are plotted. Note that  $M_1^2 - M_2^2 = (M_1 - M_2) \cdot (M_1 + M_2)$ . If this is a constant,  $M_1 - M_2$  scales with  $1/M$ . (Thus there is rather an invariance and not an independence under flavour rotations.) It is extremely surprising to see that the  $\rho$ - $\pi$  mass square splitting is very similar to that for  $J/\psi$ - $\eta_c$ . For the latter we invoke the magnetic interaction due to one-gluon exchange. For the pion, the full machinery of chiral symmetry and Goldstone bosons is needed to explain its low mass. The  $\eta_b(1S)$  has so far not been detected [109]. Using a theoretical prediction from Godfrey and Rosner [110], the  $\Upsilon(1S)$ - $\eta_b(1S)$  mass square difference is  $(1.08 \text{ GeV}/c^2)^2$ , confirming the trend to larger negative values seen already in the  $c\bar{c}$  family. We note that the ALEPH collaboration found in their 6-track event sample one event which was compatible  $\gamma\gamma \rightarrow \eta_b(1S)$ , and with the expected background rate [111]. In [1], mass and decay mode of the  $\eta_b(1S)$  candidate event are given.

The  $\Delta(1232)$  and nucleon wave functions differ by a flip in spin (and isospin). The mass splitting

is similar to the one observed when the spin is flipped in mesons (like in  $\rho$  and  $\pi$ ). In the language of instanton-induced forces: there is one  $q\bar{q}$  pair in the  $\pi$  which is affected by instantons, in the  $\rho$  there is none. And their is one  $qq$  pair in the nucleon affected by instantons and none in the  $\Delta(1232)$ . In both cases, the mass square is reduced by the same amount. Adding one or two strange quarks does not introduce large changes in the decuplet-octet mass splittings. More tricky are the  $\Lambda$  states. The mass difference here is between flavour singlet and octet states instead of octet and decuplet. In the flavour singlet states, there are 3 quark pairs which are antisymmetric in spin and flavour, in octet states there is only one. The fraction of quark pairs which are antisymmetric in spin and in flavour is however reduced in odd angular momentum excitations by a factor 2. In total, we expect and observe the same splitting as in the case of the  $\Delta(1232)$  and nucleon. The mass square splitting in Fig. 6 is proportional the fraction in the wave function which is antiysmmetric in spin and in flavour [112].

Orbital angular momentum excitations and the spin-spin interactions lead to very similar mass splittings over a very wide range of meson masses demanding a unified description. This viewpoint was often stressed by Isgur [113].

### 1.2.7 The light meson spectrum and quark model assignments

Apart from ground state mesons and those on the leading Regge trajectories, a large number of meson resonances is known. In the following three figures the experimental spectrum of light flavoured mesons is displayed. Figure 7 shows isoscalar mesons, Fig. 8 isovector mesons, and Fig. 9 the experimental Kaon spectrum. Included in the figures are all entries in the Review of Particle

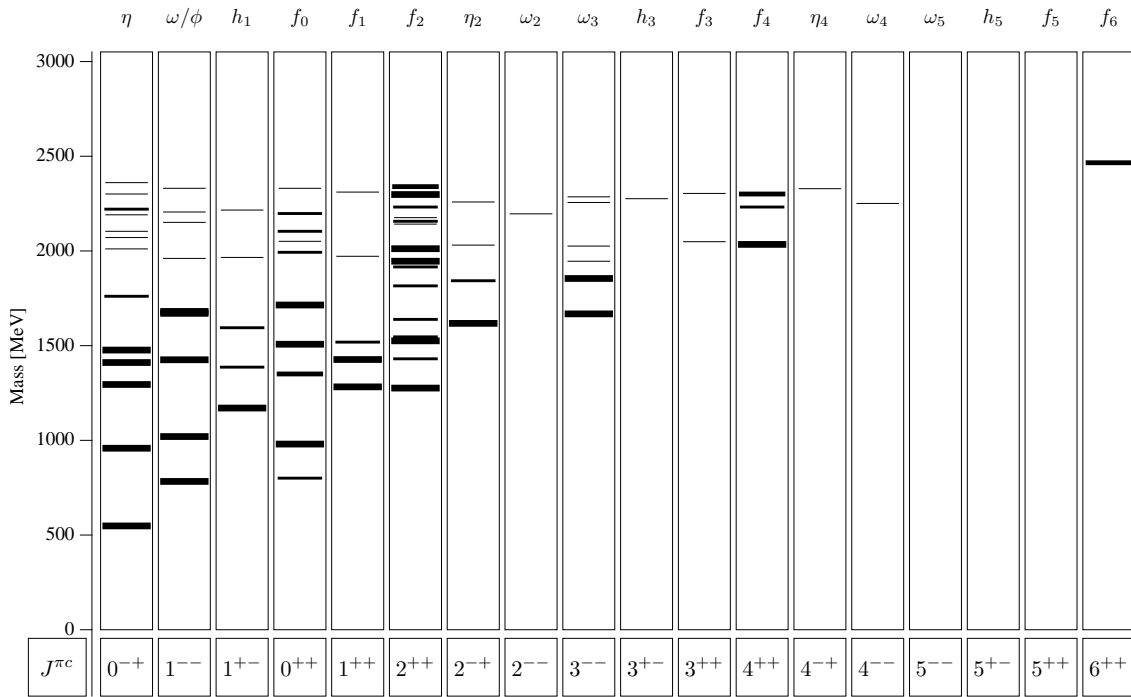


Fig. 7. Experimental light flavoured isoscalar meson spectrum. Data are from [1]. Mean values of resonance positions are indicated by thick lines, less established resonances are represented by medium thick lines, 'further states' by very thin lines.

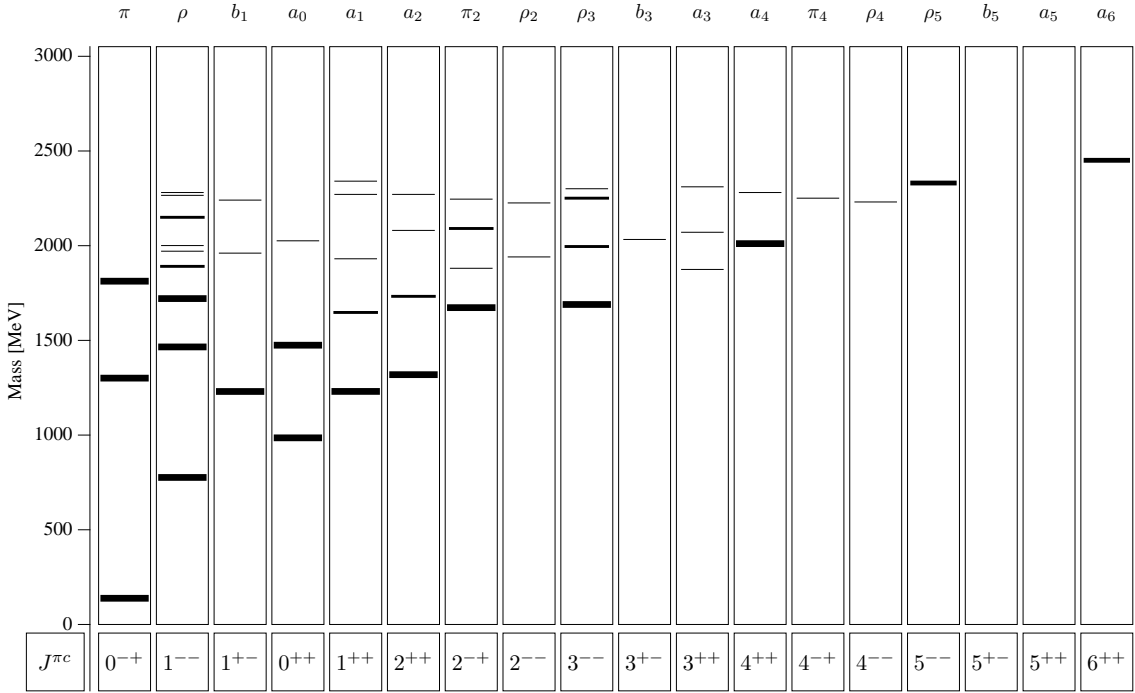


Fig. 8. Experimental light flavoured isovector meson spectrum. Data are from [1]. Mean values of resonance positions are indicated by thick lines, less established resonances are represented by medium thick lines, 'further states' by very thin lines.

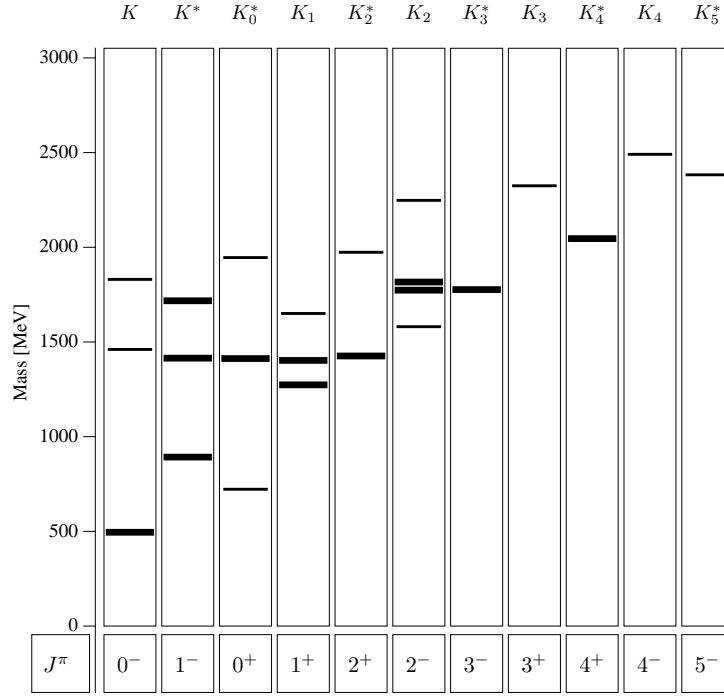


Fig. 9. Experimental strange-meson spectrum. Data are from [1]. Mean values of resonance positions are indicated by thick lines, less established resonances are represented by medium thick lines.

Properties [1], also those which are less well established and which are *omitted from the summary table*. The Particle Data Group has a third classification, *further states*, a collection of candidates which are not considered to have a good chance to survive future experiments. In spite of this warning, we include the results based on analyses of Crystal Barrel data by the QMC-Rutherford-Gatchina group [49] since these are the only data providing a systematic view of the high-mass region of meson resonances.

These mesons have known spin and parity, their flavour structure is however unknown. In some cases, like  $\omega$ ,  $\phi$ ,  $f_2(1270)$  and  $f'_2(1520)$ , the decay pattern reveals their  $n\bar{n}$  and  $s\bar{s}$  nature. The nature of other mesons is more difficult to establish. For the isospin quartet  $a_0^{\pm,0}(980)$ ,  $f_0(980)$  numerous interpretations exist. A solid knowledge of the spectrum of  $q\bar{q}$  mesons is mandatory if other forms of hadronic matter like glueballs, hybrids, tetraquark states,  $N\bar{N}$  bound states and resonances, or meson-meson molecules bound by nuclear forces are to be discriminated against the ‘background’ of  $q\bar{q}$  mesons.

Of course, these different forms of hadronic matter are not realised in nature as separate identities. Mesons should rather be considered as complex objects with a Fock space expansion to which different configurations make their contribution, even though at an unknown level. So the question arises if leading configurations can be identified by comparing simplified models with experimental data. From the patterns of the well established resonances in these figures we infer:

- With the exception of pseudoscalar and scalar mesons, for every isovector resonance there exist an isoscalar partner almost degenerate in mass within  $50 \text{ MeV}/c^2$ . Prominent pairs are:

$$\begin{array}{lll} \rho(770) - \omega(782) & a_1(1260) - f_1(1285) & a_2(1320) - f_2(1270) \\ \rho_3(1690) - \omega_3(1670) & a_4(2040) - f_4(2050) & a_6(2450) - f_6(2510) . \end{array}$$

From this one can conclude that in these sectors  $n\bar{n} \leftrightarrow s\bar{s}$  flavour mixing does not play a significant rôle.

- Again with the exception of (pseudo)scalars, spin-orbit splittings seem to be small, note *e.g.* the approximate degeneracy of

$$\begin{array}{lll} f_1(1285) - f_2(1270) & a_1(1260) - a_2(1320) & K_1(1400) - K_2^*(1430) \\ K_2(1770) - K_3^*(1780) & K_4(2500) - K_5^*(2380) . \end{array}$$

- Also, again with the exception of (pseudo)scalars, spin-spin splittings are not very large, see *e.g.* the near degeneracy of

$$\begin{array}{lll} b_1(1235) - a_1(1260) - a_2(1320) & h_1(1170) - f_1(1285) - f_2(1270) \\ \pi_2(1670) - \rho_3(1690) & \eta_2(1645) - \omega_3(1670) . \end{array}$$

- for the (pseudo)scalar mesons distinguished spin-spin splitting and flavour mixing is observed, the most prominent example being the  $\pi - \eta - \eta'$ -pattern.

These regularities help to assign spectroscopic quantum numbers to the states. Of course, these quantum numbers are an interpretation. The  $\rho(1700)$  e.g. could be the second  $\rho$  radial excitation with spectroscopic quantum numbers  $3^3S_1$  or the ground state with intrinsic orbital angular momentum  $L = 2$ ,  $1^3D_1$ . The external quantum numbers are  $J^{PC} = 1^{--}$  in both cases. In general, the physical state can be mixed. An assignment of the dominant part in an expansion of the physical state into states with spectroscopically defined quantum numbers can be made by comparison with models, for its mass and for the decay modes.

Table 2 displays the spectrum of light  $q\bar{q}$  mesons having small intrinsic orbital angular momenta

( $L = 0, 1, 2$ ). It is surprising how many states are still unobserved; this deficiency certainly increases with increasing mass. Even more intriguing are those states, indicated by question marks in Table 2, which are expected to have low masses, in the region between 1000 and 1600 MeV/c<sup>2</sup>, for which candidates exist but for which our knowledge of the meson spectrum does not suffice for an unambiguous interpretation.

Table 2

The light meson spectrum. Mesons masses marked *xxxx* are so far unobserved, those marked with *????* will be discussed in detail in this report.

$L$	$S$	$J$	$n$	$I = 1$	$I = 1/2$	$I = 0$	$I = 0$	$J^{PC}$	$n^{2s+1}L_J$
0	0	0	1	$\pi$	$K$	$\eta$	$\eta'$	$0^{-+}$	$1^1S_0$
0	1	1	1	$\rho$	$K^*$	$\phi$	$\omega$	$1^{--}$	$1^3S_1$
0	0	0	2	$\pi(1370)$	$K(1460)$	$\eta(????)$	$\eta(????)$	$0^{-+}$	$2^1S_0$
0	1	1	2	$\rho(1450)$	$K^*(1410)$	$\phi(1680)$	$\omega(1420)$	$1^{--}$	$2^3S_1$
1	0	1	1	$b_1(1235)$	$K_{1B}$	$h_1(1380)$	$h_1(1170)$	$1^{+-}$	$1^1P_1$
1	1	0	1	$a_0(????)$	$K_0^*(1430)$	$f_0(????)$	$f_0(????)$	$0^{++}$	$1^3P_0$
1	1	1	1	$a_1(1260)$	$K_{1A}$	$f_1(1510)$	$f_1(1285)$	$1^{++}$	$1^3P_1$
1	1	2	1	$a_2(1320)$	$K_2^*(1430)$	$f_2(1525)$	$f_2(1270)$	$2^{++}$	$1^3P_2$
2	0	2	1	$\pi_2(1670)$	$K_2(1770)$	$\eta_2(1870)$	$\eta_2(1645)$	$2^{-+}$	$1^1D_2$
2	1	1	1	$\rho(1700)$	$K^*(1680)$	$\phi(xxxx)$	$\omega(1650)$	$1^{--}$	$1^3D_1$
2	1	2	1	$\rho_2(xxxx)$	$K_2(1820)$	$\phi_2(xxxx)$	$\omega_2(xxxx)$	$2^{--}$	$1^3D_2$
2	1	3	1	$\rho_3(1690)$	$K_3^*(1780)$	$\phi_3(1850)$	$\omega_3(1670)$	$3^{--}$	$1^3D_3$

From deep inelastic scattering we know that mesons do not have a simple  $q\bar{q}$  structure; the coloured quarks distort the QCD vacuum, the quark and gluon condensates become polarised and the mesonic wave function contains further virtual  $q\bar{q}$  pairs and violent gluonic field configurations. From lattice QCD and from QCD-inspired models we expect states beyond the ordinary spectrum of  $q\bar{q}$  mesons, glueballs, hybrids, and multiquark states. These additional states may have unusual production and/or decay properties which may support an identification with non- $q\bar{q}$  states. Their identification as glueballs, hybrids, or multiquark states requires comparison between model calculations and experiment, and a subtle discussion of the experimental conditions under which they have been observed. States which have served as meaningful candidates for glueballs, hybrids and multiquark states are in the focus of this review.

## 2 From QCD to strong interactions

### 2.1 Quantum Chromo Dynamics

#### 2.1.1 The QCD Lagrangian

When quarks were first introduced by Gell-Mann and Zweig in 1964 [95,114], the quark model was often interpreted as a merely useful scheme for classifying hadrons, and the lack of any experimental evidence for free quarks was not considered to be a real problem. The absence of isolated quarks became an urgent issue only with the successes of the quark-parton model and of quantum chromo dynamics as a fundamental theory of strong interactions [115]. QCD provides a frame within which experimental findings in hadron physics are discussed even though the physical consequences of the theory are often not worked out. The QCD Lagrangian [116,117] has a structure similar to its analogue in QED:

$$\mathcal{L}_{QCD} = \bar{q}_i (i\partial_\mu \gamma^\mu \delta_{ij} + g \frac{\lambda_{ij}^a}{2} A_\mu^a \gamma^\mu - m \delta_{ij}) q_j - \frac{1}{4} F_{\mu\nu}^a F^{a\mu\nu} \quad (2.1)$$

with

$$F_{\mu\nu}^a = \partial_\mu A_\nu^a - \partial_\nu A_\mu^a + g f_{abc} A_\mu^b A_\nu^c. \quad (2.2)$$

where  $q_i$  are the quark fields with colour indices  $i = 1, 2, 3, \dots$ ,  $\frac{\lambda^a}{2}$  are the generators of colour  $SU(3)$ ,  $A_a^\mu$  are the gluon fields which transform according to the adjoint representation of  $SU(3)$  with  $a = 1, \dots, 8$ ,  $g$  is the bare coupling,  $m$  is the quark mass. As in QED, the Lagrangian can be derived from the equation for free Dirac particles by requiring invariance under local gauge transformations,  $U(1)$  in case of QED or  $SU(3)$  for QCD.

Eq. (2.1) shows that quarks couple to gluons like electrons to photons. The electromagnetic current  $e\gamma^\mu$  of QED is replaced by  $g\gamma^\mu \frac{\lambda}{2}$  of QCD. t'Hooft showed in the early 1970's [118] that a gauge theory with a local  $SU(3)$  colour symmetry is renormalisable; divergences can be absorbed by a redefinition of the parameters of the Lagrangian in all orders of perturbation theory.

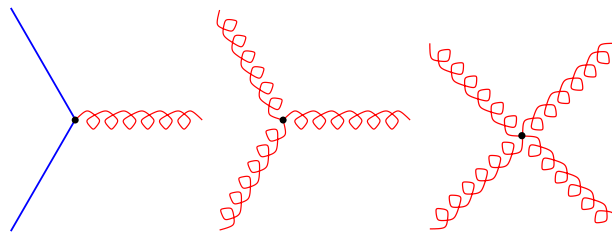


Fig. 10. Interactions in QCD at the tree level.

In comparison to QED, QCD has important additional components arising from the special structure of the (non-Abelian)  $SU(3)$  group. The electric charge is a single-valued number while quarks come in coloured triplets. Photons carry no electric charge, gluons in QCD are colour octet states. The nonlinear terms in the field strength  $F^{\mu\nu}$  give rise to trilinear and quadratic vertices in the theory so that gluons couple to themselves in addition to interacting with quarks as depicted in Fig. 10. This self-interaction leads to important consequences:

- (1) The self-interaction between gluons makes the theory nonlinear and very difficult to solve. Nevertheless in some special cases approximate solutions can be found.

At low energies, an expansion in terms of the (small) pion mass and small pion momenta provides a frame which connects different hadronic reactions. This expansion is known as Chiral Perturbation Theory ( $\chi$ PT). The dynamics of heavy quarks can be accessed in an expansion in powers of the inverse heavy quark mass known as Heavy Quark Effective Theory (HQET). In other cases, a possible solution of QCD can be obtained by numerical calculations on a lattice. With increasing computer power and the development of appropriate functions for chiral extrapolations, lattice QCD has grown to a predictive theory. However, lattice QCD often predicts numbers but does not provide intuitive understanding; the gap from QCD to intuition is bridged by so-called ‘QCD-inspired models’.

- (2) Likely, the gluon self-interaction leads to confinement of colour. Originally, the confinement hypothesis was invented to ‘explain’ the absence in Nature of free quarks, i.e. of particles with fractional electric charge. However, no fundamental principle excludes the existence of a scalar field carrying colour. A bound state of a quark and the scalar field would still have fractional charge but could be colour-neutral. Hence a modern version of the confinement hypothesis denies the existence of observable objects with non-vanishing colour charge: all observable particle states are colour singlets.
- (3) The self-interacting leads to the suggestion of the existence of new forms of hadronic matter with excited gluonic degrees of freedom, known as glueballs and hybrids.

### 2.1.2 Chiral symmetry

In the limit of vanishing quark masses, the QCD Lagrangian is invariant under chiral transformations

$$\begin{aligned} q &\rightarrow \exp(i\gamma_5\alpha^a t^a) q, \\ \bar{q} &\rightarrow \bar{q} \exp(i\gamma_5\alpha^a t^a), \end{aligned} \tag{2.3}$$

where  $t^a$  are the generators of the flavour symmetry group -  $SU(2)$  for isotopic symmetry or  $SU(3)$  for symmetry of  $u, d, s$  quarks. In this limit, positive- and negative-parity states are mass-degenerate. This degeneracy is not seen in the spectrum of low lying hadrons. For example, the negative-parity companion of the nucleon,  $N(1535)S_{11}$ , is separated from the nucleon by about  $600 \text{ MeV}/c^2$ . This mass shift is substantial and indicates that chiral symmetry is broken. The spontaneous symmetry breaking is signalled by a  $\bar{q}q$  vacuum expectation value, the chiral condensate [119]. The value of the quark condensate density is known with high precision [120] from the Gell-Mann-Oakes-Renner relation:

$$\langle \bar{q}q \rangle = -\frac{f_\pi^2 m_\pi^2}{2(m_u + m_d)} = -(240 \pm 10 \text{ MeV})^3 \tag{2.4}$$

for which higher-order corrections are small.

Spontaneously broken chiral symmetry is associated with the existence of eight Goldstone bosons, of eight massless pseudoscalar mesons. Pseudoscalar mesons observed in Nature,  $\pi^\pm, \pi^0, \eta, K^\pm, K^0, \bar{K}^0$ , are not massless; for small quark masses, chiral symmetry is broken explicitly leading to finite (but still small) masses. The  $\eta'$  mass, however, is not small; the  $\gamma_5$ -invariance is broken on the quantum mechanical level due to an anomaly which implies that the divergence of the flavour singlet axial vector current  $A_\mu = \bar{q}\gamma_\mu\gamma_5 q$  does not vanish:

$$\partial_\mu A_\mu(x) = N_f q(x), \quad \text{where} \tag{2.5}$$

$$q(x) = -\frac{1}{32\pi^2} \epsilon_{\mu\nu\alpha\beta} G_{\mu\nu}^a(x) G_{\alpha\beta}^a(x) \quad (2.6)$$

is called topological charge density.

### 2.1.3 Instantons

The QCD vacuum has a nontrivial topological structure. There are trivial vacua having vanishing classical fields ( $A_\mu^a = 0, G_{\mu\nu}^a = 0$ ) with small perturbative oscillations near this zero. In addition, there are infinitely many other solutions with  $G_{\mu\nu}^a = 0$  which can not be reduced to  $A_\mu^a = 0$  by a continuous gauge transformation [121]. These different solutions are labelled by an integer number, called winding number. The tunnelling transitions between different vacua leads to non-perturbative field configurations [122, 123] called instantons and anti-instantons. The tunnelling decreases the vacuum energy making it negative.

The theory of the instanton vacuum is far from being completed. Its inferences of any of its consequences for the real world requires the use of models and of experimental data. Nevertheless it can be used as powerful approximation to evaluate nonperturbative effects. We refer the reader to reviews by Schäfer and Shuryak [124], Forkel [125] and Diakonov [126]. As a qualitative guide we can consider instantons as nonperturbative fluctuations with a very strong field in a relatively small volume ( $r \approx 1/3$  fm) with average space-time density  $n \approx 1 \text{ fm}^{-4}$  which provide a significant contribution to the gluon condensate.

Right-handed and left-handed quarks can propagate in this highly non-trivial vacuum in zero modes of definite chirality (left handed for instantons, right handed for anti-instantons). As there is exactly one zero mode per flavour, only the propagation of quark pairs of opposite chirality are influenced by instantons. This has important consequences for meson spectroscopy: direct instanton effects should be expected for pseudoscalar mesons *and* for scalar mesons.

Instantons influence the dynamics of quarks in two ways: i) The quark and antiquark propagators get dressed and obtain a dynamical mass [126]. ii) Quark and antiquark may scatter off instantons leading to an effective quark interaction. Such processes are described by non-local  $2N_f$ -quark interactions known as 't Hooft vertices [123]. They generate the dominant instanton effects in the light-quark sector. The 't Hooft vertices manifestly break the axial  $U_A(1)$  symmetry of the QCD Lagrangian with  $m_q = 0$  and thereby resolve (at least qualitatively) the  $U_A(1)$  problem, i.e. they explain why the  $\eta'$  meson has almost twice the mass of the  $\eta$  meson and why it cannot be considered as a (quasi) Goldstone boson.

## 2.2 Chiral Perturbation Theory $\chi$ PT

Chiral Perturbation Theory [51–54] is based on the construction of an effective Lagrangian which respects the QCD symmetries, and contains  $\pi, K$  and  $\eta$  mesons as elementary ingredients of the theory. These particles are the Goldstone bosons of spontaneous chiral symmetry breaking of massless QCD and are the low-energy degrees of freedom of the theory. In the chiral limit, all amplitudes vanish at zero momentum. This fact allows one to construct  $\chi$ PT as an expansion in even powers of momenta, generically denoted as  $O(p^2), O(p^4)$ . At each order in  $p^2$ ,  $\chi$ PT is the sum of all terms compatible with the symmetries, each multiplied by a free parameter. Once a set of parameters up to a given order is determined, it describes, to that order, any other process involving mesons. In the leading order, the only parameters are masses and decay constants; 10 further

chiral parameters are needed to describe meson-meson interactions in second order ( $p^4$ ). The natural range within which  $\chi$ PT can be applied is governed by the parameter  $\Lambda_\chi \sim 4\pi f_\pi$  at about  $1 \text{ GeV}/c^2$ . The low-mass scalar interactions can be derived from the leading order Lagrangian and unitarity, from which the existence of a  $\sigma(485)$  and  $\kappa(700)$  was deduced (see section 9). In [127–129], second order corrections and coupled channels effects were calculated and meson-meson cross section data up to  $1.2 \text{ GeV}/c^2$  described in a consistent way. Resonances were constructed by extrapolation of the  $\chi$ PT amplitude via the Inverse Amplitude Method [130] which avoids conflicts with unitarity.

For sufficiently light quarks, chiral perturbation theory can be used to estimate quark mass ratios [131]. To first order, the squared masses of pseudoscalars are proportional to the quark masses. Electromagnetic interactions add to squared masses as well:

$$\begin{aligned} m_{\pi^0}^2 &= B(m_u + m_d) \\ m_{\pi^+}^2 &= B(m_u + m_d) + \Delta_{em} \\ m_{K^0}^2 &= B(m_d + m_s) \\ m_{K^+}^2 &= B(m_u + m_s) + \Delta_{em} \end{aligned} \quad (2.7)$$

Here,  $B$  and  $\Delta_{em}$  are unknown constants. From these equations quark mass ratios can be determined with high precision:

$$m_u/m_d = (2m_{\pi^0}^2 - m_{\pi^+}^2 + m_{K^+}^2 - m_{K^0}^2)/(m_{K^0}^2 - m_{K^+}^2 + m_{\pi^+}^2) = 0.56 \quad (2.8)$$

$$m_s/m_d = (m_{K^0}^2 - m_{\pi^+}^2 + m_{K^+}^2)/(m_{K^0}^2 - m_{K^+}^2 + m_{\pi^+}^2) = 20.1 \quad (2.9)$$

Higher order  $\chi$ PT corrections change these ratios by  $\approx 10\%$ . To estimate absolute values of quark masses we have to use sources from outside of chiral perturbation theory. As a first estimate we can assume that, as a result of chiral symmetry breaking, the same mass is added to all bare masses. In this approximation

$$m_s = (m_\phi - m_\rho)/2 \approx 120 \text{ MeV}/c^2. \quad (2.10)$$

More refined approaches based on sum rules [132] give an  $s$ -quark mass of about  $100 \text{ MeV}/c^2$ , with about  $10\%$  precision. Thus,  $u$  and  $d$  quarks are very light on a hadronic scale of  $1 \text{ GeV}/c^2$ :  $m_u \approx 4 \text{ MeV}/c^2$ ,  $m_d \approx 7 \text{ MeV}/c^2$ . This is a justification of the low mass approximation of  $\chi$ PT. Masses of constituent quarks cannot be determined without addressing the model in which they are used.

### 2.3 Lattice QCD

Lattice QCD aims at simulating full QCD on a discrete Euclidean space-time lattice and seems to be the most promising technique to calculate the properties of hadrons from the QCD Lagrangian. The four dimensions of space and time are discretised with a regular lattice of points separated by a spacing  $a$  in a volume  $L^3 T$ . Anisotropic lattices use more lattice points in the time direction than in the space directions. The time is chosen to be Euclidean, i.e. the metric tensor is definite. The reciprocal spacing  $1/a$  should be much smaller than the masses or momenta involved in the calculation. It acts as a ultra-violet cut-off parameter while maintaining gauge invariance of the theory. In the formulation defined by Wilson [133], quarks are placed on the sites of the lattice, while the gluonic fields are represented by links connecting neighbouring sites. Every field configuration receives a Boltzmann weight  $\exp\{-S\}$  where  $S$  is the Euclidian action. Expectation

values of physical quantities are estimated from ensemble averages. Lattice QCD provides a non-perturbative regularisation of QCD and a means by which observables can be predicted. The advantage of this approach is that it is based on first principles of QCD and that its approximations are controllable. The mass of a state is e.g. extracted from the decay of a two-point correlation function

$$C(t) = \langle \Phi(t)\Phi(0) \rangle \propto e^{-Mt} \quad (2.11)$$

where  $\Phi(t)$  is a lattice operator that creates or annihilates the state of mass  $M$  at time  $t$ . After some thermalisation, the correlation function falls off exponentially, the fall-off is given by the particle mass. Excited states fall off much more rapidly and are thus difficult to extract on the lattice. A further problem originates from the Wilson-Dirac operator which does not respect chiral symmetry: light quarks of lattice QCD are too massive,  $\sim 50$  MeV/c<sup>2</sup>. A remedy is the so-called chiral extrapolation: at low momenta, the interactions e.g. in  $\pi - \pi$  scattering and  $\pi - N$  scattering are weak and can be treated perturbatively. The results depend on the assumed quark mass which can be made large. Hence the dependence of an observable as a function of the pion mass can be determined and a chiral expansion to the true quark masses can be performed; this limit often reproduces accurately physical quantities.

Still, the inclusion of dynamical quarks is a major problem. In many calculations, quark loops are neglected, the calculations are done in *quenched approximation*. Unquenching is very computer time consuming, additionally it suffers very often from too large quark masses.

### 2.3.1 Confinement

The non-observation of free quarks has led to the general conviction that quarks (or colour sources, to be more precise) are confined. It is assumed but not proven that quantum chromodynamics confines quarks due to some special class of gauge field configurations like Abelian monopoles or centre vortices which are supposed to dominate the QCD vacuum at large distance scales. We refer the reader to a few reviews for more detailed discussions of the ideas [134, 135] and the present status [136, 137].

Lattice simulations have also confirmed properties of the static quark potential and the string-like behaviour of the QCD flux tube. In Fig. 11, the potential energy is shown as a function of the separation between two static quarks. The potential energy can be described very well by the superposition of a Coulomb-like potential and a linearly rising (confinement) potential. At sufficiently large separations, for  $R \approx 0.12$  fm, the total energy suffices to allow mesons to decay into two (colour-neutral) mesons: spring breaking occurs. Spring breaking can be simulated on a lattice [139–141]. The right panel in Fig. 11 displays the energy levels due to a  $q\bar{q}$  and a two-meson system in an adiabatic approximation. In a hadronic reaction, the sudden approximation – where the system follows the straight line – is more realistic, and  $q\bar{q}$  pairs can be excited to much higher energies.

### 2.3.2 Glueballs

The calculation of the glueball mass spectrum belongs to the early achievements of lattice QCD and is still of topical interest. A convenient way to represent the results was given by Morningstar and Peardon [143] who calculated a large number of spin-parity configurations, see Fig. 12. The

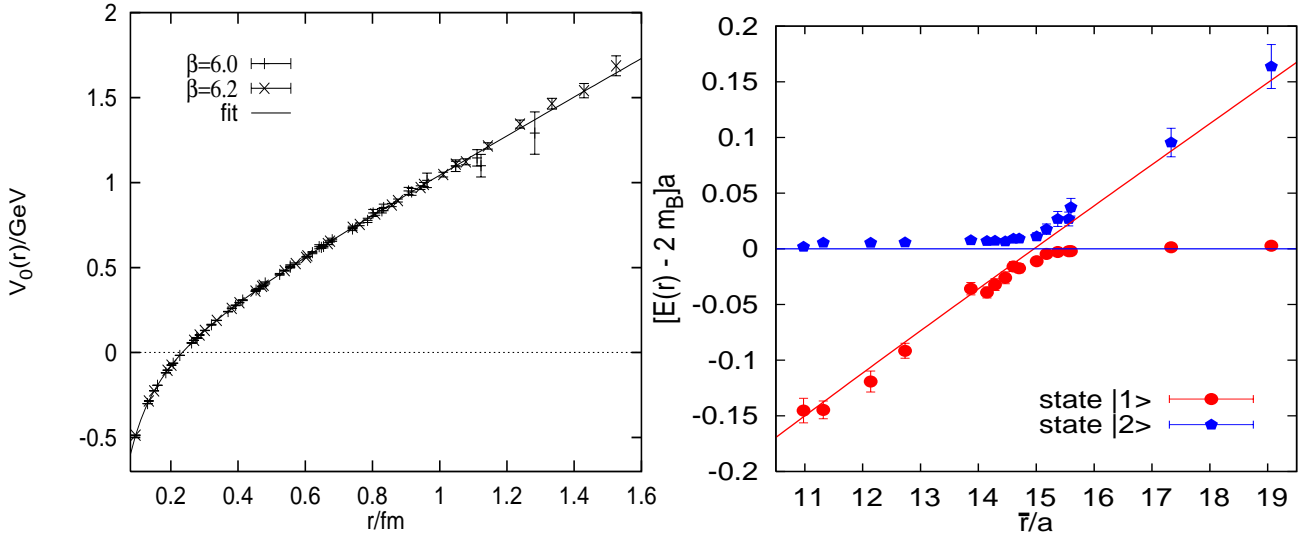


Fig. 11. Left: The potential energy between two heavy quarks (with fixed positions) as a function of their separation from lattice QCD. The solid line represents a potential in the form  $V(r) = \frac{4}{3} \frac{\alpha_s}{r} + b \cdot r$ ; from [138]. Right: In full QCD, a sea quark-antiquark can be created from the vacuum and at large distances, two-meson states are energetically preferred. For static quarks, the levels cross at some distance  $R$  (with  $a \approx 0.083$  fm), the string breaking introduces mixing of the energy levels defined by the potential  $V(R)$  and the threshold  $2m(B)$  [139–142].

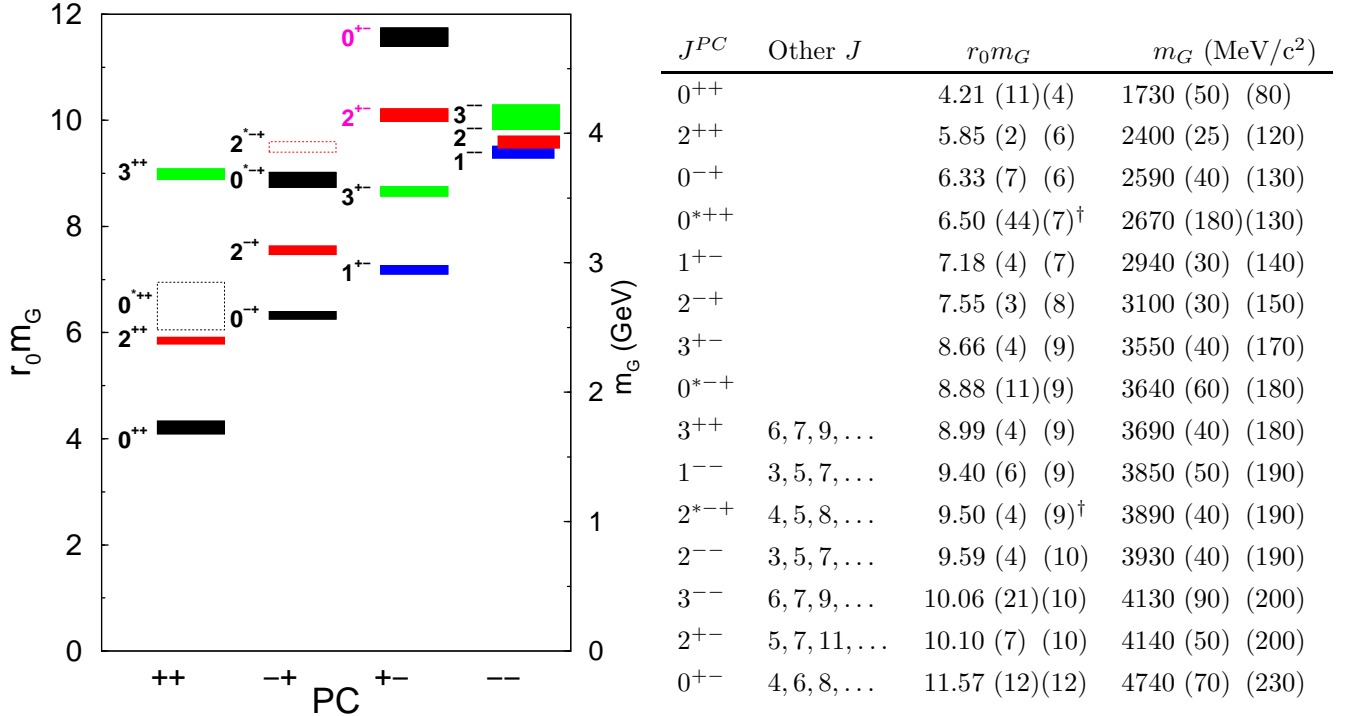


Fig. 12. The mass spectrum of glueballs in pure  $SU_C(3)$  gauge theory [143]. The masses are given in units of the hadronic scale  $r_0$  along the left vertical axis and in  $\text{GeV}/c^2$  along the right vertical axis. The mass uncertainties indicated by the vertical extents of the boxes do *not* include the uncertainty in  $r_0$ . Numerical results are listed in tabular form. In some cases, the spin-parity assignment for a state is not unique. The figure shows the smallest  $J$  value, the other possibilities are indicated in the second column of the table. In column 3, the first error is the statistical uncertainty from the continuum-limit extrapolation and the second is the estimated uncertainty from the anisotropy. In the final column, the first error comes from the combined uncertainties in  $r_0 m_G$ , the second from the uncertainty in  $r_0^{-1} = 410(20)$  MeV/ $c^2$ . The dagger indicates states for which the authors of [143] suggest further studies before interpreting them.

numerical results are reproduced here as well; for noisy states, the right  $J^{PC}$  assignment is difficult to extract.

There exists a large number of papers, partly using different techniques, to extract glueball properties. We refer the reader to a recent calculation [144] where references to previous work and to different methods are given. Essentially all calculations agree that the lowest mass scalar glueball should have a mass between 1.6 to 1.8 GeV/c<sup>2</sup>, followed by a tensor glueball and a pseudoscalar glueball at about 2.3 and 2.5 GeV/c<sup>2</sup>, respectively. It can be shown that unquenching the lattice does not lead to significant changes in the glueball mass spectrum [145]. However, in these calculations the sea quarks still have sizable masses corresponding to  $m_\pi/m_\rho \sim 0.7$ .

The lattice glueballs are compact objects, the scalar glueball has a radius of about 0.3 fm [146].

### 2.3.3 Ground-state $q\bar{q}$ mesons

A precise calculation of the light hadron spectrum in quenched QCD, i.e. without quark loops, was carried out by the CP-PACS Collaboration. Their results are summarised in the plot shown in Fig. 13. The agreement is impressive: quenched QCD describes the light hadron spectrum at the level of 10 %. Still, there remain some significant deviations from the experimentally observed spectrum, dynamical quarks do play a rôle even though at a surprisingly low level.

The CP-PACS results in Fig. 13 do not yet show any  $SU(3)$  flavour singlet meson. Pseudoscalar and scalar flavour singlet mesons are deeply affected by the topological structure or quantum fluctuations of the QCD vacuum. The quenched approximation thus misses the most important aspects of the  $\eta$  and  $\eta'$  and of their controversial scalar counterparts. An introduction to objectives and methods to overcome these difficulties, at least in part, can be found in some lectures notes [148]. The masses

$$M_\eta = 292 \pm 31 \text{ MeV}/c^2, \quad M_{\eta'} = 686 \pm 31 \text{ MeV}/c^2. \quad (2.12)$$

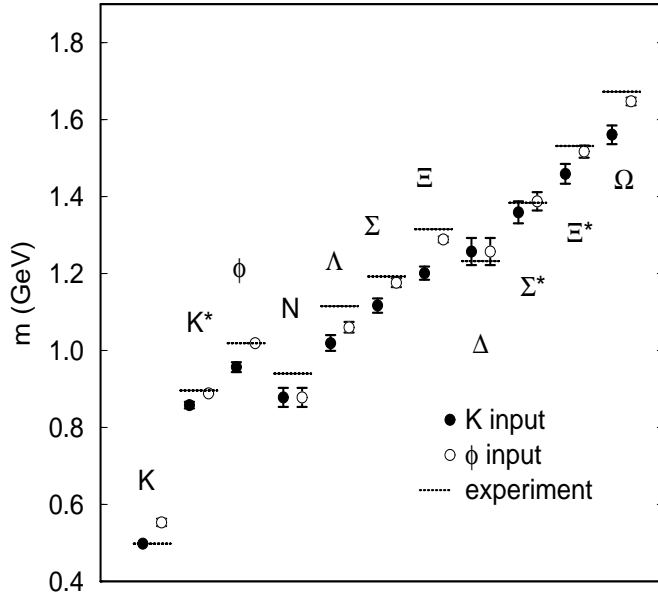


Fig. 13. Light hadron spectra in quenched QCD [147].

are low with respect to experimental values but yield a mass splitting that compares well with data. A similar study for scalar isoscalar mesons has not been made but calculations of the  $a_0(980)$  and  $K^*(1430)$  masses have been carried out [149].

The spectrum of scalar mesons is hotly debated. The glueball of lowest mass has scalar quantum numbers, and every reliable information how to organise the scalar nonet is extremely welcome. In Table 3 recent results on the mass of the ground-state scalar isovector meson  $a_0$  are collected. The results are spread over a wide range: lattice QCD can support the identification of the  $a_0(980)$ , of the Crystal Barrel  $a_0(1475)$ , or of the Obelix  $a_0(1290)$  state as the ground state scalar isovector  $q\bar{q}$  state,.

Table 3  
The mass of the  $a_0$  meson from lattice QCD

Group	Method	$m_{a_0}$ GeV/c <sup>2</sup>
Bardeen et al. [150]	quenched	1.34(9)
Hart et al. [151]	$n_f = 2$ , partially quenched,	$1.0 \pm 0.2$
Prelovsek et al. [152]	$n_f = 2$ , unquenched,	$1.58 \pm 0.34$
Prelovsek et al. [152]	partially quenched	$1.51 \pm 0.19$
Burch et al. [153]	quenched	$\sim 1.45$
McNeile and Michael [149]	$n_f = 2$ , unquenched,	$1.01 \pm 0.04$

This is a puzzling situation: lattice QCD predicts meson and baryon masses of undisputed states, in close agreement with experiment. When open physical questions are involved, there is often no guidance provided.

Recently, masses of scalar flavour singlet mesons were calculated in ( $n_f = 2$ ) unquenched lattice QCD [154] and it was shown that the mass of the lightest  $0^{++}$  meson is much lower than the mass of the  $0^{++}$  glueball in quenched QCD. The lowest-mass scalar flavour singlet meson could hence be identified with  $f_0(980)$  or even with  $\sigma(485)$ . It was stressed that for scalar mesons, there is a strong dependence on lattice spacing. Strong mixing between scalar glueball and scalar mesons is found, again with a significant lattice-spacing dependence, demanding future calculations with finer lattice spacing, dynamical simulations with light quarks (plus a strange quark in the sea), and large statistics. The main effect of unquenching the glueball is to drive its mass from 1.6 GeV to 1 GeV. The authors conclude that “it is not clear that a mixing scheme based on only the states  $f_0(1370)$ ,  $f_0(1500)$ , and  $f_0(1710)$  is complete enough to determine the fate of the quenched glueball”.

### 2.3.4 Hybrids

Hybrid mesons are mesons in which the gluonic degrees of freedom are excited. Most fascinating is the possibility that they may acquire spin-exotic quantum numbers which cannot be created from a  $q\bar{q}$  state with unexcited glue. However, spin-exotic mesons can also be formed by  $q\bar{q}q\bar{q}$  systems or by meson-meson interactions.

The lowest-lying hybrids are expected to have  $J^{PC} = 1^{-+}$ . Hybrids in the  $\Upsilon$  family are predicted in the range 10.7 to 11.0 GeV/c<sup>2</sup>, above the  $\Upsilon(4S)$  and with 20 MeV/c<sup>2</sup> width. Bottomonium hybrids are expected to decay with a width of about 100 MeV/c<sup>2</sup> into one of the  $\chi_b$  states and an isoscalar scalar meson, via its coupling to its flavour-singlet component [155–157]. In the charmonium family, hybrids are predicted at 4.34 GeV/c<sup>2</sup> [158–160] with an estimated uncertainty of 100 to

200 MeV/c<sup>2</sup>. The predicted mass is above the  $Y(4260)$  (which we interpret as  $\psi(4S)$ , see section 5.2.3). Light-quark hybrids should have masses at about 2 GeV/c<sup>2</sup> [161] but even masses as low as 1.5 GeV/c<sup>2</sup> are not excluded [162]. Hybrid decay widths depend of course on the hybrid mass. For masses around 2.2 GeV/c<sup>2</sup>, typical partial widths are  $(400 \pm 120)$  or  $(90 \pm 60)$  MeV/c<sup>2</sup> for  $\pi b_1$  and  $\pi f_1$  decays [163] and about 60 MeV/c<sup>2</sup> for  $\pi a_1$  decays [164].

## 2.4 QCD sum rules

In the method of QCD sum rules [165], problems due to long-distance interactions are avoided by considering only quarks propagating at short distances. Hadrons are represented by their interpolating currents taken at large virtualities, i.e. at large, space-like momenta  $Q^2 \equiv -q^2 \gg \Lambda_{QCD}^2$ . For normal mesons, the interpolating currents are constructed from  $q$  and  $\bar{q}$ . In the case of glueballs, the currents are given by gluonic interpolating fields, e.g. by  $O_S(x) = \alpha_s G_{\mu\nu}^a(x) G^{a\mu\nu}(x)$  for a scalar glueball. The correlation function of these currents is introduced as

$$\Pi_G(-q^2) = i \int d^4x e^{iqx} \langle 0 | T O_G(x) O_G(0) | 0 \rangle \quad (2.13)$$

and treated in the framework of the operator product expansion where the short distance interactions are calculated using QCD perturbation theory. Long-distance interactions are parametrised in terms of universal vacuum condensates. The result of the QCD calculation is then matched, via dispersion relation, to a sum over hadronic states

$$\Pi_G(Q^2) = \frac{1}{\pi} \int_0^\infty ds \frac{\text{Im}\Pi_G(-s)}{s + Q^2}. \quad (2.14)$$

The spectral function is usually parametrised by one or more resonances and a step-like continuum

$$\text{Im}\Pi_G^{(ph)}(s) = \text{Im}\Pi_G^{(pole)}(s) + \text{Im}\Pi_G^{(cont)}(s), \quad (2.15)$$

leading to the following representation:

$$\Pi(q^2) = \frac{q^2 f^2}{m^2(m^2 - q^2)} + q^2 \int_{s_0^h}^\infty ds \frac{\rho^h(s)}{s(s - q^2)} + \Pi(0). \quad (2.16)$$

After a Borel transformation, a more convenient form of the sum rule is obtained

$$\Pi(M^2) = f^2 e^{-m^2/M^2} + \int_{s_0^h}^\infty ds \rho^h(s) e^{-s/M^2}, \quad (2.17)$$

where contributions from high masses are suppressed. Shifman, Vainshtain and Zakharov [165] related the short distance behaviour of current correlation functions to the vacuum expectation values of gluon operators and thus deduced the magnitude [120] of the gluon condensate:

$$\left\langle \frac{\alpha_s}{\pi} G^2 \right\rangle = (0.012 \text{ GeV})^4 \pm 30\%. \quad (2.18)$$

QCD sum rules have the advantage that they deal with fundamental parameters like current quark masses and vacuum condensate densities, contrary to phenomenological models which use not so well defined objects like constituent quarks etc. An impressive number of results on light quark spectroscopy were obtained using sum rules. For a discussion of perspectives and limitations of sum rules, we refer the reader to the review of Colangelo and Khodjamirian [120].

Narison has calculated glueball masses and widths in the QCD sum rule approach and low-energy theorems [166]. In the scalar sector, he found a gluonium state having a mass  $M_G = (1.5 \pm 0.2)$

GeV, which should decay into the flavour octet (!)  $\eta\eta'$  channel and into  $4\pi^0$ . In addition, he suggests wide gluonium states at low masses which he identifies with the  $\sigma(485)$ . In a more recent paper, Narison proposed that the two isoscalar resonances  $\sigma(485)$  and  $f_0(980)$  result from a maximal  $q\bar{q}$ -glueball mixing. The scalar states  $f_0(1500)$ ,  $f_0(1710)$ ,  $f_0(1790)$  are suggested to have a significant glueball component [132].

## 2.5 Flux-tube model

The flux tube approach describes mesons in a dynamical nonrelativistic model motivated by the strong coupling expansion of lattice QCD [167]. In this model quarks are connected by a string of massive beads, with a linear confining potential between the beads. By analogy with lattice QCD only locally transverse spatial fluctuations of the bead positions are possible. For a string of  $N$  mass points which connects a quark at site 0 to an antiquark at site  $N + 1$  the flux tube model Hamiltonian is written as

$$H = H_{quarks} + H_{flux\;tube}, \quad (2.19)$$

$$H_{quarks} = -\frac{1}{2m_q}\vec{\nabla}_q^2 - \frac{1}{2m_{\bar{q}}}\vec{\nabla}_{\bar{q}}^2 + V_{q\bar{q}},$$

$$H_{flux\;tube} = b_0 R + \sum_n \left[ \frac{p_n^2}{2b_0 a} + \frac{b_0}{2a}(y_n - y_{n+1})^2 \right],$$

Here  $m_q$  and  $m_{\bar{q}}$  are the quark and antiquark masses,  $m_b$  is the bead mass,  $y_n$  is the transverse displacement of the  $n$ th bead,  $p_n$  is its momentum,  $b_0$  is a string tension, and  $R = (N + 1)a$  is the separation between the static quarks. The potential  $V_{q\bar{q}}$  is meant to describe the colour Coulomb interaction. When the flux tube is in its ground state, the excitation of  $q\bar{q}$  yields the conventional meson spectrum. Flux-tube excitations lead to a new kind of hadronic states called hybrids. The Schrödinger equation with Hamiltonian (2.19) can be solved in adiabatic approximation thus giving the masses of ordinary and of hybrid mesons. The excitations of the flux tube are characterised by  $\Lambda$ , the projection of the flux tube orbital angular momentum along the  $q\bar{q}$  axis. For a single flux tube excitation,  $\Lambda = \pm 1$ . With this additional degree of freedom the quantum numbers of hybrid mesons with the  $q\bar{q}$  spin  $S = 0$  are  $J^{PC} = 1^{++}, 1^{--}$ ; for  $S = 1$  the quantum numbers  $J^{PC} = 2^{+-}, 2^{-+}, 1^{+-}, 1^{-+}, 0^{+-}, 0^{-+}$  are accessible. The list contains exotic quantum numbers,  $J^{PC} = 0^{-+}, 1^{-+}, 2^{+-}$ , which cannot be generated by normal  $q\bar{q}$  states. The lightest hybrid states are predicted to have masses  $M \approx 2.0 \text{ GeV}/c^2$  [168].

Mesons can decay via flux-tube breaking at any point along its length, producing a  $\bar{q}q$  pair in  $J^{PC} = 0^{++}$  state. Hybrid states have a node along the initial  $q\bar{q}$  axis leading to a suppression of hybrid decays into two mesons with identical spatial wave functions: hybrid decays into two pseudoscalar mesons or one pseudoscalar and one vector meson are forbidden. Instead, hybrids prefer decays into one  $S$ -wave and one  $P$ -wave meson. Typical examples are decays into  $\pi b_1(1235)$  or  $\pi f_1(1285)$ . Hybrids can therefore be observed only in complicated final states and at rather high masses. These conditions make experimental searches for them very difficult.

The decay widths can be calculated using some models for wave functions of the mesons involved and assuming a universal string breaking constant for all decays [169]. This universality is of course a rather restrictive assumption.

To estimate the reliability of the flux-tube model we can compare its results on hybrids with those of lattice QCD. Figure 14 shows the flux tube potential for the ground state (solid line) and the first excited state (dotted line) [168]. These are compared to lattice computations of the

same adiabatic potentials (points) [170]. At a  $q\bar{q}$  separation of about 1 fermi, both models nearly coincide while at smaller separations the flux tube model potential overestimates the strength of the attractive Coulomb potential, at large separations, it underestimates the string tension. Hybrid mesons at small  $q\bar{q}$  separations can be treated as states formed by a  $q\bar{q}$  pair and a gluon. The gluon field carries colour, the  $q\bar{q}$  form a colour octet and thus their interaction is repulsive.

Apart from these details, flux-tube-model and lattice potential are rather similar, and the flux tube provides a viable model and a very convenient language. It has significant predictive power and a sufficient number of tuneable parameters for further development.

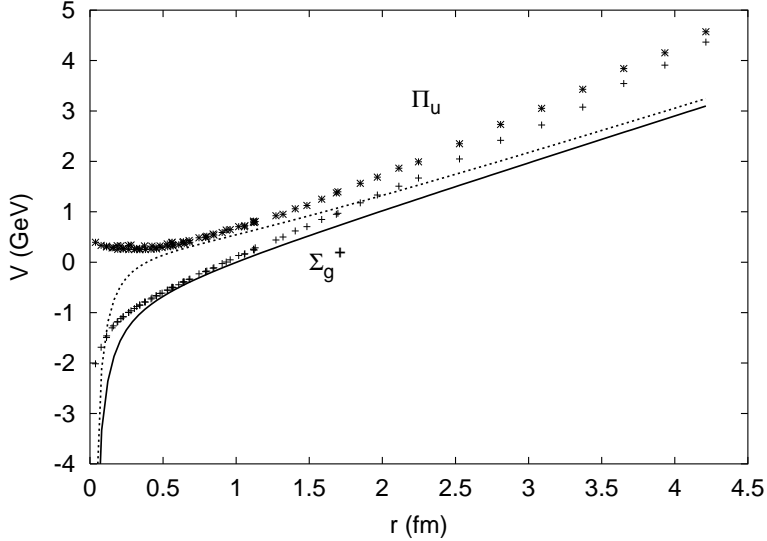


Fig. 14. Comparison of the flux-tube potentials represented by a solid line (dotted line first excited state) with lattice gauge calculations given by crosses [170].

## 2.6 Quark models

The quark model still plays an important rôle in the interpretation of the mass spectra of mesons. Quark models assume that a meson is composed of a constituent quark and an antiquark; their masses may arise from the spontaneous breaking of chiral symmetry, they are free parameters of the model. Between quark and antiquark a confining potential is assumed to rise linearly with the interquark distance. The confinement potential is however not sufficient to explain details of the spectra and some additional quark-quark interaction is required to reproduce the known meson masses. The main differences between different quark models are related to the choice of the appropriate spin-dependent quark interactions which find their roots in either One-Gluon-Exchange, Goldstone-Boson-Exchange or instanton effects.

### 2.6.1 Gluon-exchange interactions

The first unified constituent quark model for all  $q\bar{q}$ -mesons was developed by Godfrey and Isingur [171]. It is widely used as a reference for comparison of new experimental data, and has had a very significant impact on the development of the field. The model starts from a Hamiltonian

$$H\Psi = (H_0 + V)\Psi = E\Psi, \quad H_0 = \sqrt{m_q^2 + |\vec{p}|^2} + \sqrt{m_{\bar{q}}^2 + |\vec{p}|^2}, \quad (2.20)$$

with  $\vec{p}'$  the relative momentum in the centre-of-mass frame. The interaction is written as

$$V = H^c + H^{SS} + H^{LS} + H^A$$

which contains a central potential – linear confinement  $br + c$  and Coulomb potential –, a spin-spin and a spin-orbit interaction, and an annihilation contribution for flavour-neutral mesons.

The potential is generated from gluon exchange with a running coupling constant for which a parametrisation

$$G(Q^2) = -\frac{4}{3}\alpha_s(Q^2)\frac{4\pi}{Q^2}$$

is chosen where  $\alpha_s(Q^2) = \sum_k \alpha_k e^{-\frac{Q^2}{4\gamma_k^2}}$ , with  $\alpha_s(0)$  finite, and  $\vec{Q} = \vec{p}' - \vec{p}$ . These potentials are “smeared out” to avoid singularities at the origin. Relativistic effects are partly taken into account, but spin-orbit forces are suppressed; *there are no spin-orbit forces in the Hamiltonian*. The excuse for this suppression is the experimental observation that these are weak or absent in the data. From the theoretical side, spin-orbit forces are at least partly compensated by the so-called Thomas precession, a relativistic generalisation of Coriolis forces. The  $\rho$ - $\pi$ -splitting is assigned to the magnetic interaction caused by one-gluon exchange.

Annihilation is taken into account by parametrising the annihilation amplitude, one for non-pseudoscalar flavour-neutral mesons and a different one for pseudoscalar mesons. All mesons are assumed to be “ideally mixed”, except the pseudoscalar mesons.

### 2.6.2 Exchange of Goldstone particles

The model proposed by Vijande, Fernandez, and Valcarce [172] uses a quark-antiquark potential which includes a (screened) confinement potential in the form

$$V_{con}(\vec{x}) = (\Delta - a_c(1 - \exp(-\mu_c|\vec{x}|))) \lambda_q^{(c)} \cdot \lambda_{\bar{q}}^{(c)}, \quad (2.21)$$

a short range one-gluon-exchange inspired potential and Goldstone Boson exchanges in the form of modified Yukawa potentials

$$V(\vec{x}) = \sum_{\mu=\pi,\sigma,K,\eta} V_\mu(\vec{x}), \quad (2.22)$$

where the isoscalar ( $\sigma$ ) part contains a central and a spin-orbit term, and the other potentials ( $\pi, K, \eta$ ) consist of central, spin-spin and a tensor contribution. Flavour mixing for pseudoscalar mesons is induced through the flavour dependence of Goldstone boson exchange. Spectra range from light quark mesons to heavy flavours.

### 2.6.3 Instanton-induced interactions

In the Bonn quark model [173, 174], the residual interactions (in addition to a linear confining potential) are induced by instantons. Meson mass spectra, wave functions and transition matrix elements are calculated from a homogeneous, instantaneous Bethe-Salpeter equation. In this relativistic model, confinement is described by a linear potential with a suitable Dirac structure. In the Bonn model, two different Dirac structures were used to calculate the meson mass spectra. The first one has a scalar and a time-like vector structure in the form

$$\frac{1}{2}(\mathbb{I} \cdot \mathbb{I} - \gamma_0 \cdot \gamma_0) \quad (2.23)$$

where  $\mathbb{I}$  is the identity operator. Alternatively, a confinement potential invariant under  $U_A(1)$  was assumed:

$$\frac{1}{2}(\mathbb{I} \cdot \mathbb{I} - \gamma_5 \cdot \gamma_5 - \gamma^\mu \cdot \gamma_\mu). \quad (2.24)$$

In the limit of vanishing quark masses, this structure leads to parity doublets in the meson spectrum. The two variants define two models, called  $\mathcal{A}$  and  $\mathcal{B}$  in [173, 174]. Instanton-induced interactions lead to  $u\bar{u} \rightarrow d\bar{d}$  and  $u\bar{u} \rightarrow s\bar{s}$  transitions with adjustable strengths; their values were determined to describe the ground state pseudoscalar mesons.

Instanton-induced forces have been ‘invented’ to explain the  $U_A(1)$  anomaly, the large value of the  $\eta'$  mass [176]. Hence it is not surprising that a model based on instanton-induced forces does well in describing pseudoscalar meson masses. Instantons in mesons induce coherent spin flips for quark and antiquark; such transitions are possible only in pseudoscalar mesons where spin *up* and spin *down* can be interchanged, or in scalar mesons where the spins of quark and antiquark may flip and the orbital angular momentum changes its direction. Fig. 15 shows the influence of instantons for pseudoscalar and scalar ground-states mesons [175]. Instantons lead to substantial mass splittings; the  $\rho\pi$  splitting is now due to a shift in mass of the pseudoscalar pion which is absent in  $\rho$  mesons. Particularly interesting is the fact that scalar mesons organise themselves into a high-mass flavour-octet and a low-mass flavour singlet state. The predicted  $f_0(1470)$  is easily identified with the known  $f_0(1500)$ ; the  $K_0^*(1470)$  is correctly reproduced. The authors in [175] identified the predicted  $a_0(1320)$  with the  $a_0(1450)$ , in spite of a larger discrepancy. The predicted  $f_0(980)$  was identified either with the  $f_0(980)$ ; (this assignment leads to an asymmetric treatment of the twins  $a_0(980)$  and  $f_0(980)$ ); alternatively, it was identified with the wide scalar ‘background’ called  $f_0(1000)$  by Au, Morgan, and Pennington [177] (and nicknamed ‘red dragon’ by Minkowski and Ochs [178]). Later, we will call it  $f_0(1300)$ .

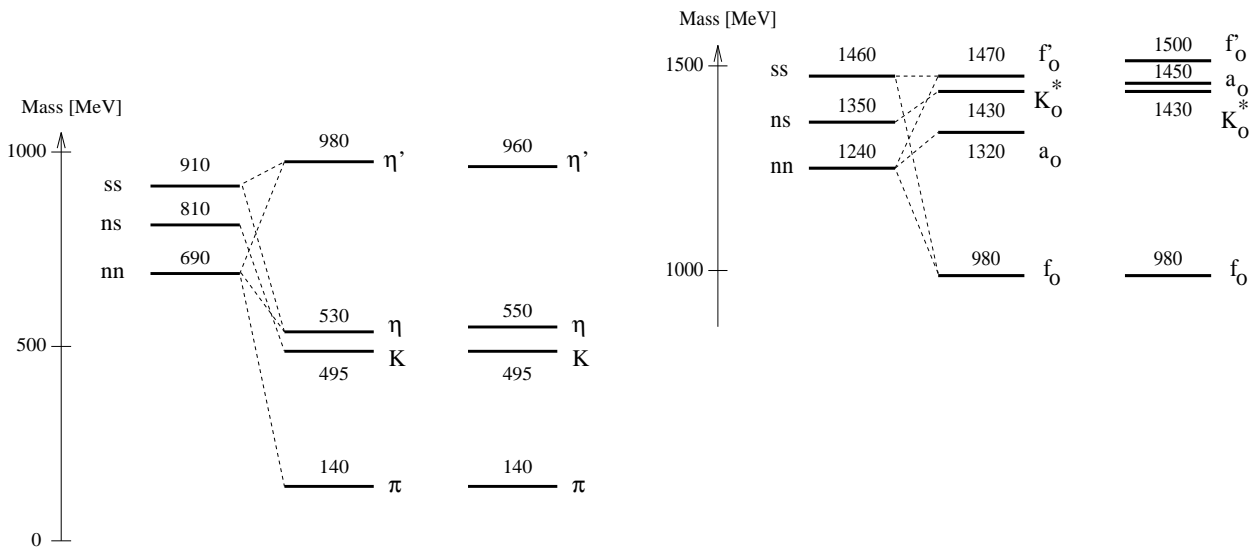


Fig. 15. Schematic splitting of pseudoscalar (left panel) and scalar (right panel) flavour nonets with confinement interaction (left), with confinement and instanton-induced force (middle) compared to data (right) [175].

## 2.6.4 Heavy Quark Symmetry

Heavy quark symmetry [179–181] exploits the large separation of mass scales in hadronic bound states of a heavy quark with light constituents (quarks, antiquarks and gluons) : the Compton wave length of the heavy quark ( $\lambda_Q \sim 1/m_Q$ ) is much smaller than the size of the hadron containing the heavy quark ( $R_{\text{had}} \sim 1/\Lambda_{\text{QCD}}$ ). This symmetry is widely used in the analysis of semileptonic decays of heavy-light hadrons and in spectroscopy (see review [182] by Neubert). In the rest frame of the heavy quark, relativistic effects such as colour magnetism vanish as  $m_Q \rightarrow \infty$  since the heavy-quark spin decouples from the light-quark degrees of freedom. For  $N_h$  heavy-quark flavours, there is thus an  $SU(2N_h)$  spin-flavour symmetry group, under which the effective strong interactions are invariant. (The flavour symmetry is analogous to the fact that different isotopes have the same chemistry, since to a good approximation the wave function of the electrons is independent of the mass of the nucleus; the nuclear spin decouples in the limit  $m_e/m_N \rightarrow 0$ ). Symmetry-breaking corrections in heavy-light systems can be studied in a systematic way within the Heavy Quark Effective Theory (HQET) where these effects depends on few phenomenological parameters. Here we limit ourselves to spectroscopic applications and do not touch semileptonic decays, most extensively studied within HQET.

In the limit  $m_Q \rightarrow \infty$ , the spin of the heavy quark and the total angular momentum  $j$  of the light quark inside a hadron are separately conserved by the strong interactions. Because of heavy-quark symmetry, the dynamics is independent of the spin and mass of the heavy quark. Hadronic states can thus be classified by the quantum numbers (flavour, spin, parity, etc.) of the light-quark degrees of freedom. Instead of the usual LS coupling scheme,  $Q\bar{q}$  mesons are more efficiently characterised in the  $jj$  coupling scheme. The total spin of a  $Q\bar{q}$  meson then decomposes into the spin  $\vec{s}_Q$  and the angular momentum  $\vec{j}_q = \vec{\ell}_q + \vec{s}_q$  where  $\vec{\ell}_q$  and  $\vec{s}_q$  are angular momentum and spin of the light quark. The total spin-parity is then given by  $J^P = \frac{1}{2}^- \otimes j_q^p$ . In this basis, the lowest states comprise three doublets labelled by  $j_q^p = \frac{1}{2}^-, \frac{1}{2}^+, \text{ and } \frac{3}{2}^+$ . Table 4 lists the classification of  $Q\bar{q}$  states in the two coupling schemes.

The different bases impose different multiplet structures on the  $D$  spectrum. For small spin-orbit interactions, the spectroscopic  $LS$  basis has an  $S$ -wave ( $D, D^*$ ) doublet and a  $P$ -wave quadruplet, the  $(jj)$  scheme has three doublets. The light components of heavy-quark-symmetry wave functions do not depend on the spin of the heavy quark. This leads to predictions [183] for the decay-width ratios for hadronic transitions between different  $jj$  multiplets like  $D_1 \rightarrow D + \pi$ ,  $D_1 \rightarrow D^* + \pi$ ,  $D_0 \rightarrow D + \pi$ ,  $D_2 \rightarrow D + \pi$ , which are found to be in good agreement with experiment.

The predictions of heavy quark effective field theory will be used as a guide to appreciate the significance of recently discovered  $D$  and  $D_s$  resonances.

Table 4  
Low-lying  $Q\bar{q}$  states in the LS and JJ coupling scheme.

	$D$	$D^*$	$D_0^*$	$D_1$	$D'_1$	$D_2^*$
$J^P$	$0^-$	$1^-$	$0^+$	$1^+$	$1^+$	$2^+$
$(2S+1)L_J$	${}^1S_0$	${}^3S_1 - {}^3D_1$	${}^3P_0$	${}^3P_1 - {}^1P_1$	${}^3P_1 - {}^1P_1$	${}^3P_2$
$\ell_q$	0	0	1	1	1	1
$j_q^p$	$\frac{1}{2}^-$	$\frac{1}{2}^-$	$\frac{1}{2}^+$	$\frac{1}{2}^+$	$\frac{3}{2}^+$	$\frac{3}{2}^+$
decay	–	–	$(DP)_S$	$(D^*P)_S$	$(D^*P)_D$	$(DP)_D$

## 2.7 Meson decays

Lattice gauge calculations have shown how hadronic decays may occur: when a meson is excited, the string connecting quark and antiquark is expanded until it reaches an energy excitation from which a transition to a meson-meson final state is allowed. It is natural to assume that the  $q\bar{q}$  pair just created carries the quantum numbers of the vacuum.

The  $^3P_0$  model of strong decays was suggested nearly 40 years ago by Micu [184] and further developed by the Orsay group [185, 186]. Extensive calculations were carried out by Barnes and collaborators [58–60]; references to earlier work can be found in these papers. The results provide an important auxiliary tool in the discussion of the nature of new states.

Other approaches were attempted. The discovery of the charmonium system with its positronium-like level pattern motivated the use of a one-gluon-exchange potential and of the assumption that hadronic decays proceed via time-like gluons [187, 188]. Instantons induce transitions not only from one  $q\bar{q}$  pair by a four-point interaction but also transitions of type  $u\bar{u} \rightarrow (d\bar{d}s\bar{s})$ . Due to their nature, instantons become effective only for decays of scalars into two pseudoscalar mesons and for pseudoscalar decays into a pseudoscalar plus a scalar meson. Results of first calculations were reported in [189]. Of course, instanton-induced decays could interfere with other decay mechanisms; an assignment of scalar and pseudoscalar mesons to flavour multiplets or glueballs using arguments based on a particular decay model is therefore extremely difficult or even impossible.

## 2.8 Effective chiral symmetry restoration

For light-quark mesons and for sufficiently high radial or orbital excitations both, chiral symmetry and  $U_A(1)$  symmetry, could be effectively restored as suggested by Glozman [190]. The momenta of valence quarks could increase at large hadron excitation energies and could then decouple from the chiral condensates of the QCD vacuum. As a consequence, the dynamical quark mass is reduced. For the physics of low-lying hadrons, the chiral-symmetry-breaking condensates are crucially important. The physics of highly-excited states is suggested to be decoupled from these chiral symmetry breaking effects. Asymptotically, the states may approach a regime where their properties are determined by the underlying unbroken chiral symmetry (i.e. by the symmetry in the Wigner-Weyl mode). In this case hadrons should gradually decouple from the Goldstone bosons [191] and form new multiplets. If chiral symmetry is restored, the states fall into approximate multiplets of  $SU(2)_L \times SU(2)_R$  [192]. In the usual potential model classification  $I, J^{PC}$ , chiral symmetry restoration leads to the following mass relations:

$$\begin{aligned} \mathbf{J} = \mathbf{0} \quad & 1, 0^{-+} \leftrightarrow 0, 0^{++}; \quad 1, 0^{++} \leftrightarrow 0, 0^{-+} \\ \mathbf{J} = 2\mathbf{k} \quad & 0, J^{--} \leftrightarrow 0, J^{++}; \quad 1, J^{-+} \leftrightarrow 0, J^{++}; \quad 1, J^{++} \leftrightarrow 0, J^{-+}; \quad 1, J^{++} \leftrightarrow 1, J^{--} \\ \mathbf{J} = 2\mathbf{k} - \mathbf{1} \quad & 0, J^{++} \leftrightarrow 0, J^{--}; \quad 1, J^{+-} \leftrightarrow 1, J^{--}; \quad 1, J^{--} \leftrightarrow 0, J^{+-}; \quad 1, J^{--} \leftrightarrow 1, J^{++} \end{aligned}$$

The  $U_A(1)$  symmetry connects opposite-parity states of the same isospin but from different  $SU(2)_L \times SU(2)_R$  multiplets, for example  $1, 0^{-+} \leftrightarrow 1, 0^{++}$ . Chiral symmetry restoration requires a doubling of some of the radial and angular Regge trajectories for  $J > 0$ . At large excitations, some of the  $\rho$ -mesons have  $a_1$  mesons as their chiral partners, while the other  $\rho$ -meson excitations are chiral partners of  $h_1$  mesons. In section 6, the predictions will be confronted with experimental results.

## 2.9 Solvable models

The relation between the spectroscopy of excited hadrons in the resonance region and their partonic degrees of freedom observed in deep inelastic scattering is one of the most challenging tasks in strong interaction physics. A promising direction has been proposed by Maldacena [193] who proposed a connection between the strongly coupling limit of a conformal field theory (CFT) defined on the AdS asymptotic boundary [194, 195], and the propagation of weakly coupled strings in a higher dimensional Anti-de-Sitter (AdS) space, where physical quantities can be computed. QCD is not a conformal theory but for an approximately constant coupling constant and for vanishing quark masses, QCD is similar to a strongly-coupled conformal theory. Holographic duality requires a higher dimensional warped space with negative curvature and a four-dimensional boundary. The equations of motion in the AdS space are expressed as effective light-front equations which describe holographic light-front eigenmodes dual to QCD bound states [108]. The eigenvalues of the effective light-front equation reproduce the mass spectra of light-quark mesons and baryons, the eigensolutions their valence wavefunctions. Confinement can be modelled by a ‘hard wall’ cutting off AdS space in the infrared region [107] or spacetimes can be capped off smoothly by a ‘soft wall’ [106].

On the basis of this ADS/CDF correspondence, a number of results on nonperturbative QCD were obtained: from chiral symmetry breaking [196, 197] to the pattern of highly excited states [106, 108], to meson decay constants, form factors, and to exclusive scattering amplitudes [198]. From these amplitudes, valence, sea-quark and gluon distributions, and generalized parton distributions measured in deeply virtual Compton scattering can be determined. A survey of the achievements can be found in recent papers of Brodsky and de Teramond [199, 200].

## 2.10 Have we gained insight from $q\bar{q}$ mesons?

“The purpose of computing is insight not numbers”, a memorable phrase used repeatedly by Hamming throughout his book on Numerical Methods for Scientists and Engineers [201]. Quark models have the intent to provide insight: to identify the leading mechanisms which result in the observed spectrum of hadron resonances and their decays. However, there are three fully developed quark models; one could try to identify the model with the best  $\chi^2$  for a minimum number of parameters as matching physics reality best, but a good  $\chi^2$  does not prove that the model is correct.

All calculations reproduce the  $\pi - \eta - \eta'$  splitting, although the underlying dynamics differ widely. In the relativised quark model of Godfrey and Isgur [171], the non-degeneracy of  $\pi$  and  $\eta$  is due to the inclusion of an extra annihilation amplitude, whereas in the other models it is attributed to an explicit flavour dependence in the quark-antiquark interaction. In the Bonn quark model these are based on instanton effects, which simultaneously accounts for the  $\rho/\omega - \pi$ ,  $K^* - K$  and  $\pi - \eta - \eta'$  splittings through non-vanishing  $u\bar{u} \leftrightarrow d\bar{d}$ ,  $u\bar{u} \leftrightarrow s\bar{s}$ , and  $d\bar{d} \leftrightarrow s\bar{s}$  amplitudes. In the Goldstone-boson-exchange model these splittings are due to the explicit flavour dependence of the various meson exchanged. The largest differences turn up for the scalar mesons: Whereas the relativised quark model concurs with the usual folklore to yield degenerate isoscalar and isovector states around  $1 \text{ GeV}/c^2$ , and the strange scalar state around  $1.25 \text{ GeV}/c^2$ , the other models predict that the scalar spectrum show splittings similar to the pseudoscalar case but of opposite sign.

All models account very well for the position of the lowest state in each flavour sector even up to the highest masses and total angular momenta. Note however, that Vijande, Fernandez and

Valcarce [172] only quote results for  $J \leq 3$ , related to their choice of a “screened” confining potential. The two models which include one-gluon exchange account somewhat better for the observed splittings (and mixing) of radially excited vector meson states. The Bonn quark model contains only the confining potential in this sector and has nearly no spin-orbit and/or tensor interactions. Thus the spin-singlet and spin triplet  $1^+$  strange mesons are in fact degenerate. None of the models produces more than one  $\eta$  states between 1 and  $1.5 \text{ GeV}/c^2$  (where the PDG [1] lists 3), for a discussion see section 8.

Obviously, strong interaction dynamics can be based on very different physical pictures, and still give reasonable descriptions of experimental data. Lattice QCD can serve here as additional support for the assumptions underlying the different quark models. Instantons can be observed in lattice QCD by cooling the highly fluctuating field configurations [202]. Cooling removes the perturbative part of the gauge fields and leaves the classical configurations. Likely, the rapid field changes in the initial phase are caused by one-gluon exchange dynamics. The  $\rho - \pi$  and the  $N - \Delta$  splitting can e.g. originate from one-gluon exchange; in this case, cooling would be expected to lead to a shrinkage of this mass splitting. If instantons are responsible, the splittings should not be effected by cooling. It turned out (Chu et al. [203]) that most particle masses, in particular also the  $\rho$  and  $\pi$  masses, changed very little when the gauge configurations were cooled. The observation suggests that the mass splittings are largely due to instantons. However, the mass splitting between the nucleon and  $\Delta$  was reduced by smoothing; thus one-gluon exchange dynamics seems to be responsible for the  $N - \Delta$  splitting. However, Chu et al. [203] assigned the latter observation to a technical problem. We are not aware that this important question was addressed more recently.

### 3 Major experiments

The importance of the development of new scientific instruments for particle physics cannot be overestimated. New experimental methods have often opened new directions while new demands and new questions stimulated important technical achievements. In this section we give a short description of major detectors with which the results to be presented and discussed in this report were obtained. The section is not meant to review the achievements in detector technology; rather it should serve the reader as short reference information on experimental aspects when physics results are discussed.

#### 3.1 Diffractive and charge exchange experiments

##### 3.1.1 *The CERN-Munich experiment*

The CERN-Munich spectrometer at the CERN Proton Synchrotron is described in detail in [204]. The spectrometer was used to study final states with two charged particles originating from the interaction of a  $\pi^-$  beam with hydrogen and transversely-polarised butanol targets. The beam particles were momentum analysed and tagged by a beam spectrometer and Cherenkov counter. A 1 mm thick scintillation counter behind the target was used to determine the charged particle multiplicity. The particle trajectories were measured, using proportional chambers and magnetoresistive spark chambers, in front and behind of a magnetic spectrometer with  $50\text{ cm} \times 150\text{ cm}$  aperture. Scintillation counters and a hodoscope were used in the trigger. Particle identification was provided by two multicell threshold Cherenkov counters. The target – suspended inside a 2.5 T magnetic field – was surrounded by a veto box of tungsten-scintillation shower counters which vetoed events with  $\pi^0$ 's and charged recoil multiplicities above one. A 36-element hodoscope measured the azimuthal angle of the recoil proton to ensure, for events with  $|t| > 0.08 (\text{GeV}/c)^2$ , coplanarity of the reaction. Most of the data were recorded at  $17.2\text{ GeV}/c$  momentum and a trigger requiring two charged particles in the final state. The results of the CERN-Munich collaboration are published in [204–211]. For later data, a polarised target was used (CERN-Munich-Krakow collaboration) [212, 213].

##### 3.1.2 *The WA3 experiment*

The experiment WA3 carried out by the ACCMOR collaboration started data taking at CERN SPS in 1977. In the initial stage it used secondary beams of  $60\text{ GeV}/c$  and  $93\text{ GeV}/c$  momenta tagged with Cherenkov counters. The apparatus comprised a two-magnet forward spectrometer with 80 magnetoresistive wire spark chamber planes and two multicellular Cherenkov detectors. The 50 cm liquid-hydrogen target was surrounded with scintillator-lead sandwiches. Proportional chambers and scintillation hodoscopes were used to select the forward charged-particle multiplicity. Veto sandwiches around the target and in front of magnets were used to suppress events with secondaries out of aperture. Most results on meson spectroscopy are devoted to diffractive production of meson resonances in pion and Kaon beams [214–219]. In these studies two triggers were used, either an unbiased trigger asking only for a preset multiplicity in forward direction, or a trigger with an additional cut on the momentum squared transfer,  $|t| > 0.16 (\text{GeV}/c)^2$ . In 1981 this detector was upgraded to study inclusive production of charmed particles.

### 3.1.3 The LASS experiment

The LASS facility was a general purpose spectrometer at SLAC designed primarily for meson spectroscopy [220, 221]. It had  $4\pi$  geometrical acceptance with excellent angular and momentum resolution, full azimuthal symmetry, particle identification, and high-rate data acquisition capability. LASS contained two magnets filled with tracking detectors. The first magnet was a superconducting solenoid with a 2.24 T field parallel to the beam direction. This magnet was followed by a 3 Tm dipole magnet with a vertical field. The solenoid was used in measurements of interaction products having large production angles and relatively low momenta. High-energy secondaries with small polar angle passed through the dipole for measurements of their tracks. Particle identification was provided by a Cherenkov counter, a time-of-flight hodoscope which filled the exit aperture of the solenoid, and by a Cherenkov counter at the exit of the dipole spectrometer. In addition,  $dE/dx$  ionisation energy loss was measured in a cylindrical drift chamber surrounding the liquid  $H_2$  target to separate wide-angle protons from pions at momenta below 600 MeV/c. LASS was situated in an RF-separated beam line delivering a 5–16 GeV/c Kaon beam of high purity. Cherenkov counters were used to tag Kaons. The poor duty factor of the SLAC beam limited the useful flux to  $\sim 250 \div 500$  particles per second. The trigger accepted all interactions in the target except all-neutral final states. The total LASS Kaon program contained 135 million events collected in 1982. The results were published in [220, 222–226].

### 3.1.4 The VES experiment

The detector VES at Protvino was designed to study multiparticle decays of mesonic resonances produced in  $\pi^-N$  and  $K^-N$  interactions at beam momenta of  $20 \div 40$  GeV/c produced in the 70 GeV/c proton synchrotron (Fig. 16). The beam particles were tagged with three threshold Cherenkov counters and their coordinates measured at the entrance to the spectrometer with

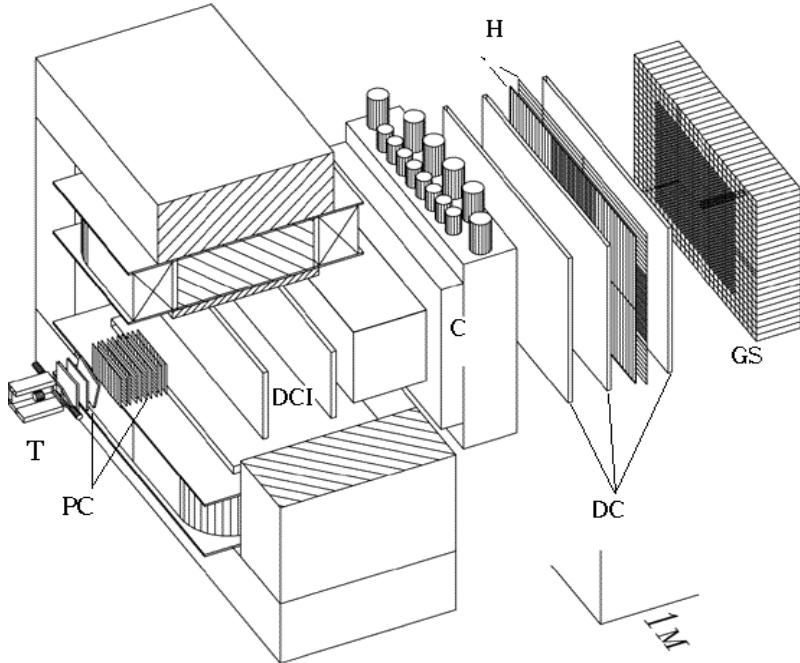


Fig. 16. Experiment VES [227]: T - target with veto counters and lead-scintillator sandwiches, PC - proportional chambers, DCI - inner drift chambers, DC - drift chambers, C - Cherenkov counter, H - hodoscope, GS - gamma spectrometer.

proportional chambers. A beryllium target of 4 cm in diameter and 4 cm in length was used. On both sides, a 3 cm aluminium shield absorbed low momentum charged particles; veto scintillation counters were used in the trigger, lead-scintillator sandwiches to tag events in which  $\pi^0$  mesons were emitted into the backward hemisphere in the centre of mass of the reaction. In forward direction the required multiplicity was selected with scintillation counters near the target and two coordinate scintillation hodoscopes  $H$  behind the wide aperture ( $100\text{ cm} \times 150\text{ cm}$ ) magnet. Tracking was provided by 16 planes of proportional chambers ( $PC$ ) in front of the magnet, four planes of minidrift chambers ( $DCI$ ) inside the magnet, and nine planes of drift chambers behind the magnet. Particles were identified with multicell Cherenkov counters ( $C$ ) which discriminate pions and Kaons in the  $4.4 \div 18\text{ GeV}/c$  momentum range. Photons were registered in a multicell lead glass spectrometer (in total 1200 cells). Veto sandwiches in front of the magnet and behind it made the spectrometer nearly completely hermetical for charged particles and photons. Most data were collected with a trigger on two or more charged particles in forward direction and a veto on high-momentum charged particles in side direction. The results on meson spectroscopy are published in [228–246].

### 3.1.5 Experiment E852 at BNL

The Multi-Particle spectrometer (MPS) shown in Fig. 17 was located at the Brookhaven Alternating Gradient Synchrotron. All data were obtained in a  $18\text{ GeV}/c \pi^-$  beam. The basic element of this detector was a 5 m long wide-aperture magnet. The apparatus [247] consisted of 3 regions: target, tracking, and downstream region. The target region was located in the middle of the magnet and contained a liquid hydrogen target, multilayer wire-chambers used to trigger on recoil protons, and a 198-element cylindrical thallium-doped caesium iodide array ( $CsI$ ) capable of rejecting events with wide-angle photons. Main components of the tracking system were located at the downstream end of the magnet where 3 proportional wire chambers and 6 drift chamber modules with 7 planes each were placed. Interspersed among these were three proportional wire chambers for trigger purposes, a window-frame lead-scintillator photon veto counter

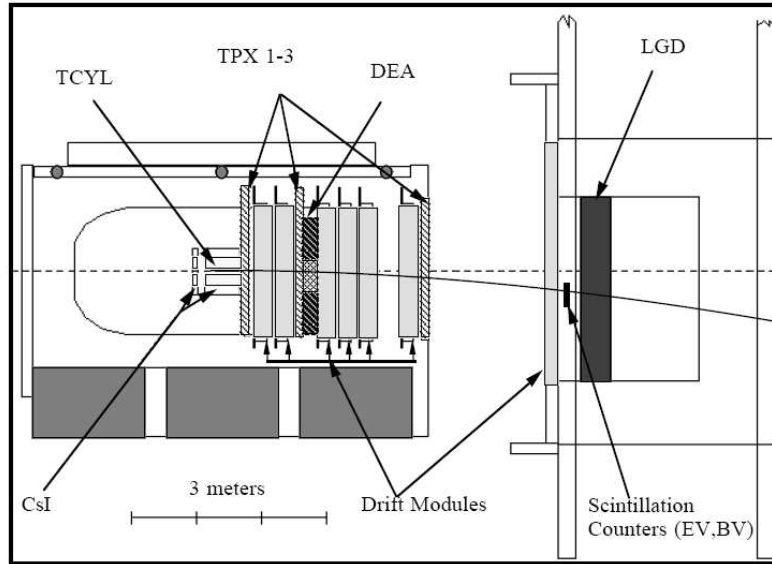


Fig. 17. Experiment E 852 at BNL [247]: TCYL: four-layer cylindrical drift chamber,  $CsI$ : caesium iodide array, DEA: lead scintillator sandwich photon veto counter, TPX1-3: proportional wire chambers, LGD: lead glass detector.

to ensure photon hermeticity, a scintillation counter to veto forward charged tracks for neutral triggers, and scintillation counters to identify charged particles entering the photon veto counter. The downstream region contained a 3045 element lead-glass calorimeter. For some experiments, multicell Cherenkov counters were used for particle identification of secondaries. The experiment was mainly devoted to the study of mesonic states with exotic quantum numbers. The results can be found in [247–262].

### 3.2 Central production experiments

#### 3.2.1 The WA76 and WA91 experiments

The WA76 experiment was designed to study mesons produced centrally at the largest beam momenta available. First data were taken at 85 GeV/c; the majority at 300 GeV/c and some data at 450 GeV/c. The experiment was based on the CERN  $\Omega$  spectrometer. The hadron (pions, protons) beam impinged on a 60 cm long  $H_2$  target; two Cherenkov counters identified the beam particle. Excitation of the target proton was vetoed in horizontal scintillation slabs surrounding the target. One (and only one) fast particle had to traverse the forward particle region, equipped with multi-wire proportional chambers, but should not hit veto counters defining non-interacting beam particles. At least two particles were required in the two drift chambers near the target. Cherenkov counters were used to identify pions and Kaons.

The experiment was devoted to the study of meson resonances and the search for glueballs. The results can be found in [263–275]. A few related results were published by the WA91 experiment [276–278] using a similar setup.

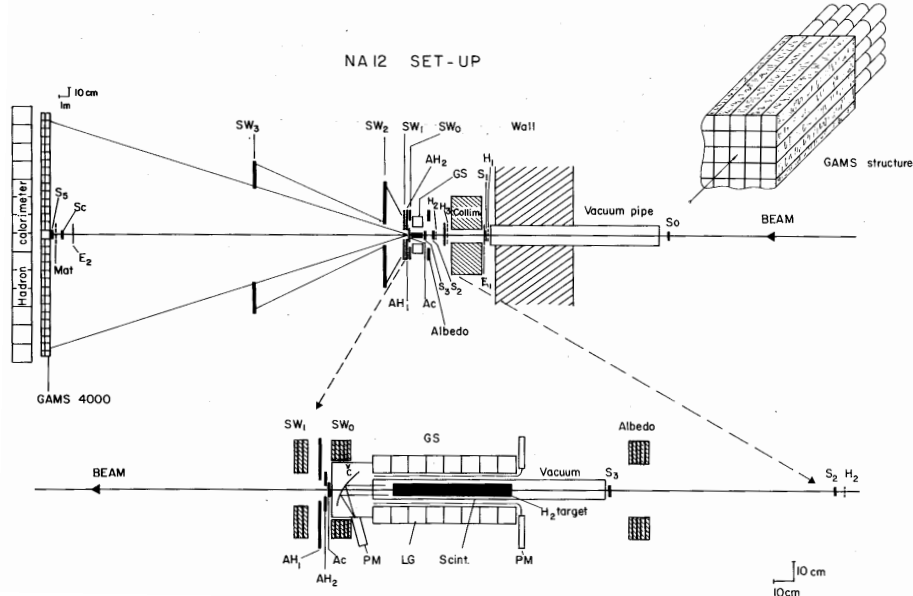


Fig. 18. Schematic view of the GAMS-4000 experiment at CERN.  $S$ : beam scintillation counters;  $H$ : beam hodoscope;  $SW$  and albedo: lead-scintillator sandwich counters;  $AC$ ,  $AH$ : scintillation counters [279].

### 3.2.2 The GAMS experiment

The GAMS experiment was designed to detect neutral mesons decaying into photons in high-energy reactions. Its main component was a wall of lead glass cells. 2000 cells were combined for experiments at IHEP, Protvino, in a 40 GeV/c pion beam; GAMS-4000 was built for experiments at the CERN SPS. The latter setup is reproduced in Fig. 18. The pion beam traversed the 50 cm long liquid H<sub>2</sub> target and was detected in scintillation counters and by Cherenkov light produced in H<sub>2</sub>. The opening angle of the light cone was used to determine the longitudinal coordinate of the interaction point. A range of scattering angles was allowed in forward scintillators. Target fragmentation or excitation of the target proton was suppressed by scintillators and lead glass counters surrounding the target.

The lead glass wall consists of 4092 cells and covers an area of 5 m<sup>2</sup>. A 100 GeV photon was measured with a precision of about 1.5 GeV in energy; the impact point was localised to 1 mm<sup>2</sup>. Results from GAMS can be found in [280–291].

### 3.2.3 WA102 experiment

The WA102 experiment was built as combined effort of the former WA76 and GAMS collaborations. The WA76 served as charged-particle tracker, the GAMS-4000 detector was installed in the forward region to detect photons. This combination provided the possibility to study events with charged and neutral particles and thus extended the range of the WA76 and GAMS experiments considerably. The results of the experiment were reported in a series of letter publications [292–314].

## 3.3 Antiproton-proton annihilation

### 3.3.1 The Asterix experiment

The Asterix experiment studied  $\bar{p}p$  annihilation from *S*- and *P*-wave orbitals by stopping antiprotons in H<sub>2</sub> gas at room temperature and pressure and observing the coincident X-ray spectrum. The detector consisted of a gas target (45 cm length and 14 cm in diameter), a X-ray drift chamber and seven multi-wire proportional chambers, partly with cathode readout to provide spatial resolution along the wires. Two end-cap detectors with three wire planes and cathode readout on both sides gave large solid-angle coverage. The assembly was situated in a homogeneous magnetic field of 0.8 T. The energy resolution of the detector for 8 keV X-rays was about 20%. The momentum resolution for  $\bar{p}p \rightarrow \pi^+\pi^-$  events at 928 MeV/c was 3%. Pions and Kaons could be separated up to 400 MeV/c. The detector is fully described in [315]. Physics results related to meson spectroscopy were published in [316–322].

### 3.3.2 The Crystal Barrel experiment

The Crystal Barrel spectrometer is shown in Fig. 19. A detailed description of the apparatus, as used for early data-taking (1989 onwards), is given in [323]. In 1995, a microstrip vertex detector surrounding the target was added [324]. Target and vertex detector were surrounded by a cylindrical jet drift chamber having 30 sectors with each sector having 23 sense wires. The coordinate along the wire was determined by charge division. A momentum resolution for pions of less than

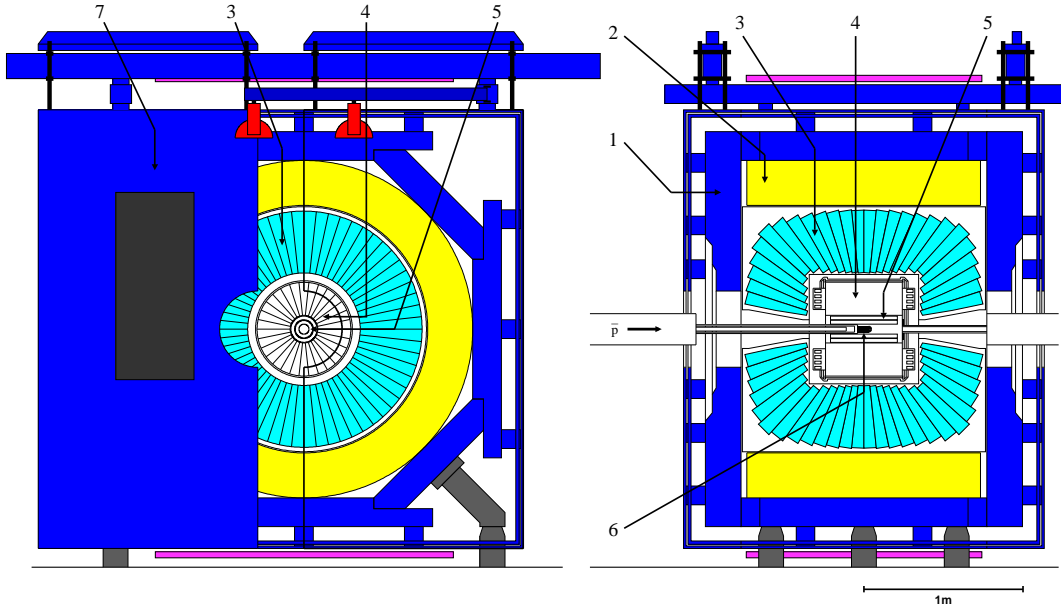


Fig. 19. Overall layout of the Crystal Barrel detector showing (1) magnet yoke, (2) magnet coils, (3)  $CsI$  barrel, (4) jet drift chamber, (5) proportional chamber, (6) liquid hydrogen target, (7) one half of endplate. Left - longitudinal cross section; Right- transverse view.

2% at  $200\text{ MeV}/c$  was obtained, rising to 4.2% at  $1\text{ GeV}/c$  for those tracks traversing all layers of the JDC. The JDC also provided  $\pi/K$  separation below  $500\text{ MeV}/c$  by ionisation sampling. The whole detector was situated in a  $1.5\text{ T}$  solenoidal magnet with the incident antiproton beam direction along its axis.

Physics results related to meson spectroscopy are published in [325–357]. Most Crystal Barrel data on  $\bar{p}p$  annihilation in flight were analyzed by the QMC-Rutherford-Gatchina group [358–382]. Meson spectroscopy with the Crystal Barrel is reviewed for  $\bar{N}N$  annihilation at rest by Amsler [46] and Amsler and Tornqvist [48], and in flight by Bugg [49].

### 3.3.3 The Obelix experiment

The Obelix spectrometer is based on the open-axial field magnet which had previously been used for experiments at the ISR. The magnet provides a field of  $0.5\text{ T}$  in an open volume of about  $3\text{ m}^3$ . A full description of the detector can be found in [383].

The Obelix detector consists of an imaging vertex detector with three-dimensional readout for charged tracks and X-ray detection, a jet drift chamber (JDC) for tracking and particle identification by  $dE/dx$  measurement with 3280 wires and flash-analog-to-digital readout, a system of two coaxial barrels of plastic scintillators consisting of 30 (84) slabs positioned at a distance of 18 cm (136 cm) from the beam axis for time-of-flight (TOF) measurements, and a high-angular-resolution gamma detector (HARGD) [384]. The momentum resolution for monoenergetic pions (with  $928\text{ MeV}/c$ ) from the reaction  $\bar{p}p \rightarrow \pi^+\pi^-$  was determined to 3.5%,  $\pi^0$  were reconstructed with a mass resolution of  $\sigma_{\pi^0} = 10\text{ MeV}/c^2$  and a momentum-dependent efficiency of 15 to 25%. The detector system was used with a liquid  $H_2$  ( $D_2$ ) target, a gaseous  $H_2$  target at room temperature and pressure, and a target at low pressures (down to 30 mbar). The wide range of target densities provided detailed information about the influence of the atomic cascade on the annihilation process. For part of the time, a  $\bar{n}$  beam was produced by charge exchange in a liquid  $H_2$  target

(positioned 2 m upstream of the centre of the main detector). The intensity of the collimated beam was about  $40 \bar{n}/10^6 \bar{p}$  of which about 30% interact in the central target. The  $\bar{n}$  beam intensity was monitored by a downstream  $\bar{n}$  detector.

The Obelix Collaboration had a broad program of experiments covering atomic, nuclear and particle physics [383]. Main results related to meson spectroscopy can be found in [385–395].

### 3.3.4 Experiment E760/E835 at FNAL

Antiproton-proton annihilation in flight was studied by the E760/E835 experiment at Fermilab [396] (see figure 20). Antiprotons were produced by bombarding a target with high-energy

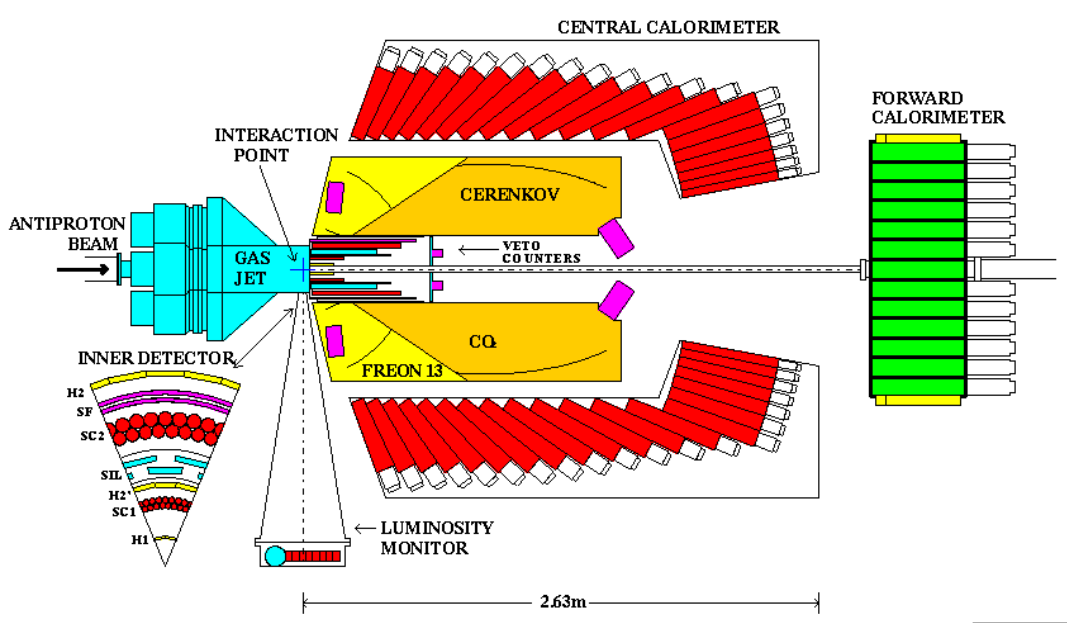


Fig. 20. Experiment E760/E835 at FNAL [396].

protons. The antiprotons were cooled in phase space in a storage ring and then accelerated to study  $\bar{p}p$  collisions at extremely high energies. A fraction of the antiprotons were used for medium-energy physics:  $8 \cdot 10^{11}$  antiprotons circulated in the Fermilab accumulator ring with a frequency  $f_{rev} = 0.63$  MHz. At each revolution, antiprotons passed through a hydrogen gas jet target, with  $\rho_{jet} = 3 \cdot 10^{14} \text{H}_2/\text{cm}^3$ , which results in a luminosity  $L = N_{\bar{p}} f_{rev} \rho_{jet}$  of  $2 \cdot 10^{31}/\text{cm}^2\text{s}$ . The energy of the antiproton beam, and thus the invariant mass of the  $\bar{p}p$  system, could be tuned very precisely according to  $\sqrt{s} = m_p \cdot \sqrt{2(1 + E_{\bar{p}}/m_p)}$ . The observed rate  $R = 2 \cdot 10^6/\text{s}$  due to the hadronic background is related to the luminosity by  $R = \sigma \cdot L$ .

Most data taken at this experiment were devoted to a study of the charmonium system. We give reference to a few of them [397–402]. E760 also produced results on light meson spectroscopy [403–405].

### 3.4 Electron-positron annihilation experiments at $\Phi$ and $c\bar{c}$ factories

#### 3.4.1 VEPP

The collider VEPP-2M was constructed at BINP, Novosibirsk, in 1974 and stopped in 2000. Its main parameters were:

$$2E = 0.4\text{--}1.4 \text{ GeV} \quad L_{max} = 4 \times 10^{30} \text{ cm}^{-2}\text{s}^{-1}$$

total integrated luminosity  $\approx 80 \text{ pb}^{-1}$        $10^9$  recorded events.

For 25 years this facility was one of the main sources of information on  $e^+e^-$  annihilation at relatively low energies. Precision data in this region are important not only for hadron spectroscopy but for precision electroweak physics as well. Indeed, this region gives the main hadronic contribution to the muon anomalous magnetic moment [406].

One of the well known achievements of this laboratory is the method of high precision mass measurements by resonant depolarisation. It was proposed and developed at BINP [407, 408] and widely used by BINP and by other laboratories. Electrons and positrons in storage rings can become polarised due to emission of synchrotron radiation. Spins of polarised electrons (positrons) precess around the vertical magnetic field with frequency  $\Omega$  which is related to the particle energy  $E$  and the revolution frequency  $\omega$ :

$$\Omega = \omega(1 + \gamma \cdot \mu_a / \mu_0) \quad (3.1)$$

where  $\gamma = E/m_e$ ,  $m_e$  is the electron mass,  $\mu_a$  and  $\mu_0$  are anomalous and normal parts of the electron magnetic moment. The precession frequency can be measured using resonant depolarisation. The polarised beam is exposed to an external electromagnetic field with the frequency  $\Omega_D$ :

$$\Omega \pm \Omega_D = \omega \cdot n \quad (3.2)$$

with any integer  $n$ . The frequency  $\Omega_D$  is scanned. At resonance, the polarisation disappears. This allows them to measure the value of  $E = \gamma \times m_e$  with very high precision. The relative mass precision achieved with this method is  $3 \cdot 10^{-5}$  for  $\phi(1020)$ ,  $5 \cdot 10^{-6}$  for  $J/\psi(1S)$  and  $2 \cdot 10^{-5}$  for  $\Upsilon(1S)$ .

First results at VEPP-2M were obtained with the nonmagnetic detectors OLYA [409] and ND [410]. Later two more advanced detectors SND [411, 412] and CMD [413] were commissioned. The main part of the SND (Spherical Neutral Detector, Fig. 21) was a three-layer spherical highly granulated NaI(Tl) calorimeter, consisting of 1632 individual crystals. The calorimeter thickness was 13.5 radiation lengths, its total mass 3.6 tons. Its energy resolution for photons as a function of their energy was determined to  $\sigma_E/E = 4.2\% / E_{[\text{GeV}]}^{1/4}$ . The inner part of the detector was a cylindrical drift chamber system for tracking of charged particles. The solid angle coverage for the inner chamber was 96% of  $4\pi$ . Outside of the calorimeter muon veto detectors were installed consisting of streamer tubes and scintillation counters. Results of this experiment related to meson spectroscopy are published in [414–434].

The detector CMD-2 (Cryogenic Magnetic Detector) was commissioned at BINP in 1990. The detector consisted of a cylindrical drift chamber surrounding the collision region, with  $250\mu$  resolution in the plane transverse to the beam axis, and a double-layer multiwire cylindrical proportional chamber. Both chambers were placed inside of a very thin (0.38 radiation lengths) superconducting solenoid with a field of  $B = 1.5 \text{ T}$ . The barrel  $CsI$  calorimeter – with a thickness of  $8.1X_0$  –

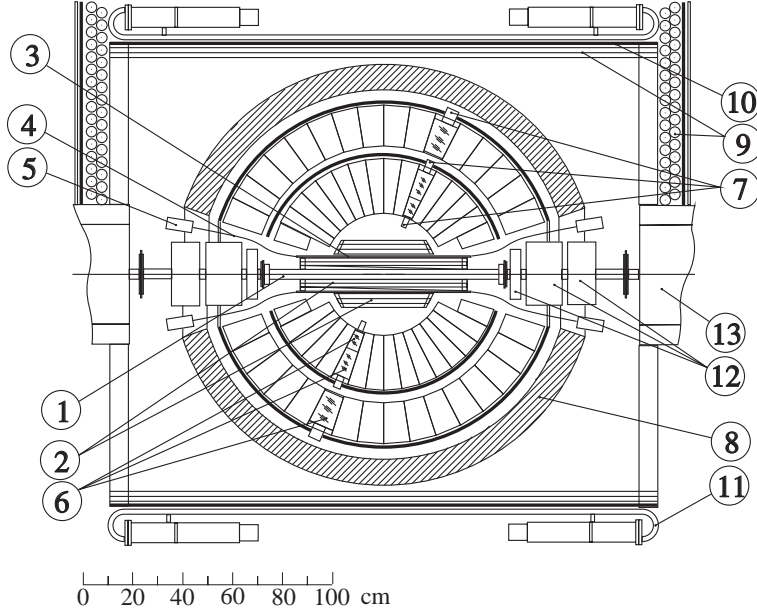


Fig. 21. Experiment SND [420]. Side view: 1 - beam pipe, 2 - drift chambers, 3 - scintillation counters, 4 - fiber lightguides, 5 - PMTs, 6 - NaI(Tl) counters, 7 - vacuum phototriodes, 8 - iron absorber, 9 - streamer tubes, 10 - iron plates, 11 - scintillation counters, 12 - magnetic lenses, 13 - bending magnets.

and a muon range detector were placed outside of the solenoid. The energy resolution for photons in the energy range from 100 to 700 MeV was about 9%, the angular resolution of the order of 0.02 radians. End-cap BGO calorimeters of  $13.4X_0$  thickness were placed inside the solenoid. The detector was nearly fully hermetic for photons. Results of this experiment related to meson spectroscopy are published in [435–455]. In the near future, both detectors – SND and CMD-2 – will work at the new high-luminosity  $e^+e^-$  collider VEPP2000 presently being constructed at BINP.

Recently one more modern facility, KEDR, started data taking at BINP. It occupies one interaction region at the VEPP-4M -  $e^+e^-$  collider. VEPP-4M will reach a maximum beam energy of  $E = 6\text{ GeV}$  and a luminosity of  $L = 10^{31}\text{ cm}^{-2}\text{ s}^{-1}$ . The main goal of the experiments at this facility are very high precision measurements of the  $\tau$ -meson [456] and of the  $\psi$  [457] and  $\Upsilon$  families as well as two-photon physics using a dedicated zero-angle spectrometer for scattered electrons and positrons. The KEDR detector consists of a vertex detector, drift chamber, time of flight system of scintillation counters, a particle identification system based on aerogel Cherenkov counters, a calorimeter (with liquid krypton in the barrel part and  $CsI$  crystals in the end caps), and a muon tube system inside and outside of the magnet yoke.

### 3.4.2 KLOE at Daphne

DAPHNE, the Frascati  $\phi$  factory, is an  $e^+e^-$  collider working at  $2E \approx m_\phi \approx 1.02\text{ GeV}$  with a design luminosity of  $5 \cdot 10^{32}\text{ cm}^{-2}\text{ s}^{-1}$ .  $\phi$  mesons are produced essentially at rest with a cross section of  $\approx 3.2\mu b$ . The main decay modes are  $K^+K^-$  and  $K_S^0K_L^0$  pairs so that pure and monochromatic  $K_S^0, K_L^0, K^+$  and  $K^-$  beams can be obtained. A survey of tests of CP and CPT invariance is given in [458]. This facility is used also to study light quark spectroscopy.

The KLOE detector consists of a drift chamber [459] surrounded by an electromagnetic calorimeter

[460] and a superconducting solenoid providing a 0.52 T magnetic field. The drift chamber is of cylindrical shape, 4 m diameter and 3.3 m in length. This unusually big volume is needed to detect  $K_L^0$  decays. The momentum resolution is  $\sigma_p/p \leq 0.4\%$ . The electromagnetic calorimeter is a lead-scintillating-fiber calorimeter consisting of a barrel and two endcaps covering 98% of the solid angle. The energy resolution is  $\sigma_E/E = 5.7\%/\sqrt{E}$  ( $E$  in GeV). This detector has taken data for two years (2001  $\div$  2002) with a maximum luminosity of up to  $7.5 \cdot 10^{32} \text{ cm}^{-2}\text{s}^{-1}$ . An integrated luminosity of  $450 \text{ pb}^{-1}$ , equivalent to  $1.4 \cdot 10^9 \phi$  decays, was achieved. In 2004, KLOE resumed data taking with an upgraded machine. The KLOE results related to meson spectroscopy are published in [461–469].

### 3.4.3 Argus, Mark3 and DM2

Significant progress in meson spectroscopy came from the Argus (DESY), Mark3 (SLAC) and DM2 (Orsay) detectors. They stopped operation more than 20 years ago, and often their contributions are now replaced by new data with higher statistics. Some results are important still today; these will be discussed in the appropriate sections. Detectors, their performance and their achievements have been reviewed by Köpke and Wermes [470]. A report of the physics achievements of the ARGUS collaboration can be found in [471].

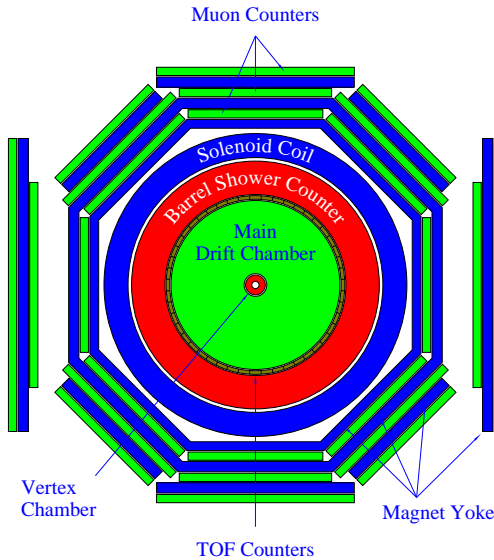
### 3.4.4 BES

The detector BES is installed at the  $e^+e^-$  collider BEPC at IHEP, Peking. The collider has a maximum energy of  $2E = 4.4 \text{ GeV}$  and a luminosity reaching  $10^{31} \text{ cm}^{-2}\text{s}^{-1}$ . It started to work in 1989. A very significant upgrade is planned for 2007 aiming at  $L = 10^{33} \text{ cm}^2\text{s}^{-1}$  luminosity. Up to now this facility provided record samples of  $J/\psi$  ( $64 \cdot 10^6$ ) and  $\psi'$  ( $18 \cdot 10^6$ ). The detector BES is based on a conventional solenoidal magnet. BES II is an upgraded version of the initial BES I detector. The layout is shown in Fig. 22. Inner tracking is provided by a 12-layer vertex chamber and a main drift chamber. The vertex detector is used in the trigger. Particle identification relies on  $dE/dx$  measurements in the drift chamber (with  $\approx 8\%$  resolution) and an array of 48 time of flight counters ( $\approx 200\text{ps}$  time resolution). Neutral particle detection is provided by a lead-gas shower detector with  $\sigma_E/E = 28\%/\sqrt{E}$  ( $E$  in GeV). The iron return yoke is instrumented with counters for muon identification. There is a large number of papers giving precise branching ratios for  $J/\psi$  and  $\psi'$  decays. The branching ratios and the comparison of  $J/\psi$  and  $\psi'$  decays is an interesting subject; here we just mention the 12% rule. Results on meson spectroscopy are published in [472–512].

## 3.5 Heavy-quark spectroscopy

### 3.5.1 Experiments at FNAL

Charmed quarks are copiously produced in high energy hadron beams owing to the high cross section, reaching a few hundreds  $\mu b$  at beam momenta of a few hundred  $\text{GeV}/c$ . As a rule, these events are singled out with precision microvertex detectors. A number of experiments were performed to study heavy quark physics in hadron and photon beams. Early studies at CERN [514–516] had only exploratory character and this direction of physics was given up. At Fermilab, important results were achieved by E687 [517] upgraded to the FOCUS experiment [518], by E691 [519], upgraded to E791, and the SELEX experiment. Here we describe the SELEX experiment as an



End view of the BES detector

Fig. 22. Experiment BES [513].

example of this approach. Experiment E760/E835 has been discussed in section 3.3.4.

The SELEX experiment used the Fermilab charged hyperon beam at 600 GeV/c to produce particles in a set of thin target foils of Cu or diamond. The negative beam was composed of about 50%  $\Sigma^-$  hyperons and 50%  $\pi^-$ . The positive beam had 90% protons. The main goal of the experiment was the study of particles carrying charm and strangeness. The beam particles were unambiguously identified with a transition radiation detector. The trajectories of charged secondaries were reconstructed in a three-stage magnetic spectrometer providing momentum resolution of  $\sigma_P/P < 1\%$  for a 150 GeV/c proton. A 10 m long Ring-Imaging CHERENKOV detector separated  $\pi$  from  $K$  up to 165 GeV/c. Three-stage lead glass spectrometers were used for electromagnetic calorimetry. A very high precision silicon vertex detector provided an average proper-time resolution of 20 fs for charm decays. A scintillation trigger was used to select events with the required topology. Charm candidates were selected using an online secondary vertex algorithm.

A large variety of results was obtained. Those relevant in the context of this paper were published in [520–539]. It may be a surprise that even the  $D\bar{\emptyset}$  and CDF experiments working on  $\bar{p}p$  collisions at  $\sqrt{s}=1.96$  TeV have made significant contributions to meson spectroscopy [540–543].

### 3.5.2 CLEO

The Cornell  $e^+e^-$  storage ring CESR is a symmetric collider which started to work in 1979. Since then, the CLEO collaboration has conducted studies of  $b, c, \tau$  and  $\gamma\gamma$  physics in  $e^+e^-$  interactions near 10 GeV [544]. Successive detector upgrades have been performed in parallel with luminosity improvements to CESR, which has delivered over  $9\text{fb}^{-1}$  integrated luminosity. The CLEO-II detector [545], operational since 1989, consisted of drift chambers for tracking and  $dE/dx$  measurements, time-of-flight counters, a 7800-element  $CsI$  electromagnetic calorimeter, a 1.5 T superconducting solenoid, iron for flux return and muon identification, and muon chambers. A three-layer silicon vertex detector was added in 1995. The CLEO-II detector was the first to combine a large magnetic volume with a precision crystal electromagnetic calorimeter. A major upgrade, the CLEO-III

detector [546,547], was installed in 1999. It contained a new four-layer silicon-strip vertex detector,

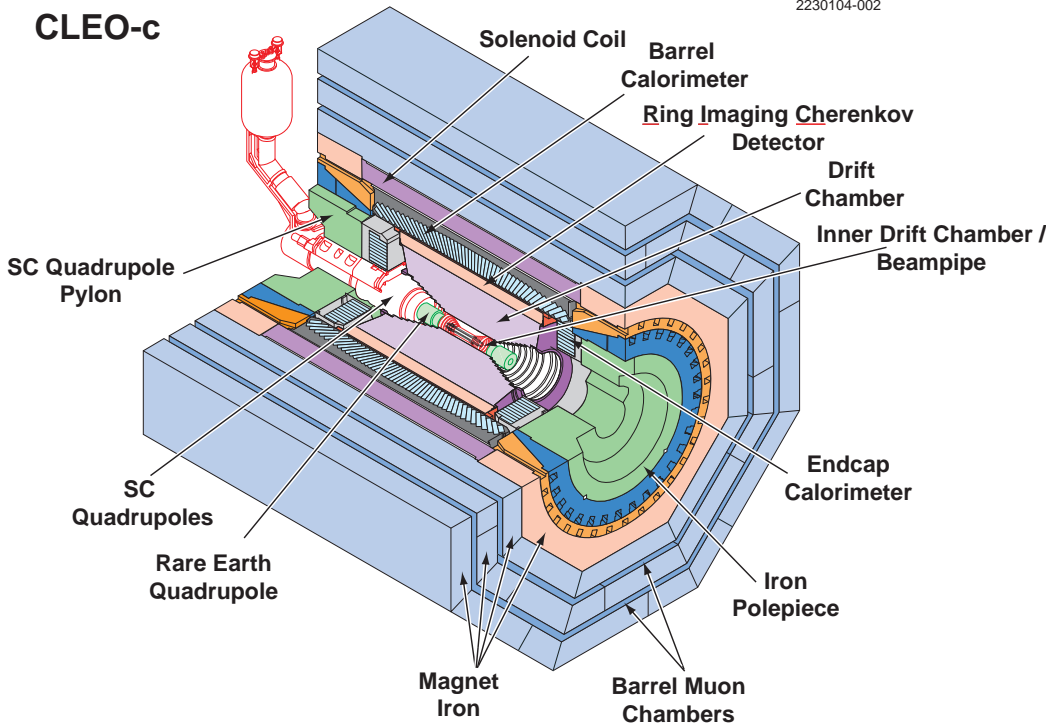


Fig. 23. Experiment CLEO-c

a new wire drift chamber and a particle identification system based on Cherenkov ring imaging. The integrated luminosity accumulated by the CLEO-III detector in 1999–2003 was  $16\text{fb}^{-1}$ . In 2003 the detector was transformed into CLEO-c (Fig. 23) aiming for charm physics at  $3 \div 5\text{ GeV}$  centre-of-mass energy at very high luminosity [548]. The silicon detector was replaced with a wire chamber that has significantly less material, the magnetic field was lowered from  $1.5\text{ T}$  to  $1\text{ T}$ . Selected results of the CLEO-collaboration on meson spectroscopy are published in [401,548–585].

### 3.5.3 Meson spectroscopy at the $\bar{b}b$ factories BaBar and BELLE

In 1999, two general purpose detectors BaBar and BELLE started data taking at the SLAC and KEK  $e^+e^-$  B-factories. Both facilities operate at the  $\Upsilon(4S)$  resonance to produce pairs of  $B\bar{B}$  mesons to study time-dependent  $CP$  asymmetries in their decays. Owing to the very high luminosity of the  $e^+e^-$  colliders and the universality of the detectors, these facilities have excellent potential for the study of meson spectroscopy. Five groups of reactions can be used for this purpose:

- decays of B-mesons produce a broad spectra of final states with hidden charm, open charm and with no charm;
- $c\bar{c}$  pairs are produced with a cross section comparable with  $\Upsilon(4S)$  production;
- even- $C$  parity states can be produced in  $\gamma\gamma$  collisions;
- vector mesons can be produced in  $e^+e^-$  interactions with sufficiently high-energy initial state radiation (radiative return);
- flavour tagging reactions like  $e^+ e^- \rightarrow J/\psi \eta_c$  can be used to study charmonium states.

The SLAC PEP-II B-factory operates at  $10.58\text{ GeV}$ , with energies of the colliding electron and

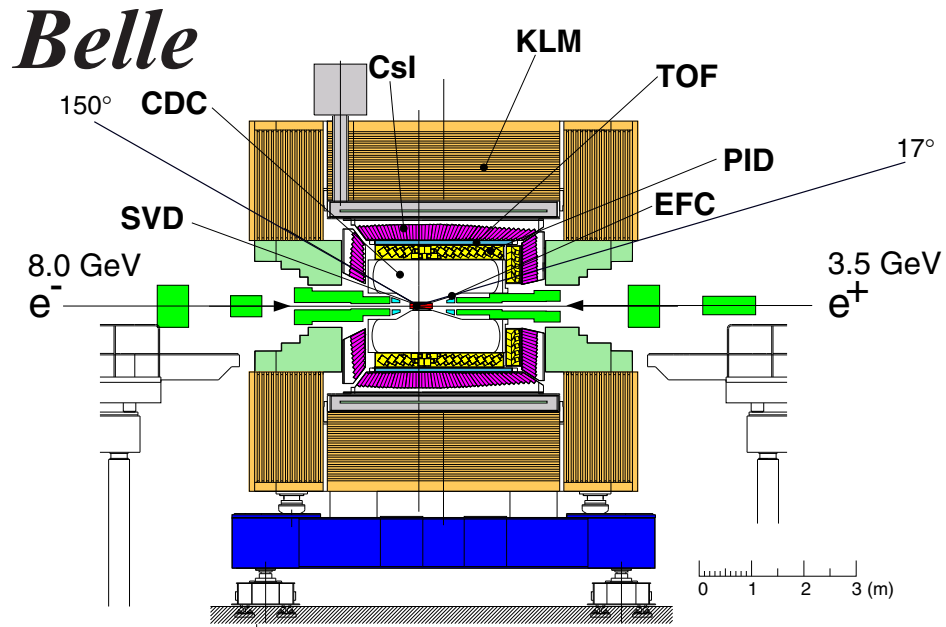


Fig. 24. Experiment BELLE

positron beam of 9 GeV and 3.1 GeV, respectively, resulting in a Lorentz boost of the centre of mass of  $\beta = 0.55$ . The maximum luminosity is  $\sim 9 \cdot 10^{33} \text{ cm}^{-2}\text{s}^{-1}$ , the peak cross section for formation of the  $\Upsilon(4S) \sim 1 \text{ nb}$ . Thus about  $10^9 B$  mesons were recorded. The detector BaBar [586] is asymmetric along the beam which reflects the asymmetry in the beam energies. The inner part of the detector includes tracking, particle identification and electromagnetic calorimetry. It is surrounded by a superconductive solenoid providing a magnetic field of 1.5 T. The tracking system is composed of a Silicon Vertex Tracker (SVT) and a drift chamber. The SVT is used for precision measurements of primary and secondary decay vertices as well as for measurements of low-momentum tracks. A 40-layer drift chamber is used to measure particle momenta and the ionisation loss  $dE/dx$ . Charged particles are identified with momenta up to  $\approx 700 \text{ MeV}/c$ , the momentum resolution is about  $\sigma_{p_t} \approx 0.5\%$  at  $p_t = 1.0 \text{ GeV}/c$  and the resolution for the track impact-parameter is about 25 and  $40 \mu\text{m}$  in the transverse plane and along the detector axis, respectively. Separation of pions and Kaons at momenta from  $0.5 \text{ GeV}/c$  to  $4 \text{ GeV}/c$  is provided by a novel ring-imaging detector based of fused silica bars. The electromagnetic calorimeter is a finely segmented array of  $CsI(Tl)$  crystals with energy resolution of  $\sigma_E/E \approx 2.3\% \cdot E^{-1/4} + 1.9\%$  ( $E$  in GeV). The iron return yoke is instrumented with resistive plate chambers and limited streamer tubes for detection of muons and neutral hadrons. Results related to meson spectroscopy are published in [586–627].

The BELLE detector is located at the KEKB  $e^+e^-$  collider at the KEK laboratory in Tsucuba, Japan. The KEKB storage rings have asymmetric energies: 8 GeV for electrons and 3.5 GeV for positrons, that provides to the  $\Upsilon(4S)$  resonance a Lorentz boost of  $\beta\gamma = 0.425$ . At KEKB the world record in luminosity of  $1.4 \cdot 10^{34} \text{ cm}^{-2}\text{s}^{-1}$  was achieved. The side view of the Belle detector [628] is shown at Fig. 24. Tracking, identification and calorimetric systems are placed inside a 1.5 T superconducting solenoid magnet of 1.7 m radius. Precision tracking and vertex measurements are provided by a silicon vertex detector and central drift chamber. The four-layer double-sided silicon detector with strip pitches of  $75 \mu\text{m}(z)$  and  $50 \mu\text{m}$  surrounds the beryllium beam pipe having 1.5 cm radius. The central drift chamber has 50 layers of anode wires for tracking and  $dE/dx$  measurements. The momentum resolution of the tracking system is  $\sigma_{p_t}/p_t = (0.30/\beta + 0.19p_t)\%$ ,

where  $p_t$  is the transverse momentum in GeV/c. The Kaon/pion separation is achieved using the central drift chamber, time of flight counters with rms resolution of 0.95 ps and aerogel Cherenkov counters with refractive indices from 1.01 to 1.03, depending on polar angle. The electromagnetic calorimeter consists of 8737  $CsI(Tl)$  crystals of projective geometry with energy resolution for photons of  $\sigma(E)/E \approx 1.8\%$  at  $E_\gamma$  above 3 GeV. The flux return is instrumented with 14 layers of resistive plate chambers for muon identification and detection of neutral hadrons. Results on meson spectroscopy can be found in [629–662].

### 3.6 Meson spectroscopy at LEP

The main goal of the LEP program was the study of electroweak physics in  $e^+e^-$  collisions on and above the  $Z^0$ . The operation of the LEP collider at CERN started in August 1989 and stopped in November 2000. LEP had four intersection regions, each surrounded by a particle detector. The detectors (DELPHI, ALEPH, L3 and OPAL) were optimised differently to study various aspects of physics. The initial LEP energy was chosen to be around 91 GeV as to produce  $Z^0$  particles. Since the end of 1995, LEP has moved away from the  $Z^0$  and entered its second phase. Its energy was doubled to study the production of  $Z^0Z^0$  and  $W^+W^-$  pairs, and to search for new particles, in particular the Higgs boson and/or supersymmetric particles. Even though the main goal of these experiments was electroweak physics, very significant results in meson spectroscopy were obtained by all four detectors. In the first data taking period, about  $5 \times 10^6$  of  $Z^0$  decays were collected in each of the four detectors. Owing to the high branching ratios of  $Z^0$  decays to heavy quarks ( $BR(Z^0 \rightarrow c\bar{c}) = 11.8\%$ ,  $BR(Z^0 \rightarrow b\bar{b}) = 15.1\%$ ), considerable statistic was collected with heavy quarks in the final state. This data is especially fruitful to study heavy-light mesons. In the second phase, the very high luminosity, up to  $10^{32} \text{ cm}^{-2}\text{s}^{-1}$ , in combination with the high energy provided unique possibilities to study  $\gamma\gamma$  interactions.

#### 3.6.1 The Aleph experiment

ALEPH was a  $4\pi$  detector designed to give detailed information on complex events from high-energy  $e^+e^-$  collisions [663]. A superconducting coil, 5 m in diameter and 6 m long, produced a uniform 1.5 T field in beam direction. Closest to the interaction point, a silicon vertex detector was installed with  $12 \mu\text{m}$  resolution in  $r - \phi$  and  $r - z$  and capability to identify secondary vertices in decays of  $\tau$ -leptons, and of  $c$  and  $b$  quarks. The vertex detector was surrounded, in order of increasing radius, by a drift chamber (Inner Tracking Chamber), a Time Projection Chamber (TPC) of 3.6 m diameter and 4.4 m length, and an electromagnetic calorimeter. A resolution in transverse momentum of  $\sigma(p_t)/p_t = 0.0006 \cdot p_t + 0.005$  ( $p_t$  in GeV/c) was reached. The electromagnetic calorimeter, consisting of 2 mm lead sheets with proportional wire sampling, has an energy resolution for electromagnetic showers of  $\sigma_E/E = 0.18/\sqrt{E} + 0.0009$  ( $E$  in GeV). Outside of the coil, a 1.2 m thick iron return path was used as hadron calorimeter, a double layer of drift tubes provided muon identification. Strong points of the detector are precision of momentum measurements for charged particles due to a high magnetic field and a TPC, good identification of electrons and muons, and good spatial resolution in electron and  $\gamma$  calorimetry. A silicon-tungsten calorimeter installed in 1992 provided high precision of the luminosity measurement via Bhabha scattering. Results on meson spectroscopy are published in [664–672].

### 3.6.2 The Delphi experiment

DELPHI was a general purpose detector offering 3-dimensional information on curvature and energy deposition with fine spatial granularity, as well as identification of leptons and hadrons over most of the solid angle [673]. A superconducting coil provided a 1.2 T solenoidal field of high uniformity. Tracking relied on a microvertex detector, an inner detector (a multiwire proportional chamber), a Time Projection Chamber (TPC) measuring up to 16 space points per track, an outer detector with 5 layers of drift tubes, and forward drift chambers. The 3-layer silicon microvertex detector was used for precision measurements of the interaction vertex and of decay vertices of short-lived particles such as bottom and charm hadrons and  $\tau$  leptons. The single-hit resolution was found to be  $9\ \mu\text{m}$  in  $z$ -direction and  $7.6\ \mu\text{m}$  in  $r - \phi$ -direction. A Ring Imaging Cherenkov detector (RICH) used gaseous ( $C_5F_{12}$ ) and liquid ( $C_6F_{14}$ ) radiators. As a result, particle identification was achieved at nearly all momenta: below 1 GeV/c with  $dE/dx$  measurements in the TPC, from 0.7 GeV/c to 8 GeV/c with the liquid radiator and from 2.5 GeV/c to 25 GeV/c with the gaseous radiator. Electromagnetic showers were measured in the barrel with high granularity by a High Density Projection Chamber (HPC), and in the endcaps by 1 x 1 degree projective towers composed of lead glass. A segmented magnet yoke served for hadron calorimetry and as a filter for muons which were identified in two drift chamber layers. In addition, scintillator systems were implemented in the barrel and forward regions. A small-angle Shashlik-type calorimeter was used to monitor the luminosity. Results on meson spectroscopy are reported in [674–679].

### 3.6.3 The L3 experiment

The detector L3 consisted of a large-volume ( $\mathcal{O} = 11.9\ \text{m}$ ,  $L = 12\ \text{m}$ ) low-field (0.5 T) solenoidal magnet, a small central tracking detector with high spatial resolution, a high-resolution electromagnetic calorimeter encapsulating the central detector, a hadron calorimeter acting also as a muon filter, and high-precision muon tracking chambers [680]. The detector was designed to measure energy and position of leptons with the highest obtainable precision allowing a mass resolution  $\delta(m)/m$  of about 2% in di-lepton final states. Hadronic energy flux was detected by a fine-grained calorimeter, which also served as a muon filter and a tracking device. The outer boundary of the detector was given by the iron return yoke of a conventional magnet. The muon momentum measurement was performed with a precision of  $\sigma(p)/p \approx 2.5\%$  by three sets of high precision drift chambers with long lever arm in the central detector region. A forward-backward muon detection system extended the polar angle coverage to 22 degrees in the forward region. Radially inwards was a combined hadron calorimeter and muon absorber. The electromagnetic energy flow was determined by approximately 11000 BGO crystals. Full electromagnetic shower containment over nearly  $4\pi$  solid angle coverage was achieved. The energy resolution varied from 5% at 100 MeV to 1.4% at high energy. Surrounding the 10 cm diameter beam pipe, a high-precision Silicon Microstrip Detector and a small drift chamber operating in the time expansion mode acted as charged particle vertex detectors, providing momentum resolution  $\sigma(p_t)/p_t = 0.021 \cdot p_t$  ( $p_t$  in GeV/c). Results on meson spectroscopy can be found in [681–693].

### 3.6.4 The Opal experiment

The general purpose detector OPAL was designed to study a wide range of unexplored physics at LEP [694]. The tracking system of the apparatus, in order of increasing distance from the interaction point, were a silicon microvertex detector providing single hit resolution of  $5\ \mu\text{m}$  in  $r - \phi$  and  $13\ \mu\text{m}$  in  $z$ , central detectors consisting of a vertex and a jet chamber, and a barrel-

shaped chambers for precise  $z$ -measurements. The main tracking with the jet chamber provided up to 159 space points per track. It was used for tracking and for particle identification using  $dE/dx$ . The momentum resolution was  $\sigma_p/p = 0.0022 \cdot p$  ( $p$  in GeV/c). A warm conductor solenoid provided a uniform magnetic field of 0.4 T. A TOF scintillator barrel detector, complemented by a scintillating tile endcap detector allowed particle identification at momenta up to 2.5 GeV/c. Electromagnetic showers were measured in a multi-cell  $10 \times 10 \text{ cm}^2$  lead glass electromagnetic calorimeter with resolution of about  $\sigma(E)/E = 0.05/\sqrt{E}$  ( $E$  in GeV). Hadrons were measured with streamer tubes and thin-gap wire chambers. Muons were detected in an external muon identifier composed of four layers of drift chambers. The luminosity was measured via Bhabha scattering into a forward small-angle silicon-tungsten calorimeter. Results on meson spectroscopy are published in [695–699].

## 4 Experimental methods

A variety of experimental techniques has been developed to search for new meson resonances and to establish properties of known states. In *production* experiments, the total energy is shared between a recoil particle and a multi-meson final state. Angular momentum can be transferred, and the multi-meson system can contain contributions from several resonant partial waves with different angular momenta. The quantum numbers of the multi-meson system are restricted only by conservation laws; production of partial waves with exotic quantum numbers, i.e. of quantum numbers which cannot be attributed to a  $q\bar{q}$  system, is allowed. In *formation* experiments, there is no recoil particle, mass and quantum numbers of the final state are given by the initial state. Formation of mesons with exotic quantum numbers in  $e^+e^-$  or  $p\bar{p}$  annihilation is thus forbidden.

Consider, i.e., antiproton-proton annihilation in flight. Nucleon and antinucleon provide their mass and their momentum to a mesonic final state. When all final-state mesons are combined, their invariant mass is determined by the invariant mass  $\sqrt{s}$  of the initial state. By scanning the total energy by variation of the antiproton momentum, the mass of the final state can be tuned to cover the range of masses in which meson resonances are to be studied. The mass resolution is given by the precision with which the beam energy can be kept stable. The quantum numbers of  $q\bar{q}$  mesons which can be formed are restricted to those of the  $p\bar{p}$  system which contains no exotic partial wave.

Alternatively, the initial momentum can be kept fixed, antiproton-proton annihilation can e.g. be studied at rest. Meson resonances can now be produced recoiling against another meson, often a pion. In case of three pions in the final state, each pion recoils against the other two pions possibly forming a resonance. In the analysis, one has to take into account all three possibilities. Of course, not their probabilities but their amplitudes have to be added. The mass of resonances is reconstructed from the measured particle momenta in the final state, the mass resolution is given by the accuracy with which the final-state particles are measured.

### 4.1 Meson resonances in production experiments

#### 4.1.1 Charge exchange and strangeness exchange scattering

The model of Reggeised particle exchange was developed in the 60's of the last century; it provides efficient tools for the analysis of two-body hadronic reactions. It was named after T. Regge who proposed the method of complex angular momentum in nonrelativistic quantum mechanics [700, 701]. In field theory this method links the two-body scattering amplitude at high energy with the amplitude in the crossed channel. Consider the reaction

$$a + b \rightarrow c + d \quad (4.1)$$

at high energy  $s \gg m^2$  and fixed transfer momentum squared  $|t| \sim m^2$ . The amplitude for  $t$ -channel exchange of a particle with mass  $m$  and spin  $J$  can be expressed as

$$T(s, t) = \frac{1}{k} g_1 g_2 \left( \frac{s}{s_0} \right)^J (m^2 - t)^{-1} \quad (4.2)$$

where  $s_0=1$  GeV<sup>2</sup> is a scale and  $g_1, g_2$  are coupling constants. For exchanges with  $J \geq 2$  this amplitude violates the Froissart limit,  $T(s, t) \sim \ln^2(s)$  for  $s \rightarrow \infty$ , for binary reactions [702]. This

problem appears as (4.2) gives the correct amplitude only near the  $m^2$  pole which is very far from the physical region of the reaction (4.1), where  $t$  is negative. At very high  $s$  and moderate  $t$ , the Regge model predicts a simple functional form for the extrapolation of the amplitude from the  $t$ -channel resonance region to the physical region of reaction (4.1) :

$$R(s, t) \sim \frac{1}{k} \beta(t) \left(\frac{s}{s_0}\right)^{\alpha_i(t)} \eta(\alpha_i(t)) \quad (4.3)$$

where  $\alpha_i(t)$  is a smooth function of  $t$ , called Regge trajectory.  $J$  is the spin of the lightest particle in the  $t$ -channel (0 for the  $\pi$  trajectory, 1 for  $\rho$ ,  $\frac{1}{2}$  for  $N$  etc.),  $\eta(\alpha_i(t)) = -\left(\frac{1+\sigma_i e^{-i\pi\alpha_i(t)}}{\sin \pi\alpha_i(t)}\right)$  is a signature factor for Regge pole  $i$  with trajectory  $\alpha_i(t)$ , signature  $\sigma_i = \pm 1$ . The amplitude (4.3) represents  $t$ -channel exchange of objects having identical flavour quantum numbers (labelled by  $i$ ) and all possible spins.

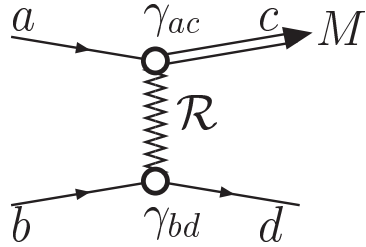


Fig. 25. The diagram for a two-body reaction with Reggeon exchange.

The differential cross section of the reaction (4.1) can be obtained by squaring the amplitude (4.3)

$$\frac{d\sigma}{dt} = f(t) \left(\frac{s}{s_0}\right)^{2\alpha_i(t)-2}. \quad (4.4)$$

The trajectories  $\alpha_i(t)$  are supposed to be linear near  $t = 0$

$$\alpha_i(t) = \alpha_i(0) + \alpha'_i(0)t. \quad (4.5)$$

From (4.4) we see that  $\alpha_i(0)$  determines the dependence of  $\frac{d\sigma}{dt}(t = 0)$  on energy while  $\alpha'_i(0)$  describes the  $t$ -dependence on energy. The parameters  $\alpha_i(0)$  and  $\alpha'_i(0)$  for different Regge trajectories are known from experiments. The extrapolation of  $\alpha_i(t)$  from small negative  $t$  (reaction 4.1) to positive  $t$  (reaction  $a + \bar{c} \rightarrow \bar{b} + d$ ) shows that  $\alpha_i(m_r^2) = J$  as suggested by the model ( $J$  is the spin of the resonance  $r$ ). Most trajectories have almost equal slopes,  $\alpha'(0) \approx 1 \text{ GeV}^{-2}$ , except the trajectory with vacuum quantum numbers. The intercept of the Regge trajectory  $\alpha_i(0)$  can be estimated to  $\alpha_i(0) = J - m_r^2/\alpha'(0)$ . It gives  $\alpha(0) \approx 0.5$  for the  $\rho$  trajectory and  $\alpha(0) \approx 0$  for the  $\pi$ -trajectory. Using (4.4) we conclude that for reactions with  $\rho$ -trajectory exchange, like  $\pi^- p \rightarrow \pi^0 n$ , the differential cross section  $\frac{d\sigma}{dt}(t = 0)$  falls off with energy as  $1/s$ , for  $\pi^- p \rightarrow \rho^0 n$  (with  $\pi$  and  $a_1$ -trajectory exchange) the cross section drops as  $1/s^2$ .

The trajectory with vacuum quantum numbers plays a very special rôle in Regge-phenomenology. It gives the dominant contribution to elastic scattering at asymptotically high energies. From the optical theorem

$$\sigma_{tot} = \frac{4\pi}{k} Im R(t = 0) \quad (4.6)$$

and (4.3) we derive that  $\alpha(0) = 1$  leads to a constant total cross section. This trajectory was called Pomeron after I.Ya. Pomeranchuk who proposed arguments in favour of asymptotically constant total cross sections [703]. At the first glance, the upper limit for any trajectory intercept should be  $\alpha(0) = 1$  since for  $\alpha(0) > 1$ , the Froissart limit is violated. This assumption is however not supported by data showing an asymptotically rising total cross sections of hadron-hadron interactions at high energy. To describe the total hadronic cross sections, the Pomeron cannot be represented by a simple  $t$ -channel Regge pole; it has to be replaced by a more complicated object [704] with  $\alpha(0) \approx 1.1$  and  $\alpha'(0) \approx 0.3$ , modified by absorption and inelastic intermediate states. It is a still debated question if such a complicated object can be linked to any resonances (possibly glueballs) in the crossed channel. The physics of Pomerons is, e.g., highlighted in the excellent book by Donnachie, Dosch, Nachtmann and Landshoff [705].

To get information on the function  $\beta(t)$  in (4.3) we have to rely on considerations beyond the Regge model. By looking at Fig. 25 it is natural to assume that the function  $\beta(t)$  in (4.3) can be represented in factorised form

$$\beta(t) = (-t)^{n/2} \gamma_{acr}(t) \gamma_{bdr}(t) \quad (4.7)$$

The functions  $\gamma_{acr}$  and  $\gamma_{bdr}$  can be written as  $\gamma_{acr} = g_{acr} \exp(r_{acr} t)$  and  $\gamma_{bdr} = g_{bdr} \exp(r_{bdr} t)$ . Here,  $g_{acr}$  and  $g_{bdr}$  are coupling constants,  $r_{acr}$  and  $r_{bdr}$  are slope parameters representing formfactors. At  $t \rightarrow 0$ , the amplitude can be suppressed at some power of  $\sin\theta \sim \sqrt{(-t)}$  to provide a net helicity ( $\lambda_i$ ) flip, and the extra flip to guarantee parity conservation  $n = |\lambda_c - \lambda_a| + |\lambda_d - \lambda_b|$ .

#### 4.1.2 Two-photon fusion

Production of resonances by two-photon fusion, as well as decays of resonances into two photons, provide important information on hadron structure. For  $q\bar{q}$  mesons the matrix element for these processes is proportional to  $\Sigma Q_i^2$ . The decay width of a neutral meson with isospin  $I = 1$  ( $M = \frac{1}{\sqrt{2}}(u\bar{u} - d\bar{d})$ ) is thus proportional to  $\frac{1}{2}(Q_u^2 - Q_d^2)^2$ , for  $I = 0$   $SU_3$ -octet mesons, it is proportional to  $\frac{1}{3}(Q_u^2 + Q_d^2)^2$  and for  $SU_3$ -singlet mesons to  $\frac{1}{6}(Q_u^2 + Q_d^2 - 2Q_s^2)^2$ . From a comparison with data, singlet-octet mixing angles can be derived. For pseudoscalar mesons the mixing angle is  $\theta_P \approx -20^\circ$ , for tensor mesons ( $f_2$ ,  $f'_2$ ) it is  $\theta_T \approx 28^\circ$ . The latter mixing angle leads to an accidental suppression of two-photon decays of  $f'_2$  due to an approximate cancellation of the  $u\bar{u} + d\bar{d}$  and  $s\bar{s}$  contributions. Two-photon fusion is studied at  $e^+e^-$  colliders (Fig. 26).

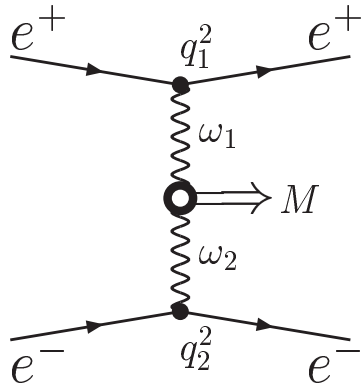


Fig. 26. The diagram describing meson production in  $e^+e^-$  annihilation. Here  $q_i^2 = (p - p')^2$  and  $p(p')$  are the momenta of the initial (final) electrons,  $\omega_i$  are the energies of the virtual photons.

Common sense, as well as specific models, tell us that  $\gamma\gamma$  decay of non- $q\bar{q}$  mesons like glueballs, hybrids, multiquark objects, or mesonic molecules is suppressed. The two-photon width can therefore be used to identify non- $q\bar{q}$  states. Production of glueballs can, e.g., be expected in radiative  $J/\psi$  decays via two gluons  $J/\Psi \rightarrow \gamma gg$ , but in two-photon fusion it should be suppressed because of their small  $\gamma\gamma$  coupling. A convenient estimator called stickiness was proposed by Chanowitz [706] to discriminate glueballs and  $q\bar{q}$  mesons. The stickiness of a resonance  $R$  with mass  $m_R$  and two-photon width  $\Gamma_{R \rightarrow \gamma\gamma}$  is defined as

$$S_R = N_l \left( \frac{m_R}{K_{J \rightarrow \gamma R}} \right)^{2l+1} \frac{\Gamma_{J \rightarrow \gamma R}}{\Gamma_{R \rightarrow \gamma\gamma}}, \quad (4.8)$$

where  $K_{J \rightarrow \gamma R}$  is the energy of the photon in the  $J$  rest frame,  $l$  is the orbital angular momentum of the two initial photons or gluons ( $l = 1$  for  $0^-$ ),  $\Gamma_{J \rightarrow \gamma R}$  is the  $J$  radiative decay width for  $R$ , and  $N_l$  is a normalization factor chosen to give  $S_\eta = 1$ .

The gluiness ( $G$ ) was introduced [707, 708] to quantify the ratio of the two-gluon and two-photon coupling of a particle and is defined as

$$G = \frac{9 e_q^4}{2} \left( \frac{\alpha}{\alpha_s} \right)^2 \frac{\Gamma_{R \rightarrow gg}}{\Gamma_{R \rightarrow \gamma\gamma}}, \quad (4.9)$$

where  $e_q$  is the relevant quark charge.  $\Gamma_{R \rightarrow gg}$  is the two-gluon width of the resonance  $R$ , calculated from equation (3.4) of ref. [707]. Stickiness is a relative measure, gluiness is a normalised quantity and is expected to be near unity for  $q\bar{q}$  mesons.

The cross section for  $e^+e^- \rightarrow M$  can be related to the cross section for  $\gamma\gamma \rightarrow Me^+e^-$  in the equivalent photon approximation:

$$d\sigma_{e^+e^- \rightarrow e^+e^- M} = dn_1 dn_2 d\sigma_{\gamma\gamma \rightarrow M}(W^2) \quad (4.10)$$

where  $n_{1,2}$  is number of photons with energy  $\omega_{1,2}$  and four-momentum squared  $q_{1,2}^2$ ,

$$dn_{1,2} = \frac{\alpha}{\pi} \left[ 1 - \frac{\omega_{1,2}}{E_{1,2}} + \frac{\omega_{1,2}^2}{2E_{1,2}^2} - \frac{m_e^2 \omega_{1,2}^2}{(-q_{1,2}^2) E_{1,2}^2} \right] \frac{d\omega_{1,2}}{\omega_{1,2}} \frac{d(-q_{1,2}^2)}{-q_{1,2}^2}. \quad (4.11)$$

The photon spectrum peaks very sharply at  $(-q^2) \rightarrow (-q^2)_{min} = m_e^2 \omega^2 / E(E - \omega)$ . The peak is much narrower than any hadronic form factor, most photons are therefore nearly real ( $q^2 \approx 0$ ). After integration of (4.10) over  $q_{1,2}^2$  and  $\omega_{1,2}$ , the cross section for production of resonance  $M$  via two-photon fusion is

$$\sigma_{e^+e^- \rightarrow e^+e^- M} = (2J+1) \frac{8\alpha^2 \Gamma_{M \rightarrow \gamma\gamma}}{m_M^3} G(s, m_M, f) \quad (4.12)$$

where  $G(s, m_M, f)$  is a known function of  $s$ ,  $m_M$ , and the form factor slope  $f$ . The dependence on the form-factor slope is very weak and can be neglected in most of cases. In the equivalent photon approximation, two-photon fusion looks like a formation experiment in a wide-band photon beam with known spectra ( $dn \approx \frac{\alpha}{\pi} \frac{d\omega}{\omega} \frac{d(-q^2)}{(-q^2)}$ ).

Not all positive-charge-parity states can couple to two real photons. Consider a system of two spin-one particles,  $s_1 = s_2 = 1$ . The total spin of these two particles is composed of spin  $S = 0, 1, 2$

and orbital angular momentum  $L = 0, 1, 2, 3\dots$ . With these  $S$  and  $L$ , one positive parity state and one negative parity state exist for  $J = 0$ , three positive parity states and four negative parity states for  $J = 1$ , and five positive parity states and four negative parity states for any  $J > 1$ . Only few of these states can be realised in a system of two real photons since real photons have only two helicities ( $\lambda = \pm 1$ ) and obey Bose symmetry. Neither  $J^p = 1^-$  nor  $J^p = 1^+$  states couple to two real photons. This statement is called Landau-Yang theorem: the cross section for production of  $J^{PC} = 1^{++}$  states like  $f_1(1285)$ ,  $f_1(1420)$  or  $a_1(1260)$  in two-photon fusion with nearly real photons is strongly suppressed. If at least one of the two photons is sufficiently virtual having  $|q^2| \sim m_h^2$  then all the three helicities are allowed ( $\lambda = 1, 0, -1$ ) and production of  $J = 1$  states in two-photon fusion is no longer suppressed. Events with larger  $|q^2|$  can be selected by applying a cut on the scattering angle of the electron or positron (single tag) or both (double-tag).

Some other reactions can also be used to study two-photon fusion, like production of mesons in Coulomb field of nuclei  $\gamma Z \rightarrow MZ$  (Primakoff reaction) and production of mesons in peripheral interactions of nuclei  $Z_1 Z_2 \rightarrow Z_1 Z_2 M$ . In both cases, photons are selected by requiring very small  $|q^2|$ . The first reaction is used to study light mesons since in fixed-target experiments, production of heavy mesons is suppressed by the minimal transfer-momentum squared  $-q_{min}^2$  which increases with the mass  $m$  of the produced meson:  $-q_{min}^2 \approx m^4/4E_{beam}^2$ .

#### 4.1.3 Central production

Central production is a process similar to two-photon fusion. Two hadrons at a large energy scatter, keeping their identity and loosing a small fraction of their energy. In a fixed target experiment, a hadron  $h_{beam}$  (mostly protons were used but also pions or Kaons), scatters off a target proton  $p_{target}$  and produces a particle or system of particles  $X$

$$h_{beam} p \rightarrow h_{fast} X p_{slow} \quad (4.13)$$

where the subscripts 'fast' and 'slow' indicate the fastest and slowest particles in the laboratory respectively. The fast hadron scatters into forward direction emitting a Reggeon. The fast (slow) hadron transfers a squared four-momentum  $t_1(t_2)$  to the central system. (See Fig. 27 for definitions.) The centre of mass energy of the scattered particle is reduced by  $x_1$ . The target-proton

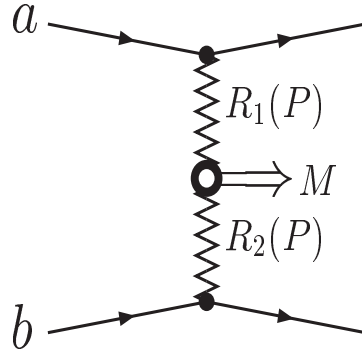


Fig. 27. Central production of a system  $X$ . The momentum transfer is defined by  $q_i = (p_i - p'_i)$  where  $p_i, p'_i$  are the in- and outgoing momenta of the two hadrons.  $\omega_i$  are the energies transferred to  $X$ .

is slow in the laboratory system; it emits a Reggeon and its centre of mass energy is reduced by  $x_2$ . The two virtual particles collide producing a particle or system of particles  $X$  with mass  $M \sim \sqrt{s}(1 - x_1)(1 - x_2)$  where  $s$  is the squared centre-of-mass energy. For  $\sqrt{s} \sim 30 \text{ GeV}/c^2$  and

$1 - x_1, 1 - x_2$  in the range from 0.0 to 0.1 the available phase space is limited to about  $3.0 \text{ GeV}/c^2$ . In the centre of mass system, particle X carries only a small fraction  $x_F$  of the momenta of the scattered particles; they are produced centrally, see Fig. 28. Scattered hadron and target proton keep a large fraction  $x_F$  of their total energy. The two scattering particles transfer a four-momenta  $t$  to the central system.

At sufficiently high energy  $s_{1,2} >> 1 \text{ GeV}^2$  and moderate momentum transfer  $-t_{1,2} < 1 \text{ GeV}^2$  the amplitude for double Regge production of the resonance can be written as (see [709] and references therein):

$$T_{\lambda_1 \lambda_2}^{\lambda_3 \lambda_h \lambda_4}(s_1, s_2, t_1, t_2, \phi) = \sum_{i,k} g_{\lambda_1 \lambda_3}(t_1) g_{\lambda_2 \lambda_4}(t_2) \left(\frac{s_1}{s_0}\right)^{\alpha_i(t_1)} \left(\frac{s_2}{s_0}\right)^{\alpha_k(t_2)} \eta(\alpha_i(t_1)) \eta(\alpha_k(t_2)) g_{ik}^{\lambda_h}(t_1, t_2, \phi) \quad (4.14)$$

Here,  $\phi$  is the angle between the transverse momenta  $\vec{p}_{3\perp}$  and  $\vec{p}_{4\perp}$  of the outgoing protons and  $\eta(\alpha_i(t))$  is the signature of Regge pole  $i$  with trajectory  $\alpha_i(t)$ . The vertex couplings for different helicities are the same as in single-Regge exchange (4.7). This amplitude looks as a very natural choice if we compare Fig. 25 with Fig. 28 and amplitude (4.3) with (4.14).

The spin structure of the central vertex  $g_{ik}^{\lambda_h}(t_1, t_2, \phi)$  depends on the product of the naturalities of particle  $h$  and the exchanged Reggeons. With this amplitude, the cross section for production of resonances with  $J^{PC} = 0^{++}, 0^{-+}, 1^{++}$  can be expressed as

$$\begin{aligned} \frac{d\sigma(0^{++})}{dt_1 dt_2 d\phi} &\sim G_E^{p^2}(t_1) G_E^{p^2}(t_2) [F_1^2(t_1, t_2, \vec{p}_{3\perp} \cdot \vec{p}_{4\perp}, M^2) + \frac{\sqrt{t_1 t_2}}{\mu^2} \cos(\phi) \times F_2^2(t_1, t_2, \vec{p}_{3\perp} \cdot \vec{p}_{4\perp}, M^2)]^2 \\ \frac{d\sigma(0^{-+})}{dt_1 dt_2 d\phi} &\sim t_1 t_2 G_E^{p^2}(t_1) G_E^{p^2}(t_2) \sin^2(\phi) \times F^2(t_1, t_2, \vec{p}_{3\perp} \cdot \vec{p}_{4\perp}, M^2) \\ \frac{d\sigma(1^{++})}{dt_1 dt_2 d\phi} &\sim G_E^{p^2}(t_1) G_E^{p^2}(t_2) [(\sqrt{t_1} - \sqrt{t_2})^2 \times F_3^2(t_1, t_2, \vec{p}_{3\perp} \cdot \vec{p}_{4\perp}, M^2) \\ &\quad + \sqrt{t_1 t_2} \sin^2(\phi/2) \times F_4^2(t_1, t_2, \vec{p}_{3\perp} \cdot \vec{p}_{4\perp}, M^2)] \end{aligned} \quad (4.15)$$

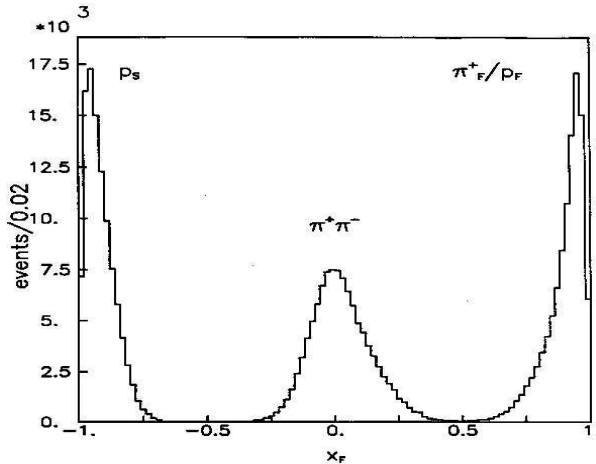


Fig. 28. The distribution of the Feynman variable  $x_F$  in the reaction  $pp \rightarrow p_s(\pi^+\pi^-)p_f$ . In the lab system, the scattered proton goes forward as fast proton  $p_f$ . Little momentum is transferred to the target proton  $p_s$ . The  $\pi^+\pi^-$  pair is slow in the centre-of-mass system [272].

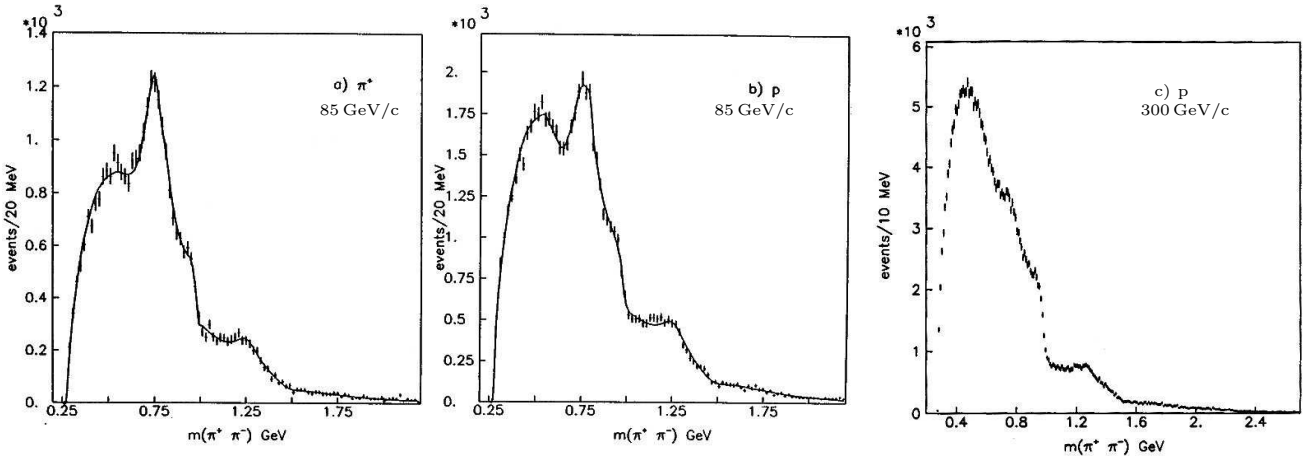


Fig. 29. The  $\pi^+\pi^-$  invariant mass distribution using a  $85 \text{ GeV}/c$  pion (a), proton (b), or a  $300 \text{ GeV}/c$  proton beam [272].

The experimental data agrees with these predictions. It is important to note that these predictions follow from general rules of the Regge model and do not tell us anything on the structure of Reggeons or mesons. The physics of resonances and their interactions with Reggeons is hidden in unknown formfactors  $F^2(t_1, t_2, \vec{p}_{3\perp} \cdot \vec{p}_{4\perp}, M^2)$ .

Several processes may compete in central production; scattering of two Reggeons, Pomeron-Reggeon scattering or Pomeron-Pomeron scattering. The cross section for Pomeron-Pomeron scattering should be independent of  $s$  while collisions of two Reggeons in the central region are predicted to scale with  $1/s$  and Pomeron-Reggeon scattering as  $1/\sqrt{s}$  [710]. The nature of Pomerons is a topic of intense discussions. Here it is sufficient to recall that Pomerons have no valence quarks. It has therefore been argued that central production is a good place to search for glueballs [711, 712]. Likewise, Pomeron-Reggeon exchange may be well suited for the study of hybrid mesons.

The suggested scaling of cross sections as a function of  $\sqrt{s}$  is evidenced in Fig. 29. It shows the centrally produced  $\pi^+\pi^-$  invariant mass using a  $85 \text{ GeV}/c$  proton and  $\pi^+$  beam, and a  $300 \text{ GeV}/c$  proton beam [272]. A low-mass enhancement is seen, followed by  $\rho$  production and a sharp drop of intensity due to  $f_0(980)$ . As expected, production of  $\rho$  disappears with increasing  $\sqrt{s}$ . This is also seen when the pion is replaced by a proton. The very fast decrease of the cross-section with energy can be explained by a Reggeised pion-pion contribution to  $\rho$  production which decreases with energy as  $\approx 1/s^2$ . The low-mass enhancement remains as dominant feature when  $\sqrt{s}$  increases.

The production rate for  $\eta'$  production is reduced by a factor  $0.72 \pm 0.16$  when going from WA92 ( $\sqrt{s} = 12.7$ ) to WA102 ( $\sqrt{s} = 29.1$ ) [308]. The reduction factor is nearly compatible with the predicted 1 for Pomeron-Pomeron fusion and incompatible with the prediction of 0.2 for  $\rho\rho$  fusion<sup>3</sup>.

A large number of centrally produced final states X has been studied by the WA102 collaboration, like  $\pi, \eta, \eta'$  [295],  $\pi\pi$  and  $K\bar{K}$  [301–303, 305],  $\eta\pi$  [309],  $\eta\eta$  [310],  $\eta\eta'$  and  $\eta'\eta'$  [306],  $3\pi$  [298, 314],  $\pi^+\pi^-\eta, \rho\gamma$ , and  $\phi\gamma$  [296, 304],  $4\pi$  [293, 307, 311],  $K\bar{K}\pi$  [294],  $\omega\omega$  [312],  $\phi\phi$  [297],  $K^*\bar{K}^*$  and  $\phi\omega$  [299], baryon-antibaryon [300] and charmonium states [313]. Earlier experiments investigated the same

<sup>3</sup> These numbers should not be stressed to much. In [713], a preliminary value  $0.20 \pm 0.05$  was given for  $\sigma_{\eta'}(\sqrt{s}=29.1 \text{ GeV})/\sigma_{\eta'}(\sqrt{s}=12.7 \text{ GeV})$  and used to argue that pseudoscalar meson production is suppressed in double Pomeron exchange. The ratio for central production  $\sigma_\eta/\sigma_\omega = 0.09 \pm 0.01$  at  $\sqrt{s} = 29.1 \text{ GeV}$  was given in [295] and compared to  $\sigma_\eta/\sigma_\omega = 0.20 \pm 0.02$  at  $\sqrt{s} = 12.7 \text{ GeV}$ . From Table 5, this ratio is  $0.52 \pm 0.06$  at  $\sqrt{s} = 29.1 \text{ GeV}$ . The large discrepancies demonstrate the difficulty of extracting absolute cross section. The systematic errors were obviously not fully under control.

channels but had smaller statistics. Here we discuss only the latest results and refer to earlier publications only when needed.

At a first view, a lab momentum of 450 GeV/c seems to guarantee that we deal with an asymptotic hadron-hadron scattering situation. However, this is not automatically the case. Let us consider central production of events in which both scattered hadrons are protons and loose the same energy in their centre of mass system. The two protons with four-momenta  $p_1, p_2$  have a total energy  $\sqrt{s}$ . After scattering, the two protons have four momenta  $p_3, p_4$ , the central system is described by the mass  $M_X^2$  and four-momentum  $p_5$ . Then  $s = (p_1 + p_2)^2$ ,  $s_1 = (p_3 + p_5)^2$ ,  $s_2 = (p_4 + p_5)^2$  where  $s_1, s_2$  are the invariant masses squared of scattered protons with particle  $X$ . When both protons scatter at zero angle,  $s_1 = s_2 = M_X \sqrt{s} + M_p^2$  which is, for 450 GeV/c lab momentum, about  $(5 \text{ GeV})^2/c^4$  at  $M_X = 1 \text{ GeV}/c^2$ , and  $(2.2 \text{ GeV})^2/c^4$  at  $M_X = M_\pi \text{ GeV}/c^2$ . This is a regime where not only Pomeron exchange but also other trajectories should make significant contributions. Hence it is not surprising that both Regge-Regge and Pomeron-Pomeron scattering contribute to central production under the experimental conditions of the WA102 experiment.

A compilation of important cross sections [714] is presented in Table 5. Pomerons are expected to have positive parity and charge conjugation. Double Pomeron Exchange should thus lead to production of isoscalar particles  $X$  with positive  $G$ -parity; isovector particles require the exchange of Reggeons. The production of mesons by Double Pomeron Exchange is predicted to yield a fall-off with squared momentum transfer  $t$  in the form  $e^{bt}$  [710]. Scalar mesons (discussed in chapter 10.2) show compatibility an exponential  $e^{bt}$  distribution but also axial vector mesons and some tensor mesons including the  $a_2(1320)$ .

Table 5

Compilation of cross sections for resonance production at  $\sqrt{s}=29.1 \text{ GeV}$  in the WA102 collaboration [714]. The error quoted represents the statistical and systematic errors summed in quadrature.

$J^{PC}$	Resonance	$\sigma$ ( $\mu\text{b}$ )	$J^{PC}$	Resonance	$\sigma$ ( $\mu\text{b}$ )
$0^{-+}$	$\pi^0$	$22.0 \pm 3.3$	$1^{--}$	$\rho(770)$	$3.1 \pm 0.25$
	$\eta$	$3.9 \pm 0.4$		$\omega(782)$	$7.4 \pm 0.6$
	$\eta'$	$1.7 \pm 0.2$		$\phi(1020)$	$0.06 \pm 0.02$
$0^{++}$	$a_0(980)$	$0.64 \pm 0.06$	$2^{++}$	$a_2(1320)$	$1.7 \pm 0.2$
	$f_0(980)$	$5.7 \pm 0.5$		$f_2(1270)$	$3.3 \pm 0.4$
	$f_0(1370)$	$1.8 \pm 0.6$		$f_2(1525)$	$0.07 \pm 0.01$
	$f_0(1500)$	$2.9 \pm 0.3$		$f_2(1910)$	$0.53 \pm 0.04$
	$f_0(1710)$	$0.25 \pm 0.07$		$f_2(1950)$	$2.8 \pm 0.18$
	$f_0(2000)$	$3.1 \pm 0.5$		$f_2(2150)$	$0.12 \pm 0.2$
$1^{++}$	$a_1(1260)$	$10.0 \pm 0.9$	$2^{-+}$	$\pi_2(1670)$	$1.5 \pm 0.15$
	$f_1(1285)$	$6.9 \pm 1.3$		$\eta_2(1645)$	$1.9 \pm 0.2$
	$f_1(1420)$	$1.1 \pm 0.4$		$\eta_2(1870)$	$1.9 \pm 0.2$

The largest cross section is given by single  $\pi^0$  production. Its large yield is explained by the large  $\pi p$  scattering contribution at small effective energies ( $\sqrt{s_1} \approx \sqrt{s_2} \approx 2.2 \text{ GeV}/c^2$ ). The strong yield of  $f_0$  resonances and the large fraction of high-mass tensor mesons in vector-vector final states are compatible with Double Pomeron exchange. Double Pomeron Exchange is often considered as flavour blind (even though structure functions reveal that the nucleon contains more  $\bar{n}n$  than  $\bar{s}s$  quarks). Production of  $f_2(1525)$  is however strongly suppressed, by a factor  $\sim 50$  compared to  $f_2(1270)$ ,  $\phi$  production by  $\sim 100$  compared to  $\omega$ : flavour symmetry is badly broken. Donnachie

and Landshoff [715] have suggested that there may be two Pomerons; a so-called soft Pomeron with  $y$  axis intercept at  $1.08 \text{ GeV}^2$  on the Chew-Frautschi plot and a hard Pomeron with intercept at  $\sim 1.4 \text{ GeV}^2$ . The soft Pomeron should have a weaker coupling to heavier quarks, and thus SU(3) symmetry can be broken. For Regge exchange, breaking of flavour symmetry is not a problem. Regge trajectories of  $s\bar{s}$  mesons have a higher intercept on the Chew-Frautschi plot, and their exchange falls off with  $s$  faster than the exchange of normal Regge trajectories.

The abundant  $a_1(1260)$  production definitely requires at least one Reggeon. Apart from single  $\pi^0$  production, it provides the largest cross section. The isovector  $a_1(1260)$  is observed in central production with a larger cross section than the isoscalar  $f_1(1285)$  though the two mesons have the same  $J^{PC}$  and about the same mass. Similarly,  $\pi_2(1670)$  is produced with a similar rate as  $\eta_2(1645)$ . The hypothesis that central production at  $\sqrt{s} = 29.1 \text{ GeV}$  is dominated by Pomeron-Pomeron collisions cannot hold true for all reactions.

Further information can be obtained from  $t$  distributions and from angular distributions. The cross sections fall off with  $t \cdot e^{bt}$  for mesons like  $\eta$ ,  $\eta'$ ,  $f_2(1270)$ ,  $f_2(1525)$ ,  $\eta_2(1645)$ , and  $\eta_2(1870)$  while for other mesons (all scalar mesons,  $\rho$ ,  $\Phi$ ,  $a_1(1260)$ ,  $f_1(1285)$ ,  $a_2(1320)$ ), a simple fall-off with  $e^{bt}$  as expected for Double Pomeron Exchange is observed. Other mesons ( $\pi^0$ ,  $\omega$ ,  $\eta_2(1645)$ ) show a mixed behaviour, possibly indicating different reaction mechanisms. The WA91 collaboration noticed that the yield of centrally produced resonances depends on the vector *difference* of the transverse momentum recoil of the final state protons [278]. For fixed four-momentum transfers in the transverse plane,  $t_1 \sim -k_{T1}^2$ ,  $t_2 \sim -k_{T2}^2$ , the quantity  $dk_T \equiv |\vec{k}_{T1} - \vec{k}_{T2}|$  can vary from configurations where two protons are scattered into the same direction or into opposite directions. Generalising this concept, an angle  $\phi$  (in the plane perpendicular to the beam) between slow and fast proton can be defined [716].

The  $dk_T$  (or  $\phi$ ) dependence of central production has been studied intensively in nearly all WA102 publications; its implications are discussed in a series of papers by Close and collaborators [713, 716–721]. The study revealed two surprises. First, many  $q\bar{q}$  mesons show an angular distribution as those produced in double-tag events in two-photon fusion. The exchanged particle must have  $J > 0$ ,  $J = 1$  is the simplest assumption. Using  $\gamma^*\gamma^*$  collisions as an analogy, Close and Schüler [713] calculated the  $\phi$  dependencies for the production of resonances with different quantum numbers. They have found that for a  $J^{PC} = 0^{-+}$  state

$$\frac{d^3\sigma}{d\phi dt_1 dt_2} \propto t_1 t_2 \sin^2 \phi. \quad (4.16)$$

For the  $J^{PC} = 1^{++}$  states the model predicts that  $J_Z = \pm 1$  should dominate, and

$$\frac{d^3\sigma}{d\phi dt_1 dt_2} \propto (\sqrt{t_2} - \sqrt{t_1})^2 + \sqrt{t_1 t_2} \sin^2 \phi / 2. \quad (4.17)$$

The WA102 data were found to be consistent with these calculated angular distributions. If Pomeron-Pomeron scattering were the leading contribution in central production, the angular distribution would imply a vectorial interaction of Pomerons [716]. Here we have to stress that these  $\phi$  dependencies are of merely kinematical origin in Regge phenomenology [709]. In [722], the concept is generalised to exchanges of mesons with arbitrary spin with subsequent reggeisation. Absorptive effects are taken into account by unitarisation of the production amplitudes.

The angular distributions revealed a further unexpected phenomenon. For some states, the angular

distributions were found to be markedly different from those for most well established  $q\bar{q}$  mesons having the same quantum numbers. It has been suggested that the angular distribution identifies intrinsic angular momenta [717]. Thus scalar and tensor mesons in  ${}^3P_0$  or  ${}^3P_2$   $q\bar{q}$  configurations with internal orbital angular momentum  $L = 1$  behave differently than glueballs or  $K\bar{K}$  molecules which need no intrinsic angular momentum. Thus it is suggested that a cut in  $dk_T$  may act as a *glueball filter* separating non- $q\bar{q}$  objects from ordinary  $q\bar{q}$  mesons. This question will be resumed in section 10.2 on scalar mesons in central production.

A final word of caution seems appropriate on the assumption that central production is dominated by Pomeron-Pomeron fusion. This assumption relies on the evolution of  $\rho$  and  $\eta'$  production with  $s$ . While  $\rho$  production decreases with increasing  $s$  indicating Regge exchange as production mechanism,  $\eta'$  production remains approximately constant. This is a behaviour predicted for Pomeron-Pomeron fusion [710]. The large yield of isovector mesons in central production makes it however unlikely that Pomeron-Pomeron fusion is the dominant feature of central production. Fusion of two Regge trajectories must play an important rôle. The scattering of two vector mesons can create scalar, pseudoscalar or axial vector and tensor mesons, and also  $\eta_2$  and  $\pi_2$  couple to  $\omega\omega$  (and  $\rho\rho$ ) and to  $\rho\omega$ , respectively. For  $J^{PC} = 0^{-+}, 1^{++}, 2^{-+}$  mesons, the high yield of isovector mesons and the angular distribution make it likely that at  $\sqrt{s} = 30$  GeV, the dominant mechanism for central production is still fusion of two Regge trajectories. For scalar mesons we notice an one order of magnitude reduction for the  $a_0(980)$  cross section compared to  $f_0(980)$  production; the  $a_0(1450)$  remained unobserved [309] while  $f_0(1500)$  is seen. The  $t$  dependence of scalar mesons shows the expected  $e^{bt}$  behaviour. Hence scalar mesons are compatible with Pomeron-Pomeron fusion as main source of their production mechanism. The rôle of tensor mesons is less clear. The  $a_2(1320)/f_2(1270)$  production ratio is about 1/2. At higher masses, little is known about isovector states. Isoscalar tensor mesons from central production of  $\rho\rho$ ,  $\rho\omega$ ,  $\omega\omega$  and  $\phi\omega$  have been reported by WA102 [297, 299, 312] but data on  $\rho\omega$  are missing. WA76, using a 300 GeV/c proton beam, studied the centrally produced  $\omega\rho$  and  $\omega\omega$  systems. They found  $304 \pm 50$   $\omega\rho$  events. From their distributions one can estimate  $200 \pm 100$   $\omega\omega$  events. Since  $\omega\rho$  requires at least one Regge trajectory to participate, there is no real evidence that two centrally produced vector mesons originate from Pomeron-Pomeron fusion. Obviously, at  $\sqrt{s} = 29.1$  the regime of double Pomeron exchange is not yet fully reached and depends on the quantum numbers of the produced system: scalar meson production is compatible in all aspects with Pomeron-Pomeron fusion, production of tensor mesons seems to receive contributions from both, Regge and double Pomeron exchange while pseudoscalar, vector and axial vector mesons are still in the regime of Reggeon exchange.

#### 4.1.4 The Deck effect

In the study of quasi-two body reactions one has to take into account production of resonances as well as nonresonant production of final states. A specific model was proposed by Deck [723] to describe nonresonant effects in quasi-two body reactions at high energy. Consider e.g. the reaction  $\pi^- p \rightarrow p \rho\pi$  in the region of the  $a_1(1260)$  meson, with the  $\rho\pi$  system having  $I^G J^{PC} = 1^{-1}^{++}$  quantum numbers. This reaction can proceed via direct  $a_1$  production (Fig. 30 (a)), via  $\pi$  exchange (Fig. 30 (b)) and via  $\pi$  exchange with rescattering (Fig. 30 (c)). The Deck model amplitude has the form [724]:

$$\frac{A}{k} \cdot e^{i\delta} \cdot \sin\delta + B \cdot e^{i\delta} \cdot (\cos\delta + \frac{\alpha}{k} \cdot \sin\delta) \quad (4.18)$$

where  $A$  represents  $a_1(1260)$  production and  $B$  the Deck amplitude with a pion propagator. The elastic  $\rho\pi$  phase shift  $\delta$  is given by a Breit-Wigner amplitude,  $k$  is the  $\rho\pi$  phase space. The predictions of this model are far from being trivial. It gives the intensities and phases of

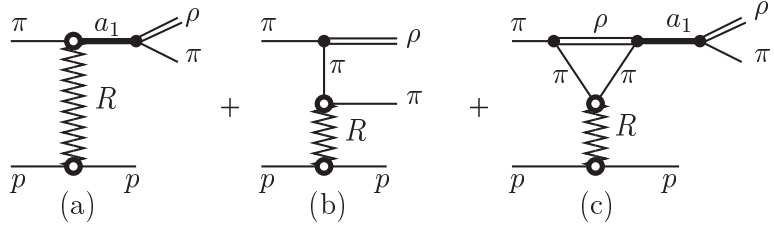


Fig. 30. Direct resonance production (a) and the Deck mechanism via  $\pi$  exchange (b) and via  $\pi$  exchange and rescattering (c).

nonresonant contributions in different final  $J^{PC}$  states with different isobars as well as the  $t$  dependence of all these contributions. In particular with increasing squared momentum transfer  $|t|$ , the nonresonant contribution has to decrease since the nonresonant  $\rho\pi$  system has a larger spatial extension than the  $a_1(1260)$ . In diffractive reactions, the Deck model predictions are in reasonable agreement with experimental results [214].

#### 4.1.5 Antiproton-proton annihilation

In  $N\bar{N}$  annihilation, a nucleon and an antinucleon undergo a transition from the baryonic world to the quanta of strong interactions, to mesons. Even for annihilation at rest, mesons of up to  $1.7 \text{ GeV}/c^2$  can be produced. The mass of meson resonances carrying open strangeness is restricted to about  $1.4 \text{ GeV}/c^2$ . The OZI rule disfavours production of mesons with hidden strangeness even though in some reactions,  $\phi$  production was found to surprisingly large. There is an abundant literature on the question if the large  $\phi$  production rate signals an  $s\bar{s}$  component in the proton wave function [725], or the  $\phi$ 's are produced via rescattering of Kaons in the final state [726, 727]. See [728] for a review.

A large number of meson resonances has been studied in  $N\bar{N}$  annihilation at rest [46, 48] and in flight [49]. The annihilation process and the formation of  $\bar{p}p$  atoms preceding annihilation has been reviewed in some detail in [729, 730]; here we emphasize a few points relevant for the further discussion.

In  $N\bar{N}$  annihilation at rest in  $H_2$  or  $D_2$ , annihilation is preceded by capture of an antiproton by a hydrogen or deuterium atom. Collisions between the protonium atom and surrounding molecules induce transitions from high orbital angular momentum states via Stark mixing; and this mixing is fast enough to ensure dominant capture from  $S$ -wave orbitals when antiprotons are stopped in liquid  $H_2$  or  $D_2$ . In gas, the collision frequency is reduced and  $P$ -wave annihilation makes significantly larger contributions. In particular at very low target pressures the  $P$ -wave fractional contribution is very large. Alternatively, rather pure samples of  $P$ -wave annihilation can also be studied by coincident detection of X-rays emitted in the atomic cascade of the  $\bar{p}p$  system (which feed mostly the  $2P$  level).

Proton and antiproton both carry isospin  $|I, I_3\rangle = |\frac{1}{2}, \pm\frac{1}{2}\rangle$ . The two isospins couple to  $|I = 0, I_3 = 0\rangle$  or  $|I = 1, I_3 = 0\rangle$  with  $I_3 = 0$ . In the absence of initial state interactions between proton and antiproton the relation

$$\bar{p}p = \sqrt{\frac{1}{2}} (|I = 1, I_3 = 0\rangle + |I = 0, I_3 = 0\rangle).$$

holds. One could expect processes of the type  $\bar{p}p \rightarrow \bar{n}n$  in the initial state but charge exchange - which would lead to unequal weight of the two isospin components - seems to be not very important [731].

The quantum numbers of the  $\bar{p}p$  system are the same as those for  $q\bar{q}$  systems; both are bound states of fermion and anti-fermion. Since isospin can be  $I = 0$  or  $I = 1$ , every atomic  $\bar{p}p$  state may have  $G$ -parity +1 or -1. Table 6 lists the quantum numbers of atomic levels from which annihilation may occur. The  $\bar{p}n$  system has always  $I = 1$ , and every atomic level has defined  $G$ -parity. For annihilation into specific final states, selection rules may restrict the number of initial states. Annihilation into any number of  $\pi^0$  and  $\eta$  mesons is e.g. forbidden from all initial states with negative  $C$ -parity .

Table 6  
Quantum numbers of levels of the  $\bar{p}p$  atom from which annihilation may occur.

$^{2S+1}L_J$	$I^G (J^{PC})$		$^{2S+1}L_J$	$I^G (J^{PC})$	
$^1S_0$	$1^-(0^{-+})$	$0^+(0^{-+})$	$^1P_1$	$1^+(1^{+-})$	$0^-(1^{+-})$
$^3S_1$	$1^+(1^{--})$	$0^-(1^{--})$	$^3P_0$	$1^-(0^{++})$	$0^+(0^{++})$
			$^3P_1$	$1^-(1^{++})$	$0^+(1^{++})$
			$^3P_2$	$1^-(2^{++})$	$0^+(2^{++})$

Unlike other processes, annihilation dynamics has no preference of producing low-mass mesons compared to mesons having a large mass. In central production or two-photon fusion, the meson mass spectrum falls off with  $1/M^2$  (with  $M$  being the meson mass); there is no similar suppression of high masses in  $p\bar{p}$  annihilation. Rather,  $N\bar{N}$  annihilation can be described as if the final state would be produced as ‘white’ spectrum distributed according to the phase space which then needs to be multiplied with a dynamical weight accounting for final-state interactions. Experiment shows [732] that the angular momentum barrier (for  $\ell = 0, 1$  or 2) does not play a significant rôle: the ratio of  $\omega\eta'$  to  $\omega\eta$  annihilation frequencies is about 1/2. The angular momentum in the reaction is  $\ell = 1$ , the linear momenta differ by a factor 2. Hence a reduction in the order of  $2^{2\ell+1} = 8$  due to phase space and angular momentum barrier should be expected, in addition to a factor 0.5 accounting for the larger  $n\bar{n}$  component of the  $\eta$  wave function (compared to the  $\eta'$  wave function). The reduction found experimentally is about 0.5, compatible with the smaller  $n\bar{n}$  component of the  $\eta'$  wave function from which the  $\bar{p}p$  system decouples. Likewise, production of  $a_2(1320)\pi$  – requiring  $\ell = 2$  between  $a_2(1320)$  and  $\pi$  – is as frequent as production of  $\rho\pi$  with  $\ell = 1$ .

The initial  $N\bar{N}$  state contains three constituent quarks and three antiquarks. In annihilation into two mesons, two  $q\bar{q}$  pairs are going out.  $N\bar{N}$  annihilation is a superposition of quark-antiquark annihilation and rearrangement diagrams, with an intermediate state of quarks and gluons. One may therefore expect  $N\bar{N}$  annihilation to be a good process to search for multiquark (tetraquark- or baryonium) states and for hybrids. Glueballs can be produced by their mixing with  $q\bar{q}$  mesons.

#### 4.1.6 Flavour tagging

4.1.6.1 *Charge and strangeness exchange scattering:* In the charge exchange reaction,  $\pi^- + \text{proton} \rightarrow \text{neutron} + \text{meson}$ , charged mesons like  $\pi$  or  $b_1$  (unnatural parity exchange) or  $\rho/a_2$  (natural parity exchange) are exchanged and mesons are produced with a preferred  $n\bar{n}$  flavour structure. For incident  $K^-$ , the baryon in the final state can be neutron or a  $\Lambda$ . Under these

experimental conditions, mesons with open ( $n\bar{s}$ ) and with hidden ( $s\bar{s}$ ) flavour are produced dominantly, see Fig. 31. This method was extensively exploited by the LASS collaboration [733, 734]. At high energies, the incoming meson can be excited without changing its flavour structure. Such processes are often called Pomeron exchange reaction even though  $f_2$  exchange leads to the same flavour in the final state.

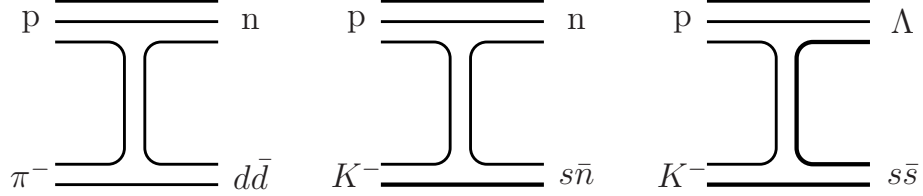


Fig. 31. Flavour tagging in scattering experiments. Up and down quarks are shown as thin, strange quarks as thick lines. In the first two reactions, a charged  $n\bar{n}$  meson is exchanged, and the meson in the final-state meson is neutral and carries the strangeness of the incoming pion or Kaon. If a hyperon is detected in coincidence, the produced meson is likely to carry hidden strangeness.

**4.1.6.2  $J/\psi$  decays:** The mass of the  $J/\psi$  is below the threshold for decay into mesons having *open* charm, hence the  $c\bar{c}$  pair must annihilate and new particles have to be created (see figure 32). Such processes are suppressed. The  $c\bar{c}$  bound state converts into gluons carrying a large four-momentum, and the coupling is small. Hence the  $J/\psi$  is narrow. The OZI rule can be exploited to tag the flavour of mesons produced in  $J/\psi$  decays in cases where one of the two mesons has a known flavour content. If it is a  $\bar{u}u + \bar{d}d$  meson like the  $\omega$ , the recoiling meson is produced via its  $\bar{u}u + \bar{d}d$  component. If a  $\phi(1020)$  is produced, the recoiling meson is produced through its  $\bar{s}s$  component. In this way, the flavour structure of mesons can be determined. This was done e.g. for the  $\eta$  and  $\eta'$  mesons [735, 736] and led to the pseudoscalar mixing angle as discussed in section 1.2.3. Flavour tagging of scalar mesons has led to surprising results which will be discussed in section 10.6.

**4.1.6.3  $D$ ,  $D_s$  and  $B$  decays:** Due to their large mass,  $D$  and  $D_s$  decays are well suited to study the light meson mass spectrum. A number of different three- and four-body final states has been analysed and interesting results, particularly on scalar mesons, were obtained. The results from partial wave analyses will be discussed in section 10.5. Here we restrict ourselves to general considerations.

$D$  and  $D_s$  mesons may decay via different mechanisms depicted in Fig. 33. A  $c$  quark converts into a quark  $q$  ( $q = d, s, b$ ) by emission of a virtual  $W^+$ . The  $W^+$  decays into a  $q\bar{q}$  meson. The  $q\bar{q}$  meson may escape; this is the leading diagram (a). Quark and antiquark may split to find

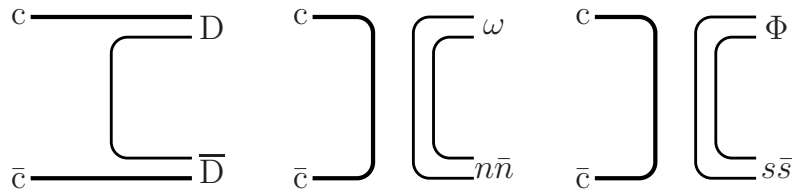


Fig. 32. Decays of charmonium states into  $\bar{D}\bar{D}$  are allowed only above the  $\bar{D}\bar{D}$  threshold, the  $J/\psi$  (and the  $\eta_c$  and  $\chi$  states) can decay only into light quarks. A  $\omega$  or  $\Phi$  signal determines the  $\bar{u}u + \bar{d}d$  and  $\bar{s}s$  component, respectively, of the recoiling meson. The thick lines represent charmed quarks.

a antiquark-quark pair. Now the colours have to match, the process is colour suppressed (b). Finally, the initial  $c\bar{q}$  may annihilate directly into a virtual  $W^+$  (c). The diagrams can be Cabibbo allowed or suppressed. The  $c$  quark prefers to convert into an  $s$  quark, conversion into a  $d$  quark is suppressed by the matrix element  $|V_{cd}|^2 = (0.224 \pm 0.012)^2$  of the CKM matrix. Likewise, the  $W^+$  can convert into  $u\bar{d}$  or  $u\bar{s}$  where the latter is Cabibbo suppressed, too. We estimate the relevance of the contributions by comparing branching ratios of simple reactions.

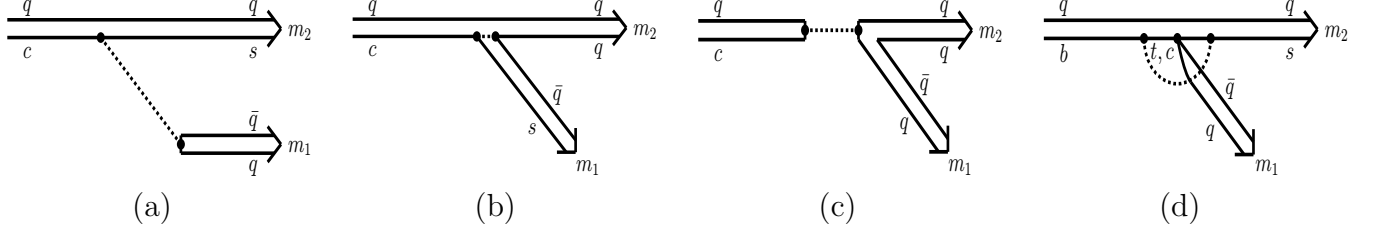


Fig. 33. Decays of charmed meson: a) leading mechanism, b) colour suppressed diagram, c) annihilation diagram. Here,  $q$  can be  $d$  or  $s$  quarks. d)  $B$  decays into light quarks prefer penguin diagrams to which  $b$  quarks contribute, too.

$D^0 = c\bar{u}$  mesons cannot decay via the annihilation diagram (c). In colour allowed decays, the  $W^+$  converts into a positively charged meson; in an Cabibbo allowed decay mode, this is a  $\pi^+$ . The  $c$  quark converts in a Cabibbo allowed transition into an  $s$  quark making a  $K^-$  by picking up the 'spectator'  $\bar{u}$  quark. In colour suppressed decays, the strange quark picks up the  $u$  quark from internal  $W^+$  conversion, the  $\bar{d}$  and the  $s$  quark form a  $\bar{K}^0$  or  $\bar{K}^{0*}$ . Table 7 compares these two types of decay branching ratios. The colour-suppressed reactions are observed with branching ratios which are smaller by a factor 2. This factor depends on the particular reaction, the factor 2 provides an order of magnitude estimate for further discussions.

Table 7  
Branching ratios for  $D^0$  decays [1].

	colour allowed	colour suppressed
$\pi^+ K^-$	$(3.80 \pm 0.09)\%$	$\pi^0 \bar{K}^0$ $(2.30 \pm 0.22)\%$
$\rho^+ K^-$	$(10.1 \pm 0.8)\%$	$\rho^0 \bar{K}^0$ $(1.55^{+0.12}_{-0.16})\%$
		$\omega \bar{K}^0$ $(2.3 \pm 0.4)\%$
$\pi^+ K^{*-}$	$(5.9 \pm 0.5)\%$	$\pi^0 \bar{K}^{*0}$ $(2.8 \pm 0.4)\%$

In a similar spirit we derive an estimate for the fraction of annihilation in  $D_s^+$  decays. The fraction of leptonic and semileptonic decay modes is about 25%, the branching ratio for  $D_s^+ \rightarrow \tau^+ \nu_\tau$  is  $(6.4 \pm 1.5)\%$ . For  $D_s^+ \rightarrow \tau^+ \nu_\tau$ , helicity conservation plays no rôle since  $\frac{v}{c} = 0.09$ ; decays into lighter particles are suppressed. For constituent quark masses of 350 MeV,  $\beta \sim 0.85$ . There is the colour factor 3 but still, we expect an annihilation contribution to hadronic decay modes of a few percent only.

Due to its high mass,  $B$  decays offer access to a wide range of spectroscopic issues. In  $B$  decays, the first three diagrams in Fig. 33 lead to charmed mesons. Here we use one example, the  $\eta_c(2S)$ , to show the power of this method. The BELLE collaboration searched for the  $\eta_c(2S)$  in the reaction  $B^\pm \rightarrow K^\pm \eta_c(2S)$  and  $B^0 \rightarrow K_S^0 \eta_c(2S)$  with  $\eta_c(2S)$  decaying into  $K^\pm \pi^\mp K_S^0$  [737]. After cuts to reduce background from non  $B$  events, a spectrum shown in Fig. 34 is obtained. The fit to the mass spectrum yields  $39 \pm 11$  events centred at  $3654 \pm 6$  MeV/c<sup>2</sup>. The width was determined to  $15^{+24}_{-15}$  MeV/c<sup>2</sup>. The properties of the resonance, mass, width, production and decay mode, are

compatible with it being the  $\eta_c(2S)$ . The peak was confirmed by BaBar [590] and CLEO [738] in  $\gamma\gamma$  fusion; the angular distributions favour  $0^{-+}$  so that the interpretation of the peak as  $\eta_c(2S)$  seems to be settled.

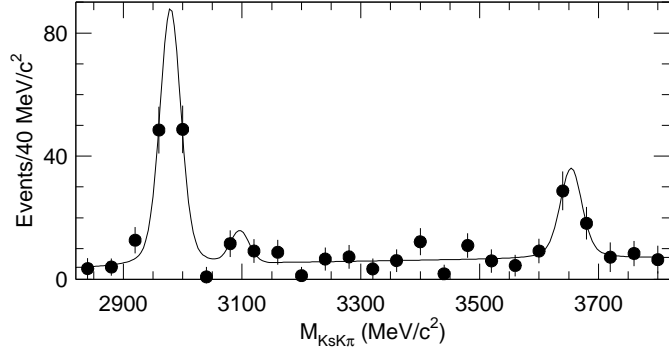


Fig. 34. The  $K_S^0 K\pi$  mass distribution from  $B^\pm \rightarrow K^\pm (K_S^0 K\pi)$  events. The two peaks are assigned to  $B^\pm \rightarrow K^\pm \eta_C(1S)$  and  $B^\pm \rightarrow K^\pm \eta_C(2S)$  events [737].

Production of light mesons by one of the diagrams in Fig. 33 proceeds via the matrix element  $|V_{bu}|$  which is only  $(0.00367 \pm 0.00047)$ . The (rare) hadronic decays into final states containing no  $c$  quarks make use of so-called Penguin diagrams (Fig. 33d) in which the  $b$  quark converts into a  $u, c$  or  $t$  quark by emission of a  $W^-$  which is reabsorbed to produce a  $d$  or  $s$  quark.

Flavour symmetry can be invoked to relate charmless two-body decay modes [739] into two pseudoscalar mesons. The large branching ratio for reactions like  $B \rightarrow K\eta'$  can be understood when a phenomenological flavour singlet amplitude is introduced which takes into account the  $\eta'$  affinity to gluons in the initial state. This observation motivated Minkowski and Ochs [740] to extend their study to  $B$  to scalar- and pseudoscalar-meson decay modes and to discuss scalar glueball contributions in  $B$  decays.

## 4.2 Meson resonances in formation experiments

### 4.2.1 $e^+e^-$ annihilation

A typical example of a *formation* experiment is annihilation of a  $e^+e^-$  pair into hadrons. The energies of an electron and positron beam (in  $e^+e^-$  storage rings these are often the same, except for the  $b$  factories) are tuned to the desired value and the probability to produce hadronic final states is determined. The cross sections are then obtained by scanning the  $e^+e^-$  total energy  $\sqrt{s}$  over the desired energy range.

Fig. 35 shows the total cross section for  $e^+e^-$  annihilation into hadrons. Peaks are seen which can be identified with  $\rho$ ,  $\omega$  and  $\phi$ . The series of narrow resonances belongs to the  $c\bar{c}$  and  $b\bar{b}$  families; at the highest energy, the  $Z$ , the neutral weak interaction boson, is seen. The reaction is dominated by a one-photon intermediate state; hence only resonances with quantum numbers  $J^{PC} = 1^{--}$  are formed. Strangeness, charm beauty (and truth) are conserved in electromagnetic interactions,  $K^*$ 's are not seen  $e^+e^-$  formation (but can be produced with a recoiling Kaon).

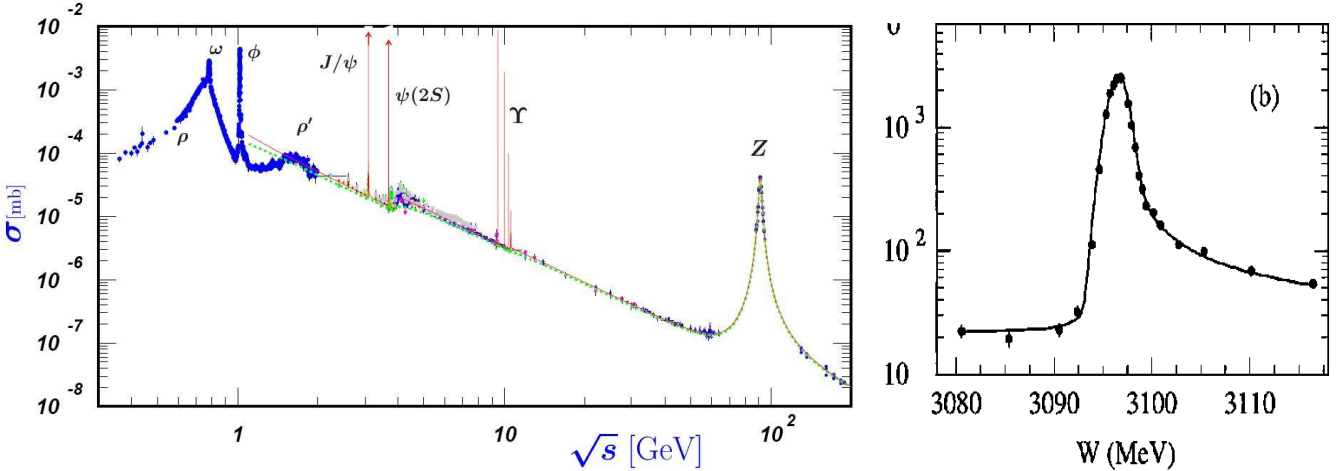


Fig. 35. a:  $e^+e^-$  hadronic cross section (from [1]). b:  $e^+e^-$  cross section (in nb) for the reaction  $e^+e^- \rightarrow \rho\pi$  [741].

#### 4.2.2 Width of the $J/\psi$

Fig. 35b shows an expanded view of the  $J/\psi$  region for the reaction  $e^+e^- \rightarrow \rho\pi$  [741]. A clear peak at the  $J/\psi$  mass is observed. The asymmetry of the line shape is due to the loss of some energy by initial state radiation which is taken into account in the fit. The width of the curve is completely dominated by the momentum spread of the beam; the natural width of the  $J/\psi$  is too narrow to be determined directly from the scan. However, the width is related to the total cross section observed in a specific reaction. The cross section can be written in the form

$$\sigma(E) = (4\pi)(\lambda^2/4\pi^2) \frac{\Gamma_{e^+e^-}\Gamma_{final}/4}{[(E - E_R) + \Gamma^2/4]} \frac{2J+1}{(2s_1+1)(2s_2+1)} \quad (4.19)$$

with  $\lambda/2\pi = 1/p = 2/E$  being the de Broglie wavelength of  $e^+$  and  $e^-$  in the centre-of-mass system (cms),  $E$  the cms energy, and  $\Gamma$  the total width. The first quotient of the right-hand side of (4.19) is the usual Breit-Wigner function describing a resonant behaviour. The second quotient sums over the spin components in the final state and averages over the spin components in the initial state.  $s_1 = s_2 = 1/2$  are electron and positron spin;  $J = 1$  is the  $J/\psi$  total angular momentum.  $\Gamma_{e^+e^-}$ ,  $\Gamma_{final}$  are the partial widths for the decay into the initial and final state, respectively. Integration over the cross section yields

$$\int_0^\infty \sigma(E_{e^+e^- \rightarrow e^+e^-, \mu^+\mu^-, \text{hadrons}}) dE = \frac{6\pi^2}{E_R^2 \Gamma} \Gamma_{e^+e^-} \Gamma_{(\mu^+\mu^-, \text{hadrons})}. \quad (4.20)$$

for the three final states  $e^+e^-$ ,  $\mu^+\mu^-$ , and hadrons. The total width is given by the sum of the partial decay width

$$\Gamma = \Gamma_{e^+e^-} + \Gamma_{\mu^+\mu^-} + \Gamma_{\text{hadrons}}. \quad (4.21)$$

Imposing  $\Gamma_{e^+e^-} = \Gamma_{\mu^+\mu^-}$  yields 3 equations and thus 3 unknown widths.

The  $J/\psi$  has a mass of  $3096.87 \pm 0.04$  MeV/c<sup>2</sup> and  $87 \pm 5$  keV/c<sup>2</sup> width. We may compare this to the  $\rho$  mass, 770 MeV, and its width 150 MeV/c<sup>2</sup>. Obviously the  $J/\psi$  is extremely narrow. This can

be understood by assuming that the  $J/\psi$  is a bound state of a new kind of quarks called charmed quarks  $c$ , and that

$$J/\psi = c\bar{c}.$$

The Okubo-Zweig-Ishida (OZI) rule then explains why the  $J/\psi$  is so narrow. Historically, the discovery of the  $J/\psi$  was a major breakthrough in particle physics and a final proof of the quark model.

#### 4.2.3 Initial state radiation

The shape of  $J/\psi$  signal in Fig. 35 differs from a Breit-Wigner one (4.19) for two main reasons - the energy spread of the  $e^+$  and  $e^-$  beams and for initial state radiation. In  $e^+e^-$  colliders, the energy spread is driven mainly by quantum fluctuations of synchrotron radiation. The spread depends on the magnetic fields, a typical value is a few MeV/c<sup>2</sup>. For this reason, narrow resonances like  $J/\psi$  are significantly distorted; the visible peak cross section is reduced by  $\Gamma(J/\psi)/\delta(E_{cm})$  (where  $\delta(E_{cm})$  is the spread of the total energy) and the visible width is close to  $\delta(E_{cm})$ .

The effects of initial state radiation (ISR) can be illustrated in the reaction  $e^+ e^- \rightarrow \mu^+ \mu^- \gamma$  in the vicinity of  $J/\psi$  peak. The Born cross section for  $J/\psi$  production is given by

$$\frac{d\sigma_{J/\psi(s,x)}^{Born}}{dx} = W(s, x) \times \sigma_0(s(1-x)) \quad (4.22)$$

where  $\sqrt{s}$  is the  $e^+ e^-$  invariant mass,  $x = 2E_\gamma/\sqrt{s}$ ,  $E_\gamma$  is the photon energy in the CMS, and  $\sigma_0$  is the Born cross section for  $e^+ e^- \rightarrow J/\psi \rightarrow \mu^+ \mu^-$ . The function

$$W(s, x) = \frac{2\alpha}{\pi x} \times \left(2\ln\frac{\sqrt{s}}{m_e} - 1\right) \times \left(1 - x + \frac{x^2}{2}\right) \quad (4.23)$$

describes the probability of ISR photon emission. To first approximation, the Born cross section for  $e^+ e^- \rightarrow J/\psi \rightarrow \mu^+ \mu^-$  is given by the Breit-Wigner formula (4.19). For a narrow resonance like  $J/\psi$  we can replace the Breit-Wigner function by a  $\delta$  function, integrate over the photon energy and find

$$\sigma_{J/\psi}^{Born}(s) = \frac{12\pi^2\Gamma_{ee}B_{\mu\mu}}{m s} \times W(s, x_0), \quad x_0 = 1 - \frac{m^2}{s} \quad (4.24)$$

The asymmetry of  $J/\psi$  signal (tail to high  $s$ ) is clearly seen. Interference of  $J/\psi$  resonant and QED nonresonant amplitudes has of course to be accounted for. By detecting the ISR photon, one can study vector final states with masses well below the energy of  $e^+ e^-$  collider. This effect is called radiative return [742–744]. The method is a new tool in meson spectroscopy, in particular for the study of vector mesons. It has been exploited in Frascati, using the Daphne detector, to measure the hadronic cross section for  $e^+e^-$  annihilation in the region below the  $\phi$  mass [745]. The BaBar collaboration, with a collider energy set to the  $\Upsilon(4s)$ , covered the mass range from low-energies up to the bottomonium states. The dynamics of  $e^+e^-$  annihilation into several final states were studied from  $\pi^+\pi^-\pi^0$  to  $2(\pi^+\pi^-)K^+K^-$  [593, 601, 619].

#### 4.2.4 Decay of $\tau$ mesons

The vector and axial vector couplings in  $\tau$  decays gives access to studies of the properties of  $\rho(1450)$  and  $a_1(1260)$  mesons. Evidence is also observed for a radial excitation at  $1700 \text{ MeV}/c^2$ . We refer the reader to [746] for more detailed information. In  $\pi$  scattering,  $a_1(1260)$  is obscured by the Deck effect and unstable results were obtained for a long time.

#### 4.2.5 The $\chi$ states in $\bar{p}p$ annihilation

The charmonium  $\chi$  states can be observed in  $\bar{p}p$  annihilation by a scan of the antiproton momenta. Of course,  $c\bar{c}$  states couple only weakly to  $p\bar{p}$  since all 3 quarks and antiquarks in the initial state have to annihilate into gluons before a meson with hidden charm can be produced. The  $\chi$  states radiate down to the  $J/\psi$  ground state which then decays into an electron-positron or  $\mu^+\mu^-$  pair. Lepton pairs with having a large invariant mass are rarely produced in  $p\bar{p}$  annihilation; hence high-mass lepton pairs can be used as very selective trigger.

The decisive advantage of this approach is the possibility to study the  $\chi$  states in formation. The observed width is determined by the spread of beam momenta, and this can be made narrow. Figure 36 shows scans of the  $\chi_{c1}(1P)$  and  $\chi_{c1}(2P)$  regions. The experimental resolution, given by the precision of the beam momentum, is shown as a dashed line. The observed distributions are broader: the natural widths of the states due to their finite life time can be directly determined.

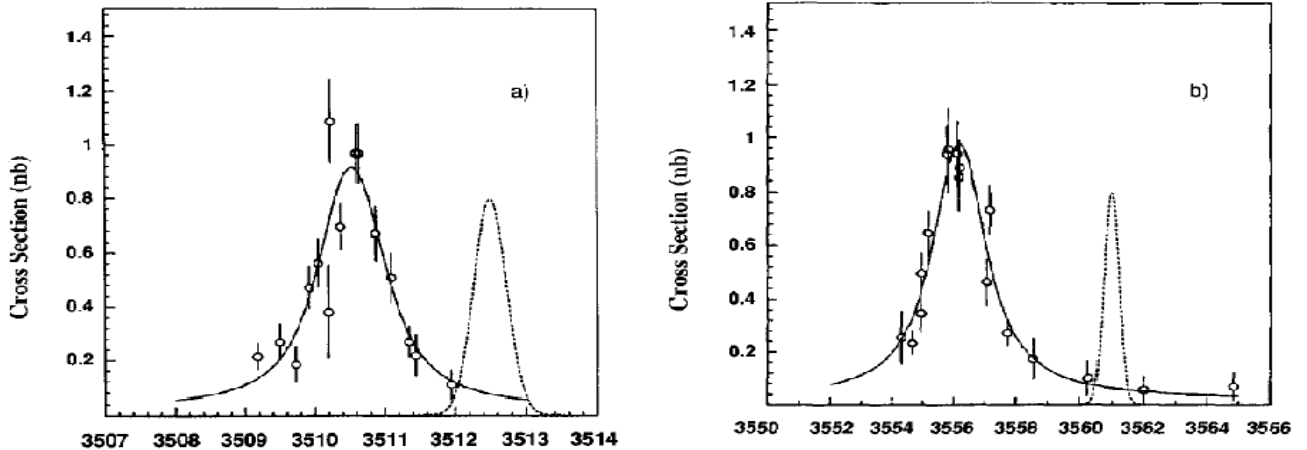


Fig. 36. The number of  $J/\psi$  as a function of the  $\bar{p}p$  mass in the  $\chi_1$  (a) and  $\chi_2$  (b) mass regions [396].

The impressive gain in accuracy achieved in a formation experiment can be visualised in a comparison with the  $\chi$  states as observed in production. Figure 37 shows the inclusive photon spectrum from the  $\psi(2S)$  states [747]. A series of narrow states is seen identifying the masses of intermediate states. The level scheme assigns the lines to specific transitions as expected from charmonium models. The width of the lines is given by the experimental resolution of the detector; the charmonium states are *produced*. The lowest mass state, the  $1^1S_0$  state, is called  $\eta_c$ . It is the analogue of the  $\eta'$ -meson.

### 4.3 Glueball rich processes

QCD, at least in its formulation on a lattice, predicts the existence of glueballs, of bound states of gluons with no constituent quarks. The search for these states and their possible rôle within

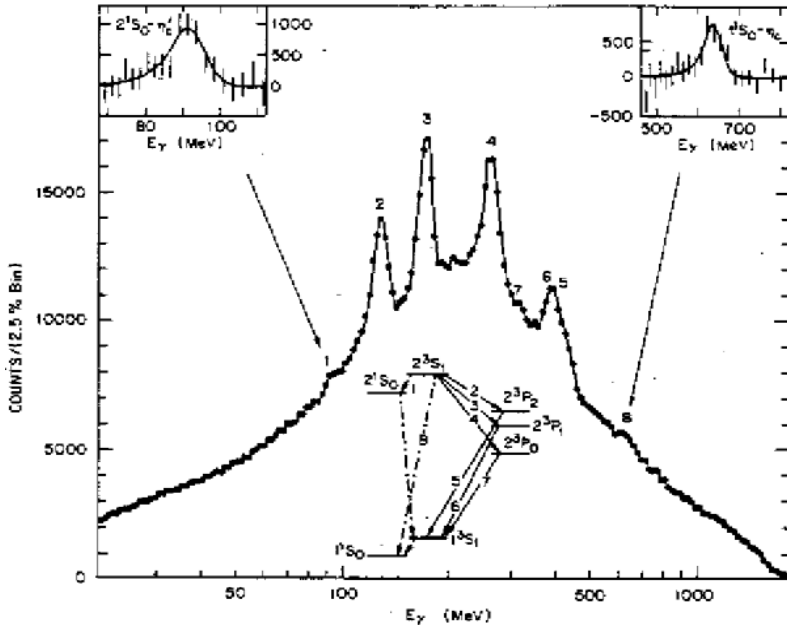


Fig. 37. Radiative transitions between charmonium levels [747]).

the family of  $q\bar{q}$  mesons is one of the topical issues of this review. There is an extensive folklore on how to hunt for glueballs [711] and which distinctive features should identify them as non- $\bar{q}q$  mesons. Glueballs should, e.g., be produced preferentially in so-called gluon-rich processes; some are depicted in Fig. 38.

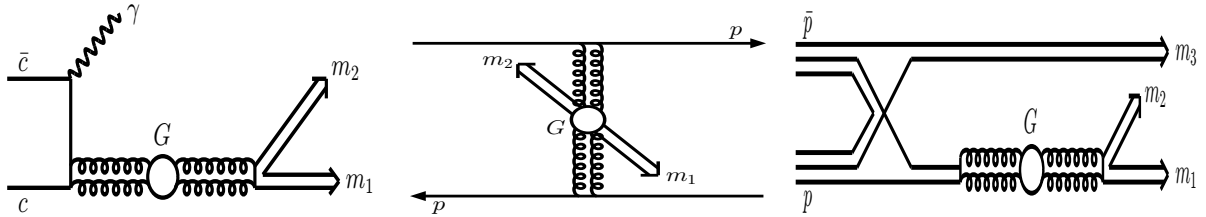


Fig. 38. Diagrams possibly leading to the formation of glueballs: radiative  $J/\psi$  decays, Pomeron-Pomeron collisions in hadron-hadron central production, and in  $p\bar{p}$  annihilation.

The most suggestive process is the radiative  $J/\psi$  decay. The  $J/\psi$  is narrow; the  $D\bar{D}$  threshold is above the mass of the  $J/\psi$  and the OZI rule suppresses decays of the  $c\bar{c}$  system into light quarks. In most decays, the  $J/\psi$  undergoes a transition into 3 gluons which then convert into hadrons. But  $J/\Psi$  can also decay into 2 gluons and a photon. The photon can be detected, the two gluons interact and must form glueballs - if they exist.

Central production is another process in which glueballs should be abundantly produced. In central production two hadrons pass by each other ‘nearly untouched’ and are scattered diffractively into forward direction. No valence quarks are exchanged. The process is often called Pomeron-Pomeron scattering or double Pomeron exchange. The absence of valence quarks in the production process makes central production a good place to search for glueballs.

In  $p\bar{p}$  annihilation, quark-antiquark pairs annihilate into gluons, they interact and may form glueballs. Glueballs decay into hadrons and hence hadro-production of glueballs is always possible. The probability that two gluons escape from the  $p\bar{p}$  system to form a glueball is a bit remote.

Production of glueballs should be suppressed in  $\gamma\gamma$  collisions since photons couple to the intrinsic

charges. So we should expect a glueball to be strongly produced in radiative  $J/\psi$  decays but not in  $\gamma\gamma$  fusion. Radial excitations might be visible only weakly in  $J/\psi$  decays but they should couple to  $\gamma\gamma$ . Further distinctive features can be derived from their decays (glueballs are flavour singlets). Decays to  $\eta\eta'$  identify a flavour octet; radiative decays of glueballs are forbidden. All these arguments have to be taken with a grain of salt: mixing of a glueball with mesons having the same quantum numbers can occur and would dilute any selection rule.

## 5 Heavy-quark spectroscopy

The discovery of a narrow high-mass resonance at Brookhaven National Laboratory (BNL) in the process proton + Be  $\rightarrow e^+e^- + \text{anything}$  [84] and at the Stanford University in  $e^+e^-$  annihilation to  $\mu^+\mu^-$ ,  $e^+e^-$  and into hadrons [85] initiated the ‘November revolution of particle physics’. In the subsequent years, several narrow charmonium states were observed. The states below the  $D\bar{D}$  threshold have a small available phase space for decays mode into other charmonium states; they may also decay into mesons with light quarks only, via gluonic intermediate states. The strong interaction fine structure constant  $\alpha_s$  is already sufficiently small at these momentum transfers ( $\alpha_s \sim 0.3$ ) resulting in small strong interaction widths.

The quark model predicts a rich spectrum of charmonium states. Fig. 39 gives a survey of observed and expected states. Some transitions are indicated by arrows. The  $h_c(1P)$  – shown as  $^1P_1(3254)$  – is, for example, forbidden to decay into  $J/\psi$  radiatively; allowed are decays into  $\pi^0 J/\psi$  or  $\gamma \eta_c(1S)$  (as E1 transition).

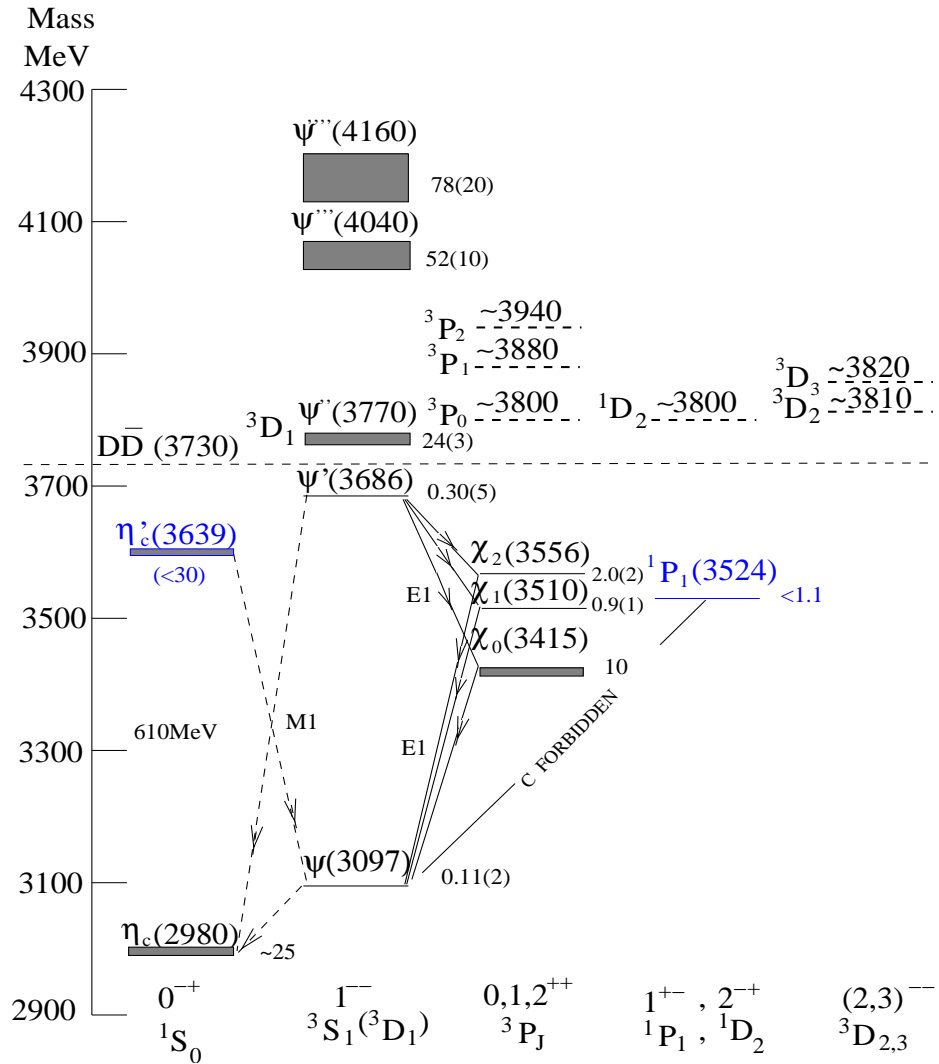


Fig. 39. The charmonium family of states and transitions between them [748]. Established resonances are shown as solid lines, predicted states as dashed lines. Widths and their errors are added as small numbers. In the bottomonium family, the  $3S$  and  $2P$  states are also stable against decays into  $B\bar{B}$ .

The physics of  $c\bar{c}$  states has found renewed interest due to the discovery of a series of unexpectedly narrow states, and several excellent review articles have been written which document the achievements [50, 63, 748–751]. Here, we give a short survey of the field. This will allow us to emphasize the intimate relation between the spectroscopy of heavy quarks and of their light cousins.

## 5.1 The $J/\psi$ states below the $D\bar{D}$ threshold

In  $e^+e^-$  annihilation, charmonium states with  $J^{PC} = 1^{--}$  can be observed and their mass be determined with the (high) precision with which the frequency of the circulating beam can be determined (see section 3.4.1). Positive  $C$ -parity states can be detected via radiative transitions from the  $\psi(2S)$  resonance but only with the (poorer) accuracy of the photon energy measurement [747]. This limitation can be overcome by  $p\bar{p}$  formation experiments as discussed in section 3.3.4. Exploiting this technique, the E835 experiment added to our knowledge an impressive amount of high-precision data on the  $c\bar{c}$  system. From BES and earlier experiments, a large number of branching ratios of the charmonium states is known. Their discussion will be resumed when they provide information on light-quark spectroscopy. A comparison of charmonium decay modes with model calculations is beyond the scope of this review. The two states  $\eta_c(2S)$  and  $h_c(1P)$  were observed only recently. Their discovery will be briefly discussed.

### 5.1.1 The $h_c(1P)$

The  $h_c(1P)$  was searched for intensively by the E760/835 collaboration in the reaction chain  $p\bar{p} \rightarrow h_c(1P) \rightarrow \pi^0 J/\psi \rightarrow \pi^0 e^+e^-$  but, at the end, no conclusive evidence was found [401]. Stimulated by an observation of the CLEO collaboration [575] discussed below, E835 studied the reaction  $p\bar{p} \rightarrow h_c \rightarrow \gamma\eta_c(1S) \rightarrow 3\gamma$  and reported a  $3\sigma$  signal [401] which was assigned to  $h_c(1P)$ . Its mass was determined to  $M(h_c) = 3525.8 \pm 0.2 \pm 0.2 \text{ MeV}/c^2$ , its width  $\Gamma(h_c) < 1 \text{ MeV}/c^2$ .

The best evidence for the  $h_c(1P)$  stems from the CLEO collaboration searching for the isospin-violating reaction  $\psi(2S) \rightarrow \pi^0 h_c \rightarrow (\gamma\gamma)(\gamma\eta_c)$ . The  $\eta_c$  is measured inclusively giving a larger yield, and exclusively in several hadronic decays modes. Both data sets are shown in Fig. 40. The data yield a  $h_c(1P)$  with  $M(h_c) = 3524.4 \pm 0.6 \pm 0.4 \text{ MeV}/c^2$ . This mass can be compared with the

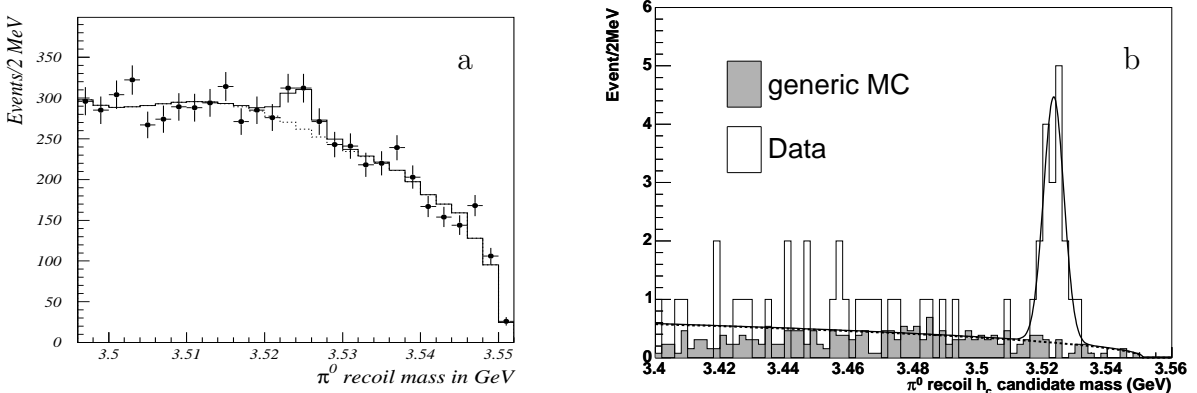


Fig. 40. Observation of  $h_c(1^1P_1)$  in  $\psi(2S) \rightarrow \pi^0 h_c \rightarrow (\gamma\gamma)(\gamma\eta_c)$  with  $\eta_c$  observed inclusively (a) or exclusively (b) [575].

centre-of-gravity of the triplet charmonium states

$$\begin{aligned} \langle M_{\chi(3P_J)} \rangle - M_{h_c(1P_1)} &= +1.0 \pm 0.6 \pm 0.4 \text{ MeV}/c^2 \\ \text{with } \quad \langle M_{\chi(3P_J)} \rangle &= \frac{1}{9} (5 \cdot M_{\chi_{c2}} + 3 \cdot M_{\chi_{c1}} + M_{\chi_{c0}}). \end{aligned} \quad (5.1)$$

With the new BES mass measurements of  $\chi_{cJ}(1P)$  states [504], the centre of gravity  $\langle M_{\chi(3P_J)} \rangle = 3524.85 \pm 0.32 \pm 0.30 \text{ MeV}/c^2$  is even closer to the  $h_c(1P)$  mass.

In leading order, the difference in Eq. (5.1) vanishes for a  $c\bar{c}$  central potential composed of a vector Coulomb ( $\sim 1/r$ ) and a scalar confining potential ( $\sim r$ ). Spin-spin interactions and tensor interactions are expected to be small [752]. The result is thus an important confirmation of the assumptions on which most quark models rely.

### 5.1.2 The $\eta_c(2S)$

The transition to  $\eta_c(2S)$  (often called  $\eta'_c$ ) was first reported by the Crystal Ball Collaboration [753], see Fig. 37 in section 4, but the signal was later shown to be a fluctuation. Evidence for the  $\eta_c(2S)$  was deduced from the  $b$ -factories, where  $\eta_c(2S)$  is now observed in three different reactions.

The  $\eta_c(2S)$  resonance was discovered by the BELLE collaboration as a narrow peak in the  $K_S^0 K^- \pi^+$  mass distribution in a sample of exclusive  $B \rightarrow K K_S^0 K^- \pi^+$  decays [737]. Fig. 41 (left) shows the  $K_S^0 K^- \pi^+$  mass distribution. There is a significant excess of events at about  $3.65 \text{ GeV}/c^2$ . A narrow peak is expected only if it belongs to the charmonium family;  $c\bar{c}$  states can be produced in  $B$  decays via the penguin diagram (see Fig. 33d in section 4.1.6.) The peak was also observed by the BaBar collaboration in the same reaction [611].

The BaBar collaboration reported the observation of  $\eta_c(2S)$  in two-photon fusion with two untagged photons (i.e. with unobserved electrons) [590]. It was detected through its  $K_S^0 K^- \pi^+$  decay mode. The relevant part of the spectrum exhibits a narrow peak shown in Fig. 41 (centre). The full spectrum (not shown here) contains a large peak due to  $\eta_c(1S)$  and a smaller  $J/\psi$  peak. The latter is assigned to initial state radiation. The production characteristics of the  $J/\psi$  and  $\eta_c(1S)$  are different;  $\eta_c(2S)$  production is compatible with  $J^{PC} = 0^{-+}$  quantum numbers. At Cornell,

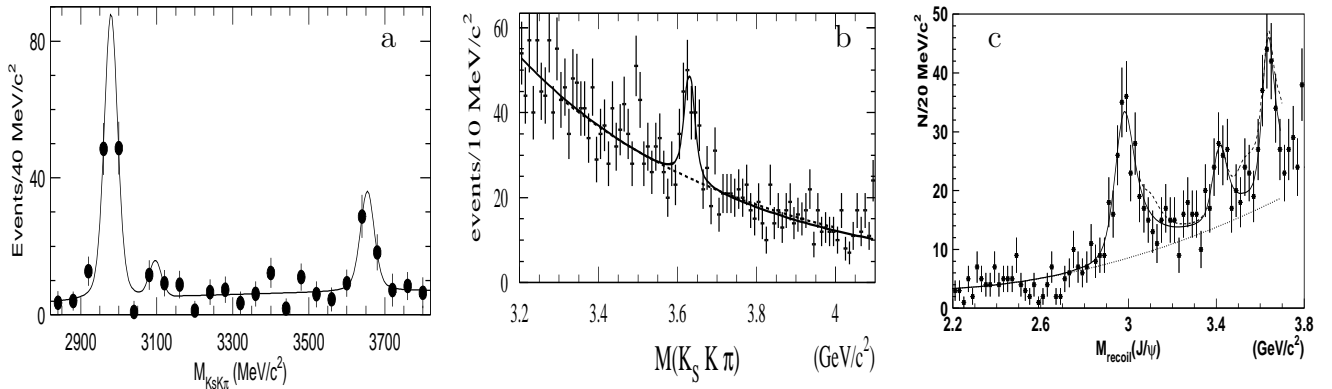


Fig. 41. a:  $K_S^0 K^- \pi^+$  mass distribution in exclusive  $B \rightarrow K K_S^0 K^- \pi^+$  decays [737]. The distribution shows a strong peak at the  $\eta_c(1S)$  mass, a few events due to  $J/\psi$  production and a third peak assigned to  $\eta_c(2S)$ . b:  $K_S^0 K^- \pi^+$  mass distribution from two-photon fusion [590]. c: The mass of the  $c\bar{c}$  system recoiling against a reconstructed  $J/\psi$  in inclusive  $e^+e^- \rightarrow J/\psi X$  events. The  $\eta_c(1S)$  and  $\eta_c(2S)$  resonances are observed, the small peak above  $3.4 \text{ GeV}/c^2$  is assigned to  $\chi_{cJ}$  production [754].

$\eta_c(2S)$  was found in CLEOII and CLEOIII data; the two-photon width was estimated, assuming similar  $K_S^0 K^- \pi^+$  branching ratios for  $\eta_c(1S)$  and  $\eta_c(2S)$  [738].

The third type of reaction uses flavour tagging [754, 755], see Fig. 32 in section 4.1.6. In  $e^+e^-$  annihilation, two  $c\bar{c}$  pairs can be produced. If a  $J/\psi$  is observed, the recoiling system must be a  $c\bar{c}$  state. The virtual photon enforces negative  $C$  parity of the final state and hence positive  $C$  parity for the recoiling  $c\bar{c}$  system. The  $c\bar{c}$  mass spectrum recoiling against the reconstructed  $J/\psi$  in inclusive  $e^+e^- \rightarrow J/\psi X$  events produced in  $e^+e^-$  annihilation at  $\sqrt{s} = 10.6 \text{ GeV}/c^2$  is shown in Fig. 41 (right). Peaks due  $\eta_c(1S)$ ,  $\chi_{cJ}(1P)$  – mostly  $\chi_{c0}(1P)$  – and  $\eta_c(2S)$  can be identified.

Instead of reporting the results from the individual measurements, we compare in Table 8 the PDG mean values of the most important properties of  $\eta_c(1S)$  and  $\eta_c(2S)$ .

Table 8  
Properties of  $\eta_c(1S)$  and  $\eta_c(2S)$  [1].

$\eta_c$ state	Mass	Width	$\Gamma_{\gamma\gamma}$
$\eta_c(1S)$	$2980.4 \pm 1.2 \text{ MeV}/c^2$	$25.5 \pm 3.4 \text{ MeV}/c^2$	$6.7^{+0.9}_{-0.8} \text{ keV}/c^2$
$\eta_c(2S)$	$3638 \pm 4 \text{ MeV}/c^2$	$14 \pm 7$	$1.3 \pm 0.6 \text{ keV}/c^2$

The two-photon width measures the density of the wave function at the origin which is smaller by  $0.19 \pm 0.09$  for  $\eta_c(2S)$  compared to  $\eta_c(1S)$  (see last column, Table 8). In positronium, this factor is 1/8. The reduction of the  $e^+e^-$  widths of  $\psi(2S)$  and  $\psi(3770)$  charmonium and of bottomonium vector states – for which recently very precise results were reported [756] – is much smaller:

$$\begin{aligned} \frac{\Gamma_{ee}(\psi(2S))}{\Gamma_{ee}(J/\psi(1S))} &= 0.393 \pm 0.008 & \frac{\Gamma_{ee}(\psi(3770))}{\Gamma_{ee}(J/\psi(1S))} &= 0.045 \pm 0.006 & [1] \\ \frac{\Gamma_{ee}(\Upsilon(2S))}{\Gamma_{ee}(\Upsilon(1S))} &= 0.461 \pm 0.008 \pm 0.003 & \frac{\Gamma_{ee}(\Upsilon(3S))}{\Gamma_{ee}(\Upsilon(1S))} &= 0.318 \pm 0.007 \pm 0.002 & [756]: \end{aligned}$$

The  $e^+e^-$  width  $\Gamma_{ee}(\psi(3770))$  is much smaller than expected for a  $3S$  level;  $\psi(3770)$  is (dominantly) the charmonium  $1^3D_1$  state.

The discovery of the  $h_c(1P)$  and  $\eta_c(2S)$  resonances marks an important step: all charmonium states below the  $D\bar{D}$  threshold predicted by quark models have been found, and no extra state.

### 5.1.3 The 12% rule and the $\rho\pi$ puzzle

The largest  $J/\psi$  decay fraction supposedly proceeds via 3-gluon intermediate states. Appelquist and Politzer [757] have shown that this fraction decreases for  $\psi(2S)$ . Using perturbative arguments, they find

$$\frac{\mathcal{B}_{\psi \rightarrow ggg}}{\mathcal{B}_{\psi \rightarrow \rho\pi}} = \frac{\Gamma_{e^+e^-}(\psi(2S)) \cdot \Gamma_{tot}(\psi(1S))}{\Gamma_{e^+e^-}(\psi(1S)) \cdot \Gamma_{tot}(\psi(2S))} = (12.37 \pm 0.03)\% \quad (5.2)$$

This is the famous 12% rule: hadronic decays are expected to be reduced to 12% when  $\psi(2S)$  hadronic decays are compared to  $J/\psi$  ( $=\psi(1S)$ ) decays. A large fraction of  $\psi(2S)$  does not decay hadronically via three-gluon intermediate states; the largest fraction goes instead into  $J/\psi$  plus hadrons. We note in passing that the same argument can be made for the  $\chi_{cJ}$  decays via  $n$  gluons,  $\Gamma_{\chi \rightarrow ng}$ . The branching fractions for decays into  $\Lambda\bar{\Lambda}$  are:

$J/\psi$	$\chi_{c0}(1P)$	$\chi_{c1}(1P)$	$\chi_{c2}(1P)$	$\psi(2S)$	$\rightarrow \Lambda\bar{\Lambda}$
$15.4 \pm 1.9$	$4.4 \pm 1.5$	$2.4 \pm 1.0$	$2.7 \pm 1.3$	$2.5 \pm 0.7$	$\times 10^{-4}$

The branching fraction for  $\Lambda\bar{\Lambda}$  decays from  $\psi(2S)$  is reduced to  $(16 \pm 5)\%$  of the fraction for  $J/\psi$ ; the reduction is compatible with the 12% rule. For the  $\chi_{cJ}$  states, the mean reduction is about  $(19 \pm 5)\%$  of the  $J/\psi$  branching fraction to  $\Lambda\bar{\Lambda}$ . In all cases, the error in the individual quantities is large enough to cover the 12% rule.

In general, the 12% rule is valid only approximately. Fig. 42 gives a survey of results compiled by Brambilla *et al.* [63]. There seems to be no obvious preference why some of these ratios are large and some small. The suppression of  $\rho\pi$  from  $\psi(2S)$  is most striking, it is known as  $\rho\pi$  puzzle. In the report of Brambilla *et al.* [63], several interpretations of the  $\rho\pi$  suppression are discussed. For  $\psi(3770)$ ,  $\pi^+\pi^-\pi^0$  is the only hadronic decay mode observed so far [498]. No  $\rho\pi$  contribution was found.

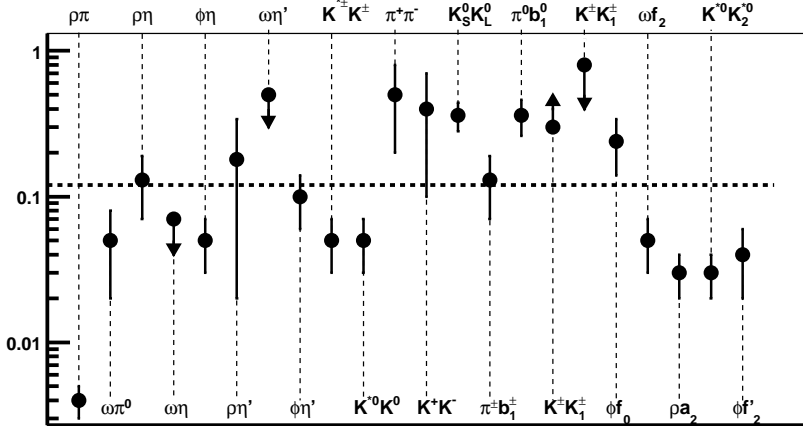


Fig. 42. The ratio of branching fractions of  $\psi(2S)$  and  $J/\psi$  decays into hadronic final states. The data are from the compilation of Brambilla *et al.* [63]. The vertical line indicates the 12% rule.

### 5.1.4 Two-pion transitions

Transitions between bound  $c\bar{c}$  or  $b\bar{b}$  states give access to their dynamics at short distances. The emission of a  $\pi\pi$  pair is considered to proceed in a two step process by the emission of two gluons followed by hadronisation to pion pairs, as indicated in Fig. 43a. Due to the small mass differences between initial and final  $Q\bar{Q}$  system, the gluons are soft and cannot be handled by perturbative QCD. In models, the gluon fields are expanded into a multipole series, the pion hadronisation matrix element is calculated using current algebra, PCAC, and gauge invariance.

Data are shown in Fig. 43b-h) for  $\psi(2S) \rightarrow \pi\pi J/\psi$ ,  $\psi(3770) \rightarrow \pi\pi J/\psi$ ,  $\Upsilon(2S), \Upsilon(3S), \Upsilon(4S) \rightarrow \pi\pi\Upsilon(1S)$ , and  $\Upsilon(3S) \rightarrow \pi\pi\Upsilon(2S)$ . From the low-energy  $\pi\pi$  interactions, the  $\pi\pi$  mass spectra are expected to exhibit an intensity increasing with the  $\pi\pi$  mass, in agreement with most data in Fig. 43. Only  $\Upsilon(3S) \rightarrow \pi^+\pi^-\Upsilon(1S)$  and  $\Upsilon(4S) \rightarrow \pi^+\pi^-\Upsilon(2S)$  are significantly different. Obviously, the differences cannot be assigned to  $\pi\pi$  interactions. The anomalous behaviour in Fig. 43e,h could signal the existence of an unknown tetraquark resonance [758–760]. However, the  $\Upsilon(3S) \rightarrow \pi^+\pi^-\Upsilon(1S)$  decay mode is suppressed, and interfering non-leading diagrams could be

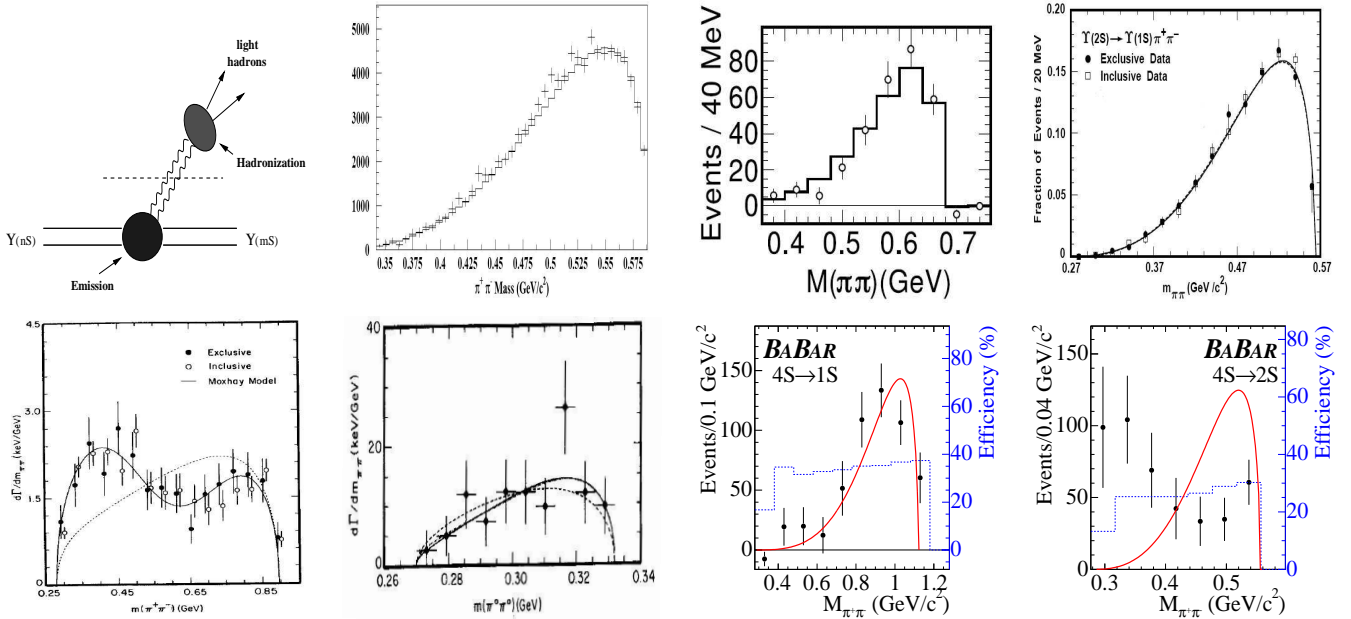


Fig. 43. a)  $\Upsilon(nS) \rightarrow \Upsilon(mS)\pi\pi$  decays as a two-step process with the emission of two gluons followed by hadronisation to pion pairs. Other diagrams:  $M_{\pi\pi}$  mass distributions from two-pion emission of heavy quarkonia. The solid lines represent fits or expected distributions; (b)  $\psi(2S) \rightarrow \pi\pi J/\psi$  [475]; (c) for  $\psi(3770) \rightarrow \pi\pi J/\psi$  [572], the latter distribution contains a 1/3 contribution from  $\psi(2S) \rightarrow \pi\pi J/\psi$  decays; (d)  $\Upsilon(2S) \rightarrow \pi\pi\Upsilon(1S)$  [559]; (e)  $\Upsilon(3S) \rightarrow \pi\pi\Upsilon(1S)$ ; (f)  $\Upsilon(3S) \rightarrow \pi\pi\Upsilon(2S)$  [555, 556]; (g)  $\Upsilon(4S) \rightarrow \pi\pi\Upsilon(1S)$ ; (h)  $\Upsilon(4S) \rightarrow \pi\pi\Upsilon(2S)$  [617] (see also [656]). The dotted histograms in (g) and (h) represent the efficiency.

the cause for the deviations from the expected shape [761]. The rôle of nodes in the wave functions of radially excited states is not fully explored. For a more detailed discussion, we refer the reader to a recent review on this subject [762].

## 5.2 The $J/\psi$ states above the $D\bar{D}$ threshold

A few years ago, the charmonium region above the  $D\bar{D}$  threshold was uncharted territory. Now, five states are known, one reasonably well established and observed in different reactions and by different collaborations. The remaining four states were observed with weak statistical evidence only, quantum numbers are often unknown. Further experimental research is certainly needed. The best studied resonance is called  $X(3872)$ .

The new states, in particular the  $X(3872)$ , are surprisingly narrow and are often close to important thresholds. These facts motivated interpretations of some of the new states as hadronic molecules or tetraquark states. Hadronic molecules and tetraquark states with hidden charm are in the discussion since very long [763–767].

Before discussing evidence for the new meson resonances and their interpretation, we have to define what we mean when calling a resonance a molecule, tetraquark state, or a  $q\bar{q}$  meson. Any meson may have a complicated Fock space expansion, with  $q\bar{q}$ , molecular, and tetraquark components in the wave function. One possibility would be, e.g., to call a meson a molecule when the largest component of its wave function can be decomposed into two colourless objects even though it has a  $q\bar{q}$  ‘seed’. We call such states  $q\bar{q}$  mesons having molecular properties or a molecular character when we imply that the seed is required for the meson to exist, and define molecules and tetraquark

mesons as states falling outside of the  $q\bar{q}$  classification. Molecular states and  $q\bar{q}$  states could mix and form two mesons with a more complex structure. In this case, one of the states is still – from the quark model point of view – supernumerous. In this case we call one state a  $q\bar{q}$  meson with a molecular component mixed in, the other state a molecule with a  $q\bar{q}$  component. Our main concern is, e.g., if  $X(3872)$  adopts the position of the  $\chi_{c1}(2P)$  charmonium state or do we expect an additional state to fill that slot?

### 5.2.1 $X(3872)$

**5.2.1.1 Discovery and the  $X(3872)$  quantum numbers.** The  $X(3872)$  was discovered by the BELLE collaboration in the reaction chain  $B^+ \rightarrow K^+ X(3872)$ ,  $X(3872) \rightarrow \pi^+\pi^- J/\psi$  [635]. Fig. 44a shows the  $\pi^+\pi^- J/\psi$  mass distribution recoiling against a  $K^+$  in  $B^+$  decays with a strong peak above little background. It is reassuring that  $X(3872)$  is now observed, in the same decay mode, by three other collaborations. The BaBar experiment confirmed the existence of the  $X(3872)$  in the same reaction, the  $D\emptyset$  [540] and the CDF2 [541, 543] (see Fig. 44b) collaborations reported observation of  $X(3872)$  in  $p\bar{p}$  collisions at  $\sqrt{s} = 1.96$  TeV. The Particle Data Group gives a mean value  $M = 3871.2 \pm 0.5$  MeV/c $^2$  and a width  $\Gamma < 2.3$  MeV/c $^2$  at 90% confidence level. Due to its decay into  $J/\psi\pi^+\pi^-$  and its narrow width, it must contain a charm and an anti-charm quark. In  $p\bar{p}$  collisions,  $X(3872)$  and  $\psi(2S)$  are produced with very similar production patterns [540, 768]. Obviously,  $X(3872)$  is produced like a regular  $c\bar{c}$  meson, and we anticipate that at short distances,  $X(3872)$  should have a  $c\bar{c}$  structure. Important further contributions were made to determine its properties.

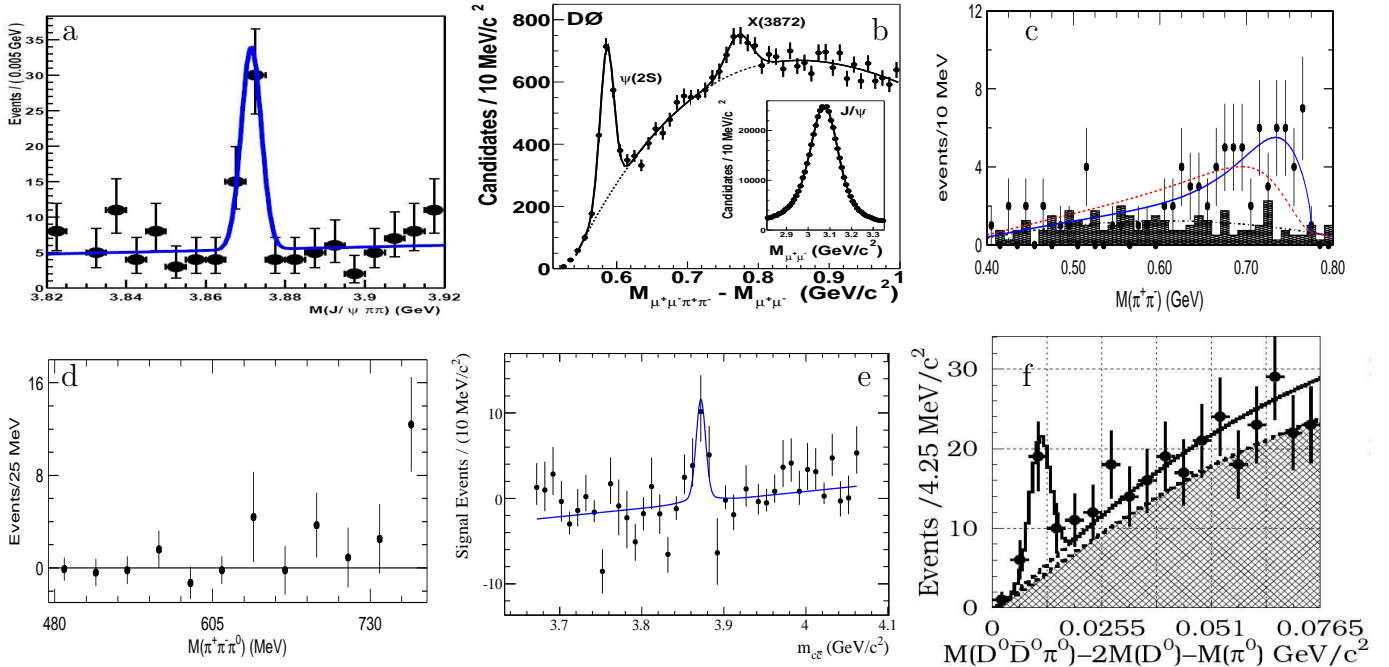


Fig. 44. a: The  $X(3872)$  in  $B^+$  decays to  $K^+(\pi^+\pi^-J/\psi)$  [635]. b: The  $\Delta M = M(\mu^+\mu^-\pi^+\pi^-) - M(\mu^+\mu^-)$  mass difference with  $\psi(2S)$  and  $X(3872)$ . The insert shows the intermediate  $J/\psi$  [540]. c: The  $\pi^+\pi^-$  recoiling against the  $J/\psi$  is compatible with a  $\rho$  and vanishing orbital angular momentum between  $J/\psi$  and the  $\rho$  [646]. d: The number of  $B^+ \rightarrow K^+(\pi^+\pi^-\pi^0 J/\psi)$  events as a function of the  $\pi^+\pi^-\pi^0$  mass [645]. e: The  $\gamma J/\psi$  invariant mass distribution [645]. f: Evidence for  $X(3872) \rightarrow D^0\bar{D}^0\pi^0$  [769].

The  $\pi^+\pi^-J/\psi$  invariant mass distribution is presented in Fig. 44c. It was noticed already in [635] that a large fraction of  $X(3872) \rightarrow \pi^+\pi^-J/\psi$  decays comes from high-mass  $\pi^+\pi^-$  pairs. The  $\pi^+\pi^-$  pair could be in *S*-wave or form a  $\rho$ . A charmonium decay into  $J/\psi\rho$  breaks isospin and may be unlikely, but it was shown that the  $\pi^+\pi^-$  invariant mass distribution enforces a  $\rho$  as intermediate state [770]. The angular momentum between  $J/\psi$  and  $\rho$  was restricted to  $L = 0$  or  $1$  [543]. Possible interpretations of the new state were given early [771–781].

The BaBar and BELLE collaborations searched for other  $X(3872)$  decay modes. These are observed with low statistics and further studies are certainly welcome. The  $X(3872)$  was seen to decay into  $\omega J/\psi$  [645],  $\gamma J/\psi$  [615, 645], and  $D^0D^0\pi^0$  [769]. The evidence for these decays is shown in Fig. 44d,e,f, respectively. The  $X(3872)$  mass is below the nominal  $J/\psi\omega$  threshold, hence only virtual  $\omega$  mesons contribute to the  $X(3872) \rightarrow \pi^+\pi^-\pi^0J/\psi$  decay mode. In Table 9, production and decay properties of  $X(3872)$  are listed. Neglecting further  $X(3872)$  decay modes, we find a total branching ratio  $\mathcal{B}\{B^+ \rightarrow K^+X(3872)\} = 1.30^{+0.20}_{-0.34} \cdot 10^{-4}$ .

The radiative  $X(3872)$  decay into  $J/\psi$ , the  $J/\psi\rho$  (with  $L = 0$ ) and the  $J/\psi\omega$  decay restrict the  $X(3872)$  quantum numbers to  $J^{PC} = 0^{++}, 1^{++}$ , and  $2^{++}$ . For a  $J^{PC} = 0^{++}$  or  $2^{++}$  state, the decay into  $D\bar{D}$  is allowed, and these states should be broader. Hence  $1^{++}$  quantum numbers are most likely. This assumption is supported by the pattern of the  $\chi_{cJ}(1P)$  state observed by BaBar. The  $\chi_{c1}$  is the only  $\chi$  state produced with a significant strength, see Fig. 45. The branching ratios for decays into  $K^+$  and  $\chi_{cJ}(1P)$  states, corrected for their  $\gamma J/\psi$  decay fractions, are given in the lower part of Table 9. The CDF collaboration measured angular distributions and correlations of the  $X(3872) \rightarrow J/\psi\pi^+\pi^-$  decay mode and constrained the possible spin, parity, and charge conjugation parity of the  $X(3872)$  to  $J^{PC} = 1^{++}$  and  $2^{-+}$  [782]. For further discussions, we assume  $J^{PC} = 1^{++}$ .

The BaBar collaboration searched for a charged partner of  $X(3872)$  in the decay mode  $X^- \rightarrow J/\psi\pi^-\pi^0$  in  $B$  meson decays  $B^0 \rightarrow X^-K^+$  and  $B^- \rightarrow X^-K_S^0$  and determined the  $X(3872)$  isospin to  $I = 0$  [598], hence the  $X(3872)$  quantum numbers correspond to  $\chi_{c1}(3872)$ . It remains to be seen if  $X(3872)$  can be identified with the  $\chi_{c1}(2P)$  charmonium state or if it requires a different interpretation.

Table 9  
 $X(3872)$  production rates and decay modes in  $B$  decays in comparison to production rates of other charmonium states.

$B^+ \rightarrow K^+X(3872)$	$X(3872)$ decay mode	Branching ratio	Ref
	$D^0D^0\pi^0$	$1.07 \pm 0.31^{+0.19}_{-0.33}$	$\cdot 10^{-4}$ [769]
	$\pi^+\pi^-J/\psi$	$(1.14 \pm 0.20)$	$\cdot 10^{-5}$ [1]
	$\pi^+\pi^-\pi^0J/\psi$	$(1.1 \pm 0.5 \pm 0.4)$	$\cdot 10^{-5}$ a
	$\gamma J/\psi$	$(1.8 \pm 0.6 \pm 0.1)$	$\cdot 10^{-6}$ [645]
	$\gamma J/\psi$	$(3.3 \pm 1.0 \pm 0.3)$	$\cdot 10^{-6}$ [615]
$B^+ \rightarrow K^+X(3872)$		$1.30^{+0.20}_{-0.34}$	$\cdot 10^{-4}$
$B^+ \rightarrow K^+\chi_{c0}(1P)$		$1.6^{+0.4}_{-0.5}$	$\cdot 10^{-4}$ [1]
$B^+ \rightarrow K^+\chi_{c1}(1P)$		$5.3 \pm 0.7$	$\cdot 10^{-4}$ [1]
$B^+ \rightarrow K^+\chi_{c2}(1P)$		$< 2.9$	$\cdot 10^{-5}$ [1]

a: using  $\mathcal{B}\{X(3872) \rightarrow \pi^+\pi^-\pi^0J/\psi\}/\mathcal{B}\{X(3872) \rightarrow \pi^+\pi^-J/\psi\} = 1.0 \pm 0.4 \pm 0.3$  [645].

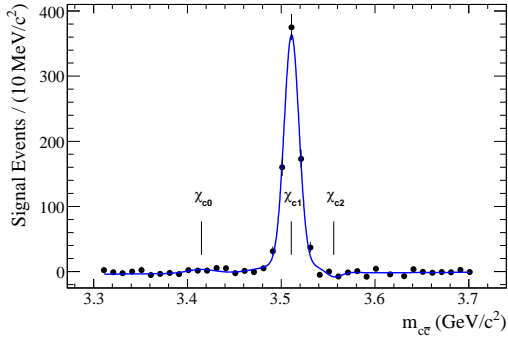


Fig. 45. The  $\chi_{cJ}$  states in  $B$  decays. The  $\chi$  states are identified via their radiative decay into  $J/\psi$  [615].

**5.2.1.2 Molecular and tetraquark interpretations of  $X(3872)$ .** There is a number of reasons not to identify  $\chi_{c1}(3872)$  with the  $c\bar{c}$  state  $\chi_{c1}(2P)$ . The most striking feature is the strong isospin breaking. The branching ratios to  $J/\psi \rho$  and  $J/\psi \omega$  are similar in magnitude; if  $\chi_{c1}(3872)$  is a loosely bound  $D^0 D^{0*}$  molecule (decoupled from  $D^+ D^{-*}$  due to the mass gap), then isospin is maximally broken. If  $\chi_{c1}(3872)$  is interpreted as a tetraquark state, isospin breaking can be implemented as well but charged partners of  $X(3872)$  are predicted; they were searched for by BaBar [598], with negative result. Matheus, Narison, Nielsen, and Richard [783] argued that  $B$  decays may prefer decays via excited  $c\bar{c}$  pairs recoiling against a cluster of light quarks and that production of neutral states with hidden charm could be favoured. Hence charged partners of  $X(3872)$  should be searched for in other reactions, too.

The second argument is based on its low mass, compared to quark-model calculations. The model of Barnes, Godfrey and Swanson [60], e.g., reproduces very well the  $\chi_{cJ}(1P)$  masses (with deviations of less than  $10 \text{ MeV}/c^2$ ) and predicts  $3925 \text{ MeV}$  for  $\chi_{c1}(2P)$ . Lattice QCD puts the state to  $4010$  [784] or  $4067 \text{ MeV}/c^2$  [785]. This  $50\text{--}200 \text{ MeV}/c^2$  mass discrepancy is too large to be bridged by parameter tuning. On the other hand, the  $X(3872)$  mass is just at the  $DD^*$  threshold<sup>4</sup> which makes it a good candidate as molecular bound state. A recent lattice calculation gave a mass of the  $\chi_{c1}(2P)$  state of  $3853 \text{ MeV}/c^2$  [786]. Obviously, there is some flexibility in the mass calculation.

Arguments based a calculation of  $B^+ \rightarrow X(3872)K^+$  in the pQCD approach are shown to be in conflict with an interpretation of  $X(3872)$  as  $2^3P_1$  charmonium state [787].

Some other important predictions fail however when compared to experimental numbers. The ratio [615, 645]

$$\frac{\mathcal{B}(X(3872) \rightarrow \gamma J/\psi)}{\mathcal{B}(X(3872) \rightarrow \pi^+ \pi^- J/\psi)} = 0.22 \pm 0.06 \quad (5.3)$$

is much larger than the value  $0.007$  predicted for a  $D^0 D^{0*}$  molecule. For a  $c\bar{c}$  state, the ratio can be as large as  $0.11$  even though also smaller values have been calculated [788]. Note that the fractional radiative yield for  $\chi_{b1}(2P) \rightarrow \gamma \Upsilon(1S)$  is  $(8.5 \pm 1.3)\%$ , that for  $\chi_{b1}(2P) \rightarrow \gamma \Upsilon(2S)$   $(21 \pm 4)\%$ . Ref. [788] has shown that this ratio depends critically on the  $X(3872)$  internal structure.

For the absolute value, only an upper limit can be given using the  $\chi_{c1}(3872)$  width  $\Gamma < 2.3 \text{ MeV}/c^2$  and the branching ratios of Table 9. The radiative rate  $\chi_{c1}(3872) \rightarrow \gamma J/\psi$  is bound by

$$\Gamma_{\chi_{c1}(3872) \rightarrow \gamma J/\psi} < 250 \text{ keV}/c^2 \quad (5.4)$$

<sup>4</sup> The  $D^0 D^{0*}$  threshold is at  $(3871.2 \pm 0.6) \text{ MeV}/c^2$ , the  $D^+ D^{-*}$  threshold at  $(3879.3 \pm 0.6) \text{ MeV}/c^2$ .

provided that there are no large unseen decay modes. This upper limit can be compared to the  $\chi_{c1}(1P) \rightarrow \gamma J/\psi$  radiative width of 288 keV/c<sup>2</sup>.

A second weak point of the molecular interpretation is the  $X(3872) \rightarrow D\bar{D}^0\pi^0$  decay branching ratio. The  $D^0\bar{D}^0\pi^0$  system shows a peak at  $3875.4 \pm 0.7^{+1.2}_{-2.0}$  MeV mass [769]. In [626],  $M = 3875.1 \pm 1.1 \pm 0.5$  MeV and  $\Gamma = 3.0^{+4.6}_{-2.3} \pm 0.9$  MeV were reported. If this state is identified with  $X(3872)$ , as suggested in [789], we have

$$\frac{\mathcal{B}(X(3872) \rightarrow D^0\bar{D}^0\pi^0)}{\mathcal{B}(X(3872) \rightarrow \pi^+\pi^-J/\psi)} = 9.4^{+3.6}_{-4.3} \quad (5.5)$$

while the prediction of the molecular model [788] is 0.054. In the fits by Hanhart *et al.* [789], the shape of the  $X(3872)$  resonance is strongly distorted. The authors conclude that  $X(3872)$  has to be of a dynamical origin; it is interpreted as a virtual state. Of course, it is difficult to exclude a  $c\bar{c}$  fraction in  $X(3872)$  which may serve as a seed to create the observed state.

The observed rates in  $B^+$  and  $B^0$  decays do not correspond to the molecular picture, neither. Experimentally [769]

$$\frac{\mathcal{B}(B^0 \rightarrow X(3872)K^0)}{\mathcal{B}(B^+ \rightarrow X(3872)K^+)} \approx 1.62 \quad (5.6)$$

while the prediction is less than 0.1 [788].

In the limit of large quark-mass ratios, tetraquarks consisting of two heavy and two light quarks should be stable against falling apart into two heavy-light mesons or into a heavy quarkonium and a light-quark meson. The light-quark degrees of freedom cannot resolve the closely bound system of two heavy quarks. Thus a tightly bound  $\bar{b}\bar{c}$  or  $\bar{b}\bar{b}$  system in colour **3** and two light quarks  $q\bar{q}$  may form a heavy-baryon configuration where the heavy quark is replaced by two heavy (anti-)quarks [790]. This exotic configuration is expected to provide more stability than the molecular (non-exotic) system consisting of two heavy-light colour-neutral mesons [766, 791, 792].

In a model calculation, Janc and Rosina [793] suggest that the most stable tetraquark configuration should not be of that of a heavy baryon but rather a molecular system. Sum rules give tetraquark masses  $M_{T_{bb}} = (10.2 \pm 0.3)$  GeV/c<sup>2</sup>, which is below the  $\bar{B}\bar{B}^*$  threshold, and  $M_{T_{cc}} = (4.0 \pm 0.2)$  GeV/c<sup>2</sup> [794].

Maiani *et al.* see  $X(3872)$  as tetraquark charmonium and predict the spectrum of new tetraquark charmonia including charged isospin partners of  $X(3872)$  [795]. Tetraquark states were constructed from diquarks in colour triplet scalar and vector clusters interacting by spin-spin interactions. Using the  $X(3872)$  as input, Maiani *et al.* predict the spectrum of new diquark charmonia shown in Fig. 46. Høgaasen *et al.* [796] postulate that  $X(3872)$  is a loosely bound tetraquark  $cu\bar{c}\bar{u}$  and  $cd\bar{c}\bar{d}$  state [796]. In [797], the interaction of two quarks and two antiquarks in  $S$ -wave is calculated including flavour-symmetry breaking. Karliner and Lipkin [798] suggested that  $bn\bar{b}\bar{n}$  and  $bn\bar{c}\bar{n}$  tetraquarks may fall below the  $B\bar{B}$  and  $B\bar{D}$  thresholds. The (four-fold) attractive forces between quarks and antiquarks may overcome the (twofold) repulsive forces between the light-quark and the heavy-quark pairs, and attraction prevails. These new states may have exotic electric charge and their decays might have striking decay patterns. The calculation might, however, depend on

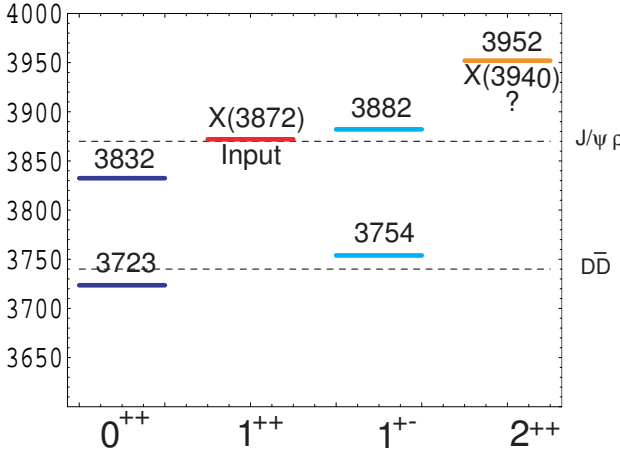


Fig. 46. Spectrum of tetraquark charmonium states [795].

the coupling scheme chosen: the interactions of two quarks with one antiquark are individually attractive; the diquark and the antiquark feel repelling forces. The charmonium spectrum is calculated by Kalashnikova [799] in a coupled channel model with couplings to  $D\bar{D}$ ,  $D\bar{D}^*$ ,  $D^*\bar{D}^*$ ,  $D_s\bar{D}_s$ ,  $D_s\bar{D}_s^*$ , and  $D_s^*\bar{D}_s^*$ , thus generating a virtual bound state just above  $D\bar{D}^*$  threshold. Coupled channels in  $S$ -wave may lead to cusps at the opening at thresholds;  $X(3872)$  may very well be such a cusp as underlined by Bugg [800].

Tetraquark models postulate a mass difference between  $B^+ \rightarrow X_{\bar{u}u}K^+$  and  $B^0 \rightarrow X_{\bar{d}d}K^0$ . BaBar determined this mass difference to  $1.7 \pm 1.1 \pm 0.2$ , a value not inconsistent with zero [598]. If molecular forces are responsible for binding the  $X(3872)$ , it is difficult to escape the conclusion that a isovector partner should be observed as well as the isoscalar  $X(3872)$ .

Summarizing, there are strong arguments that tetraquark states should exist in the heavy quark limit. Models can be made which predict tetraquarks in the charmonium system but no proof exists that in the  $cc\bar{u}\bar{d}$ ,  $cb\bar{u}\bar{d}$ , or even  $bb\bar{u}\bar{d}$  system, the heavy-quark limit is reached and that these flavour-exotic mesons are stable against colour rearrangement and do not just fall apart.

**5.2.1.3 Other interpretations of  $X(3872)$ .** Other interpretations were attempted as well. Seth proposed  $X(3872)$  to be a vector glueball [801], Li suggested a  $c\bar{c}g$  hybrid interpretation [802]. Both conjectures are at variance with the large radiative yield.

**5.2.1.4  $X(3872)$  as  $\chi_{1c}(2P)$  charmonium state.** The highest obstacles for a  $c\bar{c}$  interpretation of  $X(3872)$  are its mass and the isospin breaking effects in their  $J/\psi\omega$  and  $J/\psi\rho$  decays. Concerning

Table 10

Masses of  $\chi$  states (in MeV/c<sup>2</sup>). Cursive numbers are obtained by simple scaling. The precision is truncated at 1 MeV/c<sup>2</sup>.

$\chi_{bJ}(nP)$ states				$\chi_{cJ}(nP)$ states			
$\chi_{b0}(1P)$	9.859	$\chi_{b0}(2P)$	10.233	$\chi_{c0}(1P)$	3415	$\chi_{c0}(2P)$	$\sim 3840$
$\chi_{b1}(1P)$	9.893	$\chi_{b1}(2P)$	10.255	$\chi_{c1}(1P)$	3511	$\chi_{c1}(2P)$	$\sim 3900$
$\chi_{b2}(1P)$	9.912	$\chi_{b2}(2P)$	10.268	$\chi_{c2}(1P)$	3556	$\chi_{c2}(2P)$	$3929 \pm 5 \pm 2$

the mass, there is of course some uncertainty in the absolute scale of the predictions. Below we will identify the  $Z(3930)$  with  $\chi_{c2}(2P)$ . It has a mass of  $3931 \pm 4 \pm 2 \text{ MeV}/c^2$ , its predicted mass [60] is  $3972 \text{ MeV}/c^2$ . This is a  $40 \text{ MeV}/c^2$  discrepancy, too. We try to use the bottomonium masses to estimate the mass of the  $\chi_{c1}(2P)$  charmonium state see Table 10. Simple scaling leads to  $3900 \text{ MeV}/c^2$  as expectation for the  $\chi_{c1}(2P)$  mass, about  $28 \text{ MeV}/c^2$  above the observed  $\chi_{c1}(3872)$  mass. If the charmonium state  $\chi_{c1}(2P)$  were a separate state at about  $3900 \text{ MeV}/c^2$ , it should have been observed in the  $D^0 D^0 \pi^0$  mass distribution. Of course, a threshold can attract a pole position. This is a phenomenon known from the  $K\bar{K}$  threshold and  $a_0(980)$  and  $f_0(980)$ .

The most likely solution seems to be that  $\chi_{c1}(3872)$  is the charmonium  $\chi_{c1}(2P)$  state strongly coupled to  $D^0 D^{0*}$ . The  $D^\pm D^{\mp*}$  threshold is  $8 \text{ MeV}$  higher, the coupling to  $D^\pm D^{\mp*}$  plays no dynamical rôle in the decay thus creating large isospin breaking effects. As long as no isospin partner of  $X(3872)$  is discovered, we must conclude that the  $c\bar{c}$  component plays a decisive rôle in binding the molecular  $D^0 D^{0*}$  system. In the sense of our introductory discussion,  $X(3872)$  is a  $c\bar{c}$  meson of molecular character. When probed with high momenta like in  $p\bar{p}$  collisions, the  $c\bar{c}$  component prevails; at large separations the molecular character is revealed by its strong affinity to the  $D^0 D^{0*}$  system.

### 5.2.2 The $X, Y, Z$ resonances at $3940 \text{ MeV}/c^2$

**5.2.2.1 The  $X(3940)$**  was observed by the BELLE collaboration in the missing mass distribution recoiling against a  $J/\psi$  in  $e^+e^-$  annihilation, see Fig. 47a. Its mass and width were determined to  $(3.943 \pm 0.006 \pm 0.006) \text{ GeV}/c^2$  and  $\Gamma < 52 \text{ MeV}/c^2$  at  $90\%$  C.L. [644, 661]. It is produced in the same way as  $\eta_c(1S)$  and  $\eta_c(2S)$ . Thus it is a very good candidate for the  $\eta_c(3S)$  resonance. Evidence for  $DD^*$  decays of  $X(3940)$  was also reported [644]. The mass is unexpectedly low,  $4043 \text{ MeV}/c^2$  is expected in the model of Barnes, Godfrey and Swanson [60],  $3900 \text{ MeV}/c^2$  from our simple scaling.

**5.2.2.2 The  $Y(3940)$**  was suggested by the BELLE collaboration in the reaction  $B \rightarrow K\pi\pi\pi J/\psi$  with the three pions forming an  $\omega$  meson [642], see Fig. 47b. The  $S$ -wave Breit Wigner mass and

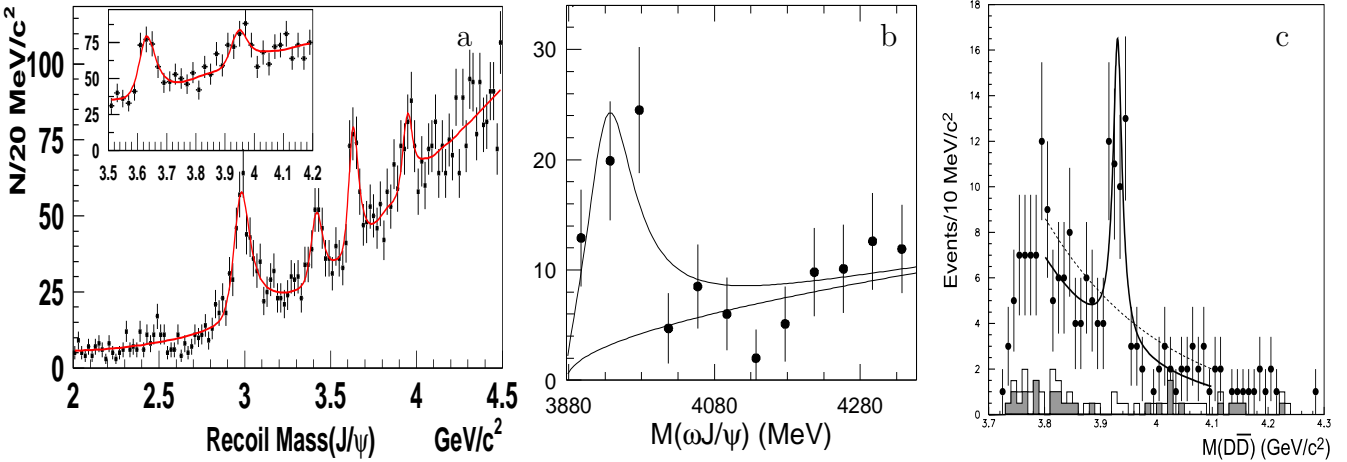


Fig. 47. a: Mass distribution in  $e^+e^- \rightarrow J/\psi + \text{charm}$  [644]. The four peaks correspond to  $\eta_c(1S)$ , a convolution of  $\chi_{cJ}(1P)$  states,  $\eta_c(2S)$  and  $X(3940)$ . b:  $\omega J/\psi$  mass distribution from  $B \rightarrow K\pi\pi\pi J/\psi$  decays [642]. c: The  $D\bar{D}$  mass distribution from two-photon fusion [803].

width were determined to be  $3943 \pm 11 \pm 13$  MeV/c $^2$  and  $87 \pm 22 \pm 26$  MeV/c $^2$ , respectively. The decay into J/ $\psi$   $\omega$  is very strange: a charmonium state at 3930 MeV/c $^2$  can decay into  $D\bar{D}$  or  $D^*\bar{D}$  while  $\omega J/\psi$  is OZI forbidden. The decay mode resembles the  $f_0(1810)$  which is observed as  $\phi\omega$  threshold enhancement in radiative J/ $\psi$  decays [508]. In section 10.7,  $f_0(1810)$  will be interpreted as a flavour octet state with large  $\frac{1}{\sqrt{6}}|\bar{u}u\bar{s}s + \bar{d}d\bar{s}s - 2\bar{u}u\bar{d}d>$  admixture; thus identification of Y(3940) as  $\bar{c}c$  state with a  $\chi_{c0}(2P) = \frac{1}{\sqrt{3}}|\bar{u}u\bar{c}c + \bar{d}d\bar{c}c + \bar{s}s\bar{c}c>$  component does not seem unlikely. The J/ $\psi$   $\omega$  decay mode is then rather natural, the mass disagrees however with the expected 3840 MeV/c $^2$  using our scaling (see Table 10). The quark model [60] yields a similar value, 3852 MeV/c $^2$ .

The width is compatible with what to expect. The  $\chi_{c2}(1P)$  width is  $2.06 \pm 0.12$  MeV/c $^2$ , the ( $\chi_{c0}(1P)$ ) width is five times broader,  $10.4 \pm 0.7$  MeV/c $^2$ . With a  $\chi_{c2}(2P)$  width of  $29 \pm 10$  MeV/c $^2$ , we can expect a  $\chi_{c0}(2P)$  width of 100–200 MeV/c $^2$ . Its high mass component decays into  $\omega J/\psi$ . This picture requires the  $\chi_{c0}(2P)$  to decay into  $D\bar{D}$  with a similar coupling constant as into J/ $\psi$   $\omega$ .

**5.2.2.3 The Z(3930)** was observed by the BELLE collaboration in  $\gamma\gamma \rightarrow D\bar{D}$  with a mass of  $3931 \pm 4 \pm 2$  MeV/c $^2$  and a width of  $20 \pm 8 \pm 3$  MeV/c $^2$  [803]. The mass distribution is reproduced in Fig. 47c. The  $D\bar{D}$  helicity distribution was determined to be consistent with  $J = 2$ , hence it was identified as  $\chi_{c2}(2P)$ . Its mass and decay mode are consistent with this identification. The predicted  $\chi_{c2}(2P)$  mass [60] is 3972 MeV/c $^2$ .

### 5.2.3 A new $\bar{c}c$ vector state Y(4260)

The Y(4260) is a stumbling stone. It was observed by the BaBar collaboration as an enhancement in the  $\pi\pi J/\psi$  subsystem in the initial state radiation (ISR), in  $e^+e^- \rightarrow \gamma_{ISR} J/\psi \pi\pi$  [606] (see Fig. 48, left). Due to the production mode, Y(4260) must have  $J^{PC} = 1^{--}$ . The mass was determined to  $4259 \pm 8 \pm 4$  MeV/c $^2$  and the width to  $88 \pm 23 \pm 5$  MeV/c $^2$ . Y(4260) was confirmed in a preliminary analysis of the BELLE collaboration [653]. The CLEO collaboration observed Y(4260) in a  $e^+e^-$  scan [582] and found the ratio of  $Y(4260) \rightarrow \pi^+\pi^-J/\psi$  and  $Y(4260) \rightarrow \pi^0\pi^0J/\psi$  events to be consistent with Y(4260) being isoscalar [583]. Three events due to  $Y(4260) \rightarrow K^+K^-J/\psi$  were reported corresponding to a  $\pi\pi/K\bar{K}$  ratio of about 1/4. A BaBar search for  $Y(4260) \rightarrow pp$  yielded a null result [599]. The BaBar collaboration searched for Y(4260) in  $B$  decays studying the reactions  $B^0 \rightarrow J/\psi \pi^+\pi^-K^0$  and  $B^- \rightarrow J/\psi \pi^+\pi^-K^-$  [614]. A weak 3- $\sigma$  signal shown in Fig. 48b was observed which is compatible with the Y(4260) parameters.

The partial width

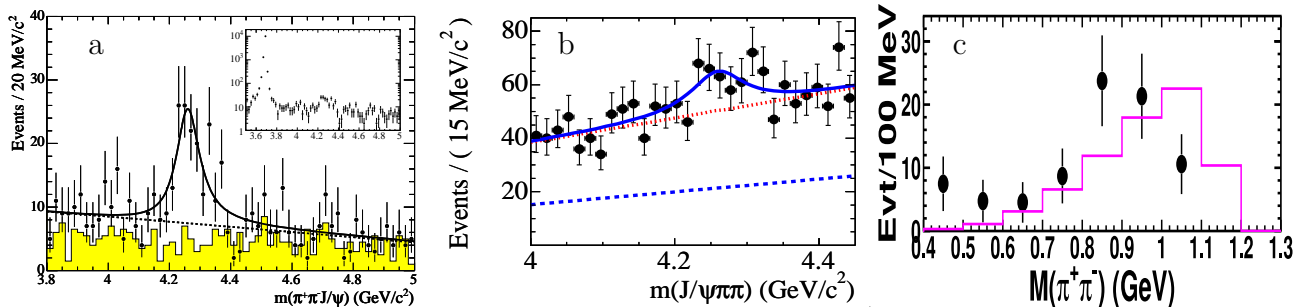


Fig. 48. a: The Y(4260) observed in  $e^+e^- \rightarrow \gamma_{ISR} J/\psi \pi\pi$  [606]. The inset shows the same spectrum over a wider range including the  $\psi(2S)$ . b: There is weak evidence for Y(4260) from  $B \rightarrow KJ/\psi \pi\pi$  decays [614]. c: The  $\pi\pi$  mass distribution recoiling against the J/ $\psi$  and the phase space distribution [583].

$$\Gamma(Y(4260) \rightarrow e^+e^-) Br(Y(4260) \rightarrow J/\psi\pi\pi) = 5.5 \pm 1.0^{+0.8}_{-0.7} \text{ eV/c}^2 \quad (5.7)$$

determined in [606] can be compared to the rate when  $Y(4260)$  is replaced by  $\psi(2S)$ :

$$\Gamma(\psi(2S) \rightarrow e^+e^-) Br(\psi(2S) \rightarrow J/\psi\pi\pi) = 672 \pm 45 \text{ eV/c}^2. \quad (5.8)$$

Either,  $Y(4260)$  must have an unusual small  $e^+e^-$  width or a very small coupling to  $J/\psi\pi\pi$  (or both).

The  $Y(4260)$  yield in  $B$  decay is anomalously low, too. The product branching ratio

$$\mathcal{B}(B^- \rightarrow K^- Y) \mathcal{B}(Y \rightarrow J/\psi\pi\pi) = (2.0 \pm 0.7 \pm 0.2) \cdot 10^{-5} \quad (5.9)$$

was interpreted as 90% C.L. upper limit at  $2.9 \cdot 10^{-5}$  [614]. The value is two orders of magnitude smaller than the branching fractions for  $KJ/\psi$  or  $K\psi(2S)$ . Again, either the coupling  $Y \rightarrow J/\psi\pi\pi$  is small, or the  $Y(4260)$  production rate is much smaller than that of  $\psi(nS)$  states.

With  $\psi(3686)$ ,  $\psi(3770)$ ,  $\psi(4040)$ ,  $\psi(4160)$ ,  $\psi(4415)$  as  $\psi(2S)$ ,  $\psi(1D)$ ,  $\psi(3S)$ ,  $\psi(2D)$ , and  $\psi(4S)$ , respectively, and a  $\psi(3D)$  at an expected mass at about  $4.5 \text{ GeV/c}^2$ , there seems to be no  $\bar{c}c$  slot available for the  $Y(4260)$ ; its mass is hence a further argument in favour of its exotic nature.

Various explanations for  $Y(4260)$  have been proposed. Its, at the first glance, anomalous properties prompted the suggestion that it might be a  $\bar{c}c$  hybrid [804–806]. Maiani *et al.* [807] interpreted the  $Y$  as first orbital excitation of a tetraquark  $[cs]_S[\bar{c}\bar{s}]_S$  state; additional states were predicted at somewhat lower masses. Alternatively, the  $Y$  could be a  $\chi_{c1}\rho$  molecule bound by  $\sigma$  exchange [808]. A  $\Lambda_c\bar{\Lambda}_c$  baryonium state is a further possibility to understand the  $Y(4260)$  [809]. The latter suggestion finds support in the claim for a  $\phi f_0$  resonance at  $2175 \text{ MeV/c}^2$  [618] and its possible interpretation as  $\Lambda\bar{\Lambda}$  bound state.

Further arguments in favour of an exotic nature can be made by analysing the  $\pi\pi$  invariant mass distribution recoiling against the  $J/\psi$  shown in Fig. 48c. The distribution is incompatible with the expectation based on normal  $\pi\pi$   $S$ -wave interactions produced without any hindrance factor. Bugg [810] fitted this spectrum, and a similar spectrum from Belle, assuming an intermediate  $\pi J/\psi$  resonance. The best fit required orbital angular momentum  $L = 1$  between the recoil pion and the  $\pi J/\psi$  resonance, and gave  $M = 4080 \text{ MeV/c}^2$  and  $\Gamma = 280 \text{ MeV/c}^2$ . The resonance is suggested to be a tetraquark state. This is an interesting conjecture but the reader should go back to Fig. 43. If  $Y(4260)$  is of exotic nature, then it may act as point-like source for decays, and the  $\pi\pi$  invariant mass distribution can be ascribed to final-state interactions. If it is a  $\psi$  radial excitation, its nodes have a significant impact.

The  $Y(4260)$  resonance was searched for in the inclusive  $e^+e^-$  annihilation cross section [811]. The cross section exhibits a dip-bump-dip structure in the  $\sqrt{s} = 4.20 - 4.35 \text{ GeV/c}^2$  region which makes it difficult to extract a reliable estimate for a possible  $Y(4260)$  contribution. Rosner assigned this dip to the opening of the  $DD_1$  channel [812]. Llanes-Estrada [813] has shown that the inclusive  $e^+e^-$  annihilation into hadrons can be explained quantitatively by  $S$ - $D$  wave interference and assuming the coupling to two pseudoscalar mesons to have positive signs for  ${}^3S_1$  and negative signs for  ${}^3D_1$  states. The  $Y(4260)$  was included in the fit as  $\psi(4S)$  state. In [811], different dynamical assumptions were made to determine an upper limit for the  $Y(4260) \rightarrow e^+e^-$  width. The largest

contribution was acceptable in fits in which the  $\psi'$  resonances were described by interfering Breit-Wigner amplitudes of constant widths with arbitrary phases. The series of resonances included  $\psi(3770)$ ,  $\psi(4040)$ ,  $\psi(4160)$ ,  $Y(4260)$ , and  $\psi(4415)$ ; a linear non-interfering background was added. The  $Y(4260)$  was given a special treatment: since it is suspected not to belong to the  $\psi'$  series, it was considered appropriate to add it partly incoherently to the cross section. It was hence split into two contributions, one interfering Breit-Wigner amplitude, a non-interfering part describing  $Y(4260)$  as threshold phenomenon. The fraction of the coherent contributions was varied between 0.7 to 0.3, and upper limits for  $\Gamma_{Y(4260) \rightarrow e^+e^-}$  were derived; 580 eV/c<sup>2</sup> for 70% coherence, 460 eV/c<sup>2</sup> for 50%, and 280 eV/c<sup>2</sup> for 30% coherence. These numbers maybe compared to  $\Gamma_{\psi(4160) \rightarrow e^+e^-} = 830 \pm 70$  eV/c<sup>2</sup> and  $\Gamma_{\psi(4415) \rightarrow e^+e^-} = 580 \pm 70$  eV/c<sup>2</sup>. The  $e^+e^-$  width of  $Y(4260)$  is not suspicious. Full coherence was not permitted in [811], extrapolating to full coherence or interpolating the two values for  $\psi(4160)$  and  $\psi(4415)$  yields our estimate of 720 eV/c<sup>2</sup> which we give in Table 11.

From eq. (5.7) and the  $Y(4260) \rightarrow e^+e^-$  width, we derive

$$\Gamma(Y(4260) \rightarrow J/\psi\pi^+\pi^-) > 670 \pm 240 \text{ keV/c}^2. \quad (5.10)$$

The yield is larger than naively expected, in particular when compared to the corresponding width for the  $\psi(3686)(2S)$  resonance. However, the  $\pi\pi$   $S$ -wave is open for a wider range in  $Y(4260)$  decays. The BESII collaboration has fitted new data on the  $R$  value in  $e^+e^-$  annihilation [512]; fits including  $Y(4260)$  were not attempted.

In Table 11 we compare charmonium vector states assuming that  $Y(4260)$  is  $\psi(4S)$ . The comparison looks very favourable. An exotic interpretation of  $Y(4260)$  may therefore not really be enforced by data. Very recently, the BELLE collaboration reported two further resonant structures in the  $\pi^+\pi^-\psi(2S)$  invariant mass distribution, at  $4361 \pm 9 \pm 9$  MeV/c<sup>2</sup> with a width of  $74 \pm 15 \pm 10$  MeV/c<sup>2</sup>, and at  $4664 \pm 11 \pm 5$  MeV/c<sup>2</sup> with a width of  $48 \pm 15 \pm 3$  MeV/c<sup>2</sup> [662]. We conjecture that these might be the  $3D$  and  $6S$  states, respectively.

### 5.2.4 Conclusions

There are four positive-parity charmonium states expected in the mass range from the  $\chi_{c2}(1P)$  to 4 GeV/c<sup>2</sup>, and four states are found,  $X(3872)$ ,  $X(3940)$ ,  $Y(3940)$ , and  $Z(3930)$ . Based on their production and decay characteristics, they can be identified with  $\chi_{c1}(2P)$ ,  $\eta_c(3S)$ ,  $\chi_{c0}(2P)$ , and  $\chi_{c2}(2P)$ , respectively. The  $Y(4260)$  finds a natural interpretation as  $\psi(4S)$  state. These conclusions were reached independently by Colangelo and collaborators [814]. Does this imply the attempts

Table 11  
Charmonium states with  $J^{PC} = 1^{--}$  in our interpretation.

$J/\psi$	$\psi(3686)$	$\psi(3770)$	$\psi(4040)$	$\psi(4160)$	$Y(4260)$	$\psi(4415)$	
	2S	1D	3S	2D	4S	5S	
$\Gamma_{e^+e^-}$	$2.48 \pm 0.06$	$0.242^{+0.027}_{-0.024}$	$0.86 \pm 0.07$	$0.83 \pm 0.07$	0.72	$0.58 \pm 0.07$	keV/c <sup>2</sup>
$\Gamma_{J/\psi\pi^+\pi^-}$	$107 \pm 5$	$44 \pm 8$	$< 360$	$< 330$	$670 \pm 240$	-	keV/c <sup>2</sup>
$M_{\psi(nS)} - M_{J/\psi}$	589	674	943	1056	1163	1318	MeV/c <sup>2</sup>
$M_{Y(nS)} - M_Y$	563		895		1119		MeV/c <sup>2</sup>

to understand these particles as exotic states were a failure? Certainly not; the tetraquark and/or molecular picture focuses the attention on the dynamics of production processes and decay rates and augment the  $\bar{q}q$  picture. Furthermore, the models serve as stringent guides to search for new phenomena. But from time to time it is necessary to recall that the quark model provides a solid foundation; claims for physics beyond the quark model have to survive critical scrutiny.

### 5.2.5 A charged charmonium state ?

After completion of the review, a narrow  $\psi'\pi^\pm$  resonance was reported by the Belle collaboration with a statistical evidence exceeding  $7\sigma$  [627]. It was observed in  $B$  decays to  $K\pi^+\psi'$ , using various  $\psi'$  decay modes. The resonance, called  $Z(4430)$ , has  $4433 \pm 4 \pm 1 \text{ MeV}/c^2$  mass and a width of  $\Gamma = 44^{+17+30}_{-13-11} \text{ MeV}/c^2$  width. It is produced with a branching fraction

$$\mathcal{B}(B \rightarrow KZ(4430)) \cdot \mathcal{B}(Z(4430) \rightarrow \pi^+\psi') = (4.1 \pm 1.0 \pm 1.3) \cdot 10^{-5} \quad (5.11)$$

It is the first charged resonance with hidden charm and can evidently not belong to the charmonium family, not even have a  $c\bar{c}$  seed. Rosner noticed that the  $Z(4430)$  mass is not far from  $D^*\bar{D}_1(2420)$  threshold and proposed that the state is formed via the weak  $b \rightarrow c\bar{c}s$  transition, creation of a light-quark pair, and rescattering of the final-state hadrons [815]. The decay  $Z(4430) \rightarrow J\psi\pi^\pm$  is not observed: the rescattering mechanism is effective only close to the production threshold.

The  $Z(4430)$  state is clearly at variance with ideas presented above. Its confirmation as resonant state (and not as effect of threshold dynamic) is very important.

## 5.3 Heavy-light quark systems

### 5.3.1 $D$ and $D_s$ mesons and their low-mass excitations

**5.3.1.1  $D$  Mesons:** Figure 49a shows the spectrum of  $D$ -meson excitations. The states of lowest mass are the  $D$  and the  $D^*$  and the four  $P$ -wave states. In the heavy-quark limit, the heavy-quark spin  $\vec{s}_c$  decouples from the other degrees of freedom and the total angular momentum of the light quark  $\vec{j}_q = \vec{L} + \vec{s}_q$  is a good quantum number. This yields the following spin-parity and light-quark angular-momenta decompositions:  $0^+(j_q = 1/2)$ ,  $1^+(j_q = 1/2)$ ,  $1^+(j_q = 3/2)$  and  $2^+(j_q = 3/2)$ , which are usually labelled as  $D_0^*$ ,  $D'_1$ ,  $D_1$  and  $D_2^*$ , respectively. The two  $j_q = 3/2$  states are narrow due to the angular-momentum barrier and have  $\sim 20 \text{ MeV}/c^2$  widths. The  $j_q = 1/2$  states decay via  $S$ -waves and are expected to be quite broad. The BELLE collaboration studied these states in  $B$  decays into  $D\pi\pi$  and  $D\pi\pi\pi$  [638]. Further support for the broad states was reported by the FOCUS [529] and the CDF [542] collaborations.

The partial wave analysis of events due to  $B^- \rightarrow D^+\pi^-\pi^-$  decays using  $D_0^*$  and  $D_2^*$  as only isobars did not give a fully satisfactory description of the  $D^+\pi^-\pi^-$  Dalitz plot. Virtual vector states as additional isobars improved the fit without changing significantly the  $D_0^*$  and  $D_2^*$  parameters. The fit results are shown in Fig. 49b. The narrow  $D_2^*$  is readily identified but there is a substantial wide ‘background’ which is mostly assigned to scalar  $D\pi$  interactions. Closer inspection reveals a spike at threshold; it is described by a virtual  $D_v^*$  (and a second one, called  $B_v^*$ ). The spin-parity of the virtual states was not tested. Below (in section 11.6.3) we suggest the existence of a subthreshold  $D_0^*(1980)$ . The spike and/or the black area in Fig. 49b could be a trace of this hypothesised state. A low mass  $D_0^*$  (at  $2030 \text{ MeV}/c^2$ ) was also suggested by Beveren and Rupp [816].

For the reaction  $B^- \rightarrow D^{*+}\pi^-\pi^-$ , an unbinned likelihood fit in the four-dimensional phase space was performed to extract the amplitudes and phases of the contributing isobars. The fit results shown in Fig. 49c exhibit three components, two narrow ones and a broad one, in line with the expectations based on Fig. 49a.

Instead of presenting the results on masses and widths of  $D$  resonances from [638] from the fits described above, we quote these quantities in Table 12 from the latest Review of Particle Properties [1]. Masses and widths will be discussed in connection with the corresponding states of the  $D_s$  family.

**5.3.1.2  $D_s$  mesons:** Fig. 50a shows the expected low-lying  $c\bar{s}$  excitations. The two ground states and two resonances above the  $D^* K$  thresholds were known since long [557, 817] from CLEO and Argus and were used to define the quark model parameters. The other two states were thought to have escaped discovery due to their large (expected) widths. It thus came as a complete surprise when  $D_{s0}^*(2317)$  was discovered by BaBar [588] as narrow and low-mass resonance, in the inclusive  $D_s^+\pi^0$  invariant mass distribution produced in  $e^+e^-$  annihilation at energies near  $10.6 \text{ GeV}/c^2$ . Fig. 50 (right) shows the  $D_s\pi^0$  invariant mass distribution with an impressive  $D_{s0}^*(2317)^+$  signal [616]. Among other (continuous) background contributions, reflections from other decay sequences are an intriguing source since they can mimic wrong signals. Particularly dangerous are reflections from  $D_s^*(2112)^+ \rightarrow D_s\gamma$  decays in which an unassociated  $\gamma$  particle is added to form a false  $\pi^0$  candidate, and from  $D_{sJ}(2460)^+ \rightarrow D_s^*(2112)^+\pi^0$  decay in which the  $\gamma$  from the  $D_s^*(2112)^+$  decay is missing. The reflections also occur in side bands and can thus be controlled quantitatively. A  $D_{s0}^*$  resonance should decay into  $D$  plus  $K$ . However, the  $D_{s0}^*(2317)$  mass is below the  $D K$  threshold. Its mass is even below the  $D_0^*(2350)$  mass, in spite of a  $n$  quark being replaced by a  $s$  quark. Since its natural decay mode is forbidden,  $D_{s0}^*(2317)$  must decay via an isospin violating mode into  $D_s\pi$ , and is narrow. The new resonance is now confirmed in several new data sets [564, 591, 596, 616, 634]. It must have natural spin-parity,  $J^{PC} = 0^{++}$  were proposed and found to be consistent with later data having higher statistics. In particular the absence of radiative transitions to the ground state supports this assignment.

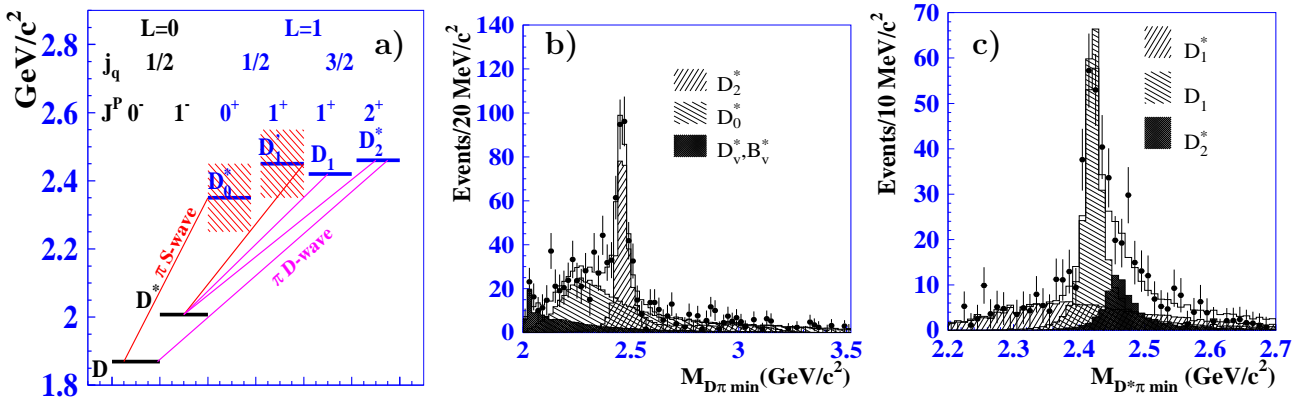


Fig. 49. (a) Spectrum of  $D$ -meson excitations. The lines indicate allowed single-pion transitions. In the heavy quark limit, the light-quark spin and orbital angular momentum couple to a total light-quark angular momentum  $j_q$ . In this approximation, one  $D_1$  decays into  $D\pi$  only via  $D$ -wave. (b) The background-subtracted minimal  $D\pi$  mass distribution in  $B^- \rightarrow D^+\pi^-\pi^-$  decays. The hatched histograms show the  $D_0^*$  and  $D_2^*$  contributions and the additional contributions from virtual intermediate states. The open histogram shows the coherent sum of all contributions. (c) The hatched histograms show the  $D_1$ ,  $D'_1$ , and  $D_2^*$  contributions, the open histogram is a coherent sum of all contributions [638].

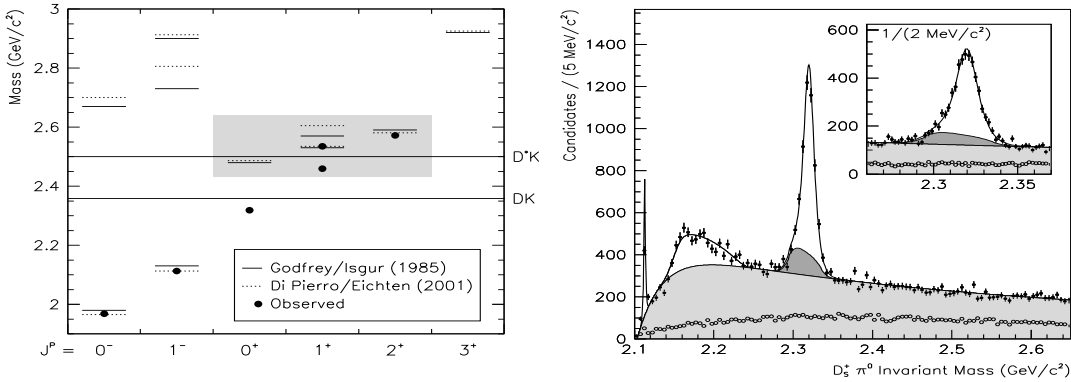


Fig. 50. Left: The spectrum of  $D_s$  excitations as predicted by Godfrey and Isgur [171] (solid lines) and Di Pierro and Eichten [818] (dashed lines) and as observed by experiment (points). The  $DK$  and  $D^*K$  mass thresholds are indicated by two horizontal lines. The  $J^P = 0^+$  state at  $2317\text{ MeV}/c^2$  has an unexpected low mass. Right: The  $D_{s0}^*(2317)^+$ . The invariant mass distribution for (solid points)  $D_s \pi^0$  candidates and (open points) the equivalent using the  $D_s$  side bins. The fit includes combinatory background (light grey) and the reflection from  $D_{sJ}(2460)^+ \rightarrow D_s^*(2112)^+ \pi^0$  decay (dark grey). The insert shows an extended view of the  $D_{s0}^*(2317)^+$  mass region [616].

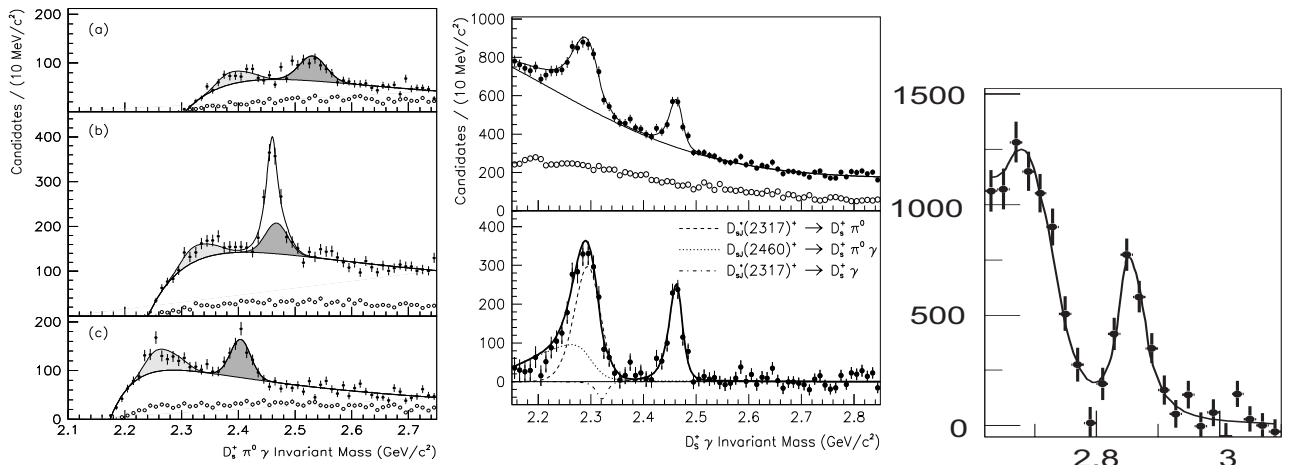


Fig. 51. Left: The  $D_{sJ}(2460)^+ \rightarrow \gamma D_s^*(2112)^+ \rightarrow D_s^+ \pi^0$  decay. Shown is the invariant mass distribution of  $D_s \pi^0 \gamma$  candidates for the  $D_s$  signal (solid points) and  $D_s$  side bands (open points). The photon energy may be compatible with a transition to  $D_s^*(2112)^+$  (b) and be too soft (a) or too hard (c). The dark grey (light grey) region corresponds to the predicted contribution from the  $D_{s0}^*(2317)^+$  ( $D_s^*(2112)^+$ ) reflection [616]. centre: The  $D_{sJ}(2460)^+ \rightarrow \gamma D_s^+$  decay. Contributions due to reflections are indicated dashed, dashed-dotted and dotted lines. The contribution  $D_{s0}^*(2317)^+ \rightarrow D_s \gamma$  is fitted to make a negative contribution (compatible with zero) [616]. Right: Observation of  $D_{sJ}(2860)^+$ . Background-subtracted  $DK$  invariant mass distributions for the sum of  $D^0$  decays into  $K^- \pi^+$  and  $K^- \pi^+ \pi^0$ , and  $D^+$  decays into  $K^- \pi^+ \pi^+$  [620].

The second missing resonance turned out to have a low mass and to be narrow, too. The  $D_{sJ}(2460)^+$  cannot decay into  $DK$  if  $J = 1$ ; its mass falls below the  $D^*K$  threshold. It was discovered shortly after  $D_{s0}^*(2317)$  [591] in pion emission to the  $D_s^*(2112)^+$  vector state and in direct radiative transitions to the  $D_s^+$  ground state. In Fig. 51 evidence for these two decay modes is displayed. The selection rules in decays of the  $D_{s0}^*(2317)^+$  and  $D_{sJ}(2460)^+$  states are consistent with  $J^P = 0^+$  and  $1^+$ , respectively. Masses and widths of the low-mass excitations of  $D_s$  are summarised in the lower part of Table 12.

It is illuminating to compare the excitation energies for the three doublets with  $(L = 0, j_q = 1/2)$ ,  $(L = 1, j_q = 1/2)$ ,  $(L = 1, j_q = 3/2)$ . We use the masses of the charged  $D$  mesons when available. For the two multiplets with  $(L = 0, j_q = 1/2)$  and  $(L = 1, j_q = 3/2)$ , the mass differences between

Table 12

Masses and width of  $D$  and  $D_s$  mesons and their excitations quoted from the Review of Particle Properties [1]. If statistical and systematic errors are given, their quadratic sum is listed below. All quantities are given in MeV/c<sup>2</sup>, except the  $D$ -meson life times which are given in fs (=10<sup>-15</sup>s) units.

Charge	$D$	$D^*$	$D_0^*$	$D'_1$	$D_1$	$D_2^*$
$\pm$ M	$1869.3 \pm 0.4$	$2010.0 \pm 0.4$	$2403 \pm 38$	$2423.4 \pm 3.1$		$2459 \pm 4$
	$1040 \pm 7$ fs	$0.096 \pm 0.023$	$238 \pm 42$	$25 \pm 6$		$29 \pm 5$
0 M	$1864.5 \pm 0.4$	$2006.7 \pm 0.4$	$2352 \pm 50$	$2422.3 \pm 1.3$	$2427 \pm 36$	$2461.1 \pm 1.6$
	$410.1 \pm 1.5$ fs	$< 2.1$	$261 \pm 50$	$20.4 \pm 1.7$	$384^{+130}_{-105}$	$43 \pm 4$
Charge	$D_s$	$D_s^*$	$D_{s0}^*$	$D'_{s1}$	$D_{s1}$	$D_{s2}^*$
$\pm$ M	$1968.2 \pm 0.5$	$2112.0 \pm 0.6$	$2317.3 \pm 0.6$	$2458.9 \pm 0.9$	$2535.35 \pm 0.61$	$2573.5 \pm 1.7$
	$98.85 \pm 0.30$	$< 1.9$	$< 4.6$	$< 5.5$	$< 2.3$	$15^{+5}_{-4}$

$D_s$  and  $D$  excitations are 99, 112, 98, 112 MeV/c<sup>2</sup>, respectively, consistent with a mass difference between  $s$  and  $d$  quark of  $\approx 105$  MeV/c<sup>2</sup>. The third multiplet resists such a simple reasoning. The mass difference for the  $D'_{s1}$  and  $D'_1$  is 37 MeV/c<sup>2</sup>, for the  $D_{s0}^*$  and  $D_0^*$  it depends on the experiment. Taking the BELLE value, the difference is -86 MeV/c<sup>2</sup>, and +9 MeV/c<sup>2</sup> for the FOCUS value.

The masses of the ( $L = 1, j_q = 1/2$ ) doublet are weird. If we expect all four  $P$  states to have similar masses, the  $D$  meson excitations concur with it, and the  $D_{s0}^*(2317)$  has exotic properties. While  $D_0^*(2400)$  is about 350 MeV/c<sup>2</sup> above the  $D\pi$  threshold,  $D_{s0}^*(2317)$  is 40 MeV/c<sup>2</sup> below the  $DK$  threshold. Hence the states do behave anomalous.

In any case, with these states, the magic number of 6 low-mass states is reached and the spectrum of  $S$ - and  $P$ -wave  $c\bar{n}$  and  $c\bar{s}$  states covered. Correspondingly, Bardeen, Eichten and Hill [819] interpreted the two new resonances  $D_{s0}(2317)$  and  $D_{sJ}(2460)$  as  $c\bar{s}$  ( $0^+, 1^+$ ) spin parity partners of the ( $0^-, 1^-$ ) doublet, and demonstrated that symmetry relation between their partial decay widths derived from chiral symmetry are fulfilled.

Recent lattice QCD calculations [820] gave an excitation energy from the  $D_s^*(2112)^+$  vector to the  $D_{s0}^*(2112)^+$  scalar state of  $(328 \pm 40)$  MeV instead of the observed 205 MeV mass gap. For their nonstrange partners the corresponding mass difference is 440 MeV on the lattice and  $(342 \pm 50)$  MeV on the experimental side. In agreement with quark model results [171, 818], the masses of  $D_{s0}(2317)$  and  $D_{sJ}(2460)$  are too low to support a straightforward interpretation as  $c\bar{s}$  states; alternative interpretations have therefore been suggested.

Barnes, Close and Lipkin argued that  $D_{s0}(2317)$  is a  $DK$  molecule and predicted the scalar  $c\bar{s}$  state at 2.48 GeV [821]. The latter state is predicted to couple strongly to the  $DK$  channel and the isoscalar  $DK$  molecule  $D_{s0}(2317)$  could be formed. The molecular forces lead to a small isovector admixture which explains its narrow width and the isospin violating decay mode  $D_s\pi$ .  $D_{s0}(2317)$  is proposed to be a dominantly I=0  $DK$  state with some I=1 admixture.

In the unitarised meson model of Van Beveren and Rupp [816],  $D_{s0}(2317)$  is created by a strong coupling to the  $S$ -wave  $DK$  threshold. The standard  $c\bar{s}$  charm strange scalar meson  $D_{s0}$  is predicted at about 2.79 GeV and with 200 MeV width. In [822], the  $D_{s0}(2317)$  is linked to the  $\kappa$  when the quark masses are lowered, and to  $\chi_{c0}$  for larger quark masses.

I. W. Lee, T. Lee, Min, and Park show that the one-loop chiral corrections could be responsible for

Table 13

Ratio of radiative and strong decay widths of  $D_{s0}^*(2317)$  and  $D'_{sJ}(2460)$ .

	BELLE [591, 634]	BaBar [596, 616]	CLEO [564]
$\Gamma_{D_{sJ}^*(2317) \rightarrow D_s^* \gamma} / \Gamma_{D_{sJ}^*(2317) \rightarrow D_s \pi^0}$	< 0.18		< 0.059
$\Gamma_{D_{sJ}(2460) \rightarrow D_s \gamma} / \Gamma_{D_{sJ}(2460) \rightarrow D_s^* \pi^0}$	$0.55 \pm 0.13 \pm 0.08$	$0.375 \pm 0.054 \pm 0.057$	< 0.49
$\frac{\Gamma_{D_{sJ}(2460) \rightarrow D_s^* \gamma}}{\Gamma_{D_{sJ}(2460) \rightarrow D_s^* \pi^0}}$	< 0.31		< 0.16
$\Gamma_{D_{sJ}(2460) \rightarrow D_{sJ}^*(2317) \gamma} / \Gamma_{D_{sJ}(2460) \rightarrow D_s^* \pi^0}$			< 0.58

the small  $D_{s0}(2317)$  mass thus supporting the picture of the new resonance as composed of a heavy quark and a light valence quark [823]. Kim and Oh used QCD sum rules study to argue that the  $D_s(2317)$  should be a bound state of scalar-diquark and scalar-antidiquark and/or vector-diquark and vector-antidiquark [824].

An interpretation of  $D_{sJ0}(2317)$  and  $D_{sJ}(2460)$  as ordinary  $c\bar{s}$  mesons derived from their decay patterns was given by Wei, Huang, and Zhu [825] who use light cone QCD sum rules. Through  $\eta - \pi^0$  mixing, their pionic decay widths are calculated which turn out to be consistent with the experimental values (or upper limits).

The unusual properties of the  $D_{s0}(2317)$  and  $D_{sJ}(2460)$  encouraged speculations that they could belong to a family of  $c\bar{s}n\bar{n}$  tetraquark states [795, 826–829]. Tetraquark states have however a common problem: many more states are predicted than found experimentally. The molecular picture is supported by calculations of strong  $D_{s0}^*$  to  $D_s \pi^0$  and radiative  $D_{s0}^*$  to  $D_s^* \gamma$  decays [830] and the leptonic decay constants  $f_{D_{s0}^*}$  and  $f_{D_{s1}}$  [831].

We come back to the discussion at the beginning of section 5.2. So far, there is no evidence for supernumerosity of states but some states certainly show an anomalous behaviour. In our language, we conclude that the states with ( $L = 1, j_q = 1/2$ ) are  $c\bar{n}$  or  $c\bar{s}$  quark model states but their coupling to the  $D\pi$  or  $D^*\pi$  ( $D_s\pi$  or  $D_s^*\pi$ ) thresholds leads to strong molecular and/or tetraquark components. More detailed information on the wave functions can probably be deduced from radiative transitions of  $D_{s0}^*(2317)$  and  $D'_{sJ}(2460)$  mesons to the  $D_s^*$  state [752]. Since the absolute width of the  $D_{s0}^*(2317)$  is expected to be in the order of  $100 \text{ keV}/c^2$ , only ratio of radiative to hadronic widths are experimentally accessible. The results, collected in Table 13 are consistent with  $c\bar{q}$  descriptions of  $D_{s0}^*(2317)$  and  $D'_{sJ}(2460)$  [819] but do not enforce this interpretation.

### 5.3.2 Further mesons with open charm

A few higher-mass states were also reported. So far, there is evidence only for one additional state belonging to the  $D$  meson family, with quantum numbers  $J^{PC} = 1^{--}$ . The  $D^*(2640)$  was observed by Delphi at LEP in  $Z^0$  decays [678]. It has a mass difference to the ground state  $D^*(2010)$  of  $630 \text{ MeV}/c^2$  which compares well with those of other vector meson, but its width is anomalously narrow, less than  $15 \text{ MeV}/c^2$ . The  $D^*(2640)$  was searched for by the Opal collaboration; an upper limit, incompatible with the Delphi result, was given [699]. If a broad resonance is present, but at the statistical limit of its observability, then it is sometimes seen due to a statistical fluctuation as a narrow peak. Without or opposite a statistical fluctuation, the resonance is ascribed to the background.

In the  $D_s$  family, a few states were reported. A  $D_{sJ}^{*+}(2630)$  was observed by the SELEX collaboration at FNAL [539] in the final states  $D^0 K^+$  and  $D_s \eta$  produced inclusively in a hyperon ( $\Sigma^-$ )

beam. The mass is determined to  $2632.6 \pm 1.6$  MeV/c<sup>2</sup> and the width to be less than 17 MeV/c<sup>2</sup> (at 90% c.l.). Due to the decay mode, it must have natural spin-parity. The ratio of the partial widths

$$\frac{\Gamma(D_{sJ}^{*+}(2630) \rightarrow D^0 K^+)}{\Gamma(D_{sJ}^{*+}(2630) \rightarrow D_s \eta)} = 0.16 \pm 0.06. \quad (5.12)$$

is unexpected since the D K mode is favoured by phase space. The width is unexpectedly narrow as well. These properties encouraged searches by other collaborations, by FOCUS (quoted from [750]), BaBar [594], and CLEO [832]. No evidence for the  $D_s(2630)^{*+}$  was found. However, SELEX is the only experiment using a hyperon beam, and it may be that this is a more favourable production mode.

The  $D_{sJ}^{*+}(2630)$  properties may evidence an exotic nature of the state. Van Beveren and Rupp [833] interpret the state in their coupled channel model. The model predicts further, partly narrow,  $D_s^*$  states at 2720, 3030, and 3080 MeV/c<sup>2</sup>. Maiani *et al.* suggest [834] that the  $D_s(2630)$  is a  $[cd][d\bar{s}]$  tetraquark. If the state does not mix with  $[cu][u\bar{s}]$ , the decay to  $D^0 K^+$  would be isospin violating, thus making the  $D_s(2630)$  narrow. Among other predictions, a close-by state with charge +2 decaying into  $D_s^+ \pi^+$  and  $D^+ K^+$  should exist.

Y.-R. Liu, Dai, C. Liu, and Zhu [835] demonstrated that the ratio (5.12) can be reproduced quantitatively when the  $D_{sJ}(2632)$  is interpreted as the  $J^P = 0^+$  isoscalar member of the **15** multiplet of tetraquarks. the meson has the quark content  $\frac{1}{2\sqrt{2}}(ds\bar{d} + sd\bar{d} + su\bar{u} + us\bar{u} - 2ss\bar{s})\bar{c}$  which leads to the relative branching ratio

$$\frac{\Gamma(D_{sJ}^+(2632) \rightarrow D^0 K^+)}{\Gamma(D_{sJ}^+(2632) \rightarrow D_s^+ \eta)} = 0.25. \quad (5.13)$$

We point out that the wave function can be reduced to  $s\bar{c}$ . In our language, the  $D_{sJ}(2632)$  is a quark model state with a tetraquark component. If, as we believe, the  $s\bar{c}$  component is essential for the binding, its flavour exotic partners – predicted in [835] – should not exist. Due to the large decay probability of the tetraquark component, this part dominates the decay properties of the state.

A  $c\bar{s}$  vector excitation was observed in a Dalitz plot analysis of  $B^+ \rightarrow \bar{D}^0 D^0 K^+$  decays [657, 658] in the  $D^0 K^+$  mass spectrum. Its mass and width are  $(2715 \pm 11^{+11}_{-14})$  and  $(115 \pm 20^{+36}_{-32})$  MeV/c<sup>2</sup>, respectively. Its spin-parity is  $J^P = 1^-$ . Fig. 52 shows a comparison of  $D_{s1}^*$  states with excitations of  $J/\psi$  and  $\rho$ . An identification of  $D_{s1}^*(2715)$  as  $D_{s1}^*(2S)$  is very convincing even though an exotic interpretation as tetraquark state has also been suggested [836].

The so-far highest mass  $c\bar{s}$  state was observed by the BaBar Collaboration [620]. Fig. 51 (right) shows the sum of the  $D^0 K^+$  and  $D^+ K_S^0$  mass distribution. Due to the decays, it must have natural spin-parity  $0^+, 1^-, 2^+, \dots$ . Its mass and width are  $2856.6 \pm 1.5 \pm 5.0$  and  $48 \pm 7 \pm 10$  MeV/c<sup>2</sup>. With weak evidence, a further state is reported with  $M = 2688 \pm 4 \pm 2$ ,  $\Gamma = 112 \pm 7 \pm 36$  MeV/c<sup>2</sup>.

Van Beveren and Rupp suggest both states to have scalar quantum numbers and identify the  $D_{sJ}^*(2860)$  as the radial excitation of the  $D_{s0}^*(2317)$  while the  $D_{sJ}^*(2690)$  is assigned to a dynamical pole originating from unitarity constraints [837]. Close, Thomas, Lakhina and Swanson use a modified quark-quark scalar potential which allows them to treat the  $D_{s0}^*(2317)$  as ordinary  $c\bar{s}$

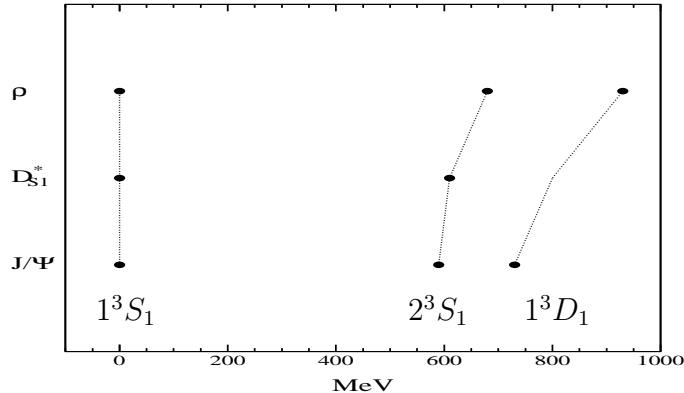


Fig. 52. Excitation energies of vector states above the  $1^3S_1$  level. Dotted lines connect states of different flavour content but the same spectroscopic quantum numbers. The charmonium states are (from left to right)  $J/\psi$ ,  $\psi(2S)$  and  $\psi(1D)$ ; the isovector vector states are  $\rho(770)$ ,  $\rho(1450)$  and  $\rho(1700)$  which are likely the  $1^3S_1$ ,  $2^3S_1$  and  $1^3D_1$  quark-model states. The  $D_{s1}^*(2715)$  is naturally assigned to a  $2^3S_1$  configuration.

meson; based on the masses, they suggest to identify  $D_{sJ}^*(2690)$  with  $D_{s1}^*(2715)$  and to interpret  $D_{sJ}^*(2860)$  as  $D_{s0}^*(2P)$  state [838]. The  $D_{sJ}^*(2860)$  may also be a  $1^-(^3D_3)$  state [839]. The centrifugal barrier then explains its narrow width.

Based on a discussion of widths and decay modes, Bo Zhang et al. [840] interpret  $D_{sJ}(2715)$  as the  $1^-(1^3D_1)$   $c\bar{s}$  state (although the  $1^-(2^3S_1)$  assignment is not excluded). An interpretation of  $D_{sJ}(2860)$  as  $1^-(2^3S_1)$  or  $1^-(1^3D_1)$  candidate was considered to be unlikely, and an assignment as  $0^+(2^3P_0)$  or  $3^-(1^3D_3)$   $c\bar{s}$  state more plausible. Obviously, more experimental data are needed to assign quantum numbers reliably.

### 5.3.3 Mesons with open beauty

Mesons with open beauty,  $b\bar{n}$  mesons, correspond closest to the classical picture of hydrogen atoms and are best suited to test ideas on heavy flavour symmetry. Experimentally, the study of  $B$  meson excitations is still in its infancy. One expects, as in the case of  $D$  meson excitations, a vector resonance  $B^*$ , two narrow states  $B_1$  and  $B_2^*$ , and two broad states  $B_0^*$  and  $B_1$ .

A pilot study was made by DØ at FNAL [841]. The  $B$  mesons were reconstructed from their  $J/\psi K$  and  $J/\psi K^*$  decays. From the inclusive  $B\pi$  mass spectrum shown in Fig. 53, the mass of the two expected 'narrow' resonances were deduced.

$$\begin{array}{lll} B_1 & M & = 5724 \pm 4 \pm 7 \text{ MeV}/c^2 \\ B_2^* & M_{B_2^*} - M_{B_1} & = 23.6 \pm 7.7 \pm 3.9 \text{ MeV}/c^2. \end{array}$$

The widths of both states were assumed to be equal and fitted to  $\Gamma = 23 \pm 12 \pm 6 \text{ MeV}/c^2$ . The results do not yet deepen our insight into heavy quark physics but rather demonstrate the feasibility of such studies.

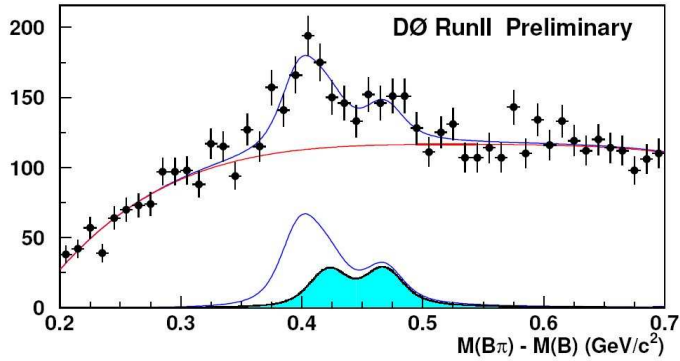


Fig. 53. The  $B\pi - B$  mass difference with the results of a fit. The 50 MeV photon from  $B^* \rightarrow \gamma B$  was not reconstructed, hence  $B_2^*$  decays to  $B_0^* \pi$  are shifted in mass. The background subtracted spectrum shows contributions assigned to  $B_2^*$  decays to  $B_0^* \pi$  and to  $B\pi$  (shaded area) and from  $B_1$  decays  $B_0^* \pi$  [841].

## 6 Radial and orbital excitations of light mesons

### 6.1 Patterns at high $l, n$

The masses of the lightest glueballs are predicted to fall into the 1.5 to 2.5 GeV/c<sup>2</sup> mass range. This is a mass interval in which a rich spectrum of meson resonances is expected, and indeed observed. This spectrum may however contain not only  $q\bar{q}$  mesons but hybrid excitations and multiquark clusters as well. Thus it is essential to develop a good understanding of the ‘background’ of  $q\bar{q}$  mesons in order to identify anomalies and to establish properties of states falling outside of this classification scheme, for their supernumerosity, for their production modes, or for their unusual decays. In the last few years, significant progress was achieved in the study of highly excited hadrons. The comprehensive analysis of various final states in  $p\bar{p}$  annihilation in flight [374, 378, 381, 382] revealed a large number of resonances with masses up to 2.4 GeV/c<sup>2</sup>. The total antiproton-proton annihilation cross section is saturated in all partial waves accessible at a given momentum, and meson resonances are excited with low and high orbital and radial quantum numbers. The simultaneous analysis of several final states gives access to all (non-exotic) quantum numbers. Many of the resonances are observed in several final states; the internal consistency of the results and the consistency of some results with earlier observations lends further credibility to the findings.

The multitude of resonances excludes a discussion of each individual state. Instead, we treat the data on a statistical basis. In Fig. 54 the number of states as a function of their squared mass is plotted. Pseudoscalars and scalars are not included in this figure for reasons discussed in the introduction (section 1.2.7). Strange particles are omitted as well. Those states which are not well confirmed are taken in the histogram with weight  $W = 0.5$  and error  $E = 0.5$ . In assigning the significance to the states we follow the judgement of Bugg [49]. The figure demonstrate clustering of

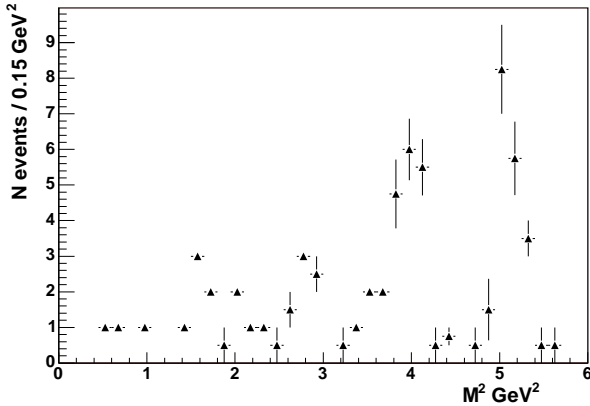


Fig. 54. The density of states versus their squared masses.

states very clearly [49]. An analogous effect of clustering is known in baryon spectroscopy [112, 842]. The spacing between bumps in Fig. 54 is about 1.1 GeV/c<sup>2</sup>, very similar to that in baryons.

A more detailed picture of light-quark mesonic states is given in Fig. 55. In this figure all light quark mesons with known quantum numbers  $I^G J^{PC}$  are plotted as a function of  $M^2$ . The ordering of states follows expectations from potential models for  $q\bar{q}$  mesons. The first four lines are occupied by states with zero orbital momentum, the next eight lines by states with  $L = 1$ , etc. States with

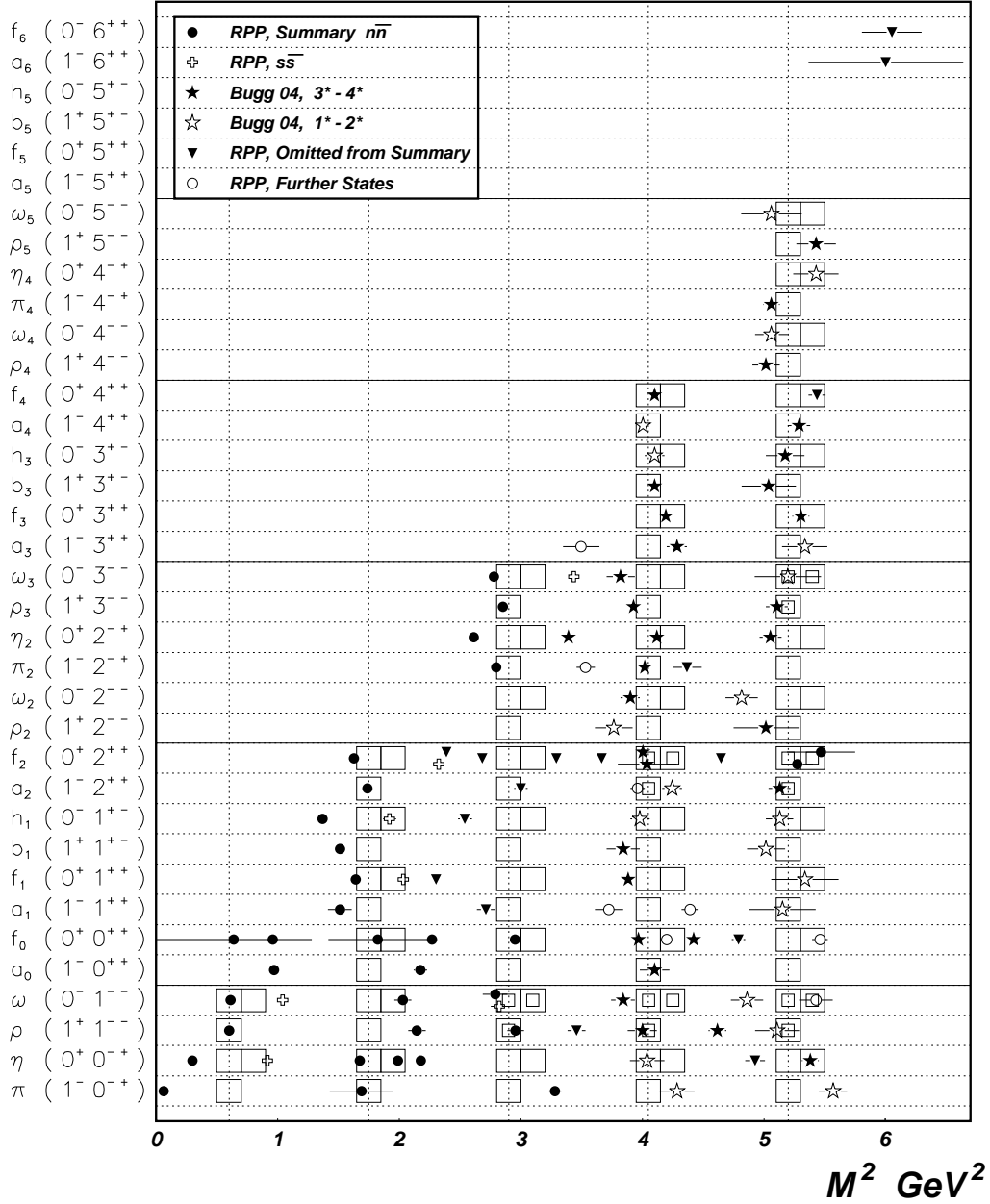


Fig. 55. The pattern of light quark meson states (adapted from [843]).

different creditability are plotted using different symbols. The empty boxes indicate the position of states in an oversimplified model in which masses of mesons are proportional to  $l + n$ , where  $l$  is the orbital and  $n$  the radial quantum number. Mesons of zero isospin have two nearby boxes for  $n\bar{n}$  and  $s\bar{s}$  states or for  $SU(3)$  singlet and octet states. Some boxes are doubled because two different states ( $J = l + 1, n$  and  $J = l - 1, n + 2$ ) can sit there.

From this amusing picture we conclude that at sufficiently high  $J$  and  $M$ , meson trajectories are nearly linear in both, in the  $M^2, J$  and in the  $M^2, n$  plane. The trajectories are parallel and equidistant. The linearity of the trajectories and the  $l, n$  degeneracy were predicted in a model based on the dual superconductor mechanism of confinement [104] and a model guided

by nonperturbative QCD [106], see section 1.2.5 in the introduction. For sake of convenience, we reproduce eq. (1.11)

$$M_n^2(l) = 2\pi\sigma \left( l + n + \frac{1}{2} \right).$$

which shows that the squared masses are linear in  $l$  and  $n$ , and degenerate in  $n + l$ .

The  $n + l$  degeneracy has been interpreted as evidence for restoration of chiral symmetry in highly excited mesons [844, 845]. A new QCD scale  $\Lambda_{CSR} = 2.5 \text{ GeV}/c^2$  is suggested at which chiral symmetry is restored [846, 847]. The string model and the conjectured restoration of chiral symmetry thus both lead to a  $n + l$  degeneracy of excited states. The two models make however different predictions for ‘stretched’ states, for states with  $J = l+s$ . The string model predicts no parity partners for  $a_2(1320)-f_2(1270)$ ,  $\rho_3(1690)-\omega_3(1670)$ ,  $a_4(2040)-f_4(2050)$ ,  $\rho_5(2350)-\omega_5$ ,  $a_6(2450)-f_6(2510)$ . On the contrary, there is no reason why these isospin doublets should not be accompanied by chiral partners, if chiral symmetry would be restored in highly excited mesons. Experimentally, there are no chiral partner for any of these 10 states. Hence data do not support the hypothesis of chiral symmetry restoration. Similar arguments have been made for baryons [848] for which restoration of chiral symmetry is suggested as well [190, 849]. From a theoretical side, Jaffe, Pirjol and Scardicchio [850] concluded that massless pions preclude chiral symmetry be restored in the hadron mass spectrum and suggested other reasons for the observed parity doublets like suppression of the violation of the flavour singlet axial symmetry  $U(1)_A$  [851].

Fig. 55 bares another important consequence: the bulk of observed mesons are compatible with a  $q\bar{q}$  assignment, with at most a few exceptions. These striking regularities suggest that at sufficiently high mass and  $J$ , exotic states (glueballs, hybrids, multiquark states, multimeson states) either do not exist or are not produced in  $p\bar{p}$  annihilation. Only a few states fall outside of the regular pattern; they deserve special attention and will be discussed below (in section 6.4).

One final word of caution. The majority of high-mass entries in Fig. 55 stems from one single experiment. Due to the early closure of LEAR, only a rather limited number of antiproton momenta was used and there is the need to extend the measurements to lower and to higher momenta. Rare channels suffered from low statistics. A confirmation with improved statistics and improved methods (e.g. an improved detector, a polarised target) is certainly highly desirable. Such experiments will become feasible again when the antiproton project at GSI comes into operation.

## 6.2 Systematic of $q\bar{q}$ mesons in $(n, M^2)$ and $(J, M^2)$ planes

In recent years, the Gatchina group has performed fits to a large number of data sets. The fits have grown in time to increasing complexity. Earlier variants can be found in [852–858]; the results presented here are taken from [371] and [859]. Recent fits include the CERN-Munich data on  $\pi^-p \rightarrow \pi^+\pi^-p$ ; GAMS data on  $\pi^-p \rightarrow \pi^0\pi^0n$ ,  $\eta\eta n$  and  $\eta\eta'n$  at small transferred momenta,  $|t| < 0.2 \text{ GeV}^2/c^2$ , and on  $\pi^-p \rightarrow \pi^0\pi^0n$  for  $0.30 < |t| < 1.0 \text{ GeV}^2/c^2$ ; BNL data on  $\pi^-p \rightarrow \pi^0\pi^0n$  at (squared) momentum transfers  $0 < |t| < 1.5 \text{ GeV}/c^2$  and on  $\pi^-p \rightarrow K\bar{K}n$ ; Crystal Barrel data on  $p\bar{p}$  annihilation at rest in liquid H<sub>2</sub> into  $\pi^0\pi^0\pi^0$ ,  $\pi^0\pi^0\eta$ ,  $\pi^0\eta\eta$ ,  $\pi^+\pi^-\pi^0$ ,  $K^+K^-\pi^0$ ,  $K_S^0K_S^0\pi^0$ ,  $K^+K_S^0\pi^-$  and  $\bar{p}n$  annihilation in liquid D<sub>2</sub> into  $\pi^0\pi^0\pi^-$ ,  $\pi^-\pi^-\pi^+$ ,  $K_S^0K^- \pi^0$ , and  $K_S^0K_S^0\pi^-$ . Data on  $\pi^0\pi^0\pi^0$ ,  $\pi^0\pi^0\eta$  for antiprotons stopping in gaseous H<sub>2</sub> were used to constrain annihilation contributions from *S*-wave and *P*-wave orbitals of the  $p\bar{p}$  atom. Such analyses have the distinctive advantage that a complete meson spectrum emerges which sums the combined knowledge from very different reactions into one unified picture.

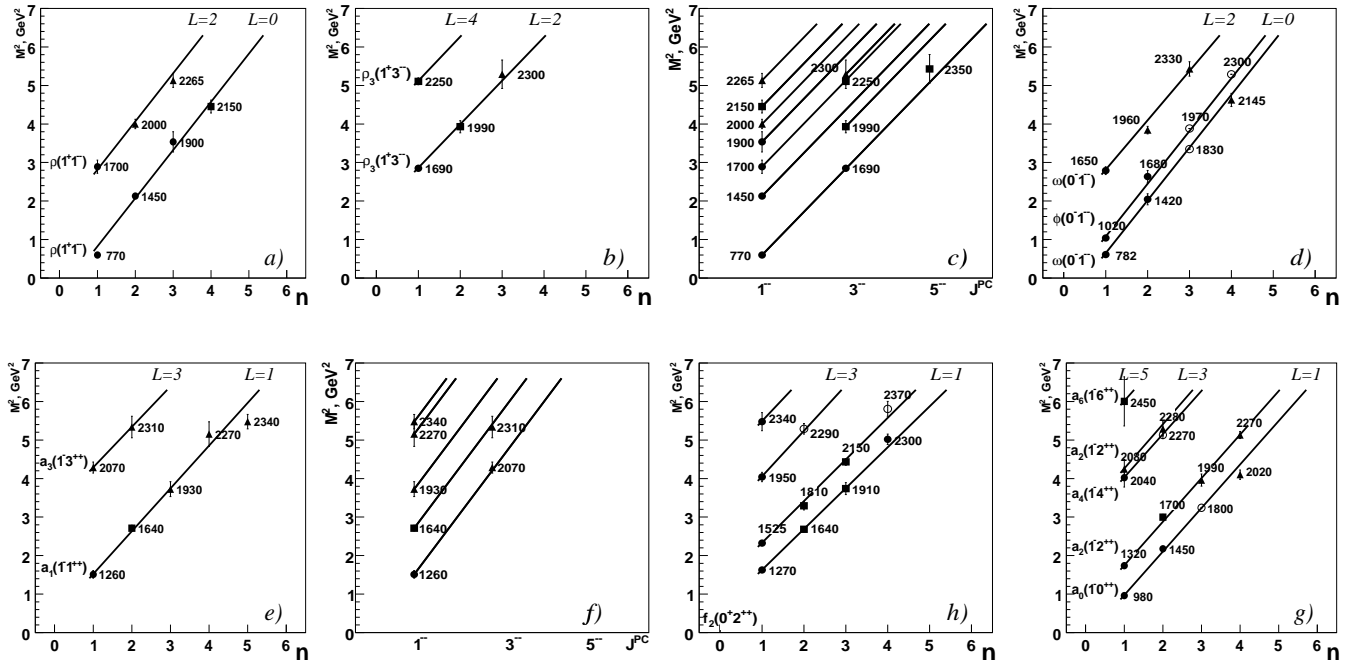


Fig. 56. Squared meson masses as functions of  $n$  and  $J$ . Particles from the PDG *Summary Table* are represented by a ●, those omitted from the *Summary Table* by a ■. ▲ represents data given by Anisovich *et al.* [371] and listed as *Further States* by the PDG, open circles predicted by their classification. a)  $(n, M^2)$ -trajectories of  $\rho(1-)$   ${}^3S_1$  and  ${}^3D_1$  mesons as functions of  $n$ ; b)  $\rho(3-)$   ${}^3D_3$  and  ${}^3G_3$  trajectories as functions of  $n$ ; c) Regge trajectories for  $\rho(770)(1^3S_1)$ ,  $\rho(1450)(2^3S_1)$ ,  $\rho(1700)1({}^3D_1)$ ,  $\rho(1900)(3^3S_1)$ ,  $\rho(2000)2({}^3D_1)$ ,  $\rho(2150)(4^3S_1)$ ,  $\rho(2265)1({}^3D_1)$ ;  $\omega(1-)$  and  $\phi(1-)$   ${}^3S_1$  and  $\omega(1-)$   ${}^3D_1$  trajectories as functions of  $n$ . e)  $(n, M^2)$ -trajectories of  $a_1(1++)$   ${}^3P_1$  and  $a_3(3++)$   ${}^3F_3$  mesons and f) the corresponding Regge trajectories; g,h)  $(n, M^2)$ -trajectories for  $a_{2J}$  and  $f_{2J}$  mesons with even spin.

The results of the Gatchina group on scalar and tensor mesons deserve a deeper discussion (see sections 6.4.3 and 11.3, respectively). Here we concentrate on general issues from a wider perspective. A.V. Anisovich, V.V. Anisovich, and Sarantsev [371] have assigned orbital and radial quantum numbers to mesonic resonances they have found in the fits described here, in the data on  $p\bar{p}$  annihilation in flight described in section 6.1, and to resonances reported elsewhere [1], and suggested a vision how to interpret the spectrum. In the mass region up to  $M < 2400$  MeV/c<sup>2</sup> the masses of mesons are plotted in  $(n, M^2)$  and  $(J, M^2)$  planes, thus suggesting their classification in terms of  $n$   ${}^{2S+1}L_J$   $q\bar{q}$  states. All trajectories are linear, with nearly the same slopes as expected from the relation  $M_n^2(l) = 2\pi\sigma \left( l + n + \frac{1}{2} \right)$ . The Figs. 56a-h characterise meson resonances by their mass; their production and decay pattern is not used to check if the interpretation based on their masses is consistent. Nevertheless, the figures can serve as guides to identify mesons beyond the  $q\bar{q}$  scheme. Further plots are shown in the section on pseudoscalar (Fig. 79) and scalar mesons (Fig. 115).

The strength of such a unified picture is evident and in most cases, the scheme provides a viable classification. Obviously, there is one missing state in the series of  $\rho$  radial excitations consisting of  $\rho(770)$ ,  $\rho(1450)$ ,  $\rho(2150)$ ; the missing state is predicted to have a mass of about 1830 MeV/c<sup>2</sup>. This is a welcome hint for further searches. The  $\rho(1700)$  is the leading resonance of the  ${}^3D_1$  series of states in which the intrinsic orbital angular momentum  $l = 2$  makes a large contribution; a small admixture of  ${}^3S_1$  is of course not excluded. Based on the mass spectrum depicted in Fig. 56a, it is unlikely that a hybrid vector meson is part of the game. A conjecture based on an

unexpected decay pattern of  $\rho(1450)$  will be discussed below. It is proposed that a hybrid vector meson may hide in the spectrum since the observed decay modes are inconsistent with a pure  $q\bar{q}$  interpretation of  $\rho(1450)$ . This is a weak point of the classifications suggested in Fig. 56: the decay modes which provide important information on the flavour structure of mesons were not considered. There is thus a potential danger in this approach: it is unclear if the scheme survives when one of the resonances disappears or shows decay modes incompatible with the assignment based on its mass. There are a few further examples where one has to be cautious:

In section 8 on pseudoscalar mesons it will be shown that  $\eta(1295)$  cannot be a  $q\bar{q}$  meson. How stable is then the classification against taken this meson out? The  $\eta_2(1870)$  resonance is produced and decays rather as  $n\bar{n}$  and not as  $s\bar{s}$  state; that is the reason to discuss this state below as hybrid candidate. In Fig. 79 it is nevertheless interpreted as  $s\bar{s}$  partner of  $\eta_2(1645)$ . In Fig. 115 the  $a_0(980)$  is needed as lowest mass scalar isovector state. Likewise, the Gatchina interpretation requires  $f_0(980)$  to be a  $q\bar{q}$  state. Both these mesons are often interpreted as non- $q\bar{q}$  objects. The  $\sigma(485)$  is tentatively interpreted as additional state beyond  $q\bar{q}$  spectroscopy generated by an amplitude singularity related to confinement, its twin brother  $\kappa(700)$  is not considered. In the Gatchina scheme,  $a_0(980)$  and  $f_0(980)$ ,  $\sigma(485)$ , and  $\kappa(700)$  are three unrelated phenomena. The  $f_0(1300)$  with  $\rho\rho$  as most prominent decay mode is interpreted in Fig. 115 as  $s\bar{s}$  state. The plots make very detailed predictions, that is of course its strength. But details may be at variance with new knowledge or interpretations. We will come back to some of these questions in the sections on pseudoscalar mesons and on the interpretation of scalar mesons.

### 6.3 Threshold dynamics

The importance of  $S$ -wave thresholds has often been underlined. Here we remind of some recent work [800, 812, 860, 861]. The best studied example is of course the  $K\bar{K}$  threshold which gave rise to many interpretational controversies. At BES II and BELLE, several threshold enhancements in baryon-antibaryon systems were observed which will be discussed briefly in section 8.4.3. At the  $p\bar{p}$  threshold, a dip is observed in  $e^+e^- \rightarrow 6\pi$  which points to an interpretation within  $N\bar{N}$  interaction physics.  $0^{-+}$  quantum numbers are suggested for the  $p\bar{p}$  threshold enhancement, the dip in  $e^+e^- \rightarrow 6\pi$  is  $1^{--}$ , so it is unclear if the two observations are related. A threshold bump at  $m = 2.175$  GeV/c $^2$  has been observed at BaBar [618] in the radiative-return reaction  $e^+e^- \rightarrow \phi f_0(980)$ . Due to its production and decay, it might be a  $\phi$  radial excitation;  $\Upsilon(nS)$  and  $\psi(nS)$  have a high chance to decay into their respective ground state plus  $\pi\pi$  in the  $S$ -wave, too. A  $\pi_2(1870)$  was observed at the threshold of its  $a_2(1320)\eta$  decay in diffractive scattering at VES [235]. In section 5 we have discussed several further states which are found close to their respective decay channels. We mention  $X(3872)$ ,  $Y(3940)$ ,  $D_{s0}(2317)$ , and  $D_{s1}(2460)$ . The three states  $X(1812)$ ,  $\phi(2175)$ , and  $Y(3940)$  have unusual decay modes; we will suggest strong tetraquark components for  $X(1812)$  ( $= f_0(1760)$ ) and  $Y(3940)$  ( $= \chi_{c0}(2P)$ ) to explain their anomalous decay.

In our view, thresholds have a significant impact on the precise mass and width of resonances. Thresholds can generate cusps, attract poles, but – as a rule – they do not generate new poles.

### 6.4 Hybrids candidates

There are a few cases where experimental findings disagree with expectations based on the quark model. These states could be glueballs, hybrids, or multiquark resonances. The most suspicious cases are found in the scalar and pseudoscalar mass spectra; these will be discussed in separate sec-

tions. Here we report on evidence for further mesons which resist a straightforward interpretation as  $q\bar{q}$  mesons.

#### 6.4.1 $J^{PC} = 1^{--}$

First evidence for the existence of a higher-mass vector meson was found in bubble chamber data on  $p\bar{p} \rightarrow \omega\pi^+\pi^-$  [862, 863] at a mass of about 1250 MeV/c<sup>2</sup>. Later, the joint analysis of data from various experiments on e<sup>+</sup>e<sup>-</sup> annihilation and photoproduction of final-states containing two or four pions proved the existence of  $\rho(1450)$  and  $\rho(1700)$  [864, 865]. In the isoscalar sector, three states are known,  $\omega(1420)$ ,  $\omega(1650)$  [866, 867], and  $\phi(1680)$  [868]. The  $\omega$  resonances are readily assigned to two states expected in the quark model, the first radial excitation  $2^3S_1$  and the first  $l = 2$  orbital excitation  $1^3D_1$ , Fig. 52 in section 5.3.2. Two  $\phi$  states are, of course, expected but only one was reported so far.

In the reaction  $J/\psi \rightarrow K^+K^-\pi^0$ , the BES collaboration found a broad enhancement in the  $K^+K^-$  invariant mass distribution. A partial wave analysis shows that the structure has  $J^{PC} = 1^{--}$ . Since it is recoiling against a pion, its quantum numbers are thus like those of the  $\rho$ . When fitted with a Breit-Wigner amplitude, a pole was found at the position  $(1576_{-55}^{+49}(stat)_{-91}^{+98}(syst))\text{MeV}/c^2 - i(409_{-12}^{+11}(stat)_{-67}^{+32}(syst))\text{MeV}/c^2$  [510]. This is an important finding: the  $K^+K^-$  enhancement is not easily assigned to any quark model state. It shows that there are background amplitudes which could be wide tetraquark resonances or generated by meson-meson interaction dynamics via  $t$ -channel exchanges. Of course, it is very difficult to prove a resonant character of such a wide background, extending over more than 1 GeV/c<sup>2</sup>. Possibly, a slow background phase motion due to molecular interactions may as well be compatible with the data.

This classification of the states  $\rho(1450)$  and  $\rho(1700)$  meets with some problems [869]:

- The experimental ratio of the  $e^+e^-$  width of the  $\rho(1700)$  to that of the  $\rho(1450)$  is too large in comparison with calculations in non-relativistic limit where this ratio is zero.
- The decay widths of these states do not follow predictions of the  ${}^3P_0$  model which often gave realistic estimates for hadronic partial widths. According to model predictions, the  $4\pi$  decays of  $\rho_{2S}$  are small and  $\rho_{1D}$  should decay into  $h_1\pi$  and  $a_1\pi$  with large and nearly equal probability. From this we would expect  $\sigma(e^+e^- \rightarrow \pi^0\pi^0\pi^+\pi^-) > \sigma(e^+e^- \rightarrow \pi^+\pi^-\pi^+\pi^-)$ , in contradiction with observations. Yet, the flux tube model – assuming  $\rho(1450)$  to be a hybrid – gave no reasonable agreement with data neither.

The assumption of an additional hybrid  $\rho_H$  state helps to solve these problems [869]. This hypothetical state is expected to decay mainly into  $a_1\pi$  and not into  $h_1\pi$ . Thus the ratio  $(\pi^0\pi^0\pi^+\pi^-)/(\pi^+\pi^-\pi^+\pi^-)$  moves into the right direction. Mixing of the two  $q\bar{q}$  states with  $\rho_H$  can reproduce the observed decay pattern.

The hybrid state needed for this scheme has to be relatively light,  $M \approx 1.6$  GeV/c<sup>2</sup>, otherwise it does not mix sufficiently with the conventional  $\rho$  state. Such a low mass of a vector hybrid imposes severe restrictions on the mass scale of other light hybrids due to predicted mass ordering  $0^{-+} < 1^{-+} < 1^{--} < 2^{-+}$  which is valid in different models [870]. The missing state of this trio could be  $\rho(1900)$  seen in  $6\pi$  final state [528], or a low mass state  $\rho(1200)$  [356].

Recently, the BES collaboration has reported an extremely broad vector state with  $(1576_{-55}^{+49}(stat)_{-91}^{+98}(syst))\text{MeV}/c^2$  mass and  $(818_{-24}^{+22}(stat)_{-134}^{+64}(syst))\text{MeV}/c^2$  width [510]. Due to its production in  $J/\psi$  decays into

$\pi(K\bar{K})$ , its isospin is likely  $I = 1$ . No attempt has been made so far to see if this state can cure these problems. In [871] it was shown that interference effects due to final state interactions could produce an enhancement around 1540 MeV in the  $K^+K^-$  spectrum but the expected intensity is smaller than the observed one. Interpretations are given by a number of authors [872–875] within tetraquark scenarios.

#### 6.4.2 $J^{PC} = 1^{++}$

The flux tube model predictions [58, 876–878] for the decay widths of  $J^{PC} = 1^{++}$   $2P$  state and of  $1^{++}$  hybrid are collected in the Table 14.

Table 14  
Partial widths (in  $\text{MeV}/c^2$ ) of  $2P(q\bar{q})$  and hybrid  $a_1(1700)$

	$\rho\pi$	$\rho\omega$	$\rho(1470)\pi$	$b_1\pi$	$f_1\pi$	$f_2\pi$	$K^*K$
$2P$	57	15	41	0	18	39	$18 \div 30$
$H$	$28 \div 40$	0	$50 \div 70$	0	$4 \div 60$	$2 \div 75$	$18 \div 24$

The most selective decay mode is  $\rho\omega$  which is supposed to be suppressed for a hybrid and strong for a  $2P$   $q\bar{q}$  state. The two alternatives differ also by their  $D/S$  ratio in  $a_1(1700) \rightarrow \rho\pi$  decay. For a  $a_1$  hybrid,  $S$ -wave dominance is expected, for a  $2D$ -state, the  $D$ -wave should exceed the  $S$ -wave.

Experiments exhibit a strong  $J^{PC} = 1^{++}$  signal at  $M \approx 1.7 \text{ GeV}/c^2$  in  $\rho\pi$  [236, 257],  $f_1\pi$  [260, 879] and  $\omega\rho$  [238]. The shapes of these signals are different, the visible width varies from  $\Gamma \approx 300 \text{ MeV}/c^2$  in the  $\rho\pi$  channel to  $\Gamma \approx 600 \text{ MeV}/c^2$  in  $\omega\rho$ . If we assume that the source of these signals is one resonance, then the decay pattern is consistent with a conventional  $2P$  meson. The  $D/S$  ratio of the  $\rho\pi$  channel ( $D > S$ ) supports the  $2P$  interpretation. The  $b_1\pi$  channels is predicted to be suppressed for both, the quark-model  $a_1(1700)(2P)$  and the hybrid  $a_1(1700)(H)$ . This suppression is observed in data; this may serve as indication that the models give a realistic estimate of decay widths. The data are presented in Fig. 57. Shown are the sum of all partial wave contributions,  $S_1(\rho\omega) + S_1(\rho_{1450}\omega)$ ,  $P_1(b_1\pi)$ ,  $D_1(\rho\omega)$ ,  $D_2(\rho\omega)$ , and the sum of the  $S_1(\rho\omega)$  and  $P_1(b_1\pi)$  waves. The latter two waves obviously do not contribute to the  $a_1(1700)$  signal. The letter  $S, P, D$  denotes the orbital angular momentum, the subscript the total spin.

The absence of a hybrid meson signal in  $J^{PC} = 1^{++}$  channel poses a real problem. According to [58] this meson should be narrow  $\Gamma \approx 100 \text{ MeV}/c^2$  and have  $\rho\pi$  as one of its dominant decays. Thus, the signal is difficult to hide. For example, it has to be seen in the charge exchange reaction  $\pi^- p \rightarrow \pi^+ \pi^- \pi^0 n$  where experiment does not show any trace of a  $1^{++}$  resonance in the  $\approx 1.6 \div 2.0 \text{ GeV}/c^2$  mass region.

#### 6.4.3 $J^{PC} = 2^{++}$ and search for the tensor glueball

The Particle Data Group [1] lists 14 isoscalar tensor mesons with masses below  $2.4 \text{ GeV}/c^2$  and considers 6 of them as established, 6 states are omitted from the Summary Table, and 2 are listed as Further States. In this mass range, 12 quark model states are expected (see Fig. 55). It would certainly be too naive to claim on this basis that there is abundance of tensor mesons. The problem is of course that the results come from a variety of different experiments and analyses. Some measurements could be wrong; more trivially, some states could be listed twice. The two candidates

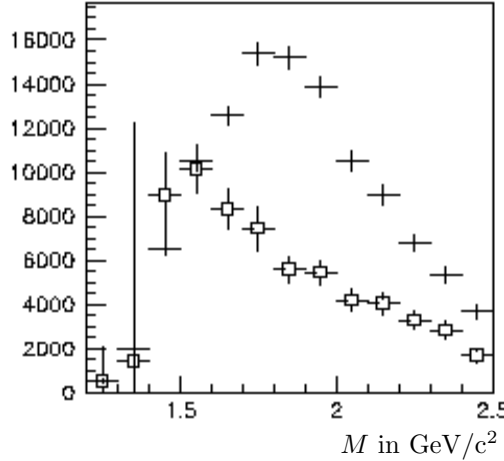


Fig. 57. The intensities of  $J^{PC} = 1^{++}$  waves in the reaction  $\pi^- N \rightarrow \omega \pi^- \pi^0 N$ : crosses - sum of all  $J^{PC} M^n = 1^{++0+}$  waves, squares - sum of two waves [238]. See text for further discussion.

$f_2(1565)$  and  $f_2(1640)$  are, e.g., very likely one state; the mass shift could be a measurement error or could be caused by the  $\omega\omega$  threshold. The only realistic chance to bring order into this mess are analyses which describe all most sensitive data with one set of amplitudes.

Such analyses have been performed by the Gatchina group; their results on tensor states were reported in [880–882]. Data on two-photon fusion into  $\pi^+\pi^-\pi^0$  [883] and into  $K_S^0 K_S^0$  [884] from L3 at LEP (see section 3.6.3) provided information on the two lowest-mass tensor nonets. The results are reproduced in Table 15. For the ground-state nonet, the  $K_2^*(1430)$  serves as a solid anchor for the mass scale; there is no  $K_2^*$  known which could play this rôle for the second nonet; an additional  $K_2^*$  should hence be expected at about 1650 MeV/c<sup>2</sup>. Both nonets are found to be nearly ideally mixed; at the first glance, this is surprising given the large mass difference between  $a_2(1730)$  and  $f_2(1560)$  which are interpreted as isospin partners. The mixing angle is however determined from the  $f_2(1560)$  and  $f_2(1750)$  couplings to  $K_S^0 K_S^0$  and not from the GMO formula.

Table 15

Parameters of resonances observed in the reaction  $\gamma\gamma \rightarrow K_S^0 K_S^0$ . The values marked with stars are fixed by using other data.

	First nonet			Second nonet		
	$a_2(1320)$	$f_2(1270)$	$f'_2(1525)$	$a_2(1730)$	$f_2(1560)$	$f_2(1750)$
Mass (MeV)	$1304 \pm 10$	$1277 \pm 6$	$1523 \pm 5$	$1730^*$	$1570^*$	$1755 \pm 10$
Width (MeV)	$120 \pm 15$	$195 \pm 15$	$104 \pm 10$	$340^*$	$160^*$	$67 \pm 12$
$g^L$ (GeV)	$0.8 \pm 0.1$	$0.9 \pm 0.1$	$1.05 \pm 0.1$		$0.38 \pm 0.05$	
$\varphi$ (deg)			$-1 \pm 3$			$-10_{-10}^{+5}$

For the higher-mass region, the authors use the Crystal Barrel data on  $\bar{p}p$  in flight discussed in section 6.1 and data on  $\bar{p}p \rightarrow \pi^+\pi^-$  data obtained with a polarised target [885]. Five tensor states were required to describe the data,  $f_2(1920)$ ,  $f_2(2000)$ ,  $f_2(2020)$ ,  $f_2(2240)$ ,  $f_2(2300)$ :

Resonance	Mass (MeV/c <sup>2</sup> )	Width (MeV/c <sup>2</sup> )
$f_2(1920)$	$1920 \pm 30$	$230 \pm 40$
$f_2(2000)$	$2010 \pm 30$	$495 \pm 35$
$f_2(2020)$	$2020 \pm 30$	$275 \pm 35$
$f_2(2240)$	$2240 \pm 40$	$245 \pm 45$
$f_2(2300)$	$2300 \pm 35$	$290 \pm 50$ .

Antiproton-proton annihilation couples primarily to the  $n\bar{n}$  states. Therefore, the three states observed at BNL in the reaction  $\pi^-p \rightarrow \phi\phi n$  by Etkin *et al.* [83, 886] were included as additional states in their discussion. In a recent reanalysis of the BNL data [887], new mass values were given; due to their decay into  $\phi\phi$ , the three states  $f_0(2120)$ ,  $f_0(2340)$ , and  $f_0(2410)$  should be discussed as  $s\bar{s}$  states or as glueballs. The group advocated since long that a tensor glueball must be present in this mass range since the  $\phi\phi$  final state can be reached only via gluonic intermediate states and the  $\phi\phi$  yield was found to be unexpectedly large, incompatible with the hypothesis that it might be due to  $\omega - \phi$  mixing.

The pair of states  $f_2(1920) + f_2(2140)$  are supposed to be contained in the  $3^3P_2$  nonet,  $f_2(2240) + f_2(2410)$  in the  $3^3P_2$  nonet, and  $f_2(2020) + f_2(2340)$  in the  $1^3F_2$  nonet. The  $f_2(2300)$  resonance is interpreted as  $2^3F_2$  quark-model state. Its  $s\bar{s}$  partner remains to be discovered. Thus all states are mapped onto quark-model expectations, except for one state at  $2\text{ GeV}/c^2$ . It has a much larger width and its couplings to final states are consistent with the assumption that it is flavour blind. Hence the data are compatible with the presence of a tensor glueball at  $2\text{ GeV}/c^2$ . Its mass is unexpectedly low, from lattice calculation  $2.4\text{ GeV}/c^2$  would be expected, or 1.6 times the scalar glueball mass. Certainly, more work is needed to solidify this interesting conjecture.

#### 6.4.4 $J^{PC} = 2^{-+}$

These quantum numbers are probably most convenient ones to search of non- $q\bar{q}$  states. The quark model  $q\bar{q}$  states with  $J^{PC} = 2^{-+}$  are relatively narrow and not distorted by mixing of  $J = L + 1$  and  $J = L - 1$  states. And the flux tube model predicts hybrids with these quantum numbers to be narrow as well [58, 876–878]. The dominant (predicted) decay modes,  $\pi_2(H) \rightarrow \rho\pi$  and  $\pi_2(H) \rightarrow f_2\pi$ , are experimentally well accessible.

There are several experimental indications suggesting the existence of  $\pi_2(1880)$ . A first signal was observed by the ACCMOR collaboration [216] in the reaction  $\pi^-p \rightarrow \pi^+\pi^-\pi^-p$ . A resonance-like signal was reported in the  $2^-D_0^+(f_2\pi)$  wave. The signal itself was confirmed by VES [236]. However, the signal could be described as well by interference of  $\pi_2(1680)$  with a broad state  $\pi_2(2100)$ . Further evidence for the  $\pi_2(1880)$  resonance, in its decay to  $a_2\eta$ , was reported in  $\pi^-N \rightarrow \eta\eta\pi^-N$  [235] and in  $p\bar{p}$  annihilation in flight into  $\eta\eta\pi^0\pi^0$  [376]. The reaction  $\pi^-p \rightarrow \pi^+\pi^-\pi^-\pi^0\pi^0p$  was analysed at BNL [261]. Three isovector  $2^{-+}$  states were seen in the  $\omega\rho^-$  decay channel, the well known  $\pi_2(1670)$  and evidence for two further states,  $\pi_2(1880)$  and  $\pi_2(1970)$ . The two resonances  $\pi_2(1670)$  and  $\pi_2(1970)$  match perfectly to the pattern displayed in Fig. 55, the  $\pi_2(1880)$  does not. In the reaction  $\pi^-p \rightarrow f_1(1285)\pi^-p$ ,  $\pi_2(1670)$  and  $\pi_2(1970)$  were found but not  $\pi_2(1880)$  [260]. Thus evidence for the existence of this state is very suggestive but not forcing. If its existence is assumed, it is a viable hybrid candidate.

Similar observations have been made in the  $\eta_2$  partial wave. Apart from the well established

$\eta_2(1645)$ , a high-mass state is reported at  $M = 2030 \pm 5 \pm 15$  MeV/c<sup>2</sup>,  $\Gamma = 205 \pm 10 \pm 15$  MeV/c<sup>2</sup> [372]. According to the systematic of Fig. 55, these two mesons well suited to represent the  $1^1D_2$  and  $2^1D_2$  quark model states. The third state,  $\eta_2(1870)$ , falls in between the two quark model states and is a natural isoscalar partner of  $\pi_2(1880)$ . In the isoscalar sector, two  $1^1D_2$  states are of course expected but the  $\eta_2(1870)$  production modes, central production and  $p\bar{p}$  annihilation, makes an  $s\bar{s}$  interpretation of  $\eta_2(1870)$  unlikely.

The  $\eta_2(1870)$  in central production is observed in its  $a_2(1320)\pi$ ,  $a_0(980)\pi$  and  $f_2(1270)\eta$  decay mode in the  $\eta\pi\pi$  final state [304], and in central production of four pions in the  $a_2(1320)\pi$  isobar [307]. In  $p\bar{p}$  annihilation it was observed just above threshold in  $f_2(1270)\eta$  with  $L = 0$  [333], and in its  $a_2(1320)\pi$  decay mode [372]. The latter analysis determines the  $a_2(1320)\pi/f_2(1270)\eta$  decay mode ratio to  $1.27 \pm 0.17$ , presumably not incompatible with the ratio 4, predicted by Barnes, Close, Page, and Swanson [58] and by Page, Swanson, and Szczepaniak [878].

These two resonances,  $\pi_2(1880)$  and  $\eta_2(1870)$ , are the best evidence for the existence of hybrids with non-exotic quantum numbers. If confirmed, they change our view of hadron spectroscopy. On the other hand, if hybrids really exist as independent identities, many more of them should be expected and it is a miracle that we have evidence for some 150 mesons, and all but two are  $q\bar{q}$  compatible. For this reason, we still maintain our general suspicion that hybrids, like tetraquark states, do not show up as separate particles but are rather part of the hadronic wave function. Observable resonances may need a  $q\bar{q}$  component which provides additional attractive forces. A way to scrutinise this conjecture is the search for resonances in exotic partial waves where  $q\bar{q}$  components are forbidden by conservation laws.

## 7 Mesons with exotic quantum numbers

### 7.1 Model predictions for exotic mesons

#### 7.1.1 Hybrid mesons

Mesons with exotic quantum numbers are non- $\bar{q}q$  objects. They may be hybrid mesons ( $q\bar{q}g$ ), multiquark states ( $q\bar{q}q\bar{q}\dots$ ) or multimeson states ( $M_1 M_2\dots$ ). Exotic quantum numbers are, e.g.

$$J_{exotics}^{PC} = 0^{--}, \quad 0^{+-}, \quad 1^{-+}, \quad 2^{+-}, \quad 3^{-+} \dots \quad (7.1)$$

The existence of hybrid mesons was suggested in 1976 by Jaffe and Johnson [888] and Vainstein and Okun [889]. Often, the symbolic notation  $q\bar{q}g$  is used which reminds of the excitation of the gluon field between the  $q\bar{q}$  pair. The spectrum of hybrid mesons was calculated in different models. A collection of results is presented in Table 16.

Table 16  
Prediction of various models for the mass of the lightest hybrid meson.

Model	Mass, Gev/c <sup>2</sup>	References
Bag model	1.3 ÷ 1.4	[890]
Flux-tube model	1.8 ÷ 2.0	[870, 876–878]
Sum rules	1.3 ÷ 1.9	[891–893]
Lattice QCD	1.8 ÷ 2.3	[894]
Effective Hamiltonian	2.0 ÷ 2.2	[895]

From the table we may conclude that the lightest  $I^G J^{PC} = 1^- 1^{-+}$  state should have a mass in the  $1.7 - 2.2$  GeV/c<sup>2</sup> region even though smaller values are not ruled out. Early estimates assumed  $\eta(1410)$  to be a pseudoscalar hybrid [890], and suggested low hybrid masses. For exotic states with quantum numbers of  $I^G J^{PC} = 1^- 1^{-+}$ , the conventional name is now  $\pi_1$ . Earlier publications called it  $\hat{\rho}$  or  $M$ . The mass of the lightest hybrids with nonexotic quantum numbers  $J^{PC} = 0^{-+}$  is predicted in the same region [870].

In recent lattice calculations [162], the mass of the  $1^{-+}$  exotic meson – created with hybrid interpolating fields – was explored with light-quark masses approaching  $25$  MeV/c<sup>2</sup> ( $m_\pi/m_\rho \simeq 1/3$ ). The results indicate that the  $1^{-+}$  exotic partial wave exhibits significant curvature close to the chiral limit, suggesting that previous linear extrapolations, far from the chiral regime, may have overestimated the mass of the  $1^{-+}$ . It was found that the  $1^{-+}$  mass can be as low as  $M_{\pi_1} \approx 1600$  MeV/c<sup>2</sup>. In line with this observation, Thomas and Szczepaniak [896] argued that chiral extrapolations may be difficult for exotics and that small quark masses are required to get reliable results.

The  $\pi_1$  partial widths for decays to  $\rho\pi$ ,  $b_1\pi$ ,  $f_1\pi$ ,  $\eta'\pi$  and  $\eta\pi$  were calculated in different models with very different results. In the potential quark model with a constituent gluon [897, 898], as well as in the flux tube model [870, 876, 878], the decays of a hybrid meson into a pair of mesons having identical spatial wave functions are forbidden; hence decays into one S-wave and one P-wave meson are favoured. This selection rule leads to the suppression of the decay  $\pi_1 \rightarrow \rho\pi$  due to the assumed similarity of the wave functions for  $\rho$  and  $\pi$  mesons. The predicted width is in the region of a few MeV/c<sup>2</sup>, even a width of a few tens of MeV/c<sup>2</sup> can be accepted in the flux-tube model [899].

Relativistic calculations [900] confirmed the  $S + P$  rule. On the other hand, calculations within QCD spectral sum rules gave  $10 \div 100$  MeV/c $^2$  [901] or even 0.6 GeV/c $^2$  [892] for the  $\rho\pi$  width. The dominant decays  $\pi_1 \rightarrow b_1\pi$  and  $\pi_1 \rightarrow f_1\pi$  have quite large widths:  $\Gamma_{\pi_1 \rightarrow b_1\pi} = 100 \div 500$  MeV/c $^2$ , and  $\Gamma_{7\pi_1 \rightarrow f_1\pi^0} = 50 \div 150$  MeV/c $^2$  were predicted [163, 878, 898, 902].

Decays of  $J^{PC} = 1^{-+}$  states into two pseudoscalars can be used to shed light onto their flavour structure. In [903] it was pointed out that an isovector  $1^{-+}$  state can belong to either the  $SU(3)$  octet or to the decuplet-antidecuplet. The former can decay only into  $\eta_1\pi$ , while the latter can decay only into  $\eta_8\pi$ , where  $\eta_1$  and  $\eta_8$  are singlet and octet  $\eta/\eta'$  combinations. Hence an octet state will decay into  $\eta\pi$  and  $\eta'\pi$  with a ratio of the squared matrix elements  $|M(\pi_1 \rightarrow \eta\pi)|^2/|M(\pi_1 \rightarrow \eta'\pi)|^2 = \tan^2 \Theta_{PS} \simeq 0.1$ ; a decuplet-antidecuplet state will decay with a ratio  $\tan^{-2} \Theta_{PS} \simeq 10$ . In other words, octet  $1^{-+}$  states decay mainly into  $\eta'\pi$ , and decuplet -antidecuplet states into  $\eta\pi$ . This result is valid for any  $J^{PC} = 1^{-+}$  systems; it does not use arguments related to a gluon-enrichment of the  $\eta'$  or  $\eta'\pi$  state. Hybrids states with  $J^{PC} = 1^{-+}$  being members of an  $SU(3)$  octet have to demonstrate this unusual ratio of  $\eta'\pi/\eta\pi$  branching fractions. As a guide for this ratio we can use the branching ratios of  $J/\psi$  radiative decays to  $\eta'$  and  $\eta$ . If radiative decays couple to the flavour singlet component only, this ratio is given by  $\tan^{-2} \Theta_{PS} \simeq 10$  as well. Experimentally, the ratio is  $R_{\eta'\pi/\eta\pi} \approx 5$ . QCD spectral sum rules expect a width of  $\pi_1 \rightarrow \eta'\pi$  decays which is relatively small,  $\Gamma_{\eta'\pi} \approx 3$  MeV/c $^2$  [893]. However, if the coupling of  $\eta'$  to two gluons through the anomaly is included into the model, the width could be as large as  $\Gamma_{\eta'\pi} \approx 1$  GeV/c $^2$  [904].

### 7.1.2 Multiquark states

In the limit of  $SU(3)$  symmetry two quarks in flavour 3 combine to  $3 \otimes 3 = \bar{3} + 6$  and two antiquarks to  $3 + \bar{6}$ . From these, the irreducible representations of the  $SU(3)$  group can be constructed for the  $qq\bar{q}\bar{q}$  system:

$$(\bar{3} + 6) \otimes (3 + \bar{6}) = \bar{3} \otimes 3 + \bar{3} \otimes \bar{6} + 6 \otimes 3 + 6 \otimes \bar{6} = \\ 1 + 8 + 8 + 10 + 8 + 10 + 1 + 8 + 27 \quad (7.2)$$

A large number of tetraquark states should be expected from the four different octets and the  $10 + \bar{10}$  and  $10 - \bar{10}$  multiplets. The  $10 + \bar{10}$  and  $10 - \bar{10}$  representations as well as the octets include exotic states with  $J^{PC} = 1^{-+}$ . The 27-plet has even spin only and does not contribute to  $J^P = 1^-$ . The  $10 + \bar{10}$ ,  $10 - \bar{10}$  and 27-plet representations include flavour exotic states.

As a rule, the decays of these states to mesons are superallowed and therefore these bag-model objects do not exist as  $T$ -matrix poles [905]. On the other hand, quarks in multiquark states can cluster to  $(qq)(\bar{q}\bar{q})$  systems. Contrary to naive expectation based on our experience with QED, the forces between two quarks can be attractive. The strongest attraction is expected in the system of two different quarks  $q$  and  $q'$  in a colour-SU(3)-antitriplet spin-singlet state. The lowest scalar nonet ( $a_0(980)$ ,  $f_0(980)$ ,  $\sigma$ ,  $\kappa$ ) is the favorite candidate for  $(qq)(\bar{q}\bar{q})$  exotics [906]. Within the bag model, the mass of the lightest  $J^{PC} = 1^{-+}$  tetraquark state is about  $M \approx 1.7$  GeV/c $^2$ . As this state has a number of superallowed decay channels it is likely too broad to be identified unambiguously. In section 11.6.2 we will argue that  $(qq)(\bar{q}\bar{q})$  systems do not bind without additional  $q\bar{q}$  forces. This is good news for hybrids with exotic quantum numbers: If a resonance with exotic quantum numbers is found, it is unlikely to be a tetraquark state. Hence it must be a hybrid.

### 7.1.3 Molecular states

A large number of states with different quantum numbers including exotic ones can be generated dynamically from a meson pair  $M_1 M_2$ . The forces between the mesons could be sufficiently attractive to form bound systems, in particular close to their thresholds. Barnes, Black and Swanson [907] have calculated two meson states with exotic quantum numbers with a quark-interchange model. In exotic waves, the annihilation process  $q \ q \bar{q} \bar{q} \rightarrow q \bar{q}$  is forbidden and therefore the interaction of the two mesons  $M_1$  and  $M_2$  is driven mainly by the exchange of quarks (antiquarks) from different mesons. The model describes rather well the low-energy scattering amplitudes in annihilation-free channels like  $I = 2 \ \pi\pi$  and  $I = 3/2 \ K\pi$  or low-energy nucleon-nucleon scattering. In particular, the model gives small negative phase shifts for  $K^+\pi^+$   $P$ -wave scattering, in agreement with experiment [908]. Low-energy  $\rho\pi \rightarrow \rho\pi$  scattering in the exotic  $J^{PC} = 1^{-+}$  wave and  $P$ -wave  $\eta\pi \rightarrow \eta\pi$  scattering were studied as well. In both processes, the phase motion was found to be small; binding of the  $\rho\pi$  or  $\eta\pi$  system in the exotic  $1^{-+}$  partial wave does not occur.

The exotic wave  $J^{PC} = 1^{-+}$  was studied with an effective Lagrangian approach. Chan and Haymaker [909] calculated the scattering amplitudes for scattering of two pseudoscalar mesons in the framework of a  $SU(3) \times SU(3)$   $\sigma$  model involving only scalar and pseudoscalar mesons. Low energy scattering of two pseudoscalars were reasonably well described; repulsive forces were predicted for the  $J^{PC} = 1^{-+}$  wave. Bass and Marco [910] included a gluonic potential to generate contributions to the  $\eta$  and  $\eta'$  masses. The model does not exclude exotic resonances in the  $\eta'\pi$   $P$ -wave. Achasov and Shestakov [911] suggested a model for scattering if a vector and a pseudoscalar meson into two pseudoscalar mesons, constructed tree-amplitudes from an ‘anomalous’ effective interaction of vector and pseudoscalar mesons with subsequent unitarisation, and calculated exotic-wave amplitudes with  $J^{PC} = 1^{-+}$  for the reactions  $\rho\pi \rightarrow \rho\pi$ ,  $\rho\pi \rightarrow \eta'\pi$ ,  $\eta\pi \rightarrow \eta\pi$ ,  $\eta\pi \rightarrow (K^*\bar{K} + \bar{K}^*)$ , and others. Depending on the choice of free parameters of the model, various resonant-like amplitudes could be generated in different channels. General, Wang, Cotanch and Llanes-Estrada [912] use an Hamiltonian approach to arrive at the conclusion that molecular-like configurations involving two color singlets are clearly favoured compared to hybrid (tetraquark) configurations in which a  $\bar{q}q$  pair (or two pairs) carry colour.

## 7.2 Experimental results for $J^{PC} = 1^{-+}$

The lightest isovector state with these quantum numbers could decay to  $\pi\eta$ ,  $\pi\eta'$ ,  $\pi\rho$ ,  $\pi b_1$ ,  $\pi f_1$ ,  $a_0\rho$ ,  $a_1\eta$ ,  $\pi\rho'$ . Most of these channels were studied at various places using GAMS/NA12 at IHEP-CERN, E179 at KEK, Crystal Barrel at CERN, E852 at BNL, Obelix at CERN and VES at IHEP (see Table 17).

### 7.2.1 The wave $J^{PC} = 1^{-+}$ in the $\eta\pi$ channel.

Diffractive reactions could be especially effective to produce hybrid mesons, as these mesons have some additional gluon-like component in their wave function and could have a strong coupling to the Pomeron. After a very early first observation of an  $J^{PC} = 1^{-+}$  exotic wave in 1981 [913], high statistics data became available from VES and KEK in 1993 [231, 914]<sup>5</sup>. In the VES experiment, events due to the exclusive reactions  $\pi^- Be \rightarrow XBe$  (where  $X$  means the aforementioned decay channels) at  $p_\pi = 37$  GeV/c were selected and subjected to a partial wave analysis (PWA). Waves

---

<sup>5</sup> An observation of  $J^{PC} = 1^{-+}$  in  $\eta\pi$ -channel by GAMS [87] was revised in [915].

Table 17  
Experimental studies of  $1^{-+}$  states.

Experiment	Reaction	final state	Reference
VES	Diffraction; charge exchange;	$\eta\pi^-$ , $\eta'\pi^-$ , $\rho\pi^-$	[231, 236, 238]
	28-,37-GeV/c $\pi^-$ beam	$f_1\pi^-$ , $b_1\pi^-$ , $\eta'\pi^0$	[240, 243, 245]
E179	Diffraction, 6.3-GeV/c $\pi^-$ beam	$\eta\pi^-$	[245, 914]
Crystal Barrel	$p\bar{p}$ annihilation	$\eta\pi^\pm$ , $\eta\pi^0$	[341, 345]
	to $\eta\pi^+\pi^-$ , $\eta\pi^-\pi^0$ , $\pi^-3\pi^0$ , $\pi^+\pi^-\pi^0\omega$	$\rho\pi$ , $b_1\pi$	[354, 357]
Obelix	$p\bar{p}$ annihilation to $\pi^+\pi^-\pi^+\pi^-$	$\rho\pi$	[395]
GAMS/NA12	Charge exchange; $\pi^-$ 32, 38, 100 GeV/c	$\eta\pi^0$	[290]
E852	Diffraction; charge exchange; 18 GeV/c	$\eta\pi^-$ , $\eta'\pi^-$ , $\rho\pi^-$	[248–250, 257]
	$\pi^-$ beam	$f_1\pi^-$ , $b_1\pi^-$	[255, 259–261]

with orbital angular momenta of  $L=0$ , 1, and 2 ( $L = S, P, D$ ) and orbital angular momentum projection of  $M = 0$  and 1 onto the Gottfried-Jackson axis with both natural and unnatural parity exchange were included in the analysis, i.e. the waves  $S, P_0, P_+, P_-, D_0, D_+, D_-$  were tested. It turned out that waves with unnatural parity exchange are not significant. The results of the VES collaboration on this channel were published in [231, 241]. The dominant wave  $J^{PC} = 2^{++}$  is peaking at the mass of the  $a_2(1320)$  meson. There is a clear signal in the exotic wave  $J^{PC} = 1^{-+}$  centered at  $M \approx 1.4$  GeV/c $^2$  (Fig. 58). The mass-dependent fits to the PWA results were reported in [241].

These results were beautifully confirmed by the E-852 collaboration [248]. When overlayed, both data sets are indistinguishable in their distributions demonstrating the reliability of both experiments with respect to detector performance, data reconstruction and partial wave analysis. Differences which turn up in the publications are due to the mass-dependent fits to the results of the mass-independent partial-wave analyses, and due to different underlying assumptions in these fits. Are meson-meson interactions dominated by resonances or do background amplitudes play an important rôle? For  $P$ -wave meson-meson scattering, this question is unsolved but it may serve as an indication that  $\pi N$  scattering even in the  $\Delta(1232)$  region proceeds not only via  $\Delta(1232)$  formation but also via a background  $P$ -wave  $\pi N$  scattering amplitude.

In the KEK experiment [914] at  $p_\pi = 6.3$  GeV/c, a very different shape of the  $P_+(\eta\pi^-)$  wave was

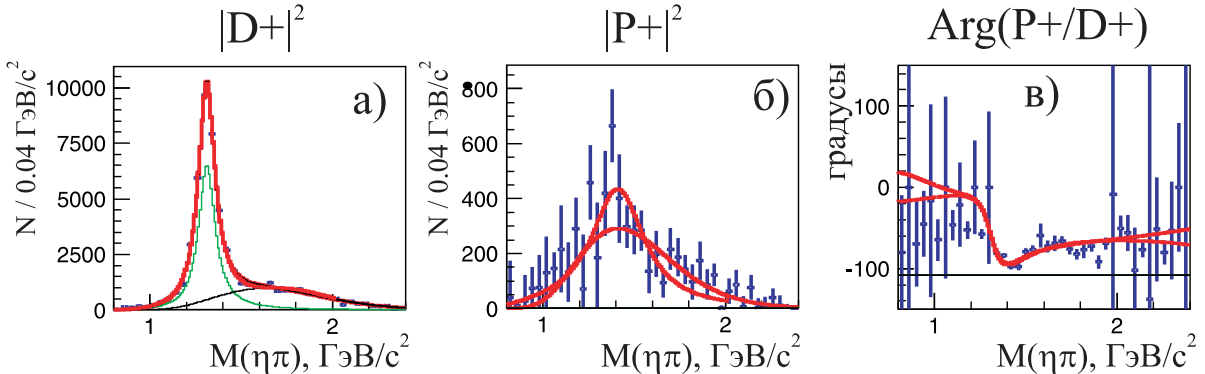


Fig. 58. Results of partial-wave analysis of the  $\eta\pi^-$  system: a) intensity of  $D_+$  wave, b) intensity of  $P_+$  wave, c) phase difference  $P_+/D_+$  [241].

found. The dominant  $D_+$  wave exhibited a clear  $a_2(1320)$ ; in the exotic  $P_+$  wave, amplitude and phase followed exactly the  $D_+$  wave. In a mass-dependent fit, an exotic resonance with parameters of the  $a_2(1320)$  shows up. This coincidence may suggest that the  $P_+$  wave signal could be driven by leakage from the dominant  $a_2(1320)$  resonance, either due to imperfections of the PWA model or due to experimental effects like acceptance, resolution or background. Possibly, the PWA model with seven waves ( $S, P_0, P_+, P_-, D_0, D_+, D_-$ ) in the  $\eta\pi$  system could be oversimplified: At  $p_{\pi^-}=6.3 \text{ GeV}/c$  contributions from baryon resonances could be important and lead to distortions in the  $\eta\pi$  system. The compatibility of the E-852 and VES results (taken at  $18 \text{ GeV}/c$  and at  $28$  and  $37 \text{ GeV}/c$ , respectively) suggests that at these momenta, baryon resonances are well enough separated and have no impact on the mesonic system.

The data in Fig. 58 exhibit a dominant  $a_2(1320)$  in the  $D_+$  and a clear bump at  $M \approx 1.4 \text{ GeV}/c^2$  in the (exotic)  $P_+$  partial wave. The E-852 collaboration [248, 250] finds that the data are consistent with a simple ansatz, assuming contributions from two resonances, one in each partial waves. The  $D_+$  wave returns the parameters of  $a_2(1320)$ , for the  $P_+$  partial wave, mass and width are determined to  $M = 1370 \pm 16^{+50}_{-30}$ ;  $\Gamma = 385 \pm 40^{+65}_{-105}$ . This observation is referred to as  $\pi_1(1400)$  by the Particle Data Group [1].

A systematic study was carried out in [241] to investigate if the observations can be explained without introducing an exotic resonance. The data were fitted with  $a_2(1320)$  and  $P_+$  and  $D_+$  backgrounds in the form

$$A_B = LIPS_l \times (m - m_t)^\alpha \exp(-\beta(m - m_t)), \quad (7.3)$$

where  $LIPS_l(m)$  is the phase space volume,  $m_t$  the threshold mass, and  $\alpha, \beta$  shape parameters. An arbitrary (constant) phase is allowed for both background amplitudes. The background amplitudes are interpreted as meson-meson interaction dynamics originating from  $t$ -channel exchange currents. The fit without  $\pi_1(1400)$  gives a perhaps acceptable  $\chi^2$  of 244 for 149 degrees of freedom. If  $\pi_1(1400)$  with E-852 parameters is added,  $\chi^2$  improves significantly by 57 units for 2 additional parameters (amplitude and phase). The two fits are presented and compared to the data in Fig. 58.

A judgement if the  $P_+$  wave carries a resonance is not only a statistical question. Obviously, there are spin-flip and spin-nonflip contributions at the baryon vertex leading to a production density matrix of rank two. For a system of two pseudoscalars, a rank-2 density matrix can not be reconstructed in a model-independent way due to a continuous ambiguity. Hence some doubts remain as to the existence of a resonant  $P_+$  wave in the  $\pi\eta$  channel.

The Indiana group [916] tested the idea that  $t$  channel exchange forces might give rise to a background amplitude which could mimic  $\pi_1(1400)$ . A model respecting chiral symmetry for meson-meson interactions was constructed in which these interactions were expanded in terms of the relative momenta<sup>6</sup>. The production amplitudes were supposed to follow the momentum dependence of the interactions. In this way,  $\pi\eta$   $P_+$ -wave interactions were constructed which are very similar to  $\pi\pi$   $S$ -wave interactions. The latter were characterised by the  $\sigma$  pole; as a consequence,  $\pi_1(1400)$  is considered as  $\sigma$ -type phenomenon in  $\pi\eta$   $P_+$ -wave interactions. In the words of the authors of [916],  $\pi_1(1400)$  is ‘not a QCD bound state’ but rather generated dynamically by meson exchange forces. This difference is subtle; the reader may like to have a look at the discussion in section 11.6.2.

---

<sup>6</sup> Even though related, the analysis is not using an effective field theory approach based on a chiral Lagrangian with low-energy constants fixed from other processes.

The  $\eta\pi$   $P_+$ -wave was also studied in the charge exchange reaction  $\pi^- p \rightarrow \eta\pi^0 n$  [259, 290]. The  $P_+$  wave is clearly seen in both experiments. Mass-dependent fits of the amplitudes required the introduction of a resonance but yielded resonance parameters which were different in the three ranges of  $t$  studied in [259]. The authors concluded that there is no evidence for a resonant signal at  $M \approx 1.4 \text{ GeV}/c^2$ . Of course, this does not rule out the existence of  $\pi_1(1400)$ . The exotic  $\eta\pi^0$   $P_+$ -wave is produced by  $t$ -channel exchange of isospin-1 natural-parity objects like  $\rho$ . From the absence of  $\pi_1(1400)$  in  $\pi^- p \rightarrow \eta\pi^0 n$  it can only be inferred that the  $\pi_1(1400) \rightarrow \rho\pi$  coupling is small in comparison to its coupling to  $\pi$ -Pomeron or  $\pi-f_1(1285)$ . On the other hand, these results point to a significant nonresonant background in the exotic  $\pi\eta$   $P_+$ -wave channel.

The Crystal Barrel Collaboration confirmed the existence of the exotic  $\pi\eta$   $P_+$ -wave in an entirely different reaction: in  $\bar{p}n \rightarrow \pi^-\pi^0\eta$  and  $\bar{p}p \rightarrow 2\pi^0\eta$  [341, 345]. The evidence for  $\pi_1(1400)$  comes from the first reaction; in the reaction  $\bar{p}p \rightarrow 2\pi^0\eta$ , a small signal was unraveled by comparison of this reaction in liquid and gaseous hydrogen where the fraction of annihilation contributions from atomic  $S$  and  $P$  states is different. Only the combined fit of these two data sets gave positive evidence for a small contribution from an exotic wave. A reanalysis [917] fitted the  $\bar{p}p \rightarrow 2\pi^0\eta$  data without the need for a narrow exotic resonance. In the annihilation reaction  $\bar{p}n \rightarrow \pi^-\pi^0\eta$ , the exotic wave is rather strong, however, and provided a contribution to the final states which is about 1/3 of the  $a_2(1320)$  contribution. The Dalitz plot is shown in Fig. 59. If fitted with only conventional mesons, a poor description of the data is achieved; the addition of the exotic  $\pi_1(1400)$  gave an excellent fit. The fit and the data are compared in Fig. 59. In the lower part the amplitudes of the resonances allowed by conservation laws were optimised but the exotic meson was omitted.

The exotic partial wave was described by a Breit-Wigner resonance. The best fit was obtained for  $M = 1400 \pm 20 \pm 20 \text{ MeV}/c^2$  and  $\Gamma = 310 \pm 50^{+50}_{-30} \text{ MeV}/c^2$  where the first error is a statistical and the second a systematic error estimated from a variety of different fits.

The Crystal Barrel and Obelix collaborations found a  $J^{PC} = 1^{-+}$  wave in  $(\rho\pi)$  in  $p\bar{p}$  annihilation

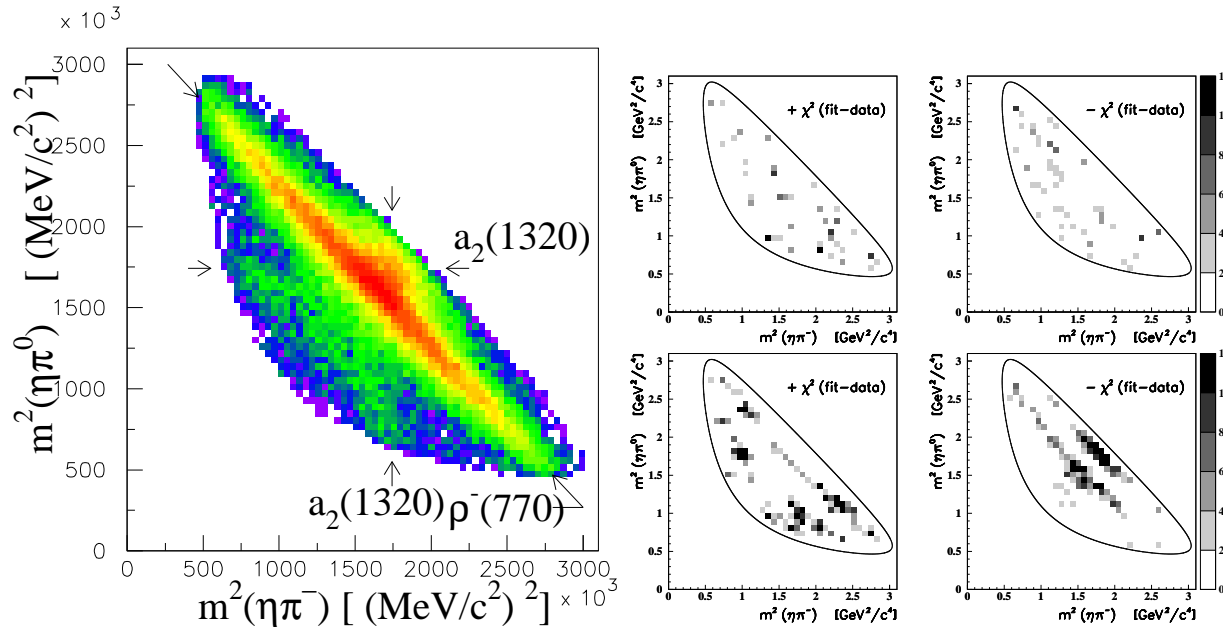


Fig. 59. Left: Dalitz plot for  $\bar{p}n \rightarrow \pi^-\pi^0\eta$ , right: Differences between data and fit (in  $\chi^2$ ) over the Dalitz plot. The  $\pi\eta$   $P$ -wave is included in (a,b) but not in (c,d). The + sign indicates that the fit exceeds the data, the - sign that data exceed the fit. All fits include the  $\rho(770)$ ,  $a_2(1320)$ ,  $a_0(980)$  and  $a_0(1450)$  [341].

to four pions. Crystal Barrel reported this observation only in a conference contribution [357] and reported  $M, \Gamma \sim 1400, \sim 400 \text{ MeV}/c^2$ . The Obelix parameters for this wave are  $M, \Gamma = (1384 \pm 28), (378 \pm 58) \text{ MeV}/c^2$  [395]. The results are not incompatible with the findings reported for the  $\pi\eta$   $P$ -wave. A major point of concern is the production mechanism. The  $\pi\eta$   $P$ -wave is seen to be produced from spin triplet states of the  $N\bar{N}$  system, in particular from the  ${}^3S_1$  state. In contrast, the exotic  $\rho\pi$  wave comes from spin singlet states, dominantly from the  ${}^1S_0$  state. Hence these must be different objects. It was pointed out by Sarantsev (A. Sarantsev, private communication, 2005) that in  $p\bar{p}$  annihilation to  $\rho\pi\pi$ , rescattering processes in the final state could lead to logarithmic singularities which could mimic a pole singularity. This argument holds true for  $\eta\pi\pi$  as well but no calculation has ever been reported.

From a wider view, the claim for an exotic  $\pi_1(1400)$  resonance in  $\pi\eta$  interactions is rather problematic.  $P$ -wave states in the  $\eta_8\pi$  channel belong to a  $SU(3)$  decuplet [903], the suggested resonance cannot be a hybrid. One can assume that  $\pi_1(1400)$  belongs to a decuplet-antidecuplet family of multiquark or mesomolecular states. The decuplet-antidecuplet includes also  $K^+\pi^+$   $P$ -wave states. The amplitude of  $K^+\pi^+ \rightarrow K^+\pi^+$  scattering was studied in [908]. It was found that the scattering amplitude is dominated by  $S$ -wave while the  $P$ -wave is strongly suppressed. The  $P$ -wave phase shift is less than a few degrees from threshold to  $M \approx 1.8 \text{ GeV}/c^2$  and does not leave room for a resonance in this mass region<sup>7</sup>. Based on  $SU(3)$  symmetry, very little phase motion should be expected for the  $\pi\eta$   $P_+$ -wave. Donnachie and Page [918] suggest that the 1.4 GeV enhancement in the VES and E852  $\eta\pi$  data can be understood as interference between a non-resonant Deck-type background and a hybrid resonance at 1.6 GeV. A hybrid should not decay into  $\pi\eta_8$  due to  $SU(3)$  arguments [903]. In [918], the suppression of hybrid  $\eta\pi$  decays is circumvented by rescattering of intermediate  $b_1(1235) - \pi$  into  $\eta\pi$ . Of course, this is difficult to accept when the suppression is due to  $SU(3)$ . The mass of  $\pi_1(1400)$  is very close to the  $f_1(1285)\pi$  threshold. A  $f_1(1285)\pi$  virtual bound state or a cusp may contribute to the scattering amplitude as well.

In summary, all experiments agree that there is a substantial contribution of the exotic  $P_+$ -wave to  $\pi\eta$  interactions. The data are well described once a resonant  $\pi_1(1400)$  is introduced. Due to  $SU(3)$  symmetry arguments, the observation cannot be due to a hybrid, the roots have to be in tetraquark dynamics. However, in tetraquark systems in decuplet-antidecuplet, no substantial phase motion is expected. Fits to the diffractively produced data without  $\pi_1(1400)$  but including  $t$ -channel exchange dynamics were successfully performed, too; the dynamical origin of the non-resonant background amplitudes was however not yet traced back to meson-meson interactions in a convincing way.

### 7.2.2 The wave $J^{PC} = 1^{-+}$ in the $\eta'\pi$ channel.

Even if interpreted as resonance, the  $\pi_1(1400)$  cannot belong to the family of hybrid mesons due to  $SU(3)$  arguments. The  $P_+$ -wave in  $\eta'\pi$  is a much better place where a true hybrid might be found. Fig. 60 shows the  $\eta'\pi^-$  system produced in a diffractive-like reaction at  $p_{\pi^-} = 18 \text{ GeV}/c$ . The data are from the E-852 collaboration [248, 250]; VES using a beam at  $p_{\pi^-} = 37 \text{ GeV}/c$  showed similar distributions [231]. The main results of the partial wave analysis of both experiments can be summarised as follows:

- waves with unnatural parity exchange are strongly suppressed;

---

<sup>7</sup> The  $K^+\pi^+ \rightarrow K^+\pi^+$  data are also at variance with the interpretation of [916] which requires a sizable phase motion in  $\pi\eta$   $P_+$ -wave

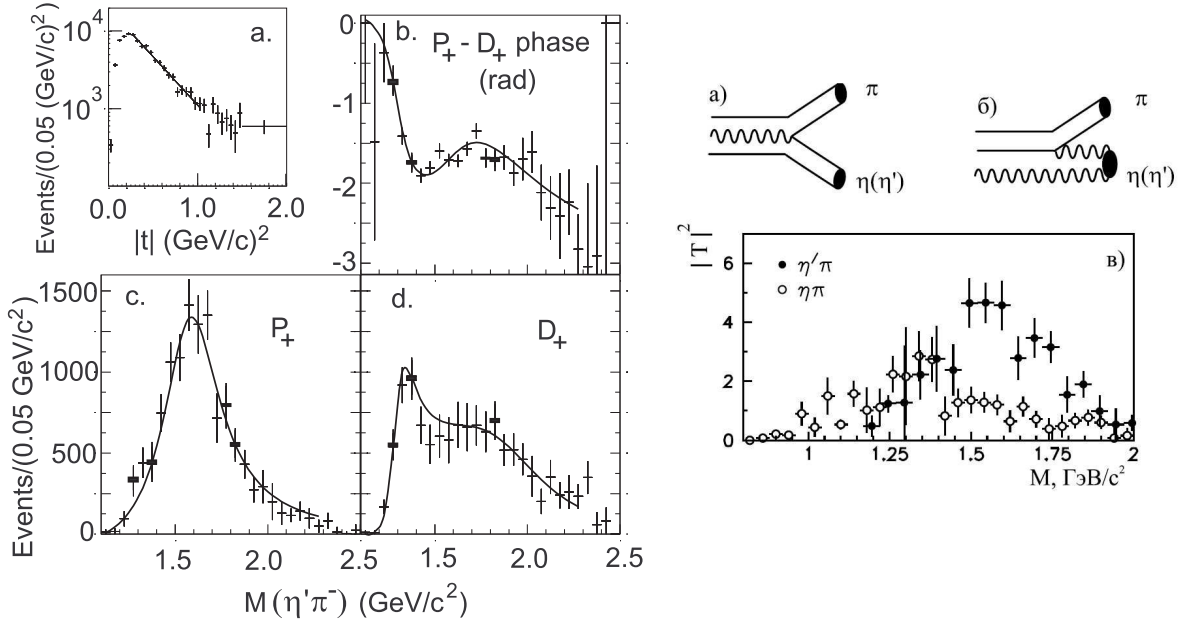


Fig. 60. Left panel, BNL data [250]: (a) The acceptance-corrected  $|t|$  distribution fitted with the function  $f(t) = ae^{bt|t|}$  (solid line). (b), (c), (d) results of a mass-independent PWA and a mass-dependent fit (solid curve) for the  $P_+$  and  $D_+$  partial waves and their phase difference. (b) The  $(P_+ - D_+)$  phase difference. (c) Intensity of the  $P_+$  and (d) of the  $D_+$  partial wave. Right panel: (a) OZI-allowed and (b) OZI-forbidden diagrams for the decay of a hybrid meson and (c) squares of matrix elements for the  $1^{-+}$  wave in the  $\eta\pi^-$  and  $\eta'\pi^-$  systems.

- the wave  $1^{-+}$  is the dominant one, it has a maximum at  $M \approx 1.6$  GeV/c<sup>2</sup>;
- in the wave  $J^{PC} = 2^{++}$  there is a  $a_2(1320)$  signal and a broad bump at  $M = 1.6 \div 2.0$  GeV/c<sup>2</sup>.
- a  $4^{++}$  wave is also clearly observed (but documented only for BNL).

The intensity of the  $1^{-+}$  wave at  $M \approx 1.6$  GeV/c<sup>2</sup> is much higher than that in the  $\eta\pi$  channel (Fig. 60); therefore this  $1^{-+}$  state belongs to  $SU(3)$  octet. This octet dominance looks very natural for diffractive-like reactions which are mediated by Pomeron exchange at sufficiently high energy. In the collision of octet pions with ( $SU(3)$  singlet) Pomerons<sup>8</sup>, only octets can be produced.

The E-852 collaboration performed a fit to these partial waves with the following ingredients: the  $2^{++}$  wave was described by  $a_2(1320)$  and either one broad (550 to 750 MeV/c<sup>2</sup>) or two narrower Breit-Wigner tensor resonances, the  $4^{++}$  wave by the  $a_4(2040)$  meson in its  $\eta'\pi^-$  decay mode. The dominant, exotic (non- $q\bar{q}$ )  $1^{-+}$  partial wave was described as a resonance with a mass of  $1.597 \pm 0.010^{+0.045}_{-0.010}$  GeV/c<sup>2</sup> and a width of  $0.340 \pm 0.040 \pm 0.050$  GeV/c<sup>2</sup>. The exotic partial wave is produced with a  $t$  dependence which is different from that of the  $a_2(1320)$  meson, indicating different production mechanisms for the two states.

The VES collaboration performed tests on the stringency with which these claims can be made. They fit the data with  $a_2(1320)$  and a phenomenological background amplitude for the  $2^{++}$  and  $1^{-+}$  with the shape given in eq. (7.3). These assumptions yield also a perfect fit. Hence the decisive question (for both reactions,  $\pi^-p \rightarrow n\pi^-\eta$  and  $\pi^-p \rightarrow n\pi^-\eta'$ ) is if  $t$  channel exchange

<sup>8</sup> The  $\bar{s}s$  suppression in the soft Pomeron induces however an octet component.

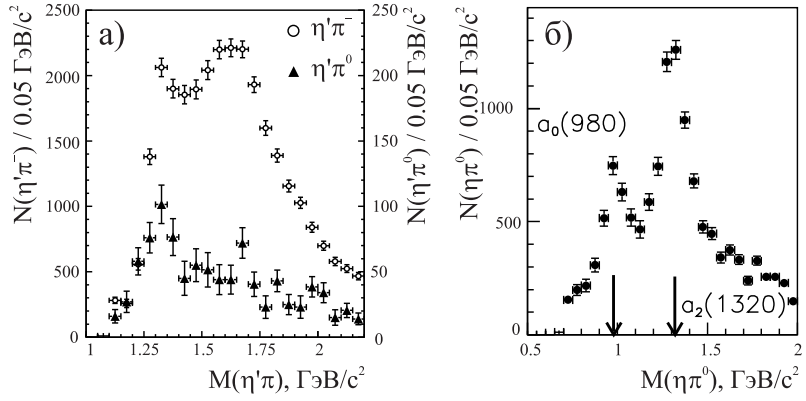


Fig. 61. The mass spectra of (a)  $\eta'\pi^-$ ,  $\eta'\pi^0$ , and (b)  $\eta\pi^0$ .

forces between  $\pi$  and  $\eta$  ( $\eta'$ ) can lead to significant background amplitudes. It is well known that a large fraction of the  $\pi\pi$   $S$ -wave phase shift and the magnitude of the scattering amplitude can be understood in terms of  $t$ -channel  $\rho$  exchange. An additional phase amplitude and phase shift is provided by  $f_2(1270)$  exchange (see e.g. [919]). Since the  $\rho$  and  $f_2(1270)$  couplings are known, absolute predictions can be made. Likewise, after projection onto the  $P$ -wave, absolute predictions of the background amplitude due to  $a_2(1320)$  exchange are possible and should be made.

The Indiana group [916] tried to expand their model on  $\pi\eta$  interactions to  $\pi\eta'$  but did not succeed to describe the data without a resonance at 1600 MeV/c<sup>2</sup> and with 300 MeV/c<sup>2</sup> width.

The  $\eta'\pi^0$  system was studied GAMS, E-852 and VES by charge exchange [243, 259, 290]. The results are again compatible; Fig. 61 shows  $\eta\pi^0$  and  $\eta'\pi^0$  mass spectra from VES. The  $\eta\pi^0$  spectrum is dominated by the  $a_2^0(1320)$  meson. The  $\eta'\pi^0$  spectrum is also dominated by  $a_2^0(1320)$  production, in spite of a strong threshold suppression ( $\sim p^5$ ). The signal at  $M \approx 1.6$  GeV/c<sup>2</sup> which dominates the  $\eta'\pi^-$  spectrum has disappeared in  $\eta'\pi^0$ . The ratio of  $P$ -wave intensities in the  $\eta'\pi^0$  and  $\eta\pi^0$  channels is

$$R = |T_{P+}^{\eta'\pi^0}|^2 / |T_{P+}^{\eta\pi^0}|^2 \approx 0.1 \pm 0.1.$$

The suppression of the  $\eta'\pi^0$  signal in charge exchange can be used to derive an upper limit on the  $\pi_1(1600)$  branching ratios.

$$Br(\pi_1(1600) \rightarrow \rho\pi) \times Br(\pi_1(1600) \rightarrow \eta'\pi) \leq 3 \times 10^{-3} \quad (7.4)$$

Obviously, the  $\rho\pi$  coupling is small. The contribution from  $\rho\pi \rightarrow \eta'\pi$   $P$ -wave scattering is of the order of the contribution expected from  $\rho\pi \rightarrow \eta_8\pi$   $P$ -wave scattering via SU(3)<sub>(10,̄10)</sub> amplitudes and standard  $\eta_1$ - $\eta_8$  mixing. Hence the octet  $\rho\pi \rightarrow \eta'\pi$   $P$ -wave scattering amplitude must be very small and is compatible with zero.

### 7.2.3 Partial wave analyses of the diffractively produced $\pi^+\pi^-\pi^-$ system

The wave  $J^{PC} = 1^{-+}$  in the  $\pi^+\pi^-\pi^-$  system is highly controversial. It was studied by two experiments in diffractive-like reactions: by the VES collaboration [236, 245] at  $p_\pi = 37$  GeV/c and by the E-852 collaboration at  $p_\pi = 18$  GeV/c [249, 257]. A new BNL data sample with 10-fold increased statistics was reported in [262].

Most of the basic parameters of the PWA models are similar in all three analyses. Up to 45 waves with total angular momenta ranging from  $J = 0$  to  $J = 4$  were used in [236, 242, 245], 21 to 27 waves in [249, 257] and 36 waves in [262]. The  $J^{PC} = 1^{-+}\rho^0\pi^-$  wave was included in PWA with three different states:  $M^\eta = 0^-$ ,  $1^-$  and  $1^+$ . In the first BNL analysis and in [262], a spin-density matrix of rank 1 or 2 was used to account for the possibility of two incoherent contributions to the reaction. In the analysis of the Protvino data, the spin-density matrix was taken in a general form without any restrictions of its rank. The reason for this approach is that any PWA model is based on some assumptions and approximations. These model imperfections could lead to a leakage from the most intensive to less intensive waves and generate spurious artificial signals. This effect seems unavoidable in a PWA model with density matrix of rank 1. PWA models based on density matrices of arbitrary rank give more freedom to waves how to interfere and leakage from intensive waves is not so dangerous. Hence it is less likely to produce spurious results; the risk is that small signals could be washed out.

The results of BNL experiment on  $J^{PC} = 1^{-+}$  waves are presented in Fig. 62. Clear peaks of compa-

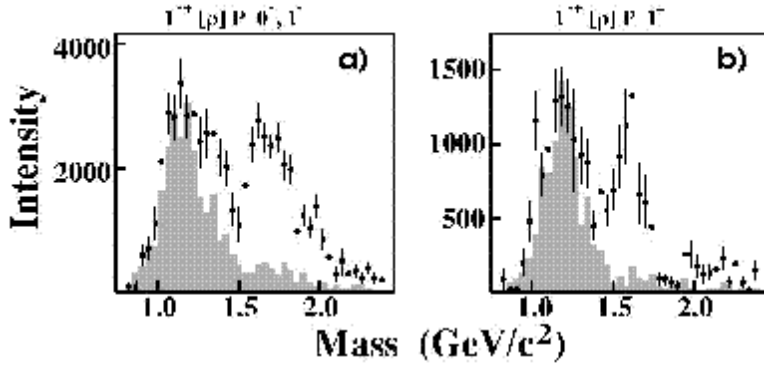


Fig. 62. Wave intensities of the  $1^{-+}(\rho\pi)P$  exotic waves: (a) the  $M^\eta = 0^-$  and  $1^-$  waves combined; (b) the  $M^\eta = 1^+$  wave. The 21-wave rank-1 PWA fit to the data is shown as points with error bars; the shaded histograms show estimated contributions from all non-exotic waves due to leakage.

rable intensities are seen at  $M \approx 1.6$  GeV/c $^2$ , both in natural parity exchange ( $J^{PC}M^\eta = 1^{-+}1^+$ ) and in unnatural parity exchange ( $J^{PC}M^\eta = 1^{-+}0^-$  and  $J^{PC}M^\eta = 1^{-+}1^-$ ). The distributions were fitted with a Breit-Wigner amplitude, the fit gave mass and width

$$M = 1593 \pm 8^{+29}_{-47} \text{ MeV}/c^2, \quad \Gamma = 168 \pm 20^{+150}_{-12} \text{ MeV}/c^2. \quad (7.5)$$

The flatness of phase difference  $\phi(1^{-+}1^+(\rho\pi)) - \phi(2^{-+}0^+(f_2\pi))$  in presence of the well established resonance  $\pi_2(1670)$  in the wave  $J^{PC}M^\eta = 2^{-+}0^+(f_2\pi)$  supports the resonance interpretation of the signal. The total intensity of the exotic wave  $J^{PC} = 1^{-+}$  at  $M \approx 1.6$  GeV/c $^2$  is about 20% of the  $a_2(1320)$  signal at its maximum.

In the second analysis of BNL data (with increased statistics), 20 partial waves were used (called low-wave set) and, alternatively, 35 partial waves (called high-wave set). Fig. 63 shows the results for the exotic  $\rho\pi$   $P$ -wave. While the peak is clearly visible in the low-wave set, it has disappeared in the high-wave set.

A similar observation was made by the VES collaboration analysing an even higher-statistics data set [236, 242, 245]. The  $3\pi$  mass distribution (a) shows a large enhancement due to  $a_1(1260)/a_2(1320)$  production, followed by a peak which is dominantly due to  $\pi_2(1670)$ . This wave is rather strong

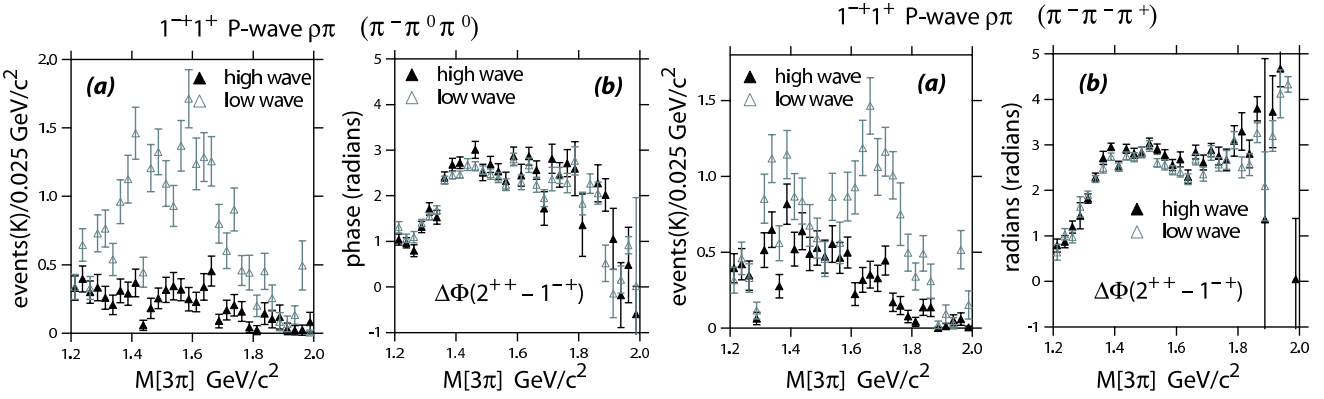


Fig. 63. Left panel: (a) The  $1^{-+}1^+$   $P$ -wave  $\rho\pi$  partial wave in the neutral mode  $(\pi^- \pi^0 \pi^0)$  for the high-wave set PWA and the low-wave set PWA and (b) the phase difference  $\Delta\Phi$  between the  $2^{++}$  and  $1^{-+}$  for the two wave sets. Right panel: (a) The  $1^{-+}1^+$   $P$ -wave  $\rho\pi$  partial wave in the charged mode  $(\pi^- \pi^- \pi^+)$  for the high-wave set PWA and the low-wave set PWA and (b) the phase difference  $\Delta\Phi$  between the  $2^{++}$  and  $1^{-+}$  for the two wave sets [262].

in the data; when full coherence is required in the PWA mode, a signal in  $J^{PC} = 1^{-+}$  waves of both parity-exchange naturalities is observed, likely due to leakage from the much stronger  $2^{-+}$  wave [245]. The  $1600 \text{ MeV}/c^2$  bump in Fig. 64(b) disappears in the full model allowing for an arbitrary incoherence in the  $2^{-+}$  wave, see Fig. 64(c). In the unnatural parity exchange sector ( $M^\eta = 0^-, 1^-$ ), the intensity of the exotic signal at  $M \approx 1.6 \text{ GeV}/c^2$  is compatible with zero.

A broad signal is seen in natural parity exchange ( $M^\eta = 1^+$ ) with maximum at  $M \approx 1.2 \text{ GeV}/c^2$ . This low mass peak can be assigned to leakage from the very intensive wave to  $J^{PC} = 1^{-+}$ . The intensity is about 2% of the  $a_2(1320)$  signal. Because of its smallness and broadness, the signal is not believed to represent a true exotic signal.

The three analyses of VES and E-852 data arrive at very different results and it is hard to decide objectively, which analysis is right. The approach in [245] and [262] allowing for more flexibility in the fit is certainly more conservative. However fitting is an art, and it is not inconceivable that too many fit parameters lead to an overparametrisation which washes out a signal which is observed only when just the right waves are introduced and no additional spurious waves. At Hadron05, Adams showed results of the partial wave analysis of Dzierba et al. (claiming absence of  $\pi_1(1600) \rightarrow \rho\pi$ ) on the  $2^{-+}$  and  $1^{-+}$  waves. Adams fitted the data of Dzierba et al. in a new mass-dependent fit which returned – within errors – the  $\pi_1(1600)$  Breit-Wigner parameters.

The BNL-E852 collaboration studied the stability of the  $1^{-+}$  signal and its phase motion with

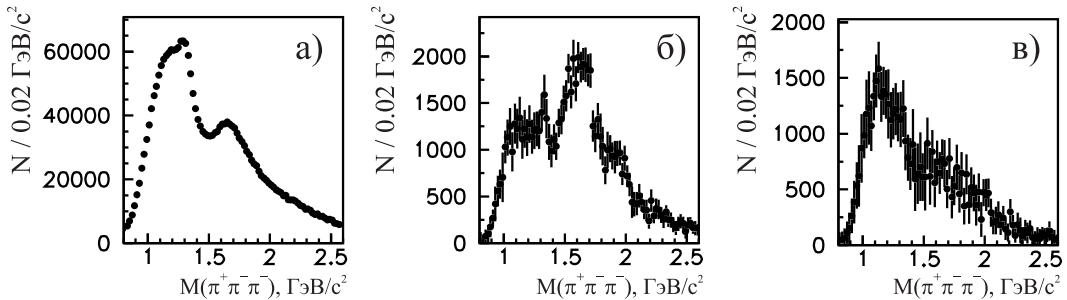


Fig. 64. Results of PWA of the  $\pi^+ \pi^- \pi^-$  system: (a) total intensity; intensity of the  $J^{PC} M^\eta = 1^{-+}1^+$  wave in the  $\rho\pi$  channel (b) under the assumption of full coherence of the  $2^{-+}$  waves and (c) in the case where this assumption is not used [245].

respect to the  $2^{-+}$  wave. The amount of the  $1^{-+}$  wave and the width proved to be unstable; it varied from a clear, unmistakable signal with 'narrow' width to a vanishingly small number of  $1^{-+}$  events and a very wide width, depending on the number of partial waves introduced and, in particular, if rank 1 or 2 of the density matrix was assumed in the analysis. It is clear that, if one attempts to claim a new state or its decay mode, its proof must remain stable against the number of waves introduced or the rank of the density matrix. For this reason they relied on the phase motion  $\Delta\phi = \phi(1^{-+}) - \phi(2^{-+})$ . In all of their numerous fits, the phase motion remained stable. So the authors were confident that their choice of the phase motion made sense. The instability in the amount and the width of  $\pi_1(1600) \rightarrow \rho\pi$  led to the highly asymmetrical error in the width given in eq. (7.5) [249, 257].

The Breit-Wigner parameters of the observed  $\rho\pi$  exotic signal [249, 257] coincide within errors with those of the signal seen in the  $\eta'\pi$  channel. However, the  $\pi_1(1600)$  in  $\eta'\pi$  is seen in natural parity exchange, and not in unnatural parity exchange. From this observation, eq. (7.4) was derived. The signal in  $\rho\pi$  is observed with comparable intensities in both, natural and unnatural parity exchange. Hence there must be two different mass degenerate objects, one decaying into  $\rho\pi$ , the other one into  $\eta'\pi$ . The need for two resonances degenerate in mass is difficult to accept and, given the differences in the published approaches and results, the  $\pi_1(1600) \rightarrow \rho\pi$  decay remains a controversial issue.

#### 7.2.4 The wave $J^{PC} = 1^{-+}$ in the $\omega\pi\pi$ channel.

The wave  $J^{PC} = 1^{-+}$  in the  $\omega(\pi^+\pi^-\pi^0)\pi^-\pi^0$  channel was studied by VES [238, 245] and E-852 [261]. Three isobars  $\omega\rho$ ,  $b_1\pi$  and  $\rho_3\pi$  were included in the PWA model, with waves in the range  $J \leq 4$ ,  $L \leq 3$ , and  $m \leq 1$ , with  $J$  as total angular momentum,  $L$  as decay orbital-angular momentum, and  $m$  as projection of  $J$  onto the beam axis.

The results of E852 are summarised in Fig. 65. Two bumps at  $M \approx 1.7 \text{ GeV}/c^2$  and at  $M \approx 2.0 \text{ GeV}/c^2$  are seen in the dominant  $2^{++}(\omega\rho)_2^S 1^+$  wave, a further peak in the  $a_2(1320)$  region is not shown. There are two intensive exotic waves  $1^{-+}(b_1\pi)_1^S 1^+$  and  $1^{-+}(b_1\pi)_1^S 0^-$  peaking at  $M \approx 1.6 \text{ GeV}/c^2$ . These three waves can be fitted with four Breit-Wigner resonances  $a_2(1700)$ ,  $a_2(2000)$ ,  $\pi_1(1600)$  and  $\pi_1(2000)$ . Mass and width of  $\pi_1(1600)$  were determined to

$$M = 1664 \pm 8 \pm 10 \text{ GeV}/c^2, \Gamma = 184 \pm 25 \pm 28 \text{ GeV}/c^2.$$

The production characteristics resembles that of the  $\pi_1(1600)$  in  $\rho\pi$ ; both have nearly equal intensities in natural and unnatural parity exchange. One more exotic resonance is suggested at  $M \approx 2.0 \text{ GeV}/c^2$  to fit the tail in the wave  $1^{-+}(b_1\pi)_1^S 1^+$ .

In the VES experiment, the dominant  $2^{++}(\omega\rho)_2^S 1^+$  wave has a broad bump at  $M \approx 1.7 \text{ GeV}/c^2$ , the signal at  $M \approx 2.0 \text{ GeV}/c^2$  is not seen. The exotic wave  $1^{-+}(b_1\pi)$  is significant only in natural parity exchange and gives a broad contribution of low intensity, about 15% of the leading  $2^{++}$  wave. A fit with a Breit-Wigner amplitude shows that the data are consistent with resonant behaviour of the amplitude with  $M \sim 1.6, \Gamma = 0.33 \text{ MeV}/c^2$  [241].

The three signals in  $b_1(1235)\pi$ ,  $\eta'\pi$  and  $\rho\pi$  have the relative strength  $1 : 1 \pm 0.3 : 1.6 \pm 0.4$  [920]. But the coherence study [242] suggested to remove  $\rho\pi$  from this comparison.

### 7.2.5 The wave $J^{PC} = 1^{-+}$ in the $f_1\pi$ channel.

The E-852 results on the reaction  $\pi^- A \rightarrow \eta\pi^+\pi^-\pi^- A$  are published in [260] and those of VES in [245]. The results of the partial wave analyses of both experiments are again very similar, and it is sufficient to show, in Fig. 66, one data set only.

The dominant wave is  $J^{PC} = 1^{-+}(f_1\pi)$ . It is broad and structureless with a maximum at  $M \approx 1.7$  GeV/c<sup>2</sup> (Fig. 66(a)). The signal in the wave  $J^{PC}M^\eta = 1^{-+}1^+$  is clearly seen (Fig. 66 (c)). It is produced via natural parity exchange; it resembles in production characteristics the  $\eta'\pi$  exotic wave.

The shape of the signal is very similar to the shape of the  $1^{++}0^+(f_1\pi)$  wave. The phase differences  $\phi(1^{-+}) - \phi(1^{++})$  and  $\phi(1^{-+}) - \phi(2^{-+})$  both fall by  $\approx 2\text{rad}$  as  $M_{\eta 3\pi}$  increases from  $M = 1.5$  GeV/c<sup>2</sup> to  $M = 2.4$  GeV/c<sup>2</sup>. Hence the  $1^{++}$  and  $2^{-+}$  phases rise faster than  $\phi(1^{-+})$ . The number of  $1^{++}$  and  $2^{-+}$  resonances which the data can accommodate thus determines the number of  $1^{-+}$  resonances.

The E-852 collaboration fits the PWA intensity distributions and phase differences with a superposition of Breit-Wigner resonances in all channels. Any type of smooth background is not admitted. In this resonance-dominated approach, several resonances are needed to get a good fit to the distributions. These are listed, with the results on masses and width, in Table 18.

Table 18  
Results of the mass-dependent fit.

Wave	Mass [MeV/c <sup>2</sup> ]	$\Gamma$ [MeV/c <sup>2</sup> ]
$1^{++}0^+ f_1\pi P$	1714 (fixed)	308 (fixed)
	$2096 \pm 17 \pm 121$	$451 \pm 41 \pm 81$
$2^{-+}0^+ f_1\pi D$	1676 (fixed)	254 (fixed)
	$2003 \pm 88 \pm 148$	$306 \pm 132 \pm 121$
$1^{-+}1^+ f_1\pi S$	2460 $\pm 328 \pm 263$	$1540 \pm 1214 \pm 718$
	$1709 \pm 24 \pm 41$	$403 \pm 80 \pm 115$
	$2001 \pm 30 \pm 92$	$333 \pm 52 \pm 49$

### 7.2.6 Conclusion on $J^{PC} = 1^{-+}$ exotics

Before coming to conclusions on  $J^{PC} = 1^{-+}$  exotics, the assumptions will be discussed which are made in the data analysis. As a rule, a partial wave analysis is performed in two steps. The first step is the mass-independent PWA which serves to construct the parameters of a density matrix  $\rho_{ij}$  which represents the final state  $X$  with mass  $M$ . In a second step, these parameters are fitted in some model in a mass-dependent fit.

The isobar model relies on the basic assumption that all processes involved can be decomposed in two-body subprocesses. For example, the reaction  $\pi^- p \rightarrow \pi^+\pi^-\pi^- p$  is considered as the sum of

$$\pi^- p \rightarrow A_i p \text{ with subsequent decays } A_i \rightarrow B_j \pi \text{ and } B_j \rightarrow \pi\pi$$

$$\pi^- p \rightarrow C_i D_j \text{ with subsequent decays } C_i \rightarrow \pi\pi \text{ and } D_j \rightarrow \pi p$$

$\pi^- p \rightarrow \pi E_j$  with subsequent decays  $E_i \rightarrow \pi F_j$  and  $F_j \rightarrow \pi p$

In general, each partial wave may have resonant and non-resonant contributions. But often it is assumed that all decay channels are saturated with reasonably narrow resonances. Even with these approximations, the large quantity of free parameters may lead to the necessity of various truncations like a reduction in the list of isobars due to limitations in  $J_{max}$  of contributing isobars.

A first assumption which is generally made supposes that the three reactions listed above live in different corners of the phase space and can be separated by kinematical cuts. At sufficiently high energy, this is the case, but at moderate energies the assumption does not need to be absolutely true. But it is essential for the extraction of weak exotic  $J^{PC} = 1^{-+}$  wave from some reactions like  $\pi^- p \rightarrow \eta \pi^- p$ . The problem is that the  $\eta p$  and  $\pi^- p$  systems are very different in nature and have different isospin decompositions. Therefore the angular distribution of the  $\eta \pi$  system on  $\theta_{GJ}$  will be asymmetric as soon as nucleon excitations are not completely ruled out. Within a standard PWA model, this asymmetry is then assigned to the interference of the dominant  $D_+$  wave and a wave of opposite parity,  $P_+$ . Thus, the effect can generate an effective resonant-like exotic wave  $J^{PC} = 1^{-+}$  in the  $a_2$  region.

Another potential sources of false signals are parametrisations of isobars and integrations over  $t$ . The different partial waves depend on  $t$  in different ways; integration over  $t$  decreases therefore the coherence between partial waves. Quite generally, any model imperfections decrease the coherence and may generate false signals in low intensity waves by leakage from most intensive waves. The importance of leakages depends on the PWA model. In case of a density matrix of rank one with  $n$  waves, there are  $n$  different functions to absorb these imperfections. As a result, leakage should be expected at the level of  $\alpha/n$ , where  $\alpha \approx 0.1$  is the scale of imperfection of the model. A density matrix of arbitrary rank has  $n(n+1)/2$  different functions resulting to a significant reduction of the leakage problem. Therefore a density matrix of highest possible rank is recommended for the study of low intensity waves. Of course, higher-rank fits require significantly higher statistics since more parameters need to be determined.

Summarizing the progress in studies of the  $J^{PC} = 1^{-+}$  hybrid mesons achieved since the first observation of the exotic wave we arrive at the following conclusions:

- Exotic waves are observed in numerous final states with comparable intensities in diffraction-like reactions. Only one of them is confirmed in a non-diffractive process, in  $\bar{p}p$  annihilation.
- Even at low energies, several different intermediate states are separately identified due to their different production characteristics:
  - (1)  $\pi\eta$  in SU(3) ( $10, \bar{10}$ ) with strong intensity at  $1400 \text{ MeV}/c^2$ .
  - (2) Possibly  $\rho\pi$  at  $1400 \text{ MeV}/c^2$  in  $\bar{p}p$  annihilation, but from a different initial  $\bar{p}p$  state.
  - (3)  $\pi\eta'$  and  $f_1(1285)\pi$  in natural parity exchange, with strong intensity at  $1600 \text{ MeV}/c^2$ .
  - (4)  $b_1(1230)\pi$  and  $\rho\pi$  in natural and unnatural exchanges, with strong intensity at  $1600 \text{ MeV}/c^2$ .
- Results requiring unnatural parity exchange are controversial.
- The data are consistent with both, resonant and non-resonant interpretations; a decision which interpretation is correct requires calculations of meson-meson interaction amplitudes.
- There is a chance that the lowest mass exotic hybrid has been discovered. It would have  $1600 \text{ MeV}/c^2$  mass and a width of  $300 \text{ MeV}/c^2$ . It couples to  $\pi\eta'$  and  $f_1(1285)\pi$ . However, more work is required to establish or to reject this possibility.

### 7.3 Further $J^{PC}$ exotic waves

#### 7.3.1 $J^{PC} = 0^{+-}, 2^{+-}$

Predictions for quantum numbers, masses, widths and branching ratios of hybrid mesons were calculated in the flux-tube model [870]. The lowest hybrids are the states with total orbital angular momentum  $l = 1$  and one phonon of transverse flux-tube vibration which carries one unit of angular momentum around the  $q\bar{q}$  axis; positive and negative parity eigenstates are found. Combined with the quark spin  $S = 0, 1$ , there are eight low-mass hybrid states with

$$J^{PC} = 1^{\pm\pm}; \quad 0^{\pm\mp}, \quad 1^{\pm\mp}, \quad 2^{\pm\mp}.$$

Three out of these eight states have exotic quantum numbers,  $J^{PC} = 0^{+-}, 1^{--}, 2^{+-}$ . Isovectors and isoscalars are expected at  $M \approx 1.8 \div 2.0 \text{ GeV}/c^2$ . The isovector exotic state with  $J^{PC} = 1^{--}$  appears to be the most convenient one for experimental studies. It is predicted to be relatively narrow ( $\Gamma \approx 0.2 \text{ GeV}/c^2$ ), it can be produced by a pion beam in diffractive-like reaction, and its dominant decay modes  $f_1\pi, b_1\pi$  are suitable for detection and for partial-wave analysis .

Other predicted isovector mesons with exotic quantum numbers ( $J^{PC} = 0^{+-}, 2^{+-}$ ) are much less appealing. These states are found to be wide  $\Gamma > 0.5 \text{ GeV}/c^2$ , their dominant decay modes end up in a tetrapion final state which is difficult for the partial wave analysis; the cross sections for production in a pion beam must be relatively small due to the positive  $G$ -parity of the states.

For searches of isoscalar exotic states, the quantum numbers  $J^{PC} = 0^{+-}, 2^{+-}$  look most promising. These states are not very wide  $\Gamma < 0.5 \text{ GeV}/c^2$  and have convenient decay modes like  $b_1\pi$ . The reaction  $\pi^-p \rightarrow b_1\pi n$  requires  $b_1$  exchange and should have a very specific broad distribution as a function of squared transfer momentum  $t$  .

Up to now all these states with exotic quantum numbers except of  $J^{PC} = 1^{--}$  remain uncharted territory.

#### 7.3.2 Isospin exotics

Non- $q\bar{q}$  resonances could manifest themselves in isospin exotic channels, like  $I = 2$  for nonstrange mesons and  $I = 3/2$  for mesons with strangeness. Detailed experimental studies of  $\pi^+\pi^+$  and  $K^+\pi^+$  scattering [211, 908] clearly show negative (repulsive) phases from thresholds to  $M \approx 1.8 \text{ GeV}/c^2$ , in  $\pi^+\pi^+$   $S$ - and  $D$ -waves and in  $K^+\pi^+$   $S$ - and  $P$ -waves. These results agree with calculations based on an Effective Lagrangian [909] and on a Quark Exchange model [907] (but are at variance with the narrow  $\pi^+\pi^+$  resonance at 1420 MeV reported by the Obelix collaboration [921]).

The situation is different in the isotensor  $I = 2$   $\rho\rho$  channel. In two-photon fusion into two  $\rho$  mesons, in  $\gamma\gamma \rightarrow \rho^0\rho^0$ , a resonance-like enhancement at  $M \approx 1.6 \text{ GeV}/c^2$  was observed in several experiments. The quantum numbers of this signal are [922]:  $(J^P, J_z, S) = (2^+, \pm 2, 2)$  (where  $J^P$  are spin and parity,  $J_z$  spin component in the beam direction and  $S$  the total spin of two  $\rho$ 's). The  $\rho^0\rho^0$  signal is much stronger than one in  $\gamma\gamma \rightarrow \rho^+\rho^-$  (Fig. 67).

This result was confirmed by L3 [689–692] with much higher statistics. If the  $\rho^0\rho^0$  bump has a defined isospin  $I = 0$  or  $I = 2$ , the ratio of  $\rho^+\rho^-$  to  $\rho^0\rho^0$  should be 2 (for  $I = 0$ ) or 1/2 (for  $I = 2$ );  $I = 1$  is forbidden for  $\rho^0\rho^0$ . The experimental ratio is about 1/5. This can be achieved assuming interference between a isotensor resonance ( $I = 2$ ) with some isoscalar contribution. The existence

of tetraquark states with  $I = 0$  and  $I = 2$  and their destructive interference in  $\gamma\gamma \rightarrow \rho^+\rho^-$  and constructive interference in  $\gamma\gamma \rightarrow \rho^0\rho^0$  was predicted a long time ago by Achasov, Devyanin and Shestakov [923] and by Li and Liu [924]. The data were thus be claimed to prove the existence of tetraquark isotensor resonances at  $M \approx 1600$  MeV/c $^2$ ,  $\Gamma \approx 500$  MeV/c $^2$  [925–927]. Calculations within QCD sum rules [928] do no exclude such resonances. However, an interpretation of the data as generated by Pomeron exchange between the two  $\rho^0$  – present due to vector meson dominance – does not seem unlikely.

Several other final states with two vector mesons were studied in  $\gamma\gamma$  fusion,  $\omega\omega$ ,  $\omega\rho^0$ ,  $K^{0*}\bar{K}^{0*}$ ,  $K^{+*}\bar{K}^{-*}$ ,  $\rho^0\phi$  and  $\omega\phi$  [929, 930]. Very wide threshold enhancements are seen in most of these channels. The cross sections vary from  $\approx 60$  nb for  $\gamma\gamma \rightarrow \rho^0\rho^0$  to  $\approx 2$  nb for  $\gamma\gamma \rightarrow \rho\phi$ . A clear  $q^2\bar{q}^2$ -resonance-dominated view did not emerge from the studies. The ratio of cross section for  $K^{0*}\bar{K}^{0*}$  and  $K^{+*}\bar{K}^{-*}$  is about 1/8. This number does not fit into any model with  $S$ -channel resonances. If a resonance would contribute, it must decay to  $\rho\phi$ ; experimentally, this channel is strongly suppressed compared to  $K^{+*}\bar{K}^{-*}$ . These features indicate that nonresonant dynamics play a decisive rôle. We have to underline that broad threshold enhancements can appear without  $s$ -channel resonance contributions; this is the case, for example, in the reaction  $K^+p \rightarrow K^0\Delta^{++}$ .

A description of the data without  $s$ -channel resonances can be achieved within a phenomenological model based on the assumption of  $t$ -channel factorisation [931]. In this model the cross section for  $\gamma\gamma \rightarrow \rho^0\rho^0$  can be calculated absolutely from experimental data on the reaction  $\gamma p \rightarrow pp$ . Even though data are successfully described by this model, it does not give a detailed microscopic picture of the processes (and does not aim for this). Quark-model calculations of these reactions are reviewed in [932].

In conclusion we have to say that the dynamics of two mesons in isotensor configuration is not yet fully understood. A detailed partial wave analysis of channels like  $\pi^+\pi^+$ ,  $\rho^+\rho^+$ ,  $\pi^+\pi^+\pi^0$ ,  $\pi^+\pi^+\eta$ ,  $\pi^+\pi^+\eta'$ ,  $\pi^+\pi^+\omega$  in different reactions could bring a better understanding of multiquark and multimeson dynamics, and possibly lead to new insights.

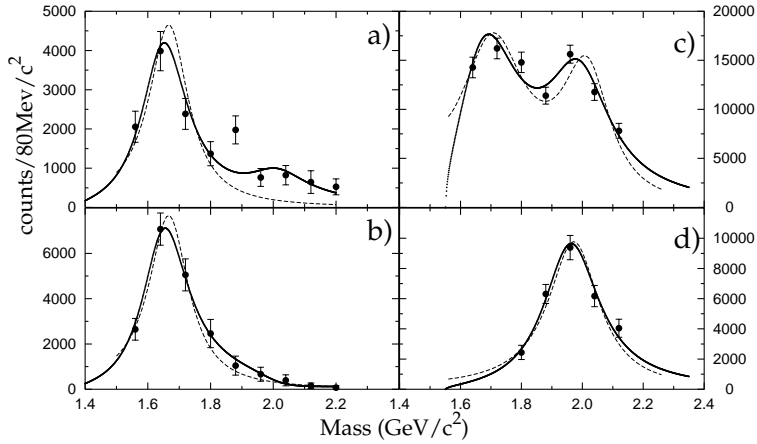


Fig. 65. Wave intensity for (a)  $1^{-+}(b_1\pi)_1^S 1^+$ , (b)  $1^{-+}(b_1\pi)_1^S 0^-$ , (c)  $2^{++}(\omega\rho)_2^S 1^+$ , and (d)  $4^{++}(\omega\rho)_2^D 1^+$ . The solid line is the result of Breit-Wigner fit for two poles and dashed line is for one.

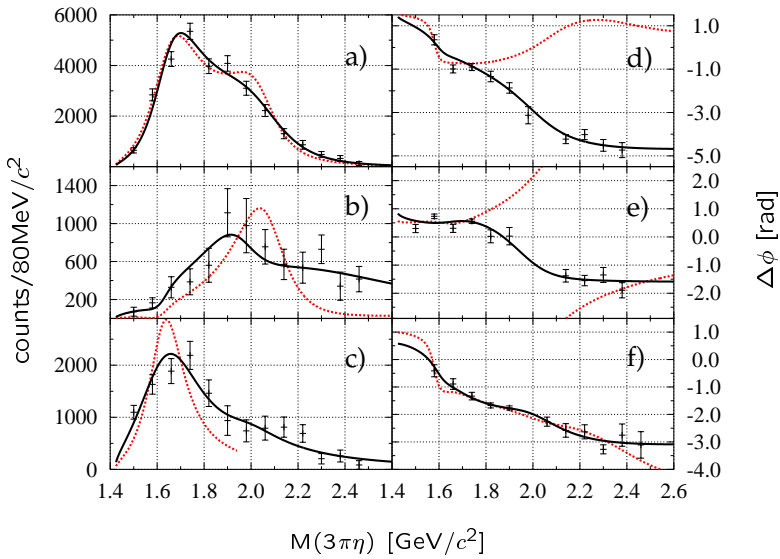


Fig. 66. PWA results:  $f_1(1285)\pi^-$  intensity distributions (a)  $1^{++}0^+f_1\pi^-P$ , (b)  $2^{-+}0^+f_1\pi^-D$ , (c)  $1^{-+}1^+f_1\pi^-S$  and phase difference distributions (d)  $\phi(1^{-+}) - \phi(2^{-+})$ , (e)  $\phi(1^{-+} - \phi(1^{++}))$ , (f)  $\phi(1^{++}) - \phi(2^{-+})$ . The results from a last squares fit are overlaid as the solid line (two poles in the  $1^{-+}f_\pi$  wave) and the dashed line (one pole in the  $1^{-+}$  wave) [260].

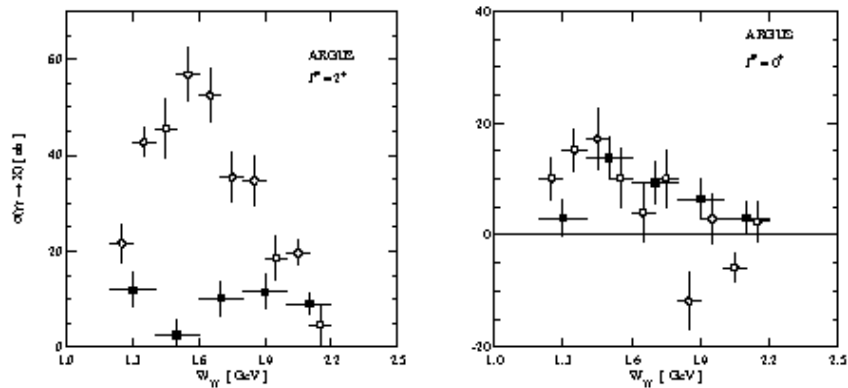


Fig. 67. Cross sections for the dominant amplitudes  $\gamma\gamma \rightarrow \rho^0 \rho^0$  (open circles) and  $\gamma\gamma \rightarrow \rho^+ \rho^-$  (full squares) [471].

## 8 Pseudoscalar mesons

The radial excitations of the pseudoscalar ground-state nonet provide answers to important questions: how do radial excitation energies of light mesons compare to the mass gap between  $\eta_c(1S)$  and  $\eta_c(2S)$ ? Due to their Goldstone nature, pseudoscalar ground-state mesons (except  $\eta'$ ) have a much smaller mass than vector mesons have; is this pattern reproduced for  $n = 2$  (and higher) excitations? The mixing angle of the ground-state nonet is far from the ideal mixing angle; what is its value for pseudoscalar radial excitations? The  $\eta'$  mass is large compared to the  $\eta$  mass due to the  $U_A(1)$  anomaly; how large is the corresponding mass difference for radial excitations? At the end of this section these questions will be resumed to see to what extend data can provide answers to them.

### 8.1 The $\pi$ radial excitations

#### 8.1.1 The $\pi(1300)$

The  $\pi(1300)$  was first reported by Daum *et al.* [214] in 1981 in a (successful) attempt to identify the  $a_1(1260)$  in  $\pi^- p$  scattering. The Deck effect (see section 4.1.4) provides a substantial background in the  $\rho\pi$   $S$ -wave and carries a phase motion in itself. Hence it was difficult to isolate the  $a_1$ . In addition to the  $a_1(1260)$  in the  $\rho\pi$   $S$ -wave, a resonance in the  $\rho\pi$   $P$ -wave was found, with quantum numbers  $(I^G)J^{PC} = (1^-)0^{-+}$  and a mass of  $\sim 1400 \text{ MeV}/c^2$ . Its mass and quantum numbers suggested its interpretation as first radial excitation of the pion. The existence of  $\pi(1300)$  was confirmed in several similar experiments, even though the measured masses scattered over a wide range [933–936].

The VES collaboration observed a clear low-mass enhancement in the  $\pi(\pi\pi)_{S\text{-wave}}$  [236], but demonstrated that there is a strong influence of the Deck effect for this partial wave which may fake a  $\pi(1300)$  at a mass of about  $1200 \text{ MeV}/c^2$ . The authors of [236] therefore refused to give any mass or width for the  $\pi(1300)$ . The importance of the Deck effect for  $\pi(1300) \rightarrow \pi(\pi\pi)_{S\text{-wave}}$  decays was not discussed in the early papers, and some of those claims may have been premature.

The E852 collaboration [257] saw the same enhancement and observed a similar phase motion in the  $\pi(\pi\pi)_{S\text{-wave}}$  as VES did. The fit to the  $\pi(\pi\pi)_{S\text{-wave}}$  proved to be very unstable and, in view of the unexplored influence of the Deck effect, observation of  $\pi(1300) \rightarrow \pi(\pi\pi)_{S\text{-wave}}$  was not claimed. In the  $(\pi\rho)_{P\text{-wave}}$ , the partial wave analysis did reveal a clear resonant behaviour which was interpreted as  $\pi(1300)$ . Mass and width are listed in Table 19.

The Obelix collaboration reported an analysis of  $\bar{p}p \rightarrow \pi^+\pi^+\pi^-\pi^-$  [387]. The solution comprised a  $\pi(1300)$  with mass and width  $(M, \Gamma) = (1275 \pm 15, 218 \pm 100) \text{ MeV}/c^2$  decaying dominantly to  $\pi(\pi\pi)_{S\text{-wave}}$ . In the Crystal Barrel experiment, data on  $\bar{p}p \rightarrow 5\pi^0$  were analysed [334]. The best

Table 19

The  $\pi(1300)$  mass and width from  $\pi(1300) \rightarrow \rho\pi$  decays

M	Γ	Ref.
$\sim 1400$		[214]
$1343 \pm 15 \pm 24$	$449 \pm 39 \pm 47$	[257]
$1375 \pm 40$	$268 \pm 50$	[352]
$1373 \pm 25$	$358 \pm 70$	mean

solution had a very low  $\pi'$  mass at 1122 MeV/c<sup>2</sup>. However, this low mass was incompatible with the  $\pi(1300)$  masses obtained when data on  $\bar{p}n \rightarrow \pi^- 4\pi^0$  and  $\bar{p}n \rightarrow 2\pi^- 2\pi^0 \pi^+$  were studied in a combined analysis. In the latter analysis, the optimum  $\pi(1300)$  parameters were  $(M, \Gamma) = (1375 \pm 40, 286 \pm 50)$  MeV/c<sup>2</sup>. The  $\pi(1300)$  was seen only in its  $\rho\pi$  decay, the coupling to  $\pi(\pi\pi)_{S-wave}$  converged to zero. The collaboration reported an upper limit of 15% for the  $\pi(\pi\pi)_{S-wave}$  decay partial width. Reanalysing the  $\bar{p}p \rightarrow 5\pi^0$  data, a nearly equally good fit was achieved without introduction of a  $\pi(1300)$  [352] while other resonance parameters were not affected (in particular the scalar mesons did not change their masses and widths). The results from [334] are therefore superseded by the more recent values, given in [352] and reproduced in Table 19.

In view of the importance of the Deck effect, we retain only results in which the  $\rho\pi$  decay mode surpasses in magnitude the  $\pi(\pi\pi)_{S-wave}$  decay mode. The existence of the latter decay mode is of course not excluded, but we do not consider it as experimentally established.

In the  ${}^3P_0$  model, the  $\rho\pi$  is expected to be the dominant mode of the  $\pi(1300)$  if interpreted as 2S  $q\bar{q}$  state. In [58], a partial width of

$$\Gamma(\pi(1300) \rightarrow \pi\rho) = 209 \text{ MeV/c}^2 . \quad (8.1)$$

is predicted while the  $\pi(\pi\pi)_{S-wave}$  decay width is expected to be small. With the latter decay mode being small, there is reasonable consistency between the value (8.1) and the average of Table 19. Thus the observed  $\pi(1300)$  is consistent with expectations for a  $2^1S_0$   $q\bar{q}$  state.

### 8.1.2 The $\pi(1800)$

The  $\pi(1800)$  was first reported by Bellini [935] and studied extensively by the VES collaboration. Its decay into  $\pi(\pi\pi)_{S-wave}$  and  $\pi(\eta\eta)_{S-wave}$  are the most prominent modes [236]. Further decay modes are  $\pi(\eta\eta')$  [231], and  $K_0^*(1430)\pi$  [233]. The VES collaboration also reported  $\pi(1800) \rightarrow \omega\pi\pi$  decays [238] even though the  $\omega\pi\pi$  resonance mass was found at a much lower value. Surprisingly, the  $\pi(1800)$  is not seen in  $\rho\pi$  or  $K^*\bar{K}$ , both of these decay modes are suppressed [233, 236, 257].

Recently, the VES collaboration performed a combined analysis of all reactions [244, 245], with only

Table 20

Ratios of  $\pi(1800)$  partial widths. The relative widths are not corrected for further decay modes; the correction factors are given in the 4<sup>th</sup> column.

Final state	subchannel	relative width	decay fraction
$\pi^+ \pi^- \pi^-$		1	
	$(\pi\pi)_{S-wave} \pi^-$	$1.1 \pm 0.1$	$2/3$
	$f_0(980) \pi^-$	$0.44 \pm 0.15$	$2/3 \cdot 0.84$
	$f_0(1500) \pi^-$	$0.11 \pm 0.05$	$2/3 \cdot 0.35$
	$\rho^0 \pi^-$	< 0.02 at 90% c.l.	$1/2$
$K^+ K^- \pi^-$		$0.29 \pm 0.10$	
	$K^*(892) K^-$	< 0.03 at 90% c.l.	$1/4$
$\eta\eta\pi^-$		$0.15 \pm 0.06$	
	$a_0(980) \eta$	$0.13 \pm 0.06$	0.8
	$f_0(1500) \pi^-$	$0.012 \pm 0.005$	0.05
$\eta\eta' \pi^-$	$f_0(1500) \pi^-$	$0.026 \pm 0.010$	0.019

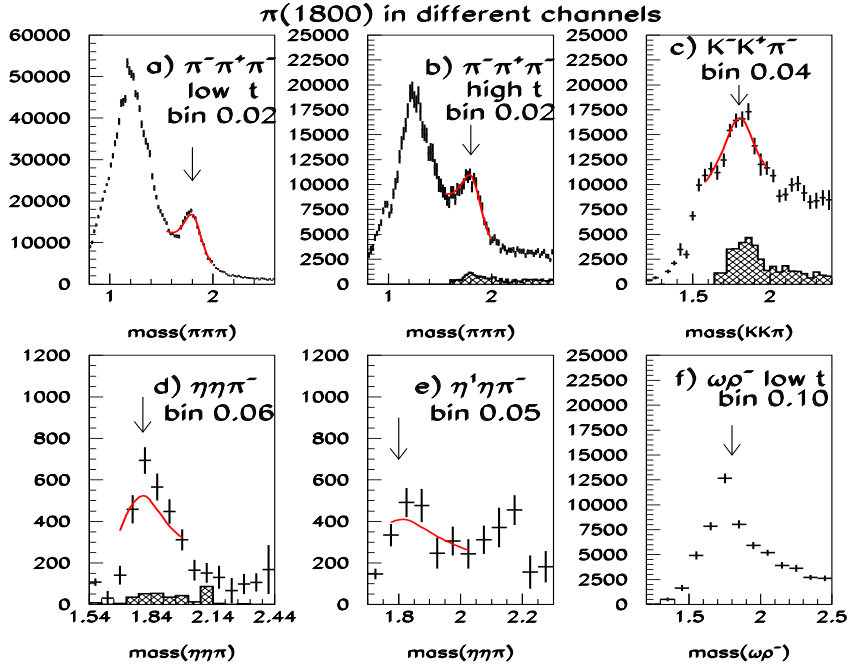


Fig. 68. Mass spectra for  $(I^G)J^{PC} = (1^-)0^{-+}$  wave. The data points represent the results of a mass-independent partial wave analysis, the solid curve a fit using a  $\pi(1800)$  with  $\Gamma = 270 \text{ MeV}/c^2$  and a polynomial background amplitude with varying phases (constrained by a 2<sup>nd</sup>-order polynomial).

the  $\rho\omega$  channel excluded. Mass and width of the global fit are compatible with  $M = 1800 \text{ MeV}/c^2$  and  $\Gamma = 270 \text{ MeV}/c^2$ . From the fit, ratios of partial width were determined which are reproduced in Table 20. Data and fit are shown in Fig. 68.

Some notations and values in the Table need explanation. For the  $(\pi\pi)_{S-wave}$  with mass up to  $\approx 1.4 \text{ GeV}/c^2$ , the parametrisation of Au, Morgan and Pennington [177] was chosen. The  $f_0(980)$  is listed as a separate resonance; its contribution was subtracted from the  $S$ -wave. The sum of decay probabilities into  $(\pi^+\pi^-)_{S-wave}\pi^-$  and into  $f_0(980)_{\pi^+\pi^-}\pi^-$  exceeds the total width of the  $(\pi^-\pi^+\pi^-)$  channel due to strong interference of these two channels. The  $K^-K^+\pi^-$  channel is not divided into the  $(K^+K^-)_{S-wave}\pi^-$  and  $K^-(K^+\pi^-)_{S-wave}$  isobars as their separation proved to be very model dependent.

Table 20 also contains the fraction with which isobars are observed in the given final state. To give partial decay widths is problematic since the results from E782 and VES are often incompatible. Furthermore, the  $\pi(1800) \rightarrow \rho\omega$  contribution and high multiplicity decays are unknown. Based on the graphs in Fig. 68 we estimate the  $\rho\omega$  contribution and assume that no other decay modes exist. The partial decay widths of Table 21 thus present an educated guess.

The decay pattern is not easily understood. Two directions were tried: the assumption that the  $1800 \text{ MeV}/c^2$  region houses two states with pion quantum numbers [58], and the hypothesis that special selection rules govern  $\pi(1800)$  decays [245]. In the mass range of the  $\pi_1(1800)$ , two pseudoscalar resonances are predicted, the second radial excitation of the pion and a hybrid meson. To distinguish these two possibilities we have to rely on model predictions. In Table 22, predictions for the two alternatives are collected [58, 876–878].

- A hybrid  $\pi_H(1800)$  and a pseudoscalar radial excitation  $\pi_{3S}$  are both predicted to have a  $\rho\pi$  partial width of  $30 \text{ MeV}/c^2$ , incompatible with the experimental finding. This may serve as

Table 21

Estimated decay partial widths of  $\pi(1800)$ . The estimate assumes absence of high multiplicity decay modes. There could be two different mesons in the mass region (see text for a discussion).

$\Gamma_{\pi(1800) \rightarrow \pi^-(\pi\pi)_{S-wave}}$	$100 \pm 25 \text{ MeV}/c^2$
$\Gamma_{\pi(1800) \rightarrow \pi^- f_0(980)}$	$50 \pm 20 \text{ MeV}/c^2$
$\Gamma_{\pi(1800) \rightarrow \pi^- f_0(1500)}$	$25 \pm 15 \text{ MeV}/c^2$
$\Gamma_{\pi(1800) \rightarrow \rho\omega}$	$60 \pm 30 \text{ MeV}/c^2$
$\Gamma_{\pi(1800) \rightarrow a_0(980)\eta}$	$16 \pm 8 \text{ MeV}/c^2$
$\Gamma_{\pi(1800) \rightarrow \rho\pi}$	$3 \pm 3 \text{ MeV}/c^2$
$\Gamma_{\pi(1800) \rightarrow K^*K}$	$6 \pm 6 \text{ MeV}/c^2$ .

Table 22

Model predictions for  $\pi_H(1800)$  and for  $\pi_{3S}$  [58, 876–878].

	$\rho\pi$	$\rho\omega$	$\rho(1470)\pi$	$f_0(1370)\pi$	$f_2\pi$	$K^*K$
$3S$	30	74	56	6	29	36
$\pi_H$	$30 \div 50$	0	$10 \div 50$	$40 \div 170$	$3 \div 8$	$5 \div 15$
Expt.	$< 6$	$60 \pm 30$	small	$100 \pm 25$	small	$< 12$

a warning that the identification of the nature of  $\pi(1800)$  is model dependent. Other well established pseudoscalar resonances like  $\pi(1300)$  and  $K(1460)$  decay dominantly into a vector and a pseudoscalar meson. The pattern resembles the  $\rho\pi$  puzzle in charmonium decays: the decay fraction  $J/\psi \rightarrow \rho\pi$  is large while  $\psi' \rightarrow \rho\pi$  is suppressed.

- A distinctive feature of  $\pi(1800)$  is the  $f_0(1370)\pi$  decay mode<sup>9</sup>. A hybrid  $\pi_H(1800)$  is predicted to have a large  $f_0(1370)\pi$  partial width (up to  $170 \text{ MeV}/c^2$ ) while  $\pi_{3S}$  is predicted to have a partial decay width for this decay of  $6 \text{ MeV}/c^2$  only.
- A hybrid  $\pi_H(1800)$  should decouple from  $\rho\omega$  while a large partial decay width ( $74 \text{ MeV}/c^2$ ) is predicted for  $\pi_{3S}$ .
- The isobars  $\rho(1470)\pi$  and  $f_2(1270)\pi$  were not needed in the partial wave analysis; presumably they are small. The  $\pi(3S)$  radial excitation is however expected to decay into these modes.
- The  $K^*K$  contribution is compatible with zero; a  $\pi_{3S}$  state is predicted to couple significantly to  $K^*K$ .

The data seem to favour the hybrid interpretation except for the large  $\rho\omega$  decay width which should vanish for a hybrid. This partial width is predicted to be strong for  $\pi(3S)$ , in agreement with the experimental result. Hence there is the possibility that two states have been observed, the  $\pi_{3S}$  and a hybrid  $\pi_H$ , as pointed out by Barnes [58]. The  $\rho\omega$  signal peaks at a lower mass than the other mass distributions in Fig. 68. The authors in [238] quote  $(M, \Gamma) = (1737 \pm 5 \pm 15, 259 \pm 19 \pm 6) \text{ MeV}/c^2$  which seems inconsistent with the nominal mass value. We also note that  $\pi(1800)$  peaks at a higher mass, at  $\sim 1830 \text{ MeV}/c^2$  in its  $\pi(\eta\eta)_{S-wave}$  and  $\pi(\eta\eta')$  decay modes which go largely via  $f_0(1500)\pi$ .

The decays into  $\pi(\pi\pi)_{S-wave}$  pose a difficulty. In the VES analysis the  $(\pi\pi)_{S-wave}$  includes the  $1300 \text{ MeV}/c^2$  region. In this mass region, there is the  $f_0(1370)$ . In Table 22, the full  $\pi(\pi\pi)_{S-wave}$  is ascribed to the  $f_0(1370)$  even though it is known that it contributes only little to  $\pi(\pi\pi)_{S-wave}$ . The  $\pi(\pi\pi)_{S-wave}$  background needs to be subtracted, unseen  $f_0(1370)$  decay modes would need to be accounted for. Both is impossible at the moment. Hence the  $\pi(1800) \rightarrow \pi^- f_0(1370)$  decay

<sup>9</sup> In section 10 it is argued that  $f_0(1370)$  is not a resonance with a proper phase motion.

mode is essentially unknown and cannot be used to assign  $q\bar{q}$  or hybrid wave functions to  $\pi(1800)$ .

The VES collaboration argued that the observed decay pattern indicates strong OZI violation in  $\pi(1800)$  decays [245]. The ratio of decays  $\pi(1800) \rightarrow K^+K^-\pi^-/\pi(1800) \rightarrow \pi^+\pi^-\pi^-$  is rather large, and also the decay rate  $\pi(1800) \rightarrow f_0(980)\pi^-$  is unexpectedly high since  $f_0(980)$  couples mainly to  $s\bar{s}$  and not to  $n\bar{n}$ . Note however, that other radial excitations have significant  $(\pi\pi)_{S-wave}$  decay modes as well, like  $\Upsilon(2s) \rightarrow \Upsilon(1s)(\pi\pi)_{S-wave}$ ,  $\omega(1470) \rightarrow \omega(\pi\pi)_{S-wave}$  or  $\eta(1405) \rightarrow \eta(\pi\pi)_{S-wave}$ .

Summarising, we do not consider the large branching to  $f_0\pi$  as convincing evidence for an exotic nature of the  $\pi 1800$ , and it will be discussed as regular second radial excitation of the pion.”

## 8.2 The $K$ radial excitations

### 8.2.1 The $K(1460)$

The  $K(1460)$  was observed in two experiments, at SLAC by Brandenburg *et al.* [937] and at CERN by Daum *et al.* [219]. The SLAC experiment reported the resonance in its  $K(\pi\pi)_{S-wave}$  decay. In view of the difficulties in identifying the  $\pi(1300)$  in its  $\pi(\pi\pi)_{S-wave}$  decay mode, we disregard this observation. The CERN analysis identified three decay modes of the  $K(1460)$  with

$$\Gamma_{K(1460) \rightarrow K^*(892)\pi} \sim 109 \quad \Gamma_{K(1460) \rightarrow K\rho} \sim 34 \quad \Gamma_{K(1460) \rightarrow K_0^*(1430)\pi} \sim 117 \quad (8.2)$$

The state was not observed in the LASS experiment.

### 8.2.2 The $K(1830)$

There is one indication for the second radial excitation of the Kaon from a study of the  $\phi K$  final state in the Omega spectrometer at CERN. Mass and width ( $M, \Gamma \sim 1830, 250$ ) MeV/c<sup>2</sup> were reported [938].

## 8.3 Isoscalar resonances

### 8.3.1 The $\eta(1295)$

In 1979, there was a claim for a new meson resonance with quantum numbers  $(I^G)J^{PC} = (0^+)0^{-+}$  at a mass of 1275 MeV/c<sup>2</sup> and 70 MeV/c<sup>2</sup> width from a phase-shift analysis of the  $\eta\pi^+\pi^-$  system produced in a 8.45 GeV/c pion beam [939]. The resonance is now called  $\eta(1295)$ ; it was later confirmed in other analyses [252, 256, 288, 940, 941] of experiments studying pion-induced reactions.

This state has a decisive influence on the interpretation of the nonet of pseudoscalar radial excitations. It is observed at a mass of  $1294 \pm 4$  MeV/c<sup>2</sup>, below the mass of the  $\pi(1300)$ , and a width of  $\Gamma = 55 \pm 5$  MeV/c<sup>2</sup> [1], much narrower than its isovector  $2^1S_0$  partner. It has been reported to decay into  $a_0(980)\pi$  and  $\eta\pi\pi$  and this may explain why it is so narrow: the most prominent decay mode of the  $\pi(1300)$  is, supposedly,  $\rho\pi$ , and there is no corresponding  $\eta(1295)$  decay mode. The  $\eta(1295)$  is the lowest-mass pseudoscalar meson with  $I = 0$  above the  $\eta'$  and is thus naturally interpreted as radial excitation of the  $\eta$  as proposed by Cohen and Lipkin [942]. It is nearly degenerate in mass with the  $\pi(1300)$ , hence the pseudoscalar radial excitations are expected to be

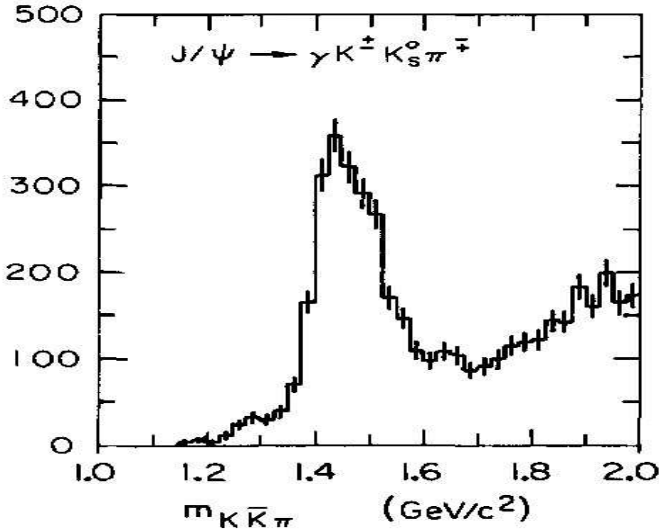


Fig. 69. The  $K\bar{K}\pi$  invariant mass distribution produced in radiative  $J/\psi$  decays by the MarkIII collaboration [470]. The structure is resolved into two pseudoscalar states and a  $J^{PC} = 1^{++}$  resonance.

ideally mixed. The isoscalar partner of  $\eta(1295)$  should then have a mass of 1500 MeV/c<sup>2</sup> [942] and should, as  $s\bar{s}$  state, decay dominantly into  $K\bar{K}^*$  +  $K^*\bar{K}$ .

### 8.3.2 The $\eta(1440)$

The  $\eta(1440)$  was discovered in 1965 in  $p\bar{p}$  annihilation at rest into  $(K\bar{K}\pi)\pi^+\pi^-$  [943]. Mass, width and quantum numbers were determined to be  $M = 1425 \pm 7$ ,  $\Gamma = 80 \pm 10$  MeV/c<sup>2</sup>, and  $J^{PC} = 0^{-+}$  [73]. In parallel, a further resonance was found in the charge exchange reaction  $\pi^-p \rightarrow nK\bar{K}\pi$ , using a 1.5 to 4.2 GeV/c pion beam [944]. It had mass and width  $M = 1420 \pm 20$ ,  $\Gamma = 60 \pm 20$  MeV/c<sup>2</sup>; quantum numbers  $J^{PC} = 1^{++}$  were suggested on the basis of the production characteristics. Even though the quantum numbers were different, both particles were called E-meson.

In 1980, the MARKII collaboration observed a strong signal in radiative  $J/\psi$  decays into  $(K^\pm K_S^0 \pi^\mp)$  [75]. Mass and width,  $M = 1440 \pm 20$ ,  $\Gamma = 50 \pm 30$  MeV/c<sup>2</sup> were compatible with those of the E-meson with which the signal was tentatively identified. In [77], pseudoscalar quantum numbers were found and the E-meson was renamed to  $\iota(1440)$  to underline the claim that a new meson was discovered and that this new meson was the  $\iota^{\text{st}}$  observed glueball. These results prompted a reanalysis of the bubble chamber data [73]. The  $J^{PC} = 0^{-+}$  quantum numbers were confirmed and  $J^{PC} = 1^{++}$  quantum numbers were shown to be incompatible with the data [74]. The Crystal Ball collaboration studied  $J/\psi \rightarrow \gamma(K^+K^-\pi^0)$  and  $\eta\pi\pi$  [77, 945]; the partial wave analysis confirmed  $J^{PC} = 0^{-+}$  quantum numbers. The Asterix experiment at LEAR deduced pseudoscalar quantum numbers for the state using arguments based on  $\bar{p}p$  annihilation dynamics [317], in agreement with the partial wave analysis of Crystal Barrel data on  $\bar{p}p \rightarrow \eta\pi^+\pi^-\pi^0\pi^0$  [332].

Higher statistics revealed that the peak at 1440 MeV/c<sup>2</sup> has a more complex structure [472, 946], see Fig. 69. The MarkIII collaboration suggested a pattern of three states, two pseudoscalar states at  $M = 1416 \pm 8^{+7}_{-5}$ ;  $\Gamma = 91^{+67+15}_{-31-38}$  MeV/c<sup>2</sup> (mainly  $a_0(980)\pi$ ) and  $M = 1490^{+14+3}_{-8-6}$ ;  $\Gamma = 54^{+37+13}_{-21-24}$  MeV/c<sup>2</sup> (mainly  $K^*K$ ), and a  $J^{PC} = 1^{++}$  resonance at 1440 MeV/c<sup>2</sup> [472]. DM2 found two pseudoscalar states, a low-mass (1420 MeV/c<sup>2</sup>) component coupling to  $K^*K$  and a high-mass (1460 MeV/c<sup>2</sup>) component decaying into  $a_0(980)\pi$ . Furthermore, DM2 studied radiative decays

into  $\eta\pi\pi$  (with  $a_0(980)\pi$  as isobar) which peaks at the lower mass. They conclude that the 1440 mass region was not yet fully understood.

In a partial wave analysis of BES data on  $J/\psi \rightarrow \gamma(K^\pm K_S^0 \pi^\mp)$  [472,482] and to  $\gamma(K^+ K^- \pi^0)$  [473], the  $\eta(1440)/\iota$  region was fitted with a Breit-Wigner amplitude with  $s$ -dependent widths. Decays into  $K^*K$ ,  $\kappa K$ ,  $\eta\pi\pi$  and  $\rho\rho$  were included ( $\kappa$  refers to the  $K\pi$  S-wave). At a  $K\bar{K}\pi$  mass of  $\sim 2040$  MeV/c $^2$ , a second peak with width  $\sim 400$  MeV/c $^2$  was seen;  $J^P = 0^-$  was preferred over  $1^+$  and  $2^-$  respectively. The authors suggested the state as candidate for a  $0^- s\bar{s}g$  hybrid partner of  $\pi(1800)$ .

The  $\eta(1440)$  region was also studied in hadronic reactions. At BNL, it was reported in  $\pi^- p$  charge exchange and in  $\bar{p}p$  annihilation in flight. With an 8 GeV/c pion beam [947] and in  $\bar{p}p$  annihilation [948], the  $\eta(1440)$  was reported at 1420 MeV/c $^2$  and with  $a_0(980)\pi$  as dominant decay mode while in a 21 GeV/c pion beam, the most prominent feature was a pseudoscalar meson at 1460 MeV/c $^2$  mass decaying into  $K^*\bar{K} + c.c.$  [949].

The  $\eta(1440)$  is a very strong signal, one of the strongest, in radiative  $J/\psi$  decays. The radial excitation  $\eta(1295)$  is not seen in this reaction; hence the  $\eta(1440)$  must have a different nature. At that time it was proposed (and often still is [1,950,951]) to be a glueball.

Table 23

Popular interpretation of the spectrum of pseudoscalar radial excitations [1,950,951].

$\pi$	$\eta$	$\eta'$	$K$
$\pi(1300)$	$\eta(1295)$	$\eta(1405)$	$\eta(1475)$
$n\bar{n}$	$n\bar{n}$	glueball	$s\bar{s}$

### 8.3.3 The split $\eta(1440)$

The Obelix collaboration at LEAR [392] studied the reaction  $p\bar{p} \rightarrow \pi^+\pi^- K^\pm K_S^0 \pi^\mp$  at 3 different densities. The  $\pi^+\pi^-$  system recoiling against  $K^\pm K_S^0 \pi^\mp$  has very little energy and is hence likely in S-wave. Likewise, there is no angular momentum to be expected between  $(\pi^+\pi^-)$  and  $(K^\pm K_S^0 \pi^\mp)$ . Then, the most likely initial state of the  $p\bar{p}$  atom from which annihilation occurs has the quantum numbers of the  $(K^\pm K_S^0 \pi^\mp)$  system [317]. This selection rule helps in the partial wave analysis.

The Obelix partial wave analysis confirmed the conjecture of MARKIII that the  $\eta(1440)$  is split into two components, an  $\eta(1405) \rightarrow a_0(980)\pi$  with  $M = 1405 \pm 5$ ,  $\Gamma = 56 \pm 6$  MeV/c $^2$  and an

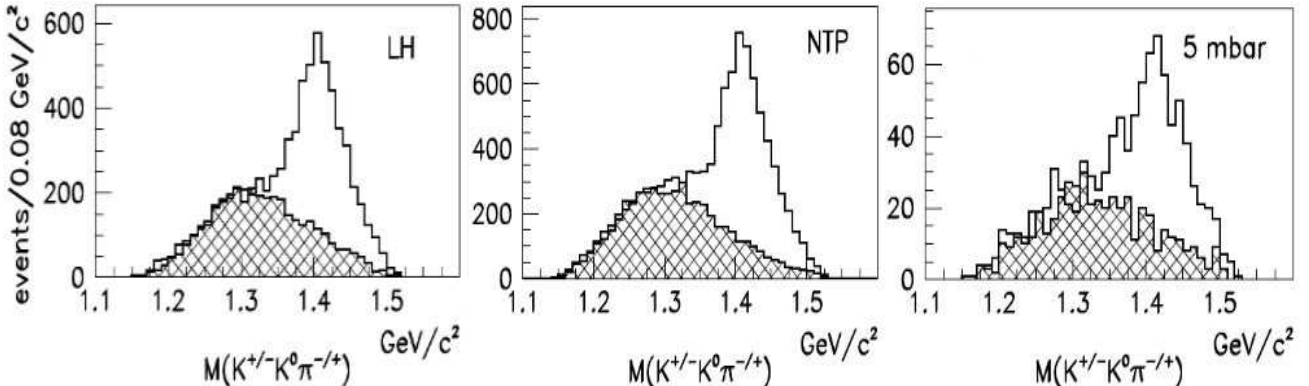


Fig. 70. The  $K^\pm K_S^0 \pi^\mp$  invariant mass distribution from  $p\bar{p}$  annihilation at rest at 3 different target densities [392]. There are two entries per event. The hatched area is the expected background from the 'wrong'  $(K^\pm K_S^0 \pi^\mp)$  combination.

$\eta(1475) \rightarrow K^* \bar{K} + \bar{K}^* K$  with  $M = 1475 \pm 5$ ,  $\Gamma = 81 \pm 11 \text{ MeV}/c^2$ . Even though a bit low in mass, the  $\eta(1475)$  fits well the properties expected for a  $s\bar{s}$  pseudoscalar radial excitation. The  $\eta(1405)$  finds no 'slot' in the spectrum of  $\bar{q}q$  resonances, it is an intruder, possibly a glueball. Since 2002, the Particle Data Group supports this interpretation of the pseudoscalar mesons with the caveat that lattice gauge calculations predict the pseudoscalar glueball mass well above 2000  $\text{MeV}/c^2$ .

Two quantitative tests have been proposed to test if a particular meson is glueball-like: the stickiness [706] and the gluiness [707] which are expected to be close to unity for normal  $q\bar{q}$  mesons. They were introduced in section 4.1.2, eqs. (4.8) and (4.9). The L3 collaboration determined [687] the stickiness to  $S_{\eta(1440)} = 79 \pm 26$  and the gluiness ( $G$ ) to  $G_{\eta(1440)} = 41 \pm 14$ . No distinction was made in [687] between  $\eta(1405)$  and  $\eta(1475)$ . These numbers can be compared to those for the  $\eta'$  for which  $S_{\eta'} = 3.6 \pm 0.3$  and  $G_{\eta'} = 5.2 \pm 0.8$  was determined, with  $\alpha_s(958 \text{ MeV}/c^2) = 0.56 \pm 0.07$ . Also  $\eta'$  is 'gluish', but much more the  $\eta(1405)$ . The  $\eta(1405)$  has properties as expected from a glueball.

The L3 data were challenged by the CLEO collaboration [578]. Fig. 71 shows their  $K_S^0 K^\pm \pi^\mp$  mass distributions for different bins of the transverse momentum transfer  $p_\perp$  from  $e^+e^-$  to the  $K_S^0 K^\pm \pi^\mp$  system. For two nearly real photons,  $p_\perp$  is small; two on-shell photons do not couple to  $J^P = 1^+$  mesons (Young's theorem) while pseudoscalar meson decays to  $2\gamma$  are allowed. The absence of signals at 1285  $\text{MeV}/c^2$  and 1440  $\text{MeV}/c^2$  in Fig. 71 proves that the signal observed for large  $p_\perp$  is due to axial vector mesons. With no pseudoscalar state observed, it is difficult to arrive at any definite conclusion concerning their nature. Both, pseudoscalar radial excitations and a pseudoscalar glueball (if it exists in this mass range) may have small couplings to  $\gamma\gamma$ .

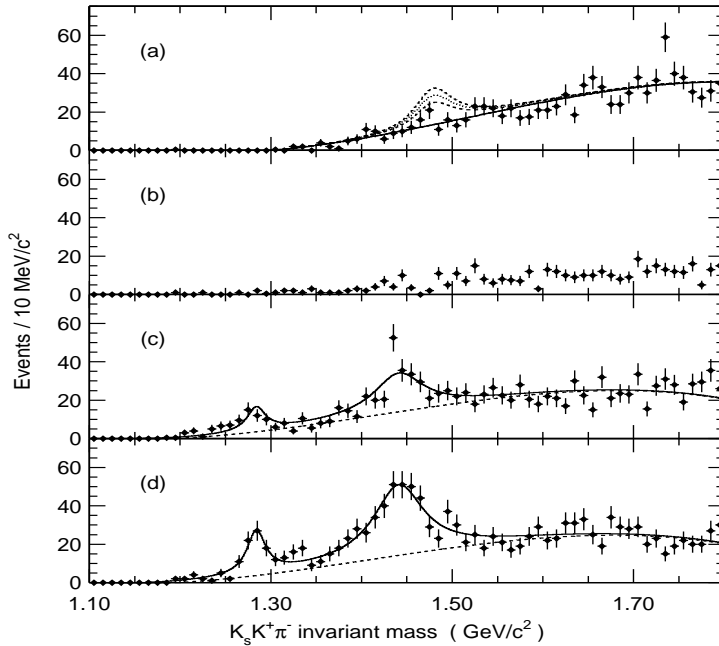


Fig. 71. The distributions of the  $K_S^0 K^\pm \pi^\mp$  invariant mass from the CLEO experiment [578]. The distributions are shown for (a)  $p_\perp \leq 100 \text{ MeV}/c$ , (b)  $100 \text{ MeV}/c \leq p_\perp \leq 200 \text{ MeV}/c$  and (c)  $200 \text{ MeV}/c \leq p_\perp \leq 600 \text{ MeV}/c$  in the untagged mode, and (d) for all  $p_\perp$  in the tagged mode. The dashed curves in (a) show the strength of the expected  $\eta(1440)$  signal according to the L3 results [687]. The solid curves represent fits with resonances and polynomial non-interfering combinatorial backgrounds. Figure (a) shows dotted and dashed distributions expected from L3, using their  $\gamma\gamma \rightarrow \eta(1440)$  yield and error.

The  $\rho\gamma$  decay mode is disturbing for the glueball interpretation. At BES,  $\eta(1295)$  and  $\eta(1440)$  were studied in  $J/\psi \rightarrow (\rho\gamma)\gamma$  and  $\rightarrow (\phi\gamma)\gamma$  [487]. A peak below 1300 MeV/c<sup>2</sup> was assigned to  $f_1(1285)$  even though a small contribution from  $\eta(1295)$  was not excluded. The  $\eta(1440)$  (observed at 1424 MeV/c<sup>2</sup>) was seen to decay strongly into  $\rho\gamma$  and not into  $\phi\gamma$ . Neither a glueball nor a  $s\bar{s}$  state should decay radiatively into a  $\rho$  meson. A small  $\bar{u}u + \bar{d}d$  component in the  $\eta(1475)$  wave function could be responsible for this decay mode but then, a large  $\phi\gamma$  decay rate should be expected. This however is not observed. The only escape is the assumption that the  $\rho\gamma$  events stem from the  $f_1(1420)$ . The spin-parity analysis prefers pseudoscalar quantum numbers for the peak at 1424 MeV/c<sup>2</sup> but  $1^{++}$  is not completely ruled out.

### 8.3.4 Isoscalar resonances revisited

There are severe inconsistencies in the scenario presented above (in section 8.3.1-8.3.3). The  $\eta(1295)$  is seen only in pion induced reactions. Radiative  $J/\psi$  decays show an asymmetric peak in the  $\eta(1440)$  region; therefore  $\eta(1405)$  and the  $\eta(1475)$  are both produced in radiative  $J/\psi$  decays. The  $\eta(1295)$  as isoscalar partner must then also be produced, but it is not - at least not with the expected yield.

There are a few reasons not to accept  $\eta(1295)$  as established resonance. It is approximately degenerate in mass and width with  $f_1(1285)$ . This is potentially dangerous. The matrix element for a pseudoscalar meson decaying into three pseudoscalar mesons does not have any peculiarities, all distributions are isotropic and flat. This decay looks like a ‘garbage can’. Any imperfection in the description of the dominant isoscalar  $1^{++}$  wave leads inevitably to the appearance of a spurious signal in the  $0^{-+}$  wave. A number of imperfections could lead to such a feedthrough: not perfectly understood acceptance or resolution, not fully justified assumptions in the PWA model like coherence of the  $1^{++}$  and/or the  $0^{-+}$  wave in production, a non-perfect parametrisation of  $f_1(1285)$  decays or any other imperfection. The feedthrough signal has a Breit-Wigner amplitude including a phase motion, but the parameters of the two resonances are similar.

The L3 observation of  $\gamma\gamma$  fusion into  $\eta(1440)$  but not into  $\eta(1295)$  is problematic. The  $n\bar{n}$  state should have larger  $\gamma\gamma$  couplings than a glueball or  $s\bar{s}$  state. However, CLEO finds neither  $\eta(1295)$  nor  $\eta(1440)$ , and there is no conflict (but also no evidence for  $\eta(1295)$ , neither).

The Crystal Barrel collaboration searched for the  $\eta(1295)$  and  $\eta(1440)$  in the reaction  $p\bar{p} \rightarrow \pi^+\pi^-\eta(xxx)$ ,  $\eta(xxx) \rightarrow \eta\pi^+\pi^-$ . The search was done by assuming the presence of a pseudoscalar state of given mass and width; mass and width were varied and the likelihood of the fit plotted. Fig. 72a shows such a plot [952]; a clear pseudoscalar resonance signal is seen at 1405 MeV/c<sup>2</sup>. Two decay modes are observed,  $a_0(980)\pi$  and  $\eta(\pi\pi)_{S-wave}$  with a ratio  $0.6 \pm 0.1$ .

A scan for an additional  $0^+0^{-+}$  resonance provides no evidence for the  $\eta(1295)$  but for a second resonance at 1490 MeV/c<sup>2</sup>, see Fig. 72b, with  $M = 1490 \pm 15$ ,  $\Gamma = 74 \pm 10$  MeV/c<sup>2</sup>. It decays to  $a_0(980)\pi$  and  $\eta(\pi\pi)_{S-wave}$  with a ratio  $0.16 \pm 0.10$ . This data could be interpreted as first evidence for  $\eta(1475) \rightarrow \eta\pi\pi$  decays.

Amsler and Masoni reinforced the existence of  $\eta(1295)$  by claiming additional evidence from four further observations, unrelated to pion induced reactions (see [1], page 591).

- In an analysis of the reaction  $p\bar{p} \rightarrow \eta\pi^+\pi^-\pi^0\pi^0$  [332], the  $\eta(1405)$  was studied and the decay mode  $\sigma\eta$  was observed for the first time. The likelihood of the fit improved when a  $\eta(1295)$  was

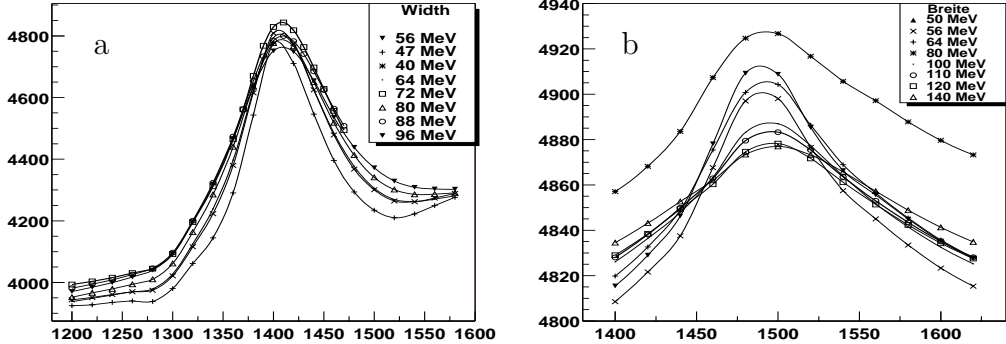


Fig. 72. Scan for a  $0^+0^{-+}$  resonance with different widths [952]. a: The likelihood optimises for  $M = 1407 \pm 5$ ,  $\Gamma = 57 \pm 9$  MeV/c $^2$ . The resonance is identified with the  $\eta(1405)$ . b: A search for a second pseudoscalar resonance (right panel) gives evidence for the  $\eta(1475)$  with  $M = 1490 \pm 15$ ,  $\Gamma = 74 \pm 10$  MeV/c $^2$ .

added. No further study was reported; in particular  $\eta(1295)$  was not replaced by  $f_1(1285)$  so that the fit likelihoods cannot be compared.

- In [953], the partial wave analysis of the reaction  $p\bar{p} \rightarrow \eta\pi^+\pi^-\pi^+\pi^-$  was directed to determine properties of  $f_0(1370)$ . A small  $\eta(1295)$  signal was found but at 1255 MeV/c $^2$ . Studies at Bonn demonstrated that the peak was faked by the Monte Carlo simulation in which the trigger condition was not sufficiently well reproduced (the same Monte Carlo data sets were used in both analyses). The small enhancement at 1260 MeV/c $^2$  in Fig. 72 is the effect which remains once the trigger condition was described more precisely in the Monte Carlo simulation.
- In another paper on  $p\bar{p} \rightarrow \eta\pi^+\pi^-\pi^+\pi^-$  by Amsler *et al.* [355] a low-mass peak  $X(1285)$  was assumed to be the  $f_1(1285)$ . A fit with  $f_1(1285)$  mass and width gave the best description. However, the possibility that the peak is due to the  $\eta(1295)$  was not excluded.
- The DM2 data on  $J/\psi \rightarrow \gamma\eta\pi\pi$  showed a small peak at 1265 MeV/c $^2$  and a larger one at 1400 MeV/c $^2$  [946]. The partial wave analysis preferred pseudoscalar quantum numbers for the peak at 1265 MeV/c $^2$  even though there is no comment on this aspect in the paper. The second peak at 1400 MeV/c $^2$  is interpreted as  $f_1(1420)/c^2$ . The  $K\bar{K}\pi$  pseudoscalar wave was fitted with two resonances in the pseudoscalar partial wave at 1420 MeV/c $^2$  in  $K^*K$  and at 1460 MeV/c $^2$  in  $a_0(980)$ , and one  $f_1(1460)$ . These findings contradict in most aspects more recent results based on larger statistical samples. We refuse to use these data as argument in favour of the existence of  $\eta(1295)$ .

We conclude that even a large number of cases which are individually not convincing do not make up a convincing argument. A major further point against the existence of  $\eta(1295)$  are internal inconsistencies: the interpretation of  $\eta(1295)$  and  $\pi(1300)$  as radial excitations would imply that the nonet of pseudoscalar radial excitation were ideally mixed. It is then not possible that the  $s\bar{s}$  state  $\eta(1475)$  is produced strongly in  $\bar{p}p$ , the  $n\bar{n}$  state  $\eta(1295)$  weakly. This behaviour would contradict violently what we have learned about the  $\bar{p}p$  annihilation process [730]. There is no way to understand why the yield of the  $s\bar{s}$  state  $\eta(1475)$  in radiative  $J/\psi$  decays is large and the  $\eta(1295)$  hardly visible. Hence  $\eta(1295)$  cannot be a  $q\bar{q}$  meson. On the other hand, we do not expect glueballs, hybrids or multiquark states so low in mass. An interpretation of  $\eta(1295)$  as exotic particle is hence unlikely even though not excluded. A possible origin of  $\eta(1295)$  might be interference of  $f_1(1285)$  with the  $\eta(\pi\pi)_{S-wave}$  Deck amplitude, faking  $\eta(1295)$ . Here, it is excluded from the further discussion.

The next puzzling state is the  $\eta(1440)$ . It is not produced as  $\bar{s}s$  state but decays with a large fraction into  $K\bar{K}\pi$  and it is split into two components. It was suggested in [954] that the origin of these anomalies is due to a node in the wave function of the  $\eta(1440)$ . This node has an impact on the decay matrix elements as calculated by Barnes *et al.* [58] within the  ${}^3P_0$  model.

The matrix elements for decays of the  $\eta(1440)$  as a radial excitation ( $=\eta_R$ ) depend on spins, parities and decay momenta of the final state mesons. For  $\eta_R$  decays to  $K^*K$ , the matrix element is given by

$$f_P = \frac{2^{9/2} \cdot 5}{3^{9/2}} \cdot x \left( 1 - \frac{2}{15} x^2 \right). \quad (8.3)$$

In this expression,  $x$  is the decay momentum in units of 400 MeV/c; the scale is determined from comparisons of measured partial widths to model predictions. The matrix element vanishes for  $x = 0$  and  $x^2 = 15/2$ , or  $p = 1$  GeV/c. These zeros have little effect on the shape of the resonance.

The matrix element for  $\eta_R$  decays to  $a_0(980)\pi$  or  $(\pi\pi)_{S-wave}\eta$  has the form

$$f_S = \frac{2^4}{3^4} \cdot \left( 1 - \frac{7}{9} x^2 + \frac{2}{27} x^4 \right) \quad (8.4)$$

and vanishes for  $p = 0.45$  GeV/c. The amplitude for  $a_0(980)\pi$  decays vanishes at 1440 MeV/c<sup>2</sup>. This has a decisive impact on the shape, as seen in Figure 73. Shown are an undistorted Breit-Wigner function, the transition matrix elements for three  $\eta(1440)$  decay modes as given by Barnes *et al.* [58], and the product of the squared matrix elements and a Breit-Wigner distribution with mass 1420 MeV/c<sup>2</sup> and width 60 MeV/c<sup>2</sup>.

The  $\eta(1440) \rightarrow a_0(980)\pi$  and  $\rightarrow K^*K$  mass distributions have different peak positions; at approximately the  $\eta(1405)$  and  $\eta(1475)$  masses. Hence there is no need to introduce  $\eta(1405)$  and  $\eta(1475)$  as two independent states. One  $\eta(1420)$  and the assumption that it is a radial excitation describe the data. Of course, the  ${}^3P_0$  model for meson decays is a model. Model-independent is however the observation that zeros in the wave functions can lead to distortions in the final states observed. If two resonances are found having identical quantum numbers and very close in mass, extreme care must be taken before far-reaching claims on the abundances of meson resonances in that partial wave can be made.

The conclusion that  $\eta(1405)$  and  $\eta(1475)$  is one single resonance can be tested further by following

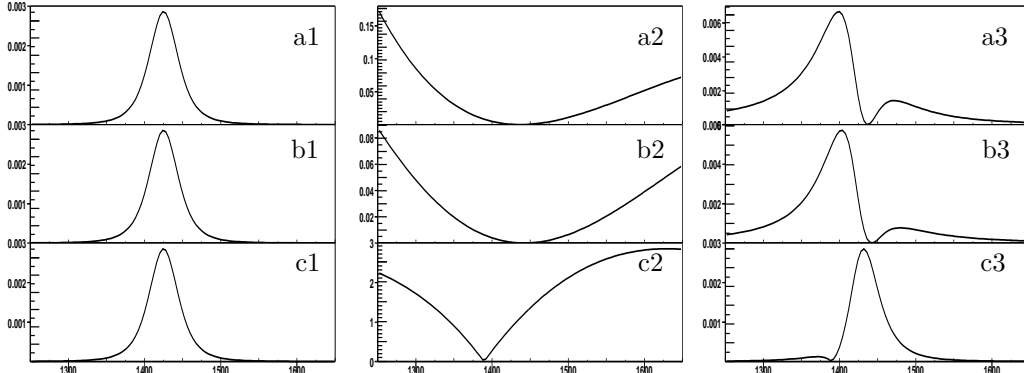


Fig. 73. Amplitudes for  $\eta(1440)$  decays to  $a_0\pi$  (a),  $(\pi\pi)_{S-wave}\eta$  (b), and  $K^*\bar{K}$  (c); the Breit-Wigner functions are shown (1), then (2) the squared decay amplitudes using eqs. (8.3),(8.4), and (3) the resulting squared transition matrix element.

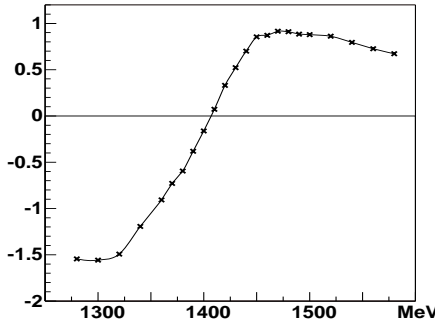


Fig. 74. Phase motion of the  $a_0(980)\pi$  isobars in  $p\bar{p}$  annihilation into  $4\pi\eta$ . In the mass range from 1300 to 1500 MeV/c<sup>2</sup> the phase varies by  $\pi$  indicating that there is only one resonance in the mass interval. The  $(\pi\pi)_{S-wave}\eta$  (not shown) exhibits the same behaviour [952].

the phase motion of the  $a_0(980)\pi$  or  $(\pi\pi)_{S-wave}\eta$  isobar [952]. The phase changes by  $\pi$  and not by  $2\pi$ , see Fig. 74.

Summarising, the results for the radial excitations of pseudoscalar mesons are as follows:

- The  $\eta(1295)$  is not a  $q\bar{q}$  meson. The source of the signal might be the Deck effect and feedthrough from the  $f_1(1285)$  wave.
- The  $\eta(1440)$  wave function has a node leading to two apparently different states  $\eta(1405)$  and  $\eta(1475)$ .
- There is only one  $\eta$  state, the  $\eta(1440)$ , in the mass range from 1200 to 1500 MeV/c<sup>2</sup> and not 3!
- The  $\eta(1440)$  is the radial excitation of the  $\eta$ . The radial excitation of the  $\eta'$  is expected at about 1800 MeV/c<sup>2</sup>.

## 8.4 Higher-mass $\eta$ excitations

### 8.4.1 Selection rules

We begin this section with a Table (24) which summarises selection rules for two-body decays of  $\eta$  excitations into pseudoscalar, scalar, and vector mesons. Decays into two pseudoscalar or two scalar mesons are forbidden due to parity and charge conjugation conservation. The selection rules are expressed by the SU(3) singlet and octet components of the (pseudo-)scalar mesons. The  $K^*K$  decays are particularly interesting since they identify octet states. For that reason,  $\eta(1440)$  must be a flavour octet state or at least have a large octet component.

Table 24  
SU(3) selection rules for excited  $\eta$  states.

$\eta_1 \rightarrow PS + V$		$\eta_8 \rightarrow PS + V$		$K^*K$
$\eta_1 \rightarrow PS + S$	$f_{0(1)}\eta_1, f_{0(8)}\eta_8, a_0\pi, K_0^*K$	$\eta_8 \rightarrow PS + S$	$f_{0(1)}\eta_8, f_{0(8)}\eta_1, a_0\pi, K_0^*K$	
$\eta_1 \rightarrow V + V$	$\omega\omega, \rho\rho, K_0^*K_0^*$	$\eta_8 \rightarrow V + V$	$\omega\omega, \rho\rho, K_0^*K_0^*$	

#### 8.4.2 $\eta$ excitations from radiative $J/\psi$ decays

There are several candidates for pseudoscalar isoscalar excitations above  $1.5 \text{ GeV}/c^2$ . MarkIII reported evidence for dominance of the  $I^G(J^{PC}) = 0^+(0^{-+})$  partial wave below  $2 \text{ GeV}/c^2$  in radiative  $J/\psi$  decays into  $\rho\rho$  [955] and  $\omega\omega$  [956]. Summarizing MarkIII results, Eigen reported strong pseudoscalar activity below  $2 \text{ GeV}/c^2$  for  $\rho\rho$ ,  $\omega\omega$  and, above their respective thresholds, for  $K^*K^*$  and  $\phi\phi$  [957]. The analysis of DM2 data suggested 3 states,  $\eta(1500)$ ,  $\eta(1800)$ , and  $\eta(2100)$ , decaying into  $\rho\rho$  [958], and possible evidence for a  $\phi\phi$  pseudoscalar meson at  $2.24 \text{ GeV}/c^2$  [959]. Bugg noticed [960] that the three DM2 peaks coincide in mass and width with three peaks in the  $\eta\eta$  mass spectrum produced in  $\bar{p}p$  annihilation in flight into  $\pi^0\eta\eta$ . Any  $\eta\eta$  resonance must have natural spin-parity quantum numbers; a reanalysis of Mark3 data on  $J/\psi \rightarrow 4\pi$  (the DM2 data were no longer available) suggested that the decay mode should not be in the  $\rho\rho$  pseudoscalar wave but in the  $(\pi\pi)_{S\text{-wave}}(\pi\pi)_{S\text{-wave}} 0^{++}$  scalar wave [960]. The analysis was repeated with BES data; the scalar quantum numbers of the three states were confirmed [477] suggesting the three  $\rho\rho$  resonances at 1500, 1760, and 2100  $\text{MeV}/c^2$  should be interpreted as  $f_0$  mesons in their  $\sigma\sigma$  decays.

Recently, BES reported results from a partial wave analysis of radiative  $J/\psi$  decays into  $\omega\omega$  [506]. Fig. 75 shows a strong enhancement in the  $\omega\omega$  invariant mass distribution at  $1.76 \text{ GeV}/c^2$ . A partial wave analysis found pseudoscalar quantum numbers to be dominant with small scalar and tensor contributions. The large yield stimulated the collaboration to discuss if the  $\eta(1760)$  has a significant glueball content.

A pseudoscalar  $\omega\omega$  resonance at  $1760 \text{ MeV}/c^2$ , glueball or  $q\bar{q}$  state, should couple to  $\rho\rho$ . Isospin invariance would require equal radiative rates for  $\rho^0\rho^0$  and  $\omega\omega$ . This is incompatible with data. For the moment, we assume that the  $\rho\rho$  signal at  $1760 \text{ MeV}/c^2$  is completely of pseudoscalar nature (in agreement with [955, 958] and in contrast to [477, 960]). The measured yields are  $(1.44 \pm 0.12 \pm 0.21) \cdot 10^{-3}$  for  $\rho\rho$  [958] and  $(1.98 \pm 0.08 \pm 0.32) \cdot 10^{-3}$  for  $\omega\omega$  [506], respectively. The  $\rho\rho$  yield should be 3 times larger than that for  $\omega\omega$ . Thus isospin is badly broken, by about a factor 4. When the  $\rho\rho$  signal has scalar quantum numbers [477, 960], this factor is even larger. There must be a dynamical reason for the large pseudoscalar  $\omega\omega$  contribution. Possibly, the  $c\bar{c}$  converts into a photon plus two gluons which hadronise into two coloured  $\omega$  mesons. They then neutralise in colour in the final state and undergo final-state interactions. This process is impossible for two  $\rho$  mesons.

Further pseudoscalar signals were reported by the BES collaboration. In  $J/\psi \rightarrow \gamma K\bar{K}\pi$  [482], the  $\eta(1440)$  is seen; the PWA gave evidence for a further resonance, above  $2000 \text{ MeV}/c^2$  and called  $\eta(2050)$  here. Mass and width are given in Table 25. Data on radiative production of  $K^*K^*$  show

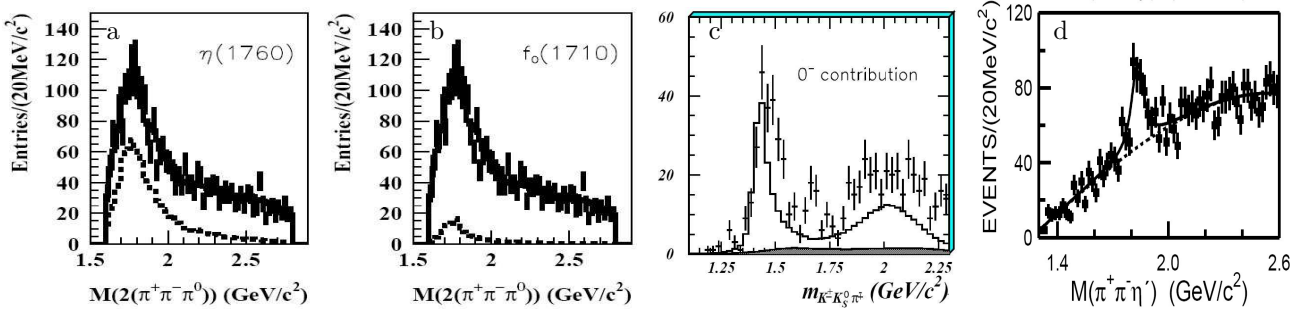


Fig. 75. Radiative decays of  $J/\psi$  to  $\omega\omega$  with pseudoscalar and the scalar wave as determined from PWA [506].  $J/\psi$  decays into  $\gamma K\bar{K}\pi$  [482] show  $\eta(1440)$  and a broad  $\eta(2040)$ . In radiative  $J/\psi$  decays into  $\pi^+\pi^-\eta'$  a narrow peak at  $1835 \text{ MeV}/c^2$  is observed [497].

(as the MarkIII data [957]) a wide pseudoscalar distribution [476] which can be fitted with a broad pseudoscalar resonance at  $\sim 1800 \text{ MeV}/c^2$ . Data on  $J/\psi \rightarrow \gamma\eta\pi\pi$  [479] confirmed previous findings on the  $\eta(1440)$  (but did not require a splitting into two components). At higher mass, two pseudoscalar states were observed with masses and widths collected in Table 25.

Bugg, Dong and Zou [961] fitted data on radiative decays of  $J/\psi$  to various final state with a single Breit-Wigner resonance having s-dependent widths proportional to the available phase space in each channel. This resonance has a K-matrix mass  $2190 \pm 50 \text{ MeV}/c^2$  and a width  $\Gamma = 850 \pm 100 \text{ MeV}/c^2$ . Within errors, decays are flavour-blind. The resonance was suggested to be a pseudoscalar glueball.

In the reaction  $J/\psi \rightarrow \gamma\pi^+\pi^-\eta'$ , a narrow peak called  $X(1835)$  was observed with a statistical significance of  $7.7\sigma$ . The data are shown in Fig. 75. A fit with a Breit-Wigner function gave mass and width  $M = 1833.7 \pm 6.1(\text{stat}) \pm 2.7(\text{syst}) \text{ MeV}/c^2$  and  $\Gamma = 67.7 \pm 20.3(\text{stat}) \pm 7.7(\text{syst}) \text{ MeV}/c^2$ , respectively, and a yield  $\mathcal{B}(J/\psi \rightarrow \gamma X) \cdot \mathcal{B}(X \rightarrow \pi^+\pi^-\eta') = (2.2 \pm 0.4_{\text{stat}} \pm 0.4_{\text{syst}}) \cdot 10^{-4}$ . No partial wave analysis has been made but based on production and decay, an interpretation as  $\eta(1835)$  is most likely. In [962],  $X(1835)$  is suggested to be the 2<sup>nd</sup> radial excitation of the  $\eta'$ . We rather believe it to be the 1<sup>st</sup>  $\eta'$  radial excitation. In this interpretation,  $X(1835)$  decays into  $\eta'$  and the singlet part of  $\sigma(485)$ . Decays into an octet  $\eta$  and the  $\sigma(485)$  octet fraction might be small leading to the observed narrow width. The BES collaboration suggests that  $X(1835)$  is related to  $p\bar{p}$  mass threshold enhancement, also observed in radiative  $J/\psi$  decays.

Table 25 collects the BES results on pseudoscalar meson production in radiative  $J/\psi$  decays. There is no clear separation into strong and weak radiative yields. The commonly used picture of radiative  $J/\psi$  decays in which the  $c\bar{c}$  system radiates off a photon and two gluons forming

Table 25

BES results on radiative  $J/\psi$  decay into pseudoscalar mesons  $X$  and tentative SU(3) assignments. The  $\eta(2000)$  is proposed as flavour-blind background, possibly the ground-state pseudoscalar glueball. The yields are in unit of  $10^{-3}$ . The singlet/octet assignment is discussed in the text.

$X$	SU(3)	Decay	Mass ( $\text{MeV}/c^2$ )	Width ( $\text{MeV}/c^2$ )	Yield $J/\psi \rightarrow \gamma X$	Ref.
$\eta$	8				$0.90 \pm 0.10$	[1]
$\eta'$	1				$4.71 \pm 0.27$	[1]
$\eta(1440)$	8	$K^*K$			$2.8 \pm 0.6$	[1]
		$a_0\pi + f_0\eta$			$0.4 \pm 0.1$	[1]
		$\rho\rho$			$1.7 \pm 0.4$	[1]
$X(1835)$		$\eta'\pi^+\pi^-$	$1833.7 \pm 6.1 \pm 2.7$	$67.7 \pm 20.3 \pm 7.7$	$0.22 \pm 0.04 \pm 0.04$	[497]
$\eta(1760)$	8(?)	$\omega\omega$	$1744 \pm 10 \pm 15$	$244^{+24}_{-21} \pm 25$	$1.98 \pm 0.08 \pm 0.32$	[506]
		$\rho\rho$	$1775 \pm 20$	$115 \pm 50$	$1.44 \pm 0.12 \pm 0.21$	[958]*
		$\eta\pi^+\pi^-$	$1760 \pm 35$	$\sim 250$	$1.2 \pm 0.5$	[479]
$\eta(2070)$	1(?)	$\rho\rho$	$2080 \pm 40$	$210 \pm 40$	$1.32 \pm 0.15 \pm 0.21$	[958]*
		$K_0^*K$	$2040 \pm 50$	$400 \pm 90$	$2.1 \pm 0.1 \pm 0.7$	[482]
$\eta(2000)$	1	$\eta\pi^+\pi^-$	$\sim 1800$		$0.72 \pm 0.03$	[479]
		$K^*K^*$	$1800 \pm 100$	$500 \pm 200$	$2.3 \pm 0.2 \pm 0.7$	[476]
		$K_0^*K$	$\sim 1800$	$\sim 1000$	$(0.58 \pm 0.03 \pm 0.20)$	[482]
		<i>coupled</i>	$2190 \pm 50$	$850 \pm 100$		[961]

\* The pseudoscalar nature of the signal was rejected in [477, 960].

a flavour singlet expects large radiative yields for singlet production and small octet yields. Of course, unseen decay modes could change the pattern significantly.

The  $X(1835)$  is particularly interesting. As it may be related to the  $p\bar{p}$  mass threshold enhancement, we present also baryon-antibaryon threshold enhancements observed in other reactions even though there are mostly no quantum number determinations.

#### 8.4.3 Baryon-antibaryon threshold enhancements

The BES collaboration [484] observed a narrow  $p\bar{p}$  threshold enhancement in radiative  $J/\psi$  decay but not in  $J/\psi \rightarrow \pi^0 p\bar{p}$  nor in  $J/\psi \rightarrow \omega p\bar{p}$  (Fig. 76). It can be fitted with an  $S$ - or  $P$ -wave Breit-Wigner function giving masses of  $1859 \pm 6$  and  $1876 \pm 0.9$  MeV/c $^2$ , respectively. The absence of the enhancement in  $J/\psi \rightarrow \pi^0 p\bar{p}$  suggests positive  $C$ -parity; parity conservation and assuming low angular momenta  $\ell = 0$  or 1 restrict quantum numbers to  $0^{-+}$ ,  $0^{++}$ ,  $1^{++}$ , and  $2^{-+}$ . The absence of the signal in recoil to an  $\omega$  must be due to a special dynamical selection. A first sight of an anomalous behaviour at the  $p\bar{p}$  threshold had already been reported by the BELLE collaboration in  $B$  decays  $B^\pm \rightarrow p\bar{p}K^\pm$  [630]. Closer inspection shows, however, that the Belle and BES observations are very different in nature. The BELLE structure seen in  $B$  decays is much broader (with a width, estimated from the graph, of about 400 MeV/c $^2$ ) and resembles perhaps the  $p\bar{p}$  signal observed by BaBar in different decay modes of  $B$  mesons into  $D\pi p\bar{p}$  final states [622]. The BES signal has a visible width of about 60 MeV/c $^2$  and fits give values which are compatible with zero, hence the two phenomena observed at Belle and BES are likely different.

There have been several attempts to explain the BES result. The Jülich group analysed the data within their  $N\bar{N}$  model and were able to reproduce the  $p\bar{p}$  data with just one normalization parameter. The isovector part of  $N\bar{N}$  interactions plays the dominant rôle; fine-tuning is possible by adding final-state interactions with  $\pi(1800)$  as intermediate state [964]. An extension to  $B$

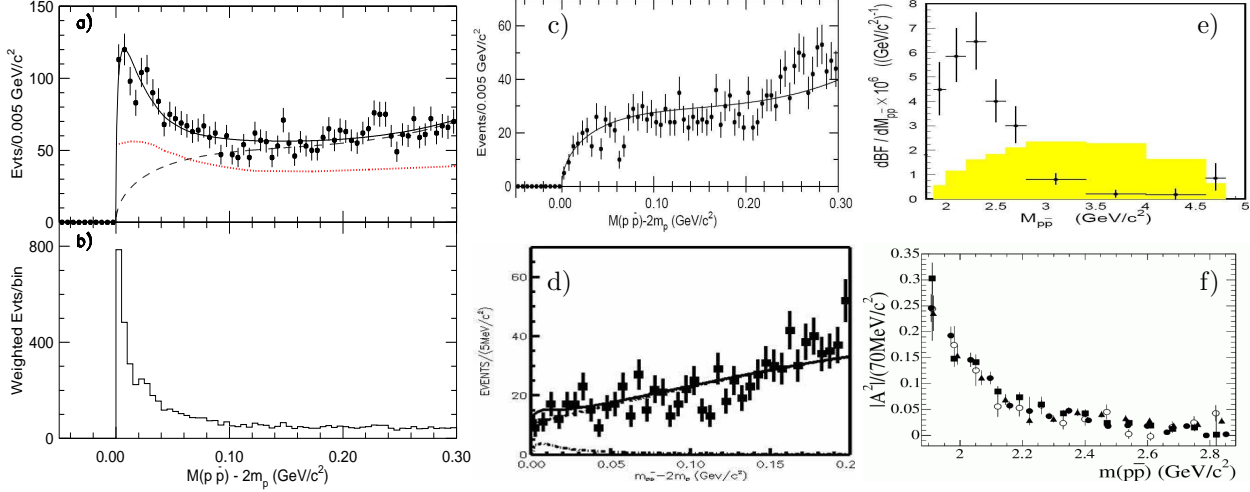


Fig. 76. a: The  $M_{p\bar{p}} - 2m_p$  distribution for  $J/\psi \rightarrow \gamma p\bar{p}$ . The data is fitted with a Breit-Wigner function plus background function represented by the dashed curve. The dotted curve gives the acceptance. b: The  $M_{p\bar{p}} - 2m_p$  distribution with events weighted by  $q_0/q$  [484]. The  $M_{p\bar{p}} - 2m_p$  distributions for c)  $J/\psi \rightarrow \pi^0 p\bar{p}$  ([484]) and for d)  $J/\psi \rightarrow \omega p\bar{p}$  ([963]) show no significant threshold enhancements. Invariant  $p\bar{p}$  mass distributions from: e)  $B^0 \rightarrow p\bar{p}K^0$ , BELLE experiment [639]; f) phase space-corrected  $p\bar{p}$  invariant mass distributions for four decay modes:  $B^0 \rightarrow \bar{D}^0 p\bar{p}$  (triangles),  $B^0 \rightarrow \bar{D}^{*0} p\bar{p}$  (open circles),  $B^0 \rightarrow D^- p\bar{p}\pi^+$  (squares), and  $B^0 \rightarrow D^{*-} p\bar{p}\pi^+$  (closed circles); BaBar experiment [622].

decays is found in [965]. Of course, production of isovector mesons like  $N\bar{N}$  with  $I = 1$  or  $\pi(1800)$  is unexpected in radiative  $J/\psi$  decays; indeed, no visible signal is observed in  $J/\psi \rightarrow \gamma\pi^+\pi^-\pi^0$  [963]. Entem and Fernandez, describing scattering data and mass shifts and broadening of  $p\bar{p}$  atomic levels in a constituent quark model, assign the threshold enhancement to final-state interactions [966,967]. Bugg interpreted the threshold  $p\bar{p}$  peak as a cusp arising from the well known threshold peak in  $p\bar{p}$  elastic scattering due to annihilation [800]. Zou and Chiang find that final-state-interaction makes an important contribution to the  $p\bar{p}$  near-threshold enhancement [968]. We just mention (without imposing a relation between the two phenomena) that the  $p\bar{p}$  threshold is not far from the dip in the six-pion photoproduction cross section observed by DM2 [969], Focus [528], and BaBar [619]. Its interpretation of the dip goes a la mode; DM2 – with low statistics – assign the peak below the dip to  $\rho(1600)$ , the Focus dip is argued to be a hybrid, BaBar suggests an interpretation as amalgamation of several broad resonances.

The BES collaboration associated the  $p\bar{p}$  threshold enhancement with the  $X(1835)$  suggesting a large affinity of both,  $p\bar{p}$  and  $\eta'$ , to gluons. From the  $p\bar{p}$  data,  $M = 1831 \pm 7 \text{ MeV}/c^2$  and a width  $\Gamma < 153 \text{ MeV}/c^2$  (at the 90% C.L.) was obtained, compatible with mass and width of the  $\eta'\pi^+\pi^-$  signal. Hence both signals might be one comparatively narrow pseudoscalar resonance. The product branching ratio for the  $X(1835)$  radiative yield

$$\mathcal{B}(J/\psi \rightarrow X_{\pi\pi\eta'}) \cdot B(X_{\pi\pi\eta'} \rightarrow \pi^+\pi^-\eta') = (2.2 \pm 0.4(\text{stat}) \pm 0.4(\text{syst})) \times 10^{-4}$$

can be compared to the branching ratio for the  $p\bar{p}$  threshold enhancement

$$\mathcal{B}(J/\psi \rightarrow X_{p\bar{p}}) \cdot B(X_{p\bar{p}} \rightarrow p\bar{p}) = (7.0 \pm 0.4(\text{stat})^{+1.9}_{-0.8}(\text{syst})) \times 10^{-5}$$

Hence the  $(p\bar{p})/(\pi^+\pi^-\eta)$  ratio is 1/3; from the absence of  $X(1835)$  in the inclusive photon spectrum measured by the Crystal Ball collaboration [747], the BES collaboration concluded that  $X$  must have a branching ratio into  $p\bar{p}$  exceeding 4% [963].

A clue to decide on the different interpretations is possibly provided by the non-observation of the  $p\bar{p}$  threshold enhancement in  $J/\psi \rightarrow \omega p\bar{p}$ . The  $\omega$  has the same quantum numbers as the photon; hence the absence of the signal in the latter data cannot be due to any kind of selection rule based on conservation of angular momentum, charge conjugation or parity. On the other hand, the  $J/\psi$  radiative yield for  $\eta'$  exceeds the  $\eta$  yield by a factor 4.8 while  $\omega\eta'$  has a branching ratio (from  $J/\psi$ ) which is 10% only of the  $\omega\eta$  yield. The observation of  $X(1835)$  in radiative  $J/\psi$  and its non-observation in  $\omega J/\psi$  may thus hint at its flavour singlet structure. This conjecture is supported by its observation in  $\eta'\pi\pi$ , its non-observation in  $\eta\pi\pi$  and assigning a large flavour singlet component to the  $\sigma(485)$ .

The  $X(1835)$  is one of the many examples where the vicinity of a threshold, in this case  $\bar{p}p$ , attracts the mass of a close by resonance. ‘Dressing’ of the  $q\bar{q}$  singlet meson with two  $q\bar{q}$  pairs can create  $N\bar{N}$ . Final state interactions enhance the probability of this transition. In this way, the  $q\bar{q}$  meson mixes with the  $\bar{p}p$  final state and its wave function develops a sizable  $\bar{p}p$  component.

Further reactions with a baryon and an antibaryon in the final state were studied by the BELLE and BES collaborations. The reactions include  $J/\psi \rightarrow \gamma p\bar{\Lambda}$  [491],  $B^0 \rightarrow D^{(*)0}p\bar{p}$ ,  $B^0 \rightarrow p\bar{\Lambda}\pi^-$ ,  $B^+ \rightarrow p\bar{p}\pi^+$ ,  $B^0 \rightarrow p\bar{p}K^0$ ,  $B^+ \rightarrow p\bar{p}K^{*+}$ ,  $B^+ \rightarrow \Lambda\bar{\Lambda}K^+$ ,  $B^- \rightarrow J/\psi\Lambda\bar{p}$ ,  $B^+ \rightarrow \bar{\Xi}_c^0\Lambda_c^+$ , and  $B^0 \rightarrow \bar{\Xi}_c^-\Lambda_c^+$  [631,636,639,640,648,650,659]. In Fig. 77 we show the  $p\bar{\Lambda}$  invariant mass distribution from  $J/\psi \rightarrow \gamma p\bar{\Lambda}$  (BES) and from  $B^0 \rightarrow p\bar{\Lambda}\pi^-$  and  $B^+ \rightarrow \Lambda\bar{\Lambda}K^+$  (Belle) decays. It is not known at present if particular spin-parities can be assigned to these threshold enhancements, and if resonances are involved. Recently, a wide  $p\bar{\Lambda}$  threshold enhancement was reported for

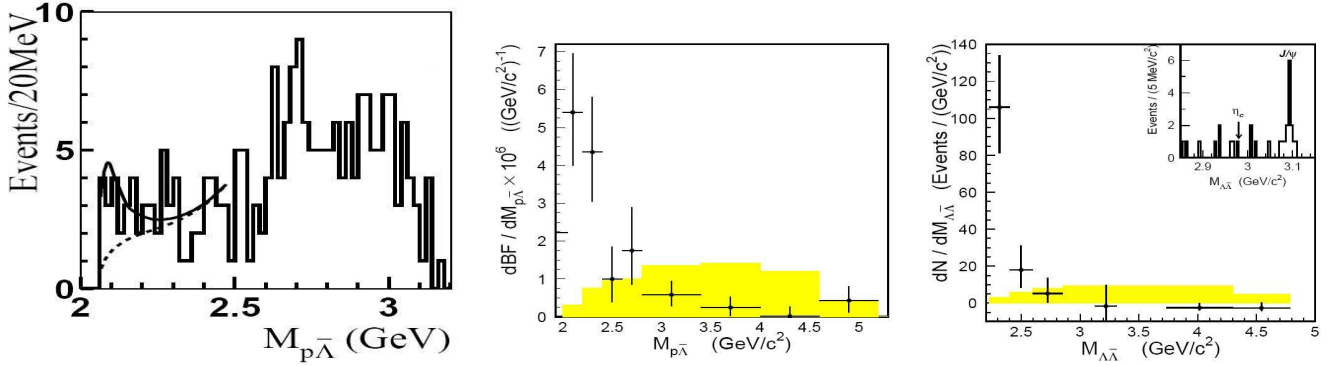


Fig. 77. Left: The  $p\bar{\Lambda}$  mass distribution from  $J/\psi \rightarrow \gamma p\bar{\Lambda}$  [491]; centre:  $p\bar{\Lambda}$  mass distribution from  $B^0 \rightarrow p\bar{\Lambda}\pi^-$ , right:  $\Lambda\bar{\Lambda}$  mass distribution from  $B^+ \rightarrow \Lambda\bar{\Lambda}K^+$  [636, 639, 640].

$B^+ \rightarrow p\bar{\Lambda}\pi^0$  [659]. We notice that the  $p\bar{\Lambda}$  mass distribution observed in radiative  $J/\psi$  decays appears to be much narrower than their counterparts from  $B$  decays. The BES data can be fitted with both,  $S$ -wave and  $P$ -wave Breit-Wigner amplitudes. If it is fitted with an  $S$ -wave Breit-Wigner resonance function, the mass is  $m = 2075 \pm 12 \pm 5 \text{ MeV}/c^2$ , the width  $\Gamma = 90 \pm 35 \pm 9 \text{ MeV}/c^2$ , and the branching ratio  $BR(J/\psi \rightarrow K^- X)BR(X \rightarrow p\bar{\Lambda}) = (5.9 \pm 1.4 \pm 2.0) \times 10^{-5}$ . It is tempting to interpret this observation as pseudoscalar  $K(2075)$ . It would certainly fit very well into the scheme suggested in Table 26 and Fig. 78. To substantiate this conjecture, a signal has to be seen in radiative  $J/\psi$  production of  $K\pi$  and  $K\pi\pi$  systems.

## 8.5 The nonet of pseudoscalar radial excitations

With  $\eta(1760)$  and  $X(1835)$ , there are two close-by resonances, likely with identical quantum numbers but with widths which differ by a factor 4. Expected are in this mass region the 2<sup>nd</sup> radial excitation of the  $\eta$  and the 1<sup>st</sup> radial excitation of the  $\eta'$ . In the SU(3) limit of  $\sigma(485)$  being a flavour singlet resonance, singlet  $\eta$  excitations decay into  $\eta'\sigma(465)$ , octets into  $\eta\sigma(485)$ . The narrow  $X(1835)$  width may thus indicate that it is a flavour singlet state. Thus we interpret  $X(1835)$  as 1<sup>st</sup>  $\eta'$  radial excitation.

In the region above  $2 \text{ GeV}/c^2$ , a few observations of isoscalar pseudoscalar resonances have been reported. Bisello *et al.* find  $2104 \text{ MeV}/c^2$  from  $J/\psi \rightarrow \gamma\rho\rho$ , BES  $M = 2040 \pm 50, \Gamma = 400 \pm 90 \text{ MeV}/c^2$  from  $J/\psi \rightarrow \gamma K\bar{K}\pi$ , Bugg *et al.* report  $2190 \pm 50 \text{ MeV}/c^2$  and a width  $\Gamma = 850 \pm 100 \text{ MeV}/c^2$  from an analysis of several final states in radiative  $J/\psi$  decays. The Queen-Mary-St. Petersburg group analysed Crystal Barrel data on  $p\bar{p}$  annihilation in flight and reported an  $\eta(2010)$  with  $M = 2010^{+35}_{-60}, \Gamma = 270 \pm 60 \text{ MeV}/c^2$ , consistent with  $\eta(2040)$ . Table 26 collects pseudoscalar

Table 26

Pseudoscalar radial excitations. The mixing angle is calculated from the linear GMO formula 8.5, the sign from 8.6. The mass differences to the respective ground states are listed as small numbers. See text for discussion of the states.

$1^1S_0$	$\pi(135)$	$K(498)$	$\eta(548)$	$\eta(958)$	$\Theta_{PS} = -24.6^\circ$	$\eta_c(2980)$
$\delta M =$	1.24	0.97	0.89	0.88		$0.66 \text{ GeV}/c^2$
$2^1S_0$	$\pi(1375)$	$K(1460)$	$\eta(1440)$	$X(1835)$	$-20.8^\circ$	$\eta_c(3638)$
$\delta M =$	1.66	1.34	1.21	1.11		$0.96 \text{ GeV}/c^2$
$3^1S_0$	$\pi(1800)$	$K(1830)$	$\eta(1760)$	$\eta(2070)$	$-30.5^\circ$	$X(3940)$

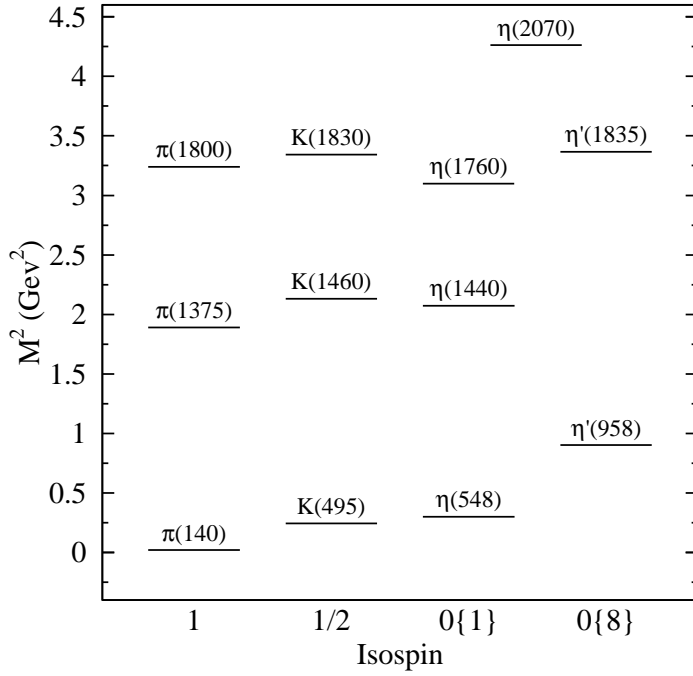


Fig. 78. The pseudoscalar radial excitations. Most of the resonances are well established. The  $\eta(1295)$  has been omitted.  $K(1830)$  and  $\eta(1760)$  are omitted from the summary table in PDG; for  $\eta(1760)$  there is new evidence from BES. For  $X(1835)$ , spin and parity are not measured.  $\eta(2070)$  relies on a weak evidence from two analyses. It might be a flavour singlet or octet state. See text for discussion and references.

ground states and radial excitations. We combine these results by introducing an  $\eta(2070)$  into the discussion, with a mass given by the mean of the two results quoting a narrow width. This state is the most uncertain one in the table. In this mass region, the 2<sup>nd</sup>  $\eta'$  and 3<sup>rd</sup>  $\eta$  radial excitation are expected.

The  $X(3940)$  resonance is seen as a narrow peak in  $e^+e^-$  annihilation in the spectrum of masses recoiling against reconstructed  $J/\psi$  [644]. The spectrum contains  $\eta_c(1S)$  and  $\eta_c(2S)$  and  $\chi_{c0}$ . Due to its production and decay (assuming  $\ell = 0$  or 1) into  $D^*D$  its quantum numbers could be  $J^{PC} = 0^{-+}, 1^{++}$  or  $2^{-+}$ . If we reserve  $1^{++}$  to  $X(3872)$ , it seems likely that  $X(3940)$  should be identified as  $\eta_c(3S)$ .

The systematic behaviour apparent in Table 26 covers the range from the pion and its excitations to the charmonium states. It is obvious that the inclusion of an  $\eta(1295)$  would be problematic. The first radial excitations as proposed here still show a singlet-octet splitting rather than ideal mixing. For the second radial excitations the uncertainties become large. The singlet-octet mixing angles are not very different for the three nonets suggesting that the radial excitations of pseudoscalar mesons are organised into singlets and octets rather than into  $n\bar{n}$  and  $s\bar{s}$  states. The mixing angles given in Table 26 are calculated from the Gell-Mann Okubo mass formula

$$\tan^2 \Theta = \frac{4m_K - m_\pi - 3m_\eta}{-4m_K + m_\pi + 3m_{\eta'}}. \quad (8.5)$$

This equation does not yield the sign of the mixing angle. One can use instead

$$\tan \Theta = \frac{4m_K - m_\pi - 3m_\eta}{m_\pi - m_K} \quad (8.6)$$

The latter formula yields mixing angles of  $-11.5^\circ$ ,  $-31.1^\circ$ , and  $-70.5^\circ$ , respectively. These values depend on small and not precisely known mass differences like  $M_{K(1830)} - M_{\pi(1800)}$  and are considered as less reliable.

In addition to the 'narrow' resonances collected in Fig. 78, a wide isoscalar  $0^+$  background amplitude is required in some analyses. It is compatible with being flavour singlet. The most straightforward interpretation assigns the background amplitude to a very wide pseudoscalar glueball, with a width of more than 800 MeV. We refrain from giving a precise pole position of this elusive object.

One final (trivial) remark. The masses of pseudoscalar and vector radial excitations are similar; radial excitations have no Goldstone character.

### 8.5.1 Other interpretations

The linear mass gaps between the pseudoscalar ground states  $\pi$ ,  $K$ ,  $\eta$  and  $\eta'$  to their first radial excitation vary slowly and can even be reasonably extrapolated to the  $\eta_c$ . The mass square gaps are however about  $1.8 \text{ GeV}^2/c^4$  for the first three mesons; for the  $\eta'$  it is even larger. This is inconsistent with the general observation outlined in section 6.2. Hence other identifications have been made in the literature. In Fig. 79a,b the interpretation of  $\pi$  and  $\pi_2$ ,  $\eta$ ,  $\eta'$ , and  $\eta_2$  by A.V. Anisovich, V.V. Anisovich, and Sarantsev is shown. The mass spectra can also be organised in linear trajectories when  $\eta(1295)$  is omitted (c,d).

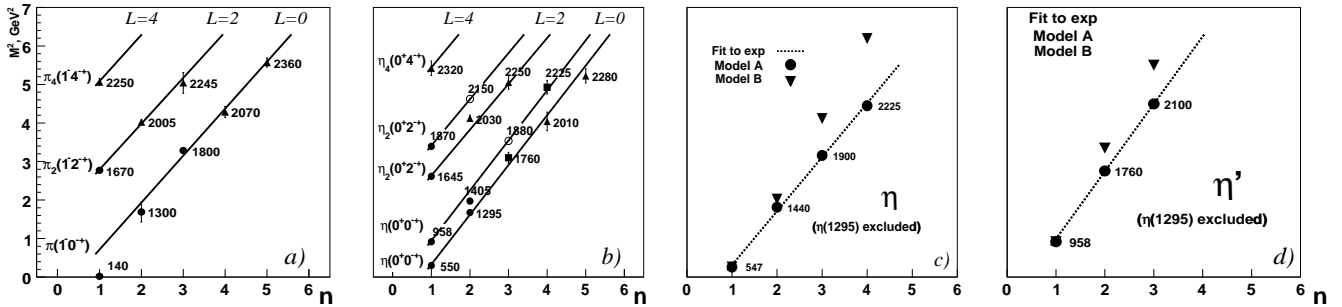


Fig. 79.  $(n, M^2)$ -trajectories. In a) and b), particles from the PDG *Summary Table* are represented by a ●, those omitted from the *Summary Table* by a ■. ▲ represents data given by Anisovich *et al.* [371] and listed as *Further States* by the PDG, open circles predicted by their classification. The number of isoscalar mesons is twice larger due to hidden strangeness;  $u\bar{u} + d\bar{d}$  and  $s\bar{s}$  components mix to form the observed states. a)  $(n, M^2)$ -trajectories of  $\pi$ ,  $\pi_2$ ,  $\pi_4$ , and b)  $\eta$ ,  $\eta_2$ , and  $\eta_4$  excitations. c) and d) give a comparison of experimental results with two model calculations of the Bonn group [174]. The lines gives a fit though the data, the points represent results of the calculations. Model B reproduces the data points when  $\eta(1295)$  is omitted.

## 9 Scalar mesons: $\sigma$ , $\kappa$ , $\delta$ , $S^*$

Scalar mesons, their mass spectrum, their decays and their interpretation, are one of the hottest subjects in meson spectroscopy; scalar mesons have been in the centre of common interest for several decades. The flavour singlet component of scalar mesons carries the quantum numbers of the vacuum and is thus intimately tied up with the rôle of quark and gluon condensates. The nine scalar mesons of lowest mass,  $a_0(980)$ ,  $f_0(980)$ ,  $f_0(485)$ ,  $K_0^*(900)$  are often called with their traditional names  $\delta$ ,  $S^*$ ,  $\sigma$ ,  $\kappa$ . Special conferences have been devoted to the question if the  $\sigma(485)$ , the low-mass  $\pi\pi$  enhancement, is a genuine resonance, if it is a tetraquark state or generated by molecular forces, by  $t$ -channel exchange dynamics [970]. A controversy has arisen on the correct formalism to determine the properties of the  $\sigma(485)$  meson and of its twin brother  $\kappa(700)$ , on achievements in the past and on the fair use of data taken by a collaboration [971, 972].

The  $\sigma(485)$  meson has a long history, and its meaning changed in the course of time. It was originally introduced to improve the description of nucleon-nucleon interactions in one-boson-exchange potentials. An isoscalar and an isovector  $\sigma_0$  and  $\sigma_1$  were invented. Modern theories of nuclear forces understand the interaction by correlated two-pion exchanges [973] with no need to introduce  $\sigma_0$  and  $\sigma_1$ . Nambu [974] and Nambu and Jona-Lasinio [975, 976] described mass generation in analogy to superconductivity and argued that spontaneous mass generation is linked to a massless pion field. Following these ideas, Delbourgo and Scadron [977] predicted a scalar companion of the pion, a  $1^3P_0$   $q\bar{q}$  state, at a mass corresponding to twice the constituent quark mass, i.e. at 600 to 700 MeV/c<sup>2</sup>. While pions get their (small) mass from the distortion of chiral symmetry by finite light-quark masses, the lowest-mass scalar mesons acquire their mass by spontaneous symmetry breaking. Thus the  $\sigma(485)$  is sometimes called the Higgs of strong interactions [978].

Experimentally, the existence of the  $\sigma(485)$  was, e.g., deduced from  $\pi\pi \rightarrow \pi\pi$  phase shifts between the  $\pi\pi$  and the  $K\bar{K}$  thresholds. In [979], a negative background phase was introduced, reflecting a “repulsive core” in  $\pi\pi$  interactions; the  $\sigma(485)$  resonance adds a full 180° phase shift. A repulsive background interaction could stem from left-hand singularities [980] which are usually omitted in fits to the data. Ishida san and collaborators interpret the  $\sigma(485)$  as a relativistic  $q\bar{q}$  state in an S-wave, making the lowest mass scalar mesons to a nonet of ‘chiralons’ [981, 982]. Weinberg [983] showed that the isoscalar  $\pi\pi$  S-wave scattering amplitude vanishes when the momenta of the pions go to zero, growing linearly with increasing  $s$ . The conflict between this consequence of chiral symmetry and unitarity requires the existence of a low-mass pole (see however [984]). These qualitative arguments can be sharpened within Chiral Perturbation Theory (see below). Related to the  $\sigma(485)$  are discussions of the existence of the  $\kappa(700)$ , a low-mass  $K\pi$  enhancement. If the  $\sigma(485)$  exists but not the  $\kappa(700)$ , the  $\sigma(485)$  must be related to the spectrum of glueballs; indeed, QCD spectral sum rules require a scalar glueball below 1 GeV [985, 986].

Uncounted is the number of papers on the  $f_0(980)$  and  $a_0(980)$ , which are fiercely defended as genuine  $q\bar{q}$  states, as tetraquark states or as  $K\bar{K}$  molecules, forming – together with  $f_0(470)$  and  $K_0^*(900)$  – a full nonet of dynamically generated resonances. The two twin brothers  $f_0(980)$  and  $a_0(980)$  have very unusual properties: both have a mass very close to the  $K\bar{K}$  threshold and a large coupling to  $K\bar{K}$ ; Weinstein and Isgur argued [987–989] that the properties can be explained assuming that they are  $K\bar{K}$  molecules. Jaffe [906, 990] had combined the  $a_0(980)$ ,  $f_0(980)$ ,  $f_0(470)$ , and  $K_0^*(700)$  (with somewhat different masses) to form a nonet of tetraquark states depicted in Fig. 80. The unusual properties were assigned to their intrinsic structure as tetraquark states where the mass scales with the number of  $s$  quarks. Their low mass – in comparison to 1.3 GeV expected for  $1^3P_0$   $q\bar{q}$  states – is due to the absence of an orbital angular momentum barrier, and

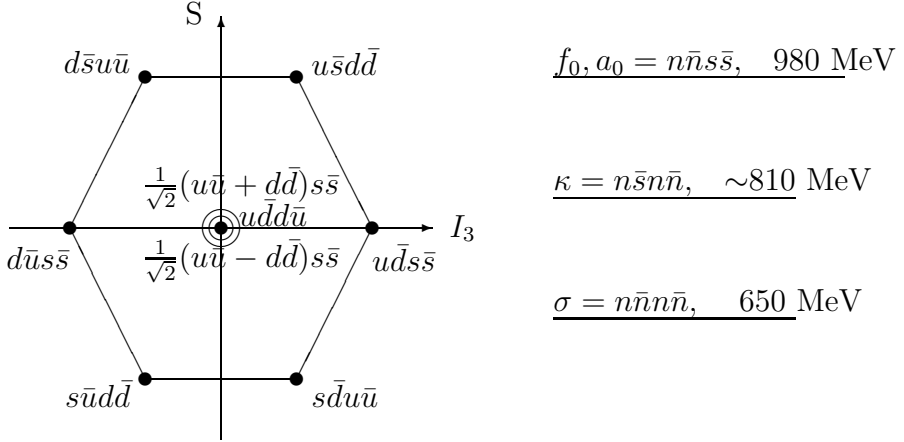


Fig. 80. The nonet of lowest-mass scalar mesons and mass ordering [906].

due to a tighter binding of  $qq$  pairs in a colour  $\bar{\mathbf{3}}$  state (and  $q\bar{q}$  pairs in colour  $\mathbf{3}$ ).

Last not least, a scalar glueball is expected. Its mass is likely to fall into the 1 to 2 GeV region; it possibly mixes with  $q\bar{q}$  states, thus creating a complex pattern of states. An orthodox view has been developed in which the 3 states  $f_0(1370)$ ,  $f_0(1500)$ , and  $f_0(1760)$ <sup>10</sup> originate from two  $q\bar{q}$  states and a glueball even though the existence of  $f_0(1370)$  is sometimes challenged.

A survey of the scalar intensity can be seen in GAMS data on  $\pi^- p \rightarrow n\pi^0\pi^0$ . The process offers the advantage that odd partial waves cannot contribute. The GAMS collaboration has studied this reaction and measured angular distribution from 0.8 to 3 GeV. Fig. 81 shows the modulus of the  $S$ -wave amplitude [289]. A series of peaks and dips is observed and it is not straightforward

<sup>10</sup> The Particle Data Group quotes the  $f_0(1760)$  as  $f_0(1710)$ . The region may, however, house up to 3 isoscalar scalar resonances, called  $f_0(1710)$ ,  $f_0(1790)$ , and  $f_0(1810)$ . In this report, the unresolved structure is denoted  $f_0(1760)$ .

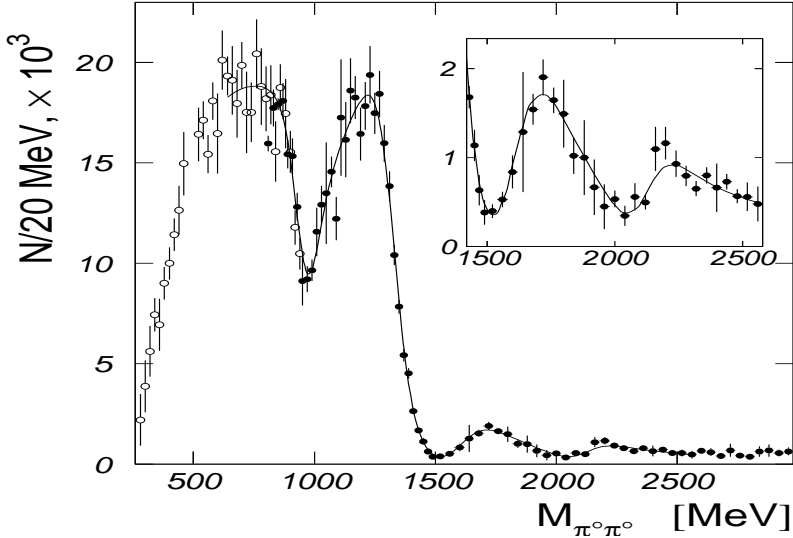


Fig. 81. The reaction  $\pi^- p \rightarrow p\pi^0\pi^0$  at 100 GeV/c for  $|t| < 0.2 \text{ GeV}^2$  [289]. Open circles represent data taken at 38 GeV. The  $S$ -wave exhibits peaks at  $600 \text{ MeV}/c^2$ ,  $1300 \text{ MeV}/c^2$ ,  $1700 \text{ MeV}/c^2$  and at  $2200 \text{ MeV}/c^2$  and dips at  $980 \text{ MeV}/c^2$ ,  $1500 \text{ MeV}/c^2$  and at  $2100 \text{ MeV}/c^2$ .

to identify the scalar resonances. Some of the peaks have traditional names:  $\sigma$  (now  $f_0(485)$ ),  $\epsilon$ , and the  $G(1590)$ . The latter peak was first observed by GAMS in the reaction  $\pi^- p \rightarrow \eta\eta n$  as a peak in the  $\eta\eta$  invariant mass distribution [280], the two peaks at 1300 and 1590 MeV/c<sup>2</sup> are now understood as consequence of the  $f_0(1500)$  dip [991]. The dips correspond to well known meson resonances,  $f_0(980)$ ,  $f_0(1500)$  and to the less well established  $f_0(2100)$ . In other experiments the dips are observed as peaks. For  $f_0(980)$  and  $f_0(1500)$  phase motions have been observed; there is no doubt that these are resonances. It is thus tempting to try to understand the  $\pi\pi$  *S*-wave as a global phenomenon generated by a very broad object  $f_0(1000)$  [177, 178], possibly generated by *t*-channel exchanges, interspersed with  $q\bar{q}$  resonances represented by dips. The peaks may house additional resonances, like  $f_0(1370)$ ,  $f_0(1710)$ , and  $f_0(1760)$ , and deserve a deeper discussion.

## 9.1 $\pi\pi$ scattering

Scalar resonances coupling to two pions can be studied by scattering negatively charged pions off protons to produce  $\pi^+\pi^-$  or  $\pi^0\pi^0$  pairs. A proton can dissociate into neutron and  $\pi^+$ , and scattering may take place off the virtual pion. If the four-momentum transfer  $q$  (with  $t = -q^2$ ) to the proton is small, the pion is nearly on-shell and the process can be considered as a scattering experiment in which a beam scatters off a pion target [992]. A simultaneous analysis of  $\pi^+\pi^-$  and  $\pi^0\pi^0$  provides for a decomposition of the scattering amplitude into isoscalar and isotensor contributions.

A classic experiment to determine the  $\pi\pi$  scattering amplitude was carried out at CERN in the sixties by the CERN-Munich collaboration (see section 3.1.1). A 17.2 GeV/c  $\pi^-$  beam and an unpolarised target were used. The data were expanded into Legendre polynomials from which  $\pi\pi$  amplitudes can be extracted. In the general case, the  $S, P_0, P_+, P_-$  amplitudes and their relative phases depend on the nucleon helicities. Without using a polarised target, these partial waves cannot be deduced from the moments without further assumptions [993, 994]. Without polarisation data, there are no unambiguous solutions and additional assumptions are necessary. At low  $q^2$ , the one pion exchange mechanism dominates which prefers spin flip at the nucleon vertex. Under these conditions, the rank of the spin-density matrix is reduced to one and all density matrix elements can be fixed. In [204, 205] it was thus assumed that for small values of  $t$ , the proton spin-flip amplitude is dominant. More generally speaking, it was assumed that the  $\pi\pi$  phase does not depend on the projection of the orbital angular momentum onto the flight direction with which it is produced (phase coherence) and that the ratio of flip and non-flip amplitudes is universal ('spin coherence'). Later, the experiment (performed by a CERN-Krakow-Munich collaboration) included a polarised target [212], and the assumptions on spin and phase coherence were verified to a good approximation in a model-independent analysis. For large  $t$ , neither phase nor spin coherence is granted, and feedthrough of higher partial waves into the scalar wave cannot be excluded without exploiting a polarised target.

The threshold region is of particular importance. The most precise data stem from  $K^+ \rightarrow \pi^+\pi^-e^+\nu_e$  decays [995] (see [996, 997] for recent data). This type of data is often included in partial wave analyses in order to constrain the low energy behaviour of the scattering amplitude. A recent reanalysis of the CERN-Munich data yielded the  $\pi\pi$  *S*-wave amplitude and phase (and other partial wave amplitudes) in a  $\pi\pi$  mass range from 600 MeV/c<sup>2</sup> to 1600 MeV/c<sup>2</sup> [998]. However, it was still not possible to reconstruct all partial waves unambiguously. There is a long history of 'up' or 'down' solutions (and 'flat' or 'steep') which gave equally good descriptions of the moments. Steep solutions violate unitarity and can be discarded. The remaining ambiguity can be resolved by invoking crossing symmetry. Crossing symmetry relates a partial wave amplitude to

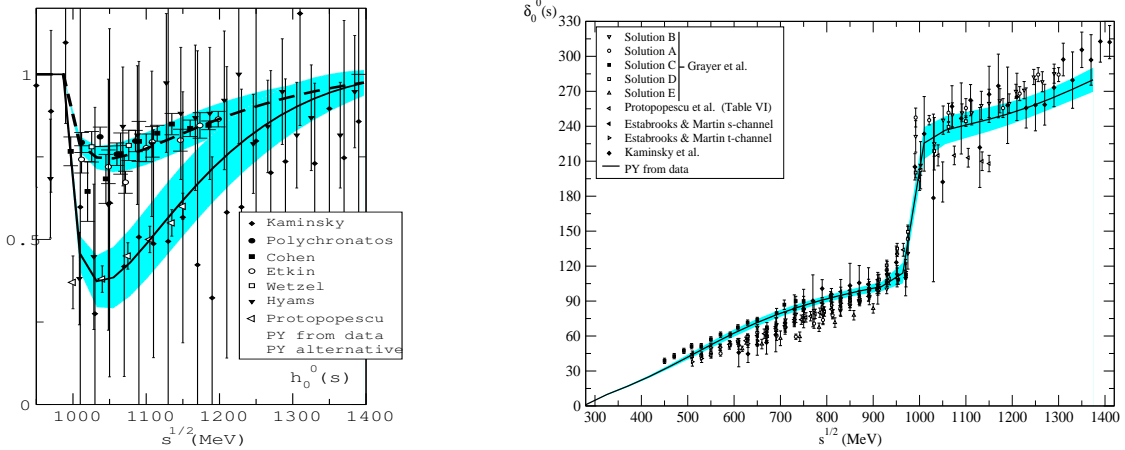


Fig. 82. The  $I = 0$ ,  $S$ -wave inelasticity and phase shift (with error band) with a fit by Pelaez and Ynduráin [1005]. Data points from  $K$  decays are not shown. The inelasticity derived from  $\pi\pi$  elastic scattering (marked PY from data) is much larger than that from  $\pi\pi \rightarrow K\bar{K}$  (PY alternative).

the imaginary part of the amplitude, integrated from threshold to infinity (Roy's equations [999]). The integral is dominated by the threshold region and was evaluated using some approximations. It turns out that only the ‘down-flat’ is compatible with Roy's equations and satisfies crossing symmetry [1000]. The ‘down-flat’ solution is also compatible [1001] with the BNL [253] and GAMS results [289] which we discuss further down.

Many more experiments and analyses have been carried out [177, 204, 205, 210, 1001–1004]; Fig. 82 collects isoscalar scalar phase shifts deduced from these experiments. The solid line is a fit by Pelaez and Ynduráin [1005], a refined analysis by Kaminski, Pelaez and Ynduráin is presented in [1006].

The following observations can be made. The  $\pi\pi$   $S$ -wave scattering amplitude vanishes at some small value of  $s$ . This is the Adler or Adler-Weinberg zero [983, 1007]. With increasing mass  $m_{\pi\pi}$ , amplitude and phase rise slowly until they reach the 1 GeV region where the phase increases rapidly (from  $\sim 90^\circ$  to  $\sim 240^\circ$ ) and where the amplitude exhibits a dip. These effects are due to  $f_0(980)$ ; the phase advance signals a resonance, the dip is a unitarity effect. The coupling of  $f_0(980)$  to  $K\bar{K}$  can be determined from the intensity missing in  $\pi\pi$ , and as observed intensity in the  $K\bar{K}$  final state. These two quantities disagree as shown in Fig. 82a. The dashed and dotted lines in Fig. 82a represent fits using either  $\pi\pi \rightarrow \pi\pi$  or  $\pi\pi \rightarrow K\bar{K}$  data, respectively. The phase shifts are fitted directly, the pole structure of the amplitude was not studied in [1005] and we refrain from a discussion of resonance parameters. At higher masses, the phase continues to increase slowly and the amplitude approaches the unitarity limit again. There is a hint that something new may occur in the 1400 to 1500 MeV/c<sup>2</sup> region. The isotensor  $S$ -wave phase shift and inelasticity are shown in Fig. 83.

The Adler-Weinberg zero is a consequence of chiral symmetry, it forces  $\pi\pi$  interactions to vanish close to the  $\pi\pi$  threshold. The zero is not necessarily present in a production experiment where the  $\sigma(485)$  may appear as a peak. The E791 collaboration analyzed the Dalitz plot of the reaction  $D^+ \rightarrow \pi^+\pi^+\pi^-$  [521] and observed an enhancement at low masses. It is clearly seen (Fig. 84) as a broad bump in the  $M_{\pi^+\pi^-}^2$  projection of the Dalitz plot. In [521] it is treated as Breit-Wigner amplitude. This is a crude approximation but the data certainly provide evidence for a substantial low-energy effect in the  $\pi\pi$  isoscalar  $S$ -wave. The Breit-Wigner mass and width were fitted to

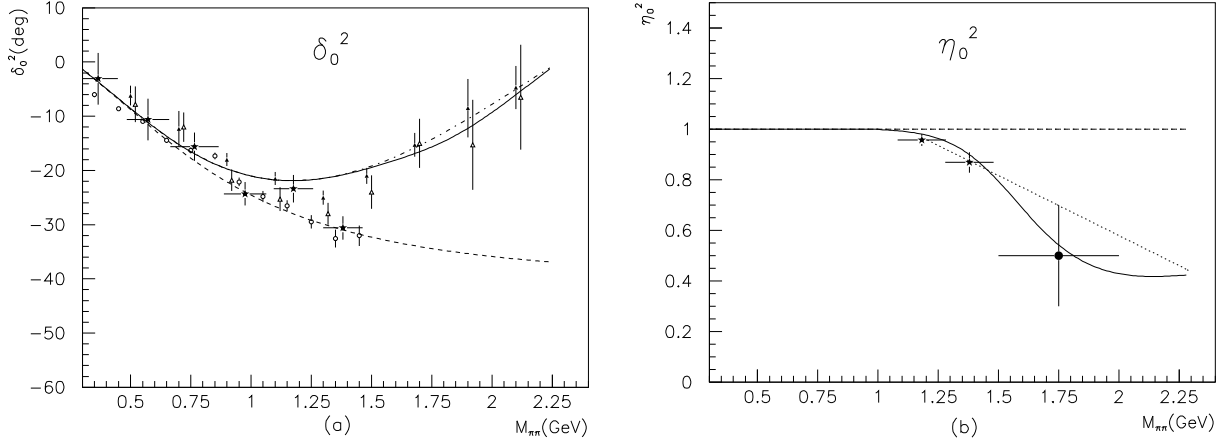


Fig. 83. The  $I = 2 \pi\pi$  S-wave phase shift  $\delta_0^2$  (a) and inelastic coefficient  $\eta_0^2$  (b). The experimental data for  $\delta_0^2$  are from [211] (circles), [1008] (stars), and [1009] (triangles); the data for  $\eta_0^2$  are from [1008] (stars), and [1009] (solid circle). The solid curves represent a fit which includes  $\rho$  and  $f_2(1270)$  exchange and a box diagram with two  $\rho$  mesons in the intermediate state. The dashed curves include only t-channel  $\rho$  exchange, the dot-dashed curves include  $\rho$  and  $f_2(1270)$  exchange. The dotted line in (b) is  $\eta_0^2 = 1.53 - 0.475m_{\pi\pi}(GeV/c^2)$  used in [1009]. Data compilation and fit are from [919].

$478^{+24}_{-23} \pm 17$  MeV/c $^2$  and  $324^{+42}_{-40} \pm 21$  MeV/c $^2$ , respectively. Very similar observations have been made by the BES collaboration in a study of  $J/\psi$  decays to  $\omega\pi^+\pi^-$ . The data will be discussed in a different context and are shown in Fig. 109. A peak at low  $\pi\pi$  masses is observed [492] to which a clear phase motion can be ascribed [1010]. The phase motion is identical to the one observed in elastic  $\pi\pi$  scattering. Mass and width of the  $\sigma(485)$  were determined to be  $(541 \pm 39) - i(252 \pm 42)$  MeV/c $^2$ . The pole was confirmed in a study of  $\psi(2S) \rightarrow \pi^+\pi^- J/\psi$  [505].

Unitarity suggests the phase of the  $\pi\pi$  interaction below the first inelastic threshold in weak or electromagnetic production processes to be the same as in elastic  $\pi\pi$  scattering; this is the famous final state interaction theorem by Watson [1011, 1012]. In the case of strong production modes, rescattering between final-state particles may lead to (likely small) additional phase shifts. It is very suspicious when a new method to identify the scalar isoscalar phase motion leads to a  $\sigma(485)$  having a phase shift from threshold to 800 MeV/c $^2$  which is compatible with a full Breit-Wigner resonance [1013] and thus incompatible with scattering data. The  $\sigma(485)$  is represented by a unique pole position in the complex energy plane; the pole must not change when going from scattering to production experiments; both types of experiments must be fitted with one amplitude. In a scattering situation, the scalar isoscalar amplitude is conveniently parametrised by multiplication

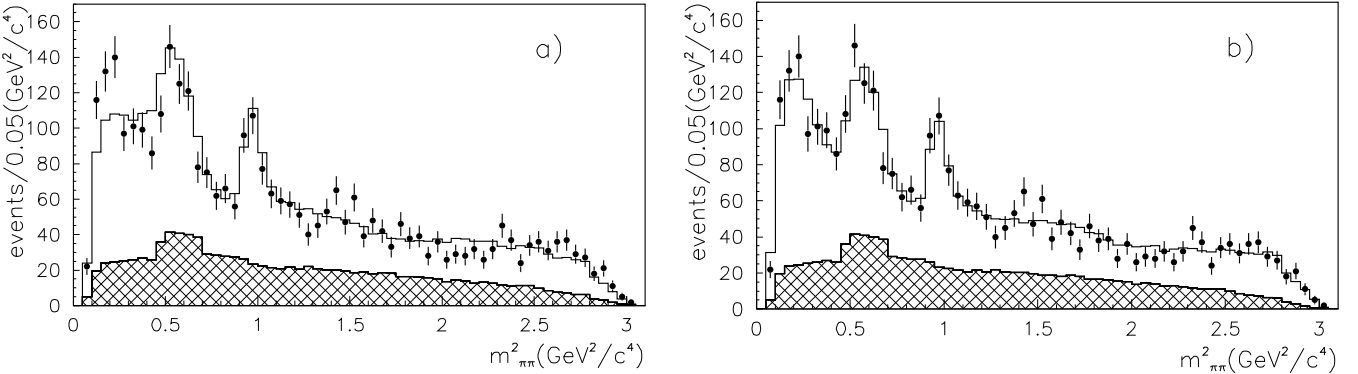


Fig. 84.  $M_{\pi^+\pi^-}^2$  distribution from  $D^+ \rightarrow \pi^+\pi^+\pi^-$  decays. Data are shown with error bars, the histogram represent a fit without (a) and with a Breit-Wigner resonance (the  $\sigma(485)$ ) [521].

with a function enforcing the Adler zero at  $s = m_\pi^2/2$ , e.g. by writing an amplitude which is  $\propto (s - m_\pi^2/2)$  in the low-energy region. Individually, isoscalar and isotensor  $\pi\pi$  phase shifts in final-state interactions and in scattering are identical; their fractional contributions might however be different in different experimental situations, and the observed total  $\pi\pi$  phase shifts (which has contributions from  $I = 0$  and  $I = 2$ ) can differ.

Current algebra or the leading order chiral Lagrangian requires  $\pi\pi$  interactions at low energies to be given by  $A = (s - m_\pi^2)/F_\pi^2$  plus corresponding terms where  $s$  is replaced by  $t$  and  $u$ . However, the amplitude cannot grow forever  $\propto s$  due to unitarity. The  $\sigma(485)$  pole resolves this conflict between chiral symmetry and unitarity. Meißner [1014] has sketched how final-state interactions between the two pions create a pole which he calls an ‘elusive’ or ‘illusory’ particle to underline its non- $\bar{q}q$  nature. Its pole position is approximately determined by the pion coupling constant  $F_\pi$  and thus not directly related to the physics of  $\bar{q}q$  mesons. Colangelo, Gasser and Leutwyler [1015] and Caprini, Colangelo and Leutwyler [1016] use further constraints from the Roy equation leading to a twice subtracted dispersion relation. The subtraction constants were expressed, using crossing symmetry, in terms of the  $S$ -wave scattering lengths which are known with high precision. The approach provides access to the scattering amplitude in the complex plane and thus to magnitude and phase below and above the pole. A pole is mandatory, the authors of [1015] quote  $M = (470 \pm 30) - i(295 \pm 20) \text{ MeV}/c^2$  while in [1016],  $M = 441_{-8}^{+16}$ ,  $\Gamma_\sigma = 544_{-18}^{+25} \text{ MeV}/c^2$  is given. The mass is lower than those from the other papers; the value was criticised by Kleefeld in [1017] for having neglected pole terms in the double subtracted dispersion relation. Bugg [1018] assigns the low value to the neglect of virtual loops due to  $K\bar{K} \rightarrow \pi\pi$  and  $\eta\eta \rightarrow \pi\pi$  below threshold. Including these channels into a fit to all data gave a pole at  $472 \pm 30 - i(271 \pm 30) \text{ MeV}/c^2$ . Leutwyler [1019] addresses this question explicitly, suggesting that in Bugg’s method, the inelastic channels pose severe problems resulting in barely controllable errors (but not in their own method). The pole structure of the low energy  $\pi\pi$  scattering amplitudes was also studied in [1020]. Low energy phase shift data were fitted by imposing chiral unitarisation and crossing symmetry. A  $\sigma(485)$  pole position at  $M_\sigma = 470 \pm 50$ ,  $\Gamma_\sigma = 570 \pm 50 \text{ MeV}/c^2$  was found. The threshold parameters were found to be in good agreement with results using the Roy equations.

The pole structure of the low energy  $\pi\pi$  scattering amplitudes was studied in [1020] using a proper chiral unitarisation method combined with crossing symmetry and the low energy phase shift data. The  $\sigma(485)$  pole position was found at  $M_\sigma = 470 \pm 50 \text{ MeV}/c^2$ ,  $\Gamma_\sigma = 570 \pm 50 \text{ MeV}/c^2$ . Kaon decays,  $K \rightarrow 3\pi$  and  $K \rightarrow \pi\pi e\nu$  decays (see, e.g. [997] for recent high-precision data from NA48/2) give the most precise data on low energy  $\pi\pi$  scattering in the  $S$ -wave. In a systematic evaluation of different data sets, Yndurain (in collaboration with Pelaez) [1021] determined a precise value for the pole position of the  $\sigma(485)$  resonance to be  $M_\sigma = (485 \pm 18) \text{ MeV}$ ,  $\Gamma_\sigma/2 = (255 \pm 12) \text{ MeV}$ . The ‘Breit-Wigner’ mass of the  $\sigma(485)$  was determined, too, and values  $M_0 = 790 \pm 25 \text{ MeV}/c^2$  and half width of  $\Gamma_0/2 = 560 \pm 60 \text{ MeV}/c^2$  were obtained.

We believe the  $\sigma(485)$  to be established and quote

$$M_\sigma = (485 \pm 40) \text{ MeV}, \Gamma_\sigma = (565 \pm 60) \text{ MeV} \quad (9.1)$$

as final value which we use for further discussion.

The mass of the  $\sigma(485)$  is driven by the value of  $f_\pi$ . Does this require the  $\sigma(485)$  to be unrelated to  $q\bar{q}$  spectroscopy? The situation remotely resembles the need to introduce weakly interacting bosons into Fermi’s four-point theory of weak interactions. The linear rise of the  $\bar{\nu}_e e^-$  cross section and unitarity clash at 300 GeV; there must be a  $W^-$ . But of course, this is not a  $\bar{\nu}_e e^-$  bound state.

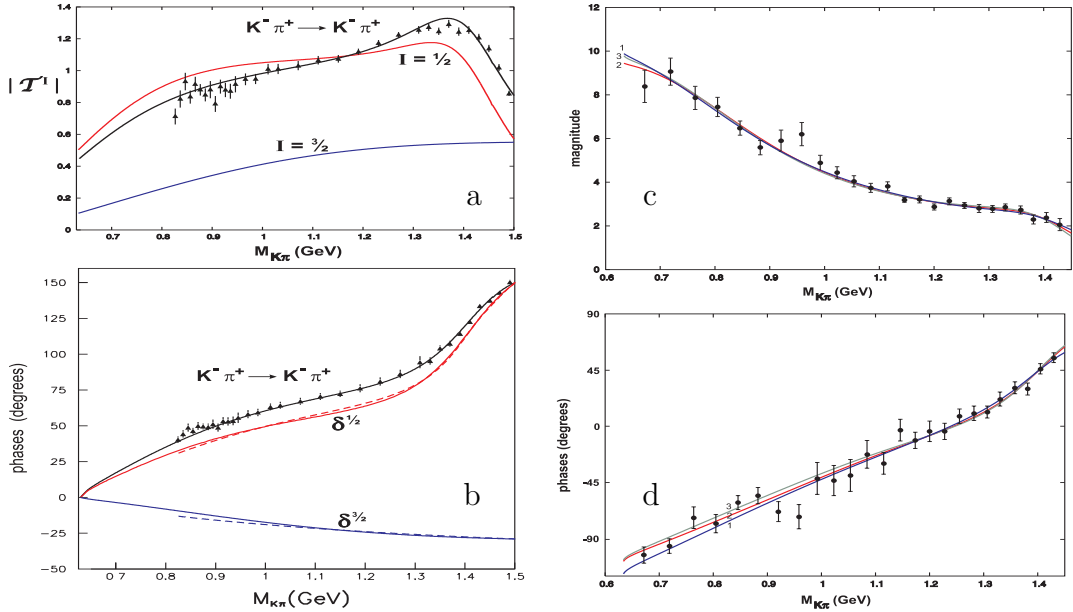


Fig. 85. Magnitudes (a) and phases (b) of the  $I = 1/2$  and  $3/2$  amplitudes. The data points are from LASS [223]. The solid line represent a fit by Boglione and Pennington [1025] compatible with constraints from current algebra. Magnitude (c) and phase (d) of the  $S$ -wave amplitude from E791 results on  $D$  decays. The fit curve (labelled 2) to these data allows for an  $s$ -dependent fraction of  $I = 1/2$  and  $3/2$  amplitudes [1025]. Curves 1 and 3 mark one standard deviation away from the optimal fit.

## 9.2 $K\pi$ scattering

The LASS experiment at SLAC, carried out in the 70ties of the last century and described in session 3.1.3, was the last one to scatter low-momentum ( $11 \text{ GeV}/c$ ) kaons off protons. For small momentum transfer to the target proton, the scattering process  $K^- p \rightarrow K^- \pi^+ n$  is dominated by  $K^- \pi^+$  scattering. The two isospin contributions,  $I = 1/2$  and  $I = 3/2$ , can be separated by measuring also  $K^+ p \rightarrow K^+ \pi^+ n$ . From the angular distributions, both  $S$ -wave scattering amplitudes can be determined. The LASS collaboration described the data (see Fig. 85, left panel) by a  $K_0^*(1430)$  and a range parameter which gives an amplitude rising linearly with  $\sqrt{s}$ . Current algebra or Chiral Perturbation Theory demands an Adler zero of the amplitude at about  $(s - m_K^2 + \frac{1}{2}m_\pi^2)$  and an amplitude rising with  $s$  [1022, 1023]. The range parametrisation is hence incompatible with chiral symmetry. In production experiments, there is no Adler-zero suppression, and this is the reason that the existence of the  $\kappa(700)$  became transparent in the analysis of the E791 Collaboration of data on  $D^+ \rightarrow K^- \pi^+ \pi^+$  [522]. Fig. 106d shows the Dalitz plot of the reaction. The vertical line shows the large contribution of the  $K^* \pi$  isobar. The intensity vanishes in the centre of the  $K^* \rightarrow K\pi$  decay angular distribution due to interference with the  $K^* \pi$   $S$ -wave amplitude: The  $P$ -wave amplitude has an angular distribution  $\propto \sin \Theta$ , the  $S$ -wave amplitude is constant. Thus the interference changes from a destructive to a constructive one for low  $K\pi$  masses; the opposite is true for high  $K\pi$  masses. Thus the scalar phase can be deduced from the interference pattern [523]. The same feature is observed in Fig. 106d with the  $\phi$  in  $K\bar{K}$   $P$ -wave and  $f_0(980) \rightarrow K\bar{K}$  in  $S$ -wave. The fit to the data from [522] revealed the existence of a  $\kappa(700)$  having mass and width, respectively, of  $M - i\Gamma/2 = (797 \pm 19 \pm 43) - i(205 \pm 22 \pm 44) \text{ MeV}/c^2$  [522], in agreement with a further analysis by Bugg, finding  $(750 \pm 30 \pm 55) - i(342 \pm 60) \text{ MeV}/c^2$  [1024].

The BES collaboration found further evidence for  $\kappa(700)$  from the reaction  $J/\psi \rightarrow \bar{K}^*(892)^0 K^+ \pi^-$  and deduced a pole at  $(841 \pm 30^{+81}_{-73}) - i(309 \pm 45^{+48}_{-72}) \text{ MeV}/c^2$  by averaging values deduced from two different methods. Bugg reanalysed also these data and found a pole position at  $(760 \pm 20_{\text{stat}} \pm$

$40_{syst} - i(420 \pm 45_{stat} \pm 60_{syst})$  MeV/c<sup>2</sup> [1026]. As shown in [1027–1029], the LASS data alone yield a  $\kappa(700)$  with (nearly) consistent parameters when analyticity and chiral symmetry are respected.

How can we reconcile these results with the strict statement of Cherry and Pennington [1030], ‘there is no  $\kappa(900)$ ’? The authors of [1030] performed a ‘model-independent analytic continuation of the LASS data’, determined the number and position of resonance poles, and concluded that there is a  $K_0^*(1430)$ , and no  $\kappa(900)$ . These conclusions were confirmed in an analysis presented in [1031]. However, both groups admitted that the LASS data cannot rule out a  $\kappa(700)$  well below 825 MeV/c<sup>2</sup>. Both, new data between the  $K\pi$  threshold and 825 MeV/c<sup>2</sup> (where LASS data set in) and the proper inclusion of chiral symmetry, have finally revealed the existence of a broad  $\kappa(700)$ . Very recently, Descotes-Genon and Moussallam used constraints from the Roy equations for  $\pi K$  scattering [1032], the existence of the  $\kappa(700)$  was confirmed and mass and width of  $M_\kappa = 658 \pm 13$  and  $\Gamma_\kappa = 557 \pm 24$  MeV/c<sup>2</sup> were given.

In our judgement, a low mass  $K_0^*$  exists, which we will call it  $K_0^*(700)$  or  $\kappa(700)$  with

$$M_\kappa = 700 \pm 80 \text{ MeV/c}^2, \quad \Gamma_\sigma = 650 \pm 120 \text{ MeV/c}^2. \quad (9.2)$$

The central value and the errors are chosen to include the (most reliable) result of [1032], not rejecting completely other evaluations giving higher mass values.

### 9.3 Isovector $\pi\eta$ interactions

#### 9.3.1 The reaction $\pi^- p \rightarrow \eta\pi^0 n$

The reaction was studied by the GAMS collaboration using the 38 GeV/c  $\pi^-$ -beam of the IHEP U-70 accelerator [290]. The  $\eta\pi$  mass spectrum shows two peaks corresponding to  $a_0(980)$  and  $a_2(1320)$  formation, no shoulder is observed which could house the  $a_0(1450)$ . For  $-t < 1$  (GeV/c)<sup>2</sup>,  $a_2(1320)$  dominates in the spectrum, at small momentum transfer, for  $-t < 0.05$  (GeV/c)<sup>2</sup>, the intensities of both peaks are actually similar. Production of  $a_2(1320)$  is dominated by natural spin-parity exchanges (mainly  $\rho$ -exchange) in the  $t$ -channel. For  $a_0(980)$  production, only unnatural exchanges are allowed in the  $t$ -channel, and the data are consistent with  $\rho_2$  as most significant exchange. No  $a_0(1450)$  was seen in the data. No data on  $a_0$  decay into  $K\bar{K}$  were reported.

#### 9.3.2 The $a_0(980)$ and $f_0(980)$ from $p\bar{p}$ annihilation

The Crystal Barrel detector measured both  $\pi\eta$  and  $K\bar{K}$  final states and was thus one of the few detectors capable to determine  $a_0(980)$  decays into both final states. Fig. 86a,b shows  $a_0(980)$  in  $p\bar{p} \rightarrow \pi^\pm K^0 K^\mp$ , with  $K^0 = K_L^0$  (a),  $K_S^0$  (b), respectively. In the  $\eta\pi$  mass distribution (c),  $a_0(980)$  manifests itself as a fast rise at 1 GeV. The  $f_0(980)$  is seen as a dip in  $p\bar{p}$  annihilation into  $3\pi^0$  (Fig. 86d). Its decay into  $K\bar{K}$  is difficult to disentangle from decays of neutral  $a_0(980)$ ; a coupled channel analysis is needed invoking isospin relations to determine the  $f_0(980)$  and  $a_0(980)$  contributions to the  $K_S^0 K_S^0$  mass spectrum shown in Fig. 86e.

Partial widths of resonances are usually defined at their peak position. This is of course impossible for resonances below an important threshold. One remedy is to determine ratios of partial decay widths as ratio of events in different final states. With this warning, we list the partial widths

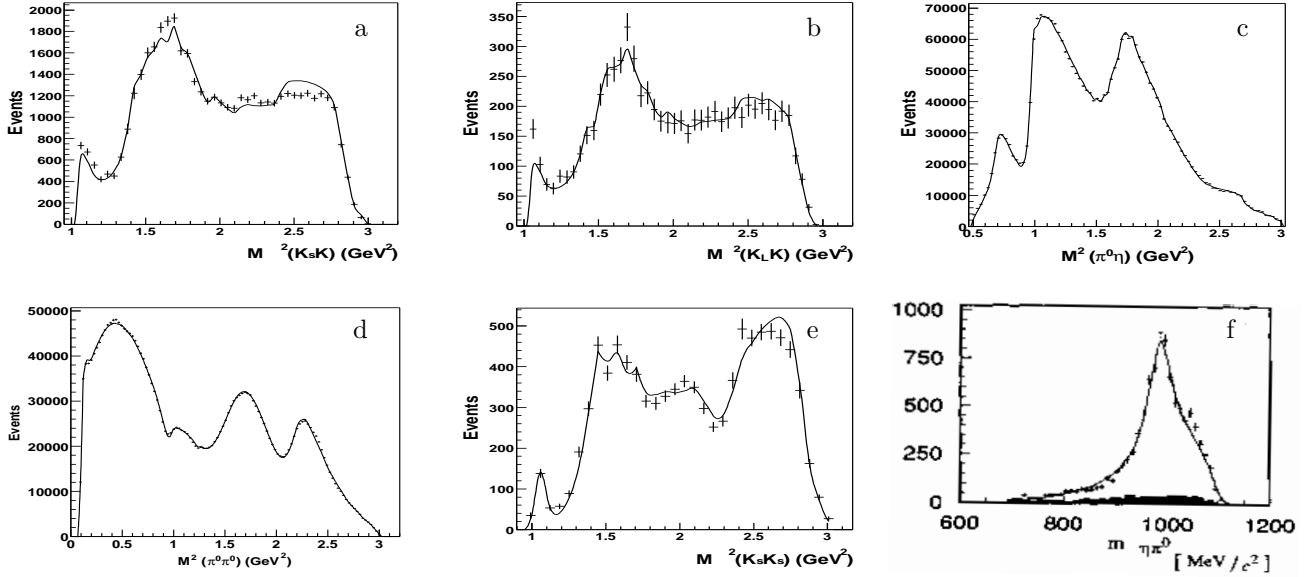


Fig. 86. Invariant mass distributions from  $p\bar{p}$  annihilation at rest. The data are from the Crystal Barrel experiment, the solid line represents a fit from [859]. a:  $K_L^0 K^\mp$  [343], b:  $K_S^0 K^\mp$ , c:  $\pi\eta$  [329], d:  $\pi^0\pi^0$  [1033], e:  $K_S^0 K_S^0$  [335] and e:  $\pi^0\pi^0$  [1033] invariant mass distributions recoiling against a pion in  $p\bar{p}$  annihilation at rest. f:  $\pi\eta$  mass distribution from  $p\bar{p} \rightarrow \omega\pi^0\eta$  with a fit using a Breit-Wigner amplitude [327].

$$a_0(980) \quad M = 984.4 \pm 1.3 \text{ MeV}/c^2 \quad \Gamma = 92 \pm 20 \text{ MeV}/c^2 \quad \frac{\Gamma_{K\bar{K}}}{\Gamma_{\pi\pi}} = 0.23 \pm 0.05 \quad [343]$$

$$f_0(980) \quad M = 994 \pm 5 \text{ MeV}/c^2 \quad \Gamma = 64 \pm 16 \text{ MeV}/c^2 \quad \frac{\Gamma_{K\bar{K}}}{\Gamma_{\pi\pi}} = 0.84 \pm 0.02 \quad [859]$$

which were deduced from the data. The widths are much more uncertain than the errors suggest. The peak widths are narrow, the decay width can be as large as 200 MeV/c<sup>2</sup>. Closer to the analysis are the parameters of the Flatté formula (9.3) giving the couplings instead of the partial widths. For  $\pi\eta$  elastic scattering or scattering into  $K\bar{K}$  via  $a_0(980)$  formation, the Flatté formula reads

$$\frac{d\sigma_i}{dm} \propto \left| \frac{m_R \sqrt{\Gamma_{\pi\eta}\Gamma_i}}{m_R^2 - m^2 - im_R(\Gamma_{\pi\eta} + \Gamma_{K\bar{K}})} \right|^2. \quad (9.3)$$

The first channel is defined by elastic scattering, with  $\Gamma_{\pi\eta} = \bar{g}_\eta q_\eta$ , and with  $g_\eta$  assumed to be constant in the vicinity of the resonance;  $q_\eta$  is centre-of-mass momentum in the  $\pi\eta$  system. The partial decay width to the second ( $K\bar{K}$ ) channel has a strong energy dependence. Above the  $K\bar{K}$  threshold, it grows rapidly and the denominator in eq. (9.3) increases leading to a reduced apparent width in the  $\pi\eta$  mass distribution.

$$\Gamma_{K\bar{K}} = \begin{cases} \bar{g}_K \sqrt{m^2/4 - m_K^2} & \text{above threshold} \\ i\bar{g}_K \sqrt{m_K^2 - m^2/4} & \text{below threshold} \end{cases}$$

The formulae are easily adapted to describe  $f_0(980)$ .

A compilation of Flatté parameters for  $a_0(980)$  and  $f_0(980)$  is reproduced from [1035] in Table 27. In the Table,  $m_R$  is the nominal mass of the resonance,  $m$  is the actual invariant mass and  $\bar{g}_\eta$  and  $\bar{g}_K$  are dimensionless coupling constants that are related to the dimensional coupling constants  $g_{\pi\eta}$  and  $g_{K\bar{K}}$  commonly used in the literature by  $\bar{g}_\eta = g_{\pi\eta}^2/(8\pi m_R^2)$  and  $\bar{g}_K = g_{K\bar{K}}^2/(8\pi m_R^2)$ , respectively.

Table 27

Flatté parameters for the  $a_0(980)$  (left) and  $f_0(980)$  (right) mesons. The values of  $m_R$ ,  $\Gamma_{\pi\eta}$ ,  $\Gamma_{\pi\pi}$  and  $E_B$  are given in MeV. Values for references labelled with the superscript <sup>a</sup> are based on a parametrisation given by Achasov [1036]. The table is adapted from [1035].

Ref.	$m_R$	$\Gamma_{\pi\eta}$	$\bar{g}_\eta$	$\bar{g}_K$	$R$	$E_R$	Ref.	$m_R$	$\Gamma_{\pi\pi}$	$\bar{g}_\pi$	$\bar{g}_K$	$R$	$E_R$
[1037]	999	143	0.445	0.516	1.16	7.6	[1038]	957	42.3	0.09	0.97	10.78	-34.3
[247]	1001	70	0.218	0.224	1.03	9.6	[438] <sup>a</sup>	975	149	0.317	1.51	4.76	-16.3
[343]	999	69	0.215	0.222	1.03	7.6	[305]	–	90	0.19	0.40	2.11	–
[422] <sup>a</sup>	995	125	0.389	1.414	3.63	3.7	[520]	977	42.3	0.09	0.02	0.22	-14.3
[462] <sup>a</sup>	984.8	121	0.376	0.412	1.1	-6.5	[421] <sup>a</sup>	969.8	196	0.417	2.51	6.02	-21.5
[1036] <sup>a</sup>	1003	153	0.476	0.834	1.75	11.6	[463] <sup>a</sup>	973	256	0.538	2.84	5.28	-18.3
[1036] <sup>a</sup>	992	145.3	0.453	0.56	1.24	0.6							

It is remarkable how large the spread in the binding energy  $E_B$  and in the ratio  $R$  of the coupling constants is. More work is certainly needed to understand the process-dependence of these quantities. The large value of  $R$  underlines the strong affinity of  $f_0(980)$  to the  $K\bar{K}$  system and can be used to argue in favour of a  $K\bar{K}$  molecular character of the two mesons; see however the discussion in section 11.6.2.

The masses of  $f_0(980)$  and  $a_0(980)$  are right at the  $K\bar{K}$  threshold; the impact of the threshold on the  $\pi\eta$  mass spectrum can be seen in Fig. 86 (bottom, right) which displays the  $\eta\pi$  spectrum recoiling against an  $\omega$  in  $p\bar{p}$  annihilation at rest. Little kinetic energy is available in this reaction, a kinematical situation which is not suppressed in  $p\bar{p}$  annihilation [730]. The small kinetic energies give the optimum detector resolution, and the non-Breit-Wigner mass distribution becomes immediately visible. The Crystal Barrel collaboration did not fit the data with the Flatté formula; also a study of  $p\bar{p} \rightarrow \omega K\bar{K}$  was not made.

## 9.4 Scalar mesons in radiative $\phi$ decays

The open interpretation of the  $f_0(980)$  and  $a_0(980)$  mesons initiated experiments aiming at exploring their nature. In the tetraquark interpretation, the 2-photon width was calculated to be suppressed [923] while large branching ratios were predicted for radiative  $\phi$  decays into  $f_0(980)$  and  $a_0(980)$  [1039]. Thus there was hope that their nature can be identified by a study of radiative  $\phi$  decays. The reactions  $\phi(1020) \rightarrow \pi^0\eta\gamma$ ,  $\phi(1020) \rightarrow \pi^0\pi^0\gamma$ , and  $\phi(1020) \rightarrow \pi^+\pi^-\gamma$  were first observed in the SND and CMD experiment at Novosibirsk (see section 3.4.1), and the  $a_0(980)$  and  $f_0(980)$  contributions were derived from fits to the data [414, 415, 421, 422, 437, 438]. The three reactions were also studied [462, 463, 467] with the Daphne detector at Frascati, described briefly in section 3.4.2. The latter experiment has the largest statistics; hence the Daphne results are shown in Fig. 87. The  $\pi^0\pi^0$  invariant mass distribution exhibits a dip at about 500 MeV/c<sup>2</sup> which is interpreted in [463] as destructive interference between two Breit-Wigner amplitudes for  $\sigma(485)$  and  $f_0(980)$  production. The results of all three experiments are summarised in Table 28.

Looking at Table 28 it seems safe to assume that the process  $\phi(1020) \rightarrow f_0(980)\gamma$  is observed with a branching fraction of about  $4 \cdot 10^{-4}$  of all decay modes. However, Boglione and Pennington [1040] criticised the KLOE analysis, reanalysed the data and found that the result depends crucially on the parametrisation of the  $\pi\pi$   $S$ -wave. The  $\pi\pi$   $S$ -wave from Au, Morgan and Pennington [177],

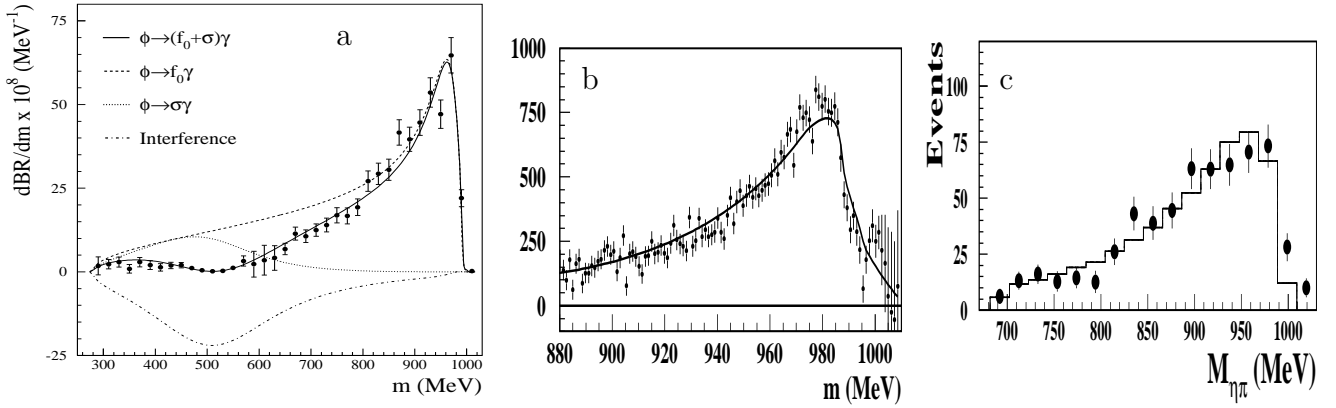


Fig. 87. Invariant mass distributions in radiative  $\phi$  decays. a:  $\pi^0\pi^0$  [463], b:  $\pi^+\pi^-$  [462], c:  $\pi^0\eta$  [467].

of Morgan and Pennington [1041], or Anisovich and Sarantsev [859] gave grossly different results,  $(0.31 \text{ or } 0.34 \text{ or } 1.92) \cdot 10^{-4}$ , respectively. The main reason for the differences between the  $S$ -waves from [177, 1041] and [859] are the different  $f_0(980)$  pole positions. A further problem arises from the dip in the  $\pi^0\pi^0$  mass distribution. In [1040] the dip is created by a zero in the production amplitude. Even when compatibility with the scattering amplitudes is maintained, the production amplitude can be shaped using different parametrisations. As a consequence, very different results on the branching fraction for  $\phi(1020) \rightarrow f_0(980)\gamma$  follow. It remains to be seen if the dip in Fig. 87 is a real effect or due to a (possibly wrong) background subtraction. Clearly, the status is unsatisfactory; appropriate methods to analyse the data need to be developed. A general parametrisation of the amplitude is proposed in [1042].

Very recently, the Daphne collaboration reported on a Dalitz plot analysis of  $e^+e^- \rightarrow \pi^0\pi^0\gamma$  events collected at  $\sqrt{s} \simeq M_\phi$  with the KLOE detector [469]. The statistics was increased very significantly; detailed studies were made to verify the dynamical assumptions of the fit. Data and fit are reproduced in Fig. 88.

In the Kaon Loop model, the two low mass scalars  $f_0(980)$  and  $\sigma(485)$  are required to adequately fit the data and a stable branching ratio of the  $\phi \rightarrow \pi^0\pi^0\gamma$  process was obtained:

Table 28

Branching ratios for radiative  $\phi$  decays (in units of  $\cdot 10^{-4}$ ). The branching ratios for  $\phi(1020) \rightarrow a_0(980)\gamma$  are corrected by using the ratio  $K\bar{K}/\eta\gamma = 0.23 \pm 0.05$  and  $K\bar{K}/\pi\pi = 0.23 \pm 0.05$  for  $\phi(1020) \rightarrow f_0(980)\gamma$ . First results from SND were obtained using  $8 \cdot 10^6 \phi$ 's, later SMD-2 and SND disposed of  $19 \cdot 10^6 \phi$  events. The first studies of KLOE were based on  $53 \cdot 10^6 \phi$ 's. In the study of  $\phi(1020) \rightarrow \pi^+\pi^-\gamma$ , an equivalent of  $3 \cdot 10^9$  events were recorded. See text for references.

Reaction	SND	CMD-2	KLOE
$\phi(1020) \rightarrow \pi^0\eta\gamma$	$0.88 \pm 0.14$	$0.90 \pm 0.24 \pm 0.10$	
$\phi(1020) \rightarrow a_0(980)\gamma$	$a_0(980) \rightarrow \eta\pi^0$	$0.83 \pm 0.23$	$0.90 \pm 0.24 \pm 0.10$
$\phi(1020) \rightarrow \pi^0\pi^0\gamma$		$1.14 \pm 0.10 \pm 0.12$	$0.92 \pm 0.08 \pm 0.06$
$3 \times \phi(1020) \rightarrow f_0(980)\gamma$	$f_0(980) \rightarrow \pi^0\pi^0$	$3.42 \pm 0.30 \pm 0.36$	$2.90 \pm 0.21 \pm 1.54$
$\frac{3}{2} \times \phi(1020) \rightarrow f_0(980)\gamma$	$f_0(980) \rightarrow \pi^+\pi^-$		$4.47 \pm 0.21$
			$1.93 \pm 0.46 \pm 0.50$
			$3.1 - 3.6$

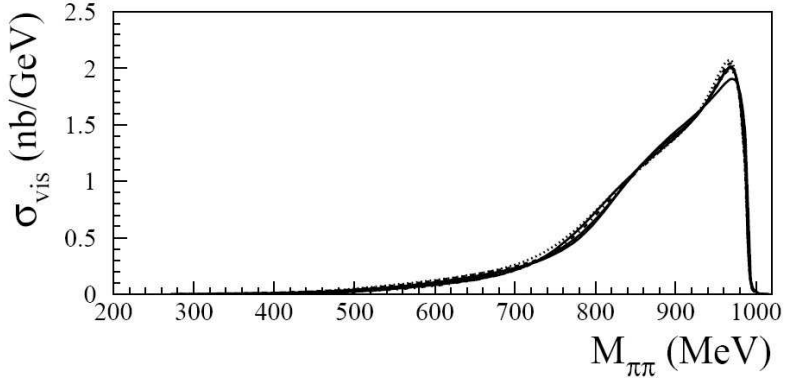


Fig. 88. The  $\pi^0\pi^0$  invariant mass distribution from Daphne [469]. Data points are represented by dots, the thick solid line is the result of a fit based on model in which  $\phi$  mesons dissociate in kaon loops radiating off photons.

$$\begin{aligned}
 \mathcal{B}(\phi \rightarrow S\gamma \rightarrow \pi^0\pi^0\gamma) &= (1.07_{-0.03}^{+0.01} \text{ fit } +0.04_{-0.02} \text{ syst } +0.05_{-0.06} \text{ mod}) \times 10^{-4} \\
 M_{f_0} &= (976.8 \pm 0.3 \text{ fit } +0.9_{-0.6} \text{ syst } +10.1 \text{ mod}) \text{ MeV}/c^2 \\
 g_{f_0 K^+ K^-} &= (3.76 \pm 0.04 \text{ fit } +0.15_{-0.08} \text{ syst } +1.16_{-0.48} \text{ mod}) \text{ GeV}/c^2 \\
 g_{f_0 \pi^+ \pi^-} &= (-1.43 \pm 0.01 \text{ fit } +0.01_{-0.06} \text{ syst } +0.03_{-0.60} \text{ mod}) \text{ GeV}/c^2.
 \end{aligned} \tag{9.4}$$

Like the experimental uncertainties in the determination of the radiative yield, the theoretical interpretation which one may find in the literature is far from being unique neither, with the  $q\bar{q}$ ,  $q\bar{q}q\bar{q}$ , and the  $K\bar{K}$  molecular picture all being pursued and compatible with data. In [1043] it is shown that the processes  $\phi(1020) \rightarrow \gamma\pi\pi$  and  $\phi(1020) \rightarrow \gamma f_0(980)$  can well be described assuming  $f_0(980)$  to be dominantly  $q\bar{q}$ . Achasov [1044] and Achasov and Kiselev argue [1045] that  $a_0(980)$  and  $f_0(980)$  production in radiative  $\phi$  decays gives new evidence in favour of their tetraquark nature. But also the molecular picture is not excluded [1046]. Radiative decays of  $\phi$  mesons into scalars are shown to require a sizable  $K\bar{K}$  component of the scalar mesons, but do not allow to discriminate between compact molecules and  $q\bar{q}$  states when they are allowed to disintegrate into a kaon loop. Close and Tornqvist [1047] propose a nonet of complex objects: near the centre they are 4-quark states, with some ( $q\bar{q}$ ) in  $P$ -wave; further out they rearrange in colour to two colourless ( $q\bar{q}$ ) pairs and finally to meson-meson states. Beveren and colleagues [822] show how light and heavy scalar mesons can be linked to one another by a continuous variation of the masses involved. They conclude that all scalar mesons can be understood as ordinary  $q\bar{q}$  states strongly distorted due to coupled channels, and suggest that labelling scalar mesons as  $q\bar{q}$  states as opposed to dynamical meson-meson resonances makes no sense, since one kind of pole can be turned into another by tiny parameter variations. For the moment, we leave the question of the nature of these states open, and discuss further data. The issue will be resumed in section 11.6.2.

## 9.5 Scalar mesons in 2-photon fusion

The radiative width of resonances, their coupling to two photons, provides another handle on their internal structure. Fig. 89 shows data on two-photon fusion into a pion pair from [1048–1050]. Identification of scalar mesons in two-photon fusion requires data with polarised photons and complete angular coverage of the hadron final state. Such data do not exist; other constraints are needed to make a partial wave separation possible. Boglione and Pennington [1051, 1052] have used several constraints to deduce the scalar part of the interaction. At low energies  $\gamma\gamma \rightarrow \pi\pi$  is dominated by a Born term. Unitarity requires that the  $\gamma\gamma \rightarrow \pi\pi$  process is related to  $\pi\pi$

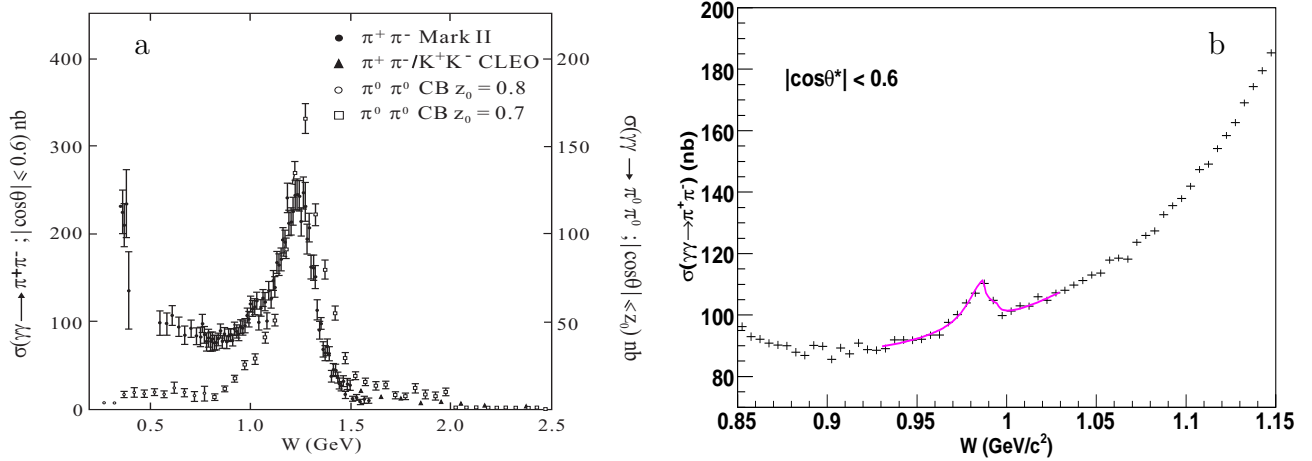


Fig. 89. a: Integrated cross-section (within  $|\cos\theta| < 0.6$ ) for  $\gamma\gamma \rightarrow \pi\pi$  as a function of c.m. energy  $W$  from Mark II [1048], Crystal Ball (CB) [1049] and CLEO [1050]. b: Expanded view of the  $f_0(980)$  region from BELLE [654] exhibiting  $f_0(980)$  as a clear peak.

scattering. At sufficiently small masses, constraints from  $\pi\pi$  and  $K\bar{K}$  intermediate states can thus be imposed. They found two solutions, in which the  $f_0(980)$  appears either as a peak or as a dip. The radiative widths of the  $f_2(1270)$ ,  $f_0(980)$  and  $f_0(485)$  for the two solutions are listed in Table 29.

New data on  $\gamma\gamma \rightarrow \pi^+\pi^-$  became available from the BELLE experiment, which supersede all previous work in statistics. A clear signal for the  $f_0(980)$  resonance is observed [654, 660]. The mass spectrum was fitted with a two-channel Breit-Wigner amplitude and interfering and non-interfering background terms. Mass and partial widths to  $\pi^+\pi^-$  and to  $2\gamma$  were determined to

$$\begin{aligned} M^{f_0} &= 985.6 {}^{+1.2}_{-1.5}(\text{stat}) {}^{+1.1}_{-1.6}(\text{syst}) \text{ MeV}/c^2, \\ \Gamma_{\pi^+\pi^-}^{f_0} &= 34.2 {}^{+13.9}_{-11.8}(\text{stat}) {}^{+8.8}_{-2.5}(\text{syst}) \text{ MeV}/c^2, \\ \Gamma_{\gamma\gamma}^{f_0} &= 205 {}^{+95}_{-83}(\text{stat}) {}^{+147}_{-117}(\text{syst}) \text{ eV}/c^2, \end{aligned} \quad (9.5)$$

respectively. Early predictions by Barnes [1053] gave the two-photon width for an internal  $n\bar{n}$  or  $s\bar{s}$  structure or a  $f_0(980)$  with molecular origin. Achasov and Shestakov interpreted the data in a model in which  $f_0(980) \rightarrow K\bar{K}$  loops play a decisive rôle [1056, 1057]; the direct  $f_0(980) \rightarrow \gamma\gamma$  coupling is shown to be negligibly small. Oller and Oset, incorporating chiral symmetry and exchange of vector and axial resonances in the crossed channels, used kaon loop diagrams to

Table 29

Radiative widths of states contributing to  $\gamma\gamma \rightarrow \pi\pi$  for the two solutions (*dip* and *peak*) from [1051] and predicted widths of scalar mesons for different compositions [1053] and recent calculations.

solution	$\Gamma(\gamma\gamma)$ keV						
	$f_2(1270)$	$f_0(980)$	$f_0(400/1200)$	prediction	$n\bar{n}$	$s\bar{s}$	$K\bar{K}$
dip	2.64	0.32	4.7	$\Gamma(0^{++} \rightarrow \gamma\gamma)$	4.5	0.4	0.6
peak	3.04	$0.13 - 0.36$	3.0			0.2	[1054]
						$0.22 \pm 0.07$	[1055]

arrive at their result [1054]. Hanhart, Kalashnikova, Kudryavtsev, and Nefediev [1055] argued for a molecular picture of  $f_0(980)$ . Their results are listed in Table 29. From an experimental point we find it hard to differentiate between a  $q\bar{q}$  or  $qq\bar{q}\bar{q}$  state (the ‘seed’) decaying into the final state via a  $K\bar{K}$  loop and, on the other hand, a truly molecular  $K\bar{K}$  state, having no seed bound by chromo-electromagnetic forces. In a recent paper, Pennington asks “Can Experiment Distinguish Tetraquark Scalars, Molecules And  $q\bar{q}$  Mesons?” [1058]. His answer is yes, with some conditional ifs, in particular only when the wave function does not have a complicated Fock space expansion. Applied to the  $\sigma(485)$ , the direct answer from its 2-photon coupling assigns a  $q\bar{q}$  nature [1059]. Obviously, such predictions have to be taken with some precaution.

## 9.6 Production of $f_0(980)$ as a function of $t$

The GAMS collaboration reported a peculiar behaviour of  $f_0(980)$  production in the reaction  $\pi^- p \rightarrow n\pi^0\pi^0$ . For small momentum transfers between the proton and the neutron ( $-t < 0.1 \text{ GeV}^2$ ), the scalar amplitudes show a dip around 1 GeV, while  $f_0(980)$  is observed as a peak for large momentum transfers ( $-t > 0.4 \text{ GeV}^2$ ). This observation has been interpreted as evidence for a hard component in the  $f_0(980)$  [35, 852, 1060, 1061]. However, the strong dependence of  $f_0(980)$ -production on the momentum transfer between proton and neutron can also well be reproduced by a change of the interference between the resonance structure and the non-resonant background when  $\pi\pi$  and  $a_1(1230)\pi$  scattering are considered, and the data are fully compatible with the molecular picture of  $f_0(980)$  [1062–1065].

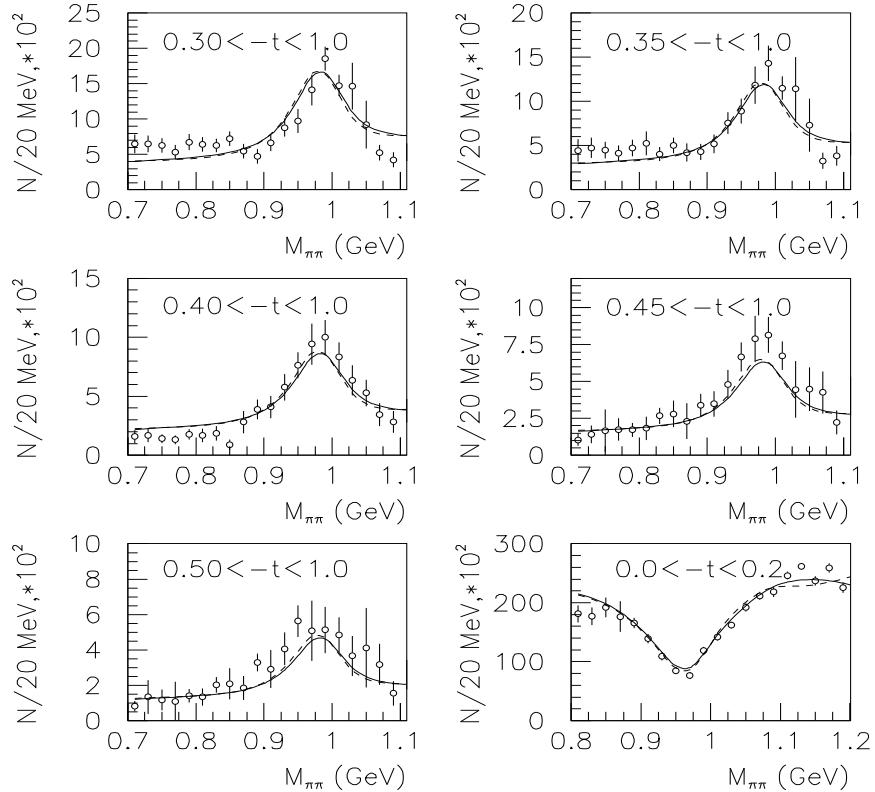


Fig. 90. The reaction  $\pi^- p \rightarrow \pi^0\pi^0n$  as a function of the momentum transfer to the  $\pi\pi$  system [285].

Table 30  
Yield of light mesons per hadronic  $Z^0$  decays as a function of the mesonic mass [1038, 1066].

	$\pi^0$	$9.55 \pm 0.06 \pm 0.75$			
	$\eta$	$0.97 \pm 0.03 \pm 0.11$			
$\eta'$	$0.14 \pm 0.01 \pm 0.02$	$a_0^\pm(980)$	$0.27 \pm 0.04 \pm 0.10$	$f_0(980)$	$0.141 \pm 0.007 \pm 0.011$
		$\phi(1020)$	$0.091 \pm 0.002 \pm 0.003$		
		$f_2(1270)$	$0.155 \pm 0.011 \pm 0.018$		

## 9.7 Scalar mesons in fragmentation

The  $f_0(980)$  and  $a_0(980)$  wave functions were tested at LEP by a study of  $Z^0$  fragmentation into quark- and gluon jets. Some total inclusive rates for meson production from  $Z^0$  fragmentation are listed in Table 30.

There is a strong mass dependence of the production rates. The three mesons  $\eta'$ ,  $f_0(980)$  and  $a_0(980)$  - which have very similar masses - have production rates which are nearly identical (the two charge modes of the  $a_0(980)^\pm$  need to be taken into account). This fact was interpreted in [1038] as evidence that at short distances, the three mesons have the same internal structure. Fig. 91 shows the production characteristics of the  $f_0(980)$  compared to those of  $f_2(1270)$  and  $\phi(1020)$  mesons, and with the Lund string model of hadronisation in which  $f_0(980)$  is treated as a conventional meson. No difference is observed in any of these comparisons between  $f_0(980)$  and  $f_2(1270)$  or  $\Phi(1020)$ . The production characteristics of  $f_0(980)$  are fully consistent with the hypothesis that it is a  $q\bar{q}$  state. Further tests were made [1038] confirming this conclusion: the total number of charged particles per event or selection criteria to enhance or suppress gluon jets or quark jets led to no significant deviations between data and Monte Carlo simulation assigning a  $n\bar{n}$  nature to  $f_0(980)$  and  $a_0(980)$  (at the moment of their creation).

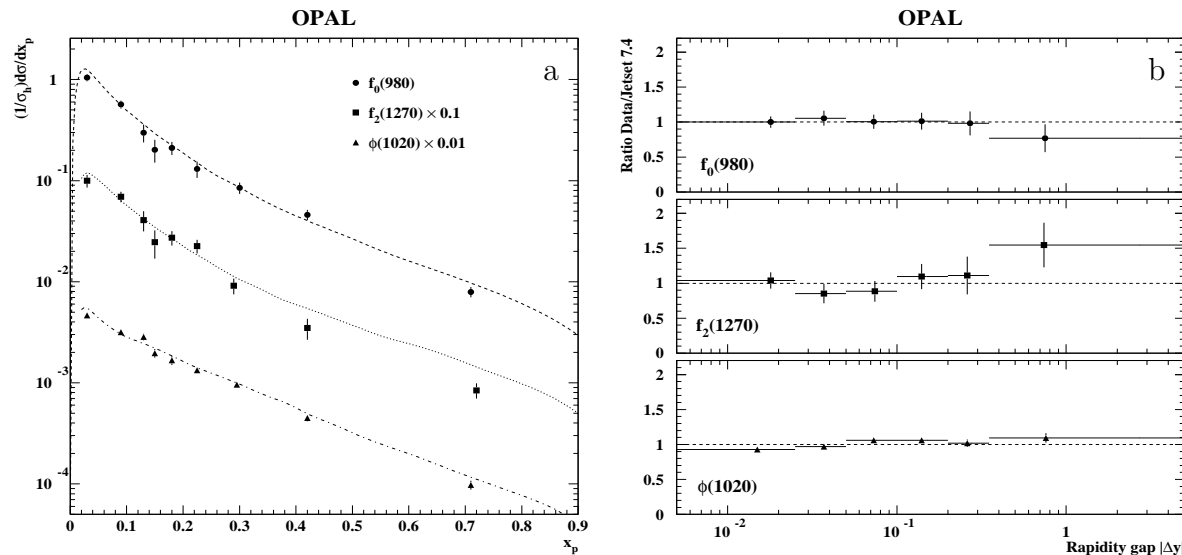


Fig. 91. Production rates for  $f_0(980)$ ,  $f_2(1270)$  and  $\phi$  compared to JETSET 7.4 simulations. a: Fragmentation functions (the  $f_2(1270)$  and  $\phi$  data are scaled by  $\times 0.1$  and  $\times 0.01$  respectively, the Monte Carlo curves are normalised to the data. b: Rates for bins of the absolute value of the rapidity difference between the meson and the nearest charged particle [1038].

## 9.8 Scalar mesons from chiral symmetry

Oller, Oset, and Pelaez used Chiral Perturbation Theory ( $\chi$ PT) to study low-mass scalar meson-meson interactions [127–129]. The authors included order  $p^4$  terms in the chiral expansion and coupled channels effects. Resonances were constructed using the Inverse Amplitude Method [130, 1067] which avoids conflicts with unitarity. The phase shifts of  $\pi\pi$  scattering, the  $\pi\pi \rightarrow K\bar{K}$  transition amplitude, the phase shifts of  $\pi K$  scattering and the  $\pi\eta$  mass distribution for the  $a_0$  resonance were well reproduced. The authors suggest that the resonances  $a_0(980)$ ,  $f_0(980)$ ,  $\sigma(485)$ , and  $\kappa(700)$  form a nonet of dynamically generated resonances, unrelated to  $q\bar{q}$  spectroscopy since they have put no ab-initio resonance into the formalism. Of course, the low energy constants may not be really independent of any resonance physics. Their conclusions are confirmed by a recent analysis of van Beveren, Bugg, Kleefeld, and Rupp [861] in which generation of  $\sigma(485)$ ,  $\kappa(700)$ ,  $a_0(980)$  and  $f_0(980)$  is a balance between attraction due to  $q\bar{q}$  loops and suppression of the amplitudes in the chiral limit. The immediate question arises: are there more dynamically generated resonances and how can they be differentiated?

In  $\chi$ PT, the dependence of low energy constants on the number of colours  $N_c$  can be derived. Then masses and widths are known as functions of  $N_c$ . The mass of a  $q\bar{q}$  meson should not depend on  $N_c$ : it does not matter if the  $q\bar{q}$  pair is red, green or blue or has additional colour options. The widths however scale with  $1/N_c$  since the newly created  $q\bar{q}$  pair must have colour and anticolour to match the colour of the mesonic  $q\bar{q}$  pair at the instant of pair creation.

Fig. 92 shows, for increasing  $N_c$ , the evolution of the pole positions of light vector and scalar mesons [1068, 1069]. The  $\rho$  and  $K^*$  masses remain constant for increasing  $N_c$  while the widths become narrower. This is the behaviour expected for ‘normal’  $q\bar{q}$  mesons. In the  $\sigma(485)$  and  $\kappa(700)$  region, the signal dilutes as it does in the  $f_0(980)$  and  $a_0(980)$  region. In the large  $N_c$  limit, the low-mass scalar mesons are lost. This behaviour does not depend critically on the renormalisation scale chosen in the range  $\mu = 0.5 – 1$  GeV. The behaviour is incompatible with these particles being  $q\bar{q}$  mesons. Only  $a_0(980)$  survives for very small values of  $\mu$ . Hence a  $q\bar{q}$  nature of  $a_0(980)$  is not fully excluded. But in this interpretation, all four states,  $\sigma(485)$ ,  $\kappa(700)$ ,  $f_0(980)$ , and  $a_0(980)$ , are dynamically generated poles probably unrelated to the physics of  $q\bar{q}$  states. The  $N_c$  dependence of light mesons was also studied by Uehara [1070]; in agreement with Pelaez it was found that  $\rho$  and  $K^*$  survive for large  $N_c$  as narrow width resonances while the scalar mesons below 1 GeV fade away already when  $N_c$  exceeds 6.

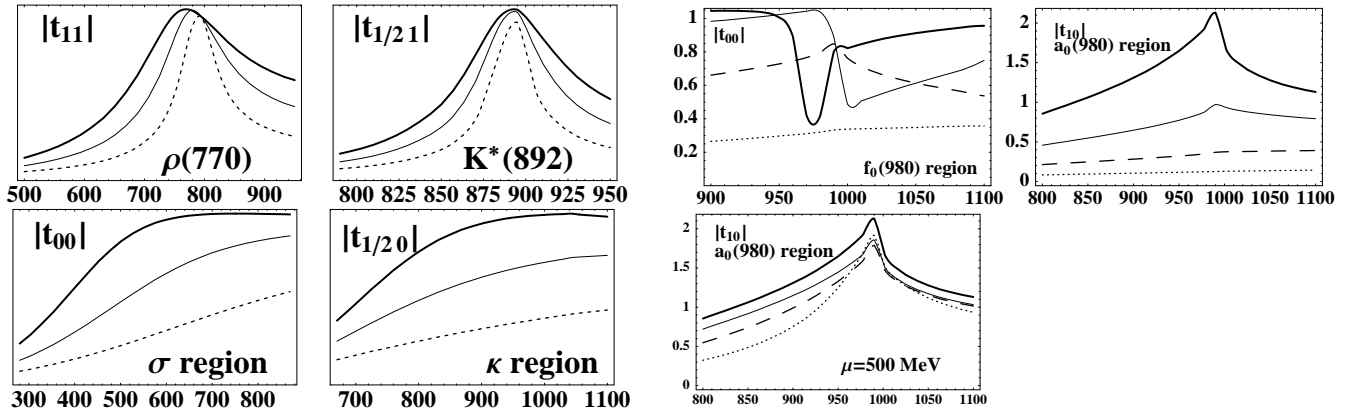


Fig. 92.  $N_c$  dependence of the pole positions of light vector and scalar mesons [1068].

## 9.9 A low-mass nonet of scalar mesons

There is now solid evidence that there are nine low-mass scalar mesons. These are  $\delta, S^*, \sigma(485)$ ,  $\kappa(700)$  or  $a_0(980)$ ,  $f_0(980)$ ,  $f_0(485)$ ,  $K_0^*(700)$ . Likely, they form a SU(3) nonet. There is, however, still ample room for different interpretations.

Hanhart, Kalashnikova, Kudryavtsev, and Nefediev [1055] and C. Hanhart, private communication, argue that the scalar nonet, in particular  $f_0(980)$ , must be interpreted as  $K\bar{K}$  molecule. If the pole position of a state is much closer to a threshold than any intrinsic scale of the problem, one can disentangle the molecular component from the compact one. The idea is based on analyticity: if the pole is predominantly generated from the non-analytic pieces that emerge from the loops of the constituents, then it deserves the name molecule. If the pole is predominantly generated from quark dynamics, it can only lead to contributions analytic in  $s$ , and it should be called a compact state.

Achasov [1044] has a different view: he sees the flow-lying scalar mesons as compact tetraquark states as they result for instance from the MIT bag model [1071, 1072]. The compact object decays virtually into a  $K\bar{K}$  loop which is responsible for the decay dynamic.

Beveren and collaborators argue that the strong coupling of  $q\bar{q}$  states to the meson-meson continuum gives rise to a doubling of states but that it makes little sense to talk about intrinsic resonances and dynamically generated poles [1073]. The  $\sigma(485)$  and  $\kappa(700)$  still have  $q\bar{q}$  seeds and the  $\sigma(485)$  still is the chiral partner of the pion. The  $D_{s0}^*(2317)$  is linked to the  $\kappa(700)$  while the next  $c\bar{s}$  quark model states are predicted to have a pole position at  $M - i\frac{1}{2}\Gamma = 2800 - i200$  MeV [1074], very far off the Godfrey-Isgur prediction [171]. Obviously it is wrong to consider the quark model states as independent of the interaction of their decay products; coupled channel effects and unitarity have a significant impact on the properties of quark model states even though the seed of these states may still be of  $q\bar{q}$  nature. It is suggested that the coupling between  $q\bar{q}$  and meson-meson systems leads to a doubling of states.

Tornqvist [1075], imposing the Adler zero and unitarity, identified low-mass scalars as  $q\bar{q}$  objects. He found ‘that in particular for the  $a_0(980)$  and  $f_0(980)$  the  $K\bar{K}$  component in the wave function is large, i.e., for a large fraction of the time the  $q\bar{q}$  state is transformed into a virtual  $K\bar{K}$  pair. This  $K\bar{K}$  component, together with a similar component of  $\eta'\pi$  for the  $a_0(980)$ , and  $\eta\eta$ ,  $\eta\eta'$  and  $\eta'\eta'$  components for the  $f_0(980)$ , causes the substantial shift to a lower mass than what is naively expected from the  $q\bar{q}$  component alone’. His view finds support in an analysis of  $D_s \rightarrow 3\pi$  decay via  $f_0(980)$  [1076]. The  $f_0(980)$  resonance is interpreted as  $s\bar{s}$  state with significant  $K\bar{K}$  component.  $D_s \rightarrow 3\pi$  decays via  $f_0(980)$  couple to its  $s\bar{s}$  component. The methods are tested using the more frequent process  $D_s \rightarrow \phi\pi$ . In a recent paper by van Beveren, Bugg, Kleefeld, and Rupp the  $\sigma(485)$ ,  $\kappa(700)$ ,  $a_0(980)$  and  $f_0(980)$  nonet is interpreted as balance between attraction due to  $q\bar{q}$  loops and the suppression of the amplitudes at the Adler zeros [861].

Boglione and Pennington used a toy model to study this phenomenon [1077]. Starting with just one bare seed for each member of a scalar nonet, they generated two isovector states which they identified with the  $a_0(980)$  and the  $a_0(1450)$ . In the  $I=1/2$  sector, they generated states with masses above 1 GeV but not the  $\kappa(700)$ . The isoscalar sector proved to be the most complicated one and the outcome was very strongly model dependent but the occurrence of numerous states was achieved. Beveren, Pennington and Tornqvist, interpret the scalar mesons as being generated by both  $q\bar{q}$  mesons and molecular forces. The interplay of direct QCD forces and molecular forces is suggested to generate two nonets but all mesons are supposed to have a similar structure: they

are  $q\bar{q}$  mesons with properties which are strongly influenced by their coupling to the continuum. If this view holds true, we should expect that scalar mesons do not behave like  $1^3P_2$   $q\bar{q}$  mesons do; the scalar mesons may be more complicated than their tensor brothers. Both scenarios agree in the number of states: when the number of scalar states is counted – to answer the question if a scalar glueball hides in the spectrum – the low-lying scalar meson nonet is supernumerous. However, there is certainly a strong model dependence in such a statement.

QCD sum rules were exploited by several authors to shed light onto the scalar mesons. Sum rules are a powerful technique to study hadrons. However, there is no direct correspondence between the constituent quark picture and the operator (current) quark picture. Diquarks are thus not a meaningful concept in sum rule approaches [1078], and care must be taken not to overinterpret the results. Brito, Navarra, Nielsen, and Bracco found that the mesons decay constants and hadronic couplings are consistent with a tetraquark structure for the light scalar mesons [1079]. Chen, Hosaka and Zhu [1080] determine the mass spectra for tetraquark and  $q\bar{q}$  scalar mesons, and find the tetraquark states below, the  $q\bar{q}$  mesons above 1 GeV. Matheus, Navarra, Nielsen and Rodrigues da Silva use QCD sum rules to argue against the tetraquark of the light scalar nonet [1081]. Obviously, this question is not yet settled.

The low masses of  $\sigma(485)$ ,  $\kappa(700)$ ,  $a_0(980)$  and  $f_0(980)$  – compared to any quark model prediction – find a well-founded explanation by Jaffe’s tetraquark picture [906]. These tetraquark states are not compact objects like those of Achasov. The difference can be understood discussing a toy model to illustrate the relation between a ‘molecular’ state and a state bound by chromodynamic forces, see [1082] and Jaffe, private communication. In the toy model, the four quarks are bound very weakly inside of a strong interaction volume; outside, the  $K\bar{K}$  system is supposed not to interact. If the colour forces are strong enough to bind the system, its small binding energy forces the system to become large. Thus  $f_0(980)$  does not need to be a compact object but four quark correlations are still a decisive element. The  $f_0(980)$  is bound by mesonic forces. But the forces are chromodynamic in origin and do not have a simple representation in terms of meson-exchange forces between the nucleons.

The  $1/N_c$  expansion identifies the low-mass scalar mesons as non- $q\bar{q}$  objects. In the  $1/N_c$  expansion, scalar mesons certainly behave differently than vector mesons do. This does not imply that the low-mass scalar mesons have no  $q\bar{q}$  component. Scalar mesons have a strong coupling to their  $S$ -wave decays, and this may already be sufficient to dilute their existence in the large  $N_c$  limit. At present, it is not clear if any scalar meson survives the  $1/N_c$  test as a  $q\bar{q}$  state.

It would be very illustrative to try to differentiate the  $1/N_c$  behaviour of the  $f_1(1420)$  and  $f_1(1510)$ . Both mesons decay into  $K^*K$  in  $S$ -wave. Based on the Gell-Mann-Okubo mass formula and SU(3) symmetry of meson decays, Gavillet *et al.* [1083] concluded that  $a_1(1260)$ ,  $f_1(1510)$ ,  $f_1(1285)$ ,  $K_{1A}$  and  $b_1(1260)$ ,  $h_1(1170)$ ,  $h_1(1380)$ ,  $K_{1B}$  form two nearly ideally mixed nonets, with  $K_{1A}$ ,  $K_{1B}$  mixing to form the observed  $K_1(1280)$  and  $K_1(1400)$ . The  $f_1(1420)$  was interpreted by Longacre [1084] as molecular fluctuation between a pion, orbiting in  $P$ -wave around a scalar  $s\bar{s}$  core, and a  $K^*K$  in  $S$ -wave. Based on their glueball- $q\bar{q}$  filter (discussed in section 10.2), Close and Kirk [713] interpreted the  $f_1(1420)$  as SU(3) partner to the  $f_1(1285)$  and determined a flavour singlet-octet mixing angle of approximately 50 degrees. The latter interpretation is adopted by the Particle Data Group [1].

There are thus still many dissenting views of the low lying scalar mesons. Different interpretations of the low-mass region often entails different interpretations of the mass region above 1 GeV. One has to accept that at present, some questions do not find a unique answer: the  $q\bar{q}$ , the tetraquark, and the molecular picture all give e.g. reasonable descriptions of the process  $\phi \rightarrow \gamma\pi\pi$  and  $\rightarrow \gamma\pi\eta$ .

Even though we assign  $\sigma(485)$ ,  $\kappa(700)$ ,  $a_0(980)$  and  $f_0(980)$  to one nonet, we will, in section 11 on ‘Scalar mesons and their interpretation’, present different views as well. We will discuss the mesons below 1 GeV as originating from meson-meson dynamics, with or without  $q\bar{q}$  and  $q\bar{q}q\bar{q}$  fractions being mixed in. On the other hand, 1 GeV exceeds perhaps the range of applicability of chiral symmetry, and we will also discuss views of scalar mesons in which  $a_0(980)$  and  $f_0(980)$  are interpreted as members of a regular nonet of  $q\bar{q}$  mesons and in which only  $\sigma(485)$  and  $\kappa(700)$  are generated dynamically (even though we do not share this view). The  $\sigma(485)$  is certainly better established than the  $\kappa(700)$ ; thus interpretations accepting the  $\sigma(485)$  and ignoring the  $\kappa(700)$  will also not be discarded in the discussion. Last not least, the full nonet of light scalar mesons may have a  $q\bar{q}$  seed with properties strongly influenced by their couplings to two pseudoscalar mesons as proposed in section 11.6.2.

## 10 Scalar mesons above 1 GeV

In this section data will be presented and discussed which contribute to the spectrum of scalar mesons above 1 GeV. The main focus will be on the existence and the properties of isoscalar scalar candidates which have been suggested,  $f_0(1370)$ ,  $f_0(1200 - 1600)$ ,  $f_0(1500)$ ,  $f_0(1670)$ ,  $f_0(1710)$ ,  $f_0(1790)$ ,  $f_0(1810)$ ,  $f_0(2000)$ ,  $f_0(2100)$ . This is an unexpected large number; the quark model expects 4 (possibly 6) states, QCD predicts one scalar glueball in this mass range. Of course, there might be  $qq\bar{q}\bar{q}$  and hybrid states in addition. On the other hand, it is also not unlikely that some of these states do not survive critical discussions of their viability. In a first scan, we present results from individual experiments; at the end of this section results from combined fits to several data sets will be presented. This allows us to define the impact of individual experiments and to emphasize the virtue of getting a consistent picture of a large number of meson resonances from fits to many reactions.

### 10.1 Charge exchange

The CERN-Munich experiment (see section 3.1.1) on the charge exchange reaction  $\pi^- p \rightarrow n\pi^+\pi^-$  covered the meson mass range from 600 to 1900 MeV. The data are still used to constrain modern partial wave analyses. General features of apparatus and of the data were presented in [204], production mechanism and  $t$  dependence studied in [206]. The results of energy-dependent and energy-independent partial wave analyses on the  $\pi^+\pi^-$  system can be found in [205, 210]. Isotensor  $\pi\pi$  interactions were studied in [208, 211]. Later, the  $H_2$  target was replaced by a polarised target providing for ‘model-independent analyses’ of the  $\pi^+\pi^-$  [212] and  $K^+K^-$  systems [1085]. Partial wave analyses of the CERN-Munich data were also performed by Estabrooks and Martin [994, 1002, 1086] and Martin and Pennington [1087]. The scalar isoscalar phase motion above 1 GeV of the CERN-Munich data is presented in Fig. 93 for the four different CERN-Munich solutions. In all four cases, the phase motion exhibits a resonance-like behaviour in the 1500 MeV region,

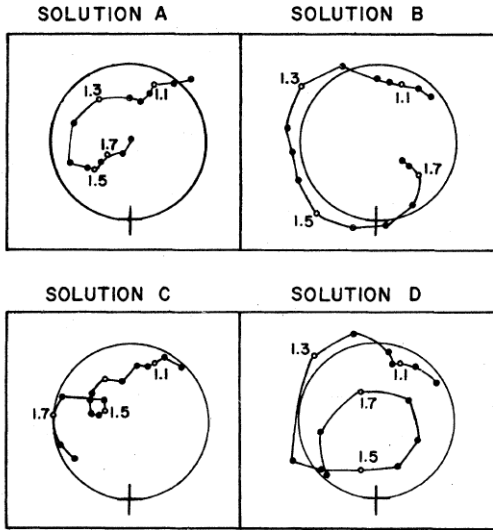


Fig. 93. The scalar isoscalar phase from CERN-Munich data on  $\pi^- p \rightarrow n(\pi^+\pi^-)_{S-\text{wave}}$  for four different solutions [1002, 1086]. A  $K$ -matrix fit to the yields consistent parameters for  $f_0(980)$  and one second resonance at a mass between 1.5 and 1.6 GeV [1088].

and a hint for a further phase advance above 1.7 GeV. Estabrooks fitted the data (plus the data below 1 GeV and the  $\pi\pi \rightarrow K\bar{K}$  data) using a two-channel  $K$ -matrix [1088]. Two resonances and a slowly varying background amplitude were sufficient to get a good fit. The  $f_0(980)$  mass and width were consistent in all four fits, the  $f_0(1500)$  – as it is called now – came out with mass and width between 1.5 and 1.6 GeV and 140 and 320 MeV, respectively.

A recent energy dependent fit to the CERN-Munich data was performed by L. Li, B. S. Zou, and G. I. Li [991]. Ambiguities were not discussed, but constraints from knowledge of other experiments was built into the analysis. The authors used  $t$ -channel  $\rho$  exchange to fit the  $\pi\pi$  isotensor interaction and fixed the  $\rho$  exchange contribution to the isoscalar interaction by the relation  $T^{Born}(I=2) = -\frac{1}{2}T^{Born}(I=0)$ . This part of the amplitude gave rise to a  $\sigma(485)$  pole at  $(0.36 - 0.53i)$  GeV. Two relatively narrow resonances were found,  $f_0(980)$  and  $f_0(1500)$ , and a broad one with a pole at  $(1.67 - 0.26i)$  GeV. The  $f_0(1370)$  and  $f_0(1710)$  mesons were not observed.

The exchange character of the interaction can be seen in Fig. 94 where the  $S$ -wave intensity is shown as a function of the squared momentum transfer  $|t|$ . The data stem from a charged exchange experiment (E852) at BNL using a 18.3 GeV/c pion beam [253]. A short description of the detector was given in section 3.1.5. For large momentum transfers to the proton, not only pions but also heavier mesons, in particular  $a_1(1260)$ , are exchanged. The quantum numbers of the exchange particles are restricted by conservation laws. Of course, when a pion is exchanged, the  $\pi(1300)$  can also be exchanged. Generalising the concept, the exchange of  $q\bar{q}$  pairs is referred to as Reggeon exchange.

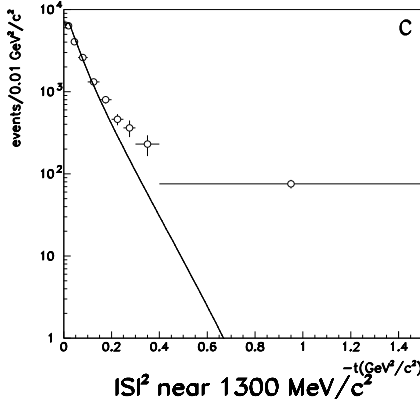


Fig. 94. The  $S$ -wave intensity as a function of  $|t|$  at  $1.30 \text{ GeV}/c^2$  compared with one-pion exchange. At small  $|t|$  data are well described. At higher  $|t|$ , additional exchange currents like  $a_1(1260)$  exchange start to contribute [253]. A turnover expected at low  $t$  was not observed.

The  $S$ -wave mass distributions for different intervals of  $t$  are shown in Fig. 95 together with a fit by Anisovich and Sarantsev [859]. The contribution of  $a_1(1260)$  deserves some comments. Apart from  $\pi$  and  $a_1(1260)$  exchanges, there is the possibility of significant  $\pi(1370)$  or  $a_2(1320)$  exchange contributions. The  $S, P_0, P_+, P_-$  amplitudes and their relative phases depend on the nucleon helicities [993]. Without using a polarised target, the partial waves  $P_0$  and  $P_+$  cannot be deduced from the moments without further assumptions. At low  $q^2$  and for pion exchange, the phase between  $P_0$  and  $P_+$  can be shown to vanish; the  $\pi\pi$  phase is then the same for spin-flip and spin-non-flip at the  $\pi N$  vertex. This is expected in the chiral limit and holds true for the reconstructed amplitudes. Under these conditions, the rank of the spin-density matrix is one, and all amplitudes can be fixed (apart from the  $2^n$  fold ambiguities when the real part of the amplitudes

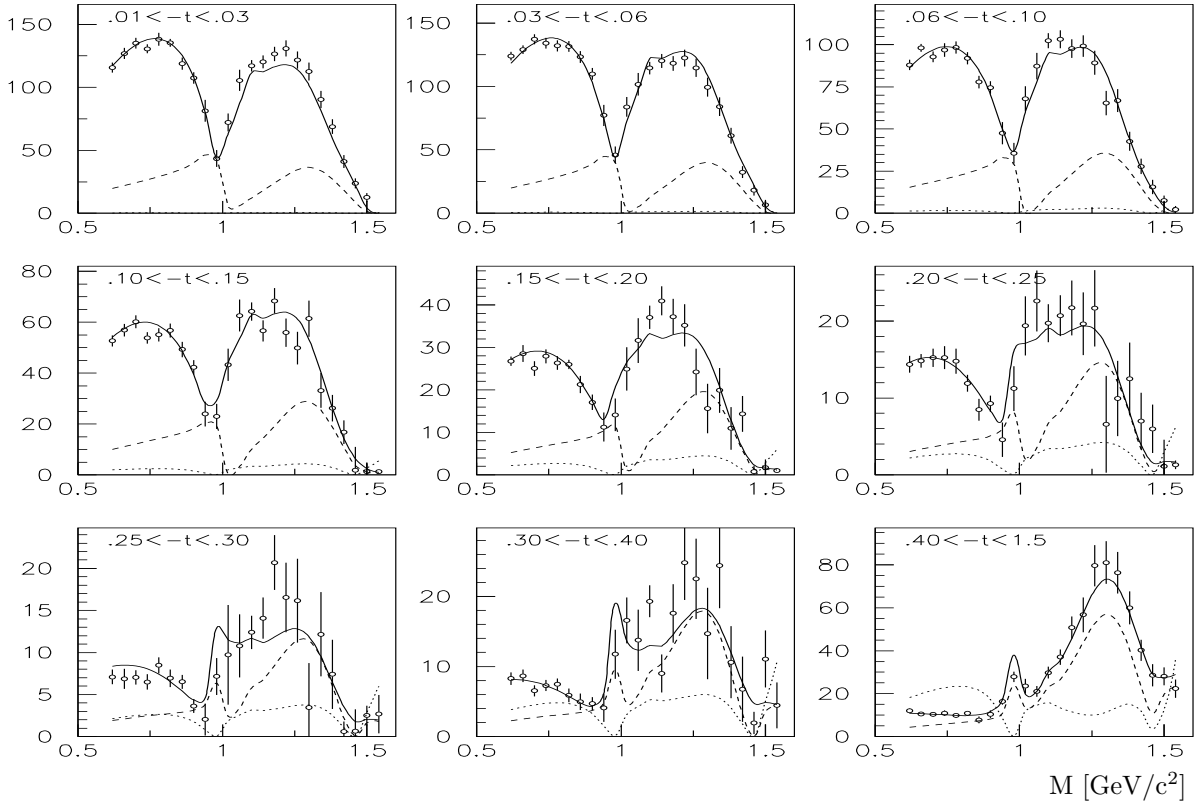


Fig. 95. The reaction  $\pi^- p \rightarrow p\pi^0\pi^0$  18.3 GeV/c for different  $t$ -intervals [253]. The dashed curve shows the contribution of the  $a_1$ -trajectory, the dotted curve of the pion trajectory [859].

has  $n$  zeros). For large  $t$  and complex exchange currents the hypothesis does not need to be fulfilled, and the bump in the  $\pi\pi$  mass distribution could receive large contributions from a feedthrough of  $f_2(1270)$  production. The warning is important since the data are used to argue that the existence of  $f_0(1370)$  follows unambiguously from this data (and similar data on  $\pi\pi \rightarrow K\bar{K}$ ).

Above the  $K\bar{K}$  threshold, inelastic reactions set in. As seen in Fig. 81, the  $\pi\pi$  S-wave intensity exhibits dips at the  $f_0(980)$  and  $f_0(1500)$  masses. In the mass range up to 1500 MeV, open channels are  $\pi\pi \rightarrow K\bar{K}, \eta\eta$ , and  $4\pi$ . Fig. 96 shows data on the former two channels. The  $K_S^0 K_S^0$  mass distribution falls off from a maximum value due to  $f_0(980)$  formation, show a dip-bump structure at and decreases sharply at 1500 MeV. The  $\eta\eta$  mass distribution exhibits a striking dip at this mass. The data were recently fitted by Bugg [1089], with and without introduction of an amplitude for  $f_0(1370)$ . The  $K_S^0 K_S^0$  mass distribution is better described when  $f_0(1370)$  is introduced even though the phase motion is still problematic for masses below 1.25 GeV. The discussion if a resonance  $f_0(1370)$  exists or not will be resumed in section 10.4.

## 10.2 Scalar resonances from central production

Double Pomeron Exchange is one of the reactions which are supposed to reveal the existence of glueballs. Double Pomeron Exchange ( $PP \rightarrow M_X$ ) is expected to contribute a large fraction to central production even though the systematic of meson production provides only limited support for this conjecture. The technique of central production experiments and a survey of results was presented in section 4.1.3. Pseudoscalar, axial vector and  $J^{PC} = 2^{-+}$  mesons seem to be produced mainly via Reggeon-Reggeon fusion ( $RR \rightarrow M_X$ ). For tensor mesons, the available data are not conclusive while production of scalar mesons follows closely the expectation from Double Pomeron

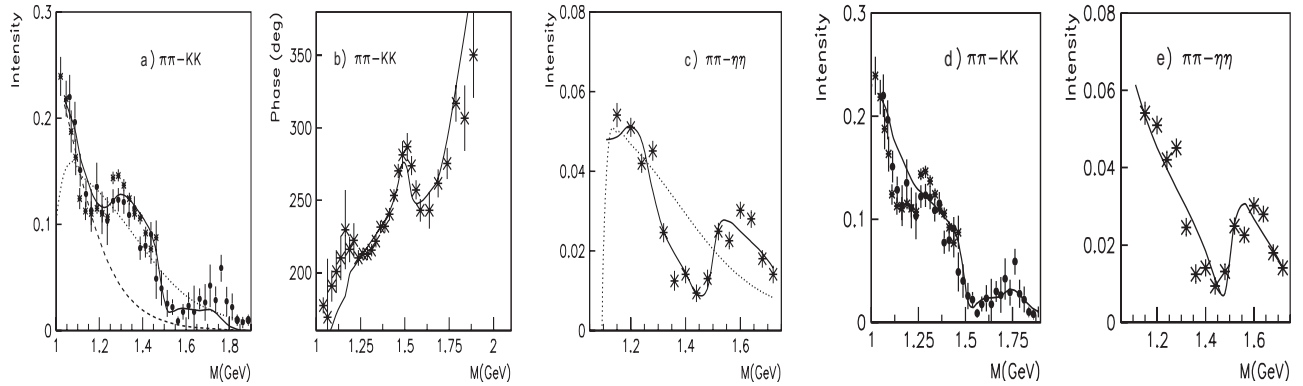


Fig. 96. . Scalar partial wave produced in  $\pi p$ -collisions at small momentum transfers  $t$ . a + d)  $\pi\pi \rightarrow K\bar{K}$ , crosses show data from Martin and Ozmutlu, circles those of Lindenbaum and Longacre [1090, 1091]. b) phases of Etkin et al. [1092]. c + e)  $\pi\pi \rightarrow \eta\eta$ , data from Binon et al. [82]. The solid lines in a,b,c) show the best fit by Bugg [1089] which includes  $f_0(1370)$ , in d,e) the  $f_0(1370)$  resonance is omitted from the fit. The dashed curve shows the intensity of  $f_0(980)$  and the dotted curves that from  $\sigma(485)$ .

Exchange: in central production at  $\sqrt{s} = 29.1$  GeV, the  $a_0(980)/f_0(980)$  ratio is  $\sim 1/10$ ,  $f_0(1500)$  production is observed,  $a_0(1470)$  production not, and the frequency of scalar mesons as a function of the four-momentum transfer is compatible with the expected  $e^{bt}$  distribution. In this section we restrict the discussion to scalar mesons and assume that the dominant production process is Pomeron-Pomeron fusion.

The WA102 results on central production of  $\pi^+\pi^-$  [314] are summarised in Fig. 97. The figure shows (a) the so-called Ehrlich distribution (square of the transverse missing mass) suggested in [1093] with a peak at the squared pion mass. A cut  $-0.3 \leq M_X^2 \leq 0.2$  GeV $^2$  selects events for further analysis. The  $p_{fast}\pi^\pm$  effective mass spectra are plotted in Fig. 97b,c, respectively. In the  $p_{fast}\pi^+$  mass distribution (Fig. 97b),  $\Delta^{++}(1232)$  is observed, while in  $p_{fast}\pi^-$  (Fig. 97c) there is obviously also significant production of  $\Delta^*$ 's or  $N^*$ 's at higher mass. Both  $\Delta(1232)$  signals were

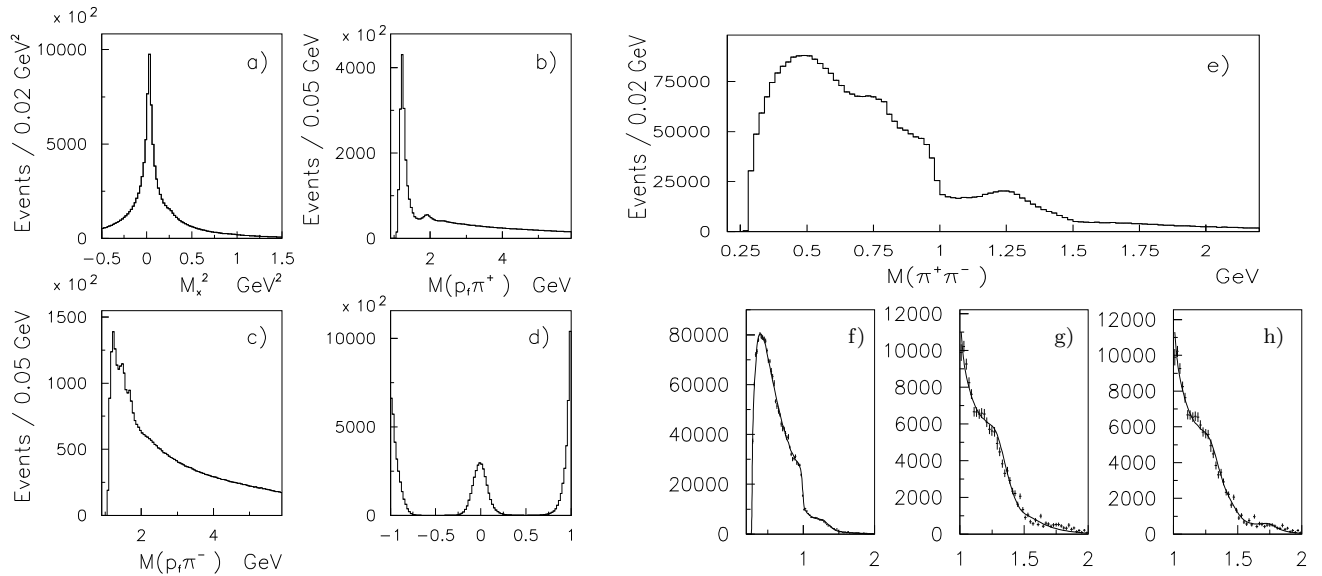


Fig. 97. Extraction of centrally produced  $\pi^+\pi^-$  pairs. a) The Ehrlich mass squared distribution, b) the  $M(p_f\pi^+)$  and c) the  $M(p_f\pi^-)$  mass spectra. d) The  $x_F$  distribution for the slow and the fast particle, and for the  $\pi\pi$  system. e) The centrally produced  $\pi\pi$  invariant mass distribution. The physical solution from the PWA of the  $\pi\pi$  final state. Full mass range (f); the 1 to 2 GeV region without (f) and with (h) inclusion of  $f_0(1710)$  in the fit [314].

removed by a cut  $M(p_{fast}\pi) > 1.5$  GeV; there is a similar cut on *slow*-proton excitations. It was verified by a cut  $M(p\pi) > 2.0$  GeV that production of high-mass baryon resonances does not lead to significant changes in the final results. The Feynman  $x_F$  distributions for the ‘slow’ and ‘fast’ particles and the  $\pi\pi$  system are shown in Fig. 97d. The central region is clearly seen to lie within  $|x_F| \leq 0.25$ . The resulting centrally produced  $\pi\pi$  mass distribution is shown in Fig. 97e. A small  $\rho^0(770)$  signal and some  $f_2(1270)$  can be seen and a sharp drop at 1 GeV which is due to interference of  $f_0(980)$  with the  $S$ -wave background. A second dip develops at 1.5 GeV due to  $f_0(1500)$ . The partial wave analysis of this data was performed assuming the  $\pi\pi$  system to be produced by the collision of two objects (e.g. two Pomerons or Reggeons) and full coherence of the final state. As discussed above, the latter assumption is a strong but untested constraint. The data was divided into mass bins and expanded into multipoles from which the partial wave amplitudes were derived. A system with  $S, P$  and  $D$  waves has eight solutions for each mass bin. In each mass bin, one of these solutions was found from the fit to the experimental angular distributions while the other seven can then be calculated by a method described by Chung [1094]. The solutions in adjacent mass bins were required to be analytical function of mass [289]. Under favourable circumstances, the linking procedure leads to eight global solutions. They all give identical moments but differ in the physical content. Differentiation between the solutions requires additional input such as the requirement that, at threshold, the  $S$ -wave is the dominant wave. Apart from the  $S$ -wave, the data show clear evidence for  $\rho(770)$  in the  $P^-$  wave and for  $f_2(1270)$  in the  $D^-$  wave, produced dominantly with  $m = 0$ .

The  $S$ -wave of the surviving solution is shown in Fig. 97f-h. The data exhibit a strong threshold enhancement followed by drops in intensity at 1 GeV and at 1.5 GeV as seen already in the global spectrum. The  $S$ -wave was fitted with a background of the form  $a(m - m_{th})^b e^{(-cm-dm^2)}$  – with  $m$  as  $\pi\pi$  mass,  $m_{th}$  as  $\pi\pi$  threshold mass and  $a, b, c, d$  as fit parameters – and three interfering Breit-Wigner amplitudes to describe  $f_0(980)$ ,  $f_0(1370)$  and  $f_0(1500)$ . The fit is shown in Fig. 97f for the entire mass range and in Fig. 97g for masses above 1 GeV. A forth state,  $f_0(1710)$ , leads to a significant improvement of the fit, see Fig. 97h. We quote here parameters (pole positions on sheet II) which were determined from a coupled channel analysis on centrally produced  $\pi\pi$  and  $K\bar{K}$  pairs [305]

$$\begin{array}{lllll} f_0(980) & M = & 987 \pm 6 \pm 6 & -i(48 \pm 12 \pm 8) & \text{MeV} \\ f_0(1370) & M = & 1312 \pm 25 \pm 10 & -i(109 \pm 22 \pm 15) & \text{MeV} \\ f_0(1500) & M = & 1502 \pm 12 \pm 10 & -i(49 \pm 9 \pm 8) & \text{MeV} \\ f_0(1710) & M = & 1727 \pm 12 \pm 11 & -i(63 \pm 8 \pm 9) & \text{MeV} \end{array}$$

which are consistent with the PDG [1] values for these resonances.

In the  $K\bar{K}$   $S$ -wave (Fig. 98a), a strong threshold enhancement is observed due to  $f_0(980)$  with a long tail which may comprise  $f_0(1370)$ ,  $f_0(1500)$  and  $f_0(1710)$ . The latter two resonances are seen as peaks. Partial decay widths of  $f_0(1370)$  and  $f_0(1500)$  will be discussed below (see Table 32), here we quote

$$\frac{\mathcal{B}_{f_0(1710) \rightarrow K\bar{K}}}{\mathcal{B}_{f_0(1710) \rightarrow \pi\pi}} = 5.0 \pm 0.6 \pm 0.9 \quad (10.1)$$

The  $f_0(1710)$  must have a large  $s\bar{s}$  component. The  $D$ -wave (Fig. 98b) resonates at the  $f_2(1270)$  and  $f_2(1525)$  masses, and at 2.15 GeV. The latter resonance is also seen in the D-wave  $\eta\eta$  mass distribution (Fig. 98d) to which also  $f_2(1270)$  contributes. The scalar wave (Fig. 98c) evidences  $f_0(1500) \rightarrow \eta\eta$  decays. There is a shoulder at low  $\eta\eta$  masses which is assigned to  $f_0(1370)$ .

The  $\eta\eta'$  mass distribution (Fig. 98e) is interpreted by two Breit-Wigner amplitudes with  $(M; \Gamma) =$

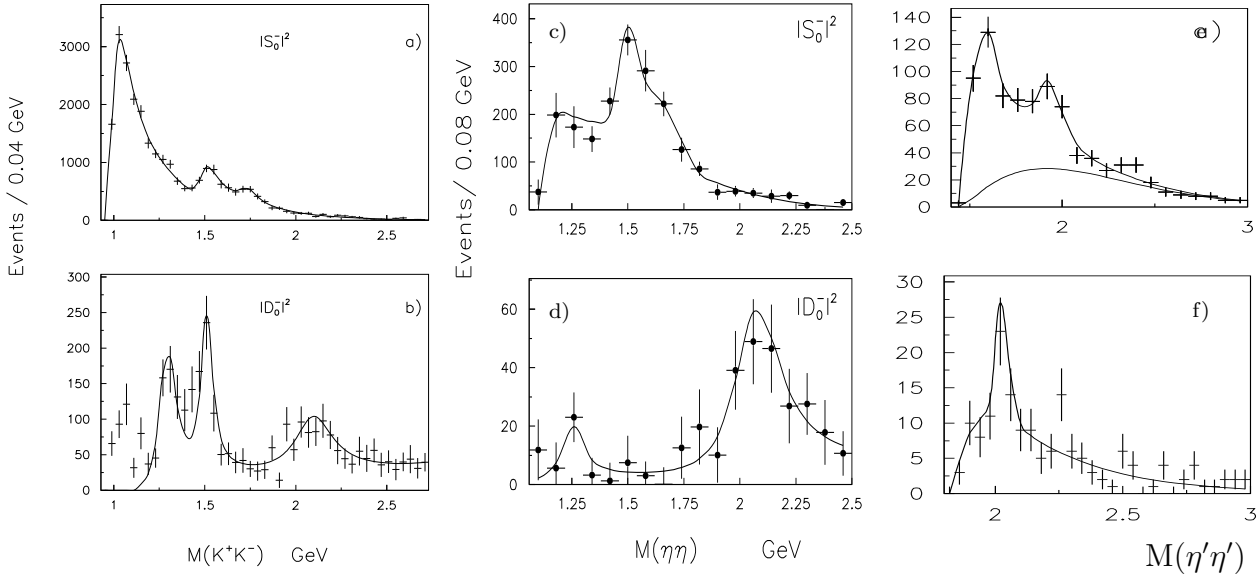


Fig. 98. The S (a,c) and D (b,d) wave for  $K\bar{K}$  [301] and  $\eta\eta$  [310] in central production. e) the  $\eta\eta'$  and f)  $\eta'\eta'$  mass distributions [306].

$(1515 \pm 12; 55 \pm 12)$  MeV and  $(1934 \pm 16; 141 \pm 41)$  MeV, respectively, and a phenomenological background in the form  $a(m - m_{th})^b e^{-cm-dm^2}$ , where  $m$  is the  $\eta\eta'$  mass. The higher-mass resonance was observed before by GAMS [281], also in  $\eta\eta'$ . It should be remembered that GAMS had observed an  $\eta\eta$  enhancement at 1590, the so-called G(1590) [280]. The  $\eta\eta$  distribution showed a pronounced peak just below 1.6 GeV which was interpreted as a resonance. The data is now explained as bump following a dip at the  $f_0(1500)$  mass [859]. Possibly, (Fig. 98e) should be interpreted by dips at 1500 and 1710 MeV (and possibly at 2100 MeV) in an  $\eta\eta'$  background spectrum. In the  $\eta'\eta'$  mass distribution (Fig. 98e), a prominent peak at about 2 GeV is observed. Its decay angular distribution suggests tensor quantum numbers. It could be related to the  $D$ -wave resonance in  $K\bar{K}$  and  $\eta\eta$  even though the masses are not fully consistent.

It is interesting to compare the  $2\pi$  distributions from central production (Fig. 97f) with those on the  $\pi\pi_{S\text{-wave}}$  from charge exchange in a 100 GeV pion beam (Fig. 81). In charge exchange, there is a background amplitude with a dip due to the  $f_0(980)$ . The  $\pi\pi$  elastic scattering amplitude is at the unitarity limit; above the  $K\bar{K}$  threshold the amplitude is still close to it. In central production, a very large low-mass enhancement is observed. Minkowski and Ochs argue that this large  $S$ -wave contribution is a new effect specific for central production and originating from Pomeron-Pomeron fusion [950]. The large intensity is however as well expected from the  $1/M^2$  dependence of the central production yield.

A bump-dip-bump structure is observed in central production of four pions, too. Fig. 99 shows  $4\pi$  invariant mass spectra from the WA102 experiment [311]. In the  $\rho\rho$  scalar intensity distribution, a large peak at 1370 MeV is seen followed by a dip in the 1500 MeV region and a further (asymmetric) bump. This behaviour is in sharp contrast to the  $\sigma\sigma$  invariant mass distribution showing an isolated peak at 1500 MeV. This is confirmed by the  $4\pi^0$  invariant mass distribution which can receive contributions from  $\sigma\sigma$  but not from  $\rho\rho$ .

The  $f_0(1710)$  is observed neither in  $\sigma\sigma$  nor in  $\rho\rho$ . Instead, a new scalar isoscalar  $\rho\rho$  resonance,  $f_0(2000)$ , is suggested. Masses and widths of  $f_0(1370)$  and  $f_0(1500)$

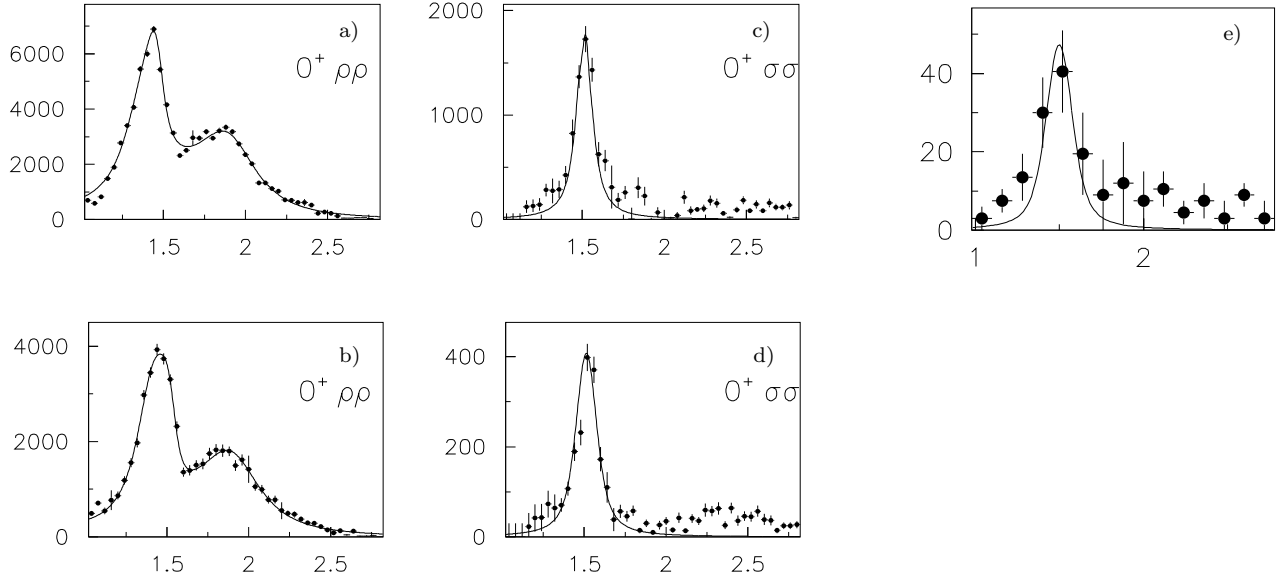


Fig. 99.  $4\pi$  invariant mass (in GeV) spectra from central production. a)  $\rho\rho$  S-wave from  $2\pi^+2\pi^-$ ; b)  $\rho\rho$  S-wave from  $\pi^+\pi^-2\pi^0$ ; c)  $\sigma\sigma$  S-wave  $2\pi^+2\pi^-$ ; d)  $\sigma\sigma$  S-wave from  $\pi^+\pi^-2\pi^0$ ; e)  $\sigma\sigma$  S-wave  $4\pi^0$ .

$$\begin{array}{lll} f_0(1370) & M = & 1309 \pm 24 -i(163 \pm 26) \text{ MeV} \\ f_0(1500) & M = & 1513 \pm 12 -i(58 \pm 12) \text{ MeV} \\ f_0(2000) & M = & 1989 \pm 22 -i(224 \pm 42) \text{ MeV} \end{array}$$

are compatible with the findings from central production of  $\pi\pi$  and  $K\bar{K}$ . The state at 1989 MeV could be related to the  $\eta\eta'$  enhancement in Fig. 98e and to similar observations in  $p\bar{p}$  annihilation in flight [366, 405], see the end of section 10.3. From the data and the fits, ratios of partial decay rates were derived given in Table 32. They will be discussed jointly with results from  $p\bar{p}$  annihilation experiments. The  $f_0(980)$  couplings were observed with  $g_\pi = 0.19 \pm 0.03 \pm 0.04$ ,  $g_K = 0.40 \pm 0.04 \pm 0.04$ .

The data on central production of four pions [307, 311] are well suited to highlight the rôle of the Close-Kirk glueball filter [713, 717]. Fig. 100 shows the scalar  $4\pi$  mass distribution for events in which the fast and the slow protons are scattered (a) into the same direction ( $\phi \sim 0^\circ$ ) or (b) into opposite directions ( $\phi \sim 180^\circ$ ).

A rotation in angle  $\phi$  leads to a significant change of the  $RR \rightarrow M$  kinematics and to a dramatic change of production mechanism. As example we consider the symmetrical case where the two scattered protons reduce their longitudinal momenta by the same value (in the cms), i.e.  $|P_{1L}| = |P_{2L}|$ , and obtain equal transverse momenta  $|P_{1T}| = |P_{2T}|$ . The transverse momenta  $\vec{P}_{1T}$  and  $\vec{P}_{2T}$  may point into the same direction, then  $\phi$  vanishes; or they may point into opposite directions with  $\phi = 180^\circ$ . For a specified mass of the centrally produced system,

$$M_X^2 = 4(t + P_L^2 + P_T^2 \sin^2(\phi/2)) \quad (10.2)$$

holds where  $t$  the momentum transfer to system  $X$  by each proton. The  $\phi$  dependence observed in Fig. 100 is thus related to a considerable variation in  $t$ .

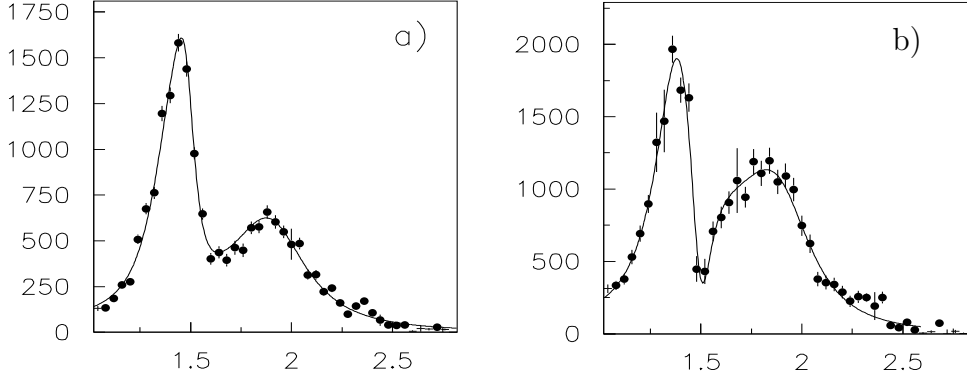


Fig. 100. The  $J^{PC} = 0^{++}$   $\rho\rho$  wave from centrally produced  $\pi^+\pi^-\pi^+\pi^-$  as a function of  $\phi$ . a)  $|\phi| \leq 45^\circ$ , b)  $|\phi - 180^\circ| \leq 45^\circ$ .

Such effects are observed in various reactions. We give a few examples:

- in diffractive production of  $\rho\pi$  by pions, the signal in the  $a_1$  region is dominated by the Deck effect at small  $-t$  and by a “true”  $a_1$  signal at large  $-t$ ;
- in the reaction  $\pi^-p \rightarrow \pi\pi n$ , the interference of  $f_0(980)$  with the wide  $\pi\pi$   $S$ -wave is purely destructive at small  $-t$  due to unitarity and mainly constructive at large  $-t$ , where unitarity constraints are relaxed.

Three interpretations were offered to explain the change in the mass distribution when different  $\phi$  ranges are selected.

- Close and Kirk compared the  $\phi$  dependence of different mesons and noticed that unconventional states have a large chance to be produced with  $|\phi| \leq 45^\circ$  while established  $q\bar{q}$  mesons have a better chance to be seen with  $|\phi - 180^\circ| \leq 45^\circ$  [713, 717]. It was suggested that at small  $dk_T$ , the production of glueball candidates is enhanced and the production of mesons is suppressed. At large  $dk_T$ , there is ample production of mesons and little production of glueballs. In the fits [307, 311], the strong enhancement at  $\sim 1.4$  GeV was assigned to  $f_0(1370)$ , the  $f_0(1500)$  produces a dip. In this view, three processes contribute to central production, gluon-gluon fusion (Fig. 101a),  $q\bar{q}$  production (Fig. 101b) and a general unspecified background.
- Ochs and Minkowski [178] assigned the dips to production of  $q\bar{q}$  mesons. The wide background is produced by diagram Fig. 101a and is called *red dragon*. It is argued that the  $f_0(1370)$  does not exist; instead, the slow background phase motion seen in  $\pi\pi$  scattering is due to a very broad resonance  $f_0(1000)$ , and this is believed to represent the scalar glueball.
- A third explanation of these effects was offered in [35]. The starting point of the interpretation is the similarity of the dips observed in  $\pi\pi$  scattering (Fig. 81) and in  $4\pi$  central production (Fig. 100b). The peak at 980 MeV in Fig. 81 disappears gradually when the kinematical regime is changed (Fig. 94) and may even turn into a peak. The gradual disappearance of the  $4\pi$  dip in Fig. 100a compared to Fig. 100b suggests that the same mechanism is at work. The dip is pronounced for small values of  $t$ . For opposite side scattering, the object  $M$  is produced by nearly real Pomerons ( $t' \approx 0$ ). Unitarisation of the sum of elastic background amplitude and the resonant  $f_0(1500)$  amplitude causes the observed dip. In case of one side scattering just the object  $M$  is balancing the transverse momentum of both protons and the object  $M$  is produced by highly virtual Pomerons ( $t' \approx -P_T^2$ ), and unitarisation has a reduced influence only. Since a background amplitude and unitarity effects were not taken into account in the analysis [307, 311],

the results could be misleading.

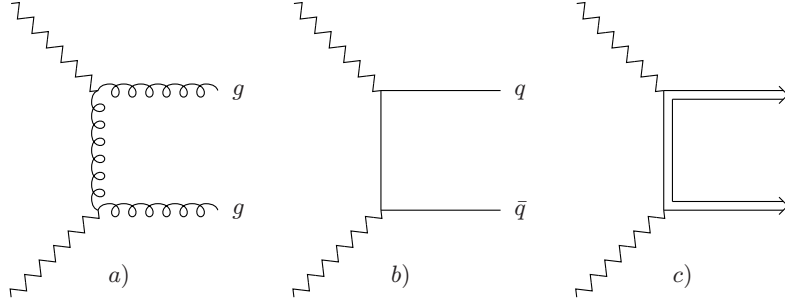


Fig. 101. Processes contributing to double Pomeron exchange. a) Glueballs may be produced by couplings of two Pomerons to glue. b) Exchange of a quark leads to production of  $q\bar{q}$ . a) and b) are short range processes. c) At large distances, mesons can be exchanged between two Pomerons.

The spectacular effects (Fig. 100 shows one example) are well explained without requiring introduction of new states. We believe that two mechanisms compete, producing mesons and a general background. The latter process is probably more peripheral (smaller  $-t$ ). In [35], the two processes depicted in Fig. 101b and c to are supposed to contribute to the  $4\pi$  system: quark exchange at short distances and a long-range exchange creating a background amplitude. To produce a  $\rho\rho$  background amplitude, a  $\rho$  trajectory needs to be exchanged between the two Pomerons; to produce  $\pi\pi$ , a pion trajectory is needed. Thus there is not one red dragon but a whole family of red dragons. For peripheral interactions, they exchange e.g. a  $\rho$  meson and two  $\rho$ 's are seen in the final state. This process yields a background amplitude. For large  $-t$ , the interaction is short range, a quark can be exchanged and Pomeron-Pomeron fusion leads to production of scalar  $q\bar{q}$  mesons which interfere destructively with the background amplitude. Experimental data show that there is no  $\sigma\sigma$  background; the  $\sigma\sigma$  final state can only be reached via formation of a  $q\bar{q}$  resonance, see Fig. 100.

### 10.3 Scalar resonances from $p\bar{p}$ annihilation

The Crystal Barrel collaboration studied scalar mesons in  $\bar{p}p$  annihilation at rest. The detector is briefly described in section 3.3.2, experimental methods are discussed in 4.1.5. Annihilation in liquid H<sub>2</sub> takes place predominantly from  $S$ -wave orbitals of the  $\bar{p}p$  atom which is formed when antiprotons come to rest. The angular momenta are restricted, and scalar mesons are produced abundantly in this process. Two scalar isoscalar mesons were discovered, the  $f_0(1370)$ ,  $f_0(1500)$ , and one isovector  $a_0(1450)$ . Their main properties were derived from six Dalitz plots [326, 329, 331, 335, 1033], shown in figure 102, and from the analysis of different five-pion final states [328, 334, 350, 352]. The Dalitz plot for  $\bar{p}p$  annihilation into  $3\pi^0$  is shown in Fig. 102a. It is based on 700.000 events. The population along the  $\pi\pi$  mass band marked  $f_2(1270)$  increases at the edges of the Dalitz plot indicating that one  $\pi^0$  is preferentially emitted along the flight direction of the resonance. This is typical for high-spin resonances. In  $\bar{p}p$  annihilation at rest, resonances with  $J = 4$  are hardly produced; the band is produced by the  $f_2(1270)$  decaying with the angular distribution  $(3\cos^2\theta - 1)^2$  from  ${}^1S_0$ . The  $f_0(980)$  appears as a narrow dip in the  $\pi\pi$   $S$ -wave. In addition, a narrow band of about constant intensity is observed. It is marked  $f_0(1500)$  in Fig. 102a. The partial wave analysis revealed contributions from a further scalar state at 1370 MeV mass. The enhancement labelled  $f_2(1520)$  originates from the constructive interference of the two low-mass  $\pi\pi$   $S$ -waves. In addition, some contribution from the  $f_2(1565)$  is required in the fit.

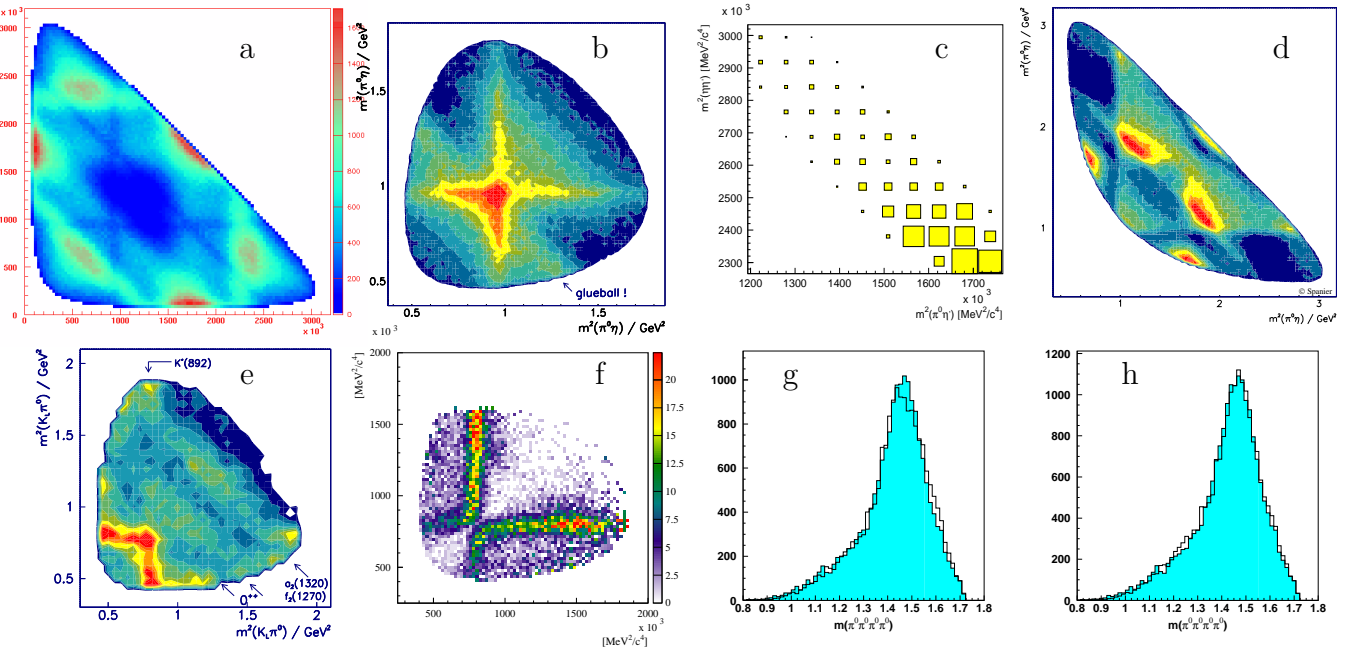


Fig. 102. Dalitz plots for  $p\bar{p}$  annihilation at rest into  $3\pi^0$  (a),  $\pi^0 2\eta$  (b),  $\pi^0 \eta\eta'$  (c),  $2\pi^0 \eta$  (d),  $K^\pm K_L^0 \pi^\mp$  (e),  $K_L^0 K_L^0 \pi^0$  (f). Plots (g,h) show the  $4\pi^0$  invariant mass in the reaction  $\bar{p}n \rightarrow \pi^- 4\pi^0$ . A fit (including other amplitudes) with one scalar state fails; two scalar resonances at 1370 and 1500 MeV give a good fit. Note that a event-based likelihood fit was performed and not a fit to the mass projection shown here. The data are from [326, 329, 329, 331, 335, 343, 350, 1033]. The  $f_0(1500)$  resonances contributes to all reactions except to (d,f); the  $f_0(1370)$  is used to all fits except (c,f). From the Dalitz plots (a,d,e,f) the properties of  $a_0(980)$ ,  $f_0(980)$  and  $a_0(1450)$  are determined.

The reaction  $\bar{p}p \rightarrow \pi^0 \eta\eta$  leads to a Dalitz plot with  $2 \cdot 10^5$  events; it is shown in Fig. 102b. The  $a_0(980)$  decaying to  $\eta\pi^0$  is seen as a horizontal and a vertical band. In the second diagonal, two homogeneously populated bands can be observed which correspond to two states decaying to  $\eta\eta$ . These are marked  $f_0(1370)$  and  $f_0(1500)$  in Fig. 102b.

In the  $\pi^0 \eta\eta'$  Dalitz plot (Fig. 102c) a strong threshold enhancement in the  $\eta\eta'$  invariant mass is seen; it can be traced to the observation of  $f_0(1500)$  in its  $\eta\eta'$  decay mode. The  $\eta$  and  $\eta'$  are orthogonal states in SU(3). The strength of this decay mode indicates a substantial SU(3) octet component in the  $f_0(1500)$  flavour wave function.

The Dalitz plot for  $\bar{p}p \rightarrow \pi^0 \pi^0 \eta$  with  $2.8 \times 10^5$  events is shown in Fig. 102d. It is characterised by a sharp increase of intensity at a  $\pi^0 \eta$  mass of  $\sim 1 \text{ GeV}/c^2$  due to  $a_0(980)$  production and a diagonal band due to  $f_0(980)$  decaying to  $\pi\pi$ . The most prominent irregular pattern with sharp maxima and minima is due to  $a_2(1320) \rightarrow \eta\pi$ . Two corners (top and right) show additional intensity which requires to introduce a scalar isovector resonance, the  $a_0(1450)$ . The strength of the interference pattern suggests that only one single  $\bar{p}p$  atomic state ( ${}^1 S_0$ ) makes a significant contribution to this annihilation mode ( $\sim 92\%$  [345]). Similar  $P$ -wave contributions are found in  $\bar{p}p \rightarrow 3\pi$  and  $\pi^0 \eta\eta$ .

The  $K_L^0 K_L^0 \pi^0$  Dalitz plot shown in Fig. 102d is based on events in which one  $K_L^0$  is detected in the Crystal Barrel detector while the second one is missing. Due to the large  $K_L^0$  mass, the final state can be identified in a kinematical fit with a surprisingly low background of a few %. It has prominent  $K^*$  bands; it is the interference with the  $f_0(1500)$  which makes the intensity so large in the lower left corner. Finally, the Dalitz plot for reaction  $\bar{p}p \rightarrow K^\pm K_L^0 \pi^\mp$  with a missing  $K_{\text{miss}}^0$  (likely  $K_L^0$ ) is given in Fig. 102f.

The reactions  $p\bar{p} \rightarrow \pi^+ \pi^- 3\pi^0$  [328],  $p\bar{p} \rightarrow 5\pi^0$  [334],  $p\bar{n} \rightarrow \pi^- 4\pi^0$  [350] and  $p\bar{n} \rightarrow 2\pi^- 2\pi^0 \pi^+$

Table 31  
Scalar mesons  $f_0(1370)$  and  $f_0(1500)$  as observed in  $p\bar{p}$  annihilation at rest.

$f_0(1370)$	M	$\Gamma$	$f_0(1500)$	M	$\Gamma$	f.s.	Ref.	Note
	$1386 \pm 30$	$310 \pm 50$				$\bar{n}p \rightarrow 5\pi$	[1095]	BW
	$1330 \pm 50$	$300 \pm 80$		$1500 \pm 15$	$120 \pm 25$	$\bar{p}p \rightarrow 3\pi^0$	[1033]	Pole
	$1360 \pm 70$	$450 \pm 150$		$1505 \pm 15$	$120 \pm 30$	$\bar{p}p \rightarrow \pi^0 2\eta$	[331]	Pole
				$1545 \pm 25$	$100 \pm 40$	$\bar{p}p \rightarrow \pi^0 \eta\eta'$	[326]	BW
	$1330 \pm 50$	$300 \pm 80$		$1500 \pm 15$	$120 \pm 25$	$\bar{p}p \rightarrow \pi^0 K\bar{K}$	[335]	Pole
	$1395 \pm 40$	$275 \pm 55$		$1500 \pm 15$	$120 \pm 25$	$\bar{p}n \rightarrow \pi^- 4\pi^0$	[350]	BW
	$1449 \pm 20$	$108 \pm 33$		$1507 \pm 15$	$130 \pm 20$	$\bar{p}p \rightarrow 3\pi$	[386]	BW

[352] were studied to determine meson decays into 4 pions. The data required two scalar states,  $f_0(1370)$  and  $f_0(1500)$  with masses and widths given in Table 31. It was found that the  $4\pi$ -decay width of  $f_0(1370)$  is about 6 times larger than the sum of all observed partial decay widths to two pseudoscalar mesons; the four-pion decays have important contributions from two pion pairs in  $S$ -wave and in  $P$ -wave (from  $\sigma\sigma$  and  $\rho\rho$ ). The  $4\pi$ -decays of the  $f_0(1500)$  represent about half of its total width.

Like CERN, Fermilab developed an intense antiproton source primarily for high-energy proton antiproton collisions. The E760/E835 experiment used a fraction of the antiproton beam at low momenta and a  $H_2$  gas jet target, see section 3.3.4. The main motivation were studies of the charmonium states formed in  $p\bar{p}$  annihilation. However, some background events were analysed,  $p\bar{p} \rightarrow 3\pi^0, 2\pi^0\eta$  [404],  $\pi^0 2\eta$ , and  $3\eta$  [403]. In particular the data on  $p\bar{p} \rightarrow \pi^0 2\eta$  show very exciting structures. The data are shown in Fig. 103. A fit yields 3 resonances with masses and widths, respectively, of

$$M = 1488 \pm 10 \text{ MeV}/c^2 \quad M = 1748 \pm 10 \text{ MeV}/c^2 \quad M = 2104 \pm 20 \text{ MeV}/c^2 \\ \Gamma = 148 \pm 17 \text{ MeV}/c^2 \quad \Gamma = 264 \pm 25 \text{ MeV}/c^2 \quad \Gamma = 203 \pm 10 \text{ MeV}/c^2.$$

The first peak is also seen in their  $\pi^0\pi^0$  mass distribution [404], the other two not. The most natural interpretation is that all three states are scalar resonances. For scalar resonances,  $\eta\eta$  decays are less suppressed by the centrifugal barrier than tensor resonances, and thus scalars survive more visibly (compared to the background) in their  $\eta\eta$  decay mode.

Recently, the data on  $p\bar{p} \rightarrow \eta\eta\pi^0$  in flight were subjected to a partial wave analysis [405]. Four  $f_0$ -states decaying into  $\eta\eta$  were reported, with masses and widths, respectively, of  $(1473 \pm 5, 108 \pm 9)$ ;  $(1747 \pm 5, 188 \pm 13)$ ;  $(2037 \pm 8, 296 \pm 17)$ ;  $(2105 \pm 8, 236 \pm 14)$ . The splitting of the  $2100 \text{ MeV}/c^2$  peak into two scalar states is also suggested by the QMC-Gatchina analysis of Crystal Barrel

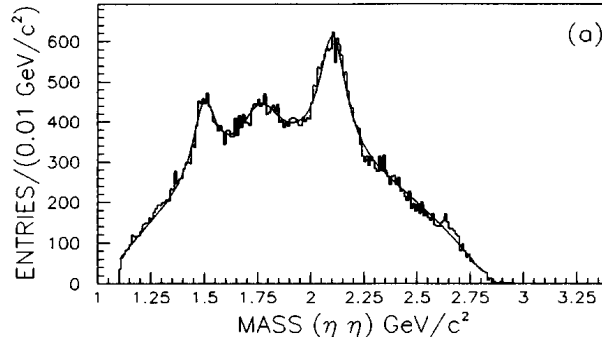


Fig. 103. The  $\eta\eta$  mass distribution from  $p\bar{p} \rightarrow \pi^0 2\eta$  at  $3 \text{ GeV}/c^2$  cms energy [403].

data on  $p\bar{p}$  annihilation in flight for 900-1900 MeV/c momenta, reporting masses and widths of  $(2005 \pm 30)$ ,  $(305 \pm 50)$  MeV/c $^2$  and  $(2105 \pm 15)$ ,  $(200 \pm 25)$  MeV/c $^2$  [366]. The agreement between these two analyses is impressive, not to say seductive; from general arguments we would expect that two overlapping resonances decouple in their respective decay modes.

## 10.4 The $f_0(1370)$ and $f_0(1500)$ resonances

### 10.4.1 The $f_0(1370)/f_0(1500)$ partial decay widths

Table 32 lists ratios of partial widths of scalar mesons as derived from  $\bar{p}p$  annihilation at rest and from central production. The intention is not to replace the PDG average values but rather to test if the same particles are observed in the two reactions. For the  $f_0(1500)$ , this is obviously the case. Most ratios are reasonably consistent except  $\Gamma_{\rho\rho}/\Gamma_{4\pi}$ . The Crystal Barrel value from  $\bar{p}p$  annihilation is much smaller than the one from central production (WA102). One source of the discrepancy could be the inclusion of  $\pi(1300)\pi$  and  $a_1(1260)\pi$  decays which were large for  $f_0(1500)$  decays in [350] and not considered in [311]. Large inconsistencies are observed for  $f_0(1370)$ . The three values of  $\Gamma_{K\bar{K}}/\Gamma_{tot}$  derived from Crystal Barrel data [394, 859, 1096] scatter wildly and are inconsistent with the WA102 result [305]. Suspicious are the small  $f_0(1370)$   $\Gamma_{\eta\eta}$  and  $\Gamma_{\sigma\sigma}$  partial widths in central production. In radiative  $J/\psi$  decays into four pions (see section 10.7) and in  $\bar{p}p$  annihilation, three scalar mesons are observed,  $f_0(1500)$ ,  $f_0(1750)$ ,  $f_0(2100)$ , which all have large  $\sigma\sigma$  and  $\eta\eta$  couplings. It is strange that just the  $f_0(1370)$  resonance should decouple from  $\sigma\sigma$  and from  $\eta\eta$  as found in central production. This observation and the dip in Fig. 100 seem to suggest that  $f_0(1370)$  is generated by  $\rho\rho$  interaction dynamics. Background amplitudes like the one shown in Fig. 101 representing Pomeron-Pomeron scattering via exchange of isovector mesons ( $\pi$  and  $\rho$  trajectories) cannot lead to  $\eta\eta$  or  $\sigma\sigma$ ; these are the decay modes missing in central production of the  $f_0(1370)$ .

### 10.4.2 Is $f_0(1370)$ a resonance?

A further point of concern is the absence of any measured  $f_0(1370)$  phase motion. The scalar isoscalar amplitude of the CERN-Munich data was already shown in Fig. 93. A rapid change of the phase is seen at 1000 and 1500 MeV/c $^2$ ; a fit with  $f_0(980)$  and  $f_0(1500)$  but without  $f_0(1370)$

Table 32  
Relative branching ratios of isoscalar scalar mesons from central production (CP) and  $\bar{p}p$  annihilation.

	$f_0(1370)$		$f_0(1500)$	
	$\bar{p}p$	CP	$\bar{p}p$	CP
$\Gamma_{\pi\pi}/\Gamma_{tot}$	$0.15 \pm 0.05^1$		$0.349 \pm 0.023^2$	
$\Gamma_{K\bar{K}}/\Gamma_{tot}$	$0.17 \pm 0.17^3$	$0.07 \pm 0.02^4$	$0.070 \pm 0.014^5$	$0.09 \pm 0.02^6$
$\Gamma_{\eta\eta}/\Gamma_{tot}$	$0.022 \pm 0.013^7$	$0.004 \pm 0.002^8$	$0.058 \pm 0.012^9$	$0.063 \pm 0.011^{10}$
$\Gamma_{\eta\eta'}/\Gamma_{tot}$			$0.015 \pm 0.004^{10}$	$0.033 \pm 0.009^{11}$
$\Gamma_{4\pi}/\Gamma_{tot}$	$0.80 \pm 0.05^{12}$		$0.76 \pm 0.08^{13}$	$0.48 \pm 0.05^{14}$
$\Gamma_{\rho\rho}/\Gamma_{4\pi}$	$0.26 \pm 0.07^{13}$	$\sim 0.9^{14}$	$0.13 \pm 0.08^{13}$	$0.74 \pm 0.03^{14}$
$\Gamma_{\sigma\sigma}/\Gamma_{4\pi}$	$0.51 \pm 0.09^{13}$	$\sim 0^{14}$	$0.26 \pm 0.07^{13}$	$0.26 \pm 0.03^{14}$

(1): educated guess, (2): from PDG, otherwise, mean and spread of results are listed. (3): [394, 859, 1096]; (4): [305]; (5): [335, 343, 394, 859, 1096] (6): [305]; (7): [859]; (8): [310]; (9): [330, 331, 859]; (10): [326]; (11): [306]; (12): [1095]; (13): [350]; (14): [311].

describes the data very well. The final conclusions of the CERN-Munich analysis were phrased by Estabrooks [1088]: ‘we found no evidence for more than three resonances’ beyond  $\sigma(485)$ ,  $f_0(980)$  and  $f_0(1500)$ . The same conclusion were obtained by Long Li, Bing-song Zou, and Guang-lie Li [1031] who decomposed the scalar amplitudes of the CERN-Munich data into  $t$ -channel  $\rho$  meson exchange plus  $s$ -channel resonances  $f_0(X)$ . The  $\rho$  exchange amplitude was fixed by the isotensor  $\pi\pi \rightarrow \pi\pi$   $S$ -wave scattering. The fit required  $f_0(980)$ ,  $f_0(1500)$ , and a broad  $f_0(1670)$  background amplitude – tentatively assigned to the scalar glueball – while  $f_0(1370)$  was not needed.

The phases of the  $4\pi$  scalar isoscalar partial wave was studied in data on  $\bar{p}p$  annihilation at rest into five pions,  $2\pi^- 2\pi^0 \pi^+$  and  $\pi^- 4\pi^0$ , respectively [350] using a method described in [1097]. In that analysis, scans were made in which the likelihood of fits were determined when the mass of a scalar resonance was changed in steps while all other variables were refitted. The scalar isoscalar  $4\pi$  intensity was described by one or two Breit-Wigner resonances. The Breit-Wigner magnitude is multiplied with a free phase factor  $e^{i\phi}$  where the phase is defined relative to the  $\rho(1450)\pi$  isobar. The optimum choice of the phase is made when the phase of the Breit-Wigner amplitude, shifted by  $\phi$ , agrees with the scalar isoscalar phase of the data. Using a single Breit-Wigner amplitude, the phase  $\phi$  (represented by  $x$  in Fig. 105a,b) follows closely the expected Breit-Wigner shape of a  $100 - 120$  MeV/c $^2$  wide resonance at 1500 MeV/c $^2$  (solid lines). When two amplitudes are offered in the fit, the complex sum of these two amplitudes has a phase which is reproduced in Fig. 105a as small dots. The resulting phase adjusts itself as to mimic the phase motion of a single resonance. Attempts were made to fit the data with the  $f_0(1370)$  amplitude being replaced by an amplitude with no phase motion. Then, the sum of the two amplitudes for  $f_0(1370)$  and  $f_0(1500)$  cannot mimic a Breit-Wigner resonance and the fit quality is worse.

Recently, Bugg has reported a ‘study in depth of  $f_0(1370)$ ’ [1098]. Fits to four data sets show a highly significant improvement (in  $\chi^2$ ) when the  $f_0(1370)$  is included as resonance. Obviously, the fit hypothesis ‘there is no  $f_0(1370)$ ’ at all is worse than the hypothesis that  $f_0(1370)$  exists. A study of the width dependence shows however that the  $f_0(1370)$  expected line shape depends only marginally on its width. When the partial width  $\Gamma_{2\pi}$  of the  $f_0(1370)$  was increased to 800 MeV/c $^2$  (and  $\Gamma_{\text{tot}}$  to 1 GeV/c $^2$ ),  $\chi^2$  of the fit changed very little. A very wide  $f_0(1370)$  is however fully compatible with the red dragon of Minkowski and Ochs, and with our view.

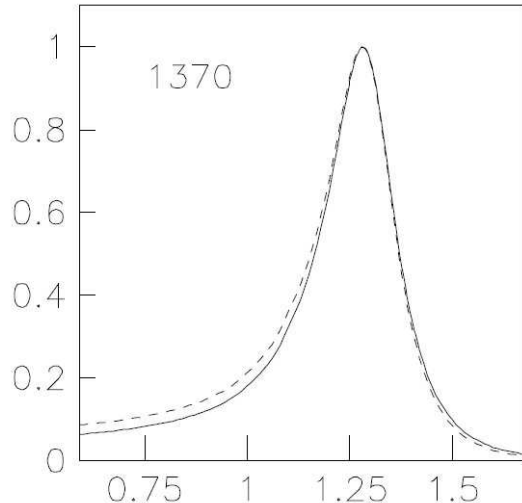


Fig. 104. Line-shapes of  $f_0(1370)$  within the phase space of  $p\bar{p}$  annihilation at rest into  $3\pi^0$ , normalised to 1 at its peak height, for  $\Gamma_{2\pi} = 325$  MeV/c $^2$  (solid line) and 800 MeV/c $^2$  (dashed line) [1098].

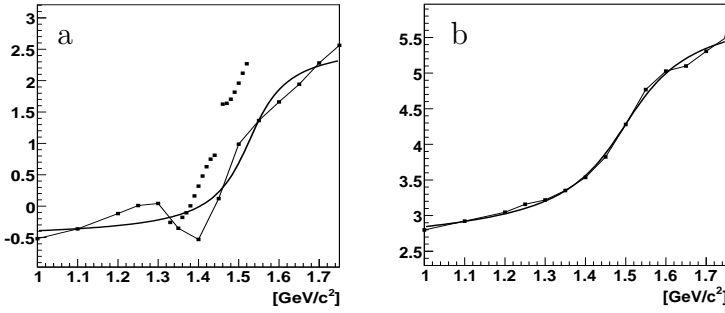


Fig. 105. The scalar isoscalar phase from  $\bar{p}n \rightarrow \pi^-(2\pi^0\pi^+\pi^-)_{S-wave}$  (a) and from  $\bar{p}n \rightarrow \pi^-(4\pi^0)_{S-wave}$  (b). The phases are represented by x connected with a thin line. The thick line gives the phase motion expected for  $f_0(1500)$ . The small squares in (a) give the effective phase when the scalar intensity is fitted with two resonances.

As a conclusion, we do not consider the  $f_0(1370)$  as established resonance. In the discussion (section 11) we present interpretations of the scalar meson spectrum with and without assuming its existence.

## 10.5 Scalar mesons in $D$ , $D_s$ and $B$ decays

Fig. 106 shows a series of  $D^0$ ,  $D^+$ , and  $D_s^+$  Dalitz plots for different decay modes. The comparison of  $D^0$ ,  $D^+$ , and  $D_s^+$  decays into three pions reveals an interesting but not yet fully understood phenomenology. A summary of Dalitz plot analyses is given by Asner in the Review of Particle Properties [1]. Analyses of the same Dalitz plot made in different collaborations mostly arrive at similar conclusions concerning contributing resonances and their fractional contributions except for some – partly important – details. We give here a description of a few Dalitz plots to underline their potential for meson spectroscopy.

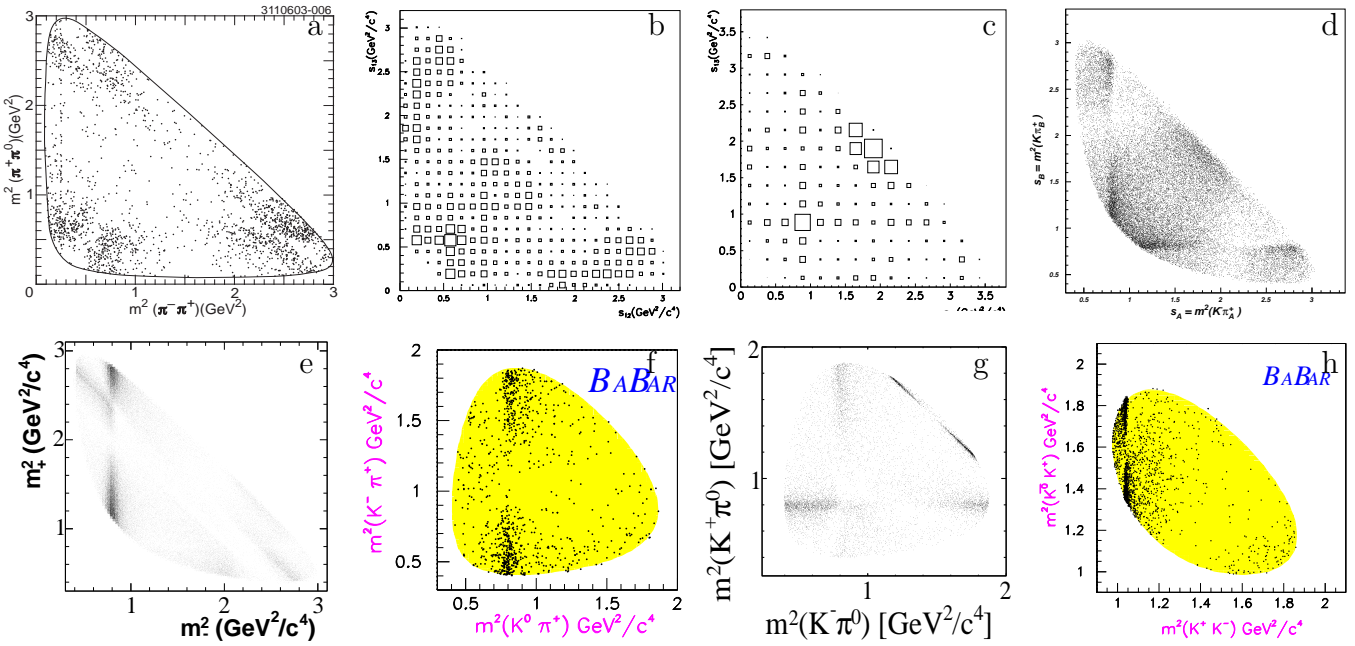


Fig. 106. Dalitz plots for decays.  $D^0$  (a),  $D^+$  (b) and  $D_s^+$  (c) decays into  $3\pi$ ; [520, 521, 565];  $D^+ \rightarrow K^-\pi^+\pi^+$  (d), [523].  $D^0 \rightarrow K_S^0\pi^+\pi^-$  (e) [604];  $D^0 \rightarrow K^0K^-\pi^+$  (f) [1099];  $D^0 \rightarrow \bar{K}^0K^+\pi^-$  (g) [623];  $D^0 \rightarrow \bar{K}^0K^+K^-$  (h) [609].

In  $D^0 \rightarrow 3\pi$  decays, a  $c$  quark converts into a  $d$  quark, the transition is Cabibbo suppressed. The CLEO Dalitz plot [565] shows significant structures due to  $\rho^+\pi^-$  production and weaker contributions from  $\rho^0\pi^0$  and  $\rho^-\pi^+$ . There are depletions along the three diagonal lines separating the three charge states of the  $\rho$  indicating destructive interference between the three amplitudes at appropriate mass values. The dominance of  $\rho^+\pi^-$  is unexpected; the leading diagram (see Fig. 33) produces  $\rho^-\pi^+$ , the annihilation diagram cannot contribute, colour suppressed diagrams lead to equal production of all three charge states. Possibly, constructive and destructive interference between leading and non-leading diagrams are responsible for the inversion of the expected yields. So far, CLEO is the only experiment which reported results from this reaction, and only in conference proceedings.

The leading diagram for  $D^+ \rightarrow 2\pi^+\pi^-$  decays produces a  $\pi^+$  and a neutral meson. In the Dalitz plot of E791 at Fermilab [521], bands due to  $\rho(770)$ ,  $f_0(980)$  and  $f_2(1270)$  can be recognised. The  $\rho$  band is depleted in the centre due to the  $\cos^2\theta$  angular distribution expected for a transition from a pseudoscalar initial state to a vector plus pseudoscalar meson. The asymmetry along the angular distribution points to a substantial interference between even and odd partial waves. The partial wave analysis found strong evidence for the  $\sigma(485)$  with mass  $478^{+24}_{-23} \pm 17$  MeV/c $^2$  and width  $324^{+42}_{-40} \pm 21$  MeV/c $^2$  accounting for approximately half of all decays. Recently, the CLEO collaboration performed a Dalitz plot study of  $D^+ \rightarrow \pi^+\pi^+\pi^-$  decays [585] using different S-wave parametrisations. They confirm the large  $\sigma(485)\pi^+$  yield ( $41.8 \pm 2.9\%$ ). The isobar fit used in addition  $\rho^0\pi^+$  ( $20.0 \pm 2.5\%$ ),  $f_2(1270)\pi^+$  ( $18.2 \pm 2.7\%$ ), and  $f_0(980)\pi^+$  ( $4.1 \pm 0.9\%$ ). The region above 1 GeV/c $^2$  was described by two Breit-Wigner amplitudes for  $f_0(1370)$  and  $f_0(1500)$  contributing with  $2.6 \pm 1.9\%$  and  $3.4 \pm 1.3\%$ , respectively. The existence of  $f_0(1370)$  was not questioned; when its mass was introduced as a free fit parameter,  $M = 1260$  MeV/c $^2$  was found.

A surprise in the  $D_s^+ \rightarrow \pi^+\pi^+\pi^-$  Dalitz plot shown in Fig. 106c is the large yield and the large scalar intensity [526]. In  $D_s^+ = c\bar{s}$  decays, the leading contribution stems from the process shown in Fig. 33a in which the  $c$  quark converts – by emission of a  $W^+ \rightarrow \pi^+$  – into an  $s$  quark forming an  $s\bar{s}$  state. However, the  $\pi^+$  recoils against a  $\pi^+\pi^-$  (and not the expected  $K^+K^-$ ) pair. Obviously, some resonances offer a bridge from primary  $s\bar{s}$  states to pionic final states. Such a behaviour is known from pseudoscalar mesons which have large  $n\bar{n}$  and  $s\bar{s}$  components. Likely, scalar mesons have flavour wave functions which do not correspond to an ideal mixing angle. A more subtle interpretation of the  $s\bar{s} \rightarrow \pi\pi$  transition is discussed in section 11.6 where we give our own interpretation of the scalar mesons. The  $\sigma(485)$  is not required in fits to  $D_s^+$  decays; it is generated dynamically from  $\pi\pi$  interactions and seems to have weak coupling to  $s\bar{s}$ ;  $\rho$  production is nearly absent.

The largest contribution stems visibly from  $f_0(980)\pi^+$ . There is a second structure at about 2 GeV $^2$ /c $^4$  which partial wave analyses assign to  $\rho(1450)\pi^+$ ,  $f_2(1270)\pi^+$ , and  $f_0\pi^+$ . A very important aspect is the mass of the scalar resonance. E687 [526] determined the scalar meson mass to 1475 MeV/c $^2$  with 100 MeV/c $^2$  width, Focus [531] found  $M = 1475 \pm 10$  MeV/c $^2$  and  $\Gamma = 112 \pm 24$  MeV/c $^2$ . These results are not incompatible with the standard  $f_0(1500)$ . E791 [520] imposed the  $f_0(1370)$  mass; when left free, the parameters optimised for  $M = 1434 \pm 18 \pm 9$  MeV/c $^2$  and  $\Gamma = 172 \pm 32 \pm 6$  MeV/c $^2$ . In [530], four scalar mesons above 1 GeV/c $^2$  were used to describe the data,  $f_0(1370)$ ,  $f_0(1500)$ ,  $f_0(1750)$ , and a wide  $f_0(1200 - 1600)$ . It is thus an open question if the enhancement at  $M^2 \sim 2$  GeV $^2$  in  $D_s^+ \rightarrow 2\pi^+\pi^-$  is due to  $f_0(1370)$  or  $f_0(1500)$  production, to production of both, or due to some dynamical effect. The reason why  $\rho(1450)$  makes a large contribution to  $D_s$  decays (and  $\rho(770)$  at most weakly) while  $\rho(770)$  is observed in  $D$  decays (and  $\rho(1450)$  not) is not understood.

Table 33

$D^+$  and  $D_s^+$  fit fractions and phases with the isobar model [531]. The results from [520, 521] are shown as small numbers for comparison.

resonance	$D^+ \rightarrow 2\pi^+\pi^-$		$D_s^+ \rightarrow 2\pi^+\pi^-$	
	fit fraction(%)	phase (deg)	fit fraction(%)	phase (deg)
NR	$9.8 \pm 4.3$	$145.9 \pm 17.7$	$25.5 \pm 4.6$	$246.5 \pm 4.7$
	$7.8 \pm 6.6$	$246.5 \pm 20.3$	$0.5 \pm 2.2$	$181 \pm 107$
$\rho(770)\pi^+$	$32.8 \pm 3.8$	$208.8 \pm 16.8$	-	
	$33.6 \pm 3.9$	0 (fixed)	$5.8 \pm 4.4$	$109 \pm 25$
$\rho(1450)\pi^+$	-		$4.1 \pm 1.0$	$187.3 \pm 15.3$
	-		$4.4 \pm 2.1$	$162 \pm 31$
$f_2(1275)\pi^+$	$12.3 \pm 2.1$	$146.7 \pm 17.7$	$9.8 \pm 1.3$	$140.2 \pm 9.2$
	$19.4 \pm 2.6$	$246.5 \pm 6.0$	$19.7 \pm 3.4$	$133 \pm 31$
$f_0(485)\pi^+$	$18.9 \pm 5.3$	$49.0 \pm 30.7$	-	
	$46.3 \pm 9.3$	$40.7 \pm 9.5$	-	
$f_0(980)\pi^+$	$6.7 \pm 1.5$	0(fixed)	$94.4 \pm 3.8$	0(fixed)
	$6.2 \pm 1.4$	0(fixed)	$56.5 \pm 6.4$	0(fixed)
$f_0(1475)\pi^+$	$1.8 \pm 1.2$	$28.2 \pm 25.8$	$17.4 \pm 3.1$	$249.7 \pm 6.4$
$f_0(1370)\pi^+$	$2.3 \pm 1.8$	$270.4 \pm 17.8$	$32.4 \pm 7.9$	$198 \pm 33$

The Focus collaboration reported an interesting analysis of both data sets,  $D^+$  and  $D_s^+$  decays into  $2\pi^+\pi^-$  using the same resonances [531]. An equivalent fit using a  $K$  matrix for the S-wave was also used, but this approach does not give easy access to the fractional yields of S-wave resonances. The Focus data were also fitted [530] using a highly flexible set of amplitudes proposed by Anisovich and Sarantsev [859]; the latter results will be discussed in section 11.3.

The  $D_s^+ \rightarrow \pi^-\pi^+\pi^+$  Dalitz plot of the E791 collaboration [520] was reanalysed using  $K$ -matrices in  $P$ -vector approach, or Breit-Wigner amplitudes and a Flatté parametrisation to describe  $f_0(980)$  [1100]. As in other analyses,  $f_0(980)$  resonance provided the most significant contribution. The emphasis was laid on the question if  $f_0(1370)$  is required to describe the data. The answer was no. When  $f_0(1500)$  and  $f_0(1710)$  were used in the fit, the uncertainty in the mass increased and  $M = 1458 \pm 37 \text{ MeV}/c^2$  was found which is  $1.2\sigma$  compatible with the PDG mass.

In Table 33 results are collected of the analysis [531] using Breit-Wigner amplitudes to describe the dynamics of the process. The physical content of the results are similar to those obtained by E687 [526] even though some numbers are different (in particular a larger fraction of the data was assigned to a nonresonant (NR) amplitude in [526]. The results of [520] and [521] are presented as small numbers in Table 33. Recently, CLEO reported a preliminary analysis of  $D^+ \rightarrow 3\pi$  [1101] with different numbers but similar results. In an analysis of  $D^0 \rightarrow K^+K^-\pi^0$  decays [580], the existence of both,  $f_0(1370)$  and  $f_0(1500)$  is assumed but not explored further.

The data on  $D^+ \rightarrow K^-\pi^+\pi^+$  [523] shown in Fig. 106d were used to develop a model-independent partial-wave analysis of the S-wave component of the  $K\pi$  system. The amplitudes were determined for ranges of  $K^-\pi^+$  invariant mass down to threshold. This was an essential extension of the LASS data and thus helped to extract the  $K_0^*(750)$  discussed in section 9.2 (see also [613]).

The four BaBar Dalitz plots on  $D^0$  decays in the lower row evidence the importance of  $S$ - $P$  interference and the potential of charm decays for light meson spectroscopy. The  $D^0 \rightarrow K^0\pi^+\pi^-$  Dalitz plot reveals strong interference effects between  $K^*(892)$  and  $(K\pi)_{S-\text{wave}}$  interfering with

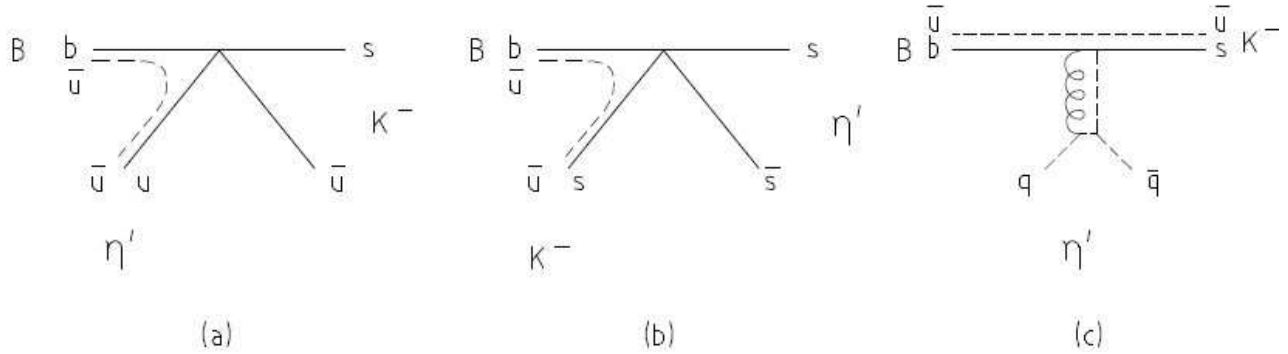


Fig. 107. Two-body decay  $B^- \rightarrow K^- \eta'$  with amplitudes in which transitions take place with (a)  $s \rightarrow K^-$ , (b)  $s \rightarrow \eta'$  and (c)  $K^- \eta'$  production via intermediate gluons. The dashed lines represent 'soft' QCD [740].

$\rho$  and the  $(\pi\pi)_{S\text{-wave}}$  [604]. The decays  $D^0 \rightarrow K^0 K^- \pi^+$  were shown at a conference [1099]; no visible structure except  $K^*(892)$  production is observed. There are hints for interference with the  $K\pi$  S-wave. The  $D^0 \rightarrow K^+ K^- \pi^0$  Dalitz plot [623] shows significant contributions from  $K^*(892)$  and  $\phi(1020)$ . The fits assigned the largest fraction to the  $(K\pi)_{S\text{-wave}}$ . The LASS parametrisation and a fit using the  $(K\pi)_{S\text{-wave}}$  from [523] both resulted in acceptable fits. Finally, the reaction  $D^0 \rightarrow K^0 K^- K^+$  [609] shows strong  $K^0 \phi(1020)$  production interfering with  $K^0 a_0(980)^0$ . The yield of  $K^- a_0(980)^+$  is significant, the two doubly-Cabibbo suppressed decay modes  $K^+ a_0^-(980)$  and  $\bar{K}^0 f_0^+(980)$  make no significant contributions. There is some additional contribution, which can be described by the tail of a broad resonance peaking well outside the phase space.

Decays of  $B$  mesons offer a wide phase space at the expense of small event numbers per MeV. Charmless decays may proceed via the Penguin diagram in which the  $b$  quark converts under  $W$  emission into a  $u$ ,  $c$ , or  $t$  quark. The latter quark reabsorbs the  $W$  turning into an  $s$  (or  $d$ ) quark. Based on a comparison of data on  $B$  decays into two pseudoscalar mesons, Minkowski and Ochs argue that a large fraction of  $\eta'$  production has to proceed via a gluonic amplitude (see Fig. 107c). This amplitude is very similar to the one needed in radiative  $J/\psi$  production.

The BABAR and BELLE collaboration have analysed the Dalitz plots for the three-body charmless decays  $B^+ \rightarrow K^+ K^+ K^-$  and  $B^+ \rightarrow K^+ \pi^+ \pi^-$  [641], and for  $B^0 \rightarrow K^+ K^- K_S^0$  and  $B^0 \rightarrow K_S^0 \pi^+ \pi^-$  [605, 612]. These data, even though low in statistics, provide an important key to the dynamics of scalar mesons. The BELLE data are based on 152 million  $B\bar{B}$  pairs produced on the  $\Upsilon(4S)$  resonance. Three significant structures were observed, the  $f_0(980)$  and a small enhancement in the  $\pi\pi$  mass distribution at about  $1.3 \text{ GeV}/c^2$ , denoted as  $f_X(1300)$ , and resonant structure at  $1.5 \text{ GeV}/c^2$  in the  $K\bar{K}$  mass distribution. The latter is best described as a scalar resonance; mass and width are compatible with standard values for  $f_0(1500)$ .

Now, there is a problem: if the  $f_0(1500)$  were the same particle as observed in other experiments, it would decay to  $\pi^+ \pi^-$  about five times more frequently than to  $K^+ K^-$ . This is not observed. In the  $\pi^+ \pi^-$  mass distribution there is, instead, a peak at  $1300 \text{ MeV}/c^2$ . Both these aspects were confirmed in the BABAR data. The BABAR collaboration concludes that the nature of the  $f_0(1500)$  contribution remains unclear. Identification of this state as the  $f_0(1500)$  leads to inconsistency with the measurement of the  $B^0 \rightarrow f_0(1500) K_S^0$ ,  $f_0(1500) \rightarrow \pi^+ \pi^-$  decay.

Fig. 108 shows the  $\pi^+ \pi^-$  and  $K^+ K^-$  mass spectra from  $B \rightarrow K \pi^+ \pi^-$  and  $B \rightarrow K K^+ K^-$ , respectively, and a fit to the data by Minkowski and Ochs [740]. The  $\pi^+ \pi^-$  exhibits a clear  $f_0(980)$  signal and some additional intensity which can be described by  $f_0(1370)$ . However, this interpretation is very problematic: the  $K^+ K^-$  peak at  $1500 \text{ MeV}/c^2$ , if assigned to  $f_0(1500)$ , must

be accompanied by a peak in  $\pi^+\pi^-$ . This is not the case. Hence a new scalar state would need to be introduced which couples strongly to  $K^+K^-$  and weakly to  $\pi^+\pi^-$ . (This very argument is used to identify two scalar mesons  $f_0(1710)$  and  $f_0(1790)$ , see section 10.6). Minkowski and Ochs have shown that both spectra can be explained by assuming a broad SU(3) isoscalar background amplitude (which they identify with a scalar glueball) and  $f_0(980)$  plus  $f_0(1500)$  with standard properties [740]. Fig. 108 shows how the destructive interference creates a fall off of intensity at  $1.5 \text{ GeV}/c^2$  in the  $\pi^+\pi^-$  invariant mass distributions and a peak in the  $K^+K^-$  due to constructive interference. A  $f_0(1370)$  is not needed in the fit. The main difference in this analysis compared to the analyses of the BABAR and BELLE collaborations is the treatment of unitarity: the  $f_0(1370)$  resonance decaying to  $\pi\pi$  and a second (new)  $f_0(1500)$  resonance decaying into  $K\bar{K}$  is not needed if there is a background amplitude close to the unitarity limit plus resonant amplitudes which are added in a unitarity conserving way, in a  $K$ -matrix or using the Dalitz-Tuan formalism. Even in a production experiment, unitarity constraints play a decisive rôle. This may be unexpected. The strong dip in the centrally produced  $\rho\rho J^{PC} = 0^{++}$  wave in Fig. 100b at exactly  $1.5 \text{ GeV}/c^2$  underlines the importance of unitarity constraints.

The change of the  $f_0(1500)$  interference phase from constructive (in  $K\bar{K}$ ) to destructive (in  $\pi\pi$ ) suggests that the  $f_0(1500)$  wave function has a minus sign between its  $n\bar{n}$  and  $s\bar{s}$  component. The background amplitude is assumed to be flavour singlet. The minus sign was already found in [178] from a comparison of the Argand phase motion for  $\pi\pi \rightarrow \eta\eta$  and to  $K\bar{K}$ . Obviously,  $f_0(1500)$  is flavour-octet like. This is in agreement with its large coupling to  $\eta\eta'$ .

## 10.6 Scalar mesons in hadronic $J/\psi$ decays

Hadronic decays of  $J/\psi$  into  $\omega$  and  $\phi$  mesons recoiling against a meson  $X$  give access to the flavour content of  $X$ . Due to the OZI rule,  $J/\psi \rightarrow \omega X$  couples to the  $n\bar{n}$  component of  $X$  while  $J/\psi \rightarrow \phi X$  couples to  $s\bar{s}$ . The BESII detector – described briefly in section 3.4.4 – has recorded  $58 \cdot 10^6$   $J/\psi$  decays. The results on  $J/\psi$  decays to  $\omega$  or  $\phi$  recoiling against two pseudoscalar mesons are summarised in Table 34; important mass spectra are collected in Fig. 109. Fig. 109a,b show  $\pi\pi$

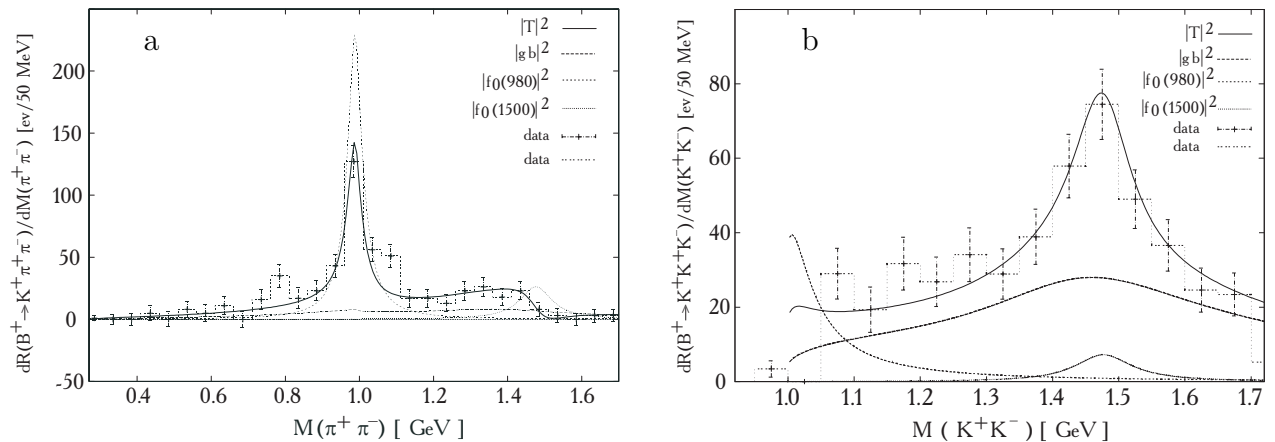


Fig. 108.  $\pi^+\pi^-$  (a) and  $K^+K^-$  (b) mass spectra in  $B$ -decays as [641] measured by BELLE in comparison with a model amplitude  $|T|^2$  of the coherent superposition of  $f_0(980)$ ,  $f_0(1500)$  and a broad background amplitude. Also shown are the individual resonance terms  $|T_R|^2$ . The background interferes destructively with both  $f_0(980)$  and  $f_0(1500)$  in their  $\pi^+\pi^-$  decays while there is constructive interference between background and  $f_0(1500)$  in case of  $f_0(1500) \rightarrow K^+K^-$  [740].

and  $K\bar{K}$  systems recoiling against an  $\omega$ , Fig. 109c,d those recoiling against a  $\phi$ . Data on radiative  $J/\psi$  decays into  $\pi^+\pi^-$  (e) and  $K\bar{K}$  (f,g) are also included in the figure.

The following observations can be made:

- The region below  $1 \text{ GeV}/c^2$ :

The  $\pi\pi$  mass distribution from  $J/\psi \rightarrow \omega\pi^+\pi^-$  shows a significant peak at about  $600 \text{ MeV}/c^2$  (discussed as  $\sigma(485)$  in section 9), the  $\pi\pi$  mass distribution recoiling against the  $\phi$  not. This apparent puzzle was explained recently [1103] by the difference of the strange and non-strange formfactors of the pion: the  $J/\psi \rightarrow \phi\pi^+\pi^-$  process is mainly driven by the strange scalar pion formfactor which vanishes in leading order in chiral perturbation theory. The non-strange formfactor is not suppressed at small energies, and the  $\sigma(485)$  appears. A second remarkable feature is the high visibility of  $f_0(980)$  in the  $\pi\pi$  mass spectrum recoiling against a  $\phi$ . The corresponding  $K\bar{K}$  spectrum shows, up to the  $f_0(1500)$ , no significant features. In the recoil against an  $\omega$ ,  $f_0(980)$  gives only small contributions. Careful inspection of the  $\pi\pi$  spectrum in the latter reaction reveals a small dip (Fig. 4 in [1103]); the fit in [1103] demonstrates compatibility of  $f_0(980)$  – generated by meson-meson interactions – with all four reactions. The singlet/octet fraction varies as a function of the mass in the  $K\bar{K}$  threshold region, and we refrain from assigning a singlet or octet flavour wave function to it.

- The  $1.3 - 1.6 \text{ GeV}/c^2$  region:

Above  $1 \text{ GeV}/c^2$ , the  $\pi\pi$  mass distribution from  $J/\psi \rightarrow \omega\pi^+\pi^-$  is dominated by a strong  $f_2(1270)$  peak. The partial wave analysis finds nearly no scalar contribution. In  $\phi\pi\pi$  the scalar contribution is substantial and peaks at about  $1400 \text{ MeV}/c^2$  followed by a dip at about  $1520 \text{ MeV}/c^2$ . In both  $K\bar{K}$  spectra, there are peaks due to  $f'_2(1525)$ . In  $K\bar{K}$  recoiling against  $\phi$ , a significant scalar component is found beneath the  $f'_2(1525)$  which is assigned to  $\phi f_0(1500)$ . The best evidence for  $f_0(1370)$  (if any) stems from  $J/\psi \rightarrow \phi\pi^+\pi^-$ .

- The  $1.6 - 1.9 \text{ GeV}/c^2$  region:

The  $1700-1800 \text{ MeV}/c^2$  region is the most complicated part of the spectrum. In the  $K\bar{K}$  mass distributions recoiling against  $\omega$  mesons, a striking peak is observed at  $1710 \text{ MeV}/c^2$  which is absent in the spectrum recoiling against  $\phi$ 's. On the contrary, a  $\pi^+\pi^-$  peak at about  $1770 \text{ MeV}/c^2$  is seen in  $\phi\pi^+\pi^-$  which is absent in  $\phi K\bar{K}$ . This is very puzzling. The BES collaboration suggests

Table 34

Masses, widths and branching fractions (in  $10^{-4}$ ) of scalar resonances recoiling against  $\omega$  and  $\phi$  mesons in  $J/\psi$  decays. Masses and width are given from the data with the largest branching fraction. The yields given as  $\leq$  were derived from fits with imposed masses and widths with no forcing evidence for presence of the contribution.

Channel	Mass ( $\text{MeV}/c^2$ )	Width ( $\text{MeV}/c^2$ )	$\mathcal{B}(J/\psi \rightarrow \omega X,$ $X \rightarrow \pi\pi)$	$\mathcal{B}(J/\psi \rightarrow \omega X,$ $X \rightarrow K\bar{K})$	$\mathcal{B}(J/\psi \rightarrow \phi X,$ $X \rightarrow \pi\pi)$	$\mathcal{B}(J/\psi \rightarrow \phi X,$ $X \rightarrow K\bar{K})$
$\sigma$	$541 \pm 39$	$504 \pm 84$	$\sim 20$		$1.6 \pm 0.6$	$0.2 \pm 0.1$
$f_0(980)$	Flatté formula		$\leq 1.2$	fixed	$5.4 \pm 0.9$	$4.5 \pm 0.8$
$f_0(1370)$	$1350 \pm 50$	$265 \pm 40$			$4.3 \pm 1.1$	$0.3 \pm 0.3$
$f_0(1500)$	PDG	PDG	$\leq 1.2$		$1.7 \pm 0.8$	$0.8 \pm 0.5$
$f_0(1710)$	$M = 1738 \pm 30$	$\Gamma = 125 \pm 20$	$\leq 0.5$	$13.2 \pm 2.6$		$2.0 \pm 0.7$
$f_0(1790)$	$1790^{+40}_{-30}$	$270^{+60}_{-30}$			$6.2 \pm 1.4$	$1.6 \pm 0.8$

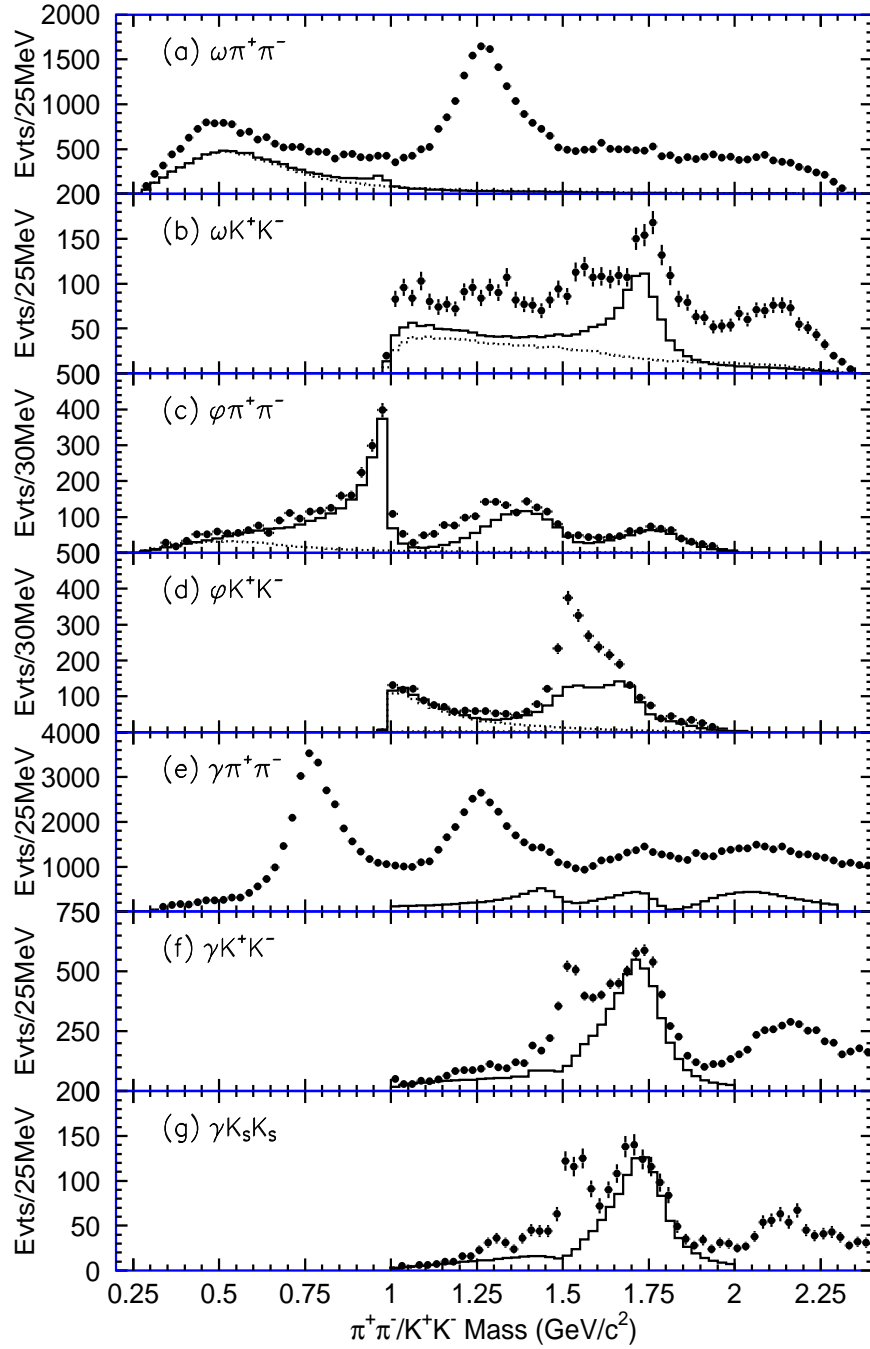


Fig. 109. The invariant mass distributions of the pseudoscalar meson pairs recoiling against  $\omega$ ,  $\phi$ , or  $\gamma$  in  $J/\psi$  decays measured at BES-II. The dots with error bars are data, the solid histograms are the scalar contribution from PWA, and the dashed lines in (a) through (c) are contributions of  $\sigma(485)$  from the fits, while the dashed line in (d) is the  $f_0(980)$ . Not the full mass spectra are analyzed in (e), (f), and (g). The figure is taken from [1102].

that the phenomena originate from production of two different resonances, a  $f_0(1710)$  mainly  $s\bar{s}$  state decaying into  $\bar{K}K$ , and a  $f_0(1790)$  mainly  $n\bar{n}$  state decaying into  $\pi\pi$ . At the present stage, it is a mystery why the mainly  $s\bar{s}$   $f_0(1710)$  state is produced recoiling against an  $\omega$ , and the mainly  $n\bar{n}$   $f_0(1770)$  state is seen in its recoil against a  $\phi$ .

## 10.7 Scalar mesons in radiative $J/\psi$ decays

Radiative  $J/\psi$  decays bare the promise to reveal unambiguously the presence of glueballs. In this process, the  $\bar{c}c$  system supposedly decays into one photon and two interacting gluons. If their interaction resonates, a glueball is formed. Because of the importance of  $J/\psi$  radiative decays for the discussion of scalar mesons and their interpretation, it seems appropriate to highlight some important historical aspects.

We have already discussed the  $\eta(1440)$  or  $\iota(1440)$ , which was interpreted in section 8.3.4 as  $\eta$  radial excitation but was believed to be a glueball when first seen in radiative  $J/\psi$  decay. With a pseudoscalar glueball at  $1.4 \text{ GeV}/c^2$ , a tensor glueball was expected below  $2 \text{ GeV}/c^2$ , and there was great excitement when a broad bump in the radiatively produced  $\eta\eta$  mass spectrum was discovered by the Crystal Ball collaboration [1104]. The bump extended from  $1450$  to  $1800 \text{ MeV}/c^2$ , was found with a yield of  $(4.9 \pm 1.4 \pm 1.0) \cdot 10^{-4}$ , and was called  $\Theta(1640)$ . The  $2^{++}$  quantum numbers originated from an excess of four events above  $|\cos \theta| > 0.95$ . If these events are neglected, scalar quantum numbers follow. We now believe that the bump comprises contributions from  $f_0(1500)$  and  $f_0(1760)$  which we estimate to be in the order of 1:4. Then

$$\begin{aligned}\mathcal{B}_{J/\psi \rightarrow \gamma f_0(1500) \rightarrow \gamma\eta\eta} &= (1.0 \pm 0.3 \pm 0.2 \pm 0.3) \cdot 10^{-4} \\ \mathcal{B}_{J/\psi \rightarrow \gamma f_0(1760) \rightarrow \gamma\eta\eta} &= (3.9 \pm 1.1 \pm 0.8 \pm 0.3) \cdot 10^{-4},\end{aligned}\quad (10.3)$$

where the first error is of statistical nature, the second the systematic error, and the third one (introduced here) estimates the uncertainty in dividing the signal into two components. The  $\eta\eta$  peak was confirmed by the GAMS collaboration in central production, another glue-rich environment. GAMS reported  $M = 1755 \pm 8 \text{ MeV}/c^2$  [282] and, with higher statistics,  $M = 1744 \pm 15$ ,  $\Gamma < 80 \text{ MeV}/c^2$  [284]. The branching ratio (10.3) and other ratios are collected in Table 35.

MARKIII [1106] observed the  $\Theta$  at  $1720 \text{ MeV}/c^2$  in  $J/\psi \rightarrow \gamma K^+ K^-$  (and possibly  $\gamma\pi^+\pi^-$ ), found  $2^{++}$  quantum numbers and a yield  $\mathcal{B}_{J/\psi \rightarrow \gamma f_J(1710) \rightarrow \gamma K^+ K^-} = (4.8 \pm 0.6 \pm 0.9) 10^{-4}$ . A reanalysis by Dunwoodie [1107] identified the  $\Theta$  as scalar resonance and reported contributions from two scalar states

Table 35

Branching fraction  $\times 10^4$  for production of scalar mesons in  $J/\psi$  radiative decays. The  $f_0(1500)$  yield is calculated from the  $\eta\eta$  and  $\sigma\sigma$  and the known  $f_0(1500)$  decay branching ratios.

Decay channel	$f_0(980)$	$f_0(1500)$	$f_0(1710)$ , $f_0(1790)$ , $f_0(1810)$	$f_0(2100)$	reference
$\omega\omega$		-	$3.1 \pm 0.6$		[506]
$\omega\phi$		-	$  2.61 \pm 0.27 \pm 0.65$		[508]
$\sigma\sigma$ (or $\rho\rho$ )		$8.0 \pm 3.5$	$9.0 \pm 1.3$	$13 \pm 5$	[1105]
$\pi\pi$	$\leq 4$	$1.00 \pm 0.03 \pm 0.42$	$3.96 \pm 0.06$		[507]
$\eta\eta$		$1.0 \pm 0.3 \pm 0.2 \pm 0.3$	$3.9 \pm 1.1 \pm 0.8 \pm 0.3$		Eq. (10.3)
$K\bar{K}$		-	$9.62 \pm 0.29^{+2.11+2.81}_{-1.86-0.00}  $		[485]
total	$\leq 5$	$16 \pm 7$	$31.6 \pm 4.1$	$> 13 \pm 5$	

$$\begin{aligned}
M &= 1429_{-37}^{+43} \quad \Gamma = 169_{-76}^{+111} \quad \mathcal{B}_{J/\psi \rightarrow \gamma f_0(1430)} = (4.3_{-1.3}^{+2.7}) \cdot 10^{-4} \\
&\qquad \Gamma [f_0(1430) \rightarrow K\bar{K}] / \Gamma_{f_0(1430) \rightarrow \pi\pi} = 0.15_{-0.13}^{+0.22} \\
M &= 1704_{-23}^{+16} \quad \Gamma = 124_{-44}^{+53} \quad \mathcal{B}_{J/\psi \rightarrow \gamma f_0(1710)} = (9.5_{-2.0}^{+2.5}) \cdot 10^{-4} \\
&\qquad \Gamma_{f_0(1710) \rightarrow \pi\pi} / \Gamma_{f_0(1710) \rightarrow K\bar{K}} = 0.27_{-0.12}^{+0.17}
\end{aligned}$$

where the yields  $\mathcal{B}$  refer to the sum of the two decay modes.

BES I [1108] decomposed the structure at about  $1750 \text{ MeV}/c^2$  into a (small) scalar component at  $1781 \text{ MeV}/c^2$  plus a large tensor component at  $1696 \text{ MeV}/c^2$ . Hence the situation remained unclear.

Data on radiative  $J/\psi$  decays into  $\pi\pi$  [507] and  $K\bar{K}$  [485] from BESII were already shown in Fig. 109e,f,g. In the reaction  $J/\psi \rightarrow \gamma\pi^+\pi^-$ , the recoiling photon has a large energy when the  $\pi^+\pi^-$  masses are small; a large background due to three-pion production (with one  $\pi^0 \rightarrow \gamma\gamma$  and one  $\gamma$  lost) cannot be avoided, and the authors have limited the partial wave analysis to the region above  $1 \text{ GeV}/c^2$ . The reaction reveals a strong  $f_2(1270)$  contribution. The scalar part rises slowly, peaks at about  $1430 \text{ MeV}/c^2$  followed by a faster fall-off with minimum at  $1520 \text{ MeV}/c^2$ , rises again to a bump at  $1710 \text{ MeV}/c^2$  and has a second dip at  $1820 \text{ MeV}/c^2$ . It is legitimate to ask whether the bumps or the dips should be identified as resonances. The BES Collaboration uses Breit-Wigner amplitudes without a coherent background amplitude; hence the bumps are identified with scalar resonances. The first resonance was found at a mass of  $1466 \pm 6 \pm 20 \text{ MeV}/c^2$  and a width of  $108_{-11}^{+14} \pm 21 \text{ MeV}/c^2$ . The branching fraction is given in Table 35. The second  $0^{++}$  resonance parameters are determined to  $M = 1765_{-3}^{+4} \pm 12 \text{ MeV}/c^2$  and  $\Gamma = 145 \pm 8 \pm 69 \text{ MeV}/c^2$ . A joint analysis of the two reactions  $J/\psi \rightarrow \gamma K^+K^-$  and into  $\gamma K_S^0 K_S^0$  did not require introduction of  $f_0(1500)$ , and gave mass and width  $M = 1740 \pm 4 \text{ MeV}/c^2$  and  $\Gamma = 166_{-8}^{+5} \text{ MeV}/c^2$ , respectively, for the  $f_0(1710)$ .

Radiative decay  $J/\psi \rightarrow \gamma\pi^+\pi^-\pi^+\pi^-$  had been observed by DM2 and MARKIII [955, 958]. The data were interpreted as a series of pseudoscalar resonances at about  $1.5$ ,  $1.75$  and  $2.1 \text{ GeV}/c^2$ . Bugg noticed the similarity of the pattern of  $\eta\eta$  resonances observed in antiproton-proton annihilation at  $2950 < s^{1/2} < 3620 \text{ MeV}/c^2$  [404], the data are reproduced in Fig. 103. The  $\eta\eta$  states cannot have pseudoscalar quantum numbers. This observation motivated a reanalysis [960] suggesting scalar quantum numbers for the three structures in  $J/\psi \rightarrow \gamma\pi^+\pi^-\pi^+\pi^-$  [958]. This conjecture was confirmed by BES [477]. Fig. 110a shows the resulting  $4\pi$  invariant mass distribution and the fraction assigned to the scalar partial wave which was found to originate from  $\sigma\sigma$  decays. A study of radiative  $J/\psi$  decays into  $\omega\omega$  [506] found a peak at  $1.76 \text{ GeV}/c^2$ , just above the  $\omega\omega$  threshold. Analysis of angular correlations assigned predominantly pseudoscalar quantum numbers to the  $\omega\omega$  system below  $2 \text{ GeV}/c^2$ . A partial wave found small  $0^{++}$  and  $2^{++}$  contributions in addition, with a product branching fraction  $\mathcal{B}(J/\psi \rightarrow \gamma f_0(1710)) \cdot \mathcal{B}(f_0(1710) \rightarrow \omega\omega) = (3.1 \pm 0.6) \cdot 10^{-3}$ . In a recent discussion of  $f_0(1790)$ , Bugg included a small fraction of  $\rho\rho$  decays and estimated the  $\omega\omega$  contribution [1105]. The decays into  $\pi^+\pi^-\pi^+\pi^-$  via  $\rho\rho$  or  $\sigma\sigma$  lead to different Clebsch-Gordan corrections, 2.25 and 3 respectively, for the total four-pion yield. We use  $2.6 \pm 0.4$  to determine the total  $4\pi$  branching ratio from the  $\pi^+\pi^-\pi^+\pi^-$  contribution.

For  $f_0(1500)$ ,  $\omega\omega$  is not open. For the four-pion state, the Crystal Barrel Collaboration found a mixture of  $\rho\rho$ ,  $\sigma\sigma$  and other decays. Again, we use  $2.6 \pm 0.4$  to calculate the total  $f_0(1500) \rightarrow 4\pi$  contribution from the  $J/\psi \rightarrow \gamma\pi^+\pi^-\pi^+\pi^-$  yield.

A threshold enhancement was observed in the doubly OZI suppressed decay  $J/\psi \rightarrow \gamma\omega\phi$  [508],

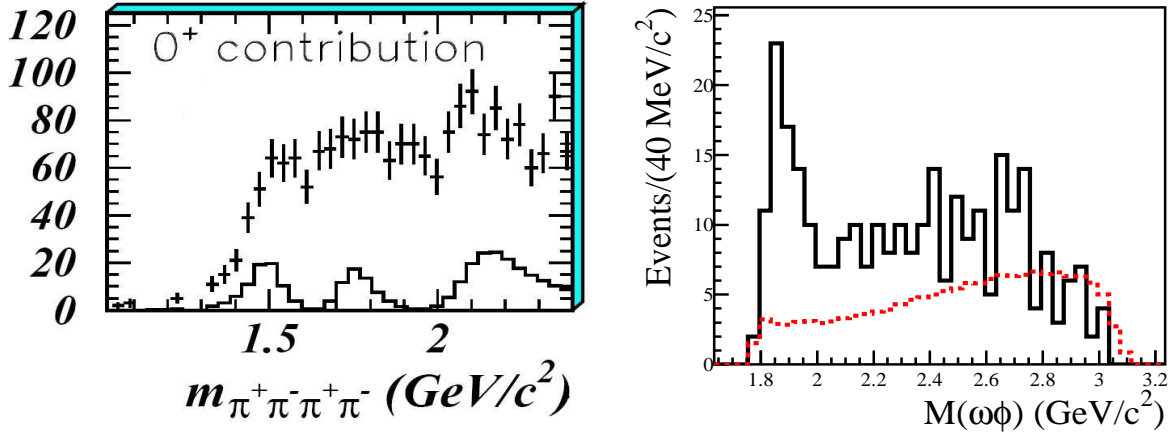


Fig. 110. Left:  $\pi^+\pi^-\pi^+\pi^-$  invariant mass for  $J/\psi \rightarrow \gamma\pi^+\pi^-\pi^+\pi^-$  and the scalar contribution (from an isobar fit). Right: The  $K^+K^-\pi^+\pi^-\pi^0$  invariant mass distribution in radiative  $J/\psi$  decays for events in which the  $\pi^+\pi^-\pi^0$  mass is compatible with the  $\omega$  mass and the  $K^+K^-$  mass with the  $\phi$  mass. The dashed curve represents the  $\omega\phi$  acceptance.

see Fig. 110b. The partial wave analysis favoured scalar quantum numbers with the  $\omega\phi$  system in S-wave. Mass and width of the enhancement were determined to be  $M = 1812^{+19}_{-26} \pm 18 \text{ MeV}/c^2$  and  $\Gamma = 105 \pm 20 \pm 28 \text{ MeV}/c^2$ , respectively, the product branching fraction was  $\mathcal{B}(J/\psi \rightarrow \gamma X) \cdot \mathcal{B}(X \rightarrow \omega\phi) = (2.61 \pm 0.27 \pm 0.65) 10^{-4}$ . It is suggested to be an 'unconventional' state and stimulated a variety of different interpretations. These will be discussed in section 11.

Is  $f_0(1810)$  an additional state? First we note that, in the limit of SU(3) invariance, decays into  $\phi\omega$  are forbidden from an isoscalar-singlet state;  $f_0(1810)$  must have a strong octet component. The nominal  $\phi\omega$  threshold mass is  $1802 \text{ MeV}/c^2$ , the  $K^*K^*$  system has a (mean) threshold at  $1788 \text{ MeV}/c^2$ . Thus both thresholds fall into the  $f_0(1760)$  natural widths, and  $\phi$  formation by  $K^*\bar{K}^*$  rescattering could be a natural explanation. A study of  $J/\psi \rightarrow \gamma K^*K^*$  [476] found however a broad pseudoscalar state ( $M, \Gamma = 1800, 500 \text{ MeV}/c^2$ ). Zou, Dong and Bugg [961] reanalysed the data using the Flatté formula and dispersive corrections for the opening of decay channels. Changing the formalism shifted the resonance mass to  $2190 \text{ MeV}$  and the width to  $800 \text{ MeV}$ . In both analyses, there was little scalar intensity. If  $f_0(1760)$  does not decay into  $K^*K^*$  with a significant yield, the interpretation of  $f_0(1810) \rightarrow \phi\omega$  decays by a rescattering mechanism seems to be excluded.

The process  $J/\psi \rightarrow \gamma f_0(980)$  was not yet observed. There is a small threshold enhancement in the  $K^+K^-$  mass distribution from which we estimate (using  $\Gamma_{f_0(980) \rightarrow K\bar{K}}/\Gamma_{tot} = 0.16$ ) an order of magnitude of

$$\mathcal{B}_{J/\psi \rightarrow \gamma f_0(980)} \leq 5 \cdot 10^{-4}. \quad (10.4)$$

A summary of results on radiative production of scalar mesons in  $J/\psi$  decays is given in Table 35. The radiative yield of scalar isoscalar mesons increases with increasing mass. This is an important observation. Naively, one might expect an increase of radiative yields with the third power of the photon momentum. However, if the reaction is viewed as  $J/\psi \rightarrow \gamma gg$ , the chance of two gluons to be produced with a low mass vanishes with  $m^{-3}$ .

The energy and spin-parity distribution of a two-gluon system recoiling against the photon were calculated by Billoire *et al.* [1109] assuming that the two gluons are massless. The distributions are shown in Fig. 111a. For small  $M_X$ , the scalar intensity vanishes. Assuming gluon-hadron duality

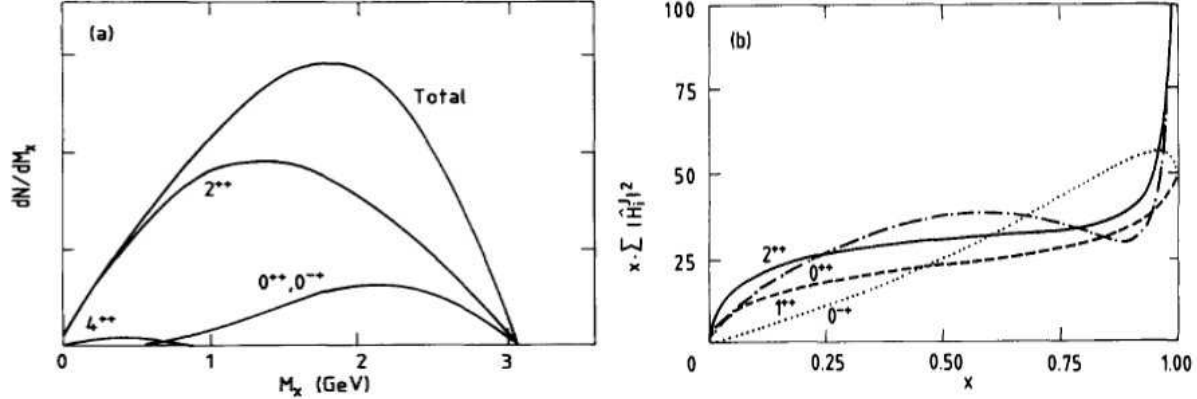


Fig. 111. Energy and spin-parity distributions of a two-gluon system recoiling against a photon in radiative decays of heavy quarkonia as functions of the produced mass (a) or as function of  $x = M_{gg}/M_{Q\bar{Q}}$ . For  $x \rightarrow 1$ , a soft photon is radiated. a) is calculated for massless gluons [1109], b) for off-shell gluons [1110].

we can expect that these predictions are valid for hadrons as well.

Körner *et al.* [1110] consider virtual gluons as well. Quark loop integrals are calculated in nonrelativistic approximation. Their distributions, shown in Fig. 111b, does not predict the reduction of the scalar intensity at  $M_x \rightarrow 0$ , ( $x \rightarrow 1$ ). On the other hand, Billoire *et al.* predict absence of the  $1^{++}$  wave which is forbidden in their model due to the Landau-Yang theorem. The model of Körner *et al.* predicts sizable  $f_1$  radiative yields, in agreement with experiment. Both calculations use perturbative methods, and the limit of applicability seems to be reached.

We have assigned flavour octet wave functions to both  $f_0(1500)$  and  $f_0(1760)$ ; we conjecture that  $f_0(2100)$  is octet as well. Is this assignment compatible with them being produced in radiative  $J/\psi$  decays? First, also octet mesons are produced in radiative  $J/\psi$  decays, see Table 25. The summation of all seen radiative yields into isoscalar  $0^{-+}$  mesons gives 2.25%. All isoscalar  $0^{++}$  mesons give a yield of 0.63% (see Table 35). Of course, this is an estimate since we do not know what fractions are missing. From the calculation of [1109] shown in Fig. 111, scalar and pseudoscalar mesons are expected with similar yields. SU(3) symmetry breaking, final state radiation and/or singlet-octet mixing may contribute to the production of the observed scalar mesons.

## 10.8 Scalar mesons in radiative $\Upsilon$ decays

The CLEOIII collaboration studied  $21 \cdot 10^6$   $\Upsilon$  annihilations. As in the case of  $J/\psi$ , radiative decays give access to a final states which are supposedly glueball-rich. Compared to  $J/\psi$ , radiative decays of the  $\Upsilon$  are a challenge. The ratio

$$\frac{\Gamma_{\Upsilon}^{rad}}{\Gamma_{\Upsilon}^{tot}} = \left( \frac{\alpha_S(\Upsilon)}{\alpha_S(J/\psi)} \right)^4 \left( \frac{\Gamma_{\Upsilon \rightarrow e^+e^-}}{\Gamma_{\Upsilon}^{tot}} \cdot \frac{\Gamma_{J/\psi}^{tot}}{\Gamma_{J/\psi \rightarrow e^+e^-}} \cdot \frac{\Gamma_{J/\psi}^{rad}}{\Gamma_{J/\psi}^{tot}} \right) \approx 0.013, \quad (10.5)$$

instead of 8% for  $J/\psi$ 's and we expect a suppression of about a factor  $\sim 6$ . However, there is a second important reduction factor from the energy and spin-parity distribution of the two-gluon system recoiling against the photon, see Fig. 111a. The  $2^{++}$  contribution peaks at half the quarkonium mass; for tensor mesons a factor 2 reduction is predicted at the mass of the  $f_2(1270)$ . For scalar mesons the factor is about 20 for the  $f_0(1760)$  and increases rapidly for smaller masses.

Table 36

Comparison of observed [577] and expected yields (in units of  $10^{-5}$ ) in radiative decays into tensor and scalar mesons.

Reaction	observed yield	expected yield
$\mathcal{B}_{\Upsilon \rightarrow \gamma f_2(1270)}$	$10.5 \pm 1.6 \text{ (stat)}^{+1.9}_{-1.8} \text{ (syst)}$	$\approx 10$
$\mathcal{B}_{\Upsilon(1S) \rightarrow \gamma f_0(1500)}$	$< 1.17$	$\approx 0.5$
$\mathcal{B}_{\Upsilon \rightarrow \gamma f_2(1760), f_2(1760) \rightarrow 2\pi^0}$	$< 1.2$	$\approx 1$

With  $\mathcal{B}_{J/\psi \rightarrow \gamma f_2(1270)} = 1.38 \cdot 10^{-3}$  and the scalar radiative yields from Table 35 we expect yields which are compared in Table 36 to the CLEOIII results [577].

The comparison shows that searches for a scalar glueball are much more sensitive in radiative  $J/\psi$  decays. In  $\Upsilon$  radiative decays, the scalar mass spectrum is dominated by the tensor contributions. A tensor glueball, expected at about  $2.4 \text{ GeV}/c^2$ , might be detectable in  $\Upsilon$  radiative decays if it exists with a reasonably small width, and if the statistics can be increased significantly.

## 10.9 Scalar mesons in $\chi_{cJ}$ decays

A first study of  $\chi_{c0}$ ,  $\chi_{c1}$ , and  $\chi_{c2}$  decays into three mesons was reported in [579]. For  $\chi_{c1}$  to  $\pi^+ \pi^- \eta$ ,  $K^+ K^- \pi^0$ , and  $\pi^+ K^- K_S^0$ , Dalitz plot analysis were presented showing the potential of these decays for light-meson spectroscopy.

## 10.10 Scalar mesons in two-photon fusion

The ALEPH collaboration at LEP searched for  $\gamma\gamma$  production of the glueball candidates  $f_0(1500)$  and  $f_J(1710)$  via their decay to  $\pi^+ \pi^-$ . No signal was observed; upper limits to the product of  $\gamma\gamma$  width and  $\pi^+ \pi^-$  branching ratio of the  $f_0(1500)$  and the  $f_J(1710)$  were reported to be  $\Gamma_{\gamma\gamma \rightarrow f_0(1500)} \cdot BR(f_0(1500) \rightarrow \pi^+ \pi^-) < 0.31 \text{ keV}/c^2$  and  $\Gamma_{(\gamma\gamma \rightarrow f_J(1710))} \cdot BR(f_J(1710) \rightarrow \pi^+ \pi^-) < 0.55 \text{ keV}/c^2$  at 95% confidence level [669]. From the decay branching ratios given above we estimate  $\Gamma_{\gamma\gamma \rightarrow f_0(1500)} < 1.6 \text{ KeV}/c^2$  and  $\Gamma_{(\gamma\gamma \rightarrow f_J(1710))} < 6 \text{ KeV}/c^2$  assuming that the 1700 to 1800  $\text{MeV}/c^2$  region is dominated by one scalar meson (no  $f_0(1790)$  and no  $f_2(1720)$ ). The expected width is zero for a pure glueball not mixing with  $q\bar{q}$  mesons,  $4.5 \text{ keV}/c^2$  for a  $n\bar{n}$ , and  $0.4 \text{ keV}/c^2$  for a  $s\bar{s}$  meson [1053].

## 11 Scalar mesons and their interpretation

### 11.1 Global views of scalar mesons and the scalar glueball

The interpretation of the spectrum of scalar mesons is still highly controversial. The foundations of the different interpretations are not well enough established to allow us to decide which scenario is closest to the physical truth. The main differences arise because of ambiguities in the interpretation of the following parts:

- (1) Are  $f_0(980)$  and  $a_0(980)$  genuine  $q\bar{q}$  resonances, or are they additional states? If the latter is the case, they may be  $qq\bar{q}\bar{q}$  states (Jaffe),  $K\bar{K}$  molecules (Isgur), or generated by a doubling of states due to strong coupling of scalar states to the meson-meson continua (Beveren, Tornqvist)? Do  $\sigma(485)$ ,  $\kappa(700)$ ,  $f_0(980)$ , and  $a_0(980)$  form a nonet?
- (2) Is  $f_0(1370)$  a true  $q\bar{q}$  resonance or generated by  $\rho\rho$  molecular dynamics? The resonance is needed to fit very different data sets and is accepted by the Particle Data Group as established particle. However, the evidence is much weaker when individual channels are discussed. A proper  $f_0(1370)$  phase motion has never been established. On the contrary, wherever the scalar phase motion was tested, no evidence for an additional resonance between  $f_0(980)$  and  $f_0(1500)$  was found.
- (3) Are  $f_0(1710)$  and  $f_0(1790)$  distinct objects? In mixing scenarios discussed below there must be a scalar resonance in this mass range with a sizable  $s\bar{s}$  component. The  $f_0(1710)$  has a large coupling to  $K\bar{K}$ , the  $f_0(1790)$  not. At the first glance, it is plausible to assign a large  $s\bar{s}$  component to  $f_0(1710)$  while  $f_0(1790)$  could be the radial excitation of  $f_0(1370)$ . However,  $f_0(1710)$  is observed recoiling against  $\omega$  in  $J/\psi$  decays. Thus,  $f_0(1710)$  is produced via its  $n\bar{n}$  component and decays via its  $s\bar{s}$  component.  $f_0(1790)$  decaying into  $\pi\pi$  is produced in recoil against  $\phi$ , via its  $s\bar{s}$  component. There is a clear conflict.
- (4) The  $f_0(1810)$  is intriguingly close to  $f_0(1790)$  and to two thresholds,  $K^*\bar{K}^*$  and  $\phi\omega$ . It is observed in the latter decay mode. The yield in radiative  $J/\psi$  decays is too large to assign it to a conventional  $f_0(1790)$ . Its production and decay is doubly OZI rule violating. The most obvious interpretation is that of a tetraquark resonance. Is it separate from  $f_0(1790)$ ? Possibly, the three observations at 1710, 1790, and 1810 MeV/c<sup>2</sup> are traces of one resonance,  $f_0(1760)$ .
- (5) Is  $f_0(2100)$  a respectable resonance? It is seen as a dip in the GAMS data on  $\pi\pi$  scattering, shown in Fig. 81, as a  $\eta\eta$  peak of unknown (even) spin in  $\bar{p}p$  annihilation in flight into  $\pi^0\eta\eta$  (Fig. 103), and is suggested to make a significant contribution to  $J/\psi$  radiative decay into four pions, see Fig. 110.
- (6) Does the  $f_0(2100)$  region house two components,  $f_0(2000)$  reported in central production [311] and possibly confirmed in  $\bar{p}p$  annihilation in flight [366, 405] and  $f_0(2100)$  seen in [366, 405] and observed in  $J/\psi \rightarrow \gamma 4\pi$  [477]?
- (7) What is the dynamical origin of the broad scalar component shown in Fig. 112?

The low mass part (up to  $\sim 1.2$  GeV/c<sup>2</sup>) can well be described by  $t$ -channel  $\rho$  and some  $f_2(1270)$  exchange. Thus it seems plausible that it is generated by  $t$ -channel exchange dynamics. At high energies, cross sections can be described by a series of  $s$ -channel resonances;  $t$ -channel amplitudes reproduce the mean cross section averaging over the many individual resonances. Possibly, the broad  $\pi\pi$  S-wave scattering background amplitude – let it be called  $f_0(1000)$  – is equivalent to

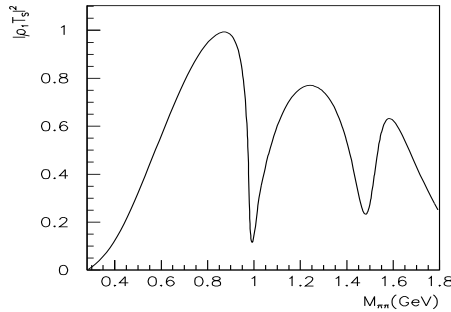


Fig. 112. The  $I = 0 \pi\pi$  S-wave amplitude squared [991].

a series of  $t$ -channel exchange processes. Duality arguments then assign a  $q\bar{q}$  nature to  $f_0(1000)$ . On the other hand, it is also very attractive to assume that the broad component is the scalar glueball.

Figure 113 compares the scalar mass spectrum with those of other nonets. Vector and tensor nonets show ideal mixing and a very regular pattern. Axial vector mesons exhibit a similar pattern even though modified due to  $K_{1A} - K_{1B}$  mixing (see section 1.2.3). The pseudoscalar and low-mass scalar spectra are similar but inverted. In all these cases, nine mesons with identical  $J^{PC}$  fall into a limited mass gap which identifies the nine mesons as one single nonet. The scalar mesons at higher mass resist such a simple pattern. In a reasonable mass gap of  $400 \text{ MeV}/c^2$ , ten scalar states are reported [1]. A popular interpretation assigns these ten states to a scalar nonet plus a scalar glueball. The three isoscalar states are supposed to mix forming the three observed states.

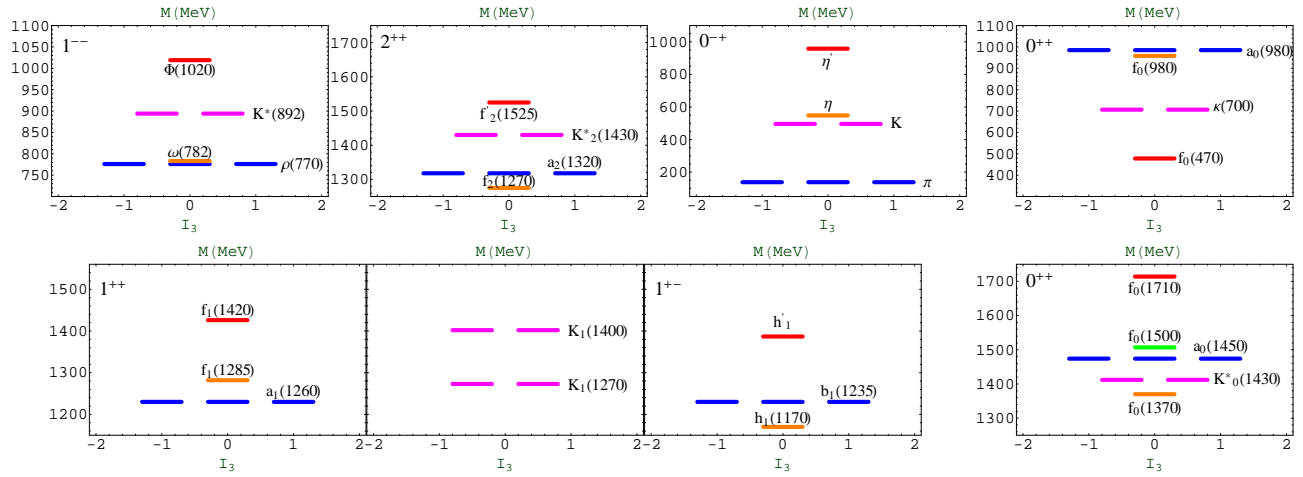


Fig. 113. Mass spectra of the lowest lying meson multiplets. Most multiplets show a high-mass  $s\bar{s}$  state, an isospin doublet of strange mesons (plus their antiparticles), and an isotriplet which is approximately mass degenerate with the  $n\bar{n}$  state. The strange  $K_1$  mesons are mixtures of the two  $K_{1A}$  and  $K_{1B}$  states (belonging to the  $J^{PC} = 1^{+\pm}$  nonets). The pseudoscalar mesons have no ideal mixing, the  $\eta$  is much heavier than the  $\pi$ . The lower-mass scalar nonet has a structure like vector, tensor, and axialvector mesons have, but it is inverted. The other scalar mesons may form a decuplet possibly evidencing the intrusion of a glueball into a scalar meson nonet. The figure is adapted from [1111].

## 11.2 Glueball- $q\bar{q}$ mixing scenarios

The most popular view of the scalar mesons assumes that  $\sigma(485)$ ,  $\kappa(700)$ ,  $f_0(980)$ , and  $a_0(980)$  are bound by molecular forces or are  $qq\bar{q}\bar{q}$  states, unrelated to  $q\bar{q}$  spectroscopy. In the approach of Beveren and Tornqvist and their collaborators, these mesons acquire a large  $q\bar{q}$  fraction, but the

number of the lowest-lying scalar states is still doubled due to the molecular forces between the decay products of scalar mesons. Thus the lowest mass scalar nonet can still be discarded in as far as the abundance of scalar mesons is in the focus of interest.

Then, there are three states,  $f_0(1370)$ ,  $f_0(1500)$ , and  $f_0(1760)$  which need to be interpreted. One of them,  $f_0(1760)$ , couples strongly to  $K\bar{K}$  and could be the  $1^3P_0$   $s\bar{s}$  state. The two remaining states,  $f_0(1370)$  and  $f_0(1500)$ , cannot both be  $1^3P_0$   $n\bar{n}$  states; hence there must be one non- $q\bar{q}$  state. Since the lowest mass scalar glueball is predicted to fall into this mass range, it is natural to assume that a glueball has intruded the spectrum of scalar mesons, mixes with them thus forming the 3 observed states  $f_0(1370)$ ,  $f_0(1500)$ , and  $f_0(1760)$ . An extension is offered when  $f_0(1760)$  is split into a  $1^3P_0$   $s\bar{s}$   $f_0(1710)$  and a  $2^3P_0$   $n\bar{n}$   $f_0(1790)$  state.

Different mixing scenarios have been developed in which the primordial glueball has a mass above or in between the two  $q\bar{q}$  states. The differences between the models lie in the assumed mass of the glueball – which can be taken from lattice gauge calculation – and in imposing (or not) the known decay branching ratios of scalar mesons. These mixing scenarios were pioneered by two papers by Amsler and Close [1112, 1113]. In these papers, it was shown that the properties of  $f_0(1370)$  and  $f_0(1500)$  are incompatible with them both being  $q\bar{q}$  mesons. In contrast,  $f_0(1500)$  mass and decays are compatible with it being the ground state glueball mixed with the nearby states of the  $0^{++}$   $q\bar{q}$  nonet. These conclusion were confirmed when data from central production were included in the analysis [721, 1114]. The  $s\bar{s}$  state predicted in [1112, 1113] was identified with the  $f_0(1710)$ . Further support for a glueball nature of  $f_0(1500)$  was presented in [1115]. The upper limits on the two-photon widths of  $f_0(1500)$  and  $f_0(1710)$  suggest that these two mesons cannot have sizable  $n\bar{n}$  components. Hence they must have glueball and  $s\bar{s}$  wave functions, the decay pattern assigns the larger glueball content to  $f_0(1500)$ . The production rates of  $f_0^i$  ( $i = 1, 2, 3$  corresponding to  $f_0(1710)$ ,  $f_0(1500)$ , and  $f_0(1370)$ ) in  $J/\psi \rightarrow V f_0 \rightarrow VPP$  ( $V$ =vector,  $P$ =pseudoscalar meson) were also exploited to test glueball and  $q\bar{q}$  nonet mixing scenarios. In [1116] it is shown that the peculiar patterns in these branching ratios can be understood by assuming the presence of significant glueball fractions in the scalar wavefunctions. Recently, branching ratios from  $J/\psi$  decays into a vector and a scalar meson were used to determine the mixing [1116, 1117]; OZI rule violating is required to play a significant rôle [1118].  $J/\psi$  decays were found to be very sensitive to the structure of scalar mesons. The analysis confirmed the claim for a glueball in the  $1.5 - 1.7$   $\text{GeV}/c^2$  region, in line with Lattice QCD. The mixing parameters were compatible with previous analyses.

Starting from lattice results on the scalar glueball mass, Weingarten and Lee [1119, 1120] see the main glueball component in  $f_0(1710)$  while  $f_0(1500)$  is believed to be dominantly  $s\bar{s}$ . The decay pattern of scalar mesons was not included in the analysis. De-Min Li *et al.* studied the influence of the position of the primordial glueball mass on the mixing parameters [1121]. Crystal Barrel results on  $4\pi$  decays of scalar mesons were included in the analysis by Fässler and collaborators [1122, 1123]. In this analysis, slightly more than 50% of the  $f_0(1500)$  wave function is of gluonic nature, the  $f_0(1710)$  comprises 32% and the  $f_0(1370)$  12% of glue. Refined variants of this approach can be found in [1124–1126]. A viable mass matrix can however also be constructed with the largest glueball fraction assigned to  $f_0(1370)$  [1127].

In a relativistic quark model Celenza *et al.* [1128] find a good fit to the scalar mass spectrum by adding a glueball with mass of about  $1700 \text{ MeV}/c^2$ . The scalar meson nonet is nearly ideally mixed, with the  $f_0(980)$  interpreted as having a 10%  $s\bar{s}$  component. The  $f_0(1370)$  is the dominantly  $s\bar{s}$  state, while  $f_0(1500)$  is a  $n\bar{n}$  state having a single node. The next radial excitation is expected at  $1843 \text{ MeV}/c^2$ . Thus,  $f_0(1760)$  was identified as the state with the largest glueball component [1128].

The scheme can be extended to contain not only  $q\bar{q}$  mesons and glueballs but also tetraquarks [1111, 1129] or hybrids [1118]. The possible discovery of a further scalar meson at  $1810 \text{ MeV}/c^2$  may require the extension into one of these directions.

Based on QCD spectral sum rules, Narison interprets  $\sigma, \kappa, \delta, S^*$  as nonet of  $1^3P_0$  ground state  $q\bar{q}$  mesons. The properties of the isoscalar states are strongly influenced by their coupling with a low-mass glueball. He suggests that  $f_0(1370)$  is mostly  $n\bar{n}$  while  $f_0(1500)$ ,  $f_0(1710)$ , and  $f_0(1790)$  should have significant gluonium components in their wave functions [132]. Invoking sum rules as well, Zhang, and Steele [1078] interpret the light scalar meson nonet as nonet of tetraquarks.

A few recently suggested interpretations of the scalar mesons below  $1 \text{ GeV}/c^2$  and decompositions of  $f_0(1370)$ ,  $f_0(1500)$ , and  $f_0(1710)$  into their  $n\bar{n}$ ,  $s\bar{s}$  and glueball components are collected in Fig. 114. Close and Kirk (Fig. 114a) interpret  $\sigma(485)$  and  $S^*$  as molecules with small  $q\bar{q}$  admixture; the largest glueball component is contained in  $f_0(1500)$  [1114]. Maiani, Piccinini, Polosa, and Riquer interpret  $\sigma, \kappa, \delta, S^*$  as nonet of tetraquark states. A decuplet consisting of  $f_0(1370)$ ,  $K_0^*(1430)$ ,  $a_0(1475)$ ,  $f_0(1500)$ , and  $f_0(1710)$  is suggested to originate from a nonet of tetraquark states plus a glueball. The isoscalar mesons mix, the mixing fractions are shown in Fig. 114b;  $f_0(1500)$  is nearly a pure glueball [1111]. Fariborz starts from a nonlinear chiral Lagrangian, developed in [1130, 1131], and studies mixing of two scalar meson nonets, a two-quark nonet and a tetraquark nonet, and a scalar glueball [1132]. The observed isoscalar states receive contributions from  $gg$ ,  $q\bar{q}$ , and  $qq\bar{q}\bar{q}$  with fractions displayed in Fig. 114c. Bugg underlines the unusual  $\phi\omega$  decay mode in the scalar wave, having a peak position at  $1810 \text{ MeV}/c^2$  [1105]. He combines it with the  $1790 \text{ MeV}/c^2$  peak and derives decay properties of an scalar resonance which require a large  $q\bar{q}$  - glueball mixing. Bicudo, Cotanch, Llanes-Estrada, and Robertson argue in favour of a glueball interpretation [1133]. Fig. 114d reminds of this possibility. None of the papers mentions that glueball decays into  $\phi\omega$  violate SU(3) symmetry.

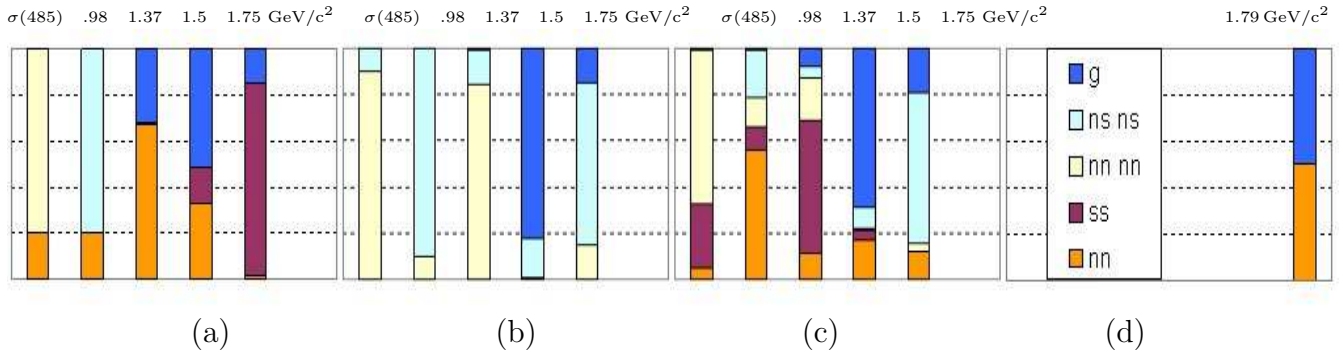


Fig. 114. Decomposition of scalar isoscalar states into different components. a)  $n\bar{n}, s\bar{s}$  and glueball [1114]. b)  $q\bar{q}, \bar{q}, q\bar{q}\bar{q}$  and glueball [1111]. c)  $n\bar{q}, s\bar{s}, q\bar{q}\bar{q}\bar{q}$  and glueball [1132]. d) The  $f_0(1790)$  and  $f_0(1810)$  are treated as one state with very large glueball content [1105]. Notation:  $n\bar{n} = \frac{1}{\sqrt{2}}(u\bar{u} + d\bar{d})$ ,  $q\bar{q} = 8_F \oplus 1_F$ .

### 11.3 The Anisovich-Sarantsev picture

The Gatchina group fitted a large set of different reactions and final states as outlined in section 6.2. Here we discuss the S-wave which is parameterised by a K-matrix. In a simplified version, the scalar partial wave amplitude is written in the form

$$\hat{A}(s) = \hat{K}(s) \left[ 1 - i\hat{\rho}\hat{K}(s) \right]^{-1}, \quad \hat{K} = \begin{vmatrix} K_{11}, K_{12}, \dots \\ K_{21}, K_{22}, \dots \\ \dots \end{vmatrix}, \quad \hat{\rho} = \begin{vmatrix} \rho_1, 0, \dots \\ 0, \rho_2, \dots \\ \dots \end{vmatrix}$$

with a  $5 \otimes 5$  matrix which includes the decay modes 1,2,3,4 and 5 and  $1 = \pi\pi$ ,  $2 = K\bar{K}$ ,  $3 = \eta\eta$ ,  $4 = \eta\eta'$ ,  $5 = \pi\pi\pi\pi$ . Threshold singularities are taken into account correctly. The phase space elements were defined as

$$\rho_{\pi\pi} = \sqrt{\frac{s - 4m_\pi^2}{s}}, \quad \rho_{K\bar{K}} = \sqrt{\frac{s - 4m_K^2}{s}}, \quad \dots$$

The definition of the amplitudes became more complex in the course of time and with an increasing number of reactions studied.

Fit parameters are the K-matrix elements, represented by a sum of pole terms  $g_a^{(n)}g_b^{(n)}/(\mu_n^2 - s)$ , and a smooth  $s$ -dependent term  $f_{ab}(s)$ :

$$K_{ab} = \sum_n \frac{g_a^{(n)}g_b^{(n)}}{\mu_n^2 - s} + f_{ab}(s),$$

$M_n$ ,  $g_a$ ,  $g_b$  are K-matrix parameters. The full amplitudes used recently in fitting procedure are documented in [859]. From the fits, positions of poles (masses and total widths of the resonances) and pole residues and hence partial widths to meson channels  $\pi\pi$ ,  $K\bar{K}$ ,  $\eta\eta$ ,  $\eta\eta'$ ,  $\pi\pi\pi\pi$  were deduced. Masses and widths of scalar mesons are given in Table 37, the decay branching ratios in Table 38. The  $\sigma(485)$  was not required in the fits but its existence was not excluded. Possibly, its absence is due to the threshold behaviour of the amplitudes which were not constrained by chiral symmetry. A small modification of the threshold behaviour of the amplitudes would likely accommodate  $\sigma(485)$  and  $\kappa(700)$  as additional resonances. In [1134] it is suggested that the  $\sigma(485)$  resonance, if it exists, may originate from the singularity of a flavour singlet Coulomb-like potential at  $r \rightarrow 0$ . The  $\kappa(700)$  was not mentioned.

The interpretation of the Gatchina group [859] started from the quark model assignments presented in Figs. 56 and 79 – shown in sections 6.2 and 8.5.1, respectively – and in Fig. 115. The two scalar

Table 37

Pole positions of scalar mesons from a fit to a large number of data sets [859].

$f_0(980)$	$a_0(980)$	$K_0^*(1430)$	$f_0(1370)$
$(1015 \pm 15) - i(43 \pm 8)$	$988 \pm 5^1$	$(1415 \pm 25) - i(165 \pm 25)$	$(1310 \pm 20) - i(160 \pm 20)$
$f_0(1500)$	$a_0(1450)$	$K_0^*(1800)$	$f_0(1760)$
$(1496 \pm 8) - i(58 \pm 10)$	$(1490 \pm 5) - i(70 \pm 10)$	$(1820 \pm 40) - i(125 \pm 50)$	$(1780 \pm 30) - i(140 \pm 20)^2$
Glueball: $f_0(1530)$			$(1530_{-250}^{+90}) - i(560 \pm 140)$

<sup>1</sup> $g_{\pi\eta} = 0.436 \pm 0.02$ ,  $\left(\frac{g_{K\bar{K}}}{g_{\pi\eta}}\right)^2 = 1.23 \pm 0.10$

<sup>2</sup>Alternative solution:  $(1780 \pm 50) - i(220 \pm 50)$

Table 38

Partial decay widths of scalar mesons [859].

Resonance	$\Gamma_{\pi\pi}$	$\Gamma_{K\bar{K}}$	$\Gamma_{\eta\eta}$	$\Gamma_{\eta\eta'}$	$\Gamma_{\pi\pi\pi\pi}$	$\Gamma_{tot}$
$f_0(980) :$	$55 \pm 5$	$10 \pm 1$	–	–	$2 \pm 1$	$68 \pm 10$
$f_0(1300) :$	$66 \pm 10$	$6 \pm 4$	$5 \pm 2$	–	$230 \pm 50$	$300 \pm 40$
$f_0(1500) :$	$23 \pm 5$	$6 \pm 2$	$3 \pm 1$	$0.1 \pm 0.1$	$80 \pm 10$	$110 \pm 10$
$f_0(1760) :$	$30 \pm 5$	$100 \pm 10$	$5 \pm 3$	$7 \pm 3$	$5 \pm 5$	$140 \pm 40$
	$105 \pm 10$	$2 \pm 1$	$8 \pm 1$	$5 \pm 3$	$170 \pm 40$	$300 \pm 50$

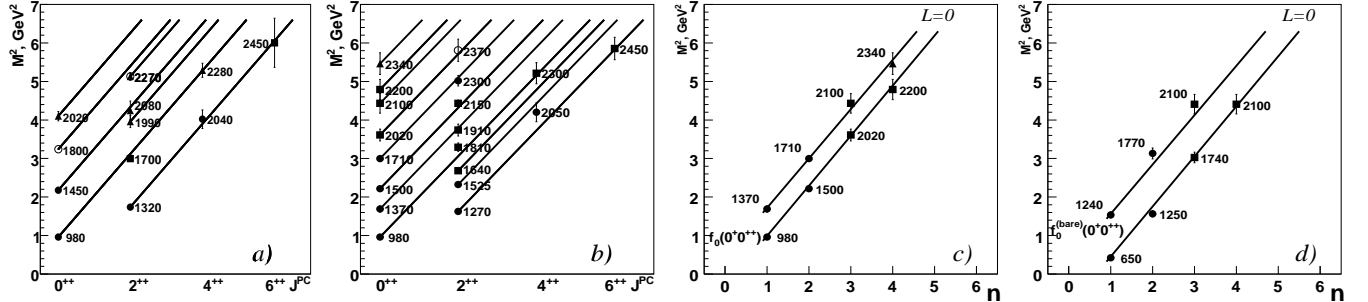


Fig. 115. Leading and daughter Regge trajectories of isovector (a) and isoscalar (b) positive-parity mesons with even  $J$ . Different symbols are used to identify states belonging to the same trajectory. Fig. (b) contains separate straight lines for mesons with a larger and a smaller  $s\bar{s}$  component. In particular the isoscalar scalar states reveal a rich spectrum. The  $f_0(00^{++})$ -trajectories for the physical states (c) and for the K-matrix pole positions (d) [371].

mesons  $f_0(980)$ ,  $a_0(980)$  were interpreted as  $q\bar{q}$  mesons. The main reasons for this assignment were found in the consistency of their masses with trajectories on  $(n, M^2)$  and  $(J, M^2)$  planes, in the high yield of  $f_0(980)$  in  $D_s$  decays, in the fact that  $\phi$  radiative yields of  $f_0(980)$  and  $a_0(980)$  agree with calculations assuming a  $q\bar{q}$  structure of these mesons, and in the need of their presence in K-matrix fits and a consistent interpretation of K- and T-matrix poles (see below) [1135].

With  $f_0(980)$  and  $a_0(980)$  as  $q\bar{q}$  states, the following spectroscopic assignments were suggested:

$$\{ a_0(980), f_0(1300), f_0(980), K_0^*(1430) \} \quad \{ a_0(1450), f_0(1760), f_0(1500), K_0^*(1430) \}$$

for the ground state scalar nonet and its first radial excitation. These are the pole positions of the scattering matrix or T-matrix. They correspond to the experimentally observed states. These poles did not suffice to get a good description of the data, a wide background amplitude was needed in addition. When parametrised as  $s$ -channel resonance, its mass was found to be

$$0^{++} \text{ glueball: } M = 1530_{-250}^{+90} ; \quad \Gamma = 560 \pm 140 .$$

Its decay couplings to the channels  $\pi\pi$ ,  $K\bar{K}$ ,  $\eta\eta$ ,  $\eta\eta'$  were found to be flavour neutral; the state is a flavour singlet state. This gave the reason to consider this state as the lightest scalar glueball.

The K-matrix poles are direct fit parameters but do not correspond to observables quantities. However, when the coupling of T-matrix poles are reduced (and then set to zero), the T-matrix poles approach the K-matrix pole (and coincide with them for vanishing couplings). It is thus tempting to identify the K-matrix poles with the quark model states in the absence of decays. A full dynamical model of strong interactions would include meson decay couplings but such calculations are not available. To remedy this situation the Gatchina group suggested that the K-matrix pole may represent the bare states and that dressing of bare  $q\bar{q}$  states (which results in observable meson resonances) can be mimicked by switching on the couplings of K-matrix poles to the respective final states. This is an untested but very intuitive assumption. Hence the positions of the K-matrix poles and their couplings to meson channels were identified as masses and couplings of 'bare' states. For the first nonet, the K-matrix poles were found to have, within 20%, the same SU(3) coupling, for second nonet members the coupling was nearly identical. (Of course, the SU(3) couplings had to be multiplied with the appropriate isoscalar coefficients.)

The bare states were interpreted as  $q\bar{q}$  states before dressing, before the couplings to meson-meson final states are turned on, and these are the states which should be compared to quark model calculations. It is only after coupling to the meson-meson continuum that the quark-model states

acquire finite widths. When the couplings to the meson continua were turned on, for the fitted values of the coupling constants  $g_\alpha$ , the physical states evolve. Their masses can be determined by inspecting the T-matrix; their poles positions give the physical masses and the total widths, the residues give the partial decay widths. These are the quantities which are independent of the production process.

On this basis, the bare states can be classified into quark-antiquark nonets. In particular it can be imposed that (or checked if) two scalar isoscalar mesons assigned to the same multiplet have orthogonal flavour wave functions and that a 5<sup>th</sup> scalar isoscalar state has couplings of a SU(3) isosinglet state, of a glueball candidate. Its position differs in different solutions and the authors quote  $f_0(1200 - 1600)$ . It is a rather broad state, with a width between 1 and 2 GeV/c<sup>2</sup>. It is interpreted as the descendant of a primary glueball (even though mixing with SU(3) isoscalar mesons cannot be excluded).

The strongest argument in favour of the Anisovich-Sarantsev approach is the beautiful agreement between their K-matrix poles and the meson mass spectrum calculated in the Bonn quark model using instanton-induced interactions (see section 2.6.3). The comparison of K-matrix poles and of the calculated masses is shown in Table 39.

Table 39

Comparison of K-matrix poles [859] and meson masses calculated in a relativistic quark model with instanton-induced forces [175].

$1^3P_0 q\bar{q}$ :	$f_0^{bare}(720 \pm 100)$	$a_0^{bare}(960 \pm 30)$	$K_0^{bare}(1220^{+50}_{-150})$	$f_0^{bare}(1260 \pm 30)$
Model	$f_0(665)$	$a_0(1057)$	$K_0^*(1187)$	$f_0(1262)$
$2^3P_0 q\bar{q}$ :	$f_0^{bare}(1230^{+150}_{-30})$	$a_0^{bare}(1650 \pm 50)$	$K_0^{bare}(1885^{+50}_{-100})$	$f_0^{bare}(1810 \pm 30)$
Model:	$f_0(1262)$	$a_0(1665)$	$K_0^*(1788)$	$f_0(1870)$

The agreement is very impressive. The identification of K-matrix poles and quark model states (which are calculated by neglecting their coupling to the meson-meson continuum) seems very plausible even though one has to admit that K-matrix poles are not observable quantities. Even worse, there is no one-to-one correspondence of K- and T-matrix poles. The position of K-matrix poles can be changed by a large amount, and the T-matrix poles can still remain at the same position. Only in the limit of narrow resonances, K-matrix and T-matrix poles remain at similar values. Quantitative details on the spread of K-matrix poles for a given T-matrix pole can be found in a recent paper by Jaffe [1082].

The mass and width of the wide state are not well defined, the mass were found in the range 1200 to 1600 MeV/c<sup>2</sup>, the width between 1000 and 2000 MeV/c<sup>2</sup>. The large width is accumulated from its mixing with  $q\bar{q}$  states. Anisovich, Bugg, and Sarantsev developed the idea of width accumulation of an exotic state which overlaps with  $\bar{q}q$  resonances [1136]. The idea can best be followed in a concrete example. Let  $Re M_1^2$  and  $Re M_2^2$  be different but  $M_1\Gamma_1 = M_2\Gamma_2 = M\Gamma$ . Then,

$$M_1^2 = M_{R1}^2 - iM\Gamma, \quad M_2^2 = M_{R2}^2 - iM\Gamma. \quad (11.1)$$

The diagonalisation of the mass matrix yields:

$$M_{A,B}^2 = \frac{1}{2}(M_{R1}^2 + M_{R2}^2) - iM\Gamma \pm \sqrt{\frac{1}{4}(M_{R1}^2 - M_{R2}^2)^2 - M^2\Gamma^2}. \quad (11.2)$$

In the limit  $2M\Gamma \ll |M_{R1}^2 - M_{R2}^2|$ , there is no mixing and the location of the two poles remains unchanged. For  $|M_{R1}^2 - M_{R2}^2| \ll 2M\Gamma$  the two poles coincide in mass, with one state being almost stable while the width of the other resonance is close to  $2\Gamma$ . Of course, this is a simplified example. The two quark model states  $K_{1A}$  and  $K_{1B}$  mix to form  $K_1(1270)$  and  $K_1(1400)$ . Their total widths are similar, 90 and 174 MeV/c<sup>2</sup>, respectively. But they acquire different partial widths:  $K_1(1270)$  couples to  $K^*\pi$  with  $(16 \pm 5)\%$  branching ratio and  $(53 \pm 6)\%$  to  $K\rho$  and  $K\omega$ ;  $K_1(1400)$  decays with  $(94 \pm 6)\%$  to  $K^*\pi$  and with  $(5 \pm 4)\%$  to  $K\rho$  and  $K\omega$ . In this example, none of the states acquires a broad total width; rather they decay into two orthogonal final states.

## 11.4 The red dragon of Minkowski and Ochs

Minkowski and Ochs [178] interpret the isoscalar states  $f_0(980)$  and  $f_0(1500)$  together with  $a_0(980)$  and  $K_0^*(1430)$  as members of the  $q\bar{q}$  nonet with  $J^{PC} = 0^{++}$  of lowest mass. They show that the  $f_0(980)$  and  $\eta'$  have very similar production patterns in  $J/\psi$  decay when recoiling against an  $\omega$  or  $\phi$ , and that  $f_0(1500)$  has a flavour wave function in which the  $n\bar{n}$  and  $s\bar{s}$  components have opposite signs. The data are compatible with  $f_0(980)$  as isoscalar singlet and  $f_0(1500)$  as isoscalar octet member of the scalar nonet. Hence flavour mixing in the scalar sector resembles more the one observed in the pseudoscalar nonet even though with inverted masses. Scalar mesons do not follow the ideal mixing pattern of vector and tensor mesons and as most other meson nonets do. The pair  $f_0(980)$  and  $\eta'$  forms a (nearly) mass-degenerate parity doublet of scalar isoscalar states.

In the mass range from 400 MeV/c<sup>2</sup> up to about 1700 MeV/c<sup>2</sup>, the  $\pi\pi$  amplitude describes a full loop in the Argand diagram after the  $f_0(980)$  and  $f_0(1500)$  states are subtracted. This background amplitude is called *red dragon* and identified with the expected glueball. The  $\sigma(485)$  and  $f_0(1370)$  are considered to be part of the red dragon and not to be genuine resonances. It should be noted that the authors interpret  $\eta(1440)$  as pseudoscalar glueball (see however section 8), and  $f_J((1710)$  with  $J = 2$  as tensor glueball.

The glueball scenario suggested by Minkowski and Ochs has some similarity with the Anisovich-Sarantsev picture even though the scalar  $q\bar{q}$  nonets are completely different. Minkowski and Ochs interpret the observed T-matrix poles at 980 MeV/c<sup>2</sup> and at 1500 MeV/c<sup>2</sup> as  $q\bar{q}$  states; the  $f_0(1370)$  is put into question, the  $f_0(1760)$  is argued to have tensor quantum numbers and suggested to be the tensor glueball. Jointly with  $a_0(980)$  and  $K_0^*(1430)$ , one scalar nonet is suggested. Anisovich and Sarantsev identify two full scalar nonets. Their T-matrix poles, the observable resonances, are given by  $f_0(980)$ ,  $f_0(1370)$ ,  $f_0(1500)$ ,  $f_0(1760)$ ,  $a_0(980)$ ,  $a_0(1450)$ ,  $K^*(1430)$  and  $K_0^*(1760)$ . Common in both pictures is the glueball: it is a broad about 1 GeV/c<sup>2</sup> wide object with a mass of 1 to 1.5 GeV/c<sup>2</sup>.

## 11.5 Scalar mesons with instanton-induced interactions

In 1995, a quark model was suggested [175] which is based on quarks having an effective constituent quark mass, a linear interaction modelling confinement and a residual interaction based on instanton effects [123, 1137]. The model had the virtue of reproducing near exactly the mass spectrum of the ground-state pseudoscalar mesons and their flavour mixing. The instanton-induced interaction inverts their sign when going from the pseudoscalar to the scalar world. Thus they lower the mass of states whose SU(3) flavour structure is dominantly flavour singlet and pushes the dominantly flavour octet states to higher masses, see Fig. 15 in section 2.6.3. The calculated masses of the

ground state scalar mesons were predicted to be

$$a_0(1370), \quad K_0^*(1430), \quad f_0(980), \quad f_0(1470) \quad (11.3)$$

which can be compared to the observed states

$$a_0(980)/a_0(1450), \quad K_0^*(1430), \quad f_0(980), \quad f_0(1500). \quad (11.4)$$

The  $f_0(980)$  is calculated to have a nearly pure flavour singlet wave function and  $f_0(1500)$  to be a flavour octet state, in accordance with its large coupling to  $\eta\eta'$ <sup>11</sup>.

Preserving the molecular picture of the  $a_0(980)$ ,  $f_0(980)$  doublet yields a nonet of a scalar  $q\bar{q}$  nonet

$$a_0(1450), \quad K_0^*(1430), \quad f_0(1000), \quad f_0(1500). \quad (11.5)$$

In this case, the broad background component is identified with the ground-state scalar meson. In the dual Regge picture, the scattering amplitude can be described by a sum of  $s$ -channel resonances or by a sequence of  $t$ -channel exchanges. The Pomeron belongs to the allowed  $t$ -channel exchanges, it is dual to a ‘background’ in the direct  $s$ -channel and can possibly be identified with a contribution of a glueball. From  $\pi\pi$  scattering, amplitudes for  $t$ -channel exchanges with defined isospin  $I_t$  was constructed by Quigg [1138]. The  $I_t = 0$  amplitude rises with energy and is sizable already below 1 GeV. This amplitude could be due to Pomeron exchange which would suggest that the broad background component could be a glueball. Of course, exchanges of isoscalar  $q\bar{q}$  mesons like  $f_2(1270)$  contribute to this amplitude, hence the broad isoscalar scalar background could also be of  $q\bar{q}$  nature. Its width may speak against this interpretation, but the analysis of Ritter, Metsch, Münz, and Petry [189] has shown that instanton induced interaction can make significant contributions to the decay amplitude for the decay of scalar mesons into two pseudoscalar mesons. The solution space for interference of this amplitude and a conventional  ${}^3P_0$  decay amplitude is not yet explored. Hence very different widths within a scalar nonet are not ruled out.

If  $f_0(1370)$  does not exist as  $q\bar{q}$  resonance, if  $f_0(1000)$  is of  $q\bar{q}$  nature, and if the lowest mass scalar meson form a separate nonet there is, below  $1.7 \text{ GeV}/c^2$ , no room left for the scalar glueball [35].

The eminent rôle played by the  $U_A(1)$  symmetry-breaking t’ Hooft interaction in scalar mesons was underlined by Dmitrasinovic [1139] in the Nambu-Jona-Lasinio model. He derived an approximate sum rule

$$m_{\eta'}^2 + m_\eta^2 - 2m_K^2 = m_{f'_0}^2 + m_{f_0}^2 - 2m_{K_0}^2 \quad (11.6)$$

linking the mass splittings between the pseudoscalar and the scalar singlet and octet mesons. The splitting must have the same size but opposite signs. A scalar nonet was suggested to comprise

$$a_0(1320), \quad K_0^*(1430), \quad f_0(1000), \quad f_0(1590) \quad (11.7)$$

Burakovsky, partly with Goldman, calculated the mass spectra of P-wave mesons using a non-relativistic quark model [1140, 1141]. The calculation assumed degeneracy of tensor and scalar mesons, except for the scalar isosinglet state. Its mass is put in ‘by hand’ using eq. (11.6). In the Nambu-Jona-Lasinio model with instanton-induced interactions, a SU(3) multiplet mass formula was obtained consistent with this assignment [1139].

---

<sup>11</sup> The ratio  $0.38 \pm 0.16$  of partial widths  $f_0(1500) \rightarrow \eta\eta'$  to  $f_0(1500) \rightarrow \eta\eta$  is rather large in spite of the much more favourable phase space for  $\eta\eta$  decays. A isoscalar singlet can of course not decay into  $\eta\eta'$  while an octet is allowed to decay into  $\eta\eta$ .

## 11.6 Our own interpretation

### 11.6.1 Light scalar nonets

The starting point of our interpretation is  $f_0(1500)$ . It is a mainly SU(3) octet state; this follows from its strong  $\eta\eta'$  decay mode [326], from the phase motion of the scalar wave in  $\pi^- p \rightarrow p\eta\eta$  and  $pK_S^0 K_S^0$  [178], and from the constructive interference of  $B^\pm \rightarrow K^\pm f_0$ ,  $f_0 \rightarrow (K\bar{K})$  and destructive interference in  $B^\pm \rightarrow K^\pm f_0$ ,  $f_0 \rightarrow (\pi\pi)$  [740]. The different interference patterns in these two reactions would lead, if not properly taken into account, to the necessity to introduce three scalar states, a scalar state at about  $1350 \text{ MeV}/c^2$  coupling to  $\pi\pi$ , the standard  $f_0(1500)$ , and a new state at  $1500 \text{ MeV}/c^2$  with strong coupling to  $K\bar{K}$  and weak coupling to  $\pi\pi$  [605, 612, 641]. The latter state would have properties incompatible with the standard Crystal Barrel state which decays into  $\pi\pi$  four times more frequent than into  $K\bar{K}$ . We refuse this interpretation. Instead, we enforce the interpretation of Minkowski and Ochs [740] that the  $f_0(1500)$  with standard properties interferes with a scalar isoscalar background.

The  $f_0(1500) \rightarrow (K\bar{K})$  peak would require introduction of a new resonance if interference effects were not properly taken into account. With this warning, we examine the BES puzzle on  $J/\psi$  decays into a scalar mesons recoiling against an  $\omega$  and a  $\phi$  meson. The  $1700\text{-}1800 \text{ MeV}/c^2$  region is often supposed to be split into a low-mass  $f_0(1710)$  and a high-mass  $f_0(1790)$ . The problem is that the low mass state  $f_0(1710)$  is produced in  $J/\psi \rightarrow \omega f_0(1710)$  as a mainly  $n\bar{n}$  state. But is only observed decay mode is  $K\bar{K}$ . The  $f_0(1790)$  is produced in  $J/\psi \rightarrow \phi f_0(1790)$  as a mainly  $s\bar{s}$  state. But the latter state decays into  $\pi\pi$ . At the first glance, this is completely contradictory. To increase the complexity of the pattern, a scalar structure was observed in radiative  $J/\psi$  decays which decays into  $\phi\omega$ . Decays into  $\phi\omega$  are OZI rule violating; radiative production of such a state violates the OZI rule as well. The BES collaboration announced the observation as doubly OZI rule violating effect.

We start with the assumption that the three observations  $f_0(1710)$ ,  $f_0(1790)$ , and  $f_0(1810)$  represent one single state with unusual properties which we call  $f_0(1760)$ . In the SU(3) limit,  $\phi\omega$  is flavour octet. The radiative yield of  $f_0(1760)$  is large, hence it does not have only a small octet component, its flavour structure must be octet-like (with a negative sign between  $\bar{n}n$  and  $\bar{s}s$ ). Production of flavour-octet mesons in radiative  $J/\psi$  decays is unexpected. Initial state radiation in  $J/\psi$  decays produces a system of pure glue (with minimum of two gluons in a perturbative picture). These cannot couple to one flavour-octet meson. However, final state radiation could play a significant rôle as well. Here it is worthwhile to recall that bremsstrahlung is produced proportional to  $m^{-3}$  of the radiating system. These factors counterbalance arguments based on the number of gluons. Production of octet mesons seems therefore not implausible.

A  $q\bar{q}$  octet state can decay into  $\rho\rho$ ,  $\omega\omega$ , and  $K^*K^*$  but not into  $\phi\omega$ . However, a tetraquark S-wave configuration with the two antisymmetric quark pairs may be energetically favoured compared to  $q\bar{q}$  in P-wave. An octet-state tetraquark wave function is derived by adding a second  $q\bar{q}$  pair to the  $q\bar{q}$  wave function in a way suggested by Jaffe. In this way one obtains

$$f_0^8 = \frac{1}{\sqrt{6}} |\bar{u}u + \bar{d}d - 2\bar{s}s> \quad \Rightarrow \quad \frac{1}{\sqrt{6}} |2\bar{u}u\bar{d}d - \bar{u}u\bar{s}s - \bar{d}d\bar{s}s> \quad (11.8)$$

which decays naturally, by falling apart, into  $\pi\pi$ ,  $K\bar{K}$ ,  $\rho\rho$ ,  $\omega\omega$ ,  $K^*K^*$ , and into  $\phi\omega$ . The tetraquark flavour singlet wave function

$$f_0^1 = \frac{1}{\sqrt{3}} |u\bar{u} + d\bar{d} + s\bar{s}\rangle \quad \Rightarrow \quad \frac{1}{\sqrt{3}} |u\bar{u}d\bar{d} + u\bar{u}s\bar{s} + d\bar{d}s\bar{s}\rangle . \quad (11.9)$$

has the same decay modes as the octet state. It is important to emphasize that a small tetraquark fraction in the flavour wave function and a large decay probability of this component is sufficient to result in a significant impact on the observed decay pattern.

Likely, SU(3) singlet and octet amplitudes contribute to the final state as in the case of  $B$  decays discussed above (see Fig. 108 and their discussion in the text). Interference between singlet and octet amplitudes could be responsible for the weird production and decay pattern in  $J/\psi$  decays into scalar mesons recoiling against an  $\omega$  or  $\phi$ . Note that adding or subtracting eqs. (11.8) and (11.9) with appropriate factors yields pure  $\bar{u}u\bar{d}\bar{d}$  and  $\bar{u}u\bar{s}s - \bar{d}d\bar{s}\bar{s}$  states. The former state does not couple to  $K\bar{K}$ , the latter not to  $\pi\pi$ .

The  $a_0(1475)$  mass is larger than that of  $K_0^*(1430)$  even though the latter state carries strangeness, the former one not. This ‘inverse’ mass pattern has been discussed often and used as an argument against  $a_0(1475)$  and  $K_0^*(1430)$  belonging to the same SU(3) nonet. In Jaffe’s scalar tetraquark nonet,  $a_0$  masses are heavier than  $K_0^*$  masses by  $150 \text{ MeV}/c^2$ , see Fig. 80. This for tetraquark states, the inverse mass pattern emerges naturally. Mixing with  $q\bar{q}$  can obviously reproduce the observed masses.

When  $f_0(980)$ ,  $f_0(1500)$ , and  $f_0(1760)$  are interpreted as SU(3) octet states, where are the associated singlet resonances? Scalar isosinglet resonances couple directly to the QCD vacuum, in contrast to the octet states. Thus isosinglet states can become very broad. We suggest that all flavour-singlet scalar mesons get absorbed into a wide structure; the transition from the flavour-singlet  ${}^3P_0$  mesons to the vacuum by emission of two pseudoscalar mesons, of two Goldstone bosons, is too fast to support the existence of individual resonances. The scalar glueball could be part of this broad background. The background is thus ‘gluish’ in the same sense as  $\eta'$  mesons are gluish. But the coupling to the QCD vacuum is much stronger for  ${}^3P_0$  quantum numbers than for the flavour-singlet pseudoscalar  $\eta'$ . The isoscalar scalar amplitude manifests itself only by interference with the narrow octet scalar mesons.

In the schematic view of Fig. 112, the wide scalar background amplitude is assumed to be isoscalar, the interspersed narrow resonances octet states. The  $\sigma(485)$  is partner of  $f_0(980)$ , the other isosinglet partners are not easily identified due to their large widths. Fig. 116 sketches this scenario.

We see immediately one problem: interpreted as octet state,  $f_0(1760)$  needs an isovector and isodoublet partner. Hence either  $f_0(1760)$  is isosinglet (and the problematic production and decay pattern observed in  $J/\psi$  decays remains an unsolved issue), or we need to postulate the existence of a  $a_0(1720)$  and a  $K_0^*(1680)$  resonance, where the masses are estimates. It is not unrealistic that these two states have escaped detection so far. The two isovector states  $a_0(1475)$  and  $a_0(2020)$  were both discovered in  $\bar{p}p$  annihilation, the  $a_0(1475)$  in  $\bar{p}p$  annihilation at rest, the  $a_0(2020)$  in  $\bar{p}p$  annihilation in flight, in formation. Both techniques do not give access to an eventual  $a_0(1720)$ . The  $K_0^*(1720)$  may have escaped observation due to dominant contributions of  $K_0^*(1680)$  and  $K_1(1720)$ . In the discussion of tensor mesons [880–882] (see section 6.4.3), an additional  $K_2^*(1650)$  was predicted. Hence, the non-observation of these two missing states may not be a decisive argument against our view.

The mass of isoscalar scalar mesons is speculative. Nevertheless we suggest a scenario which may

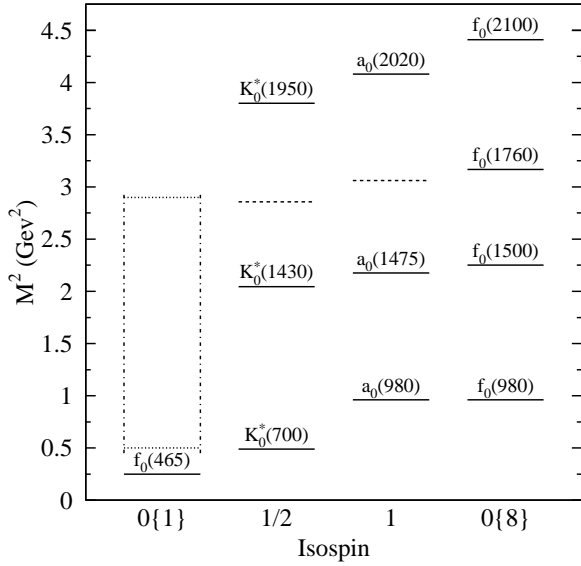


Fig. 116. Scalar mesons with 4 octets:  $\{a_0(980), K_0^*(700), f_0(980)\}$ ,  $\{a_0(1475), K_0^*(1430), f_0(1500)\}$ ,  $\{a_0(xxx), K_0^*(xxx), f_0(1760)\}$ ,  $\{a_0(2020), K_0^*(1950), f_0(2100)\}$ . The ninth members are flavour SU(3) singlets. They are not separated into individual resonances. A glueball component is possible but unproven.

have some plausibility even though it is not enforced by data. Instanton induced interactions increase the mass of the pseudoscalar isoscalar  $q\bar{q}$  mesons, of  $\eta'$  and  $\eta(1835)$ . Their masses lie well above other all S-wave ground-state mesons and above all other first radial excitations, respectively. The same forces lower the masses of scalar isoscalar  $q\bar{q}$  mesons, by about the same amount. However, scalar mesons are not dominantly  $q\bar{q}$  and the action of instanton induced forces is likely reduced for the latter component. Instead of a mass shift of  $400 \text{ MeV}/c^2$  ( $m_{\eta'} - m_\eta$ ), we estimate the mass shift to  $\sim 200 \text{ MeV}/c^2$ . Thus we estimate isoscalar masses to be  $1300 \text{ MeV}/c^2$ ,  $1560 \text{ MeV}/c^2$ ,  $1900 \text{ MeV}/c^2$ . The lower two masses are close to values found in partial wave analyses:  $f_0(1370)$  is considered as established resonance; we believe it to exist but to be narrowed artificially by the  $f_0(980)$  and  $f_0(1500)$  resonances. Anisovich and Sarantsev find a scalar isoscalar resonance with a pole at  $(1530^{+90}_{-250}) - i(560 \pm 140)$ . Possibly the same pole was found at a somewhat larger mass, at  $(1.67 - 0.26i) \text{ GeV}$  in [991].

Why is there so little phase motion for  $f_0(1300)$ ? A likely answer can be seen looking at the  $\sigma(485)$  phase motion. The  $90^\circ$  phase is reached at  $750 \text{ MeV}/c^2$ , a further  $45^\circ$  shift (corresponding to a half width) is reached (subtracting  $f_0(980)$ ) at  $1200 \text{ MeV}/c^2$ . A pole far from the real axis has a slow phase motion and a  $180^\circ$  phase shift may never be reached.

Where is the scalar glueball? We believe it to be dissolved as well into the wide scalar background amplitude. We recall that the wide scalar component of low-energy  $\pi\pi$  scattering can be described quantitatively by molecular forces between the pions, by  $t$ -channel exchange of  $\rho$  and  $f_2(1270)$ . Duality arguments link amplitudes for  $t$ -channel exchange of  $\rho$  and  $f_2(1270)$  mesons to  $s$ -channel  $q\bar{q}$  resonances. A sum of broad S-wave resonances can thus be represented by a sum of a few meson  $t$ -channel exchanges. The  $t$ -channel exchange may contain a contribution from Pomeron exchange which in  $s$ -channel corresponds to a glueball. This scenario is a possibility how the glueball may hide; at present there is no evidence for this in reality.

The question arises how we can understand the absence of a narrow scalar glueball which is so firmly predicted by QCD inspired models and by QCD on the lattice. The reasons have to be the approximations made on the lattice. QCD on the lattice neglects the coupling of the gluon field to  $q\bar{q}$  pairs. This is called quenched approximation. Recent glueball mass calculations on the lattice include couplings to fermion loops [1142] but pions are still too heavy to represent the true chiral limit. It is hence not excluded that the scalar glueball is very broad.

To clarify this question, high precision data on  $J/\psi$  decays into a vector meson ( $\gamma$ ,  $\omega$  and  $\phi$ ) and two pseudoscalar mesons ( $\pi\pi$ ,  $K\bar{K}$ ,  $\eta\eta$ ,  $\eta\eta'$ ) are needed, and detailed studies of the decay of scalar mesons including radiative decays [1143]. Ultimately, a series of Rosner plots as functions of the scalar mass will be required. A Rosner plot for pseudoscalar mesons was shown in Fig. 3 in section 1.

### 11.6.2 Dynamical generation of resonances and flavour exotics

We have seen that there are severe arguments which justify interpreting some mesons as being generated from molecular forces between the mesons into which they decay. For the isospin quartet ( $a_0(980)$ ,  $f_0(980)$ ) the discussion [1035, 1039, 1043, 1046, 1056, 1144] concentrates, with refutation [1145] and counter-arguments [1146], and a recent detailed analysis [1055, 1147], on the question if data are compatible with or enforce one of the favoured interpretations, if  $a_0(980)$  and  $f_0(980)$  are dynamically generated,  $q\bar{q}$ , or tetraquark states.

The mesonic flavour wave function of  $a_0^+(980)$  can be expanded into its Fock components

$$|a_0(980)^+\rangle = \alpha|u\bar{d}\rangle + \beta|u\bar{d}s\bar{s}\rangle + \gamma|K^+\bar{K}^0\rangle + \dots \quad (11.10)$$

plus higher order configurations. In this expansion, quark and antiquark in  $u\bar{d}$  are in P-wave while the  $u\bar{d}s\bar{s}$  and  $K^+\bar{K}^0$  systems are in S-wave. The Pauli principle forbids to add a  $|u\bar{d}u\bar{u}\rangle$  or  $|u\bar{d}d\bar{d}\rangle$  component. The two components  $|u\bar{d}s\bar{s}\rangle$  and  $|K^+\bar{K}^0\rangle$  differ in their colour configuration: in the latter wave function,  $u\bar{s}$  and  $s\bar{d}$  are colour singlets, in the former this is not imposed. The tetraquark wave function contains the molecular picture. The dynamical assumptions are of course different in these two cases.

Jaffe has reminded us recently that tetraquark configurations and the molecular picture cannot be meaningfully distinguished when the state is near or above important thresholds [1082]. He considered a toy model in which the four quarks are very weakly bound inside of a strong interaction volume; outside, the  $K\bar{K}$  system is supposed not to interact. Then he assumed the colour forces are strong enough to bind the system but with a small binding energy. The small binding energy forces the system to become large. Is that system of tetraquark nature or of molecular character? The origin of that state lies certainly in the colour forces. The wave function exhibits molecular character.

Similar arguments have been raised in baryon spectroscopy. In the quark model, the  $N(1535)S_{11}$  resonance with  $J = 1/2$  is the twin brother of  $N(1520)D_{13}$  with  $J = 3/2$ . They both have intrinsic orbital angular momentum  $\ell = 1$  and the 3 quarks spins couple to  $s = 1/2$  (some  $s = 3/2$  component can be mixed into the wave function. On the other hand, the decay properties of the  $N(1535)S_{11}$  resonance can very well be understood from the S-wave meson-baryon interaction in the energy range around the  $\eta N$  threshold using a coupled channel chiral Lagrangian with  $\pi N$ ,  $\eta N$ ,  $K\Lambda$ ,  $K\Sigma$  in the isospin-1/2,  $l = 0$  partial wave. A fit to scattering data then yielded parameters, supporting a quasi-bound  $K\Sigma$ -state which can be identified with the  $N(1535)S_{11}$

resonance [1148]. Does this observation require two states, a quark model state *and* a quasi-bound  $K\Sigma$ -state? We do not believe so. Meson-nucleon scattering is partly driven by resonances which in turn can be reconstructed from the scattering amplitude. The quark model and dynamically generated resonances are, as we believe, different views of the same object.

Coming back to the low-lying scalar mesons. The main topic of this discussion is if we can expect two states, a  $|u\bar{d}\rangle$  and a  $|us\bar{d}\bar{s}\rangle$  meson (or  $K\bar{K}$  molecule), possibly mixing but creating two (or even three) states. This is a dynamical question to which answers can be given within a model or by looking at the observed pattern of states. The two orthogonal components  $\alpha|u\bar{d}\rangle + \beta|us\bar{d}\bar{s}\rangle$  and  $-\beta|u\bar{d}\rangle + \alpha|us\bar{d}\bar{s}\rangle$  may both form resonances. Yet it is possible as well that one of them disappears as scattering state. In SU(3), the number of tetraquark wave functions is 9, see Fig. 80. This is just the number of  $q\bar{q}$  states. This situation does not repeat in the case of SU(4). Charm provides an additional degree of freedom, and it is rewarding to include  $u, d, s, c$  quarks into the discussion. In SU(4), there are 16  $q\bar{q}$  states but 36 tetraquark configurations which have quark pairs which are antisymmetric in spin and flavour: 9 tetraquark states with  $u, d, s$  quarks only, 20 tetraquark states with open charm or anti-charm, and 9 tetraquark states with hidden charm. The 16  $q\bar{q}$  states are the light-quark nonet, a  $D^+, D^0, \bar{D}^0, D^-$  quartet, a  $D_s^+$ , and  $D_s^-$ , and the  $c\bar{c}$  state; three of them carry charm (and three anticharm). The 10 tetraquark states with open charm have wave functions:

$$\begin{array}{lllll} c\bar{d}u\bar{u} & ; & c\bar{d}s\bar{s} & ; & c\bar{d}d\bar{s} \\ c\bar{u}d\bar{d} & ; & c\bar{u}s\bar{s} & ; & c\bar{u}u\bar{s} \\ & & & & c\bar{u}s\bar{d} \\ & & & & c\bar{u}d\bar{s} \end{array} \quad (11.11)$$

These tetraquark combinations can all have  $qq$  in colour **3** and spin  ${}^1S_0$ . Thus mesons with wave functions  $1/\sqrt{2}|c\bar{s}(\bar{u}u+\bar{d}d)\rangle$  and  $1/\sqrt{2}|c\bar{s}(\bar{u}u-\bar{d}d)\rangle$  could exist. However, the last two wave functions in both rows of (11.11) are flavour exotic, and such states have never been observed.

Out of the 10 wave functions in (11.11), three can mix with  $q\bar{q}$ , the other seven tetraquark wave functions cannot. Phenomenologically, none of the seven extra states has been found. We conjecture that the forces in the tetraquark system and the molecular forces are not strong enough to provide binding, they fall apart as suggested by Jaffe [906, 990]. Only those tetraquark configurations exist which can mix with  $q\bar{q}$ . The tetraquark component plays a significant rôle for scalar mesons with masses close to or above their respective thresholds for OZI rule allowed decays. The tetraquark flavour wave functions of scalar charmed states are given by  $c\bar{d}(\bar{u}u+\bar{s}s)$ ,  $c\bar{u}(\bar{d}d+\bar{s}s)$ ,  $c\bar{s}(\bar{u}u+\bar{d}d)$ . We identify  $c\bar{s}(\bar{u}u+\bar{d}d)$  with  $D_s^*(2317)$ . The  $c\bar{d}(\bar{u}u+\bar{s}s)$  and  $c\bar{u}(\bar{d}d+\bar{s}s)$  ground states might be  $D_0^{*,0}(2350)$ . We believe that these are the first excited scalar states, and that the ground state  $D^{*,0}(1980)$  is not yet found. At such a low mass, SU(3) symmetry breaking will reduce the  $\bar{s}s$  component; in high excitations, the  $\bar{s}s$  component may play a rôle.

The conjecture of just three tetraquark scalar states with open charm can be tested at the  $D_s K_S^0$  threshold. A  $(c\bar{s})(s\bar{d}) = (c\bar{d})(s\bar{s})$  tetraquark state could exist and should be observed as narrow peak in the  $D^+ \pi^0$  mass distribution. Its decay would be OZI rule violating. Fig. 117 would suggest it to have a mass  $\sim 50 \text{ MeV}/c^2$  below the  $D_s^*(2317)K^0$  threshold, i.e. about  $2750 \text{ MeV}/c^2$ . It should show up as peak in Fig. 49b. Clearly, considerably more statistics is needed to exclude its existence. We predict that it will not be found.

It should be noted that the existence or not of flavour-exotic tetraquark states is of considerable importance. If tetraquark states not allowed to mix with  $q\bar{q}$  states are unstable – as we claim – then any resonance with exotic quantum numbers must be of hybrid nature. In the light-quark sector, all non-exotic tetraquark states in Jaffe configuration can mix with  $q\bar{q}$  and arguments in

favour of tetraquark states have to rely on their abundance. In the charm sector, flavour-exotic tetraquark states might still exist; their discovery or quantitative upper limits are urgently needed. Even if they should not exist, QCD may support tetraquark bound states in very heavy plus light quark systems, like  $b\bar{c}\bar{u}\bar{d}$  (Richard, private communication).

### 11.6.3 Scalar states from the $\sigma$ to $\chi_{b0}(1P)$

In this last section we summarise our view of the mass spectrum of scalar ground states and of their first radial excitation. In Fig. 117a we display our view.

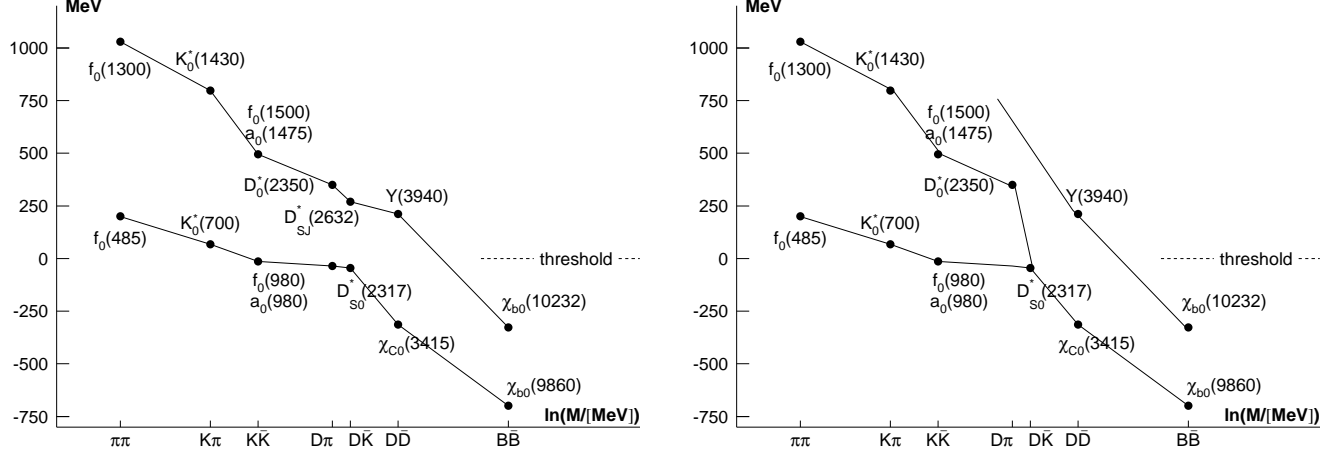


Fig. 117. Excitation energy of scalar mesons above their respective thresholds for OZI allowed decays. The diagram suggests that the  $\chi_{b0}(1P)$  would change its mass continuously down to the  $\sigma(485)$  mass, and the  $\chi_{b0}(2P)$  to the  $f_0(1300)$  mass, when the quark masses are reduced continuously from  $b\bar{b}$  to  $n\bar{n}$ . The horizontal scale is given by the logarithmic threshold masses.

The nine mesons  $\{a_0(980), K_0^*(700), f_0(465), f_0(980)\}$  form a low-mass scalar nonet. Their Fock space expansion contains  $q\bar{q}$ ,  $qq\bar{q}\bar{q}$ , and meson-meson components. In this sense we interpret  $\{a_0(980), K_0^*(700), f_0(465), f_0(980)\}$  as nonet of  $q\bar{q}$  mesons, with diquark (and antidiquark) having colour wave functions in  $\{\bar{\mathbf{3}}\}$  (and  $\mathbf{3}$ ) representation and spins in  ${}^1S_0$ , and with the two  $q\bar{q}$  subsystems spending most of the time as  $K$  or  $\bar{K}$ . So far, we have presented an accepted (even though not undisputed) view. However, we interpret  $f_0(980)$  as flavour octet and  $f_0(465)$  as flavour singlet state even though flavour SU(3) is broken at such a low mass, and  $f_0(465)$  is expected to have a small  $\bar{s}s$  component only. With  $K_0^*(700)$  as lowest scalar state carrying strangeness, there is consensus that  $K_0^*(1430)$  is the first excitation above it. Controversies will arise from our assignment of  $f_0(1500)$  and  $a_0(1475)$  as octet states and  $K_0^*(1430)$  partners. We omit the disputed narrow  $f_0(1370)$  and interpret the broad scalar isoscalar background  $f_0(1300)$  – the old  $\epsilon(1300)$  – as  $f_0(465)$  excitation. The puzzling mass pattern of  $D_0^*(2350)$  and  $D_{s0}^*(2317)$  – with the  $c\bar{n}$  state heavier than its  $c\bar{s}$  companion – is resolved by interpreting the former state as excited, the latter one as ground state. A  $D_0^*$  ground state is then expected at about  $1980 \text{ MeV}/c^2$ , below the  $D\pi$  threshold. In the limit of chiral symmetry, the  $D\pi$  interaction vanishes when pion momenta approach zero. This may shift the mass of the hypothesised  $D_0^*$  state to higher masses. Beveren, Costa, Kleefeld and Rupp [822] propose it to have  $2114 \text{ MeV}$ . The  $D_{s0}^*(2317)$  radial excitation is expected at about  $2650 \text{ MeV}/c^2$ . The Selex state  $D_{sJ}^*(2632)$  has the right mass to fill this slot; however there is no obvious reason why it is so narrow. Alternatively, the  $D_{sJ}(2860)$  might play this rôle [837]. The  $Y(3940)$  fits well as radial  $\chi_{c0}$  excitation.

Bugg (private communication) pointed out that an inclusion of the rapidly growing phase space

might shift the  $D_0^*(1980)$  pole position up to 2350 MeV; if this is true, an additional  $D_0^*(1980)$  would, of course, not be needed. The Selex state  $D_{sJ}^*(2632)$  could be fake. Hanhart (private communication) insisted that  $f_0(980)$  is of molecular character and has no relation to  $q\bar{q}$  or  $qq\bar{q}\bar{q}$ , in the same way as the deuteron is a proton-neutron bound state and no six-quark state. If these two views are correct, the low-mass scalar meson nonet decouples from  $q\bar{q}$  physics becoming an independent branch, and the ground state scalar mesons are all above  $1 \text{ GeV}/c^2$ . This more conventional scenario is shown in Fig. 117b.

Our preferred interpretation is contained in Fig. 117a. Its most striking aspect is the smooth change of the excitation energy with the mass of the two pseudoscalar mesons to which the scalar mesons couple strongly. The plot suggests that the  $\chi_{b0}(1P)$  state gradually changes into  $f_0(465)$  when the quark masses are lowered continuously. Of course, this does not imply that  $f_0(465)$  and  $\chi_{b0}(1P)$  have the same structure. The  $\chi_{b0}(1P)$  is well understood as  $q\bar{q}$  state; when the quark masses get smaller, the mass approaches the threshold for OZI allowed decays and tetraquark and molecular components become important. But still,  $f_0(465)$  occupies the slot of the quark model ground state, and no light  $q\bar{q}$  scalar isoscalar meson which resembles the  $\chi_{b0}(1P)$ . Quantum chromodynamics forms states of  $q\bar{q}$  structure when both quark masses exceed one GeV; for light quarks, QCD forms bound states of a more complicated dynamical structure.

## 12 Outlook ... and a look back

We recall some novel features which we developed while writing this review. A summary of facts and ideas was already presented at the beginning of this review.

The most fascinating aspect is the new view of scalar mesons, from the  $\chi_{b0}(9860)$  to the  $\sigma$ . The scalar mesons have brought with them many puzzles: from the long-debated  $\sigma(465)$  and the twin brothers  $f_0(980)/a_0(980)$  to the hotly disputed  $f_0(1370)/f_0(1500)/f_0(1760)$  complex and its strange production and decay pattern in  $J/\psi$ ,  $B$  and  $D$  decays. It may look surprising that a view can be developed with embraces all these different observations with a minimum set of assumptions. In this view, the  $\chi_{b0}(9860)$  is, as expected, a  $b\bar{b}$  bound state and  $\chi_{c0}(3415)$  a  $c\bar{c}$  state: the  $h_{1c}(3542)$  mass coincides with the centre of gravity of the spin-triplet states. The summation includes  $\chi_{c0}(3415)$ . If  $\chi_{c0}(3415)$  would have non- $c\bar{c}$  components, the coincidence would be extremely fortuitous. With decreasing quark masses, the scalar states approach their respective thresholds for OZI allowed decays and become strongly coupled to the meson-meson continuum. The  $q\bar{q}$  seed develops a tetraquark component and, for very low mass, a molecular object is formed. The tetraquark and molecular components govern the meson masses and their decay properties. While  $\chi_{b0}(9860)$  and  $\sigma(465)$  are of very different nature, their roots are the same. But when when a light quark-antiquark pair with scalar quantum numbers is created out of the vacuum, QCD transforms the initial  $q\bar{q}$  seed into a complex object which is efficiently interpreted using methods of chiral perturbation theory instead of the conventional quark model. The light-quark isoscalar mesons seem to organise themselves into comparatively narrow octet states and into broad flavour singlet states. The latter states have the quantum numbers of the QCD vacuum and couple strongly to pions, to the lightest Goldstone bosons. The isoscalar scalar mesons are so broad that they do not show up as individual resonances, they merge into a wide background. The scalar glueball may be part of this general background. The strange production and decay patterns observed for scalar mesons can be understood by interference between the wide SU(3) singlet states and the narrow octet states and their expansion from primarily formed  $q\bar{q}$  seeds into tetraquark clusters.

Many new questions have emerged. Even though our belief in glueballs is shaken, there will be undoubtedly new experimental searches for glueballs and new attempts to interpret the scalar mesons as  $q\bar{q}$  mesons mixing with a scalar glueball. Also the search for spin-parity exotics will go on; arguments have been put forward that charmonium hybrids could be narrower and easier to detect. And optimists hope for narrow high-mass glueballs. The new excitingly narrow charmonium states lead to the expectation of flavour-exotic states, of tetraquark states which cannot be reduced to  $c\bar{c}$ . So far there is no experimental evidence for such states but it is important to clarify these conjectures.

We expect that the ‘boring’ spectrum of high-mass  $q\bar{q}$  mesons will be completed in future experiments and that some important questions will find answers. We still do not know the basic mechanisms responsible for high orbital and radial excitations. Are the agents in a  $a_6^+(2450)$  meson still a constituent  $u$  and a  $\bar{d}$  quark? Do the masses of the constituent quarks change when mesons are excited? What connects the quark and the antiquark? A gluonic string? What kind of nonperturbative fluctuations are important for small and for large separations? Do condensates play a rôle in the ‘empty’ space between quark and antiquark? Is there really something like an effective one-gluon exchange? Are there instanton-induced interactions? We believe, these are fundamental questions which need to be solved before we can claim to have understood QCD.

It appears from this review that answers often come from unexpected directions. The best evidence

for the octet character of  $f_0(1500)$  comes from  $B$  decays. The tetraquark nature of the low-mass scalar mesons was suggested 30 year ago. We believe this to be a much broader concept and found support for this view from  $J/\psi$  decays and from  $B^+ \rightarrow \omega J/\psi K^+$  decays. The new narrow charmonium and open-charm states have emphasized the rôle of the opening of new thresholds. The systematic of the mesons with open charm taught us that scalar mesons are likely not be just tetraquark states; a  $q\bar{q}$  component may be needed to bind the system. One major conclusion of the review can be drawn: hadron spectroscopy is still full of surprises, a fact which teaches us modesty. And we have learned that hadron spectroscopy does not advance by performing one experiment only. Different approaches stimulate each other and shed light from different directions on a subject which continues to be fascinating and intellectually demanding.

Physics does not deal only with objects. Physics cannot be done without the enthusiasm of colleagues and collaborators. Here we would like to render our deepest thanks to all with whom we had the privilege to cooperate in one of the experiments. Our views developed in a multitude of discussions; here we mention a few but in the conviction to have forgotten enlightening discussions with people not listed below. Nevertheless we mention here N. Achasov, R. Alkofer, C. Amsler, A.V. Anisovich\*, V.V. Anisovich\*, R. Armenteros, D. Aston, T. Barnes, Chr. Batty, K. Beck, E. van Beveren, F. Bradamante, S.J. Brodsky, D. Bugg, S. Capstick, S.U. Chung\*, F.E. Close, G.F. De Teramond, D. Diakonov, A. Donnachie, W. Dunwoodie, W. Dünnweber, St. Dytman, A. Dzierba, W. Dünnweber, P. Eugenio, A. Fässler, M. Fässler, H. Fritzsch, U. Gastaldi, K. Göke, C. Guaraldo, H. Hammer\*, C. Hanhart\*, D. von Harrach, D. Herzog, N. Isgur, S. Ishida, B. Jaffe\*, A. Kirk, K. Königsmann, F. Klein, K. Kleinknecht\*, H. Koch, K. Königsmann, S. Krewald\*, B. Kubis\*, G.D. Lafferty, R. Landua, L.G. Landsberg, S. Lange, Weiguo Li, D.B. Lichtenberg, M. Locher, R.S. Longacre, V.E. Markushin, A. Masoni, A. Martin, B. Meadows\*, U.-G. Meißner\*, V. Metag, B. Metsch\*, C.A. Meyer, P. Minkowski, L. Montanet, S. Narison, V.A. Nikonov, W. Ochs\*, L.B. Okun, S.L. Olsen, E. Oset, M. Ostrick, Ph. Page, A. Palano, E. Paul, J.R. Pelaez, M. Pennington\*, K. Peters, H. Petry, M.V. Polyakov, J. Pretz\*, Yu.D. Prokoshkin, J.M. Richard\*, A. Sarantsev\*, A. Schäfer, F. Scheck, H. Schmieden, B. Schoch, K. Seth, Jin Shan\*, Xiaoyan Shen, E.S. Swanson, W. Schwille, A.P. Szczepaniak, J. Speth, K. Takamatsu, L. Tiator, P. Truöl, U. Thoma\*, T. Tsuru, Th. Walcher, Chr. Weinheimer, W. Weise, N. Wermes, U. Wiedner\*, H. Wittig, H. Willutzki, B.S. Zou\*, and C. Zupancic. Those marked with a \* had read critically parts of the manuscript and made thoughtful suggestions. D. Bugg and B. Schoch read the full manuscript, to them our deepest thanks. Early contributions by Bernard Metsch and Mike Pennington in the initial phase of the project are kindly acknowledged. Of course, the responsibility for any remaining inaccuracies rests with the authors.

We as authors have collaborated closely with our direct colleagues. We both would like to thank them for the wonderful time we have spend with them. A.Z. would like to appreciate the collaboration with D.V. Amelin, E.B. Berdnikov, S.I. Bityukov, G.V. Borisov, V.A. Dorofeev, R.I. Dzhelyadin, Yu.P. Gouz, Yu.M. Ivanyushenkov, A.V. Ivashin, V.V. Kabachenko, I.A. Kachaev, A.N. Karyukhin, Yu.A. Khokhlov, G.A. Klyuchnikov, V.F. Konstantinov, S.V. Kopikov, V.V. Kostyukhin, A.A. Kriushin, M.A. Kulagin, S.A. Likhoded, V.D. Matveev, A.P. Ostankov, D.I. Ryabchikov, A.A. Solodkov, A.V. Solodkov, O.V. Solovianov, E.A. Starchenko, N.K. Vishnevsky, and E.A. Vlasov in common experimental efforts.

E.K. has had the privilege to work in the course of time with a large number of PhD students. The results were certainly not achieved without their unflagging enthusiasm for physics. I would like to mention O. Bartholomy, J. Brose, V. Crede, K.D. Duch, A. Ehmanns, I. Fabry, M. Fuchs, G. Gärtner, J. Junkersfeld, J. Haas, R. Hackmann, M. Heel, Chr. Heimann, M. Herz, G. Hilkert, I. Horn, B. Kalteyer, F. Kayser, R. Landua, J. Link, J. Lotz, M. Matveev, K. Neubecker, H. v.Pee, K.

Peters, B. Pick, W. Povkov, J. Reifenröther, G. Reifenröther, J. Reinnarth, St. Resag, E. Schäfer, C. Schmidt, R. Schulze, R. Schneider, O. Schreiber, S. Spanier, Chr. Straßburger, J.S. Suh, T. Sczcepanek, U. Thoma, F. Walter, K. Wittmack, H. Wolf, R.W. Wodrich, M. Ziegler. Very special thanks go to my colleague Hartmut Kalinowsky with whom I have worked with jointly for more than 35 years. Anyone familiar with one of the experiments I was working on knows and admires his competence and endurance and his invaluable contributions to our common efforts. To him my very personal thanks.

This work (A.Z.) was supported in part by the Presidential Grant 5911.206.2.

Nathan Isgur and Lucien Montanet were exceptional personalities, as individuals and as physicists, and have made outstanding contributions in many areas of physics. We are grateful for their friendship and will have them in our memories, ever.

## References

- [1] W.-M. Yao, et al., Review of Particle Physics, *Journal of Physics G* 33 (2006) 1.
- [2] M. Gell-Mann, A. H. Rosenfeld, Hyperons and heavy mesons (systematics and decay), *Ann. Rev. Nucl. Part. Sci.* 7 (1957) 407–478.
- [3] International Seminar on Vector Mesons and Electromagnetic Interactions; Dubna, Joint Inst. for Nuclear Research, USSR, 1969, JINR-P2-4816, Dubna, USSR, 1969.
- [4] R. H. Dalitz, A. Zichichi (Eds.), International Conference on Meson Resonances and Related Electromagnetic Phenomena; Bologna, Italy, 1971, Editrice Compositori, 1972.
- [5] A. H. Rosenfeld, K.-W. Lai (Eds.), 3<sup>rd</sup> International Conference on Experimental Meson Spectroscopy; Philadelphia, Pennsylvania, 1972, AIP Conf. Proc., American Inst. Phys., 1972.
- [6] D. A. Garelick (Ed.), 4<sup>th</sup> International Conference on Experimental Meson Spectroscopy; Northeastern University, Boston, Mass. 02115, 1974, Vol. 21 of AIP Conf. Proc., 1974.
- [7] E. von Goeler, R. Weinstein (Eds.), 5<sup>th</sup> International Conference on Meson Spectroscopy; Northeastern University, Boston, Mass. 02115, 1977, Northeastern University Press, 1977.
- [8] S.-U. Chung, S. J. Lindenbaum (Eds.), Experimental Meson Spectroscopy; Brookhaven Natl. Lab., Upton, NY 11973, 1981, Vol. 67 of AIP Conf. Proc., 1981.
- [9] S. J. Lindenbaum (Ed.), 7<sup>th</sup> International Conference on Experimental Meson Spectroscopy; Brookhaven Natl. Lab., Upton, NY 11973, 1983, Vol. 113 of AIP Conf. Proc., American Inst. Phys., 1983.
- [10] S. Oneda (Ed.), International Conference on Hadron Spectroscopy; Univ. of Maryland, College Park, Maryland 20742, 1985, Vol. 132 of AIP Conf. Proc., 1985.
- [11] Y. Oyanagi, K. Takamatsu, T. Tsuru (Eds.), 2<sup>nd</sup> International Conference on Hadron Spectroscopy; Natl. Lab. on High-energy Physics Tsukuba, Japan, 1987, KEK-87-7, 1987.
- [12] F. Binon, J. M. Frère, J. P. Peigneux (Eds.), 3<sup>rd</sup> International Conference on Hadron Spectroscopy; Ajaccio, Corsica (France), 1989, Editions Frontieres, 1989.
- [13] S. Oneda, D. C. Peaslee (Eds.), International Conference on Hadron Spectroscopy; Univ. of Maryland, College Park, Maryland 20742, 1991, World Scientific, 1992.
- [14] A. Taroni (Ed.), The Biennial Conference on Hadron Spectroscopy; Como, Italy, 1993, Vol. 107A of *Nuovo Cim.*, 1994, p. 1797.
- [15] M. Birse, G. D. Lafferty, J. A. McGovern (Eds.), 6<sup>th</sup> International Conference on Hadron Spectroscopy; University of Manchester, Manchester M13 9PL, England, 1995, World Scientific, 1996.
- [16] S.-U. Chung, H. J. Willutzki (Eds.), 7<sup>th</sup> International Conference on Hadron Spectroscopy; Brookhaven National Lab., Upton, NY 11973-5000, 1997, Vol. 432 of AIP Conf. Proc., 1998.
- [17] W. G. Li, Y. Z. Huang, B. S. Zou (Eds.), 8<sup>th</sup> International Conference on Hadron Spectroscopy; Beijing, China, 1999, Vol. A675 of Nuclear Physics, 2000.
- [18] D. Amelin, A. M. Zaitsev (Eds.), 9<sup>th</sup> International Conference on Hadron Spectroscopy; Protvino, Russia, 2001, Vol. 619 of AIP Conf. Proc., 2002.
- [19] E. Klemp, H. Koch, H. Orth (Eds.), 10<sup>th</sup> International Conference on Hadron Spectroscopy; Aschaffenburg, Germany, 2003, Vol. 717 of AIP Conf. Proc., 2004.
- [20] A. C. dos Reis (Ed.), 11<sup>th</sup> International Conference on Hadron Spectroscopy; Rio de Janeiro, Brazil, 2005, 2006.
- [21] D. Frekers, D. R. Gill, J. Speth (Eds.), International Meeting on Physics at KAON: Hadron Spectroscopy, Strangeness, Rare Decays; Bad Honnef, Germany, 1989, *Zeitschrift fur Physik C*, Suppl. to Vol. 46, 1990.

- [22] E. Klempt, K. Peters (Eds.), Rheinfels Workshop on Hadron Mass Spectrum; St. Goar, Germany, 1990, Nucl. Phys. B (Proc. Suppl.) 21, 1991.
- [23] K. Takamatsu, T. Tsuru (Eds.), Light Quark Meson Spectroscopy Workshop; Natl. Lab. for High Energy Physics, Tsukuba, Japan, 1992, KEK-Proceedings-92-8, 1992.
- [24] T. Bressani, A. Feliciello, A. Filippi (Eds.), Workshop on Hadron Spectroscopy (WHS 99); Rome, Frascati, Italy, 1999, Istituto Naz. Fis. Nucl., 1999, Frascati Physics Series 15, 1999.
- [25] K. Takamatsu, T. Tsuru, K. Ukai, Z. Zheng (Eds.), KEK Workshop on Hadron Spectroscopy and Chiral Particle Search in  $J/\psi$  Decay Data at BES; Tsukuba, Japan, 2003, KEK proceedings 2003-10. Home URL: <http://aries.phys.cst.nihon-u.ac.jp/symp03/>, 2003.
- [26] S. Ishida, K. Takamatsu, T. Tsuru, S. Tsai, M. Ishida, T. Komada (Eds.), International Symposium on Hadron Spectroscopy, Chiral Symmetry and Relativistic Description of Bound Systems; Tokyo, Japan, 2003, KEK proceedings 2003-7; NUP-B-2003-1, 2003.
- [27] N. Brambilla, G. M. Prosperi (Eds.), International Conference on Quark Confinement and the Hadron Spectrum; Como, Italy, 1994, World Scientific, 1995.
- [28] N. Brambilla, G. M. Prosperi (Eds.), 2<sup>nd</sup> International Conference on Quark Confinement and the Hadron Spectrum; Como, Italy, 1996, World Scientific, 1997.
- [29] N. Isgur (Ed.), 3<sup>rd</sup> International Conference on Quark Confinement and the Hadron Spectrum; Newport News, Virginia, 1998, World Scientific, 2000.
- [30] W. Lucha, K. M. Maung (Eds.), 4<sup>th</sup> International Conference on Quark Confinement and the Hadron Spectrum; Austrian Acad. of Science, Vienna, Austria, 2000, World Scientific, 2002.
- [31] N. Brambilla, G. M. Prosperi (Eds.), 5<sup>th</sup> International Conference on Quark Confinement and the Hadron Spectrum; Gargnano, Brescia, Italy, 2002, World Scientific, 2004.
- [32] N. Brambilla, U. D'Alesio, A. Devoto, K. Muang, G. M. Prosperi, S. Serci (Eds.), 6<sup>th</sup> International Conference on Quark Confinement and the Hadron Spectrum; Villasimius, Sardinia, Italy, 2004, AIP Conf. Proc. 756, 2005.
- [33] N. Brambilla, A. V. (Milano), K. M. M. (Hattiesburg), J. E. R. (Lisboa) (Eds.), 7<sup>th</sup> International Conference on Quark Confinement and the Hadron Spectrum; Ponta Delgada, Azores, Portugal 2006, AIP Conf. Proc., 2007.
- [34] H. R. Quinn, Heavy flavor physics, <http://doc.cern.ch/yellowrep/2004/2004-001/p35.pdf>, lectures given at European School of High-Energy Physics (ESHEP 2002), Pylos, Greece (2002).
- [35] E. Klempt, Meson spectroscopy: glueballs, hybrids and  $q\bar{q}$  mesons, in: D. Graudenz, V. Markushin (Eds.), Proceedings of the PSI Zuoz Summer School ‘Phenomenology of Gauge Interactions’, hep-ex/0101031, 2000, pp. 61–126.
- [36] P. R. Page, Hadron structure and modern spectroscopy, hep-ph/0009135, lectures given at the Advanced School on Quantum Chromodynamics (QCD 2000), Benasque, Huesca, Spain (2000).
- [37] K. K. Seth, Quarkonium, Prog. Part. Nucl. Phys. 50 (2003) 341–352.
- [38] B. L. Ioffe, Chiral phase transition in hadronic matter: The influence of baryon density, invited talk presented at the 58th Scottish University Summer School in Physics, St. Andrews, Scotland, hep-ph/0408238 (2004).
- [39] E. Klempt, Glueballs, hybrids, pentaquarks: Introduction to hadron spectroscopy and review of selected topics, lectures given at the 18th Annual Hampton University Graduate Studies (HUGS at JLab 2003), Newport News, Virginia, hep-ph/040427 (2003).
- [40] R. L. Jaffe, Exotica, Phys. Rept. 409 (2005) 1–45.
- [41] U. G. Meißner, H.-W. Hammer, A. Wirzba (Eds.), 4<sup>th</sup> International Workshop on Chiral Dynamics 2003: Theory and Experiment, 2003, Bonn, Germany, 2003, 8–13 Sep 2003.

- [42] A. Irving, C. McNeile, C. Michael (Eds.), 23<sup>rd</sup> International Symposium on Lattice Field Lattice 2005; Trinity College, Dublin, Ireland, 2005, Proceedings of Science, 2005.
- [43] Workshop on Hadron Structure and QCD: From Low to High Energies (HSQCD 2005); St. Petersburg, Russia, 2005, see: [hepd.pnpi.spb.ru/hsqcd/proceed.html](http://hepd.pnpi.spb.ru/hsqcd/proceed.html), 2006.
- [44] H.-C. C. Hackensack (Ed.), 10<sup>th</sup> International Symposium on Meson-Nucleon Physics and the Structure of the Nucleon (MENU 2004); Beijing, China, 2004, World Scientific, 2005. (*Int. J. Mod. Phys. A*20 (2005) 1531-2025), 2005.
- [45] S. Godfrey, J. Napolitano, Light meson spectroscopy, *Rev. Mod. Phys.* 71 (1999) 1411–1462.
- [46] C. Amsler, “Proton–antiproton annihilation and meson spectroscopy with the Crystal Barrel,” *Rev. Mod. Phys.* 70 (1998) 1293.
- [47] D.-M. Li, B. Ma, H. Yu, Quarkonia glueball structure of the ground pseudoscalar mesons, *Int. J. Mod. Phys. A*18 (2003) 3335–3346.
- [48] C. Amsler, N. A. Tornqvist, Mesons beyond the naive quark model, *Phys. Rept.* 389 (2004) 61–117.
- [49] D. V. Bugg, Four sorts of mesons, *Phys. Rept.* 397 (2004) 257–358.
- [50] S.-L. Zhu, New hadron states.
- [51] J. Gasser, H. Leutwyler, Chiral perturbation theory to one loop, *Ann. Phys.* 158 (1984) 142.
- [52] J. Gasser, H. Leutwyler, Low-energy expansion of meson form-factors, *Nucl. Phys.* B250 (1985) 517–538.
- [53] U. G. Meißner, Recent developments in chiral perturbation theory, *Rept. Prog. Phys.* 56 (1993) 903–996.
- [54] S. Weinberg, The quantum theory of fields. Vol. 2: Modern applications, Cambridge, UK: University Press (1996) 489 p.
- [55] V. Bernard, U.-G. Meißner, Chiral perturbation theory, *Ann. Rev. Nucl. Part. Sci.*, hep-ph/0611231.
- [56] J. G. Körner, G. Thompson, The heavy mass limit in field theory and the heavy quark effective theory, *Phys. Lett.* B264 (1991) 185–192.
- [57] M. Neubert, Heavy quark symmetry, *Phys. Rept.* 245 (1994) 259–396.
- [58] T. Barnes, F. E. Close, P. R. Page, E. S. Swanson, Higher quarkonia, *Phys. Rev. D*55 (1997) 4157–4188.
- [59] T. Barnes, N. Black, P. R. Page, Strong decays of strange quarkonia, *Phys. Rev. D*68 (2003) 054014.
- [60] T. Barnes, S. Godfrey, E. S. Swanson, Higher charmonia, *Phys. Rev. D*72 (2005) 054026.
- [61] C. McNeile, Meson and baryon spectroscopy on a lattice, 2003, in: *Int. Rev. Nucl. Phys.*, Vol.9, Hadronic Physics from Lattice QCD, ed. by A.M. Green, World Scientific Publishing Company (2003), hep-lat/0307027.
- [62] A. Ali Khan, Effective field theories and quantum chromodynamics on the lattice, 2004, Habilitationsschrift, Humboldt-Universität Berlin, hep-lat/0403006.
- [63] N. Brambilla, et al., Heavy quarkonium physics, CERN Yellow Report, CERN-2005-005, hep-ph/0412158 (2004).
- [64] C. M. G. Lattes, H. Muirhead, G. P. S. Occhialini, C. F. Powell, Processes involving charged mesons, *Nature* 159 (1947) 694–697.
- [65] A. Pevsner, et al., Evidence for a three-pion resonance near 550 MeV, *Phys. Rev. Lett.* 7 (1961) 421423.
- [66] B. C. Maglic, L. W. Alvarez, A. H. Rosenfeld, M. L. Stevenson, Evidence for a  $T = 0$  three pion resonance, *Phys. Rev. Lett.* 7 (1961) 178–182.
- [67] P. L. Connolly, et al., Existence and properties of the  $\phi$  meson, *Phys. Rev. Lett.* 10 (1963) 371.

- [68] G. Goldhaber, et al., Evidence for a  $\rho\pi$  interaction produced in the  $\pi^+p$  reaction at 3.65 BeV/c, Phys. Rev. Lett. 12 (1964) 336–340.
- [69] L. Bondar, et al., Experimental results on the cross section for  $\pi^-\pi^0 \rightarrow \pi^-\omega$ , Phys. Lett. 5 (1963) 209.
- [70] A. Astier, et al., Existence and properties of the C-meson as observed in  $p\bar{p}$  annihilations at rest, Nuclear Physics B10 (1969) 65–88.
- [71] D. H. Miller, et al.,  $K\bar{K}\pi$  resonance at 1280 MeV, Phys. Rev. Lett. 14 (1965) 1074–1077.
- [72] C. D'Andlau, et al., Evidence for a non-strange meson of mass 1290 MeV, Phys. Lett. 17 (1965) 347–352.
- [73] P. Baillon, et al., Further study of the E meson in antiproton proton annihilations at rest, Nuovo Cimento 50 (1967) 393.
- [74] P. Baillon, Clarifications about the E(1425) meson quantum numbers, 21<sup>st</sup> Int. Conf. on High Energy Physics, Paris, France, Jul 26–31, 1982.
- [75] D. L. Scharre, et al., Observation of the radiative transition  $\psi \rightarrow \gamma E(1420)$ , Phys. Lett. B97 (1980) 329.
- [76] M. S. Chanowitz, Have we seen our first glueball?, Phys. Rev. Lett. 46 (1981) 981.
- [77] C. Edwards, et al., Observation of a pseudoscalar state at 1440 MeV in  $J/\psi$  radiative decays, Phys. Rev. Lett. 49 (1982) 259.
- [78] W. Selove, V. Hagopian, H. Brody, A. Baker, E. Leboy, Evidence for a T=0  $\pi^+\pi^-$  resonance at 1250 MeV, Phys. Rev. Lett. 9 (1962) 272–275.
- [79] L. Goldberg, et al., Evidence for a new  $\pi^+\pi^-$  resonance at 1.67 GeV, Phys. Lett. 17 (1965) 354.
- [80] J. Bartsch, et al., Evidence for an isoscalar  $\rho\pi$  resonance at 975 MeV, Phys. Lett. 11 (1966) 167.
- [81] A. Etkin, et al., Evidence for two new  $0^{++}$  mesons and a possible scalar decuplet, Phys. Rev. D25 (1982) 2446.
- [82] F. Binon, et al., G(1590): a scalar meson decaying into two  $\eta$  mesons, Nuovo Cim. A78 (1983) 313.
- [83] A. Etkin, et al., Increased statistics and observation of the  $g_t$ ,  $g'_t$ , and  $g''_t$   $2^{++}$  resonances in the glueball enhanced channel  $\pi^-p \rightarrow \phi\phi n$ , Phys. Lett. B201 (1988) 568–572.
- [84] J. J. Aubert, et al., Experimental observation of a heavy particle J, Phys. Rev. Lett. 33 (1974) 1404–1406.
- [85] J. E. Augustin, et al., Discovery of a narrow resonance in  $e^+e^-$  annihilation, Phys. Rev. Lett. 33 (1974) 1406–1408.
- [86] J. Bartsch, et al., Observation of a ( $K\pi\pi$ ) resonance near 1800 MeV, Phys. Lett. 22 (1966) 357–360.
- [87] D. Alde, et al., Evidence for a  $1^{-+}$  exotic meson, Phys. Lett. B205 (1988) 397.
- [88] M. N. Focacci, et al., Mass spectrum of bosons from 500 to 2500 MeV in the reaction  $\pi^-p \rightarrow pX^-$  observed by a missing-mass spectrometer, Phys. Rev. Lett. 17 (1966) 890–893.
- [89] M. Gell-Mann, Symmetries of baryons and mesons, Phys. Rev. 125 (1962) 1067–1084.
- [90] T. Feldmann, P. Kroll, B. Stech, Mixing and decay constants of pseudoscalar mesons, Phys. Rev. D58 (1998) 114006.
- [91] J. L. Rosner, Quark content of neutral mesons, Phys. Rev. D27 (1983) 1101.
- [92] R. Escribano, J. Nadal, On the gluon content of the  $\eta$  and  $\eta'$  mesons, hep-ph/0703187.
- [93] T. Huang, X.-G. Wu, Determination of the  $\eta$  and  $\eta'$  mixing angle from the pseudoscalar transition form factors, Eur. Phys. J. C50 (2007) 771.
- [94] S. Okubo, Phi meson and unitary symmetry model, Phys. Lett. 5 (1963) 165–168.

- [95] G. Zweig, An SU(3) model for strong interaction symmetry and its breaking. CERN-TH-412, Feb 1964, Published in 'Developments in the Quark Theory of Hadrons'. Volume 1. Edited by D. Lichtenberg and S. Rosen. Nonantum, Mass., Hadronic Press, 1980. pp. 22-101.
- [96] J. Iizuka, Systematics and phenomenology of meson family, *Prog. Theor. Phys. Suppl.* 37 (1966) 21–34.
- [97] P. Gauron, B. Nicolescu, A possible two-component structure of the non-perturbative pomeron, *Phys. Lett.* B486 (2000) 71–76.
- [98] R. Muradian, Regge in the sky: Origin of the cosmic rotation, IC-94-143, Internal Report, Trieste, 1994.
- [99] R. M. Muradian, The Regge law for heavenly bodies, *Phys. Part. Nucl.* 28 (1997) 471–482.
- [100] M. M. Brisudova, L. Burakovsky, T. Goldman, A. Szczepaniak, Nonlinear Regge trajectories and glueballs, *Phys. Rev.* D67 (2003) 094016.
- [101] G. F. de Teramond, S. J. Brodsky, The hadronic spectrum of a holographic dual of QCD, *Phys. Rev. Lett.* 94 (2005) 201601.
- [102] F. Bigazzi, A. L. Cotrone, L. Martucci, L. A. Pando Zayas, Wilson loop, Regge trajectory and hadron masses in a Yang-Mills theory from semiclassical strings, *Phys. Rev.* D71 (2005) 066002.
- [103] Y. Nambu, QCD and the string model, *Phys. Lett.* B80 (1979) 372.
- [104] M. Baker, R. Steinke, Semiclassical quantization of effective string theory and Regge trajectories, *Phys. Rev.* D65 (2002) 094042.
- [105] M. Baker, From QCD to dual superconductivity to effective string theory, 2003, 5th International Conference on Quark Confinement and the Hadron Spectrum, Gargnano, Brescia, Italy, 10-14 Sep 2002. Published in Gargnano 2002, Quark confinement and the hadron spectrum, pp 204-210.
- [106] A. Karch, E. Katz, D. T. Son, M. A. Stephanov, Linear confinement and AdS/QCD, *Phys. Rev.* D74 (2006) 015005.
- [107] J. Polchinski, M. J. Strassler, Hard scattering and gauge/string duality, *Phys. Rev. Lett.* 88 (2002) 031601.
- [108] S. J. Brodsky, Hadron spectroscopy and structure from AdS/CFT, *Eur. Phys. J.* A31 (2007) 638–644.
- [109] A. H. Mahmood, et al., Search for  $\eta_b(1s)$  in inclusive radiative decays of the  $\Upsilon(3S)$ , 2002, 31<sup>st</sup> International Conference on High Energy Physics (ICHEP 2002), Amsterdam, The Netherlands, 24-31 Jul 2002, hep-ex/0207057.
- [110] S. Godfrey, J. L. Rosner, Production of the  $\eta_b(ns)$  states, *Phys. Rev.* D64 (2001) 074011.
- [111] A. Heister, et al., Search for  $\gamma\gamma \rightarrow \eta_b$  in  $e^+e^-$  collisions at LEP2, *Phys. Lett.* B530 (2002) 56–66.
- [112] E. Klempt, A mass formula for baryon resonances, *Phys. Rev.* C66 (2002) 058201.
- [113] N. Isgur, Comment on 'Valence QCD: Connecting QCD to the quark model', *Phys. Rev.* D61 (2000) 118501.
- [114] M. Gell-Mann, A schematic model of baryons and mesons, *Phys. Lett.* 8 (1964) 214–215.
- [115] H. Fritzsch, M. Gell-Mann, Current algebra: Quarks and what else?, 16<sup>th</sup> International Conference on High-Energy Physics, Batavia, Illinois, 6-13 Sep 1972, hep-ph/0208010.
- [116] H. D. Politzer, Reliable perturbative results for strong interactions?, *Phys. Rev. Lett.* 30 (1973) 1346–1349.
- [117] D. J. Gross, F. Wilczek, Ultraviolet behavior of non-abelian gauge theories, *Phys. Rev. Lett.* 30 (1973) 1343–1346.
- [118] G. 't Hooft, Renormalization of massless Yang-Mills fields, *Nucl. Phys.* B33 (1971) 173–199.
- [119] M. Gell-Mann, R. J. Oakes, B. Renner, Behavior of current divergences under  $SU(3) \times SU(3)$ , *Phys. Rev.* 175 (1968) 2195–2199.

- [120] P. Colangelo, A. Khodjamirian, QCD sum rules: A modern perspective, in: M. Shifman (Ed.), Boris Ioffe Festschrift 'At the Frontier of Particle Physics / Handbook of QCD', vol. 3\*, World Scientific, Singapore, 2001, pp. 1495–1576, hep-ph/0010175.
- [121] A. M. Polyakov, Compact gauge fields and the infrared catastrophe, *Phys. Lett.* **B59** (1975) 82–84.
- [122] A. A. Belavin, A. M. Polyakov, A. S. Shvarts, Y. S. Tyupkin, Pseudoparticle solutions of the Yang-Mills equations, *Phys. Lett.* **B59** (1975) 85–87.
- [123] G. 't Hooft, Computation of the quantum effects due to a four-dimensional pseudoparticle, *Phys. Rev.* **D14** (1976) 3432–3450.
- [124] T. Schäfer, E. V. Shuryak, Instantons in QCD, *Rev. Mod. Phys.* **70** (1998) 323–426.
- [125] H. Forkel, A primer on instantons in QCD, Heidelberg (unpublished), hep-ph/0009136.
- [126] D. Diakonov, Instantons at work, *Prog. Part. Nucl. Phys.* **51** (2003) 173–222.
- [127] J. A. Oller, E. Oset, J. R. Pelaez, Non-perturbative approach to effective chiral Lagrangians and meson interactions, *Phys. Rev. Lett.* **80** (1998) 3452–3455.
- [128] J. A. Oller, E. Oset, J. R. Pelaez, Meson meson and meson baryon interactions in a chiral non-perturbative approach, *Phys. Rev.* **D59** (1999) 074001.
- [129] A. Gomez Nicola, J. R. Pelaez, Meson meson scattering within one loop chiral perturbation theory and its unitarization, *Phys. Rev.* **D65** (2002) 054009.
- [130] T. N. Truong, Remarks on the unitarization methods, *Phys. Rev. Lett.* **67** (1991) 2260–2263.
- [131] S. Weinberg, The problem of mass, *Trans. New York Acad. Sci.* **38** (1977) 185–201.
- [132] S. Narison, QCD tests of the puzzling scalar mesons, *Phys. Rev.* **D73** (2006) 114024.
- [133] K. G. Wilson, Confinement of quarks, *Phys. Rev.* **D10** (1974) 2445–2459.
- [134] Y. A. Simonov, Vacuum background fields in QCD as a source of confinement, *Nucl. Phys.* **B307** (1988) 512.
- [135] A. S. Kronfeld, G. Schierholz, U. J. Wiese, Topology and dynamics of the confinement mechanism, *Nucl. Phys.* **B293** (1987) 461.
- [136] R. Alkofer, L. von Smekal, The infrared behavior of QCD Green's functions: Confinement, dynamical symmetry breaking, and hadrons as relativistic bound states, *Phys. Rept.* **353** (2001) 281.
- [137] J. Greensite, The confinement problem in lattice gauge theory, *Prog. Part. Nucl. Phys.* **51** (2003) 1.
- [138] G. S. Bali, QCD forces and heavy quark bound states, *Phys. Rept.* **343** (2001) 1–136.
- [139] P. Pennanen, C. Michael, String breaking in zero-temperature lattice QCD (unpublished), hep-lat/0001015.
- [140] C. W. Bernard, et al., Zero temperature string breaking in lattice quantum chromodynamics, *Phys. Rev.* **D64** (2001) 074509.
- [141] C. Michael, Hadronic decays, PoS LAT2005 (2006) 008.
- [142] C. Michael, Hadronic decays from the lattice, *Eur. Phys. J.* **A31** (2007) 793–798.
- [143] C. J. Morningstar, M. J. Peardon, The glueball spectrum from an anisotropic lattice study, *Phys. Rev.* **D60** (1999) 034509.
- [144] M. Loan, X.-Q. Luo, Z.-H. Luo, Monte Carlo study of glueball masses in the Hamiltonian limit of SU(3) lattice gauge theory, *Int. J. Mod. Phys.* **A21** (2006) 2905–2936.
- [145] E. B. Gregory, A. C. Irving, C. C. McNeile, S. Miller, Z. Sroczynski, Scalar glueball and meson spectroscopy in unquenched lattice QCD with improved staggered quarks, PoS LAT2005 (2006) 027.
- [146] M. Loan, Y. Ying, Sizes of lightest glueballs in SU(3) lattice gauge theory, *Prog. Theor. Phys.* **116** (2006) 169.

- [147] S. Aoki, et al., Quenched light hadron spectrum, Phys. Rev. Lett. 84 (2000) 238–241.
- [148] K. Schilling, H. Neff, T. Lippert, Computing the  $\eta$  and  $\eta'$  mesons in lattice QCD, Lect. Notes Phys. 663 (2005) 147–176.
- [149] C. McNeile, C. Michael, Properties of light scalar mesons from lattice QCD, Phys. Rev. D74 (2006) 014508.
- [150] W. A. Bardeen, A. Duncan, E. Eichten, N. Isgur, H. Thacker, Chiral loops and ghost states in the quenched scalar propagator, Phys. Rev. D65 (2002) 014509.
- [151] A. Hart, C. McNeile, C. Michael, Masses of singlet and non-singlet  $0^{++}$  particles, Nucl. Phys. Proc. Suppl. 119 (2003) 266–268.
- [152] S. Prelovsek, C. Dawson, T. Izubuchi, K. Orginos, A. Soni, Scalar meson in dynamical and partially quenched two-flavor QCD: Lattice results and chiral loops, Phys. Rev. D70 (2004) 094503.
- [153] T. Burch, et al., Excited hadrons on the lattice: Mesons, Phys. Rev. D73 (2006) 094505.
- [154] A. Hart, C. McNeile, C. Michael, J. Pickavance, A lattice study of the masses of singlet  $0^{++}$  mesons, Phys. Rev. D74 (2006) 114504.
- [155] K. J. Juge, J. Kuti, C. J. Morningstar, Ab initio study of hybrid  $\bar{b}gb$  mesons, Phys. Rev. Lett. 82 (1999) 4400–4403.
- [156] T. Manke, et al., Hybrid quarkonia with dynamical sea quarks, Phys. Rev. D64 (2001) 097505.
- [157] C. Michael, Hybrid mesons from the lattice (unpublished), hep-ph/0308293.
- [158] C. W. Bernard, et al., Exotic mesons in quenched lattice QCD, Phys. Rev. D56 (1997) 7039–7051.
- [159] T. Manke, et al., Hybrid quarkonia on asymmetric lattices, Phys. Rev. Lett. 82 (1999) 4396–4399.
- [160] Z.-H. Mei, X.-Q. Luo, Exotic mesons from quantum chromodynamics with improved gluon and quark actions on the anisotropic lattice, Int. J. Mod. Phys. A18 (2003) 5713.
- [161] C. McNeile, C. Michael, P. Pennanen, Hybrid meson decay from the lattice, Phys. Rev. D65 (2002) 094505.
- [162] J. N. Hedditch, et al.,  $1^{-+}$  exotic meson at light quark masses, Phys. Rev. D72 (2005) 114507.
- [163] C. McNeile, C. Michael, Decay width of light quark hybrid meson from the lattice, Phys. Rev. D73 (2006) 074506.
- [164] M. S. Cook, H. R. Fiebig, Exotic meson decay widths using lattice QCD, Phys. Rev. D74 (2006) 034509.
- [165] M. A. Shifman, A. I. Vainshtein, V. I. Zakharov, QCD and resonance physics. Sum rules, Nucl. Phys. B147 (1979) 385–447.
- [166] S. Narison, Masses, decays and mixings of gluonia in QCD, Nucl. Phys. B509 (1998) 312–356.
- [167] N. Isgur, J. E. Paton, A flux tube model for hadrons in QCD, Phys. Rev. D31 (1985) 2910.
- [168] E. S. Swanson, The flux tube model: Applications, tests, and extensions, Workshop on Gluonic Excitations, Newport News, Virginia, 14–16 May 2003. hep-ph/0311328.
- [169] F. E. Close, P. R. Page, The photoproduction of hybrid mesons from CEBAF to HERA, Phys. Rev. D52 (1995) 1706–1709.
- [170] K. J. Juge, J. Kuti, C. J. Morningstar, Gluon excitations of the static quark potential and the hybrid quarkonium spectrum, Nucl. Phys. Proc. Suppl. 63 (1998) 326–331.
- [171] S. Godfrey, N. Isgur, Mesons in a relativized quark model with chromodynamics, Phys. Rev. D32 (1985) 189–231.
- [172] J. Vijande, F. Fernandez, A. Valcarce, Constituent quark model study of the meson spectra, J. Phys. G31 (2005) 481.

- [173] M. Koll, R. Ricken, D. Merten, B. C. Metsch, H. R. Petry, A relativistic quark model for mesons with an instanton induced interaction, *Eur. Phys. J. A*9 (2000) 73–94.
- [174] R. Ricken, M. Koll, D. Merten, B. C. Metsch, H. R. Petry, The meson spectrum in a covariant quark model, *Eur. Phys. J. A*9 (2000) 221–244.
- [175] E. Klempert, B. C. Metsch, C. R. Munz, H. R. Petry, Scalar mesons in a relativistic quark model with instanton induced forces, *Phys. Lett. B*361 (1995) 160–166.
- [176] G. 't Hooft, Symmetry breaking through Bell-Jackiw anomalies, *Phys. Rev. Lett.* 37 (1976) 8–11.
- [177] K. L. Au, D. Morgan, M. R. Pennington, Meson dynamics beyond the quark model: A study of final state interactions, *Phys. Rev. D*35 (1987) 1633.
- [178] P. Minkowski, W. Ochs, Identification of the glueballs and the scalar meson nonet of lowest mass, *Eur. Phys. J. C*9 (1999) 283–312.
- [179] N. Isgur, M. B. Wise, Weak transition form-factors between heavy mesons, *Phys. Lett. B*237 (1990) 527.
- [180] M. A. Shifman, M. B. Voloshin, On annihilation of mesons built from heavy and light quark and  $\bar{B}^0 \leftrightarrow B^0$  oscillations, *Sov. J. Nucl. Phys.* 45 (1987) 292.
- [181] W. E. Caswell, G. P. Lepage, Effective Lagrangians for bound state problems in QED, QCD, and other field theories, *Phys. Lett. B*167 (1986) 437.
- [182] M. Neubert, Heavy-quark effective theory, 20<sup>th</sup> Johns Hopkins Workshop on Current Problems in Particle Theory: Non-Perturbative Particle Theory and Experimental Tests, Heidelberg, Germany, 27-29 Jun 1996. hep-ph/9610385.
- [183] N. Isgur, M. B. Wise, Spectroscopy with heavy quark symmetry, *Phys. Rev. Lett.* 66 (1991) 1130–1133.
- [184] L. Micu, Decay rates of meson resonances in a quark model, *Nucl. Phys. B*10 (1969) 521–526.
- [185] A. Le Yaouanc, L. Oliver, O. Pene, J. C. Raynal, Naive quark pair creation model of strong interaction vertices, *Phys. Rev. D*8 (1973) 2223–2234.
- [186] A. Le Yaouanc, L. Oliver, O. Pene, J. C. Raynal, Naive quark pair creation model and baryon decays, *Phys. Rev. D*9 (1974) 1415–1419.
- [187] E. Eichten, K. Gottfried, T. Kinoshita, K. D. Lane, T.-M. Yan, Charmonium: The Model, *Phys. Rev. D*17 (1978) 3090.
- [188] E. Eichten, K. Gottfried, T. Kinoshita, K. D. Lane, T.-M. Yan, Charmonium: Comparison with Experiment, *Phys. Rev. D*21 (1980) 203.
- [189] C. Ritter, B. C. Metsch, C. R. Munz, H. R. Petry, Instanton effects in the decay of scalar mesons, *Phys. Lett. B*380 (1996) 431–436.
- [190] L. Y. Glozman, Parity doublets and chiral symmetry restoration in baryon spectrum, *Phys. Lett. B*475 (2000) 329–334.
- [191] L. Y. Glozman, A. V. Nefediev, On Goldstone bosons decoupling from high-lying hadrons, *Phys. Rev. D*73 (2006) 074018.
- [192] T. D. Cohen, L. Y. Glozman, Chiral multiplets versus parity doublets in highly excited baryons, *Phys. Rev. D*65 (2002) 016006.
- [193] J. M. Maldacena, The large N limit of superconformal field theories and supergravity, *Adv. Theor. Math. Phys.* 2 (1998) 231–252.
- [194] I. R. Klebanov, TASI lectures: Introduction to the AdS/CFT correspondence, Theoretical Advanced Study Institute in Elementary Particle Physics (TASI 99): Strings, Branes, and Gravity, Boulder, Colorado, 31 May - 25 Jun 1999. Published in \*Boulder 1999, Strings, branes and gravity\*, pp 615-650, hep-th/0009139.
- [195] E. Witten, Anti-de Sitter space and holography, *Adv. Theor. Math. Phys.* 2 (1998) 253–291.

- [196] J. Erlich, E. Katz, D. T. Son, M. A. Stephanov, Qcd and a holographic model of hadrons, Phys. Rev. Lett. 95 (2005) 261602.
- [197] J. P. Shock, F. Wu, Y.-L. Wu, Z.-F. Xie, AdS/QCD phenomenological models from a back-reacted geometry, hep-ph/0611227.
- [198] S. J. Brodsky, G. F. de Teramond, Light-front hadron dynamics and AdS/CFT correspondence, Phys. Lett. B582 (2004) 211–221.
- [199] S. J. Brodsky, G. F. de Teramond, Light-Front Dynamics and AdS/QCD: The Pion Form Factor in Space and Time-Like Regions. In preparation.
- [200] G. F. de Teramond, S. J. Brodsky, AdS/CFT Integrability in a Semiclassical Approximation to QCD: Bosonic Modes. In preparation.
- [201] R. W. Hamming, Numerical Methods for Scientists and Engineers, McGraw-Hill Education, 1962.
- [202] J. W. Negele, Instantons, the QCD vacuum, and hadronic physics, Nucl. Phys. Proc. Suppl. 73 (1999) 92–104.
- [203] M. C. Chu, J. M. Grandy, S. Huang, J. W. Negele, Evidence for the role of instantons in hadron structure from lattice QCD, Phys. Rev. D49 (1994) 6039–6050.
- [204] G. Grayer, et al., High statistics study of the reaction  $\pi^- p \rightarrow \pi^-\pi^+ n$ : Apparatus, method of analysis, and general features of results at 17 GeV/c, Nucl. Phys. B75 (1974) 189.
- [205] B. Hyams, et al.,  $\pi\pi$  phase shift analysis from 600 MeV to 1900 MeV, Nucl. Phys. B64 (1973) 134–162.
- [206] B. Hyams, et al., t dependence and production mechanisms of the  $\rho$ ,  $f$  and  $g$  resonances from  $\pi^- p \rightarrow \pi^-\pi^+ n$  at 17.2 GeV, Phys. Lett. B51 (1974) 272.
- [207] P. Estabrooks, et al.,  $\rho - \omega$  interference in  $\pi^- p \rightarrow \pi^-\pi^+ n$  at 17.2 GeV, Nucl. Phys. B81 (1974) 70.
- [208] W. Hoogland, et al., Isospin-two  $\pi\pi$  phase shifts from an experiment  $\pi^+ p \rightarrow \pi^+\pi^+ n$  at 12.5 GeV/c, Nucl. Phys. B69 (1974) 266–278.
- [209] W. Blum, et al., Observation of a spin-4 boson resonance at 2050 MeV, Phys. Lett. B57 (1975) 403–406.
- [210] B. Hyams, et al., A study of all the  $\pi\pi$  phase shift solutions in the mass region 1.0 GeV to 1.8 GeV from  $\pi^- p \rightarrow \pi^-\pi^+ n$  at 17.2 GeV, Nucl. Phys. B100 (1975) 205.
- [211] W. Hoogland, et al., Measurement and analysis of the  $\pi^+\pi^+$  system produced at small momentum transfer in the reaction  $\pi^+ p \rightarrow \pi^+\pi^+ n$  at 12.5 GeV, Nucl. Phys. B126 (1977) 109.
- [212] H. Becker, et al., A model independent partial wave analysis of the  $\pi^+\pi^-$  system produced at low four momentum transfer in the reaction  $\pi^- p_{\text{polarized}} \rightarrow \pi^+\pi^- n$ , Nucl. Phys. B151 (1979) 46.
- [213] H. Becker, et al., Measurement and analysis of the reaction  $\pi^- p \rightarrow \rho^0 n$  on a polarized target, Nucl. Phys. B150 (1979) 301.
- [214] C. Daum, et al., Experimental proof of the existence of the  $a_1$  meson, Phys. Lett. B89 (1980) 281.
- [215] C. Daum, et al.,  $A_2$  meson production at 63 GeV and 94 GeV in the reaction  $\pi^- p \rightarrow \pi^-\pi^-\pi^+ p$ , Phys. Lett. B89 (1980) 276.
- [216] C. Daum, et al., 3  $\pi$  resonances in  $2^-$  partial waves, Phys. Lett. B89 (1980) 285.
- [217] B. Alper, et al., Evidence for a spin-5 boson resonance at 2300 MeV, Phys. Lett. B94 (1980) 422.
- [218] C. Daum, et al., Diffractive production of 3  $\pi$  states at 63 GeV and 94 GeV, Nucl. Phys. B182 (1981) 269.
- [219] C. Daum, et al., Diffractive production of strange mesons at 63 GeV, Nucl. Phys. B187 (1981) 1.
- [220] D. Aston, et al., The strange meson resonances observed in the reaction  $K^- p \rightarrow \bar{K}^0 \pi^+ \pi^- n$  at 11 GeV/c, Nucl. Phys. B292 (1987) 693.

- [221] B. Ratcliff, Future facilities for light quark spectroscopy: A perspective based on the LASS experience, in: S. Oneda, D. Peaslee (Eds.), Proceedings of the International Conference On Hadron Spectroscopy (HADRON 91) College Park, MD, 1991, U.S.A., World Scientific, 1992, pp. 825–842.
- [222] D. Aston, et al., Observation of the leading  $K^* L$  excitation series from  $J^P = 1^-$  through  $5^-$  in the reaction  $K^- p \rightarrow K^- \pi^+ n$  at 11 GeV/c, Phys. Lett. B180 (1986) 308.
- [223] D. Aston, et al., A study of  $K^- \pi^+$  scattering in the reaction  $K^- p \rightarrow K^- \pi^+ n$  at 11 GeV/c, Nucl. Phys. B296 (1988) 493.
- [224] D. Aston, et al., Evidence for two strangeonium resonances with  $J^{PC} = 1^{++}$  and  $1^{+-}$  in  $K^- p$  interactions at 11 GeV/c, Phys. Lett. B201 (1988) 573.
- [225] D. Aston, et al., A study of the  $K_S^0 K_S^0$  system in the reaction  $K^- p \rightarrow K_S^0 K_S^0 \Lambda$  at 11 GeV/c, Nucl. Phys. B301 (1988) 525.
- [226] D. Aston, et al., Evidence for two  $J^P = 2^-$  strange meson states in the  $K_2(1770)$  region, Phys. Lett. B308 (1993) 186–192.
- [227] S. I. Bityukov, et al., Observation of the decay  $a_2(1320) \rightarrow \pi^- \eta'$ , Z. Phys. C54 (1992) 235–238.
- [228] S. I. Bityukov, et al., Observation of resonance with mass  $m = 1814$  MeV decaying into  $\pi^- \eta\eta$ , Phys. Lett. B268 (1991) 137–141.
- [229] S. I. Bityukov, et al., Study of the reaction  $\pi^- p \rightarrow \omega \omega n$  at  $p_{\pi^-} = 36$  GeV/c, Z. Phys. C54 (1992) 367–370.
- [230] E. B. Berdnikov, et al., Study of the reaction  $\pi^- p \rightarrow \eta' \eta' n$ , Z. Phys. C57 (1993) 13–16.
- [231] G. M. Beladidze, et al., Study of  $\pi^- N \rightarrow \eta \pi^- N$  and  $\pi^- N \rightarrow \eta' \pi^- N$  reactions at 37 GeV/c, Phys. Lett. B313 (1993) 276–282.
- [232] D. V. Amelin, et al., Study of the decay  $f_1(1285) \rightarrow \rho^0(770)\gamma$ , Z. Phys. C66 (1995) 71–76.
- [233] E. B. Berdnikov, et al., Study of the reaction  $\pi^- A \rightarrow K^+ K^- \pi^- A$  at 37 GeV/c, Phys. Lett. B337 (1994) 219–225.
- [234] I. A. Kachaev, et al., Study of the  $\pi(1800)$  resonance in diffractive reactions, Phys. Atom. Nucl. 57 (1994) 1536–1541.
- [235] D. V. Amelin, et al., Investigation of the diffractive reaction  $\pi^- A \rightarrow \eta \eta \pi^- A$  at an incident  $p_{\pi^-}$  momentum of 37-GeV/c, Phys. Atom. Nucl. 59 (1996) 976–981.
- [236] D. V. Amelin, et al., Study of resonance production in diffractive reaction  $\pi^- A \rightarrow \pi^+ \pi^- \pi^- A$ , Phys. Lett. B356 (1995) 595–600.
- [237] D. V. Amelin, et al., Partial wave analysis of the reaction  $\pi^- p \rightarrow \pi^+ \pi^- \pi^0 n$  at  $p_{\pi^-} = 36$  GeV/c: Study of  $a_2(1320)$  and  $\omega_3(1670)$  mesons, Z. Phys. C70 (1996) 71–76.
- [238] D. V. Amelin, et al., Investigation of the reaction  $\pi^- A \rightarrow \omega \pi^- \pi^0 A$ , Phys. Atom. Nucl. 62 (1999) 445–453.
- [239] D. V. Amelin, et al., Natural parity resonances in  $\eta \pi^+ \pi^-$ , Nucl. Phys. A668 (2000) 83–96.
- [240] Y. Khokhlov, Study of  $X(1600)$   $1^{-+}$  hybrid, Nucl. Phys. A663 (2000) 596–599.
- [241] V. Dorofeev, et al., The  $J^{PC} = 1^{-+}$  hunting season at VES, AIP Conf. Proc. 619 (2002) 143–154.
- [242] I. A. Kachaev, et al., Study of reaction  $\pi^- A \rightarrow \pi^+ \pi^- \pi^- A$  at VES setup, AIP Conf. Proc. 619 (2002) 577–581.
- [243] D. V. Amelin, et al., Investigation of the reaction  $\pi^- p \rightarrow \eta' \pi^0 n$  at the VES spectrometer, Phys. Atom. Nucl. 67 (2004) 1408–1415.
- [244] V. Nikolaenko, et al., Dynamical selection rule in the decays of  $\pi(1800)$ , AIP Conf. Proc. 717 (2004) 155–159.
- [245] D. V. Amelin, et al., Investigation of hybrid states in the VES experiment at the Institute for High Energy Physics (Protvino), Phys. Atom. Nucl. 68 (2005) 359–371.

- [246] D. V. Amelin, et al., Resonances in the  $\omega\omega$  system, Phys. Atom. Nucl. 69 (2006) 690–698.
- [247] S. Teige, et al., Properties of the  $a_0(980)$  meson, Phys. Rev. D59 (1999) 012001.
- [248] D. R. Thompson, et al., Evidence for exotic meson production in the reaction  $\pi^- p \rightarrow \eta \pi^- p$  at 18 GeV/c, Phys. Rev. Lett. 79 (1997) 1630–1633.
- [249] G. S. Adams, et al., Observation of a new  $J^{PC} = 1^{-+}$  exotic state in the reaction  $\pi^- p \rightarrow \pi^+ \pi^- \pi^- p$  at 18 GeV/c, Phys. Rev. Lett. 81 (1998) 5760–5763.
- [250] S. U. Chung, et al., Evidence for exotic  $J^{PC} = 1^{-+}$  meson production in the reaction  $\pi^- p \rightarrow \eta \pi^- p$  at 18 GeV/c, Phys. Rev. D60 (1999) 092001.
- [251] G. S. Adams, et al., Experimental evidence for hadroproduction of exotic mesons, Nucl. Phys. A680 (2000) 335–341.
- [252] J. J. Manak, et al., Partial-wave analysis of the  $\eta \pi^+ \pi^-$  system produced in the reaction  $\pi^- p \rightarrow \eta \pi^+ \pi^- n$  at 18 GeV/c, Phys. Rev. D62 (2000) 012003.
- [253] J. Gunter, et al., A partial wave analysis of the  $\pi^0 \pi^0$  system produced in  $\pi^- p$  charge exchange collisions, Phys. Rev. D64 (2001) 072003.
- [254] P. Eugenio, et al., Observation of a new  $J^{PC} = 1^{+-}$  isoscalar state in the reaction  $\pi^- p \rightarrow \omega \eta n$  at 18 GeV/c, Phys. Lett. B497 (2001) 190–198.
- [255] E. I. Ivanov, et al., Observation of exotic meson production in the reaction  $\pi^- p \rightarrow \eta' \pi^- p$  at 18 GeV/c, Phys. Rev. Lett. 86 (2001) 3977–3980.
- [256] G. S. Adams, et al., Observation of pseudoscalar and axial vector resonances in  $\pi^- p \rightarrow K^+ K^- \pi^0 n$  at 18 GeV, Phys. Lett. B516 (2001) 264–272.
- [257] S. U. Chung, et al., Exotic and  $q\bar{q}$  resonances in the  $\pi^+ \pi^- \pi^-$  system produced in  $\pi^- p$  collisions at 18 GeV/c, Phys. Rev. D65 (2002) 072001.
- [258] M. Nozar, et al., A study of the reaction  $\pi^- p \rightarrow \omega \pi^- p$  at 18 GeV/c: The D and S decay amplitudes for  $b_1(1235) \rightarrow \omega \pi$ , Phys. Lett. B541 (2002) 35–44.
- [259] A. R. Dzierba, et al., A study of the  $\eta \pi^0$  spectrum and search for a  $J^{PC} = 1^{-+}$  exotic meson, Phys. Rev. D67 (2003) 094015.
- [260] J. Kuhn, et al., Exotic meson production in the  $f_1(1285)\pi^-$  system observed in the reaction  $\pi^- p \rightarrow \eta \pi^+ \pi^- \pi^- p$  at 18 GeV/c, Phys. Lett. B595 (2004) 109–117.
- [261] M. Lu, et al., Exotic meson decay to  $\omega \pi^0 \pi^-$ , Phys. Rev. Lett. 94 (2005) 032002.
- [262] A. R. Dzierba, et al., A partial wave analysis of the  $\pi^- \pi^- \pi^+$  and  $\pi^- \pi^0 \pi^0$  systems and the search for a  $J^{PC} = 1^{-+}$  meson, Phys. Rev. D73 (2006) 072001.
- [263] T. A. Armstrong, et al., Spin parity analysis of the E meson centrally produced in the reactions  $\pi^+ p \rightarrow \pi^+(K_L K^\pm \pi^\mp) p$  and  $p p \rightarrow p(K_L K^\pm \pi^\mp) p$  at 85 GeV/c, Phys. Lett. B146 (1984) 273.
- [264] T. A. Armstrong, et al., Study of the centrally produced  $K_s^0 K^\pm \pi^\mp$  system at 85 GeV/c, Z. Phys. C34 (1987) 23.
- [265] T. A. Armstrong, et al., Study of the  $K^+ K^- \pi^+ \pi^-$  system centrally produced in the reactions  $\pi^+ p \rightarrow \pi^+(K^+ K^- \pi^+ \pi^-) p$  and  $p p \rightarrow p(K^+ K^- \pi^+ \pi^-) p$  at 85 GeV/c, Z. Phys. C34 (1987) 33.
- [266] T. A. Armstrong, et al., A spin parity analysis of the  $f_1(1285)$  and  $f_1(1420)$  mesons centrally produced in the reaction  $p p \rightarrow p_f(K_s^0 K^\pm \pi^\mp) p_s$  at 300 GeV/c, Phys. Lett. B221 (1989) 216.
- [267] T. A. Armstrong, et al., Study of the  $\pi^+ \pi^- \pi^+ \pi^-$  system centrally produced by incident  $\pi^+$  and  $p$  beams at 85 GeV/c, Z. Phys. C43 (1989) 55.
- [268] T. A. Armstrong, et al., Observation of centrally produced  $\Theta/f_2(1720)$  in the reaction  $p p \rightarrow p_f(K \bar{K}) p_s$  at 300 GeV/c, Phys. Lett. B227 (1989) 186.

- [269] T. A. Armstrong, et al., Evidence for new states produced in the central region in the reaction  $pp \rightarrow p_f(\pi^+\pi^-\pi^+\pi^-)$  at 300 GeV/c, Phys. Lett. B228 (1989) 536.
- [270] T. A. Armstrong, et al., A study of the centrally produced  $K^{*0}\bar{K}^{*0}$  final state in the reaction  $p\ p \rightarrow p_f(K^+K^-\pi^+\pi^-)p_s$  at 300 GeV/c, Z. Phys. C46 (1990) 405–410.
- [271] T. A. Armstrong, et al., A study of the centrally produced  $\pi^+\pi^-\pi^0$  system formed in the reaction  $p\ p \rightarrow p_f(\pi^+\pi^-\pi^0)p_s$  at 300 GeV/c, Z. Phys. C48 (1990) 213–220.
- [272] T. A. Armstrong, et al., Study of the centrally produced  $\pi\pi$  and  $K\bar{K}$  systems at 85 GeV/c and 300 GeV/c, Z. Phys. C51 (1991) 351–364.
- [273] T. A. Armstrong, et al., Study of the  $\eta\pi^+\pi^-$  system centrally produced in the reaction  $pp \rightarrow p_f(\eta\pi^+\pi^-)p_s$  at 300 GeV/c, Z. Phys. C52 (1991) 389–396.
- [274] T. A. Armstrong, et al., Study of the centrally produced  $\omega\rho^0$  and  $\omega\omega$  systems in  $pp$  interactions at 300 GeV/c, Z. Phys. C58 (1993) 257–266.
- [275] B. R. French, et al., A partial wave analysis of the centrally produced  $K^+K^-$  system in  $pp$  interactions at 300 GeV/c, Phys. Lett. B460 (1999) 213–218.
- [276] S. Abatzis, et al., Observation of a narrow scalar meson at 1450-MeV in the reaction  $pp \rightarrow p_f(\pi^+\pi^-\pi^+\pi^-)p_s$  at 450 GeV/c using the CERN Omega Spectrometer, Phys. Lett. B324 (1994) 509–514.
- [277] F. Antinori, et al., A further study of the centrally produced  $\pi^+\pi^-$  and  $\pi^+\pi^-\pi^+\pi^-$  channels in  $pp$  interactions at 300 GeV/c and 450 GeV/c, Phys. Lett. B353 (1995) 589–594.
- [278] D. Barberis, et al., Observation of vertex factorisation breaking in central  $pp$  interactions, Phys. Lett. B388 (1996) 853–858.
- [279] M. Boutemeur, Results from GAMS, in: J. Grunhaus (Ed.), Proceedings of the 9th International Conference On Physics In Collisions, Jerusalem, 1989, no. C27 in Editions Frontieres, 1990, pp. 401–410.
- [280] D. Alde, et al., Production of G(1590) and other mesons decaying into  $\eta$  pairs by 100-GeV/c  $\pi^-$  on protons, Nucl. Phys. B269 (1986) 485–508.
- [281] D. Alde, et al., 2.22-GeV  $\eta\eta'$  structure observed in 38-GeV/c and 100-GeV/c  $\pi^-p$  collisions, Phys. Lett. B177 (1986) 120.
- [282] D. Alde, et al., Observation of a 1750-MeV narrow meson decaying into  $\eta\eta$ , Phys. Lett. B182 (1986) 105.
- [283] D. Alde, et al., Observation of the  $\omega \rightarrow \pi^0\pi^0\gamma$  decay, Phys. Lett. B340 (1994) 122–124.
- [284] D. Alde, et al., Production mechanism of the X(1740) meson, Phys. Lett. B284 (1992) 457–460.
- [285] D. Alde, et al., Study of the  $f_0(995)$  resonance in the  $\pi^0\pi^0$  decay channel, Z. Phys. C66 (1995) 375–378.
- [286] D. Alde, et al., Partial wave analysis of the  $\omega\pi^0$  system at high masses, Nuovo Cim. A107 (1994) 1867–1874.
- [287] D. Alde, et al., Study of the  $\pi^0\pi^0$  system in  $p\ p$  central collisions at 450 GeV/c, Phys. Lett. B397 (1997) 350–356.
- [288] D. Alde, et al., Partial-wave analysis of the  $\eta\pi^0\pi^0$  system produced in  $\pi^-p$  charge exchange collisions at 100 GeV/c, Phys. Atom. Nucl. 60 (1997) 386–390.
- [289] D. Alde, et al., Study of the  $\pi^0\pi^0$  system with the GAMS-4000 spectrometer at 100 GeV/c, Eur. Phys. J. A3 (1998) 361–371.
- [290] D. Alde, et al., Study of the reaction  $\pi^-p \rightarrow \eta\pi^0n$  at 32 GeV/c, 38 GeV/c, and 100 GeV/c, Phys. Atom. Nucl. 62 (1999) 421–434.
- [291] R. Bellazzini, et al., A partial wave analysis of the centrally produced  $\pi^0\pi^0$  system in  $p\ p$  interactions at 450 GeV/c, Phys. Lett. B467 (1999) 296–302.
- [292] D. Barberis, et al., A kinematical selection of glueball candidates in central production, Phys. Lett. B397 (1997) 339–344.

- [293] D. Barberis, et al., A study of the centrally produced  $\pi^+\pi^-\pi^+\pi^-$  channel in  $p\ p$  interactions at 450 GeV/c, Phys. Lett. B413 (1997) 217–224.
- [294] D. Barberis, et al., A study of the  $K\bar{K}\pi$  channel produced centrally in  $p\ p$  interactions at 450 GeV/c, Phys. Lett. B413 (1997) 225–231.
- [295] D. Barberis, et al., A study of pseudoscalar states produced centrally in  $p\ p$  interactions at 450 GeV/c, Phys. Lett. B427 (1998) 398–402.
- [296] D. Barberis, et al., A measurement of the branching fractions of the  $f_1(1285)$  and  $f_1(1420)$  produced in central  $p\ p$  interactions at 450 GeV/c, Phys. Lett. B440 (1998) 225–232.
- [297] D. Barberis, et al., A study of the centrally produced  $\phi\phi$  system in  $p\ p$  interactions at 450 GeV/c, Phys. Lett. B432 (1998) 436–442.
- [298] D. Barberis, et al., A study of the centrally produced  $\pi^+\pi^-\pi^0$  channel in  $p\ p$  interactions at 450 GeV/c, Phys. Lett. B422 (1998) 399–404.
- [299] D. Barberis, et al., A study of the centrally produced  $K^*(892)\bar{K}^*(892)$  and  $\phi\omega$  systems in  $p\ p$  interactions at 450 GeV/c, Phys. Lett. B436 (1998) 204–210.
- [300] D. Barberis, et al., A study of the centrally produced baryon antibaryon systems in  $p\ p$  interactions at 450 GeV/c, Phys. Lett. B446 (1999) 342–348.
- [301] D. Barberis, et al., A partial wave analysis of the centrally produced  $K^+K^-$  and  $K_S^0K_S^0$  systems in  $p\ p$  interactions at 450 GeV/c and new information on the spin of the  $f_J(1710)$ , Phys. Lett. B453 (1999) 305–315.
- [302] D. Barberis, et al., A partial wave analysis of the centrally produced  $\pi^+\pi^-$  system in  $p\ p$  interactions at 450 GeV/c, Phys. Lett. B453 (1999) 316–324.
- [303] D. Barberis, et al., A partial wave analysis of the centrally produced  $\pi^0\pi^0$  system in  $p\ p$  interactions at 450 GeV/c, Phys. Lett. B453 (1999) 325–332.
- [304] D. Barberis, et al., A study of the  $\eta\pi^+\pi^-$  channel produced in central  $p\ p$  interactions at 450 GeV/c, Phys. Lett. B471 (2000) 435–439.
- [305] D. Barberis, et al., A coupled channel analysis of the centrally produced  $K^+K^-$  and  $\pi^+\pi^-$  final states in  $p\ p$  interactions at 450 GeV/c, Phys. Lett. B462 (1999) 462–470.
- [306] D. Barberis, et al., A study of the  $\eta\eta'$  and  $\eta'\eta'$  channels produced in central  $p\ p$  interactions at 450 GeV/c, Phys. Lett. B471 (2000) 429–434.
- [307] D. Barberis, et al., A spin analysis of the  $4\pi$  channels produced in central  $p\ p$  interactions at 450 GeV/c, Phys. Lett. B471 (2000) 440–448.
- [308] D. Barberis, et al., Experimental evidence for a vector-like behaviour of Pomeron exchange, Phys. Lett. B467 (1999) 165–170.
- [309] D. Barberis, et al., A study of the centrally produced  $\eta\pi^0$  and  $\eta\pi^-$  systems in  $p\ p$  interactions at 450 GeV/c, Phys. Lett. B488 (2000) 225–233.
- [310] D. Barberis, et al., A study of the  $\eta\eta$  channel produced in central  $p\ p$  interactions at 450 GeV/c, Phys. Lett. B479 (2000) 59–66.
- [311] D. Barberis, et al., A study of the  $f_0(1370)$ ,  $f_0(1500)$ ,  $f_0(2000)$  and  $f_2(1950)$  observed in the centrally produced  $4\pi$  final states, Phys. Lett. B474 (2000) 423–426.
- [312] D. Barberis, et al., A study of the  $\omega\omega$  channel produced in central  $p\ p$  interactions at 450 GeV/c, Phys. Lett. B484 (2000) 198–204.
- [313] D. Barberis, et al., A search for charmonium states produced in central  $p\ p$  interactions at 450 GeV/c, Phys. Lett. B485 (2000) 357–361.

- [314] D. Barberis, et al., A study of the centrally produced  $\pi^0\pi^0\pi^0$  channel in  $p\bar{p}$  interactions at 450 GeV/c, Phys. Lett. B507 (2001) 14–18.
- [315] S. Ahmad et al., “The Asterix Spectrometer at LEAR,” Nucl. Instr. Meth. A286 (1990) 76.
- [316] S. Ahmad et al., “Search for monochromatic pion emission in  $p\bar{p}$  annihilation from atomic P states,” Phys. Lett. B152 (1985) 135.
- [317] K.D. Duch et al., “Observation and analysis of E mesons in  $p\bar{p}$  annihilation at rest in H<sub>2</sub> gas,” Z. Phys. C45 (1989) 223.
- [318] B. May et al., “Observation of an isoscalar meson AX(1565) in annihilation of the  $p\bar{p}$  atom from P states,” Phys. Lett. B225 (1989) 450.
- [319] B. May et al., “Antiproton-proton annihilation at rest in H<sub>2</sub> gas into  $\pi^+\pi^-\pi^0$ . 1: Annihilation from S states,” Z. Phys. C46 (1990) 191.
- [320] B. May et al., “Antiproton-proton annihilation at rest in H<sub>2</sub> gas into  $\pi^+\pi^-\pi^0$ . 2: Annihilation from P states,” Z. Phys. C46 (1990) 203.
- [321] E. Klempt et al., “Evidence for a multi-quark state in  $p\bar{p}$  annihilation at rest,” Nucl. Phys. A508 (1990) 317.
- [322] J. Reifenroether et al., “ $\phi$  production in  $p\bar{p}$  annihilation at rest,” Phys. Lett. B267 (1991) 299.
- [323] E. Aker, et al., The Crystal Barrel spectrometer at LEAR, Nucl. Instr. Meth. A321 (1992) 69–108.
- [324] M. Doser, et al., The Crystal Barrel Si-vertex detector, Nucl. Instr. Meth. A412 (1998) 70.
- [325] C. Amsler, et al., Proton - antiproton annihilation into  $\eta\eta\pi$ : Observation of a scalar resonance decaying into  $\eta\eta$ , Phys. Lett. B291 (1992) 347–354.
- [326] C. Amsler, et al.,  $\eta\eta'$  threshold enhancement in  $p\bar{p}$  annihilations into  $\pi^0\eta\eta'$  at rest, Phys. Lett. B340 (1994) 259–263.
- [327] C. Amsler, et al., Study of  $p\bar{p}$  annihilation at rest into  $\omega\eta\pi^0$ , Phys. Lett. B327 (1994) 425–432.
- [328] C. Amsler, et al., Observation of a scalar resonance decaying to  $\pi^+\pi^-\pi^0\pi^0$  in  $p\bar{p}$  annihilation at rest, Phys. Lett. B322 (1994) 431–440.
- [329] C. Amsler, et al., Observation of a new  $I^G(J^{PC}) = 1^-(0^{++})$  resonance at 1450 MeV, Phys. Lett. B333 (1994) 277–282.
- [330] C. Amsler, et al., Coupled channel analysis of  $p\bar{p}$  annihilation into  $\pi^0\pi^0\pi^0$ ,  $\pi^0\eta\eta$  and  $\pi^0\pi^0\eta$ , Phys. Lett. B355 (1995) 425–432.
- [331] C. Amsler, et al., High statistics study of f<sub>0</sub>(1500) decay into  $\eta\eta$ , Phys. Lett. B353 (1995) 571–577.
- [332] C. Amsler, et al., E decay to  $\eta\pi\pi$  in  $p\bar{p}$  annihilation at rest, Phys. Lett. B358 (1995) 389–398.
- [333] J. Adomeit, et al., Evidence for two isospin zero  $J^{PC} = 2^{-+}$  mesons at 1645-MeV and 1875-MeV, Z. Phys. C71 (1996) 227–238.
- [334] A. Abele, et al., A study of f<sub>0</sub>(1500) decays into  $4\pi^0$  in  $\bar{p}p \rightarrow 5\pi^0$  at rest, Phys. Lett. B380 (1996) 453–460.
- [335] A. Abele, et al., Observation of f<sub>0</sub>(1500) decay into  $K_LK_L$ , Phys. Lett. B385 (1996) 425–432.
- [336] A. Abele, et al., High mass  $\rho$ -meson states from  $\bar{p}d$  annihilation at rest into  $\pi^-\pi^0\pi^0$  plus proton spectator, Phys. Lett. B391 (1997) 191–196.
- [337] A. Abele, et al., Study of the  $\pi^0\pi^0\eta'$  final state in  $\bar{p}p$  annihilation at rest, Phys. Lett. B404 (1997) 179–186.
- [338] A. Abele, et al.,  $\rho - \omega$  interference in  $p\bar{p}$  annihilation at rest into  $\pi^+\pi^-\eta$ , Phys. Lett. B411 (1997) 354–360.
- [339] A. Abele, et al., Antiproton proton annihilation at rest into  $K_lK_s\pi^0\pi^0$ , Phys. Lett. B415 (1997) 280–288.
- [340] A. Abele, et al., Antiproton proton annihilation at rest into  $K_lK^\pm\pi^\mp\pi^0$ : manifestations of isospin interference, Phys. Lett. B415 (1997) 289–298.

- [341] A. Abele, et al., Exotic  $\eta\pi$  state in  $\bar{p}d$  annihilation at rest into  $\pi^-\pi^0\eta p_{(spectator)}$ , Phys. Lett. B423 (1998) 175–184.
- [342] A. Abele, et al., Study of  $p\bar{p} \rightarrow \eta\pi^0\pi^0\pi^0$  at rest, Nucl. Phys. B514 (1998) 45–59.
- [343] A. Abele,  $p\bar{p}$  annihilation at rest into  $K_L K^\pm\pi^\mp$ , Phys. Rev. D57 (1998) 3860–3872.
- [344] C. A. Baker, et al., The  $f_2(1565)$  in  $\bar{p}p \rightarrow \omega\omega\pi^0$  interactions at rest, Phys. Lett. B467 (1999) 147–155.
- [345] A. Abele, et al., Evidence for a  $\pi\eta$  P-wave in  $p\bar{p}$  annihilations at rest into  $\pi^0\pi^0\eta$ , Phys. Lett. B446 (1999) 349–355.
- [346] A. Abele, et al.,  $\bar{p}d$  annihilation at rest into  $\pi^+\pi^-\pi^-p_{(spectator)}$ , Phys. Lett. B450 (1999) 275–280.
- [347] A. Abele, et al., Antiproton-proton annihilation at rest into  $K^+K^-\pi^0$ , Phys. Lett. B468 (1999) 178–188.
- [348] A. Abele, et al., Observation of resonances in the reaction  $p\bar{p} \rightarrow \pi^0\eta\eta$  at 1.94-GeV/c, Eur. Phys. J. C8 (1999) 67–79.
- [349] A. Abele, et al.,  $p\bar{p}$  annihilation into  $\omega\pi^0$ ,  $\omega\eta$  and  $\omega\eta'$  at 600, 1200 and 1940 MeV/c, Eur. Phys. J. C12 (2000) 429–439.
- [350] A. Abele, et al., Study of  $f_0$  decays into four neutral pions, Eur. Phys. J. C19 (2001) 667–675.
- [351] C. Amsler, et al., A high resolution search for the tensor glueball candidate  $\xi(2230)$ , Phys. Lett. B520 (2001) 175–182.
- [352] A. Abele, et al.,  $4\pi$  decays of scalar and vector mesons, Eur. Phys. J. C21 (2001) 261–269.
- [353] C. Amsler, et al., Proton antiproton annihilation at 900-MeV/c into  $\pi^0\pi^0\pi^0$ ,  $\pi^0\pi^0\eta$  and  $\pi^0\eta\eta$ , Eur. Phys. J. C23 (2002) 29–41.
- [354] C. A. Baker, et al., Confirmation of  $a_0(1450)$  and  $\pi_1(1600)$  in  $\bar{p}p \rightarrow \omega\pi^+\pi^-\pi^0$  at rest, Phys. Lett. B563 (2003) 140–149.
- [355] C. Amsler, et al., Production and decay of  $\eta'(958)$  and  $\eta(1440)$  in  $\bar{p}p$  annihilation at rest, Eur. Phys. J. C33 (2004) 23–30.
- [356] C. Amsler, et al., Study of antiproton annihilation on neutrons into  $\omega\pi^-\pi^0$ , Nucl. Phys. A740 (2004) 130–146.
- [357] W. Dunnweber, F. Meyer-Wildhagen, Exotic states in Crystal Barrel analyses of annihilation channels, AIP Conf. Proc. 717 (2004) 388–393.
- [358] A. V. Anisovich, et al.,  $\bar{p}p \rightarrow \eta\pi^0\pi^0$  from 600-MeV/c to 1940-MeV/c, Phys. Lett. B468 (1999) 304–308.
- [359] A. V. Anisovich, et al.,  $\bar{p}p \rightarrow \eta\eta$  and  $\eta\eta'$  from 600-MeV/c to 1940-MeV/c, Phys. Lett. B468 (1999) 309–313.
- [360] A. V. Anisovich, et al., Observation of  $f_0(1770) \rightarrow \eta\eta$  in  $\bar{p}p \rightarrow \eta\eta\pi^0$  reactions from 600-MeV/c to 1200-MeV/c, Phys. Lett. B449 (1999) 154–160.
- [361] A. V. Anisovich, et al., Study of the process  $\bar{p}p \rightarrow \eta\eta\pi^0$  from 1350-MeV/c to 1940-MeV/c, Phys. Lett. B449 (1999) 145–153.
- [362] A. V. Anisovich, et al., Resonances in  $p\bar{p} \rightarrow f_2(1270)\pi$ , Phys. Lett. B452 (1999) 187–193.
- [363] A. V. Anisovich, et al., Study of  $p\bar{p} \rightarrow \pi^0\pi^0\eta$  from 600-MeV/c to 1940-MeV/c, Phys. Lett. B452 (1999) 180–186.
- [364] A. V. Anisovich, et al., Resonances formed by  $\bar{p}p$  and decaying into  $\pi^0\pi^0\eta$  for masses 1960-MeV to 2410-MeV, Nucl. Phys. A651 (1999) 253–276.
- [365] A. V. Anisovich, et al., Analysis of  $\bar{p}p \rightarrow \pi^-\pi^+, \pi^0\pi^0, \eta\eta$  and  $\eta\eta'$  from threshold to 2.5-GeV/c, Phys. Lett. B471 (1999) 271–279.
- [366] A. V. Anisovich, et al., Partial wave analysis of  $\bar{p}p \rightarrow \pi^-\pi^+, \pi^0\pi^0, \eta\eta$  and  $\eta\eta'$ , Nucl. Phys. A662 (2000) 319–343.

- [367] A. V. Anisovich, et al., Data on  $\bar{p}p \rightarrow \pi^0\pi^0, \eta\eta$  and  $\eta\eta'$  from 600-MeV/c to 1940-MeV/c, Nucl. Phys. A662 (2000) 344–361.
- [368] A. V. Anisovich, et al., Resonances in  $\bar{p}p \rightarrow \omega\pi^0\pi^0$  from 600-MeV/c to 1940-MeV/c, Phys. Lett. B476 (2000) 15–24.
- [369] A. V. Anisovich, et al., A study of  $\bar{p}p \rightarrow \eta\eta\eta$  for masses 1960-MeV/c<sup>2</sup> to 2410-MeV/c<sup>2</sup>, Phys. Lett. B496 (2000) 145–153.
- [370] A. V. Anisovich, et al., Evidence for  $\omega' \rightarrow \omega\sigma$  and  $b_1(1235)\pi$ , Phys. Lett. B485 (2000) 341–348.
- [371] A. V. Anisovich, et al., A  $J^{PC} = 0^{-+}$  enhancement at the  $f_0(980)\eta$  threshold, Phys. Lett. B472 (2000) 168–174.
- [372] A. V. Anisovich, et al., Three  $I = 0 J^{PC} = 2^{-+}$  mesons, Phys. Lett. B477 (2000) 19–27.
- [373] A. V. Anisovich, et al., Data on  $\bar{p}p \rightarrow \eta'\pi^0\pi^0$  for masses 1960-MeV/c<sup>2</sup> to 2410-MeV/c<sup>2</sup>, Phys. Lett. B491 (2000) 40–46.
- [374] A. V. Anisovich, et al., I = 0 C = +1 mesons from 1920-MeV to 2410-MeV, Phys. Lett. B491 (2000) 47–58.
- [375] A. V. Anisovich, et al., Resonances in  $\bar{p}p \rightarrow \omega\eta$  from 600-MeV/c to 1940-MeV/c, Phys. Lett. B507 (2001) 23–28.
- [376] A. V. Anisovich, et al., Study of  $\bar{p}p \rightarrow \eta\eta\pi^0\pi^0$  in flight, Phys. Lett. B500 (2001) 222–231.
- [377] A. V. Anisovich, et al., Resonances in  $\bar{p}p \rightarrow \omega\pi^0$  with masses 1960-MeV to 2410-MeV, Phys. Lett. B508 (2001) 6–16.
- [378] A. V. Anisovich, et al., Partial wave analysis of  $\bar{p}p$  annihilation channels in flight with I = 1, C = +1, Phys. Lett. B517 (2001) 261–272.
- [379] A. V. Anisovich, et al., A partial wave analysis of  $\bar{p}p \rightarrow \eta\eta\pi^0$ , Phys. Lett. B517 (2001) 273–281.
- [380] A. V. Anisovich, et al., Resonances in  $\bar{p}p \rightarrow \omega\eta\pi^0$  in the mass range 1960-MeV to 2410-MeV, Phys. Lett. B513 (2001) 281–291.
- [381] A. V. Anisovich, et al., Combined analysis of meson channels with I = 1, C = -1 from 1940 MeV to 2410 MeV, Phys. Lett. B542 (2002) 8–18.
- [382] A. V. Anisovich, et al., I = 0, C = -1 mesons from 1940-MeV to 2410-MeV, Phys. Lett. B542 (2002) 19–28.
- [383] A. Adamo, et al., First physics results from OBELIX, Sov. J. Nucl. Phys. 55 (1992) 1732–1742.
- [384] S. Affatato, et al., Electromagnetic calorimeter for the OBELIX experiment, Nucl. Instr. Meth. A325 (1993) 417–428.
- [385] A. Bertin, et al., E/ $\nu$  decays to  $K\bar{K}\pi$  in  $p\bar{p}$  annihilation at rest, Phys. Lett. B361 (1995) 187–198.
- [386] A. Bertin, et al., Spin-parity analysis of the final state  $\pi^+\pi^-\pi^0$  from  $\bar{p}p$  annihilation at rest in hydrogen targets at three densities, Phys. Lett. B408 (1997) 476–486.
- [387] A. Bertin, et al., Study of  $\bar{p}p \rightarrow 2\pi^+2\pi^-$  annihilation from S states, Phys. Lett. B414 (1997) 220–228.
- [388] A. Bertin, et al., A search for axial vectors in  $\bar{p}p \rightarrow K^\pm K_{miss}^0\pi^\mp\pi^+\pi^-$  annihilations at rest in gaseous hydrogen at NTP, Phys. Lett. B400 (1997) 226–238.
- [389] A. Bertin, et al., Study of the isovector scalar mesons in the channel  $\bar{p}p \rightarrow K^\pm K_s^0\pi^\mp$  at rest with initial angular momentum state selection, Phys. Lett. B434 (1998) 180–188.
- [390] A. Bertin, et al., Study of the f<sub>0</sub>(1500)/f<sub>2</sub>(1565) production in the exclusive annihilation  $\bar{n}p \rightarrow \pi^+\pi^+\pi^-$  in flight, Phys. Rev. D57 (1998) 55–66.
- [391] C. Cicalo, et al., Evidence for two pseudoscalar states in the 1.4 GeV to 1.5 GeV mass region, Phys. Lett. B462 (1999) 453–461.

- [392] F. Nichitiu, et al., Study of the  $K^+K^-\pi^+\pi^-\pi^0$  final state in antiproton annihilation at rest in gaseous hydrogen at NTP with the OBELIX spectrometer, Phys. Lett. B545 (2002) 261–271.
- [393] M. Bargiotti, et al., Results of the coupled channel analysis of  $\pi^+\pi^-\pi^0$ ,  $K^+K^-\pi^0$  and  $K^\pm K_s\pi^\mp$  final states from  $\bar{p}p$  annihilation at rest in hydrogen targets at different densities, Phys. Lett. B561 (2003) 233–240.
- [394] M. Bargiotti, et al., Coupled channel analysis of  $\pi^+\pi^-\pi^0$ ,  $K^+K^-\pi^0$  and  $K^\pm K_s\pi^\mp$  from  $\bar{p}p$  annihilation at rest in hydrogen targets at three densities, Eur. Phys. J. C26 (2003) 371–388.
- [395] P. Salvini, et al.,  $\bar{p}p$  annihilation into four charged pions at rest and in flight, Eur. Phys. J. C35 (2004) 21–33.
- [396] M. Ambrogiani, et al., Study of the angular distributions of the reactions  $\bar{p}p \rightarrow \chi_{c1}, \chi_{c2} \rightarrow J/\psi\gamma \rightarrow e^+e^-\gamma$ , Phys. Rev. D65 (2002) 052002.
- [397] M. Ambrogiani, et al., Search for the  $\eta_{c'}(2^1S_0)$  charmonium resonance, Phys. Rev. D64 (2001) 052003.
- [398] S. Bagnasco, et al., New measurements of the resonance parameters of the  $\chi_{c0}(1^3P_0)$  state of charmonium, Phys. Lett. B533 (2002) 237–242.
- [399] M. Ambrogiani, et al., Measurement of the resonance parameters of the charmonium ground state,  $\eta_{c1}(1^1S_0)$ , Phys. Lett. B566 (2003) 45–50.
- [400] M. Andreotti, et al., Measurement of the two photon decay of the  $\chi_{c0}(1^3P_0)$  state of charmonium, Phys. Lett. B584 (2004) 16–21.
- [401] M. Andreotti, et al., Results of a search for the  $h_c(1^1P_1)$  state of charmonium in the  $\eta_c\gamma$  and  $J/\psi\pi^0$  decay modes, Phys. Rev. D72 (2005) 032001.
- [402] M. Andreotti, et al., A study of  $\bar{p}p$  to two neutral pseudoscalar mesons at the  $\chi_{c0}(1^3P_0)$  formation energy, Phys. Rev. D72 (2005) 112002.
- [403] T. A. Armstrong, et al., Production of the  $f_2(1520)$  resonance in antiproton - proton annihilations at  $\sqrt{s} = 2980$  MeV and 3526 MeV, Phys. Lett. B307 (1993) 399–402.
- [404] T. A. Armstrong, et al., Evidence for  $\eta\eta$  resonances in antiproton - proton annihilations at  $2950 < \sqrt{s} < 3620$  MeV, Phys. Lett. B307 (1993) 394–398.
- [405] I. Uman, et al., Light quark resonances in  $p\bar{p}$  annihilations at 5.2-GeV/c, Phys. Rev. D73 (2006) 052009.
- [406] G. W. Bennett, et al., Final report of the muon E821 anomalous magnetic moment measurement at BNL, Phys. Rev. D73 (2006) 072003.
- [407] A. D. Bukin, et al., Absolute calibration of beam energy in the storage ring.  $\phi$  - meson mass measurement, In: \*Warsaw 1975, Proceedings, International Symposium on High Energy Physics\*, Dubna 1975, 138–147 and Novosibirsk Inst. Nucl. Phys. A, N - IYAF, 75-64, 14p.
- [408] Y. S. Derbenev, et al., Accurate calibration of the beam energy in a storage ring based on measurement of spin precession frequency of polarized particles, Part. Accel. 10 (1980) 177–180.
- [409] P. M. Ivanov, et al., Measurement of the charged kaon form-factor in the energy range 1.0 GeV to 1.4 GeV, Phys. Lett. B107 (1981) 297–300.
- [410] V. B. Golubev, et al., The neutral detector at VEPP-2M, Nucl. Instrum. Meth. A227 (1984) 467–469.
- [411] V. M. Aulchenko, et al., Search for the decay  $\phi \rightarrow \eta\pi^0\pi^0\gamma$ , Phys. Lett. B436 (1998) 199–203.
- [412] G. N. Abramov, et al., Upgrade of the Spherical Neutral Detector for VEPP-2000. (In Russian, unpublished) BUDKER-INP-2001-29.
- [413] R. R. Akhmetshin, et al., Measurement of  $\phi$  meson parameters with CMD-2 detector at VEPP-2M collider, Phys. Lett. B364 (1995) 199–206.
- [414] M. N. Achasov, et al., Evidence of the  $\phi \rightarrow \eta\pi^0\gamma$  decay, Phys. Lett. B438 (1998) 441–445.
- [415] V. M. Aulchenko, et al., First observation of  $\phi(1020) \rightarrow \pi^0\pi^0\gamma$  decay, Phys. Lett. B440 (1998) 442–448.

- [416] V. M. Aulchenko, et al., The decay  $\phi \rightarrow \eta'\gamma$ , JETP Lett. 69 (1999) 97–102.
- [417] M. N. Achasov, et al., Observation of the decays  $\phi \rightarrow \pi^0\pi^0\gamma$  and  $\phi \rightarrow \pi^0\eta\gamma$  in the SND experiment at VEPP-2M, Phys. Atom. Nucl. 62 (1999) 442–444.
- [418] M. N. Achasov, et al., Observation of the decay  $\phi \rightarrow \omega\pi^0$ , Phys. Lett. B449 (1999) 122–127.
- [419] M. N. Achasov, et al., Measurement of the decay  $\phi \rightarrow \mu^+\mu^-$ , Phys. Lett. B456 (1999) 304–309.
- [420] M. N. Achasov, et al., New data from SND detector in Novosibirsk, Nucl. Phys. A675 (2000) 391c–397c.
- [421] M. N. Achasov, et al., The  $\phi(1020) \rightarrow \pi^0\pi^0\gamma$  decay, Phys. Lett. B485 (2000) 349–356.
- [422] M. N. Achasov, et al., The  $\phi \rightarrow \eta\pi^0\gamma$  decay, Phys. Lett. B479 (2000) 53–58.
- [423] M. N. Achasov, et al., Study of the  $\pi\pi$  mass spectra in the process  $e^+e^- \rightarrow \pi^+\pi^-\pi^0$  at  $s^{1/2}$  approx. 1020-MeV, Phys. Rev. D65 (2002) 032002.
- [424] M. N. Achasov, et al., Measurements of the parameters of the  $\phi(1020)$  resonance through studies of the processes  $e^+e^- \rightarrow K^+K^-$ ,  $K_SK_L$ , and  $\pi^+\pi^-\pi^0$ , Phys. Rev. D63 (2001) 072002.
- [425] M. N. Achasov, et al., Dynamics of  $\eta \rightarrow 3\pi^0$  decay, JETP Lett. 73 (2001) 451–452.
- [426] M. N. Achasov, et al., Measurement of the  $\phi \rightarrow \pi^0e^+e^-$  decay probability, JETP Lett. 75 (2002) 449–451.
- [427] M. N. Achasov, et al., Study of the process  $e^+e^- \rightarrow \pi^+\pi^-\pi^0$  in the energy region  $s^{1/2}$  from 0.98-GeV to 1.38-GeV, Phys. Rev. D66 (2002) 032001.
- [428] M. N. Achasov, et al., Analysis of  $e^+e^- \rightarrow \pi^+\pi^-\pi^+\pi^-$  and  $e^+e^- \rightarrow \pi^+\pi^-\pi^0\pi^0$  processes in the energy range of  $s^{1/2} = 0.98 - 1.38$ -GeV in experiments with a spherical neutral detector, J. Exp. Theor. Phys. 96 (2003) 789–800.
- [429] M. N. Achasov, et al., Experimental study of the  $e^+e^- \rightarrow \pi^0\gamma$  process in the energy region  $s^{1/2} = 0.60$ -GeV to 0.97-GeV, Phys. Lett. B559 (2003) 171–178.
- [430] M. N. Achasov, et al., Study of the process  $e^+e^- \rightarrow \pi^+\pi^-\pi^0$  in the energy region  $s^{1/2}$  below 0.98-GeV, Phys. Rev. D68 (2003) 052006.
- [431] V. M. Aulchenko, et al., Measurement of the relative probability of the decay  $\phi \rightarrow \eta'\gamma$  in the channel  $\eta' \rightarrow \eta\pi^0\pi^0$ ,  $\eta \rightarrow \gamma\gamma$ , J. Exp. Theor. Phys. 97 (2003) 24–33.
- [432] M. N. Achasov, et al., Experimental study of the reaction  $e^+e^- \rightarrow K_SK_L$  in the energy range  $s^{1/2} = 1.04$ -GeV - 1.38-GeV, J. Exp. Theor. Phys. 103 (2006) 720–727.
- [433] M. N. Achasov, et al., Study of the  $e^+e^- \rightarrow \eta\gamma$  process with SND detector at the VEPP-2M  $e^+e^-$  collider, Phys. Rev. D74 (2006) 014016.
- [434] M. N. Achasov, et al., Update of the  $e^+e^- \rightarrow \pi^+\pi^-$  cross section measured by SND detector in the energy region 400-MeV <  $s^{1/2}$  < 1000-MeV, J. Exp. Theor. Phys. 103 (2006) 380–384.
- [435] R. R. Akhmetshin, et al., First observation of the decay  $\phi \rightarrow \eta'(958)\gamma$ , Phys. Lett. B415 (1997) 445–451.
- [436] R. R. Akhmetshin, et al., Study of the radiative decay  $\phi \rightarrow \eta\gamma$  with CMD-2 detector, Phys. Lett. B460 (1999) 242–247.
- [437] R. R. Akhmetshin, et al., First observation of the  $\phi \rightarrow \pi^+\pi^-\gamma$  decay, Phys. Lett. B462 (1999) 371.
- [438] R. R. Akhmetshin, et al., Study of the  $\phi$  decays into  $\pi^0\pi^0\gamma$  and  $\eta\pi^0\gamma$  final states, Phys. Lett. B462 (1999) 380.
- [439] R. R. Akhmetshin, et al., Cross section of the reaction  $e^+e^- \rightarrow \pi^+\pi^-\pi^+\pi^-$  below 1 GeV at CMD-2, Phys. Lett. B475 (2000) 190–197.
- [440] R. R. Akhmetshin, et al., New measurement of the rare decay  $\phi \rightarrow \eta'\gamma$  with CMD-2, Phys. Lett. B473 (2000) 337–342.

- [441] R. R. Akhmetshin, et al., Measurement of omega meson parameters in  $\pi^+\pi^-\pi^0$  decay mode with CMD-2, Phys. Lett. B476 (2000) 33–39.
- [442] R. R. Akhmetshin, et al., Observation of the  $\phi \rightarrow \eta'\gamma$  decay with four charged particles and photons in the final state, Phys. Lett. B494 (2000) 26–32.
- [443] R. R. Akhmetshin, et al., Study of the process  $e^+e^- \rightarrow \eta\gamma$  in c.m. energy range 600-MeV - 1380-MeV at CMD-2, Phys. Lett. B509 (2001) 217–226.
- [444] R. R. Akhmetshin, et al., Measurement of  $e^+e^- \rightarrow \pi^+\pi^-$  cross section with CMD-2 around  $\rho$  meson, Phys. Lett. B527 (2002) 161–172.
- [445] R. R. Akhmetshin, et al., Observation of the  $\phi\pi^+\pi^-\pi^+\pi^-$  decay, Phys. Lett. B491 (2000) 81–89.
- [446] R. R. Akhmetshin, et al., Study of the process  $e^+e^- \rightarrow \pi^+\pi^-\pi^+\pi^-\pi^0$  with CMD-2 detector, Phys. Lett. B489 (2000) 125–130.
- [447] R. R. Akhmetshin, et al., Study of the process  $e^+e^- \rightarrow \omega\pi^0 \rightarrow \pi^0\pi^0\gamma$  in cm energy range 920-MeV - 1380-MeV at CMD-2, Phys. Lett. B562 (2003) 173–181.
- [448] R. R. Akhmetshin, et al., Reanalysis of hadronic cross section measurements at CMD-2, Phys. Lett. B578 (2004) 285–289.
- [449] R. R. Akhmetshin, et al., Total cross section of the process  $e^+e^- \rightarrow \pi^+\pi^-\pi^+\pi^-$  in the cm energy range 980-MeV - 1380-MeV, Phys. Lett. B595 (2004) 101–108.
- [450] M. N. Achasov, et al., Recent results of the study of hadronic production with the CMD-2 and SND detectors at the VEPP-2M collider, Eur. Phys. J. C33 (2004) s583–s585.
- [451] R. R. Akhmetshin, et al., Study of the  $\rho$  and  $\omega$  meson decays into pseudoscalar meson and  $e^+e^-$  pair with the CMD-2 detector, Phys. Lett. B613 (2005) 29–38.
- [452] R. R. Akhmetshin, et al., High-statistics measurement of the pion form factor in the  $\rho$ -meson energy range with the CMD-2 detector, Phys. Lett. B648 (2007) 28–38.
- [453] V. M. Aulchenko, et al., Measurement of the pion form factor in the energy range 1.04-GeV - 1.38-GeV with the CMD-2 detector, JETP Lett. 82 (2005) 743–747.
- [454] R. R. Akhmetshin, et al., Study of  $\phi \rightarrow \pi^+\pi^-\pi^0$  with CMD-2 detector, Phys. Lett. B642 (2006) 203–209.
- [455] R. R. Akhmetshin, et al., Measurement of the  $e^+e^- \rightarrow \pi^+\pi^-$  cross section with the CMD-2 detector in the 370-MeV - 520-MeV cm energy range, JETP Lett. 84 (2006) 413–417.
- [456] V. V. Anashin, et al., New precise determination of the tau lepton mass at KEDR detector. 9th International Workshop on Tau Lepton Physics (Tau06), Pisa, Italy, 19-22 Sep 2006. hep-ex/0611046.
- [457] V. M. Aulchenko, et al., New precision measurement of the  $J/\psi$  and  $\psi'$  meson masses, Phys. Lett. B573 (2003) 63–79.
- [458] F. Ambrosino, et al., Determination of CP and CPT violation parameters in the neutral kaon system using the Bell-Steinberger relation and data from the KLOE experiment, JHEP 12 (2006) 011.
- [459] M. Adinolfi, et al., The tracking detector of the KLOE experiment, Nucl. Instrum. Meth. A488 (2002) 51–73.
- [460] M. Adinolfi, et al., The KLOE electromagnetic calorimeter, Nucl. Instrum. Meth. A482 (2002) 364–386.
- [461] A. Aloisio, et al.,  $\eta, \eta'$  studies with the KLOE detector at DAPHNE, Phys. Scripta T99 (2002) 123–132.
- [462] A. Aloisio, et al., Study of the decay  $\phi \rightarrow \eta\pi^0\gamma$  with the KLOE detector, Phys. Lett. B536 (2002) 209–216.
- [463] A. Aloisio, et al., Study of the decay  $\phi \rightarrow \pi^0\pi^0\gamma$  with the KLOE detector, Phys. Lett. B537 (2002) 21–27.
- [464] A. Aloisio, et al., Measurement of  $\Gamma(\phi \rightarrow \eta'\gamma)/\Gamma(\phi \rightarrow \eta\gamma)$  and the pseudoscalar mixing angle, Phys. Lett. B541 (2002) 45–51.

- [465] A. Aloisio, et al., Determination of  $\sigma(e^+e^- \rightarrow \pi^+\pi^-)$  from radiative processes at DAPHNE, Eur. Phys. J. C33 (2004) s656–s658.
- [466] A. Aloisio, et al., Measurement of  $\sigma(e^+e^- \rightarrow \pi^+\pi^-\gamma)$  and extraction of  $\sigma(e^+e^- \rightarrow \pi^+\pi^-)$  below 1 GeV with the KLOE detector, Phys. Lett. B606 (2005) 12–24.
- [467] F. Ambrosino, et al., Study of the decay  $\phi \rightarrow f_0(980)\gamma \rightarrow \pi^+\pi^-\gamma$  with the KLOE detector, Phys. Lett. B634 (2006) 148–154.
- [468] F. Ambrosino, et al., Measurement of the pseudoscalar mixing angle and  $\eta'$  gluonium content with KLOE detector, Phys. Lett. B648 (2007) 267–273.
- [469] F. Ambrosino, et al., Dalitz plot analysis of  $e^+e^- \rightarrow \pi^0\pi^0\gamma$  events at  $\sqrt{(s)} \sim m_\phi$  with the KLOE detector, hep-ex/0609009.
- [470] L. Köpke, N. Wermes,  $J/\psi$  decays, Phys. Rept. 174 (1989) 67.
- [471] H. Albrecht, et al., Physics with ARGUS, Phys. Rept. 276 (1996) 223–405.
- [472] Z. Bai, et al., Partial wave analysis of  $J/\psi \rightarrow \gamma K_S^0 K^\pm \pi^\mp$ , Phys. Rev. Lett. 65 (1990) 2507–2510.
- [473] J. Z. Bai, et al., Partial wave analysis of  $J/\psi \rightarrow \gamma(K^+K^-\pi^0)$ , Phys. Lett. B440 (1998) 217–224.
- [474] J. Z. Bai, et al., Study of the P-wave charmonium state  $\chi_{cJ}$  in  $\psi(2S)$  decays, Phys. Rev. Lett. 81 (1998) 3091–3095.
- [475] J. Z. Bai, et al.,  $\psi(2S) \rightarrow \pi^+\pi^- J/\psi$  decay distributions, Phys. Rev. D62 (2000) 032002.
- [476] J. Z. Bai, et al., Partial wave analysis of  $J/\psi \rightarrow \gamma(K^+K^-\pi^+\pi^-)$ , Phys. Lett. B472 (2000) 200–206.
- [477] J. Z. Bai, et al., Partial wave analysis of  $J/\psi \rightarrow \gamma(\pi^+\pi^-\pi^+\pi^-)$ , Phys. Lett. B472 (2000) 207–214.
- [478] J. Z. Bai, et al., Charmonium decays to axialvector plus pseudoscalar mesons, Phys. Rev. Lett. 83 (1999) 1918–1921.
- [479] J. Z. Bai, et al., Partial wave analysis of  $J/\psi \rightarrow \gamma(\eta\pi^+\pi^-)$ , Phys. Lett. B446 (1999) 356–362.
- [480] G. Xu, The analysis of decay channels  $J/\psi \rightarrow \gamma\gamma V(\rho, \phi)$ , Nucl. Phys. A675 (2000) 337c–340c.
- [481] J. Z. Bai, et al., A measurement of the mass and full width of the  $\eta_c$  meson, Phys. Rev. D62 (2000) 072001.
- [482] J. Z. Bai, et al., Partial wave analysis of  $J/\psi \rightarrow \gamma(K^\pm K_S^0 \pi^\mp)$ , Phys. Lett. B476 (2000) 25–32.
- [483] J. Z. Bai, et al., Radiative decay of the  $\psi(2S)$  into two pseudoscalar mesons, Phys. Rev. D67 (2003) 032004.
- [484] J. Z. Bai, et al., Observation of a near-threshold enhancement in the  $p\bar{p}$  mass spectrum from radiative  $J/\psi \rightarrow \gamma p\bar{p}$  decays, Phys. Rev. Lett. 91 (2003) 022001.
- [485] J. Z. Bai, et al., Partial wave analyses of  $J/\psi \rightarrow \gamma K^+K^-$  and  $\gamma K_S^0 K_S^0$ , Phys. Rev. D68 (2003) 052003.
- [486] J. Z. Bai, et al., Measurements of  $\psi(2S)$  decays into vector - tensor final states, Phys. Rev. D69 (2004) 072001.
- [487] J. Z. Bai, et al., A study of  $J/\psi \rightarrow \gamma\gamma V(\rho, \phi)$  decays with the BESII detector, Phys. Lett. B594 (2004) 47–53.
- [488] J. Z. Bai, et al.,  $\psi(2S)$  decays into  $J/\psi$  plus two photons, Phys. Rev. D70 (2004) 012006.
- [489] J.-Z. Bai, et al., Evidence of  $\sigma$  particle in  $J/\psi \rightarrow \omega\pi\pi$ , High Energy Phys. Nucl. Phys. 28 (2004) 215–224.
- [490] M. Ablikim, et al., Study of  $\psi(2S)$  decays to  $X J/\psi$ , Phys. Rev. D70 (2004) 012003.
- [491] M. Ablikim, et al., Observation of a threshold enhancement in the  $p\bar{\Lambda}$  invariant mass spectrum, Phys. Rev. Lett. 93 (2004) 112002.
- [492] M. Ablikim, et al., The  $\sigma$  pole in  $J/\psi \rightarrow \omega\pi^+\pi^-$ , Phys. Lett. B598 (2004) 149–158.

- [493] M. Ablikim, et al., Evidence for  $f_0(980)$   $f_0(980)$  production in  $\chi_{c0}$  decays, Phys. Rev. D70 (2004) 092002.
- [494] M. Ablikim, et al., Study of  $J/\psi \rightarrow \omega K^+ K^-$ , Phys. Lett. B603 (2004) 138–145.
- [495] M. Ablikim, et al., Resonances in  $J/\psi \rightarrow \phi \pi^+ \pi^-$  and  $\phi K^+ K^-$ , Phys. Lett. B607 (2005) 243–253.
- [496] M. Ablikim, et al., Measurements of  $J/\psi$  decays into  $2(\pi^+ \pi^-)\eta$  and  $3(\pi^+ \pi^-)\eta$ , Phys. Lett. B610 (2005) 192–198.
- [497] M. Ablikim, et al., Observation of a resonance  $X(1835)$  in  $J/\psi \rightarrow \gamma \pi^+ \pi^- \eta'$ , Phys. Rev. Lett. 95 (2005) 262001.
- [498] M. Ablikim, et al., Search for  $\psi'' \rightarrow \rho \pi$  at BESII, Phys. Rev. D72 (2005) 072007.
- [499] M. Ablikim, et al., Evidence for  $\kappa$  meson production in  $J/\psi \rightarrow \bar{K}^*(892)^0 K^+ \pi^-$  process, Phys. Lett. B633 (2006) 681–690.
- [500] M. Ablikim, et al., Partial wave analysis of  $\psi' \rightarrow \pi^+ \pi^- \pi^0$  at BESII, Phys. Lett. B619 (2005) 247–254.
- [501] M. Ablikim, et al., Experimental study of  $\psi(2S)$  decays to  $K^+ K^- \pi^+ \pi^- \pi^0$  final states, Phys. Rev. D73 (2006) 052004.
- [502] H.-X. Yang, Observation of  $p\bar{p}$ ,  $p\bar{\Lambda}$ ,  $K^-\bar{\Lambda}$  near-threshold enhancement at BES, Int. J. Mod. Phys. A20 (2005) 1985–1989.
- [503] W.-G. Li, General review of BES physics, achievement and future, Int. J. Mod. Phys. A20 (2005) 1560–1567.
- [504] M. Ablikim, et al., Precise measurement of spin-averaged  $\chi_{cJ}(1P)$  mass using photon conversions in  $\psi(2S) \rightarrow \gamma \chi_{cJ}$ , Phys. Rev. D71 (2005) 092002.
- [505] M. Ablikim, Production of  $\sigma$  in  $\psi(2S) \rightarrow \pi^+ \pi^- J/\psi$ .
- [506] M. Ablikim, et al., Pseudoscalar production at  $\omega\omega$  threshold in  $J/\psi \rightarrow \gamma \omega\omega$ , Phys. Rev. D73 (2006) 112007.
- [507] M. Ablikim, et al., Partial wave analyses of  $J/\psi \rightarrow \gamma \pi^+ \pi^-$  and  $\gamma \pi^0 \pi^0$ , Phys. Lett. B642 (2006) 441–448.
- [508] M. Ablikim, et al., Observation of a near-threshold enhancement in the  $\omega\phi$  mass spectrum from the doubly OZI suppressed decay  $J/\psi \rightarrow \gamma \omega\phi$ , Phys. Rev. Lett. 96 (2006) 162002.
- [509] S. Jin, BESII results on hadron spectroscopy, Int. J. Mod. Phys. A21 (2006) 613–619.
- [510] M. Ablikim, et al., Observation of a broad  $1^{--}$  resonant structure around 1.5- GeV/c<sup>2</sup> in the  $K^+ K^-$  mass spectrum in  $J/\psi \rightarrow K^+ K^- \pi^0$ , Phys. Rev. Lett. 97 (2006) 142002.
- [511] M. Ablikim, et al., Precison measurements of the mass, the widths of  $\psi(3770)$  resonance and the cross section  $\sigma(e^+ e^- \rightarrow \psi(3770))$  at  $E_{cm} = 3.7724$ -GeV.
- [512] M. Ablikim, et al., Determination of the  $\psi(3770)$ ,  $\psi(4040)$ ,  $\psi(4160)$  and  $\psi(4415)$  resonance parameters. arxiv:0705.4500 [hep-ex], 2007.
- [513] J. Z. Bai, et al., The BES upgrade, Nucl. Instrum. Meth. A458 (2001) 627–637.
- [514] M. P. Alvarez, et al., Branching ratios and properties of D meson decays, Z. Phys. C50 (1991) 11–20.
- [515] M. Adamovich, et al., WA92: A fixed target experiment to trigger on and identify beauty particle decays, Nucl. Instrum. Meth. A379 (1996) 252–270.
- [516] M. I. Adamovich, et al., Determination of the total  $c\bar{c}$  production cross section in 340 GeV/c  $\Sigma$ - nucleus interactions, Eur. Phys. J. C13 (2000) 247–254.
- [517] P. L. Frabetti, et al., Description and performance of the Fermilab E687 spectrometer, Nucl. Instrum. Meth. A320 (1992) 519–547.
- [518] V. Arena, et al., Description and performance of the FOCUS (E831) hadron calorimeter, Nucl. Instrum. Meth. A434 (1999) 271–278.

- [519] J. C. Anjos, et al., Observation of excited charmed mesons, Phys. Rev. Lett. 62 (1989) 1717.
- [520] E. M. Aitala, et al., Study of the  $D_s^+ \rightarrow \pi^-\pi^+\pi^+$  decay and measurement of  $f^0$  masses and widths, Phys. Rev. Lett. 86 (2001) 765–769.
- [521] E. M. Aitala, et al., Experimental evidence for a light and broad scalar resonance in  $D^+ \rightarrow \pi^-\pi^+\pi^+$  decay, Phys. Rev. Lett. 86 (2001) 770–774.
- [522] E. M. Aitala, et al., Dalitz plot analysis of the decay  $D^+ \rightarrow K^-\pi^+\pi^+$  and study of the  $K\pi$  scalar amplitudes, Phys. Rev. Lett. 89 (2002) 121801.
- [523] E. M. Aitala, et al., Model independent measurement of S-wave  $K^-\pi^+$  systems using  $D^+ \rightarrow K\pi\pi$  decays from Fermilab E791, Phys. Rev. D73 (2006) 032004.
- [524] P. L. Frabetti, et al., Analysis of three  $D \rightarrow K\pi\pi$  Dalitz plots, Phys. Lett. B331 (1994) 217–226.
- [525] P. L. Frabetti, et al., Analysis of the  $D^+, D_s^+ \rightarrow K^+K^-\pi^+$  Dalitz plots, Phys. Lett. B351 (1995) 591–600.
- [526] P. L. Frabetti, et al., Analysis of the  $D^+, D_s^+ \rightarrow \pi^-\pi^+\pi^+$  Dalitz plots, Phys. Lett. B407 (1997) 79–91.
- [527] P. L. Frabetti, et al., Evidence for a narrow dip structure at  $1.9\text{-GeV}/c^2$  in  $3\pi^+3\pi^-$  diffractive photoproduction, Phys. Lett. B514 (2001) 240–246.
- [528] P. L. Frabetti, et al., On the narrow dip structure at  $1.9\text{-GeV}/c^2$  in diffractive photoproduction, Phys. Lett. B578 (2004) 290–296.
- [529] J. M. Link, et al., Measurement of masses and widths of excited charm mesons  $D_2^*$  and evidence for broad states, Phys. Lett. B586 (2004) 11–20.
- [530] J. M. Link, et al., Dalitz plot analysis of  $D_s^+$  and  $D^+$  decay to  $\pi^+\pi^-\pi^+$  using the K-matrix formalism, Phys. Lett. B585 (2004) 200.
- [531] S. Malvezzi, Light quark and charm interplay in the Dalitz-plot analysis of hadronic decays in FOCUS, AIP Conf. Proc. 688 (2004) 276–292.
- [532] J. M. Link, et al., Study of the doubly and singly Cabibbo suppressed decays  $D^+ \rightarrow K^+\pi^+\pi^-$  and  $D_s^+ \rightarrow K^+\pi^+\pi^-$ , Phys. Lett. B601 (2004) 10–19.
- [533] J. M. Link, et al., Study of the  $D^0 \rightarrow K^+K^-\pi^+\pi^-$  decay, Phys. Lett. B610 (2005) 225–234.
- [534] J. M. Link, et al., A study of  $D^0 \rightarrow K_S^0 K_S^0 X$  decay channels, Phys. Lett. B607 (2005) 59–66.
- [535] L. Benussi, Measurements of masses and widths of excited charm mesons  $D_2^*$ , evidence for broad states and observation of  $D_s(2317)^+$  from FOCUS experiment, Int. J. Mod. Phys. A20 (2005) 549–553.
- [536] J. M. Link, et al., Hadronic mass spectrum analysis of  $D^+ \rightarrow K^-\pi^+\mu^+\nu$  decay and measurement of the  $K^*(892)^0$  mass and width, Phys. Lett. B621 (2005) 72–80.
- [537] V. J. Smith, The SELEX experiment at Fermilab, AIP Conf. Proc. 432 (1998) 627–630.
- [538] V. V. Molchanov, et al., Radiative decay width of the  $a_2(1320)$ -meson, Phys. Lett. B521 (2001) 171–180.
- [539] A. V. Evdokimov, et al., First observation of a narrow charm-strange meson  $D_{sJ}(2632)^+ \rightarrow D_s^+\eta$  and  $D^0 K^+$ , Phys. Rev. Lett. 93 (2004) 242001.
- [540] V. M. Abazov, et al., Observation and properties of the  $X(3872)$  decaying to  $J/\psi\pi^+\pi^-$  in  $p\bar{p}$  collisions at  $\sqrt{s} = 1.96$  TeV, Phys. Rev. Lett. 93 (2004) 162002.
- [541] D. Acosta, et al., Observation of the narrow state  $X(3872) \rightarrow J/\psi\pi^+\pi^-$  in  $\bar{p}p$  collisions at  $\sqrt{s} = 1.96$  TeV, Phys. Rev. Lett. 93 (2004) 072001.
- [542] A. Abulencia, et al., Measurement of mass and width of the excited charmed meson states  $D_1^0$  and  $D_2^{*0}$ , Phys. Rev. D73 (2006) 051104.
- [543] A. Abulencia, et al., Measurement of the dipion mass spectrum in  $X(3872) \rightarrow J/\psi\pi^+\pi^-$  decays, Phys. Rev. Lett. 96 (2006) 102002.

- [544] D. Andrews, et al., The CLEO detector, Nucl. Instr. Meth. 211 (1983) 47.
- [545] Y. Kubota, et al., The CLEO-II detector, Nucl. Instrum. Meth. A320 (1992) 66–113.
- [546] S. E. Kopp, The CLEO III detector, Nucl. Instrum. Meth. A384 (1996) 61–66.
- [547] G. Viehhauser, The CLEO III upgrade, Nucl. Instrum. Meth. A446 (2000) 97–105.
- [548] R. A. Briere, First results from CLEO-c, Int. J. Mod. Phys. A20 (2005) 375–384.
- [549] D. Andrews, et al., Observation of three  $\Upsilon$  states, Phys. Rev. Lett. 44 (1980) 1108.
- [550] D. Andrews, et al., Observation of a fourth  $\Upsilon$  state in  $e^+e^-$  annihilations, Phys. Rev. Lett. 45 (1980) 219.
- [551] K. Berkelman,  $\Upsilon$  spectroscopy at CESR, Phys. Rept. 98 (1983) 145.
- [552] A. Chen, et al., Evidence for the F meson at 1970 MeV, Phys. Rev. Lett. 51 (1983) 634.
- [553] D. Besson, et al., Observation of new structure in the  $e^+e^-$  annihilation cross-section above  $B\bar{B}$  threshold, Phys. Rev. Lett. 54 (1985) 381.
- [554] P. Avery, et al., P wave charmed mesons in  $e^+e^-$  annihilation, Phys. Rev. D41 (1990) 774.
- [555] I. C. Brock, et al., Study of  $\pi^+\pi^-$  transitions from the  $\Upsilon(3S)$  and a search for the  $h_b$ , Phys. Rev. D43 (1991) 1448–1458.
- [556] F. Butler, et al., Analysis of hadronic transitions in  $\Upsilon(3S)$  decays, Phys. Rev. D49 (1994) 40–57.
- [557] Y. Kubota, et al., Observation of a new charmed strange meson, Phys. Rev. Lett. 72 (1994) 1972–1976.
- [558] T. Bergfeld, et al., Observation of  $D_1^+(2420)$  and  $D_2^{*+}(2460)$ , Phys. Lett. B340 (1994) 194–204.
- [559] J. P. Alexander, et al., The hadronic transitions  $\Upsilon(2S) \rightarrow \Upsilon(1S)$ , Phys. Rev. D58 (1998) 052004.
- [560] M. S. Alam, et al., Further search for the two-photon production of the glueball candidate  $f_J(2220)$ , Phys. Rev. Lett. 81 (1998) 3328–3332.
- [561] C. P. Jessop, et al., Study of charmless hadronic B meson decays to pseudoscalar vector final states, Phys. Rev. Lett. 85 (2000) 2881–2885.
- [562] S. Kopp, et al., Dalitz analysis of the decay  $D^0 \rightarrow K^-\pi^+\pi^0$ , Phys. Rev. D63 (2001) 092001.
- [563] H. Muramatsu, et al., Dalitz analysis of  $D^0 \rightarrow K_S^0\pi^+\pi^-$ , Phys. Rev. Lett. 89 (2002) 251802.
- [564] D. Besson, et al., Observation of a narrow resonance of mass 2.46-GeV/c<sup>2</sup> decaying to  $D_s^{*+}\pi^0$  and confirmation of the  $D_{sJ}^*(2317)$  state, Phys. Rev. D68 (2003) 032002.
- [565] V. V. Frolov, et al., A Dalitz plot analysis of  $D^0 \rightarrow \pi^-\pi^+\pi^-$  decays in CLEO II, EPS-208, Jun 2003. 8pp. hep-ex/0306048.
- [566] M. Artuso, et al., Charm meson spectra in  $e^+e^-$  annihilation at 10.5 GeV-cms, Phys. Rev. D70 (2004) 112001.
- [567] G. Bonvicini, et al., First observation of a  $\Upsilon(1D)$  state, Phys. Rev. D70 (2004) 032001.
- [568] P. Rubin, et al., First observation and Dalitz analysis of the  $D^0 \rightarrow K_S^0\eta\pi^0$  decay, Phys. Rev. Lett. 93 (2004) 111801.
- [569] N. E. Adam, et al., Observation of  $1^-0^-$  final states from  $\psi(2S)$  decays and  $e^+e^-$  annihilation, Phys. Rev. Lett. 94 (2005) 012005.
- [570] M. Artuso, et al., Photon transitions in  $\Upsilon(2S)$  and  $\Upsilon(3S)$  decays, Phys. Rev. Lett. 94 (2005) 032001.
- [571] P. Zweber, Search for X(3872) in  $\gamma\gamma$  fusion and ISR at CLEO, J. Phys. Conf. Ser. 9 (2005) 75–78.
- [572] N. E. Adam, et al., Observation of  $\psi(3770) \rightarrow \pi\pi J/\psi$  and measurement of  $\Gamma_{ee}(\psi(2S))$ , Phys. Rev. Lett. 96 (2006) 082004.

- [573] P. Rubin, et al., Observation of the  ${}^1P_1$  state of charmonium, Phys. Rev. D72 (2005) 092004.
- [574] T. Skwarnicki, Recent CLEO results on hadron spectroscopy, Acta Phys. Polon. B36 (2005) 2329–2340.
- [575] J. L. Rosner, et al., Observation of  $h_c({}^1P_1)$  state of charmonium, Phys. Rev. Lett. 95 (2005) 102003.
- [576] M. Dubrovin, Dalitz analyses at CLEO-c, J. Phys. Conf. Ser. 9 (2005) 171–175.
- [577] D. Besson, et al., Radiative decays of the  $\Upsilon(1S) \rightarrow \gamma\pi^0\pi^0$ , and  $\gamma\eta\eta$  and  $\gamma\pi^0\eta$ , Phys. Rev. D75 (2007) 072001.
- [578] R. Ahohe, et al., The search for  $\eta(1440) \rightarrow K_S^0 K^\pm \pi^\mp$  in two-photon fusion at CLEO, Phys. Rev. D71 (2005) 072001.
- [579] S. B. Athar, et al.,  $\chi_{cJ}$  decays to  $h^+h^-h^0$ , Phys. Rev. D75 (2007) 032002.
- [580] C. Cawlfieid, et al., Measurement of interfering  $K^{*+}K^-$  and  $K^{*-}K^+$  amplitudes in the decay  $D^0 \rightarrow K^+K^-\pi^0$ , Phys. Rev. D74 (2006) 031108.
- [581] G. S. Adams,  $\chi_{c0}$  and  $\chi_{c2}$  decays into  $\eta\eta$ ,  $\eta\eta'$ , and  $\eta'\eta'$  final states, Phys. Rev. D75 (2007) 071101.
- [582] Q. He, et al., Confirmation of the  $Y(4260)$  resonance production in ISR, Phys. Rev. D74 (2006) 091104.
- [583] T. E. Coan, et al., Charmonium decays of  $Y(4260)$ ,  $\psi(4160)$ , and  $\psi(4040)$ , Phys. Rev. Lett. 96 (2006) 162003.
- [584] C. Cawlfieid, et al., A precision determination of the  $D^0$  mass, Phys. Rev. Lett. 98 (2007) 092002.
- [585] G. Bonvicini, et al., Dalitz plot analysis of the  $D^+ \rightarrow \pi^-\pi^+\pi^+$  decay, arxiv:0704.3954 [hep-ex].
- [586] B. Aubert, et al., The BaBar detector, Nucl. Instrum. Meth. A479 (2002) 1–116.
- [587] R. Bartoldus, BABAR non-CP physics results, Nucl. Instrum. Meth. A462 (2001) 66–76.
- [588] B. Aubert, et al., Observation of a narrow meson decaying to  $D_s^+\pi^0$  at a mass of  $2.32 \text{ GeV}/c^2$ , Phys. Rev. Lett. 90 (2003) 242001.
- [589] B. Aubert, et al., Observation of a narrow meson decaying to  $D_s^+\pi^0\gamma$  at a mass of  $2.458 \text{ GeV}/c^2$ , Phys. Rev. D69 (2004) 031101.
- [590] B. Aubert, et al., Measurements of the mass and width of the  $\eta_c$  meson and of an  $\eta_c(2s)$  candidate, Phys. Rev. Lett. 92 (2004) 142002.
- [591] P. Krokovny, et al., Observation of the  $D_{sJ}(2317)$  and  $D_{sJ}(2457)$  in B decays, Phys. Rev. Lett. 91 (2003) 262002.
- [592] B. Aubert, et al., Observation of the decay  $B \rightarrow J/\psi\eta K$  and search for  $X(3872) \rightarrow J/\psi\eta$ , Phys. Rev. Lett. 93 (2004) 041801.
- [593] B. Aubert, et al., Study of  $e^+e^- \rightarrow \pi^+\pi^-\pi^0$  process using initial state radiation with BaBar, Phys. Rev. D70 (2004) 072004.
- [594] B. Aubert, et al., Search for the  $D_{sJ}^{*+}(2632)$  at BaBaR, International Conference on High-Energy Physics (ICHEP 04), Beijing, China. hep-ex/0408087.
- [595] B. Aubert, et al., Study of the  $B \rightarrow J/\psi K^-\pi^+\pi^-$  decay and measurement of the  $B \rightarrow X(3872)K^-$  branching fraction, Phys. Rev. D71 (2005) 071103.
- [596] B. Aubert, et al., Study of  $B \rightarrow D_{sJ}^{(*)+}\bar{D}^{(*)}$  decays, Phys. Rev. Lett. 93 (2004) 181801.
- [597] E. Robutti, Recent BaBar results in charmonium and charm spectroscopy, Eur. Phys. J. C33 (2004) s551–s553.
- [598] B. Aubert, et al., Search for a charged partner of the  $X(3872)$  in the  $B$  meson decay  $B \rightarrow X^-K, X^- \rightarrow J/\psi\pi^-\pi^0$ , Phys. Rev. D71 (2005) 031501.
- [599] B. Aubert, et al., A study of  $e^+e^- \rightarrow p\bar{p}$  using initial state radiation with BaBar, Phys. Rev. D73 (2006) 012005.

- [600] B. Aubert, et al., Dalitz-plot analysis of the decays  $B^\pm \rightarrow K^\pm\pi^\mp\pi^\pm$ , Phys. Rev. D72 (2005) 072003.
- [601] B. Aubert, et al., The  $e^+e^- \rightarrow \pi^+\pi^-\pi^+\pi^-$ ,  $K^+K^-\pi^+\pi^-$ , and  $K^+K^-K^+K^-$  cross sections at center-of-mass energies 0.5-GeV - 4.5-GeV measured with initial-state radiation, Phys. Rev. D71 (2005) 052001.
- [602] B. Aubert, et al., Measurement of the  $B^+ \rightarrow p\bar{p}K^+$  branching fraction and study of the decay dynamics, Phys. Rev. D72 (2005) 051101.
- [603] Z. Yu, Dalitz plot analyses of charmless B decays, Int. J. Mod. Phys. A20 (2005) 3559–3561.
- [604] B. Aubert, et al., Measurement of  $\gamma$  in  $B^\pm \rightarrow D^{(*)}K^\pm$  decays with a Dalitz analysis of  $D \rightarrow K_S^0\pi^-\pi^+$ , Phys. Rev. Lett. 95 (2005) 121802.
- [605] B. Aubert, et al., Dalitz plot study of  $B^0 \rightarrow K^+K^-K_S^0$  decays, International Europhysics Conference on High Energy Physics (HEP-EPS 2005), Lisbon, Portugal, 21-27 Jul 2005.
- [606] B. Aubert, et al., Observation of a broad structure in the  $\pi^+\pi^-J/\psi$  mass spectrum around 4.26-GeV/c<sup>2</sup>, Phys. Rev. Lett. 95 (2005) 142001.
- [607] E. Robutti, Recent BaBar results on hadron spectroscopy, Acta Phys. Polon. B36 (2005) 2315–2328.
- [608] B. Aubert, et al., An amplitude analysis of the decay  $B^\pm \rightarrow \pi^\pm\pi^\pm\pi^\mp$ , Phys. Rev. D72 (2005) 052002.
- [609] B. Aubert, et al., Dalitz plot analysis of  $D^0 \rightarrow \bar{K}^0K^+K^-$ , Phys. Rev. D72 (2005) 052008.
- [610] B. Aubert, et al., Measurement of double charmonium production in  $e^+e^-$  annihilations at  $\sqrt{s} = 10.6$  GeV, Phys. Rev. D72 (2005) 031101.
- [611] B. Aubert, et al., Measurements of the absolute branching fractions of  $B^\pm \rightarrow K^\pm X_{c\bar{c}}$ , Phys. Rev. Lett. 96 (2006) 052002.
- [612] B. Aubert, et al., Measurements of neutral B decay branching fractions to  $K_S^0\pi^+\pi^-$  final states and the charge asymmetry of  $B^0 \rightarrow K^{*+}\pi^-$ , Phys. Rev. D73 (2006) 031101.
- [613] B. Aubert, et al., Measurement of  $\gamma$  in  $B^\mp \rightarrow D^*K^\mp$  and  $B^\mp \rightarrow DK^{*\mp}$  decays with a Dalitz analysis of  $D \rightarrow K_S\pi^-\pi^+$ , International Europhysics Conference on High-Energy Physics (HEP 2005), Lisbon, Portugal, 21-27 Jul 2005. hep-ex/0507101.
- [614] B. Aubert, et al., Study of  $J/\psi\pi^+\pi^-$  states produced in  $B^0 \rightarrow J/\psi\pi^+\pi^-K^0$  and  $B^- \rightarrow J/\psi\pi^+\pi^-K^-$ , Phys. Rev. D73 (2006) 011101.
- [615] B. Aubert, Search for  $B^+ \rightarrow X(3872)K^+$ ,  $X(3872) \rightarrow J/\psi\gamma$ , Phys. Rev. D74 (2006) 071101.
- [616] B. Aubert, et al., A study of the  $D_{sJ}^{*+}(2317)$  and  $D_{sJ}^+(2460)$  mesons in inclusive  $c\bar{c}$  production near  $\sqrt{s} = 10.6$  GeV, Phys. Rev. D74 (2006) 032007.
- [617] B. Aubert, et al., Observation of  $\Upsilon(4S)$  decays to  $\pi^+\pi^-\Upsilon(1S)$  and  $\pi^+\pi^-\Upsilon(2S)$ , Phys. Rev. Lett. 96 (2006) 232001.
- [618] B. Aubert, A structure at 2175 MeV in  $e^+e^- \rightarrow \phi f_0(980)$  observed via initial-state radiation, Phys. Rev. D74 (2006) 091103.
- [619] B. Aubert, et al., The  $e^+e^- \rightarrow 3(\pi^+\pi^-)$ ,  $2(\pi^+\pi^-\pi^0)$  and  $K^+K^-2(\pi^+\pi^-)$  cross sections at center-of-mass energies from production threshold to 4.5-GeV measured with initial-state radiation, Phys. Rev. D73 (2006) 052003.
- [620] B. Aubert, Observation of a new  $D_s$  meson decaying to  $DK$  at a mass of 2.86 GeV/c<sup>2</sup>, Phys. Rev. Lett. 97 (2006) 222001.
- [621] B. Aubert, et al., Dalitz plot analysis of the decay  $B^\pm \rightarrow K^\pm K^\pm K^\mp$ , Phys. Rev. D74 (2006) 032003.
- [622] B. Aubert, Measurements of the decays  $B^0 \rightarrow \bar{D}^0p\bar{p}$ ,  $B^0 \rightarrow \bar{D}^{*0}p\bar{p}$ ,  $B^0 \rightarrow D^-p\bar{p}\pi^+$ , and  $B^0 \rightarrow D^{*-}p\bar{p}\pi^+$ , Phys. Rev. D74 (2006) 051101.
- [623] B. Aubert, et al., Amplitude analysis of the decay  $D^0 \rightarrow K^-K^+\pi^0$ , arxiv:0704.3593 [hep-ex], (2007).

- [624] B. Aubert, et al., Search for neutral B-meson decays to  $a_0\pi$ ,  $a^0K$ ,  $\eta\rho^0$ , and  $\eta f_0$ . ep-ex/0703038.
- [625] B. Aubert, et al., The  $e^+e^- \rightarrow k^+k^-\pi^+\pi^-$ ,  $k^+k^-\pi^0\pi^0$  and  $k^+k^-k^+k^-$  cross sections measured with initial-state radiation, Phys. Rev. D76 (2007) 012008.
- [626] B. collaboration, Study of resonances in exclusive  $B$  decays to  $\bar{D}^*D^*K$  arxiv:0708.1565 [hep-ex], 2007.
- [627] Observation of a resonance-like structure in the  $\pi^\pm\psi'$  mass distribution in exclusive  $B \rightarrow K\pi^\pm\psi'$  decays. arxiv:0708.1790 [hep-ex] (2207).
- [628] T. Iijima, E. Prebys, Commissioning and first results from BELLE, Nucl. Instrum. Meth. A446 (2000) 75–83.
- [629] H. J. Kim, Non-CP physics at Belle, Nucl. Instrum. Meth. A462 (2001) 84–91.
- [630] K. Abe, et al., Observation of  $B^\pm \rightarrow p\bar{p}K^\pm$ , Phys. Rev. Lett. 88 (2002) 181803.
- [631] K. Abe, et al., Observation of  $\bar{B}^0 \rightarrow D^{*0}p\bar{p}$ , Phys. Rev. Lett. 89 (2002) 151802.
- [632] K. Abe, et al., Study of three-body charmless B decays, Phys. Rev. D65 (2002) 092005.
- [633] A. Garmash, et al., Study of B meson decays to three-body charmless hadronic final states, Phys. Rev. D69 (2004) 012001.
- [634] K. Abe, et al., Measurements of the  $D_{sJ}$  resonance properties, Phys. Rev. Lett. 92 (2004) 012002.
- [635] S. K. Choi, et al., Observation of a new narrow charmonium state in exclusive  $B^\pm \rightarrow K^\pm\pi^+\pi^-J/\psi$  decays, Phys. Rev. Lett. 91 (2003) 262001.
- [636] M. Z. Wang, et al., Observation of  $B^+ \rightarrow p\bar{p}\pi^+$ ,  $B^0 \rightarrow p\bar{p}K^0$ , and  $B^+ \rightarrow p\bar{p}K^{*+}$ , Phys. Rev. Lett. 92 (2004) 131801.
- [637] K. Abe, et al., Measurement of  $K^+K^-$  production in two-photon collisions in the resonant-mass region, Eur. Phys. J. C32 (2003) 323–336.
- [638] K. Abe, et al., Study of  $B^- \rightarrow D^{**0}\pi^- (D^{**0} \rightarrow D^* + \pi^-)$  decays, Phys. Rev. D69 (2004) 112002.
- [639] M. Z. Wang, et al., Observation of  $B^0 \rightarrow p\bar{\Lambda}\pi^-$ , Phys. Rev. Lett. 90 (2003) 201802.
- [640] Y. J. Lee, et al., Observation of  $B^+ \rightarrow \Lambda\bar{\Lambda}K^+$ , Phys. Rev. Lett. 93 (2004) 211801.
- [641] A. Garmash, et al., Dalitz analysis of the three-body charmless decays  $B^+ \rightarrow K^+\pi^+\pi^-$  and  $B^+ \rightarrow K^+K^+K^-$ , Phys. Rev. D71 (2005) 092003.
- [642] K. Abe, et al., Observation of a near-threshold  $\omega J/\psi$  mass enhancement in exclusive  $B \rightarrow K\omega J/\psi$  decays, Phys. Rev. Lett. 94 (2005) 182002.
- [643] M. Z. Wang, et al., Study of the baryon antibaryon low-mass enhancements in charmless three-body baryonic B decays, Phys. Lett. B617 (2005) 141–149.
- [644] K. Abe, et al., Observation of a new charmonium state in double charmonium production in  $e^+e^-$  annihilation at  $\sqrt{s} \sim 10.6$  GeV. international europhysics conference on high energy physics (hep-eps 2005), lisbon, portugal, 21-27 jul 2005. hep-ex/0507019.
- [645] K. Abe, et al., Evidence for  $X(3872) \rightarrow \gamma J/\psi$  and the sub-threshold decay  $X(3872) \rightarrow \omega J/\psi$ . 22nd International Symposium on Lepton-Photon Interactions at High Energy (LP 2005), Uppsala, Sweden, + 30 Jun - 5 Jul 2005. hep-ex/0505037.
- [646] K. Abe, et al., Experimental constraints on the possible  $J^{PC}$  quantum numbers of the X(3872)22nd International Symposium on Lepton-Photon Interactions at High Energy (LP 2005), Uppsala, Sweden, 30 Jun - 5 Jul 2005, hep-ex/0505038.
- [647] C.-C. Kuo, et al., Measurement of  $\gamma\gamma \rightarrow p\bar{p}$  production at Belle, Phys. Lett. B621 (2005) 41–55.
- [648] Q. L. Xie, et al., Observation of  $B^- \rightarrow J/\psi\Lambda\bar{p}$  and searches for  $B^- \rightarrow J/\psi\Sigma^0\bar{p}$  and  $B^0 \rightarrow J/\psi p\bar{p}$  decays, Phys. Rev. D72 (2005) 051105.

- [649] T. Ziegler, Double charmonium production and an X(3940), *J. Phys. Conf. Ser.* 9 (2005) 104–107.
- [650] R. Chistov, et al., Observation of  $B^+ \rightarrow \bar{\Xi}_c^0 \Lambda_c^+$  and evidence for  $B^0 \rightarrow \bar{\Xi}_c^- \Lambda_c^+$ , hep-ex/0510074, *Phys. Rev. D*74 (2006) 111105.
- [651] A. Drutskoy, et al., Observation of  $\bar{B}^0 \rightarrow D^* s J(2317)^+ K^-$  decay, *Phys. Rev. Lett.* 94 (2005) 061802.
- [652] A. Drutskoy, What are the  $D_{sJ}$  and X(3872) particles?, *Int. J. Mod. Phys. A*20 (2005) 3768–3770.
- [653] K. Abe, Study of the Y(4260) resonance in  $e^+e^-$  collisions with initial state radiation at Belle. 33rd International Conference on High Energy Physics (ICHEP 06), Moscow, Russia, 26 Jul - 2 Aug 2006. hep-ex/0612006 .
- [654] T. Mori, et al., High statistics study of  $f_0(980)$  resonance in  $\gamma\gamma \rightarrow \pi^+\pi^-$  production, *Phys. Rev. D*75 (2007) 051101.
- [655] W. T. Chen, S. Uehara, Measurements of  $\gamma\gamma \rightarrow K_S^0 K_S^0$  and charmonium production at BELLE, *Acta Phys. Polon. B*37 (2006) 887–892.
- [656] A. Sokolov, et al., Observation of the decay  $v(4s) \rightarrow v(1s)\pi^+\pi^-$ , *Phys. Rev. D*75 (2007) 071103.
- [657] K. Abe, et al., Observation of a new  $D_{sJ}$  meson in  $B^+ \rightarrow \bar{D}^0 D^0 K^+$  decays, 33rd International Conference on High Energy Physics (ICHEP 06), Moscow, Russia. hep-ex/0608031.
- [658] J. Brodzicka, et al., Observation of a new  $d_{sJ}$  meson in  $b^+ \rightarrow d^0 \bar{D}^0 k^+$  decays. arxiv:0707.3491 [hep-ex], 2007.
- [659] M. Z. Wang, et al., Study of  $B^+ \rightarrow p\bar{\Lambda}\gamma, p\bar{\Lambda}\pi^0$  and  $B^0 \rightarrow p\Lambda\pi^-$ . arxiv:0704.2672 [hep-ex], (2007).
- [660] T. Mori, et al., High statistics measurement of the cross sections of  $\gamma\gamma \rightarrow \pi^+\pi^-$  production, arxiv:0704.3538 [hep-ex], (2007).
- [661] K. Abe, et al., Observation of new charmonium state in double charmonium production in  $e^+e^-$  annihilation at  $\sqrt{s} \sim 10.6$  GeV, *Phys. Rev. Lett.* 98 (2007) 082001.
- [662] X. L. Wang, et al., Observation of two resonant structures in  $e^+e^- \rightarrow \pi^+\pi^-\psi(2s)$  via initial state radiation at Belle, arxiv:0707.3699 [hep-ex], 2007.
- [663] D. Decamp, et al., ALEPH: A detector for electron - positron annihilations at LEP, *Nucl. Instrum. Meth. A*294 (1990) 121–178.
- [664] D. Buskulic, et al., Production of excited beauty states in Z decays, *Z. Phys. C*69 (1996) 393–404.
- [665] D. Buskulic, et al., Production of orbitally excited charm mesons in semileptonic B decays, *Z. Phys. C*73 (1997) 601–612.
- [666] R. Barate, et al., Resonant structure and flavour tagging in the  $B\pi^\pm$  system using fully reconstructed B decays, *Phys. Lett. B*425 (1998) 215–226.
- [667] M. McNeil, Search for  $B_c$  and  $\Upsilon$  in hadronic Z decays, *Int. J. Mod. Phys. A*12 (1997) 3921–3930.
- [668] F. Muheim,  $B$  and  $D$  spectroscopy at LEP, in: H. W. Cheung, J. N. Butler (Eds.), Proceedings of the 4th Workshop on Heavy Quarks at Fixed Target (HQ 98), Batavia, IL, U.S.A., no. 459 in AIP Conference Proceedings, Springer, 1998, pp. 399–408.
- [669] R. Barate, et al., Search for the glueball candidates  $f_0(1500)$  and  $f_j(1710)$  in  $\gamma\gamma$  collisions, *Phys. Lett. B*472 (2000) 189–199.
- [670] A. Heister, et al., Production of  $D_s^{**}$  mesons in hadronic Z decays, *Phys. Lett. B*526 (2002) 34–49.
- [671] P. Bartalini, Spectroscopy of b and c hadrons at LEP, *Nucl. Phys. Proc. Suppl.* 109B (2002) 106–111.
- [672] I. Pal, Studies of two-photon collisions at LEP2, *Eur. Phys. J. C*33 (2004) s442–s444.
- [673] P. A. Aarnio, et al., The DELPHI detector at LEP, *Nucl. Instrum. Meth. A*303 (1991) 233–276.
- [674] P. Abreu, et al., Evidence for  $B_s^0$  meson production in  $Z^0$  decays, *Phys. Lett. B*289 (1992) 199–210.

- [675] P. Abreu, et al., Observation of orbitally excited  $B$  mesons, Phys. Lett. B345 (1995) 598–608.
- [676] P. Abreu, et al., Search for the  $B_c$  meson, Phys. Lett. B398 (1997) 207–222.
- [677] P. Abreu, et al., A study of the hadronic resonance structure in the decay  $\tau \rightarrow 3\pi + \nu_\tau$ , Phys. Lett. B426 (1998) 411–427.
- [678] P. Abreu, et al., First evidence for a charm radial excitation,  $D^*$ , Phys. Lett. B426 (1998) 231–242.
- [679] J. Abdallah, et al., The  $\eta_c(2980)$  formation in two-photon collisions at LEP energies, Eur. Phys. J. C31 (2003) 481–489.
- [680] B. Adeva, et al., The construction of the L3 experiment, Nucl. Instrum. Meth. A289 (1990) 35–102.
- [681] O. Adriani, et al.,  $\chi_c$  production in hadronic  $Z$  decays, Phys. Lett. B317 (1993) 467–473.
- [682] M. Acciarri, et al., Study of the  $K_s^0 K_s^0$  final state in two photon collisions, Phys. Lett. B363 (1995) 118–126.
- [683] M. Acciarri, et al., Resonance formation in the  $\pi^+ \pi^- \pi^0$  final state in two-photon collisions, Phys. Lett. B413 (1997) 147–158.
- [684] M. Acciarri, et al., Measurement of  $\eta'(958)$  formation in two-photon collisions at LEP1, Phys. Lett. B418 (1998) 399–410.
- [685] M. Acciarri, et al.,  $\chi_{c2}$  formation in two-photon collisions at LEP, Phys. Lett. B453 (1999) 73–82.
- [686] M. Acciarri, et al., Measurement of the spectroscopy of orbitally excited B mesons at LEP, Phys. Lett. B465 (1999) 323–334.
- [687] M. Acciarri, et al., Light resonances in  $K_s^0 K^\pm \pi^\mp$  and  $\eta \pi^+ \pi^-$  final states in  $\gamma\gamma$  collisions at LEP, Phys. Lett. B501 (2001) 1–11.
- [688] P. Achard, et al.,  $f_1(1285)$  formation in two photon collisions at LEP, Phys. Lett. B526 (2002) 269–277.
- [689] P. Achard, et al., Measurement of exclusive  $\rho^0 \rho^0$  production in two-photon collisions at high  $Q^2$  at LEP, Phys. Lett. B568 (2003) 11–22.
- [690] P. Achard, et al., Measurement of exclusive  $\rho^+ \rho^-$  production in high- $Q^2$  two-photon collisions at LEP, Phys. Lett. B597 (2004) 26–38.
- [691] P. Achard, et al., Measurement of exclusive  $\rho^0 \rho^0$  production in mid-virtuality two-photon interactions at LEP, Phys. Lett. B604 (2004) 48–60.
- [692] P. Achard, et al., Measurement of exclusive  $\rho^+ \rho^-$  production in mid-virtuality two-photon interactions and study of the  $\gamma\gamma^* \rightarrow \rho\rho$  process at LEP, Phys. Lett. B615 (2005) 19–30.
- [693] I. Vorobev, Analysis of  $K_S^0 K_S^0$  and  $\pi^+ \pi^- \pi^0$  final states in two photon collisions at LEP, Eur. Phys. J. C33 (2004) 569–571.
- [694] K. Ahmet, et al., The OPAL detector at LEP, Nucl. Instrum. Meth. A305 (1991) 275–319.
- [695] G. Alexander, et al., A study of  $D^{*\pm}$  production in  $Z^0$  decays, Phys. Lett. B262 (1991) 341–350.
- [696] P. D. Acton, et al., Evidence for the existence of the strange b flavored meson  $B_s^0$  in  $Z^0$  decays, Phys. Lett. B295 (1992) 357–370.
- [697] K. Ackerstaff, et al., Production of  $\chi_{c2}$  mesons in photon photon collisions at LEP, Phys. Lett. B439 (1998) 197–208.
- [698] M. Thiergen, B spectroscopy and glueball searches with the OPAL detector at LEP, Nucl. Phys. A675 (2000) 385c–390c.
- [699] G. Abbiendi, et al., A search for a radial excitation of the  $D^{*\pm}$  meson, Eur. Phys. J. C20 (2001) 445–454.
- [700] T. Regge, Introduction to complex orbital momenta, Nuovo Cim. 14 (1959) 951.

- [701] T. Regge, Bound states, shadow states and Mandelstam representation, *Nuovo Cim.* 18 (1960) 947–956.
- [702] M. Froissart, Asymptotic behavior and subtractions in the Mandelstam representation, *Phys. Rev.* 123 (1961) 1053–1057.
- [703] I. Pomeranchuk, *Zh. Exp. Theor. Fiz. [Sov. Phys. JETP]* 7 499 (1958) 34 (1958) 725.
- [704] K. A. Ter-Martirosyan, Multiple rescattering at high energy particle interaction, *Sov. J. Nucl. Phys.* 10 (1970) 600–608.
- [705] S. Donnachie, G. Dosch, O. Nachtmann, P. Landshoff, Pomeron physics and QCD, *Cambridge Monogr. Part. Phys. Nucl. Phys. Cosmol.* 19 (2002) 1–347.
- [706] M. S. Chanowitz, Resonances in photon-photon scattering, in: R. L. Lander (Ed.), *Proceedings of the 6th Int. Workshop on Photon-Photon Collisions*, Lake Tahoe, CA, Sep 10-13, 1984, World Scientific, Singapore, 1985, p. 95.
- [707] F. E. Close, G. R. Farrar, Z.-p. Li, Determining the gluonic content of isoscalar mesons, *Phys. Rev. D* 55 (1997) 5749–5766.
- [708] H. P. Paar, Study of the glueball candidate  $f_J(2220)$  at CLEO, *Nucl. Phys. Proc. Suppl.* 82 (2000) 337–343.
- [709] A. B. Kaidalov, V. A. Khoze, A. D. Martin, M. G. Ryskin, Central exclusive diffractive production as a spin parity analyser: From hadrons to Higgs, *Eur. Phys. J. C* 31 (2003) 387–396.
- [710] S. N. Ganguli, D. P. Roy, Regge phenomenology of inclusive reactions. Tata Institute of Fundamental Research, report TIFR-BC-80-2 (1980) unpublished.
- [711] D. Robson, A basic guide for the glueball spotter, *Nucl. Phys. B* 130 (1977) 328.
- [712] F. E. Close, Gluonic hadrons, *Rept. Prog. Phys.* 51 (1988) 833.
- [713] F. E. Close, A. Kirk, Implications of the glueball  $q\bar{q}$  filter on the  $1^{++}$  nonet, *Z. Phys. C* 76 (1997) 469–474.
- [714] A. Kirk, Resonance production in central p p collisions at the CERN Omega spectrometer, *Phys. Lett. B* 489 (2000) 29–37.
- [715] A. Donnachie, P. V. Landshoff, Small x: Two pomerons!, *Phys. Lett. B* 437 (1998) 408–416.
- [716] F. E. Close, Filtering glueball from  $q\bar{q}$  production in proton proton or double tagged  $e^+e^- \rightarrow e^+e^-R$  and implications for the spin structure of the Pomeron, *Phys. Lett. B* 419 (1998) 387–392.
- [717] F. E. Close, A. Kirk, A glueball  $q\bar{q}$  filter in central hadron production, *Phys. Lett. B* 397 (1997) 333–338.
- [718] F. E. Close, G. A. Schuler, Central production of mesons: Exotic states versus Pomeron structure, *Phys. Lett. B* 458 (1999) 127–136.
- [719] F. E. Close, G. A. Schuler, Evidence that the Pomeron transforms as a non-conserved vector current, *Phys. Lett. B* 464 (1999) 279–285.
- [720] F. E. Close, A. Kirk, G. Schuler, Dynamics of glueball and  $q\bar{q}$  production in the central region of p p collisions, *Phys. Lett. B* 477 (2000) 13–18.
- [721] F. E. Close, A. Kirk, The mixing of the  $f_0(1370)$ ,  $f_0(1500)$  and  $f_0(1710)$  and the search for the scalar glueball, *Phys. Lett. B* 483 (2000) 345–352.
- [722] V. A. Petrov, R. A. Ryutin, A. E. Sobol, J. P. Guillaud, Azimuthal angular distributions in EDDE as spin-parity analyser and glueball filter for LHC, *JHEP* 06 (2005) 007.
- [723] R. T. Deck, Kinematical interpretation of the first  $\pi - \rho$  resonance, *Phys. Rev. Lett.* 13 (1964) 169–173.
- [724] M. G. Bowler, A simple analytic treatment of rescattering effects in the Deck model, *J. Phys. G* 5 (1979) 203.
- [725] J. R. Ellis, M. Karliner, D. E. Kharzeev, M. G. Sapozhnikov, Abundant  $\phi$  meson production in  $\bar{p}p$  annihilation at rest and strangeness in the nucleon, *Phys. Lett. B* 353 (1995) 319–328.

- [726] M. P. Locher, Y. Lu, Rescattering mechanisms for  $\bar{p}p \rightarrow \phi X$  and the OZI rule reexamined, Z. Phys. A351 (1995) 83–87.
- [727] A. V. Anisovich, E. Klempert,  $\phi\pi$  production in  $\bar{p}p$  annihilation from S and P states and in  $J/\psi$  decays, Z. Phys. A354 (1996) 197–208.
- [728] A. Donnachie, Low-energy hadronic physics, Phys. Rept. 403-404 (2004) 281–301.
- [729] E. Klempert, F. Bradamante, A. Martin, J. M. Richard, Antinucleon nucleon interaction at low energy: Scattering and protonium, Phys. Rept. 368 (2002) 119–316.
- [730] E. Klempert, C. Batty, J.-M. Richard, The antinucleon nucleon interaction at low energy: Annihilation dynamics, Phys. Rept. 413 (2005) 197–317.
- [731] A. Abele, et al., Test of  $N\bar{N}$  potential models: Isospin relations in  $\bar{p}d$  annihilations at rest and the search for quasinuclear bound states, Eur. Phys. J. C17 (2000) 583–592.
- [732] C. Amsler, et al., Anti-proton - proton annihilation at rest into two-body final states, Z. Phys. C58 (1993) 175–190.
- [733] W. M. Dunwoodie, Strange meson and strangeonium spectroscopy: Introduction, Nucl. Phys. Proc. Suppl. 21 (1991) 3–4.
- [734] W. M. Dunwoodie, The status of strange meson spectroscopy, Nucl. Phys. Proc. Suppl. 21 (1991) 16–24.
- [735] D. Coffman, et al., Measurements of  $J/\psi$  decays into a vector and a pseudoscalar meson [Erratum-ibid. D 40, 3788 (1989)], Phys. Rev. D38 (1988) 2695–2705.
- [736] J. Jousset, et al., The  $J/\psi \rightarrow$  vector + pseudoscalar decays and the  $\eta, \eta'$  quark content, Phys. Rev. D41 (1990) 1389.
- [737] S. K. Choi, et al., Observation of the  $\eta_c(2S)$  in exclusive  $B \rightarrow KK_SK^-\pi^+$  decays, Phys. Rev. Lett. 89 (2002) 102001.
- [738] D. M. Asner, et al., Observation of  $\eta'_c$  production in  $\gamma\gamma$  fusion at CLEO, Phys. Rev. Lett. 92 (2004) 142001.
- [739] M. Gronau, Y. Grossman, G. Raz, J. L. Rosner, Suppression of flavor symmetry breaking in B decay sum rules, Phys. Lett. B635 (2006) 207–212.
- [740] P. Minkowski, W. Ochs, B decays into light scalar particles and glueball, Eur. Phys. J. C39 (2005) 71–86.
- [741] J. Z. Bai, et al., Search for a vector glueball by a scan of the  $J/\psi$  resonance, Phys. Rev. D54 (1996) 1221–1224.
- [742] A. B. Arbuzov, E. A. Kuraev, N. P. Merenkov, L. Trentadue, Hadronic cross-sections in electron positron annihilation with tagged photon, JHEP 12 (1998) 009.
- [743] S. Binner, J. H. Kuhn, K. Melnikov, Measuring  $\sigma(e^+e^- \rightarrow \text{hadrons})$  using tagged photon, Phys. Lett. B459 (1999) 279–287.
- [744] M. Benayoun, S. I. Eidelman, V. N. Ivanchenko, Z. K. Silagadze, Spectroscopy at B-factories using hard photon emission, Mod. Phys. Lett. A14 (1999) 2605–2614.
- [745] A. G. Denig, Measurement of the hadronic cross section via radiative return at DAPHNE, Int. J. Mod. Phys. A20 (2005) 1935–1938.
- [746] D. M. Asner, et al., Hadronic structure in the decay  $\tau^- \rightarrow \nu_\tau \pi^- \pi^0 \pi^0$  and the sign of the tau neutrino helicity, Phys. Rev. D61 (2000) 012002.
- [747] J. Gaiser, et al., Charmonium spectroscopy from inclusive  $\psi'$  and  $J/\psi$  radiative decays, Phys. Rev. D34 (1986) 711.
- [748] K. K. Seth, Charmonium at CLEO, AIP Conf. Proc. 814 (2006) 567–574.
- [749] C. Quigg, Hadronic physics and exotics, PoS HEP2005 (2006) 400.
- [750] E. S. Swanson, The new heavy mesons: A status report, Phys. Rept. 429 (2006) 243–305.

- [751] E. Eichten, S. Godfrey, H. Mahlke, J. L. Rosner, Quarkonia and their transitions, hep-ph/0701208.
- [752] S. Godfrey, J. L. Rosner, Production of singlet P-wave  $c\bar{c}$  and  $b\bar{b}$  states, Phys. Rev. D66 (2002) 014012.
- [753] C. Edwards, et al., Observation of an  $\eta'_c$  candidate state with mass  $3592 \text{ MeV} \pm 5 \text{ MeV}$ , Phys. Rev. Lett. 48 (1982) 70.
- [754] K. Abe, et al., Study of double charmonium production in  $e^+e^-$  annihilation at  $\sqrt{s} = 10.6 \text{ GeV}$ , Phys. Rev. D70 (2004) 071102.
- [755] K. Abe, et al., Observation of double  $c\bar{c}$  production in  $e^+e^-$  annihilation at  $\sqrt{s} \sim 10.6 \text{ GeV}$ , Phys. Rev. Lett. 89 (2002) 142001.
- [756] J. Duboscq,  $\Upsilon$  and  $\chi_b$  analyses at CLEO, PoS HEP2005 (2006) 094.
- [757] T. Appelquist, H. D. Politzer, Orthocharmonium and  $e^+e^-$  annihilation, Phys. Rev. Lett. 34 (1975) 43.
- [758] M. B. Voloshin, On a four quark isovector resonance in the  $\Upsilon$  family, JETP Lett. 37 (1983) 69.
- [759] G. Belanger, T. A. Degrand, P. Moxhay, On the spectra of the transitions  $\Upsilon(nS) \rightarrow \Upsilon(mS)\pi^+\pi^-$ , Phys. Rev. D39 (1989) 257.
- [760] V. V. Anisovich, D. V. Bugg, A. V. Sarantsev, B. S. Zou,  $\Upsilon(3S) \rightarrow \Upsilon(1S)\pi\pi$  decay: Is the  $\pi\pi$  spectrum puzzle an indication of a  $b\bar{b}q\bar{q}$  resonance?, Phys. Rev. D51 (1995) 4619–4622.
- [761] S. Chakravarty, P. Ko, On the  $\pi\pi$  spectrum in  $\Upsilon(3S) \rightarrow \Upsilon(1S)\pi\pi$ , Phys. Rev. D48 (1993) 1205–1211.
- [762] M. B. Voloshin, Two-pion transitions in quarkonium revisited, Phys. Rev. D74 (2006) 054022.
- [763] M. Bander, G. L. Shaw, P. Thomas, S. Meshkov, Exotic mesons and  $e^+e^-$  annihilation, Phys. Rev. Lett. 36 (1976) 695.
- [764] A. De Rujula, H. Georgi, S. L. Glashow, Molecular charmonium: A new spectroscopy?, Phys. Rev. Lett. 38 (1977) 317.
- [765] M. B. Voloshin, L. B. Okun, Hadron molecules and charmonium atom, JETP Lett. 23 (1976) 333–336.
- [766] J. P. Ader, J. M. Richard, P. Taxil, Do narrow heavy multi - quark states exist?, Phys. Rev. D25 (1982) 2370.
- [767] N. A. Tornqvist, Isospin breaking of the narrow charmonium state of belle at 3872-mev as a deuson, Phys. Lett. B590 (2004) 209–215.
- [768] G. Bauer, The X(3872) at CDF II, Int. J. Mod. Phys. A20 (2005) 3765–3767.
- [769] G. Gokhroo, et al., Observation of a near-threshold  $D^0\bar{D}^0\pi^0$  enhancement in  $B \rightarrow D^0\bar{D}^0\pi^0K$  decay, Phys. Rev. Lett. 97 (2006) 162002.
- [770] D. V. Bugg, The X(3872) and the 3941-MeV peak in  $\omega J/\psi$ , Phys. Rev. D71 (2005) 016006.
- [771] F. E. Close, P. R. Page, The  $D^{*0} - \bar{D}^0$  threshold resonance, Phys. Lett. B578 (2004) 119–123.
- [772] E. S. Swanson, Short range structure in the x(3872), Phys. Lett. B588 (2004) 189–195.
- [773] C.-Y. Wong, Molecular states of heavy quark mesons, Phys. Rev. C69 (2004) 055202.
- [774] T. Barnes, S. Godfrey, Charmonium options for the X(3872), Phys. Rev. D69 (2004) 054008.
- [775] E. Braaten, M. Kusunoki, Exclusive production of the X(3872) in B meson decay, Phys. Rev. D71 (2005) 074005.
- [776] E. Braaten, M. Kusunoki, S. Nussinov, Production of the X(3870) in B meson decay by the coalescence of charm mesons, Phys. Rev. Lett. 93 (2004) 162001.
- [777] M. B. Voloshin, Heavy quark spin selection rule and the properties of the X(3872), Phys. Lett. B604 (2004) 69–73.

- [778] N. A. Tornqvist, Isospin breaking of the narrow charmonium state of Belle at 3872-MeV as a deuson, Phys. Lett. B590 (2004) 209–215.
- [779] E. J. Eichten, K. Lane, C. Quigg, Charmonium levels near threshold and the narrow state  $X(3872) \rightarrow \pi^+ \pi^- J/\psi$ , Phys. Rev. D69 (2004) 094019.
- [780] M. Suzuki, The  $X(3872)$  boson: Molecule or charmonium, Phys. Rev. D72 (2005) 114013.
- [781] M. T. AlFiky, F. Gabbiani, A. A. Petrov,  $X(3872)$ : Hadronic molecules in effective field theory, Phys. Lett. B640 (2006) 238–245.
- [782] A. Abulencia, Analysis of the quantum numbers  $J^{PC}$  of the  $X(3872)$ , Phys. Rev. Lett. 98 (2007) 132002.
- [783] R. D. Matheus, S. Narison, M. Nielsen, J. M. Richard, Can the  $X(3872)$  be a  $1^{++}$  four-quark state?, Phys. Rev. D75 (2007) 014005.
- [784] M. Okamoto, et al., Charmonium spectrum from quenched anisotropic lattice QCD, Phys. Rev. D65 (2002) 094508.
- [785] P. Chen, Heavy quarks on anisotropic lattices: The charmonium spectrum, Phys. Rev. D64 (2001) 034509.
- [786] Y. Chen, C. Liu, Y. Liu, J. Ma, J. Zhang, Radially excited states of 1P charmonium and  $X(3872)$ .
- [787] X. Liu, Y.-M. Wang, Revisiting  $B^+ \rightarrow X(3872) + K^+$  in pQCD assigning to  $X(3872) 2^3P_1$  charmonium, Eur. Phys. J. C49 (2007) 643–650.
- [788] E. S. Swanson, Diagnostic decays of the  $X(3872)$ , Phys. Lett. B598 (2004) 197–202.
- [789] C. Hanhart, Y. S. Kalashnikova, A. E. Kudryavtsev, A. V. Nefediev, Reconciling the  $X(3872)$  with the near-threshold enhancement in the  $D^0 \bar{D}^{*0}$  final state. arxiv:0704.0605 [hep-ph], 2007.
- [790] C.-K. Chow, Semileptonic decays of heavy tetraquarks, Phys. Rev. D51 (1995) 3541–3543.
- [791] D. M. Brink, F. Stancu, Tetraquarks with heavy flavors, Phys. Rev. D57 (1998) 6778–6787.
- [792] B. A. Gelman, S. Nussinov, Does a narrow tetraquark  $cc\bar{u}\bar{d}$  state exist?, Phys. Lett. B551 (2003) 296–304.
- [793] D. Janc, M. Rosina, The  $T_{cc} = DD^*$  molecular state, Few Body Syst. 35 (2004) 175–196.
- [794] F. S. Navarra, M. Nielsen, S. H. Lee, QCD sum rules study of  $QQ - \bar{u}\bar{d}$  mesons, Phys. Lett. B649 (2007) 166–172.
- [795] L. Maiani, F. Piccinini, A. D. Polosa, V. Riquer, Diquark-antidiquarks with hidden or open charm and the nature of  $X(3872)$ , Phys. Rev. D71 (2005) 014028.
- [796] H. Hogaasen, J. M. Richard, P. Sorba, A chromomagnetic mechanism for the  $X(3872)$  resonance, Phys. Rev. D73 (2006) 054013.
- [797] F. Buccella, H. Hogaasen, J.-M. Richard, P. Sorba, Chromomagnetism, flavour symmetry breaking and S-wave tetraquarks, Eur. Phys. J. C49 (2007) 743–754.
- [798] M. Karliner, H. J. Lipkin, Diquarks and antiquarks in exotics: A menage a trois and a menage a quatre, Phys. Lett. B638 (2006) 221–228.
- [799] Y. S. Kalashnikova, Coupled-channel model for charmonium levels and an option for  $X(3872)$ , Phys. Rev. D72 (2005) 034010.
- [800] D. V. Bugg, Reinterpreting several narrow 'resonances' as threshold cusps, Phys. Lett. B598 (2004) 8–14.
- [801] K. K. Seth, An alternative interpretation of  $X(3872)$ , Phys. Lett. B612 (2005) 1–4.
- [802] B. A. Li, Is  $X(3872)$  a possible candidate of hybrid meson, Phys. Lett. B605 (2005) 306–310.
- [803] S. Uehara, et al., Observation of a  $\chi'_{c2}$  candidate in  $\gamma\gamma \rightarrow D\bar{D}$  production at Belle, Phys. Rev. Lett. 96 (2006) 082003.

- [804] S.-L. Zhu, The possible interpretations of Y(4260), Phys. Lett. B625 (2005) 212.
- [805] F. E. Close, P. R. Page, Gluonic charmonium resonances at BaBar and Belle?, Phys. Lett. B628 (2005) 215–222.
- [806] E. Kou, O. Pene, Suppressed decay into open charm for the Y(4260) being an hybrid, Phys. Lett. B631 (2005) 164–169.
- [807] L. Maiani, V. Riquer, F. Piccinini, A. D. Polosa, Four quark interpretation of Y(4260), Phys. Rev. D72 (2005) 031502.
- [808] X. Liu, X.-Q. Zeng, X.-Q. Li, Possible molecular structure of the newly observed Y(4260), Phys. Rev. D72 (2005) 054023.
- [809] C.-F. Qiao, One explanation for the exotic state Y(4260), Phys. Lett. B639 (2006) 263–265.
- [810] D. V. Bugg, The  $\pi\pi$  mass spectrum in  $Y(4260) \rightarrow \pi\pi J/\psi$ , hep-ex/0701002.
- [811] X. H. Mo, et al., Determining the upper limit of  $\Gamma_{e^+e^-}$  for the Y(4260), Phys. Lett. B640 (2006) 182–187.
- [812] J. L. Rosner, Effects of s-wave thresholds, Phys. Rev. D74 (2006) 076006.
- [813] F. J. Llanes-Estrada, Y(4260) and possible charmonium assignment, Phys. Rev. D72 (2005) 031503.
- [814] P. Colangelo, F. De Fazio, R. Ferrandes, S. Nicotri, New open and hidden charm spectroscopy, 7th Workshop on Continuous Advances in QCD, Minneapolis, Minnesota, 11-14 May 2006. hep-ph/0609240.
- [815] J. L. Rosner, Threshold effect and  $\pi^\pm\psi(2s)$  peak. arxiv:0708.3496 [hep-ph] (2007).
- [816] E. van Beveren, G. Rupp, Observed  $D_s(2317)$  and tentative  $D(2030)$  as the charmed cousins of the light scalar nonet, Phys. Rev. Lett. 91 (2003) 012003.
- [817] H. Albrecht, et al., Measurement of the decay  $D_{s2}^{*+} \rightarrow D^0 K^+$ , Z. Phys. C69 (1996) 405–408.
- [818] M. Di Pierro, E. Eichten, Excited heavy-light systems and hadronic transitions, Phys. Rev. D64 (2001) 114004.
- [819] W. A. Bardeen, E. J. Eichten, C. T. Hill, Chiral multiplets of heavy-light mesons, Phys. Rev. D68 (2003) 054024.
- [820] H.-W. Lin, S. Ohta, A. Soni, N. Yamada, Charm as a domain wall fermion in quenched lattice QCD, Phys. Rev. D74 (2006) 114506.
- [821] T. Barnes, F. E. Close, H. J. Lipkin, Implications of a D K molecule at 2.32-GeV, Phys. Rev. D68 (2003) 054006.
- [822] E. van Beveren, J. E. G. N. Costa, F. Kleefeld, G. Rupp, From the  $\kappa$  via the  $D_{s0}^*(2317)$  to the  $\chi_{c0}$ : Connecting light and heavy scalar mesons, Phys. Rev. D74 (2006) 037501.
- [823] I. W. Lee, T. Lee, D. P. Min, B.-Y. Park, Chiral radiative corrections and  $D_s(2317)/D(2308)$  mass puzzle, Eur. Phys. J. C49 (2007) 737.
- [824] H. Kim, Y. Oh,  $D_s(2317)$  as a four-quark state in QCD sum rules, Phys. Rev. D72 (2005) 074012.
- [825] W. Wei, P.-Z. Huang, S.-L. Zhu, Strong decays of  $D_{sJ}(2317)$  and  $D_{sJ}(2460)$ , Phys. Rev. D73 (2006) 034004.
- [826] H.-Y. Cheng, W.-S. Hou, B decays as spectroscopic for charmed four-quark states, Phys. Lett. B566 (2003) 193–200.
- [827] K. Terasaki, BaBar resonance as a new window of hadron physics, Phys. Rev. D68 (2003) 011501.
- [828] V. Dmitrasinovic,  $D_{sJ}^*(2317)$ ,  $D_J^*(2308)$  and  $D_{sJ}^*(2632)$  as candidates for open-charm tetraquarks, Int. J. Mod. Phys. A21 (2006) 5625–5632.
- [829] K. Terasaki,  $D_{s0}^+(2317)$  as an iso-triplet four-quark meson, Eur. Phys. J. A31 (2007) 676.

- [830] A. Faessler, T. Gutsche, V. E. Lyubovitskij, Y.-L. Ma, Strong and radiative decays of the  $D_{s0}^*(2317)$  meson in the  $DK$ -molecule picture, arxiv:0705.0254 [hep-ph], (2007).
- [831] A. Faessler, T. Gutsche, S. Kovalenko, V. E. Lyubovitskij,  $D_{s0}^*(2317)$  and  $D_{s1}(2460)$  mesons in two-body B-meson decays, arXiv:0705.0892 [hep-ph].
- [832] R. S. Galik, Quarkonium production and decay, 24th International Conference on Physics in Collision (PIC 2004), Boston, Massachusetts, 27-29 Jun 2004. hep-ph/0408190.
- [833] E. van Beveren, G. Rupp, Multichannel calculation for  $D_s^*$  vector states and the  $D_s(2632)$  resonance, Phys. Rev. Lett. 93 (2004) 202001.
- [834] L. Maiani, F. Piccinini, A. D. Polosa, V. Riquer, Is the anomalous decay ratio of  $D_{sJ}(2632)$  due to isospin breaking?, Phys. Rev. D70 (2004) 054009.
- [835] Y. R. Liu, S.-L. Zhu, Y. B. Dai, C. Liu,  $D_{sJ}(2632)^+$ : An excellent candidate of tetraquarks, Phys. Rev. D70 (2004) 094009.
- [836] Z.-G. Wang, Is  $d_s(2700)$  a charmed tetraquark state ? arxiv:0708.0155 [hep-ph], 2007.
- [837] E. van Beveren, G. Rupp, New BaBar state  $D_{sJ}(2860)$  as the first radial excitation of the  $D_{s0}^*(2317)$ , hep-ph/0606110, Phys. Rev. Lett. 97 (2006) 202001.
- [838] F. E. Close, C. E. Thomas, O. Lakhina, E. S. Swanson, Canonical interpretation of the  $D_{sJ}(2860)$  and  $D_{sJ}(2690)$ , Phys. Lett. B647 (2007) 159–163.
- [839] P. Colangelo, F. De Fazio, S. Nicotri,  $D_{sJ}(2860)$  resonance and the  $s_l^p = 5/2^- c\bar{s}(c\bar{q})$  doublet, Phys. Lett. B642 (2006) 48–52.
- [840] B. Zhang, X. Liu, W.-Z. Deng, S.-L. Zhu,  $D_{sJ}(2860)$  and  $D_{sJ}(2715)$ , Eur. Phys. J. C50 (2007) 617–628.
- [841] E. Cheu, Properties of heavy meson states:  $B^{**}$  and  $B_c$ , Int. J. Mod. Phys. A20 (2005) 3664–3668.
- [842] S. S. Afonin, Comment on ‘Parity doubling and  $SU(2)_L \times SU(2)_R$  restoration in the hadronic spectrum’ and ‘Parity doubling among the baryons’, hep-ph/0605102. (2006).
- [843] S. S. Afonin, Towards understanding spectral degeneracies in nonstrange hadrons. I: Mesons as hadron strings vs. phenomenology, Mod. Phys. Lett. A22 (2007) 1359–1372.
- [844] L. Y. Glozman,  $SU(2)_L \times SU(2)_R$  and  $U(1)_A$  restorations high in the hadron spectrum and what it tells us about, Phys. Lett. B539 (2002) 257–265.
- [845] L. Y. Glozman, Chiral symmetry restoration and the string picture of hadrons, Phys. Lett. B541 (2002) 115–120.
- [846] E. S. Swanson, Parity doubling in the meson spectrum, Phys. Lett. B582 (2004) 167–171.
- [847] S. S. Afonin, Experimental indication on chiral symmetry restoration in meson spectrum, Phys. Lett. B639 (2006) 258–262.
- [848] E. Klempert, Do parity doublets in the baryon spectrum reflect restoration of chiral symmetry?, Phys. Lett. B559 (2003) 144–152.
- [849] T. D. Cohen, L. Y. Glozman, Does one observe chiral symmetry restoration in baryon spectrum?, Int. J. Mod. Phys. A17 (2002) 1327–1354.
- [850] R. L. Jaffe, D. Pirjol, A. Scardicchio, Why massless pions preclude  $SU(2)_L \times SU(2)_R$  restoration in the hadron spectrum, Phys. Rev. Lett. 96 (2006) 121601.
- [851] R. L. Jaffe, D. Pirjol, A. Scardicchio, Parity doubling among the baryons, Phys. Rept. 435 (2006) 157–182.
- [852] V. V. Anisovich, A. V. Sarantsev, A. A. Kondashov, Y. D. Prokoshkin, S. A. Sadovsky, Two resonance structure of the ( $IJ^{PC} = 00^{++}$ )  $\pi\pi$  amplitude in a mass region around 1-GeV, Phys. Lett. B355 (1995) 363–373.

- [853] V. V. Anisovich, A. V. Sarantsev, K-matrix analysis of the ( $IJ^{PC} = 00^{++}$ ) amplitude in the mass region up to 1550 MeV, Phys. Lett. B382 (1996) 429–440.
- [854] V. V. Anisovich, Y. D. Prokoshkin, A. V. Sarantsev, Nonet classification of scalar/isoscalar resonances below 1900-MeV: The existence of an extra scalar state in the region 1200-MeV to 1600-MeV, Phys. Lett. B389 (1996) 388–396.
- [855] V. V. Anisovich, A. A. Kondashov, Y. D. Prokoshkin, S. A. Sadovsky, A. V. Sarantsev, The two-pion spectra for the reaction  $\pi^- p \rightarrow \pi^0 \pi^0 n$  at 38-GeV/c pion momentum and combined analysis of the GAMS, Crystal Barrel and BNL data, Phys. Atom. Nucl. 63 (2000) 1410–1427.
- [856] A. V. Anisovich, A. V. Sarantsev, K-matrix analysis of the  $K\pi$   $S$ -wave in the mass region 900-MeV to 2100-MeV and nonet classification of scalar  $q\bar{q}$  states, Phys. Lett. B413 (1997) 137–146.
- [857] A. V. Anisovich, V. V. Anisovich, A. V. Sarantsev, Scalar glueball: Analysis of the ( $IJ^{PC} = 00^{++}$ )-wave, Z. Phys. A359 (1997) 173–189.
- [858] A. V. Anisovich, V. V. Anisovich, A. V. Sarantsev, Y. D. Prokoshkin, Observation of the lightest scalar glueball, Z. Phys. A357 (1997) 123–125.
- [859] V. V. Anisovich, A. V. Sarantsev, K-matrix analysis of the ( $IJ^{PC} = 00^{++}$ )-wave in the mass region below 1900-MeV, Eur. Phys. J. A16 (2003) 229–258.
- [860] N. A. Tornqvist, From the deuteron to deusons, an analysis of deuteronlike meson-meson bound states, Z. Physik C61 (1994) 526.
- [861] E. van Beveren, D. V. Bugg, F. Kleefeld, G. Rupp, The nature of  $\sigma, \kappa, a_0(980)$  and  $f_0(980)$ , Phys. Lett. B641 (2006) 265–271.
- [862] P. Frenkiel, et al.,  $\omega\pi$  resonances and  $\pi\pi$  s wave structures as observed in  $\bar{p}p$  annihilations at rest, Nucl. Phys. B47 (1972) 61–80.
- [863] J. Ballam, et al., A search for B and  $\rho'(1250)$  production in the reaction  $\gamma p \rightarrow p\pi^+\pi^-$  neutrals at 2.8-GeV, 4.7-GeV and 9.3-GeV, Nucl. Phys. B76 (1974) 375.
- [864] A. Donnachie, H. Mirzaie, Evidence for two  $\rho'(1600)$  resonances, Z. Phys. C33 (1987) 407.
- [865] A. B. Clegg, A. Donnachie, Rho-primes in  $6\pi$  states from materialization of photons, Z. Phys. C45 (1990) 677.
- [866] A. Cordier, et al., Observation of a new isoscalar vector meson in  $e^+e^- \rightarrow \omega\pi^+\pi^-$  annihilation at 1.65-GeV, Phys. Lett. B106 (1981) 155.
- [867] A. Donnachie, A. B. Clegg, Omega-primes and glueballs, Z. Phys. C42 (1989) 663.
- [868] D. Bisello, et al., Observation of an isoscalar vector meson at approximately 1650 MeV/ $c^2$  in the  $e^+e^- \rightarrow K\bar{K}\pi$  reaction, Z. Phys. C52 (1991) 227–230.
- [869] A. Donnachie, Y. S. Kalashnikova, Hunting the vector hybrid, Phys. Rev. D60 (1999) 114011.
- [870] N. Isgur, R. Kokoski, J. Paton, Gluonic excitations of mesons: Why they are missing and where to find them, Phys. Rev. Lett. 54 (1985) 869.
- [871] X. Liu, B. Zhang, L.-L. Shen, S.-L. Zhu, X(1576) and the final state interaction effect, Phys. Rev. D75 (2007) 074017.
- [872] F.-K. Guo, P.-N. Shen, Isospin and a possible interpretation of the newly observed x(1576), Phys. Rev. D74 (2006) 097503.
- [873] Z.-G. Wang, S.-L. Wan, Analysis of the  $X(1576)$  as a tetraquark state with the QCD sum rules, Chin. Phys. Lett. 23 (2006) 3208–3210.
- [874] G.-J. Ding, M.-L. Yan,  $X(1576)$  as diquark antiquark bound state, Phys. Lett. B643 (2006) 33–40.
- [875] M. Karliner, H. J. Lipkin, A tetraquark model for the new  $X(1576) K^+K^-$  resonance. hep-ph/0607093.

- [876] F. E. Close, P. R. Page, The production and decay of hybrid mesons by flux tube breaking, Nucl. Phys. B443 (1995) 233–254.
- [877] T. Barnes, F. E. Close, E. S. Swanson, Hybrid and conventional mesons in the flux tube model: Numerical studies and their phenomenological implications, Phys. Rev. D52 (1995) 5242–5256.
- [878] P. R. Page, E. S. Swanson, A. P. Szczepaniak, Hybrid meson decay phenomenology, Phys. Rev. D59 (1999) 034016.
- [879] D. I. Ryabchikov, Study of exotic mesons on the VES setup, prepared for 6th International Conference on Hadron Spectroscopy (HADRON 95), Manchester, England, 10-14 Jul 1995.
- [880] V. V. Anisovich, A. V. Sarantsev, Observation of tensor glueball in the reactions  $p\bar{p} \rightarrow \pi\pi, \eta\eta, \eta\eta'$ , JETP Lett. 81 (2005) 417–423.
- [881] V. V. Anisovich, M. A. Matveev, J. Nyiri, A. V. Sarantsev, Sector of the  $2^{++}$  mesons: Observation of the tensor glueball, Int. J. Mod. Phys. A20 (2005) 6327–6364.
- [882] V. V. Anisovich, M. A. Matveev, J. Nyiri, A. V. Sarantsev, Observation of the tensor glueball, Phys. Atom. Nucl. 69 (2006) 520–527.
- [883] V. A. Shchegelsky, A. V. Sarantsev, A. V. Anisovich, M. P. Levchenko, Partial wave analysis of  $\pi^+\pi^-\pi^0$  production in two-photon collisions at LEP, Eur. Phys. J. A27 (2006) 199–205.
- [884] V. A. Shchegelsky, A. V. Sarantsev, V. A. Nikonov, A. V. Anisovich, The  $K_S^0 K_S^0$  final state in two-photon collisions and SU(3) tensor nonets, Eur. Phys. J. A27 (2006) 207–212.
- [885] E. Eisenhandler, et al., Measurement of differential cross-sections for anti-proton - proton annihilation into charged pion and kaon pairs between 0.79-GeV/c and 2.43-GeV/c, Nucl. Phys. B96 (1975) 109.
- [886] A. Etkin, et al., The reaction  $\pi^-p \rightarrow \phi\phi n$  and evidence for glueballs, Phys. Rev. Lett. 49 (1982) 1620.
- [887] R. S. Longacre, S. J. Lindenbaum, Evidence for a 4<sup>th</sup> state related to the three  $J^{PC} = 2^{++}, \pi^-p \rightarrow \phi\phi n$  states explainable by  $2^{++}$  glueball production, Phys. Rev. D70 (2004) 094041.
- [888] R. L. Jaffe, K. Johnson, Unconventional states of confined quarks and gluons, Phys. Lett. B60 (1976) 201.
- [889] A. I. Vainshtein, L. B. Okun, Anomalous levels of charmonium. (In Russian), Yad. Fiz. 23 (1976) 1347–1348.
- [890] M. S. Chanowitz, S. R. Sharpe, Hybrids: Mixed states of quarks and gluons, Nucl. Phys. B222 (1983) 211.
- [891] I. I. Balitsky, D. Diakonov, A. V. Yung, Exotic mesons with  $J^{PC} = 1^{-+}$  from QCD sum rules, Phys. Lett. B112 (1982) 71–75.
- [892] J. I. Latorre, P. Pascual, S. Narison, Spectra and hadronic couplings of light hermaphrodite mesons, Z. Phys. C34 (1987) 347.
- [893] S. Narison, Gluonia, scalar and hybrid mesons in QCD, Nucl. Phys. A675 (2000) 54c–63c.
- [894] C. Bernard, et al., Lattice calculation of  $1^{-+}$  hybrid mesons with improved Kogut-Susskind fermions, Phys. Rev. D68 (2003) 074505.
- [895] S. R. Cotanch, F. J. Llanes-Estrada, Relativistic many body approach to exotic and charmed hybrid mesons, Nucl. Phys. A689 (2001) 481–484.
- [896] A. W. Thomas, A. P. Szczepaniak, Chiral extrapolations and exotic meson spectrum, Phys. Lett. B526 (2002) 72–78.
- [897] M. Tanimoto, Decay patterns of  $\bar{q}qg$  hybrid mesons, Phys. Lett. B116 (1982) 198.
- [898] F. Iddir, et al.,  $\bar{q}qg$  hybrid and  $qq\bar{q}\bar{q}$  diquonium interpretation of GAMS  $1^{-+}$  resonance, Phys. Lett. B205 (1988) 564.
- [899] F. E. Close, J. J. Dudek, The 'forbidden' decays of hybrid mesons to  $\pi\rho$  can be large, Phys. Rev. D70 (2004) 094015.

- [900] N. J. Poplawski, A. P. Szczepaniak, J. T. Lonergan, Towards a relativistic description of exotic meson decays, Phys. Rev. D71 (2005) 016004.
- [901] F. De Viron, J. Govaerts, Some decay modes of  $1^{-+}$  hybrid mesons, Phys. Rev. Lett. 53 (1984) 2207–2210.
- [902] T. Burns, F. E. Close, Hybrid meson properties in lattice QCD and flux tube models, Phys. Rev. D74 (2006) 034003.
- [903] S. U. Chung, E. Klempt, J. G. Körner, SU(3) classification of p-wave  $\eta\pi$  and  $\eta'\pi$  systems, Eur. Phys. J. A15 (2002) 539–542.
- [904] J. M. Frère, S. Titard, A new look at exotic decays  $\hat{\rho}(1^{-+}, I = 1) \rightarrow \eta'\pi$  versus  $\rho\pi$ , Phys. Lett. B214 (1988) 463.
- [905] R. L. Jaffe, F. E. Low, The connection between quark model eigenstates and low-energy scattering, Phys. Rev. D19 (1979) 2105–2118.
- [906] R. L. Jaffe, Multi - quark hadrons. 1. The phenomenology of  $(2q2\bar{q})$  mesons, Phys. Rev. D15 (1977) 267.
- [907] T. Barnes, N. Black, E. S. Swanson, Meson meson scattering in the quark model: Spin dependence and exotic channels, Phys. Rev. C63 (2001) 025204.
- [908] P. Estabrooks, et al., Study of  $K\pi$  scattering using the reactions  $K^\pm p \rightarrow K^\pm\pi^+n$  and  $K^\pm p \rightarrow K^\pm\pi^-\Delta^{++}$  at 13-GeV/c, Nucl. Phys. B133 (1978) 490.
- [909] L.-H. Chan, R. W. Haymaker, Meson dynamics in the  $SU(3) \times SU(3)$  sigma model, Phys. Rev. D10 (1974) 4143.
- [910] S. D. Bass, E. Marco, Final state interaction and a light mass 'exotic' resonance, Phys. Rev. D65 (2002) 057503.
- [911] N. N. Achasov, G. N. Shestakov, Effective Lagrangians induced by the anomalous Wess-Zumino action and  $I^G(J^{PC}) = 1^-(1^{-+})$  exotic states, AIP Conf. Proc. 619 (2002) 599–602.
- [912] I. J. General, P. Wang, S. R. Cotanch, F. J. Llanes-Estrada, Light  $1^{-+}$  exotics: molecular resonances. arxiv:0707.1286 [hep-ph], (2007).
- [913] W. D. Apel, et al., Analysis of the reaction  $\pi^- p \rightarrow \pi^0 \eta n$  at 40-GeV/c beam momentum, Nucl. Phys. B193 (1981) 269–286.
- [914] H. Aoyagi, et al., Study of the  $\eta\pi$  system in the  $\pi^- p$  reaction at 6.3 GeV/c, Phys. Lett. B314 (1993) 246–254.
- [915] Y. D. Prokoshkin, S. A. Sadovsky, On the solution ambiguities in the partial wave analysis of the  $\pi^- p \rightarrow \eta\pi^0 n$  reaction, Sov. Phys. Dokl. 37 (1992) 152–154.
- [916] A. P. Szczepaniak, M. Swat, A. R. Dzierba, S. Teige, Study of the  $\eta\pi$  and  $\eta'\pi$  spectra and interpretation of possible exotic  $J^{PC} = 1^{-+}$  mesons, Phys. Rev. Lett. 91 (2003) 092002.
- [917] A. Sarantsev, Antiproton proton annihilation at rest into three pseudoscalar mesons, AIP Conf. Proc. 717 (2004) 65–71.
- [918] A. Donnachie, P. R. Page, Interpretation of experimental  $J^{PC}$  exotic signals, Phys. Rev. D58 (1998) 114012.
- [919] F. Q. Wu, B. S. Zou, L. Li, D. V. Bugg, New study of the isotensor  $\pi\pi$  interaction, Nucl. Phys. A735 (2004) 111–124.
- [920] Y. Khokhlov, Study of an exotic  $J^{PC} = 1^{-+} X(1600)$ , International Europhysics Conference on High- Energy Physics (EPS-HEP 99), Tampere, Finland, 15-21 Jul 1999.
- [921] A. Filippi, Study of isospin 2 states in  $\bar{n}p$  annihilations, AIP Conf. Proc. 619 (2002) 582–585.
- [922] H. Albrecht, et al., Observation of spin parity  $2^+$  dominance in the reaction  $\gamma\gamma \rightarrow \rho^0\rho^0$  near threshold, Z. Phys. C50 (1991) 1–10.
- [923] N. N. Achasov, S. A. Devyanin, G. N. Shestakov, To search for four - quark states in  $\gamma\gamma$  collisions, Z. Phys. C16 (1982) 55.

- [924] B. A. Li, K. F. Liu, In search of two-quark two-antiquark mesons in  $\gamma\gamma$  reactions, Phys. Lett. B118 (1982) 435.
- [925] N. N. Achasov, G. N. Shestakov, Exotic states  $X^\pm(1600)$ ,  $I^G(J^{PC}) = 2^+(2^{++})$  in photoproduction reactions, Phys. Atom. Nucl. 63 (2000) 1815–1823.
- [926] N. N. Achasov, G. N. Shestakov, Exotic  $\rho^\pm\rho^0$  state photoproduction at JLAB facility, Phys. Rev. D60 (1999) 114021.
- [927] N. N. Achasov, G. N. Shestakov, Are the reactions  $\gamma\gamma \rightarrow VV'$  a challenge for the factorized Pomeron at high energies?, Phys. Rev. D60 (1999) 117503.
- [928] W. Wei, L. Zhang, S.-L. Zhu, The possible  $J^{PC}I^G = 2^{++}2^+$  state X(1600), Int. J. Mod. Phys. A21 (2006) 4617.
- [929] H. Albrecht, et al., Observation of  $\gamma\gamma \rightarrow \phi\rho^0$  and  $\gamma\gamma \rightarrow \phi\omega$ , Phys. Lett. B332 (1994) 451–457.
- [930] H. Albrecht, et al., Measurement of  $K^*\bar{K}^*$  production in two-photon interactions, Eur. Phys. J. C16 (2000) 435–444.
- [931] G. Alexander, A. Levy, U. Maor, The threshold t channel factorization model and its application to  $\gamma\gamma$  reactions, Phys. Rev. D46 (1992) 2882–2890.
- [932] J. L. Rosner, Vector meson pair production in two-photon collisions near threshold, Phys. Rev. D70 (2004) 034028.
- [933] M. Bonesini, et al., Evidence for a new pseudoscalar meson, Phys. Lett. B103 (1981) 75–78.
- [934] R. Aaron, R. S. Longacre, Analysis of the  $J^P = 1^+$  and  $0^-$  three pion systems, Phys. Rev. D24 (1981) 1207–1217.
- [935] G. Bellini, et al., Evidence for new  $0^-$  S resonances in the  $\pi^+\pi^-\pi^-$  systems, Phys. Rev. Lett. 48 (1982) 1697–1700.
- [936] M. Zielinski, et al., Partial wave analysis of coherent  $3\pi$  production on nuclei at 200 GeV, Phys. Rev. D30 (1984) 1855.
- [937] G. W. Brandenburg, et al., Evidence for a new strangeness 1 pseudoscalar meson, Phys. Rev. Lett. 36 (1976) 1239.
- [938] T. Armstrong, et al., A partial wave analysis of the  $K^-\phi$  system produced in the reaction  $K^-p \rightarrow K^+K^-K^-p$  at 18.5 GeV/c, Nucl. Phys. B221 (1983) 1.
- [939] N. R. Stanton, et al., Evidence for axial vector and pseudoscalar resonances near 1.275 GeV in  $\eta\pi^+\pi^-$ , Phys. Rev. Lett. 42 (1979) 346–349.
- [940] A. Ando, et al., Evidence for two pseudoscalar resonances of  $\eta\pi^+\pi^-$  system in the D(1285) and E/iota regions, Phys. Rev. Lett. 57 (1986) 1296.
- [941] A. Birman, et al., Partial wave analysis of the  $K^+\bar{K}^0\pi^-$  system, Phys. Rev. Lett. 61 (1988) 1557.
- [942] I. Cohen, H. J. Lipkin, A phenomenological model for pseudoscalar meson mixing, Nucl. Phys. B151 (1979) 16.
- [943] R. Armenteros, et al., Proc. Int. Conf. Elementary Particles, Sienna, vol. 1 (1963) 287.
- [944] O. I. Dahl, et al., Strange-particle production in  $\pi^-p$  interactions from 1.5 to 4.2 BeV/c. I: Three-and-more-body final states, Phys. Rev. 163 (1967) 1377–1429.
- [945] C. Edwards, et al., Study of the decay  $J/\psi \rightarrow \gamma\eta\pi\pi$ , Phys. Rev. Lett. 51 (1983) 859.
- [946] J. E. Augustin, et al., Partial wave analysis of DM2 data in the  $\eta(1430)$  energy range, Phys. Rev. D46 (1992) 1951–1958.
- [947] S. U. Chung, et al., Spin and parity analysis of  $K\bar{K}\pi$  system in the D and E/ι regions, Phys. Rev. Lett. 55 (1985) 779.

- [948] D. F. Reeves, et al., Spin parity analysis of  $\bar{p}p \rightarrow E(1420)X$ , Phys. Rev. D34 (1986) 1960.
- [949] M. G. Rath, et al., The  $K_s^0 K_s^0 \pi^0$  system produced in  $\pi^- p$  interactions at 21.4 GeV/c, Phys. Rev. D40 (1989) 693.
- [950] P. Minkowski, W. Ochs, The glueball among the light scalar mesons, Nucl. Phys. Proc. Suppl. 121 (2003) 123–126.
- [951] L. Faddeev, A. J. Niemi, U. Wiedner, Glueballs, closed fluxtubes and  $\eta(1440)$ , Phys. Rev. D70 (2004) 114033.
- [952] J. Reinnarth, Exotische Mesonen im Endzustand  $2\pi^+ 2\pi^- \eta$  in der Antiproton-Proton-Vernichtung in Ruhe, Ph.D. thesis, University of Bonn (2003).
- [953] A. V. Anisovich, et al., Resonances in  $\bar{p}p \rightarrow \eta\pi^+\pi^-\pi^+\pi^-$  at rest, Nucl. Phys. A690 (2001) 567–594.
- [954] E. Klempert, The glueball candidate  $\eta(1440)$  as  $\eta$  radial excitation.32nd International Conference on High-Energy Physics (ICHEP 04), Beijing, China. hep-ph/0409148.
- [955] R. M. Baltrusaitis, et al., A study of the radiative decay  $J/\psi \rightarrow \gamma\rho\rho$ , Phys. Rev. D33 (1986) 1222.
- [956] R. M. Baltrusaitis, et al., Observation of  $J/\psi$  radiative decay to pseudoscalar  $\omega\omega$ , Phys. Rev. Lett. 55 (1985) 1723.
- [957] G. Eigen, Study of  $K^{*0}\bar{K}^{*0}$  production in radiative  $J/\psi$  decays, Nucl. Phys. Proc. Suppl. 21 (1991) 149–155.
- [958] D. Bisello, et al., First observation of three pseudoscalar states in the  $J/\psi \rightarrow \gamma\rho\rho$  decay, Phys. Rev. D39 (1989) 701.
- [959] D. Bisello, et al., Study of the  $J/\psi \rightarrow \gamma\phi\phi$  decay, Phys. Lett. B241 (1990) 617.
- [960] D. V. Bugg, et al., Further amplitude analysis of  $J/\psi \rightarrow \gamma(\pi^+\pi^-\pi^+\pi^-)$ , Phys. Lett. B353 (1995) 378–384.
- [961] D. V. Bugg, L. Y. Dong, B. S. Zou, The broad  $J^P = 0^-$  meson in  $J/\psi$  radiative decays, Phys. Lett. B458 (1999) 511–516.
- [962] T. Huang, S.-L. Zhu, X(1835): A natural candidate of  $\eta'$  's second radial excitation, Phys. Rev. D73 (2006) 014023.
- [963] Jin Shan, New observations on hadron spectroscopy at BESII 33rd International Conference on High Energy Physics (ICHEP 06), Moscow, Russia.
- [964] A. Sibirtsev, J. Haidenbauer, S. Krewald, U.-G. Meissner, A. W. Thomas, Near threshold enhancement of the  $\bar{p}p$  mass spectrum in  $J/\psi$  decay, Phys. Rev. D71 (2005) 054010.
- [965] J. Haidenbauer, U.-G. Meissner, A. Sibirtsev, Near threshold  $\bar{p}p$  enhancement in  $B$  and  $J/\psi$  decay, Phys. Rev. D74 (2006) 017501.
- [966] D. R. Entem, F. Fernandez, X(1859) Baryonium or something else?, Eur. Phys. J. A31 (2007) 649–652.
- [967] D. R. Entem, F. Fernandez, Final state interaction effects in near threshold enhancement of the  $p\bar{p}$  mass spectrum in  $B$  and  $J/\psi$  decays, Phys. Rev. D75 (2007) 014004.
- [968] B. S. Zou, H. C. Chiang, One-pion exchange final-state interaction and the  $p\bar{p}$  near threshold enhancement in  $J/\psi \rightarrow \gamma p\bar{p}$  decays, Phys. Rev. D69 (2004) 034004.
- [969] D. Bisello, et al., Study of the reaction  $e^+e^- \rightarrow 3\pi^+3\pi^-$  in the total energy range 1400-MeV to 2180-MeV, Phys. Lett. B107 (1981) 145.
- [970] N. A. Tornqvist, Summary talk of the conference on the  $\sigma$  resonance, Workshop on Possible Existence of the  $\sigma$  meson and its Implications to Hadron Physics ( $\sigma$ -meson 2000), Kyoto, Japan, 12-14 Jun 2000. hep-ph/0008135.
- [971] K. Takamatsu,  $\kappa$  particle in the analysis of the BESII data and chiral  $\sigma$  nonet. IHEP Seminar on Perspective for Studies of Chiral Particles at BES, Beijing, China, 2006. In: Perspectives for studies of chiral particles at BES\* 107-123. hep-ph/0612340.

- [972] D. V. Bugg, Reply to Takamatsu's paper on the  $\kappa$ , hep-ph/0701058.
- [973] U.-G. Meißner, Modern theory of nuclear forces, Nucl. Phys. A751 (2005) 149–166.
- [974] Y. Nambu, Axial vector current conservation in weak interactions, Phys. Rev. Lett. 4 (1960) 380–382.
- [975] Y. Nambu, G. Jona-Lasinio, Dynamical model of elementary particles based on an analogy with superconductivity. I, Phys. Rev. 122 (1961) 345–358.
- [976] Y. Nambu, G. Jona-Lasinio, Dynamical model of elementary particles based on an analogy with superconductivity. II, Phys. Rev. 124 (1961) 246–254.
- [977] R. Delbourgo, M. D. Scadron, Dynamical symmetry breaking and the  $\sigma$  meson mass in quantum chromodynamics, Phys. Rev. Lett. 48 (1982) 379–382.
- [978] M. R. Pennington, Scalars in the hadron world: The Higgs sector of the strong interaction, Int. J. Mod. Phys. A21 (2006) 747–756.
- [979] S. Ishida, et al., An analysis of  $\pi\pi$  scattering phase shift and existence of  $\sigma(555)$  particle, Prog. Theor. Phys. 95 (1996) 745–766.
- [980] V. E. Markushin, Z. Xiao, H. Q. Zheng, Left hand singularities, hadron form factors and the properties of the  $\sigma$  meson, Nucl. Phys. A695 (2001) 273–294.
- [981] M. Ishida, S. Ishida, Existence of  $\sigma(600)/\kappa(900)$ -particle and new chiral scalar nonet \*chiralons\*, 7th International Conference on Hadron Spectroscopy (Hadron 97), Upton, NY, 25-30 Aug 1997. hep-ph/9712231.
- [982] S. Ishida, M. Ishida, U(12): A new symmetry possibly realizing in hadron spectroscopy, Phys. Lett. B539 (2002) 249–256.
- [983] S. Weinberg, Pion scattering lengths, Phys. Rev. Lett. 17 (1966) 616–621.
- [984] M. Boglione, M. R. Pennington, Chiral poles and zeros and the role of the left hand cut, Z. Phys. C75 (1997) 113–118.
- [985] H. G. Dosch, S. Narison, Tests of the nature and of the gluon content of the  $\sigma(0.6)$  from  $D$  and  $D_s$  semileptonic decays, Nucl. Phys. Proc. Suppl. 121 (2003) 114–118.
- [986] S. Narison, Scalar mesons in QCD and tests of the gluon content of the  $\sigma$ , Nucl. Phys. Proc. Suppl. 121 (2003) 131–134.
- [987] J. D. Weinstein, N. Isgur, Do multi - quark hadrons exist?, Phys. Rev. Lett. 48 (1982) 659.
- [988] J. D. Weinstein, N. Isgur, The  $qq\bar{q}\bar{q}$  system in a potential model, Phys. Rev. D27 (1983) 588.
- [989] J. D. Weinstein, N. Isgur,  $K\bar{K}$  molecules, Phys. Rev. D41 2236.
- [990] R. L. Jaffe, Multi - quark hadrons. 2. methods, Phys. Rev. D15 (1977) 281.
- [991] L. Li, B.-S. Zou, G.-l. Li, A new decomposition of  $\pi\pi$  s-wave interaction, Phys. Rev. D63 (2001) 074003.
- [992] G. F. Chew, F. E. Low, Unstable particles as targets in scattering experiments, Phys. Rev. 113 (1959) 1640–1648.
- [993] W. Ochs, A method for the determination of density matrix elements and amplitudes of one-pion exchange reactions, Nuovo Cim. A12 (1972) 724–736.
- [994] P. Estabrooks, A. D. Martin, Analysis of  $\pi^- p \rightarrow \pi^-\pi^+ n$  data at 17.2 Gev/c, Phys. Lett. B41 (1972) 350–354.
- [995] L. Rosselet, et al., Experimental study of 30,000  $K_{e4}$  decays, Phys. Rev. D15 (1977) 574.
- [996] S. Pislik, et al., High statistics measurement of  $k_{e4}$  decay properties, Phys. Rev. D67 (2003) 072004.
- [997] L. Masetti, Measurements of  $K_{e4}$  and  $K^\pm \rightarrow \pi^0\pi^0\pi^\pm$  decays 33rd International Conference on High Energy Physics (ICHEP 06), Moscow, Russia. hep-ex/0610071.

- [998] R. Kaminski, L. Lesniak, B. Loiseau, Scalar mesons and multichannel amplitudes, *Eur. Phys. J.* C9 (1999) 141–158.
- [999] S. M. Roy, Exact integral equation for pion pion scattering involving only physical region partial waves, *Phys. Lett.* B36 (1971) 353.
- [1000] R. Kaminski, L. Lesniak, B. Loiseau, Elimination of ambiguities in  $\pi\pi$  phase shifts using crossing symmetry, *Phys. Lett.* B551 (2003) 241–248.
- [1001] R. Kaminski, L. Lesniak, K. Rybicki, A joint analysis of the S-wave in the  $\pi^+\pi^-$  and  $\pi^0\pi^0$  data, *Eur. Phys. J. direct* C4 (2002) 4.
- [1002] P. Estabrooks, A. D. Martin,  $\pi\pi$  phase shift analysis below the  $K\bar{K}$  threshold, *Nucl. Phys.* B79 (1974) 301.
- [1003] R. Kaminski, L. Lesniak, K. Rybicki, Separation of s-wave pseudoscalar and pseudovector amplitudes in  $\pi^- p_{pol.} \rightarrow \pi^+ \pi^- n$  reaction on polarized target, *Z. Phys.* C74 (1997) 79–91.
- [1004] S. D. Protopopescu, et al.,  $\pi\pi$  partial wave analysis from reactions  $\pi^+ p \rightarrow \pi^+\pi^-\Delta^{++}$  and  $\pi^+ p \rightarrow K^+ K^-\Delta^{++}$  at 7.1-GeV/c, *Phys. Rev.* D7 (1973) 1279.
- [1005] J. R. Pelaez, F. J. Yndurain, The pion pion scattering amplitude, *Phys. Rev.* D71 (2005) 074016.
- [1006] R. Kaminski, J. R. Pelaez, F. J. Yndurain, The pion pion scattering amplitude. II: Improved analysis above  $\bar{K}K$  threshold, *Phys. Rev.* D74 (2006) 014001.
- [1007] S. L. Adler, Consistency conditions on the strong interactions implied by a partially conserved axial vector current, *Phys. Rev.* 137 (1965) B1022–B1033.
- [1008] D. H. Cohen, T. Ferbel, P. Slattery, B. Werner, Study of  $\pi\pi$  scattering in the isotopic spin-2 channel, *Phys. Rev.* D7 (1973) 661.
- [1009] N. B. Durusoy, et al., Study of the  $I = 2$   $\pi\pi$  scattering from the reaction  $\pi^- d \rightarrow \pi^-\pi^- p_{sp}$  at 9.0 GeV/c, *Phys. Lett.* B45 (1973) 517–520.
- [1010] D. V. Bugg, The phase of the  $\sigma \rightarrow \pi\pi$  amplitude in  $J/\psi \rightarrow \omega\pi^+\pi^-$ , *Eur. Phys. J.* C37 (2004) 433–436.
- [1011] K. M. Watson, The effect of final state interactions on reaction cross- sections, *Phys. Rev.* 88 (1952) 1163–1171.
- [1012] K. M. Watson, Some general relations between the photoproduction and scattering of  $\pi$  mesons, *Phys. Rev.* 95 (1954) 228–236.
- [1013] I. Bediaga, J. M. de Miranda, Complex amplitude phase motion in Dalitz plot heavy meson three body decay, *Phys. Lett.* B550 (2002) 135–139.
- [1014] U. G. Meißner, Chiral dynamics: Where are the scalars?, *Comments Nucl. Part. Phys.* 20 (1991) 119–140.
- [1015] G. Colangelo, J. Gasser, H. Leutwyler,  $\pi\pi$  scattering, *Nucl. Phys.* B603 (2001) 125–179.
- [1016] I. Caprini, G. Colangelo, H. Leutwyler, Mass and width of the lowest resonance in QCD, *Phys. Rev. Lett.* 96 (2006) 132001.
- [1017] F. Kleefeld, Comment on ‘mass and width of the lowest resonance in qcd’, arxiv:0704.1337 [hep-ph] (2007).
- [1018] D. V. Bugg, The mass of the  $\sigma$  pole, hep-ph/0608081.
- [1019] H. Leutwyler, Mass and width of the  $\sigma$ , *Int. J. Mod. Phys.* A22 (2007) 257–265.
- [1020] Z. Y. Zhou, et al., The pole structure of the unitary, crossing symmetric low energy  $\pi\pi$  scattering amplitudes, *JHEP* 02 (2005) 043.
- [1021] F. J. Yndurain, Experimental status of the  $\pi\pi$  isoscalar S-wave at low energy:  $f_0(600)$  pole and scattering length, hep-ph/0701025.
- [1022] V. Bernard, N. Kaiser, U. G. Meißner, Threshold parameters of  $\pi K$  scattering in QCD, *Phys. Rev.* D43 (1991) 2757–2760.

- [1023] V. Bernard, N. Kaiser, U. G. Meißner,  $\pi K$  scattering in chiral perturbation theory to one loop, Nucl. Phys. B357 (1991) 129–152.
- [1024] D. V. Bugg, The  $\kappa$  in E791 data for  $D \rightarrow K\pi\pi$ , Phys. Lett. B632 (2006) 471–474.
- [1025] L. Edera, M. R. Pennington, Estimating the  $I = 3/2$   $K\pi$  interaction in  $D$  decay, Phys. Lett. B623 (2005) 55–64.
- [1026] D. V. Bugg, The  $\kappa$  in  $J/\psi \rightarrow K^+\pi^-K^-\pi^+$ , Eur. Phys. J. A25 (2005) 107–114.
- [1027] M. Jamin, J. A. Oller, A. Pich, S-wave  $K\pi$  scattering in chiral perturbation theory with resonances, Nucl. Phys. B587 (2000) 331–362.
- [1028] H. Q. Zheng, et al., The  $\kappa$  resonance in S wave  $\pi K$  scatterings, Nucl. Phys. A733 (2004) 235–261.
- [1029] Z. Y. Zhou, H. Q. Zheng, An improved study to the S-wave  $\pi K$  elastic scatterings and the  $\kappa$  resonance, Nucl. Phys. A775 (2006) 212–223.
- [1030] S. N. Cherry, M. R. Pennington, There is no  $\kappa(900)$ , Nucl. Phys. A688 (2001) 823–841.
- [1031] L. Li, B.-S. Zou, G.-L. Li, Studying  $K\pi$  S-wave scattering in K-matrix formalism, Phys. Rev. D67 (2003) 034025.
- [1032] S. Descotes-Genon, B. Moussallam, The  $K^{0*}(800)$  scalar resonance from Roy-Steiner representations of  $\pi K$  scattering, Eur. Phys. J. C48 (2006) 553.
- [1033] C. Amsler, et al., High-statistics study of  $f_0(1500)$  decay into  $\pi^0\pi^0$ , Phys. Lett. B342 (1995) 433–439.
- [1034] V. V. Anisovich, The lightest scalar glueball, Phys. Usp. 41 (1998) 419–439.
- [1035] V. Baru, J. Haidenbauer, C. Hanhart, A. E. Kudryavtsev, U.-G. Meissner, Flatte-like distributions and the  $a_0(980)/f_0(980)$  mesons, Eur. Phys. J. A23 (2005) 523–533.
- [1036] N. N. Achasov, A. V. Kiselev, The new analysis of the KLOE data on the  $\phi \rightarrow \eta\pi^0\gamma$  decay, Phys. Rev. D68 (2003) 014006.
- [1037] D. V. Bugg, V. V. Anisovich, A. Sarantsev, B. S. Zou, Coupled channel analysis of data on  $\bar{p}p \rightarrow 3\pi^0, \eta\eta\pi^0$ , and  $\eta\pi^0\pi^0$  at rest, with the N/D method, Phys. Rev. D50 (1994) 4412–4422.
- [1038] K. Ackerstaff, et al., Production of  $f_0(980)$ ,  $f_2(1270)$  and  $\phi(1020)$  in hadronic  $Z^0$  decay, Eur. Phys. J. C4 (1998) 19–28.
- [1039] N. N. Achasov, V. N. Ivanchenko, On a search for four quark states in radiative decays of  $\phi$  meson, Nucl. Phys. B315 (1989) 465.
- [1040] M. Boglione, M. R. Pennington, Towards a model independent determination of the  $\phi \rightarrow f_0\gamma$  coupling, Eur. Phys. J. C30 (2003) 503–512.
- [1041] D. Morgan, M. R. Pennington, New data on the  $K\bar{K}$  threshold region and the nature of the  $f_0$  ( $S^*$ ), Phys. Rev. D48 (1993) 1185–1204.
- [1042] G. Isidori, L. Maiani, M. Nicolaci, S. Pacetti, The  $e^+e^- \rightarrow P_1P_2\gamma$  processes close to the  $\phi$  peak: Toward a model-independent analysis, JHEP 05 (2006) 049.
- [1043] A. V. Anisovich, V. V. Anisovich, V. N. Markov, V. A. Nikonov, A. V. Sarantsev, Decay  $\phi(1020) \rightarrow \gamma f_0(980)$ : Analysis in the non-relativistic quark model approach, Phys. Atom. Nucl. 68 (2005) 1554–1572.
- [1044] N. N. Achasov, Radiative decays of  $\phi$ -meson about nature of light scalar resonances, Phys. Atom. Nucl. 67 (2004) 1529–1535.
- [1045] N. N. Achasov, A. V. Kiselev, Properties of the light scalar mesons face the experimental data on the  $\phi \rightarrow \pi^0\pi^0\gamma$  decay and the  $\pi\pi$  scattering, Phys. Rev. D73 (2006) 054029.
- [1046] Y. S. Kalashnikova, A. E. Kudryavtsev, A. V. Nefediev, C. Hanhart, J. Haidenbauer, The radiative decays  $\phi \rightarrow \gamma a_0/f_0$  in the molecular model for the scalar mesons, Eur. Phys. J. A24 (2005) 437–443.

- [1047] F. E. Close, N. A. Tornqvist, Scalar mesons above and below 1 GeV, *J. Phys. G* 28 (2002) R249–R267.
- [1048] J. Boyer, et al., Two photon production of pion pairs, *Phys. Rev. D* 42 (1990) 1350–1367.
- [1049] H. Marsiske, et al., A measurement of  $\pi^0\pi^0$  production in two photon collisions, *Phys. Rev. D* 41 (1990) 3324.
- [1050] J. Dominick, et al., Two photon production of charged pion and kaon pairs, *Phys. Rev. D* 50 (1994) 3027–3037.
- [1051] M. Boglione, M. R. Pennington, Determination of radiative widths of scalar mesons from experimental results on  $\gamma\gamma \rightarrow \pi\pi$ , *Eur. Phys. J. C* 9 (1999) 11–29.
- [1052] M. R. Pennington, Exclusive channels in  $\gamma\gamma$  reactions: Light at the end of the tunnel?, *Nucl. Phys. Proc. Suppl.* 82 (2000) 291–299.
- [1053] T. Barnes, Two photon decays support the ( $K\bar{K}$ ) molecule picture of the  $S^*(975)$  and  $\delta(980)$ , *Phys. Lett. B* 165 (1985) 434.
- [1054] J. A. Oller, E. Oset, Theoretical study of the  $\gamma\gamma \rightarrow$  meson meson reaction, *Nucl. Phys. A* 629 (1998) 739–760.
- [1055] C. Hanhart, Y. S. Kalashnikova, A. E. Kudryavtsev, A. V. Nefediev, Two-photon decays of hadronic molecules, *Phys. Rev. D* 75 (2007) 074015.
- [1056] N. N. Achasov, G. N. Shestakov, The shape of the  $f_0(980)$  in  $\gamma\gamma \rightarrow \pi^+\pi^-$ , *Phys. Rev. D* 72 (2005) 013006.
- [1057] N. N. Achasov, G. N. Shestakov, Dynamics of  $f_0(980)$ -resonance production in the reaction  $\gamma\gamma \rightarrow \pi^+\pi^-$ , *Phys. Atom. Nucl. Nucl. Phys. A* 69 (2006) 1510–1521.
- [1058] M. R. Pennington, Can experiment distinguish tetraquark scalars, molecules and  $\bar{q}q$  mesons? [hep-ph/0703256](#), 2007.
- [1059] M. R. Pennington, Location, correlation, radiation: where is the  $\sigma$ , what is its structure and what is its coupling to photons?, *Mod. Phys. Lett. A* 22 (2007) 1439–1458.
- [1060] A. A. Kondashov, A study of the  $\pi^0\pi^0$  system produced in charge exchange and central collisions, *Nucl. Phys. Proc. Suppl.* 74 (1999) 180–185.
- [1061] V. V. Anisovich, Systematics of quark antiquark states and scalar exotic mesons, [*Usp. Fiz. Nauk* **47** (2004) 49] *Phys. Usp.* 47 (2004) 45–67.
- [1062] N. N. Achasov, G. N. Shestakov, Mechanisms of the  $f_0(980)$  production in the reaction  $\pi^-p \rightarrow \pi^0\pi^0n$ , *Phys. Lett. B* 528 (2002) 73–80.
- [1063] F. P. Sassen, S. Krewald, J. Speth, Meson model for  $f_0(980)$  production in peripheral pion nucleon reactions, *Phys. Rev. D* 68 (2003) 036003.
- [1064] F. P. Sassen, S. Krewald, J. Speth,  $t$ -dependence of pion production in  $\pi^-p \rightarrow \pi^0\pi^0n$ , *Eur. Phys. J. A* 18 (2003) 197–199.
- [1065] N. N. Achasov, G. N. Shestakov,  $\pi\pi$  scattering S-wave from the data on the reaction  $\pi^-p \rightarrow \pi^0\pi^0n$ , *Phys. Rev. D* 67 (2003) 114018.
- [1066] A. Boehrner, Inclusive particle production in hadronic decays of the Z boson at LEP I, *Phys. Rept.* 291 (1997) 107–217.
- [1067] A. Dobado, J. R. Pelaez, The inverse amplitude method in Chiral Perturbation Theory, *Phys. Rev. D* 56 (1997) 3057–3073.
- [1068] J. R. Pelaez, On the nature of light scalar mesons from their large  $N_c$  behavior, *Phys. Rev. Lett.* 92 (2004) 102001.
- [1069] J. R. Pelaez, Light scalars as tetraquarks or two-meson states from large  $N_c$  and unitarized chiral perturbation theory, *Mod. Phys. Lett. A* 19 (2004) 2879–2894.
- [1070] M. Uehara, Large  $n_c$  behavior of light scalar meson nonet revisited, [hep-ph/0401037](#).

- [1071] A. Chodos, R. L. Jaffe, K. Johnson, C. B. Thorn, V. F. Weisskopf, A new extended model of hadrons, Phys. Rev. D9 (1974) 3471–3495.
- [1072] T. A. DeGrand, R. L. Jaffe, K. Johnson, J. E. Kiskis, Masses and other parameters of the light hadrons, Phys. Rev. D12 (1975) 2060.
- [1073] E. van Beveren, F. Kleefeld, G. Rupp, M. D. Scadron, Remarks on the  $f_0(400 - 1200)$  scalar meson as the dynamically generated chiral partner of the pion, Mod. Phys. Lett. A17 (2002) 1673.
- [1074] E. van Beveren, G. Rupp, Classification of the scalar mesons: A strange pole expedition into charm and beauty territory, Mod. Phys. Lett. A19 (2004) 1949–1967.
- [1075] N. A. Tornqvist, Understanding the scalar meson  $q\bar{q}$  nonet, Z. Phys. C68 (1995) 647–660.
- [1076] A. Deandrea, R. Gatto, G. Nardulli, A. D. Polosa, N. A. Tornqvist, The  $s\bar{s}$  and  $K\bar{K}$  nature of  $f_0(980)$  in  $D_s$  decays, Phys. Lett. B502 (2001) 79–86.
- [1077] M. Boglione, M. R. Pennington, Dynamical generation of scalar mesons, Phys. Rev. D65 (2002) 114010.
- [1078] A. Zhang, T. Huang, T. G. Steele, Diquark and light four-quark states, hep-ph/0612146.
- [1079] T. V. Brito, F. S. Navarra, M. Nielsen, M. E. Bracco, QCD sum rule approach for the light scalar mesons as four- quark states, Phys. Lett. B608 (2005) 69–76.
- [1080] H.-X. Chen, A. Hosaka, S.-L. Zhu, Scalar tetraquarks of light flavors in the QCD sum rule. hep-ph/0609163.
- [1081] R. D. Matheus, F. S. Navarra, M. Nielsen, R. Rodrigues da Silva, Do the QCD sum rules support four-quark states? arxiv:0705.1357 [hep-ph].
- [1082] R. L. Jaffe, Ordinary and extraordinary hadrons, hep-ph/0701038.
- [1083] P. Gavillet, R. Armenteros, M. Aguilar-Benitez, M. Mazzucato, C. Dionisi, Evidence for a new  $K^*\bar{K}$  state at a mass of 1530 MeV with  $(I)J^{PC} = (0)1^{++}$  observed in  $K^-p$  interactions at 4.2 GeV/c, Z. Phys. C16 (1982) 119.
- [1084] R. S. Longacre, The E(1420) meson as a  $K\bar{K}\pi$  molecule, Phys. Rev. D42 (1990) 874–883.
- [1085] L. Gorlich, et al., A model independent partial wave analysis of the reaction  $\pi^-p \rightarrow K^+K^-n$  at approximately 18 GeV/c, Nucl. Phys. B174 (1980) 16.
- [1086] P. Estabrooks, A. D. Martin,  $\pi\pi$  partial waves from 0.6 GeV TO 1.8 GeV, Nucl. Phys. B95 (1975) 322.
- [1087] A. D. Martin, M. R. Pennington, How imposing analyticity on a  $\pi\pi$  phase shift analysis can reveal new solutions, explore experimental structures and investigate the possibility of new resonances, Ann. Phys. 114 (1978) 1.
- [1088] P. Estabrooks, Where and what are the scalar mesons?, Phys. Rev. D19 (1979) 2678.
- [1089] D. V. Bugg, Reconciling  $\phi$  radiative decays with other data for  $a_0(980)$ ,  $f_0(980)$ ,  $\pi\pi \rightarrow K\bar{K}$  and  $\pi\pi \rightarrow \eta\eta$ , Eur. Phys. J. C47 (2006) 45–55.
- [1090] A. D. Martin, E. N. Ozmutlu, Analyses of  $K\bar{K}$  production and scalar mesons, Nucl. Phys. B158 (1979) 520.
- [1091] S. J. Lindenbaum, R. S. Longacre, Coupled channel analysis of  $J^{PC} = 0^{++}$  and  $2^{++}$  isoscalar mesons with masses below 2 GeV, Phys. Lett. B274 (1992) 492–497.
- [1092] A. Etkin, et al., Amplitude analysis of the  $K_S^0 K_S^0$  system produced in the reaction  $\pi^-p \rightarrow K_S^0 K_S^0 n$  at 23 GeV/c, Phys. Rev. D25 (1982) 1786.
- [1093] R. Ehrlich, et al.,  $p + \pi^+ + \pi^-$  enhancements in the reaction  $p + p \rightarrow p + p + \pi^+ + \pi^-$  at 24.8 GeV/c, Phys. Rev. Lett. 21 (1968) 1839–1842.
- [1094] S. U. Chung, Techniques of amplitude analysis for two pseudoscalar systems, Phys. Rev. D56 (1997) 7299–7316.

- [1095] M. Gaspero, Evidence for the dominance of an  $I^G J^{PC} = 0^+0^{++}$  resonance in  $\bar{p}n \rightarrow 2\pi^+3\pi^-$  annihilation at rest, Nucl. Phys. A562 (1993) 407–445.
- [1096] D. V. Bugg, B. S. Zou, A. V. Sarantsev, New results on  $\pi\pi$  phase shifts between 600-MeV and 1900-MeV, Nucl. Phys. B471 (1996) 59–89.
- [1097] E. Klempt, et al., Phase motion of baryon resonances, Eur. Phys. J. A29 (2006) 307–313.
- [1098] D. V. Bugg, A study in depth of  $f_0(1370)$ . arxiv:0706.1341 [hep-ex], (2007).
- [1099] B. Aubert, et al., Dalitz plot analysis of  $D^0$  hadronic decays  $D^0 \rightarrow K^0 K^- \pi^+$ ,  $D^0 \rightarrow \bar{K}^0 K^+ \pi^-$  and  $D^0 \rightarrow \bar{K}^0 K^+ K^-$ . 31st International Conference on High Energy Physics (ICHEP 2002), Amsterdam, The Netherlands, 2002, hep-ex/0207089.
- [1100] E. Klempt, M. Matvéev, A. V. Sarantsev, Further study of  $d_s^+$  decays into  $\pi^-\pi^+\pi^+$ , in preparation.
- [1101] G. Bonvicini, et al., Dalitz analysis of  $D^+ \rightarrow \pi^+\pi^-\pi^+$ , hep-ex/0607069.
- [1102] H. Li, Study of scalar mesons at BES-II,  $e^+e^-$  Collisions from  $\phi$  to  $\psi$ , Novosibirsk, Russia, 27 Feb - 2 Mar 2006, hep-ex/0605033.
- [1103] T. A. Lahde, U.-G. Meißner, Improved analysis of  $J/\psi$  decays into a vector meson and two pseudoscalars, Phys. Rev. D74 (2006) 034021.
- [1104] C. Edwards, et al., Observation of an  $\eta\eta$  resonance in  $J/\psi$  radiative decays, Phys. Rev. Lett. 48 (1982) 458.
- [1105] D. V. Bugg, A glueball component in  $f_0(1790)$ , hep-ph/0603018.
- [1106] J. Becker, et al., Radiative decays of the  $J/\psi$  into  $\gamma\pi^+\pi^-$  and  $\gamma K^+K^-$ , Phys. Rev. D35 (1987) 2077.
- [1107] W. Dunwoodie,  $J/\psi$  radiative decay to two pseudoscalar mesons from MARKIII, AIP Conf. Proc. 432 (1998) 753–757.
- [1108] J. Z. Bai, et al., Structure analysis of the  $f_J(1710)$  in the radiative decay  $J/\psi \rightarrow \gamma K^+K^-$ , Phys. Rev. Lett. 77 (1996) 3959–3962.
- [1109] A. Billoire, R. Lacaze, A. Morel, H. Navelet, The use of QCD in OZI violating radiative decays of vector mesons, Phys. Lett. B80 (1979) 381.
- [1110] J. G. Körner, J. H. Kuhn, M. Krammer, H. Schneider, Zweig forbidden radiative orthoquarkonium decays in perturbative QCD, Nucl. Phys. B229 (1983) 115.
- [1111] L. Maiani, F. Piccinini, A. D. Polosa, V. Riquer, Positive parity scalar mesons in the 1 GeV - 2 GeV mass range, hep-ph/0604018.
- [1112] C. Amsler, F. E. Close, Evidence for a scalar glueball, Phys. Lett. B353 (1995) 385–390.
- [1113] C. Amsler, F. E. Close, Is  $f_0(1500)$  a scalar glueball?, Phys. Rev. D53 (1996) 295–311.
- [1114] F. E. Close, A. Kirk, Scalar glueball  $q\bar{q}$  mixing above 1 GeV and implications for lattice QCD, Eur. Phys. J. C21 (2001) 531–543.
- [1115] C. Amsler, Further evidence for a large glue component in the  $f_0(1500)$  meson, Phys. Lett. B541 (2002) 22–28.
- [1116] F. E. Close, Q. Zhao, Production of  $f_0(1710)$ ,  $f_0(1500)$ , and  $f_0(1370)$  in  $J/\psi$  hadronic decays, Phys. Rev. D71 (2005) 094022.
- [1117] Q. Zhao, F. E. Close, Scalar glueball production in  $J/\psi$  hadronic decays, Int. J. Mod. Phys. A21 (2006) 821–824.
- [1118] Q. Zhao, B.-s. Zou, Z.-b. Ma, Glueball -  $Q\bar{Q}$  mixing and Okuba-Zweig-Iizuka rule violation in the hadronic decays of heavy quarkonia, Phys. Lett. B631 (2005) 22–31.
- [1119] D. Weingarten, Scalar quarkonium and the scalar glueball, Nucl. Phys. Proc. Suppl. 53 (1997) 232–235.

- [1120] W.-J. Lee, D. Weingarten, Scalar quarkonium masses and mixing with the lightest scalar glueball, Phys. Rev. D61 (2000) 014015.
- [1121] D.-M. Li, H. Yu, Q.-X. Shen, Glueball-quarkonia content of the  $f_0(1370)$ ,  $f_0(1500)$  and  $f_0(1710)$ , Commun. Theor. Phys. 34 (2000) 507–512.
- [1122] M. Strohmeier-Presicek, T. Gutsche, A. Faessler, R. Vinh Mau,  $4\pi$  decay modes of the  $f_0(1500)$  resonance, Phys. Lett. B438 (1998) 21–26.
- [1123] M. Strohmeier-Presicek, T. Gutsche, R. Vinh Mau, A. Faessler, Glueball-quarkonia content and decay of scalar-isoscalar mesons, Phys. Rev. D60 (1999) 054010.
- [1124] F. Giacosa, T. Gutsche, A. Faessler, A covariant constituent quark/gluon model for the glueball- quarkonia content of scalar-isoscalar mesons, Phys. Rev. C71 (2005) 025202.
- [1125] F. Giacosa, T. Gutsche, V. E. Lyubovitskij, A. Faessler, Scalar meson and glueball decays within a effective chiral approach, Phys. Lett. B622 (2005) 277–285.
- [1126] F. Giacosa, T. Gutsche, V. E. Lyubovitskij, A. Faessler, Scalar nonet quarkonia and the scalar glueball: Mixing and decays in an effective chiral approach, Phys. Rev. D72 (2005) 094006.
- [1127] D.-M. Li, H. Yu, Q.-X. Shen, Properties of the scalar mesons  $f_0(1370)$ ,  $f_0(1500)$  and  $f_0(1710)$ , Eur. Phys. J. C19 (2001) 529–533.
- [1128] L. S. Celenza, S.-f. Gao, B. Huang, H. Wang, C. M. Shakin, Covariant confinement model for the calculation of the properties of scalar mesons, Phys. Rev. C61 (2000) 035201.
- [1129] J. Vijande, A. Valcarce, F. Fernandez, B. Silvestre-Brac, Nature of the light scalar mesons, Phys. Rev. D72 (2005) 034025.
- [1130] D. Black, A. H. Fariborz, F. Sannino, J. Schechter, Putative light scalar nonet, Phys. Rev. D59 (1999) 074026.
- [1131] A. H. Fariborz, R. Jora, J. Schechter, Toy model for two chiral nonets, Phys. Rev. D72 (2005) 034001.
- [1132] A. H. Fariborz, Mass uncertainties of  $f_0(600)$  and  $f_0(1370)$  and their effects on determination of the quark and glueball admixtures of the  $I = 0$  scalar mesons, Phys. Rev. D74 (2006) 054030.
- [1133] P. Bicudo, S. R. Cotanch, F. J. Llanes-Estrada, D. G. Robertson, The new  $f_0(1810)$  in  $\omega\phi$  at BES: A good glueball candidate.
- [1134] V. V. Anisovich, Scalar mesons and low-mass sigma: Does the  $\sigma$  reveal the confinement singularity?, Int. J. Mod. Phys. A21 (2006) 3615–3640.
- [1135] A. V. Anisovich, et al., The riddle of the  $f_0(980)$  and  $a_0(980)$ : Are they the quark- antiquark states? hep-ph/0508260.
- [1136] V. V. Anisovich, D. V. Bugg, A. V. Sarantsev, Broad resonances as locking states and the problem of confinement, Phys. Atom. Nucl. 62 (1999) 1247–1257.
- [1137] M. A. Shifman, A. I. Vainshtein, V. I. Zakharov, Instantons in non-perturbative QCD vacuum, Nucl. Phys. B165 (1980) 45.
- [1138] C. Quigg, Meson spectroscopy and the phenomenology of high-energy collisions, AIP Conf. Proc. 22 (1974) 297–320.
- [1139] V. Dmitrasinovic, UA(1) breaking and scalar mesons in the Nambu-Jona-Lasinio model, Phys. Rev. C53 (1996) 1383–1396.
- [1140] L. Burakovsky, T. Goldman, Towards resolution of the enigmas of p-wave meson spectroscopy, Phys. Rev. D57 (1998) 2879–2888.
- [1141] L. Burakovsky, Towards resolution of the scalar meson nonet enigma, Found. Phys. 27 (1997) 315–330.
- [1142] G. S. Bali, et al., Static potentials and glueball masses from QCD simulations with Wilson sea quarks, Phys. Rev. D62 (2000) 054503.

- [1143] S. Pacetti, Unraveling the  $f_0$  nature by connecting KLOE and BABAR data through analyticity, *Eur. Phys. J.* A31 (2007) 665–671.
- [1144] V. Baru, J. Haidenbauer, C. Hanhart, Y. Kalashnikova, A. E. Kudryavtsev, Evidence that the  $a_0(980)$  and  $f_0(980)$  are not elementary particles, *Phys. Lett.* B586 (2004) 53–61.
- [1145] N. N. Achasov, A. V. Kiselev, Once more about the  $K\bar{K}$  molecule approach to the light scalars, *hep-ph/0606268*.
- [1146] Y. S. Kalashnikova, A. E. Kudryavtsev, A. V. Nefediev, J. Haidenbauer, C. Hanhart, Comment on 'once more about the  $K\bar{K}$  molecule approach to the light scalars', *hep-ph/0608191*.
- [1147] C. Hanhart, Towards an understanding of the light scalar mesons, *Eur. Phys. J.* A31 (2007) 543–548.
- [1148] N. Kaiser, P. B. Siegel, W. Weise, Chiral dynamics and the  $S_{11}(1535)$  nucleon resonance, *Phys. Lett.* B362 (1995) 23–28.